Diagenesis and Mineralogy of the British Liassic Ironstones

Volume I (II)

Stephen John James
Ph.D.

The University of Aston in Birmingham

October 1980

THE MINERALOGY AND DIAGENESIS OF THE BRITISH LIASSIC IRONSTONES

STEPHEN JOHN JAMES Ph D 1980

SUMMARY

The British Liassic Ironstones occur at the minima of regressive events and are condensed sequences. They are characterised by the presence of chamosite and/or geothite ooids.

Studies on the Frodingham, Marlstone Rock-bed and Cleveland Ironstones at outcrop and in core have shown that they are constructed of a series of different facies. The chamositic chamosite oolite facies represents the site of chamosite ooid and mud formation. Erosion of this facies provided ooids and mud for incorporation in the other facies. The depositional environment represented by the ironstone facies is thought to represent the shelf to shore-face transition zone. The Frodingham Ironstone underwent two periods of subaerial exposure leading to reddening of all the exposed facies.

Petrographic studies show that diagenesis was controlled by the depositional character of the facies. The formation of chamosite ooids was the first authigenic event and involved the activities of filamentous blue-green algae. Subsequent early diagenesis was entirely marine in nature. The exposed Frodingham Ironstone facies underwent vadose diagenesis. Late stage diagenesis in the Cleveland Ironstone involved widespread replacement of the depositional facies by siderite mudstone.

Bulk rock geochemistry shows that individual facies are characterised by a range of analyses reflecting the variation in abundance of the component minerals of the depositional and diagenetic assemblages.

X-ray diffraction, electron probe microanalysis and Mossbauer Spectroscopy show that the chamosite unit cell decreases in size with increasing Fe^{3+} concentrations. This reflects the degree of environmental oxidation undergone by chamosite specimens. The nature of the oxidation differs under wet and dry conditions.

Palaeomagnetic studies have yielded a Sinemurian palaeopole position for the Frodingham Ironstone. No stable component of magnetisation is carried by the two other ironstones.

Mineral stability considerations lead to the conclusion that both depositional mineral assemblages and diagenetic reactions could have occurred in a marine geochemical environment similar to that obtained today.

Keywords: Ironstones, Liassic, Diagenesis, Environment.

CONTENTS

LIST OF TABLES

CHAPTER 6 THE MINERALOGICAL NATURE OF CHAMOSITE X-RAY, ELECTRON PROBE MICROANALYSIS AND MOSSBAUER STUDIES

CHAPTER 7 PALAEOMAGNETIC STUDIES ON THE FRODINGHAM, MARLSTONE ROCK-BED AND CLEVELAND IRONSTONES

CHAPTER 8 CHEMICAL CONSTRAINTS ON THE DEPOSITIONAL AND DIAGENETIC ENVIRONMENTS OF THE LIASSIC IRONSTONES

LIST OF FIGURES

LIST OF PHOTOGRAPHIC PLATES

CHAPTER 2 THE FRODINGHAM IRONSTONE

CHAPTER 3 THE MARLSTONE ROCK-BED IRONSTONE

CHAPTER 4 THE CLEVELAND IRONSTONE FORMATION

CHAPTER 9 THE SEDIMENTOLOGY OF THE LIASSIC IRONSTONES: CONCLUSIONS

ACKNOWLEDGEMENTS

I wish to thank the Shell Trust for Higher Education and my parents, Dr. and Mrs. J. W. James for financial support during the three years spent on this research project.

Whilst carrying out the research, discussions with my supervisors, Dr. D. J. Vaughan and Dr. P. Turner, and with Dr. M. J. Bradshaw were invaluable in determining the course of the work. The technical staff of the Department of Geological Sciences and Metallurgy Department gave me much assistance and useful advice. A special word of thanks is due to Mr. J. Counden who prepared many excellent thin sections for petrographic study. During fieldwork on the Cleveland Ironstone Field Mr. R. J. Suttill helped in the collection of Palaeomagnetic samples.

I should like to thank Dr. D. J. Vaughan and Dr. P. Turner for critically reading the draft of this thesis and providing many useful comments. In the preparation and production of the thesis I owe many thanks for considerable help to my parents and brothers, David and Robert, to Mrs. Janet Churchyard, Mrs. Sue Fagg and Mrs. Sue Taylor for typing the manuscript, to Mr. Colin Nicholson for developing and printing the photomicrographs and to Mr. Keith Attwood for binding the thesis.

My fiancee, Miss Judith Randall, has been a continual source of support and encouragement during my work. In addition she has helped me considerably in the proof-reading of the thesis manuscript and with the preparation of diagrams. I owe her a very special vote of thanks and praise.

CHAPTER 1

INTRODUCTION

1.1 INTRODUCTION

Iron is the fourth most abundant element in the Earth's crust, constituting 5 wt % of it (Mason, 1966). It is thus not surprising that all sedimentary rocks contain a certain amount of iron. The average shale, for instance, contains 4.72 wt %, the average sandstone 0.98 wt %, and the average carbonate rock 0.38 wt % (Turekian and Wedepohl, 1961). In practice it is found that these major sedimentary rock types exhibit a spectrum of iron contents: from initially containing less than 1.0 wt % they progress to a situation where sufficient iron is present for them to be qualified as ferruginous, and finally to a point where enough iron is present for them to be considered under the heading of iron ore. At some level of iron concentration in sediments a line must be drawn between those which are normal, if somewhat ferruginous, and those which have higher iron contents. Sediments containing more than this are designated iron-rich. They have a mineralogy and textures which demand that their palaeoenvironmental parameters must have been significantly different to sediments which contain much less iron. It is into this category that the majority of the world's sedimentary iron deposits fall.

The major types of sedimentary iron deposits are tabulated in Table 1.1 according to age, thickness, areal extent, mineralogy and chemistry. The advantage of this type of classification (Turner, 1977) is that it avoids genetic interpretations. The only conclusion drawn is that since a group of deposits have similar characteristics, they might have similar origins. Of the deposits included the silicate ironstones and aluminous ironstones are economically the most important as iron reserves. The former are restricted to Precambrian shield

Aston University

Content has been removed for copyright reasons

regions and the latter to shallow marine sequences in the Phanerozoic, although some Precambrian examples do occur.

Although a considerable amount of research has been carried out on both silicate and aluminous ironstones their origins are still the subject of debate. This stems from the fact that for neither type of ironstone is a present-day analogue known. Of the two, aluminous ironstones are possibly the least well-documented as regards petrography, diagenesis and mineralogy. The research reported in the following chapters has been carried out in order to gain a better understanding of these features of aluminous ironstones and with the hope that it may yield a better understanding of their origin.

1.2 THE NATURE OF ALUMINOUS IRONSTONES

In the absence of a present-day analogue for these deposits a knowledge of their gross sedimentological and stratigraphic setting is an important aid in understanding their nature and origin. Hallam (1966) has shown that the British Liassic aluminous ironstones represent condensed sequences. A consideration of the level of occurrence of aluminous ironstones in the north-west European Jurassic and the nature of the sediments which underlie and overlie them has lead to the conclusion that they were deposited at the minima of regressive episodes (Hallam, 1978; Hallam and Bradshaw, 1979). The stratigraphic occurrence of the British aluminous ironstones is summarised in Figure 1.1. The Silurian Clinton aluminous ironstones of the United States occur in the shallow, near-shore, sediments located between the palaeocoastline and the reef-belt (Ellison, 1955). The work of Talbot (1974) on the

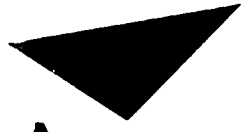

Aston University

Content has been removed for copyright reasons

Upper Oxfordian ironstones of southern England supports a near-shore site of ironstone deposition and relates it to the influx of terrigenous sediment from land areas. Many aluminous ironstones exhibit features indicative of energetic conditions of deposition such as current bedding. All aluminous ironstones contain an abundant normal epifauna and infauna which suggests that ironstone formation occurred in oxygenated waters.

Although many aluminous ironstones pass laterally into sandstones and shales there is often a marked lack of any terrigenous components within them. In order to account for this feature Hemmingway (1951) and Huber and Garrels (1953) have proposed that the site of ironstone formation was separated from the sources of clastic supply by a clastic trap. This model places the site of ironstone formation on a topographic rise in the sea floor. Terrigenous material, transported as bed-load, would be deposited around the margins of the rise. The requisite ferrous iron, aluminium, and silicon required for the formation of aluminous ironstones are transported in suspension to the topographic rise. Hallam and Bradshaw (1979) conclude that, in context of the regressive nature of ironstone formation, this is a favourable model.

In considering the transport of ferrous iron, aluminium and silicon in suspension, a point which must be raised is in what form these elements are transported. Carroll (1958) has shown that a considerable amount of iron may be transported as coatings of ferric oxides on clay platelets. Since both aluminium and silicon are both relatively immobile in the geochemical environment the possibility that soluble complexes of these two elements might be important in their transport must be investigated.

The petrography of aluminous ironstones has been reported by Hallimond (1925), Taylor (1949), Davies and Dixie (1951), Dunham (in Whitehead et al, 1952), Chowns (1968) and others. These workers report the presence of chamosite, goethite and haematite ooids, shell debris and intraclasts as the depositional components of the ironstone, and authigenic chamosite, siderite and calcite as cement phases. No detailed consideration of the diagenetic history of the aluminous ironstones has been discussed. The characteristic feature of all aluminous ironstones is the presence of ooids of chamosite or its oxidised equivalents; goethite and haematite. The presence of a ferrous alumino-silicate in such abundance in energetic, oxygenated environments is a very problematical feature. The formation of chamosite ooids has been considered by a number of workers. Their conclusions fall into three schools of thought: (i) primary formation of ooids by the mechanical accretion of a chamosite mud or gel around some core grain (Hallimond, 1925; Taylor, 1949; Knox, 1970; Talbot, 1974); (ii) replacement of originally calcite or aragonite ooids by chamosite as a result of the percolation of ground-waters rich in iron, aluminium and silicon (Sorby, 1856; Kimberley, 1974, 1979); (iii) primary formation of ooids by processes analagous to those which form present-day aragonite ooids (Chowns, 1968). The formation of chamosite ooids is considered in Chapter 9. Since chamosite ooids are quantitatively the most important primary phase of the ironstone, and therefore represent the environmental fixation of ferrous iron, aluminium and silicon, an understanding of their mode of origin is fundamental to understanding the origins of aluminous ironstones.

Although aluminous ironstones have been examined from various points of view by numerous workers very little can be concluded about their origin which is undisputed. There are four factors which need to be investigated in order to give a clearer picture of the origin of aluminous ironstones: (i) The method by which ferrous iron, aluminium, and silicon are transported in the marine environment. Ferrous iron would be expected to be oxidised to ferric iron. Aluminium and silicon are considered to be relatively immobile. (ii) Given that the geochemical environment is favourable, the mode of chamosite precipitation and its incorporation in ooids is the most important process leading to aluminous ironstone formation. (iii) Although the broad stratigraphic and sedimentological features of aluminous ironstones are well-documented the specific type of sedimentary environments represented by ironstones are unknown. This may have an important bearing on (i) and (ii). (iv) Carbonate rocks exhibit cement textures which are considered to be diagnostic of certain types of diagenetic and depositional environments. The presence of similar carbonate cement textures in ironstones would be useful in terms of (iii).

1.3 FIELD AREAS AND LABORATORY WORK

Three Liassic aluminous ironstones, the Frodingham, Marlstone Rock-bed and Cleveland Ironstones were chosen for field and laboratory study. The Frodingham Ironstone (Sinemurian) and the Marlstone Rock-bed (Domerian) were both deposited to the south of the Market Weighton

block on the East Midlands shelf (Figure 1.2). The Cleveland Ironstone (Domerian) occurs in a depositional basin (Chowns, 1968) to the immediate north of the Market Weighton block (Figure 1.2). Two of the three ironstones lie within the same area, but are separated in time, and two are contemporaneous, but occur in two different areas separated by the Market Weighton block.

Field work on the three ironstones involved the logging of sections exposed in quarries and at natural exposures and the collection of samples for laboratory work. The logging of cores provided by the British Steel Corporation (Scunthorpe Division) was a great aid in the study of the Frodingham Ironstone.

Many of the questions arising over the nature and origin of aluminous ironstones require laboratory work. A fairly extensive programme of laboratory investigation of the ironstone samples collected was therefore undertaken. The major part of this programme was the petrographic examination of the ironstone samples. This has allowed the recognition of several different ironstone facies, each characterised by its depositional grain and mud assemblage and its diagenetic history. Bulk rock chemical analysis was carried out in order to determine whether the three ironstones exhibit any chemical variation either within themselves or relative to each other. The approach to a better understanding of the nature of chamosite ooids was made by studying, in addition to petrography, the mineralogy of chamosite. This involved electron probe microanalysis, X-ray diffraction and Mossbauer spectroscopy. Although a number of conclusions can be drawn regarding the nature of chamosite ooids from petrographic work this does not yield much information on their fine structure. Scanning

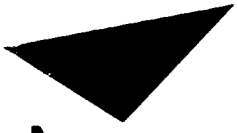

Aston University

Content has been removed for copyright reasons

electron microscopy and high-power transmission electron microscopy (this was carried out by Dr. J. R. Ashworth) were used to elucidate this. A property of sedimentary rocks, which is related to their mineralogy and diagenetic history, is their palaeomagnetic character. It would be expected that ironstones might contain magnetic minerals as a result of their iron-rich nature. Accordingly, a laboratory study of their magnetic properties was carried out.

1.4 NOMENCLATURE

It has been noted above that the British aluminous ironstones are characteristically oolitic in texture and contain a variety of minerals: chamosite, goethite or limonite, siderite, calcite, and quartz. These are distributed amongst cement and allochems, by analogy with Folk's (1959) scheme for classifying limestones. In general, chamosite and goethite (limonite) form ooids and the other minerals form either allochems, such as shell fragments, or cement. The variation in relative proportions of both allochems and cement and of individual minerals gives rise to a tremendous variety of lithologies. Taylor (1949) has proposed a scheme of nomenclature which has gained general acceptance. In this, an adjectival prefix is used for matrix and cement minerals, and a substantive prefix for those of the ooids. Thus a rock with chamosite ooids and a siderite and calcite cement is termed a sideritic calcitic chamosite oolite. In a number of cases this terminology becomes very cumbersome but does give an accurate lithological description.

In applying the nomenclature of Taylor (1949) during field work, it was found necessary to term brown or yellowish-brown ooid-forming phases limonite. This follows from the fact that crusts of limonite are the weathering product of ironstones. A lithology which is called some form of limonite oolite is, therefore, a field description. Mossbauer spectroscopy shows that the brown or yellowish-brown ooids are, in fact, goethite rather than the mixture of various types of hydrated iron compounds represented by limonite.

In the petrographic study of the ironstones several different carbonate cement fabrics were encountered. In order to describe them succintly the terminology of Friedman (1965) was used. In this terminology cement crystal size variations are taken into account by terming uniform-size cement crystals equigranular and cements in which a variation in crystal size occurs inequigranular. Both types of cement may be either idiotopic (majority of component crystals euhedral), hypidiotopic (component crystals subhedral) or xenotopic (component crystals anhedral). If a cement of any one of the six types possible contains small crystals set within a larger crystal of the cement then the overall cement type is called poikilotopic.

1.5 EXPERIMENTAL METHODS

The methods used in laboratory work are described where appropriate. One important experimental technique which has been used extensively, however, is the staining of thin sections. This has been used in order to differentiate between carbonate cement components and to recognise different iron compositions within any one component.

Due to its extensive use the method of staining thin sections is given here. The method of Dickson(1966) is used. Thin sections were stained for approximately 45 seconds in a combined solution consisting of alizarin red-S and potassium ferricyanide dissolved in dilute hydrochloric acid. The stained colour of different carbonate minerals is given in Table 1.2. The content of ferrous iron present within ferroan calcite causes a deeper blue stain with increasing composition. Lindholm and Finkelman (1972) have attempted a correlation between ferrous iron concentration and stain colour. The variables in the method of thin section staining such as seetion thickness, time of staining, acid concentration, militate against this correlation being applicable as a semiquantitative tool in the observation of large numbers of thin sections.

1.6 APPLICATION OF RESULTS

Previous studies of aluminous ironstones have been restricted to a particular ironstone or some aspect of a specific ironstone. The work reported and discussed below represents a multivariate approach to the problems of ironstone development outlined above. Three ironstones which appear to be rather different from each other have been studied. Those features which they have in common may also be shared by other aluminous ironstones and may allow some insight into the nature of ironstone formation.

Mineral	Stain colour
Non-ferroan calcite	Pink
Ferroan calcite	Blue
Non-ferroan dolomite	White (unstained)
Ferroan dolomite	Turquoise
Siderite	White (unstained)

Table 1.2. Stain colours (Dickson, 1966)

CHAPTER 2

THE FRODINGHAM IRONSTONE

THE FRODINGHAM IRONSTONE

2.1 INTRODUCTION

The Frodingham Ironstone outcrops along an escarpment immediately to the east of Scunthorpe, South Yorkshire. It has been worked as an iron-ore since 1860. This has generated its widespread exposure in a series of open-cast pits along a 2 km wide belt passing from Winterton Grange in the north to Ashby, 12 km to the south. The ironstone continues to be worked by the British Steel Corporation by both open-cast and underground methods. Figure 2.1 shows the geographic location of the Frodingham Ironstone, and Figure 2.2 the current disposition of the pits and underground workings.

The Frodingham Ironstone is the oldest of the British Liassic ironstones (Figure 1.1). It occurs in the Sinemurian stage, commencing at the base of the Semicostatum zone and extending up to the top of the Obtusum zone. The entire deposit has a lenticular form, varying in thickness over 25 km, from 9.20 m at Yarborough Pit, Scunthorpe, to 14.01 m at Warlaby (Bull. Geol. Surv. G.B., 1979), to 0.51 m at Nettleton Quarry, Claxby (Figure 2.1). In contrast, the time-equivalent strata of Yorkshire are 30 m thick, whilst those of south Lincolnshire are 60 m thick. Thus, the ironstone represents a local condensed sequence (Hallam, 1966).

The sequence beneath the Frodingham Ironstone is not well known in the area immediately surrounding Scunthorpe. Davies and Dixie (1951) report the nature of the directly underlying 3 m of sediment as alternating calcareous and grey shales. In the course of this research, a core passing through the ironstone and into the strata beneath was examined. The data obtained from this core are summarised in Figure 2.4.g

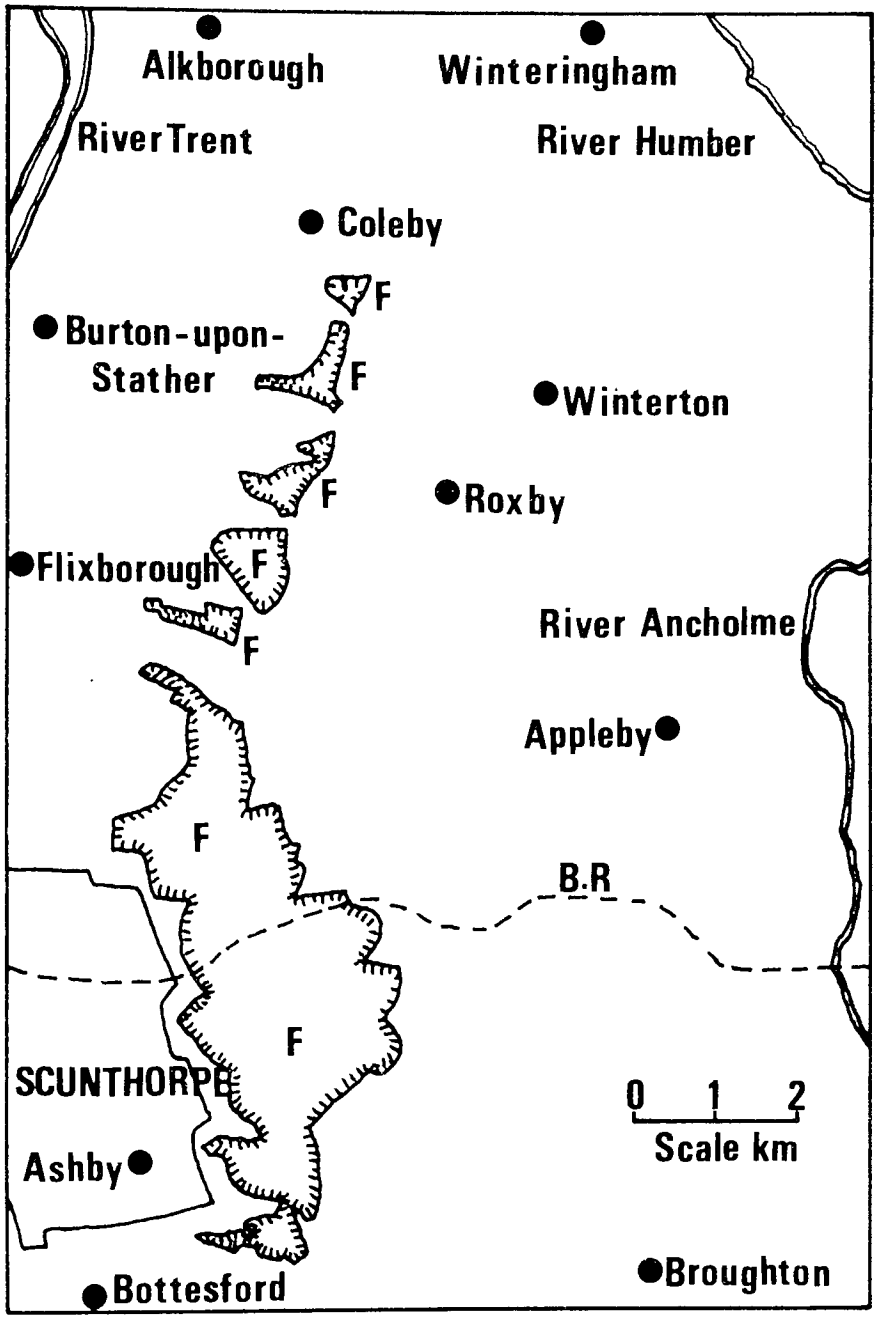

Figure 2.1: Geographical Location Of The Frodingham Ironstone Field (F)

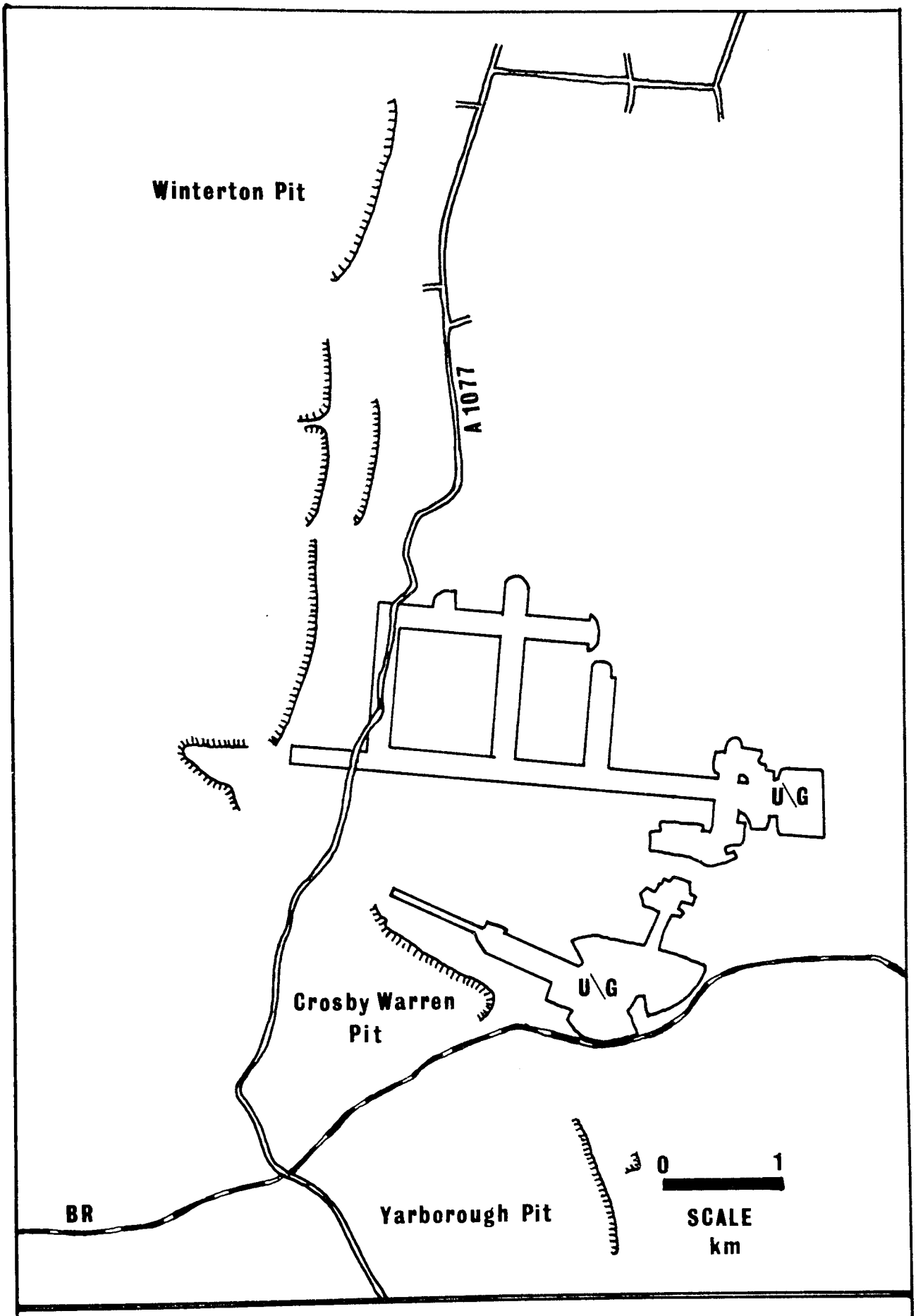

Figure 2.2: Working (Named) Pits And Underground (u\g) Mines

It was found that an alternating series of argillaceous limestones and medium to dark-grey mudstones occur beneath the ironstone. In some instances, the limestones are characterised by the presence of fragmentary bivalves. Approximately 17 m beneath the base of the ironstone, the sedimentary record becomes more uniform, being comprised of dark grey mudstones. This type of upward passage through mudstones to mudstone-limestone to ironstone is indicative of an overall shallowing or regressive event (Hallam, 1978).

The sediments which postdate the ironstone are well exposed around the northern and eastern margins of the open-cast belt where the ironstone is abruptly overlain by approximately 23 m of Upper Sinemurian and Carixian grey clays. These are interupted by a thin, heavily weathered ironstone; the Pecten Bed. A further 14 m of grey clay representing the Domerian Margaritatus zone overlies this bed and directly underlies the Marlstone Rock-bed which occupies the Domerian Spinatum zone. In the area surrounding Scunthorpe the Marlstone is a sandy ironstone (D. Elford, pers. comm.). It forms the top of this part of the Jurassic sequence in this area.

Due to Pleistocene erosive activity in the area, much of the post-ironstone cover, and some of the ironstone to the west and south-west of the open-cast belt, has been removed. The ironstone that remains is very heavily weathered and consists largely of limonite with calcite shells. This is overlain by wind-blown sands and Holocene to Recent soils.

2.2 FORM AND NATURE OF THE IRONSTONE

2.2.1 Introduction

The Frodingham Ironstone has been examined at outcrop in Winterton, Yarborough and Crosby Warren Pits, Scunthorpe. The British Steel Corporation (Scunthorpe Division) have supplied four cores from Winterton, Crosby Warren and Yarborough Pits for detailed study. The nature of the ironstone in a core drilled recently by the Oxford Heat Flow Group at Nettleton Quarry near Claxby, was also investigated. Figure 2.3 shows those localities where the ironstone has been directly examined, and those from which the above-mentioned cores were taken.

Detailed logging of the cores has been carried out. In addition, sections of the ironstone, where examined at outcrop, have been logged in the greatest detail possible. Individual graphic logs of the sections examined are presented in Figure 2.4. As a result of this research, it has been possible to distinguish several individual facies of Frodingham Ironstone. Figure 2.5 summarises the individual graphic logs in terms of these facies, and presents a tentative correlation between them.

2.2.2 Thickness Variation

It is immediately apparent from Figure 2.5 that the Frodingham Ironstone has a maximum thickness of 14.01 m in the Warlaby E. borehole (Bull. Geol. Surv. G.B., 1979). 7 km south-west of this the Yarborough Pit cores Y112 and Y113 show thicknesses of 9.20 and 9.46 m respectively. Core CW17, located approximately 1.5 km to the north-west of these, shows an ironstone thickness of 9.09 m. Core W145 from Winterton Pit reveals that the ironstone has reduced to 7.41 m in a northerly direction, over 6.5 km. The IGS Cockle Pits borehole, 10 km north of

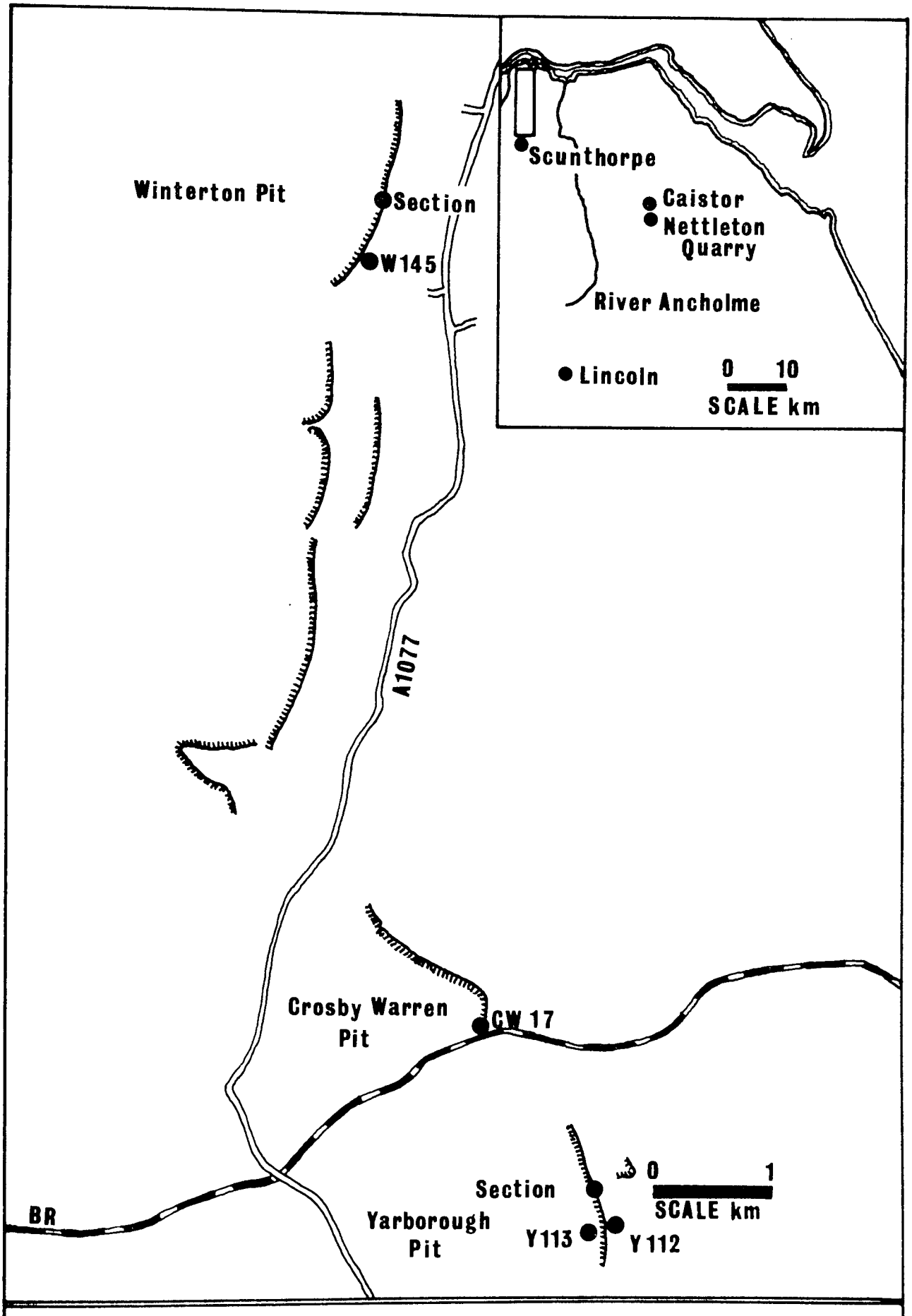

Figure 2.3: Core And Section Locations

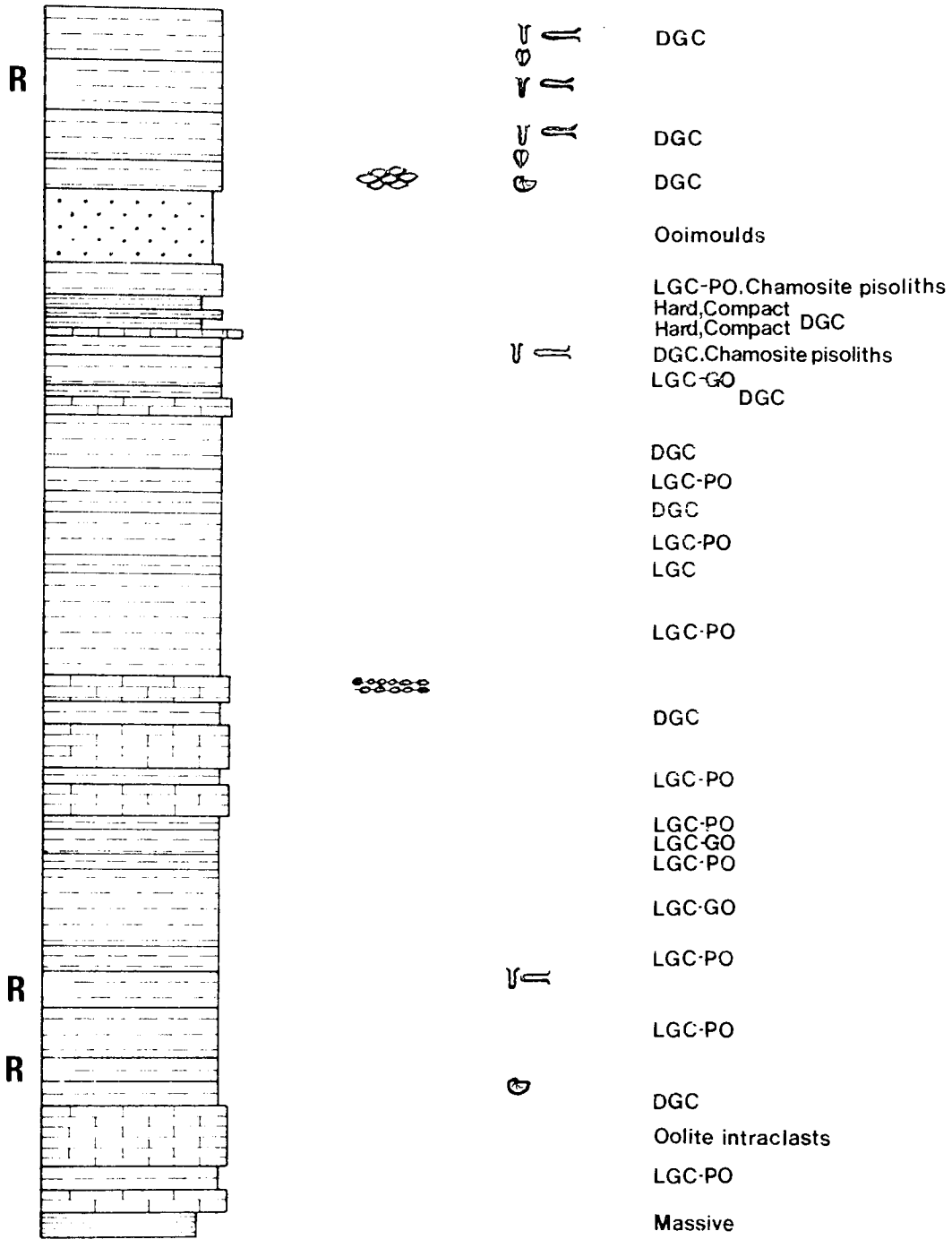

Figure 2.4a: Yarborough Core Y112 Log

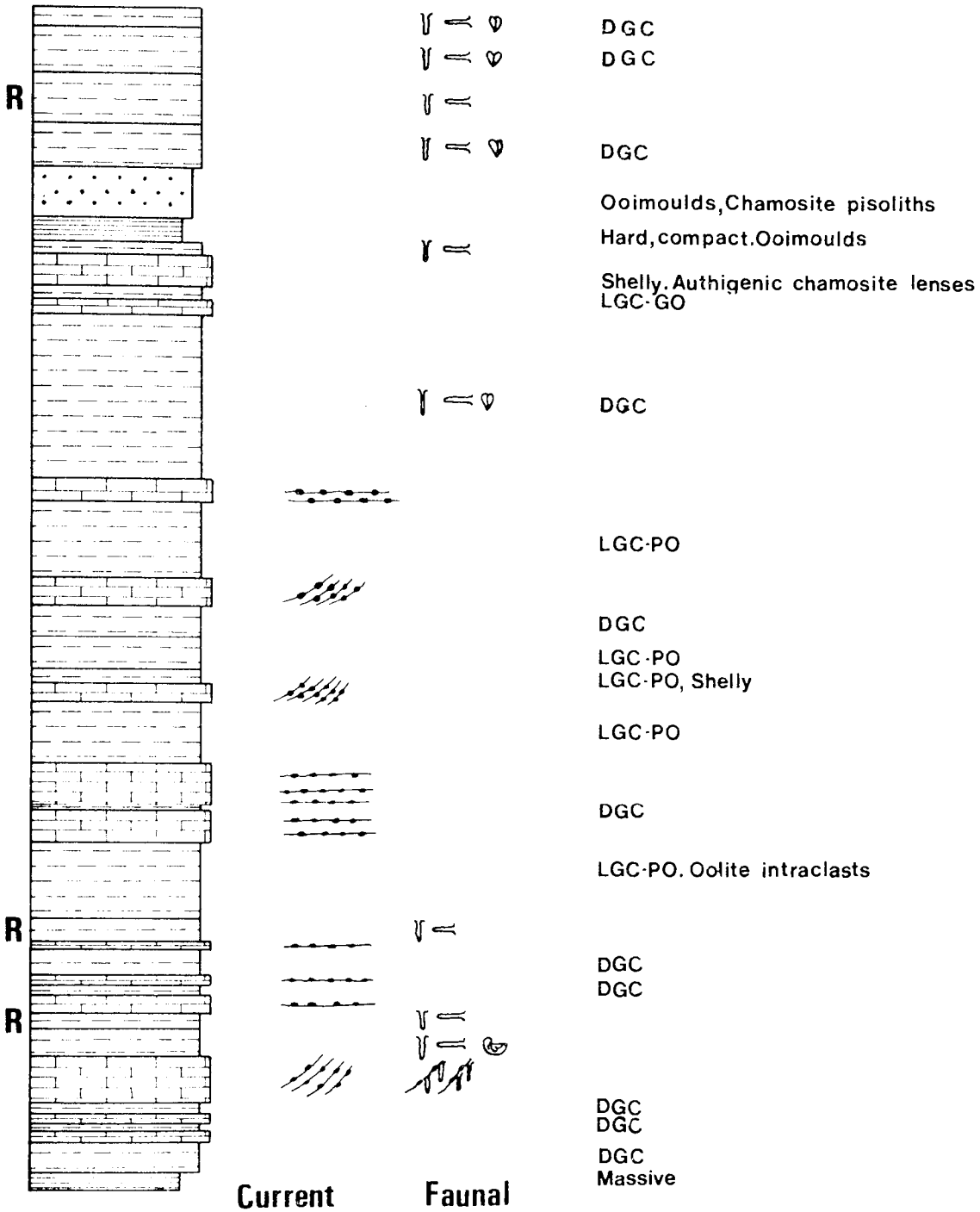

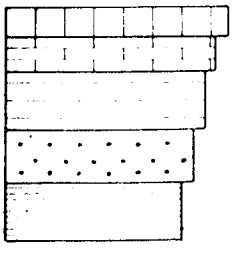

Bioclastic Limestone
Calcitic Limonite Oolite
Chamositic Limonite Oolite
Chamositic Chamosite Oolite
Chamositc Mudstone
R Red equivalent

DGC: Dark Green Chamosite Mud
LGC: Light Green Chamosite Mud;
-GO; Well formed Ooids, -PO; Poorly formed Ooids

Vertical burrows
Horizontal burrows
Burrowing bivalves
Gryphaea in life pos^{n}
Vertical burrows from foreset lamination
Ooids in horizontal lamellae
Ooids in foreset lamellae

Figure 2·4b: Yarborough Core Y113 Log

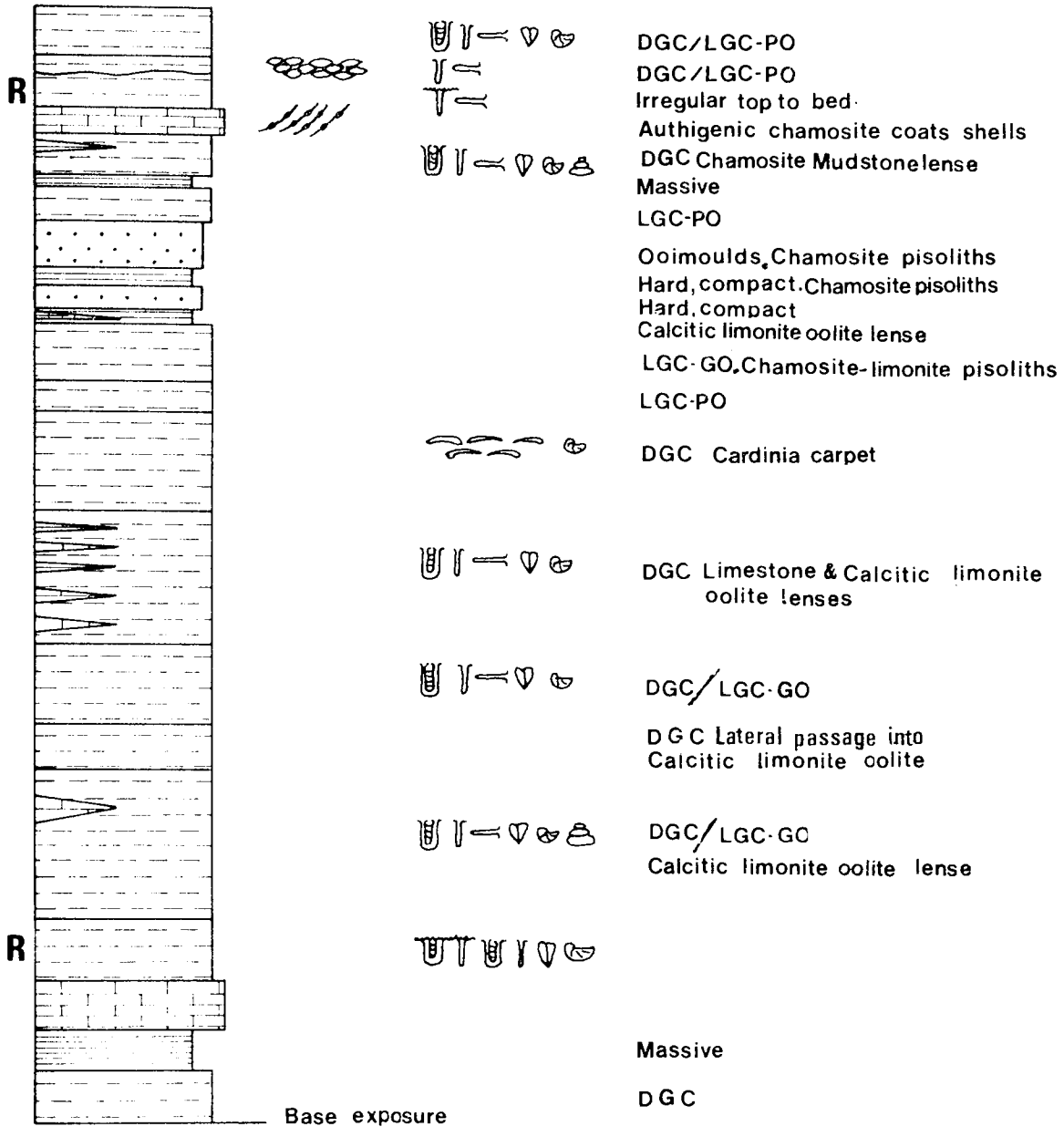

Figure 2·4c: Yarborough Pit Section Log

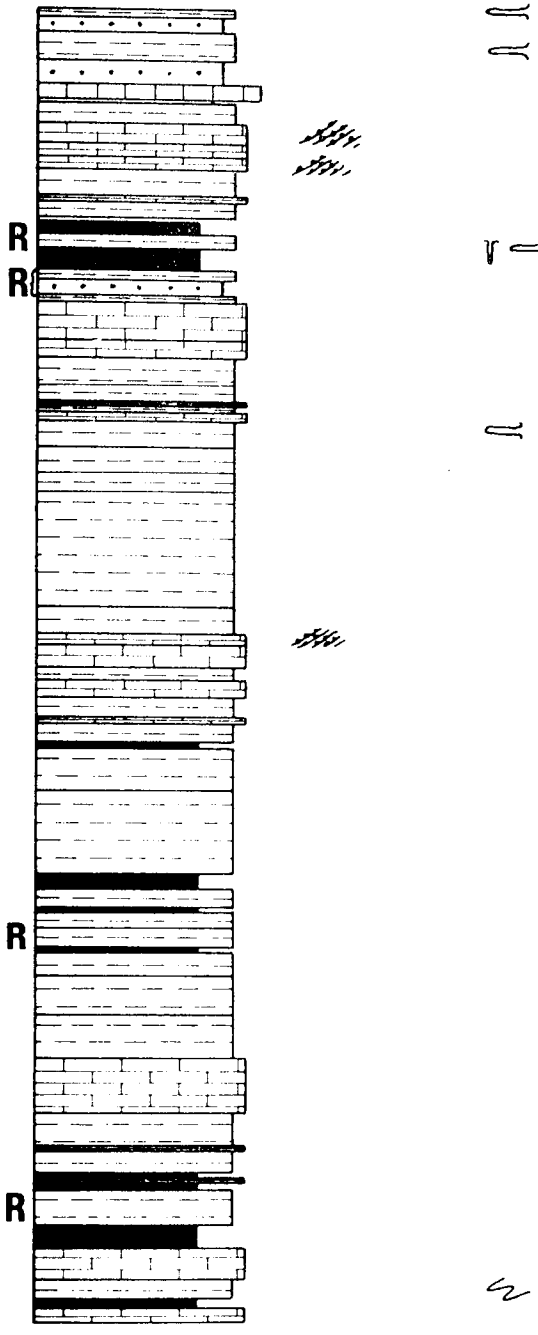

DGC Some chamosite ooids

Ooimoulds Pyritic

DGC Some chamosite ooids
Ooimoulds, Pyritic

DGC

Calcitic sideritic chamositic limonite oolite

LGC-PO

DGC

Record break

LGC-PO

Pisoliths

Calcitic sideritic chamositic limonite oolite

DGC

LGC-PO

DGC

DGC

LGC-PO

DGC

LGC-GO

LGC-GO

LGC-GO

Shelly

LGC-PO

LGC-PO

DGC

LGC-PO

LGC-PO

LGC-PO

LGC-PO

LGC-GO

LGC-PO

Intraclasts

LGC-PO

DGC

DGC

40cm

Current **Faunal**

STRUCTURES

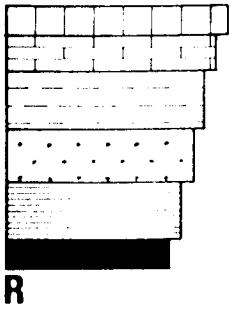

Bioclastic Limestone

Calcitic Limonite Oolite

Chamositic Limonite Oolite

Chamositic Chamosite Oolite

Chamositc Mudstone
Shale

Red equivalent

COMMENTS

Vertical burrows

Horizontal burrows

Rhizocorallium

Ooids in foreset lamellae

DGC: Dark Green Chamosite Mud
LGC: Light Green Chamosite Mud;
-GO; Well formed Ooids, -PO; Poorly formed Ooids

Figure 2.4d Crosby Warren Core CW17 Log

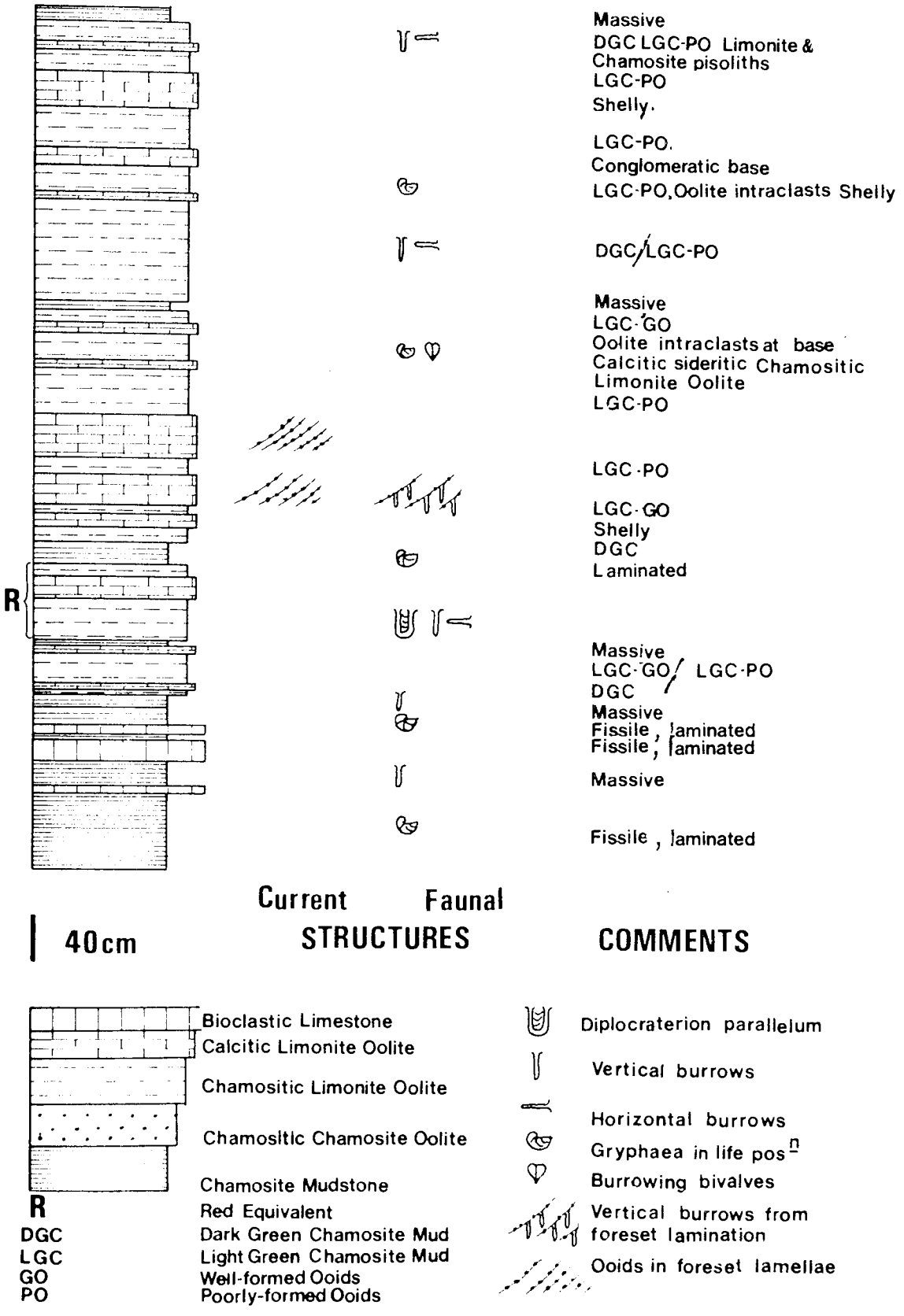

Figure 2·4e:Winterton Core W145 Log

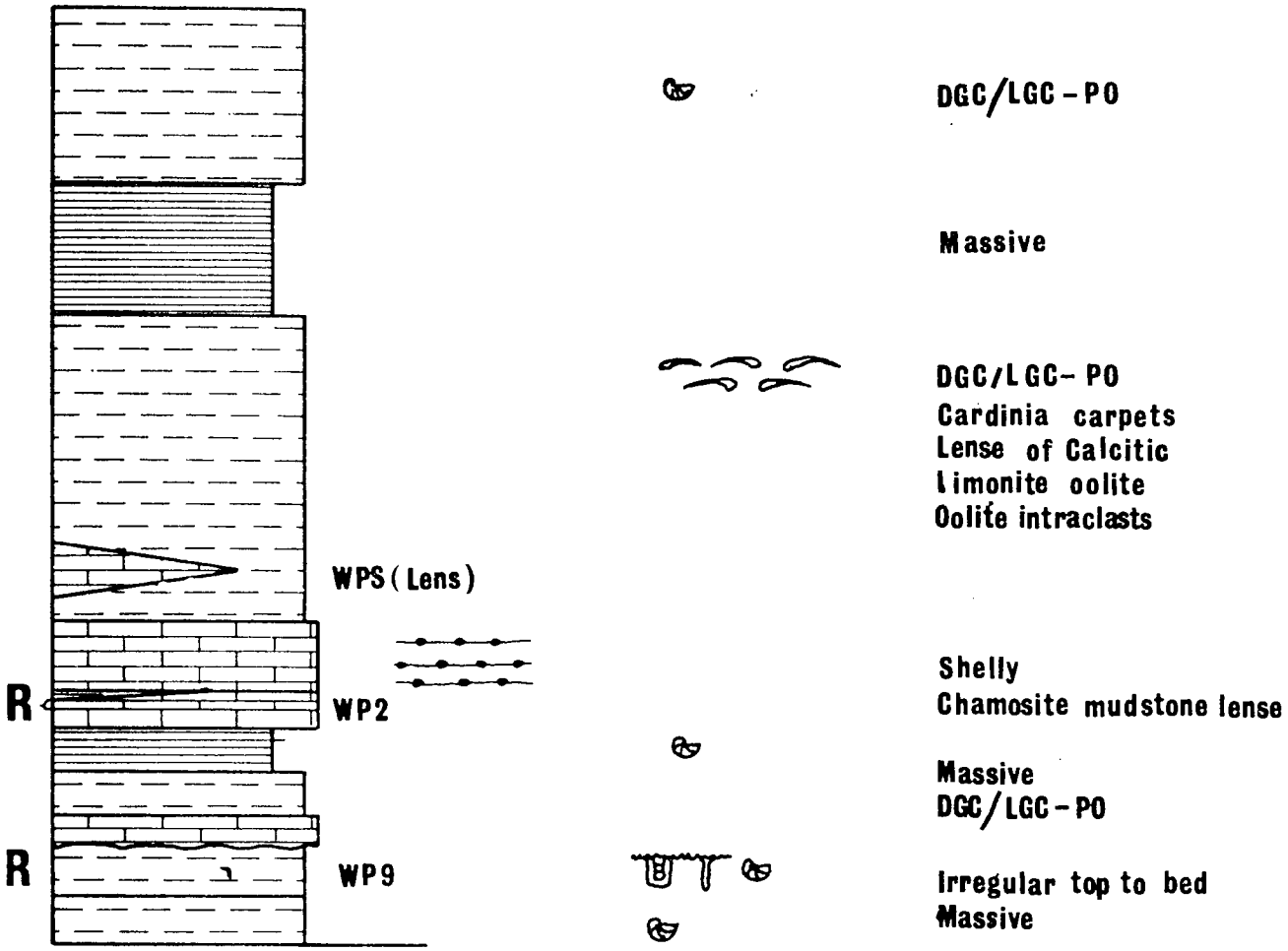

40cm

Current Faunal STRUCTURES

COMMENTS

Bioclastic Limestone

Calcitic Limonite Oolite

Chamositic Limonite Oolite

Chamositic Chamosite Oolite

Chamositic Mudstone

R Red Equivalent

DGC Dark Green Chamosite Mud

LGC-PO Light Green Chamosite Mud

Diplocraterion parallelum & vertical burrows extending from overlying bed

Gryphaea in life position

Ooids concentrated in lamellae

Figure 2·4f : Winterton Pit Section Log

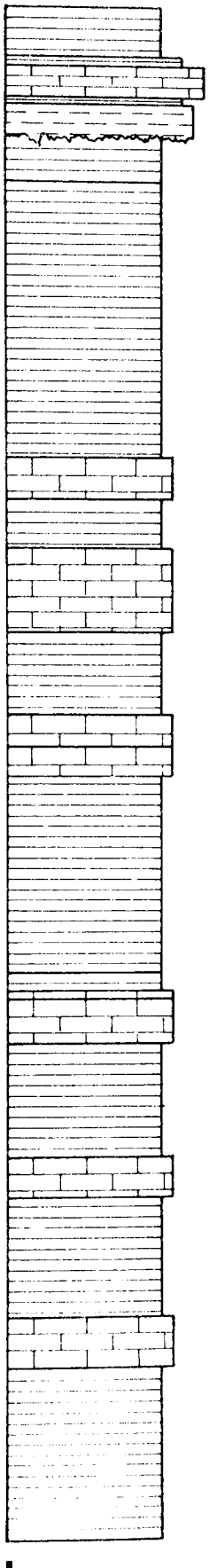

Dark grey micaceous mudstone

Chamosite mudstone
Red calcitic limonite oolite
Chamosite Mudstone
Red chamositic limonite oolite

Massive green micaceous siltstone.
Irregular top

Dark grey,well laminated,
slightly micaceous mudstone

Argillaceous limestone with basal
ball and pillow structure
Dark grey,well laminated,
slightly micaceous mudstone

Argillaceous limestone,
Vertical burrows abundant.

Dark grey,well laminated,
slightly micaceous mudstone

Argillaceous limestone with
Diplocraterion parallelum
Bioclastic Limestone

Dark grey,well laminated,
slightly micaceous mudstone

Mudstone. Limonite ooids

Bioclastic limestone

Dark grey,well laminated, mudstone

Argillaceous limestone

Dark grey micaceous mudstone

Argillaceous limestone

Dark grey,well laminated,
slightly micaceous mudstone

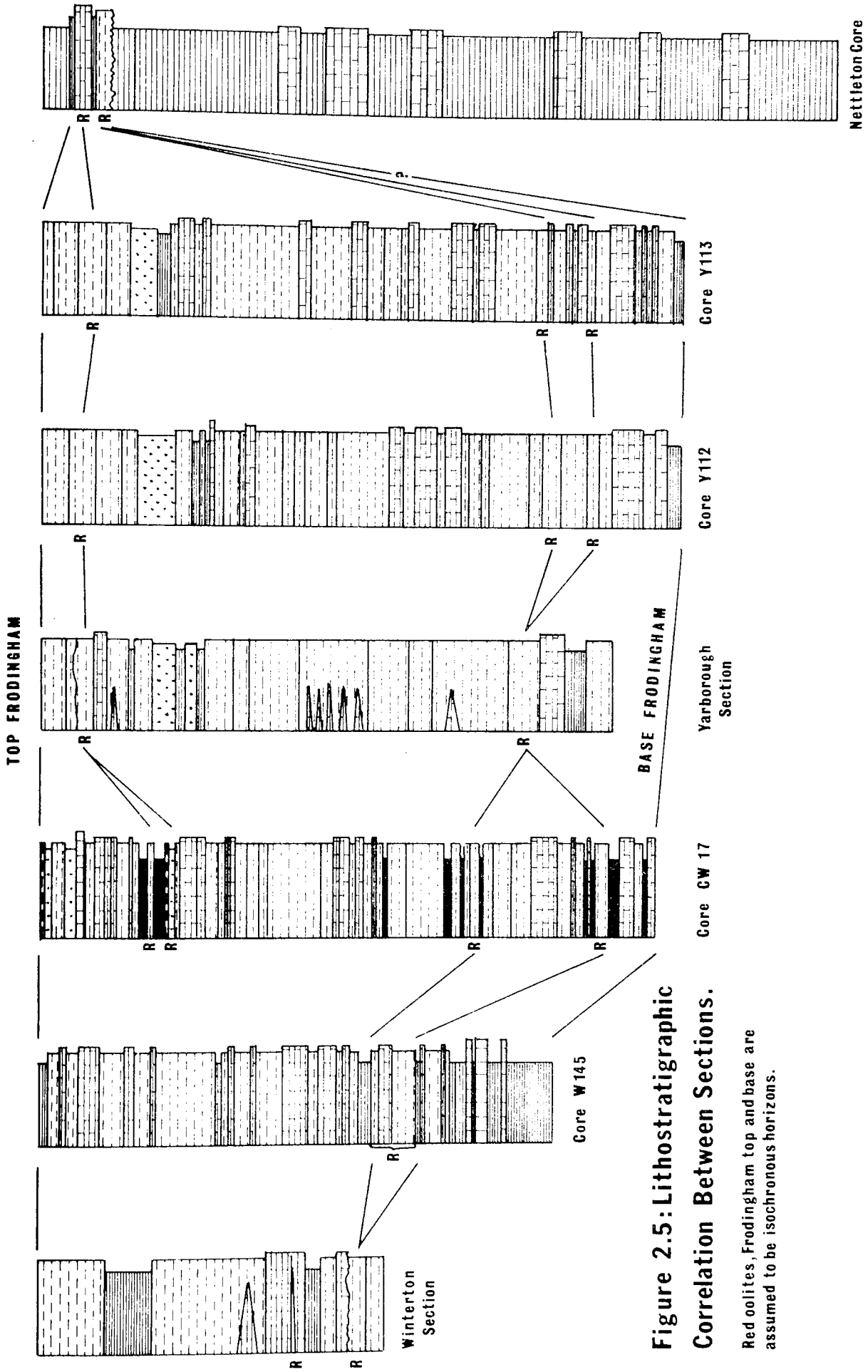

Figure 2.5: Lithostratigraphic Correlation Between Sections.

Red oolites, Frodingham top and base are assumed to be isochronous horizons.

Winterton Pit, intersected 3.07 m of Frodingham Ironstone (Ann. Rep. I.G.S., 1972). A borehole drilled by the Oxford Heat Flow Group at Nettleton Quarry, Claxby, a distance of 25 km to the south-east of Yarborough Pit, passed through 0.51 m of ironstone. The base of the ironstone in this case is marked by an erosion surface penetrated by burrows from the overlying ironstone. This is not thought to represent a major disconformity as there is an absence of a basal conglomerate of ironstone. Similarly a non-sequence does not appear possible as there is no concentration of faunal elements such as belemnites or ammonites at this horizon. The presence of burrows passing through the erosion surface tends to suggest that it represents a minor, local, episode of erosion, following which normal conditions of sedimentation and benthonic colonisation returned. The Frodingham Ironstone has not been reported from boreholes drilled through the Lower Lias sequences of the North Sea. Borehole evidence, except in the area immediately around Scunthorpe, is too sparse to allow detailed consideration of the overall form of the deposit. Furthermore, Lower Lias sediments are absent to the west of Scunthorpe. The geometry of the ironstone can, however, be seen to be broadly lenticular with a thickness maximum centred in the region of the Warlaby E borehole. It is evident that from here it thins-out to the north, south, west and east. Thinning-out of the ironstone in the former two directions appears to occur rather more rapidly than in the latter. Thus, it may be that there is a central east-west ridge passing throughout the deposit.

2.2.3 Facies of the Frodingham Ironstone

As a result of the detailed logging of both cores and quarry sections it became apparent that the Frodingham Ironstone consists of seven different

ironstone facies. Hallimond (1925) has briefly described the nature of three lithological types which he considers to be the components of the Frodingham Ironstone. Davies and Dixie (1951) have recognised four different ironstone lithologies on the basis of petrographic work. The facies recognised during the course of this work are as follows:

2.2.3.i Chamosite mudstone: This facies is represented by three slightly different sub-types, two of which are the result of differing sedimentary environments, and one of which results from subsequent diagenetic modification. Petrographic work shows that nearly all examples of the chamosite mudstone sub-types are quartzose.The distinction of the third chamosite mudstone sub-type is confirmed by petrographic evidence. This is reported in detail below, but in contrast to the other two is characterised by abundant siderite. Since siderite can usually only precipitate beneath the sediment-water interface (Curtis and Spears, 1968a) the abundance of this mineral may be taken as a measure of the degree of diagenetic modification that has occurred within the chamosite mudstones.

Generally the first and second types of mudstone are either dark green or a greyish shade of dark green in colour. A distinction is made between these on the grounds of overall physical dissimilarity. One is massive with occasional poor fissility and no lamination, although a distinct depositional fabric is seen in thin section, whilst the other is friable resulting from well-developed fissility and lamination. In this case, very thin 2 mm, or less, shell flakes are concentrated in varying amounts along the original bedding surfaces. These naturally result in the mudstone having an accentuated degree of fissility. It

seems likely that the more massive form of mudstone resulted from quick, continuous deposition, whereas the well-laminated variety resulted from deposition interspersed with frequent periods of non-deposition when shell flakes could be deposited by the processes of saltation. The fauna of these mudstone types is restricted to the derived material noted above and occasional large Gryphaea arcuata. In all cases this is only the left valve, which may be oriented either concave downwards or upwards. Therefore, it appears that these valves have also been derived. Their excellent state of preservation is explicable in terms of either a short distance of transport, or their weight resisting violent and rapid bottom transport. Hallam (1963) has noted the absence of any 'in situ' fauna in the chamosite mudstones. Occasional burrows have been observed within the chamosite mudstones but they can be demonstrated to have penetrated from different overlying lithological types.

The chamosite mudstone which has been subjected to subsequent diagenetic modification is a dark bluish-grey green in colour. It is extremely hard and compact; lamination and fissility are completely absent. This mudstone has only been encountered in Yarborough Pit, where it occurs between two beds of chamositic chamosite oolite. Here it shows common thin lenses of ooimoulds. Fabrics characterised by ooimoulds have been described by Bathurst (1975) from carbonate oolites and are considered to result from solution of original ooids. The chamosite mudstone ooimoulds are often made more noticeable by an associated honey-combe structure in which siderite forms a resistant matrix around the ooimoulds. Close examination of the siderite shows that it grades imperceptibly into the surrounding mudstone. It is likely, therefore, that the diagenetic

change undergone by this mudstone type takes the form of widespread development of siderite. Shell material is almost entirely absent.

2.2.3.ii Chamositic chamosite oolites: This facies is perhaps the least frequently occurring oolite within the Frodingham Ironstone. It is constructed of abundant whitish-green chamosite ooids. These impart a similar colouration to the rock. The individual ooids are discoidal in shape with an elliptical to ovate cross-section, parallel to the long axis. The ooids are well sorted, having an approximate size range of 0.3 - 0.4 mm when measured along the long axis. The ooids often show a preferred orientation which takes the form of their long axes being aligned parallel to bedding. The short axis may be in any orientation, but it generally lies in a plane perpendicular to bedding. Where a portion of the envelope has been removed by breakage, it can be seen that there is a void at the core of the ooid. Cut sections of these oolites show that this is a phenomenon common to the majority of the ooids present. In some instances the ooids are seen to have been replaced by pyrite.

Pisoliths are common in chamositic chamosite oolites. They have an oval cross-sectional shape. The size variation, measured along the long axis, is 1.0 - 0.5 cm. Where the pisoliths have been broken in a plane parallel to that in which the long and short axes lie, which is the usual case, the internal structure can be clearly seen. This is divisible into an envelope and a central core. The envelope is constructed of a series of rings which have a thickness maximum parallel to the long axis and a thickness minimum parallel to the short axis. These are constructed of chamosite or limonite or a mixture of the two. In the

latter case, the chamosite is concentrated in crescents at either end of the ooid long axis. Ooids with a brownish-white colour may partake in the structure of the envelope where they are oriented with their long axes tangential to the pisolith envelope. The central core of the pisoliths is often represented by an irregular void. The pisoliths may be either totally or partially replaced by pyrite.

The only faunal material present is fragmentary and represents the remnants of thin-shelled bivalves, comminuted elsewhere and subsequently washed into the site of chamosite oolite formation. In some instances, the calcite of these shells has been replaced by pyrite.

Petrographic work shows that the matrix of the chamosite oolites consists of dark green chamosite mud, interstitial to the ooids, lighter green authigenic chamosite and diagenetic siderite. The interstitial chamosite mud forms the greater portion of the matrix. Variable size areas occur, however, in which siderite is the dominant matrix mineral to abundant ooimoulds. Authigenic chamosite is associated with the siderite in this role. It is recognised as a lighter green, more resistant material than the interstitial mud. In some areas which appear to be always associated with shell material, siderite forms the matrix to dominantly complete ooids, rather than ooimoulds.

Pyrite occurs commonly as a diagenetic mineral within the matrix of the oolite. As noted above, it occurs as a replacement of a variety of allochemical grains. In addition it forms irregular or euhedral areas within the oolite which may or may not include areas of replacive pyrite.

Hallimond (1925), following the local mining terminology, has briefly described the chamositic chamosite oolites of Yarborough Pit under the heading of the 'Sulphur Bed'. The presence of ooimoulds in

a chamosite mud matrix is recorded, together with the overall morphological similarity of the occasional chamosite ooids to the limonite ooids that occur in abundance elsewhere. Hallimond points out that the name 'Sulphur Bed' derives from the abundance of pyrite.

2.2.3.iii Chamositic limonite oolites: The facies is characterised by an abundance of limonite ooids set in a chamosite matrix. Three different sub-types of the facies have been recognised. Type (i) has a dark green chamosite matrix with abundant polished limonite ooids. Type (ii) differs from this only in the colour of the chamosite which is light green. Type (iii) is similarly characterised by a light green chamosite matrix, but in contrast the limonite ooids vary from having a dull surface to being poorly developed in shape and structure.

As with the chamosite ooids of the chamositic chamosite oolites the limonite ooids of sub-types (i), (ii) and the better developed ooids of sub-type (iii) are characterised by a discoidal shape and an ovate to elliptical cross-section parallel to the long axis. Within any one bed the ooids are well sorted, but the ooid size may vary from bed to bed. Thus, an approximate size range of 0.3 - 0.4 mm, measured along the long axes, has been recorded in one bed from Yarborough Pit and another range of 0.4 - 0.5 mm in a different bed at the same locality. Hallimond (1925) and Davies and Dixie (1951) have reported that the limonite ooids are all polished. In the case of the chamositic limonite oolites of sub-types (i) and (ii) this is generally the case. Newell et al (1960), and Donahue (1965) reported from laboratory studies of carbonate ooids that a high surface polish can be derived by abrasion. Recent carbonate ooids of agitated surf zones are characterised by a

high surface polish (Bathurst, 1975). Lemoalle and Dupont (1976) report polished goethite ooids from shallow locustrine waters associated with a delta in Lake Chad, Africa. It seems likely, therefore, that the surface polish on the limonite ooids described above derives from shallow water abrasion processes. Sub-type (iii) limonite ooids are, when well developed, poorly polished. This appears to represent an 'end member' in ooid polish, shape and form, for in this sub-lithology all gredations can be recognised to a stage where the ooids have a 'relict' form. In this case the ooids are somewhat irregular, often appearing ragged, with a dull brown or ochre yellow colouration. This cannot be attributed to surface weathering processes as such ooids can be found in abundance on fresh surfaces of the sub-lithology.

The ooids show a preferred orientation, which may be recognised in all three sub-types of chamositic limonite oolites. This takes the form of the alignment of their long-axes parallel or at an angle to bedding. At the margins to burrows, ooids have often been reoriented such that their long axes have become parallel to the burrow axis. In a number of instances, burrows have been found in which the burrow infill is of limonite ooids entirely. These are all aligned with their long axes parallel to the burrow axis.

As has been noted above the matrix to the chamositic limonite oolites is either a dark green chamosite mud, as in sub-type (i), or a light green chamosite mud, as in sub-types (ii) and (iii). Petrographic work, discussed in detail below, shows that the dark green chamosite is depositional and the light green chamosite authogenic in origin. The chamosite of sub-type (i) may be limonitised to a greater or lesser extent. In some cases it may have a reddish-brown tinge. Such chamosite mud tends to be pervasive throughout the bed in question, but not uniform.

The ooids set in this type of chamosite tend to have a darker brown colour than is normally the case. The lithological type as a whole is characterised by an abundance of burrows. With the exception of a few that are infilled by limonite ooids, these are infilled entirely by chamosite mud. A few ooids of limonite may occur within the chamosite of the burrows. In contrast, chamositic limonite oolites with light green chamosite (sub-types (ii) and (iii)) lack these characteristics.

The sub-type (i) chamositic limonite oolites of Yarborough Pit show an abundance of 'in situ' fauna and burrows. A variety of infaunal elements have been collected from this locality. These include the burrowing bivalves Pholadomya sp., Pleuromya costata (Young and Bird), Mactromya sp., and the semi-infaunal burrower Modiolus scalprum (J. de Sowerby). Epifaunal sessile bivalves include Meleagrinella sp., Cardinia sp., and Pseudopecten sp. The unattached but surface-dwelling bivalve Gryphaea arcuata (Lamarck) is abundant. It can be demonstrated that these are in their life positions since they are oriented with their left valves concave downwards and, in all instances, the right valve is still attached. Death evidently came to these bivalves as a result of being quickly buried by sediment; the interior of the shell is commonly found to be completely devoid of sediment. Other faunal groups are not so well represented as the Bivalvia. Brachiopoda are represented by the occasional sessile epifaunal Rhynchonelloidella sp. The Gastropoda are represented by the vagile herbivorous Pleuratomaria sp. The occasional pelagic elements such as belemnites and the ammonite Arnioceras sp. occur. Pelagic faunas, however, reveal little about the nature of bottom conditions. A variety of burrows within the sediment indicate the presence of soft-bodied organisms which would not have been preserved.

Such trace-fossils include the ichnogenera Diplocraterion parallelum (Torell), characterised by a U-shaped burrow with an intervening spreiten, and the occasional bedding-parallel sinusoidal burrow of Rhizocorallium jenense (Zenker). Several burrows inclined at an angle to bedding can be attributed to burrowing bivalves simply because species such as Pholadomya are found at their ends. This is evidence for the occasional influx of rather a lot of sediment since such bivalves usually manage to burrow upwards until they regain contact with the surface in such circumstances.

In the chamositic limonite oolites of Yarborough and Winterton Pits, carpets of disarticulated valves of the bivalve Cardinia hybrida (J. de Sowerby) are found at certain horizons. Since C. hybrida is a moderately deep-burrowing bivalve and the valves are disarticulated, such assemblages clearly represent allochthonous or derived shell beds. Light green authigenic chamosite is often concentrated beneath the individual shells and forms a thin upper coating to them.

Hallam (1963) has discussed the paleoecology of the chamositic limonite oolites, in addition to the other facies types present. He has concluded from faunal evidence, similar to that described above, that the local bottom waters were characterised by oxygen-carrying currents. The oxygen level was enough to allow deep burrowers to survive, whilst the current energy was insufficient to excavate the burrowers or winnow away the matrix chamosite mud. This general situation, however, was evidently punctuated by periods of much greater energy, resulting in the formation of the above shell beds. Hallam (1963) reports the presence of a dwarf fauna in the 'Snap Band' of Yarborough Pit. This bed is rather higher in chamosite mud and pyrite than is normally the case amongst the chamositic limonite oolites. The most likely cause

of this is a localised diminution of oxygen levels relative to dissolved sulphur species.

The presence of three different sub-types of chamositic limonite oolites has been clearly demonstrated, but required explanation. The major difference between these is that sub-type (i) is characterised by an abundance of bioturbation, whereas sub-types (ii) and (iii) lack any such primary structures. It is these two sub-types which are characterised by light green authigenic chamosite. In sub-types (i) and (ii) the limonite ooids are well formed and polished. In sub-type (iii) the ooids are dull to 'relict' in nature. In order for the bioturbation of the sub-type (i) chamositic limonite oolites to have occurred, it is necessary that the chamosite mud matrix and limonite ooids were present at the time of bioturbation. Since sub-types (ii) and (iii) show no evidence of bioturbation it is probable that chamosite authigenesis occurred after bioturbation ceased. In any one bed of chamositic limonite oolite one, two, or all three sub-types may occur. The different nature of the limonite ooids of sub-type (iii) may reflect some diagenetic change in this phase occurring in parallel with the formation of authigenic chamosite.

2.2.3.iv Sideritic chamositic limonite oolites: A rare facies of ironstone which has been recognised in the Frodingham Ironstone Field consists of polished limonite ooids set, together with occasional pisoliths, in a matrix of light green chamosite and siderite.

The limonite ooids are a golden-brown in colour and highly polished. As before they have a discoidal shape, with an ovate to elliptical cross-section, parallel to the long axis. In the specimens examined the ooids

were found to have an approximate size range of 0.3 - 0.4 mm, measured along the long axis.

Pisoliths are a rarely occurring allochemical phase within the lithology. They are ellipsoidal in shape and may range up to 10 mm, measured along the long axis. Mineralogically, they are composed of dark green chamosite and limonite. The pisoliths are found to be constructed of a series of concordant rings, each of which is composed of one of the above two mineral species.

The matrix to the ooids and pisoliths is a mixture of light green chamosite similar in nature to that of chamositic limonite oolite sub-types (ii) and (iii), and a buff siderite. Petrographic work shows that the chamosite is entirely authigenic in origin. The siderite tends to form upstanding areas around ooids such that when a number of ooids have been removed a honey-combe surface texture to the siderite can be seen. The matrix is not an intimate mixture of chamosite and siderite, rather each mineral tends to form the matrix to the ooids over irregular, ill-defined areas.

Shell debris occurs, but is not abundant.

Davies and Dixie (1951) have briefly described a hand specimen of this facies, which corresponds to their Type A, as one in which siderite has been superficially oxidised to limonite such that the ironstone appears as a sponge-like mass of dark green chamosite, the pores in the sponge being filled with high polished ooids of brown limonite and brown aggregates of siderite.

2.2.3.v Calcitic limonite oolites: This facies corresponds to the 'Limy Stone' of Hallimond (1925). This author described the rock-type as an

aggregate of brown limonite ooids, rounded shell fragments, echinoid spines and crinoid ossicles, cemented with a clear crystalline calcite. In comparison to the other lithological types the calcitic limonite oolites are relatively simple in terms of their allochemical components and cement. Thus, little can be added to Hallimond's description.

As with the oolitic lithologies described above, the limonite ooids are a golden-brown in colour and highly polished. The degree of polish is again considered to result from abrasion. Again they are characterised by a discoidal shape with an ovate to elliptical cross-section,parallel to the long axis. The ooids are well sorted, generally having a size range of 0.3 - 0.4 mm, measured along the long axis. This varies little both within individual and beds at different levels. In contrast to the chamositic limonite oolites, all the ooids have a high polish. There is a clear preferred orientation amongst the ooids. This takes the form of an imbrication in which the ooids are oriented with their long axes lying parallel and at a high angle to bedding of between 30^{o} and 60^{o}. Commonly, high concentrations of limonite ooids define foreset lamination.

Shell fragments, and occasional complete bivalve shells, are common within the lithology. In all cases they are oriented with their long axes parallel to bedding, and generally concave downwards; their orientation has a local effect on the ooid orientation so that where in contact with shells the ooid long axis tends to be parallel to that of the shell fragments. Hallam (1963) has concluded that the shell material represents an allochthorous assemblage derived by current action from the chamositic limonite oolites. There is good evidence for periods of much reduced current activity at the time of deposition of this type of oolite. Burrows infilled with limonite ooids penetrating down from foreset laminae defined by concentrations of limonite ooids are

The cement to the limonite oolite is entirely of clear calcite. A minor cement mineral occasionally occurring is authigenic chamosite. This is usually concentrated beneath shell fragments which are oriented concave downwards. This material may also form a thin coating to the upper surface of the shell.

2.2.3.vi Bioclastic limestones: This facies comprises shell fragment material, with the occasional complete bivalve shell, generally oriented parallel to bedding and concave downwards. The cement is of calcite with occasional concentrations of authigenic chamosite. In short, it is a calcitic limonite oolite without limonite ooids.

2.2.3.vii Red oolites: From Figure 2.5 it can be seen that within the Frodingham Ironstone 'red oolites' have occasionally been deposited. Examination shows these oolites to be divisible into a red limonitic chamosite oolite, a red limonitic chamositic limonite oolite and a red calcitic limonite oolite.

The first of these oolite-types has only been found forming one bed in core CW17. It is characterised by an overall earthy red-brown colouration. It is extremely friable. Green ooids of chamosite with a discoidal shape are found set in a matrix of red-brown limonite. In places irregular patches of a buff, unaltered, siderite matrix occur.

The red limonitic chamositic limonite oolite is characterised by an overall tawny red colour. This colouration is easily distinguished from the dark reddish brown colour occasionally encountered with a patchy distribution in some chamositic limonite oolites; it is uniform throughout the red oolites of this type. The ooids of limonite present are characterised by the same morphology described above. Instead of

the golden brown colour which characterises the ooids of the other limonite oolites these are of a dark reddish brown colouration. The ooids are well sorted and have size ranges as reported for the chamositic limonite oolites. The matrix to the ooids is a fine-grained golden brown limonite. Burrows are common but are not infilled entirely with chamosite mudstone; indeed the presence of this material is confined only to the wider burrows. As before the burrows contain very few limonite ooids. Relatively thin burrows are infilled by a fine-grained red-brown material. In wider burrows this material forms an outer rim of variable thickness, surrounding an inner core of dark green chamosite mudstone.

The red calcitic limonite oolite is characterised by the widespread presence of salmon pink cement calcite. Ooid morphology is again unchanged. The ooids are well sorted with an approximate size range of 0.4 - 0.5 mm, measured along the ooid long axis. They are highly polished, with a golden-brown colouration. Occasional black ooids are present. Chamosite mud is generally rare in calcitic limonite oolites. In the lower red oolite bed in the Nettleton Core, however, a large burrow occurs which is infilled by the fine-grained red material found infilling burrows in the red limonitic chamositic limonite oolites.

At Winterton Pit, fallen material having the characteristics of the red calcitic limonite oolites was examined at the base of the logged section. This material showed a patchy development of the salmon pink matrix calcite. As with the ooids of the above described red calcitic limonite oolite, the ooids are characterised by a high polish and a golden or dark brown and less commonly, black colouration. They are relatively poorly sorted, however, with an approximate size range of 0.2 - 0.5 mm. In addition polished intraclasts are common. These are

coloured black and have a high surface polish. They vary in size from 0.5 - 1.0 cm. The smaller intraclasts tend to be equidimensional and poorly rounded, whereas the larger intraclasts have a poorly-rounded platelet form. The interior of these grains tends to be structureless, but occasional limonite ooids have been found. Faunal debris is abundant within this material. It includes ammonites, both complete and fragmentory, with a wide range of sizes. The largest ammonite found (Arnioceras sp.) was approximately 30 cm in diameter. Belemnites are common and in the majority of cases show signs of considerable abrasion. Bivalve material is common and comprises both broken and complete disarticulated valves and occasional complete shells. The size variation of this material is from a few millimetres to 15 cm. The range of bivalve fauna included in this sediment is extremely wide, including Cardinia hybrida, Pseudopecten sp., Gryphaea arcuata, Meleagrinella sp., Camptonectes sp. The range and state of preservation of the various faunal elements, the poor sorting of the ooids and the abundance of intraclasts suggests that this material represents a storm beach or a storm accumulated sediment concentration. With regard to the nature of the cementing calcite, it is interesting to note that the salmon pink cement is concentrated around shells which are coated with a red, finely crystalline material. The presence of such a coating is strange since the usual coating is of authigenic chamosite.

2.2.3.viii Non-ironstone lithologies: Unlike the other sequences of Frodingham Ironstone which have been examined core CW17 is characterised by common shale bands, and occasional beds exceeding 5 cm thickness. The shale is dark grey to black in colour. It is fissile but non-laminated. In a number of instances limonite ooids and shell flakes are present.

2.2.4 Interelationships Between Facies

Consideration of Figure 2.5 shows that there is a common tendency throughout the Frodingham Ironstone Field for certain lithologies to follow others in a vertical sequence. For instance, a chamositic limonite oolite may follow a chamosite mudstone and precede a calcitic limonite oolite. There is a clear possibility, therefore, that the facies defined above may have a cyclic interelationship. This was first suggested by Hallimond (1925) who noted that the Frodingham Ironstone shows an alternation between his 'Limy Stone' and 'chamosite mudstone'. Davies and Dixie (1951) reported that any one bed of ironstone is of one lithological type only, and that, overall, these beds have a lenticular form. Thus they considered the ironstone infrastructure to be of many superimposed lenses. These authors reported no regular alternation of lithological types either vertically or laterally.

In order to determine whether the Frodingham Ironstone is a cyclic sequence, two lines of investigation have been utilised: (i) A statistical study of the vertical sequences recorded from borehole and logged section data; (ii) a field study of the nature of any lateral variations occurring along pit faces. This approach follows from Walthers Law which proposes that vertical facies sequences reflect their lateral inter-relationships, in the absence of any major breaks in the succession. The presence of any such facies relationships has not been reported from either the Frodingham Ironstone or any other oolitic ironstone. The Frodingham Ironstone is not considered to contain any major breaks in sedimentation.

2.2.4.i Statistical study of vertical sequences: In order to test the hypothesis that the order and frequency of occurrence of individual lithological types results from a cyclic sequence of events, a facies analysis experiment was carried out using the standard Markov-I technique (Selley, 1970; Turner, 1974). The null hypothesis was that facies observed at successive points in the succession are independent of the adjacent facies. Suffice to say that in all cases the results lay outside the 95% confidence level and the null hypothesis was rejected. This indicates that the nature of deposition was non-random. The form of the statistical testing used, however, allows a further conclusion to be drawn from this result. This conclusion is that the facies at any one horizon is dependent on that of the previous facies.Hence, from the vertical sequences of Frodingham Ironstone examined it appears that the ironstone is indeed cyclic. The observed and expected data matrices are presented in Figure 2.6a, b and c, and the chi-squared value obtained for each ironstone sequence tested in this way in Table 2.1. In order for the test to be statistically valid all the recorded transitions from each pit have been combined to give a total number of transitions greater than 40 for each pit. The test therefore gives a result for each pit considered.

Having established that cyclicity is a characteristic of the ironstone it is necessary to establish the ideal sequence of facies in the ironstone cyclothem. This is accomplished simply by dividing the individual cells of the observed data matrix by the total of the row in which they lie. The matrix thus created; the transitional probability matrix, shows the probability values for the vertical transition from any one lithological type to any other. From such a matrix, a facies relationship diagram may be constructed showing diagramatically the ideal sequence

Observed

Yarborough Pit:

	1	2	3	5	6	
1	0	1	6	0	1	8
2	3	0	1	0	0	4
3	5	3	0	27	0	35
5	2	0	25	0	0	27
6	0	0	1	0	0	1
	10	4	33	27	1	75

Expected

	1	2	3	5	6
1	1.05	0.42	3.52	2.88	0.10
2	0.53	0.21	1.76	1.44	0.05
3	4.66	1.86	15.4	12.6	0.46
5	0.72	1.44	11.88	9.72	0.36
6	0.13	0.05	0.44	0.77	0.01

Figure 2.6a: Yarborough Pit.

Observed

	1	2	3	5	6	8	
1	0	0	0	0	1	0	1
2	0	0	3	0	0	0	3
3	1	1	0	12	0	8	22
5	0	0	11	0	0	3	14
6	0	1	0	0	0	0	1
8	0	1	9	2	0	0	12
	1	3	23	14	1	11	53

Expected

	1	2	3	5	6	8
1	.01	0.05	0.43	0.26	.01	.20
2	.05	.16	1.30	0.79	.05	.62
3	.41	1.24	9.54	5.81	.41	4.56
5	.26	.79	6.07	3.69	.26	2.90
6	.01	.05	.43	.26	.01	.20
8	.22	.67	5.20	3.16	.22	2.49

Figure 2.6b: Crosby Warren: (Core CW17)

Observed

	1	2	3	5	6	
1	0	0	6	1	3	10
2	0	0	0	0	0	0
3	5	0	0	14	0	19
5	1	0	14	0	0	15
6	3	0	0	0	0	3
	9	0	20	15	3	47

Expected

	1	2	3	5	6
1	1.91	0	4.25	3.19	0.64
2	0	0	0	0	0
3	3.64	0	8.08	6.06	1.21
5	2.87	0	6.38	4.97	0.96
6	0.57	0	1.28	0.96	0.19

Figure 2.6c: Winterton Pit.

1: Chamosite Mudstone, 2: Chamositic Chamosite Oolite, 3: Chamositic Limonite Oolite, 5: Calcitic Limonite Oolite, 6: Bioclastic Limestone, 8: Shale

Figure 2.6: Observed And Expected Matrices

Vertical sequence	Degrees of Freedom	$\chi^2_{0.05}$	χ^2_{obs}
Core Y112)) Core Y113)	16	7.96	1.24
) Yarborough Pit Log)			
Core CW17	25	14.61	3.79
Core W145))	16	7.96	1.32
Winterton Pit Log)			

Where Degrees of Freedom = (No. of facies - 1)^2

Table 2.1. χ^2-Test Results

of facies within the cyclothem. It is necessary to assume a lower probability value, below which vertical transitions between facies are not considered to be part of the ideal cyclothem. In this study, two minimum values have been used, 0.2 and 0.5. This has been done in order to show the most important facies transitions. Figure 2.7 shows these matrices and diagrams.

Since the development of a cyclic ironstone motif by primary, dynamic, processes is being considered it is necessary to decide which facies are primary in nature and which have been modified by post-depositional processes. In the latter case it then becomes necessary to determine what the primary facies was. A chamosite mudstone has been described which is thought to have been modified by the post-depositional precipitation of siderite; this facies was clearly deposited as a chamosite mudstone. Evidence has been brought forward regarding the chamositic limonite oolite sub-types (ii) and (iii) which shows that the matrix chamosite is authigenic in origin. Since these two lithologies are generally associated with the chamositic limonite oolite sub-type (i) and have a similar abundance of chamosite it is suggested that, as a working hypothesis, they were originally deposited as the chamositic limonite oolite sub-type (i) lithology. The sideritic chamositic limonite oolite clearly represents post-depositional modification, on the basis of the presence of siderite. The fact that the chamosite present is all of authigenic origin suggests that it may well have been a limonite oolite with a little primary chamosite mud at the time of deposition. The calcitic limonite oolites show no evidence of post-depositional change except the development of a calcite cement; evidently they were deposited as a limonite oolite from which all the primary

Yarborough Pit:

	1	2	3	5	6
1	0	0.12	0.75	0	0.12
2	0.75	0	0.25	0	0
3	0.14	0.08	0	0.77	0
5	0.07	0	0.92	0	0
6	0	0	1	0	0

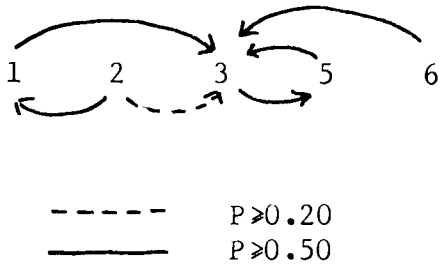

Crosby Warren (Core CW17)

	1	2	3	5	6	8
1	0	0	0	0	1.00	0
2	0	0	1.0	0	0	0
3	0.4	0.4	0	0.54	0	0.36
5	0	0	0.78	0	0	0.21
6	0	1.00	0	0	0	0
8	0	0.08	0.75	0.16	0	0

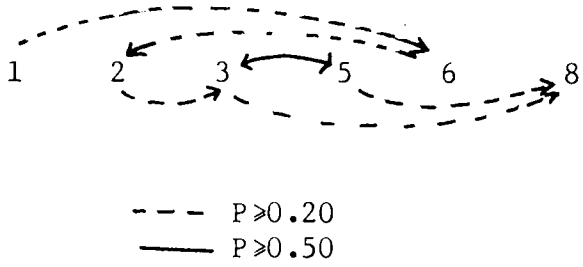

Winterton Pit:

	1	2	3	5	6
1	0	0	0.60	0.10	0.30
2	0	0	0	0	0
3	0.26	0	0	0.73	0
5	0.06	0	0.93	0	0
6	1.00	0	0	0	0

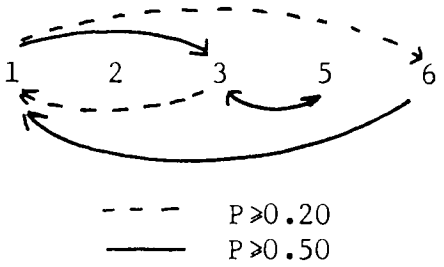

1: Chamosite mudstone, 2: Chamositic chamosite oolite, 3: Chamositic limonite oolite, 5: Calcitic limonite oolite, 6: Bioclastic limestone, 8: Shale.

Figure 2.7. Transitional Probability Matrices And Facies Relationship Diagrams

chamosite mud had been winnowed. Evidence has been accumulated regarding the Red Oolites, which is described below, to suggest that their colouration is due to post-depositional processes, and that at their time of deposition they were no different to their non-red equivalents. For the purposes of this discussion, then, the lithological types which have undergone diagenetic modification are considered as the lithologies which it is thought that they were primarily deposited as.

Reference to Figure 2.7 shows that, with the exception of core CW17, there is one sequence of facies which always occurs. This is the sequence (1) → (3) → (5), or chamosite mudstone → chamositic limonite oolite → calcitic limonite oolite. In the case of core CW17 only the latter part of the sequence i.e. (3) → (5) occurs. Since the complete reverse sequence either does not occur or when it does has a low probability of occurrence it may be concluded that the lowermost facies in the cyclothem is chamosite mudstone, followed by chamositic limonite oolite, and this by calcitic limonite oolite. A minor variant on this theme is the passage between chamosite mudstone, chamositic limonite oolites and chamositic chamosite oolites recorded in the sections from Yarborough Pit and the Crosby Warren core. The chamositic chamosite oolite lithology may thus be placed between the chamosite mudstone and chamositic limonite oolite facies in the ideal cyclothem. Since such a passage has not been recorded from the Winterton Pit sections it would seem that this lithology is not a pre-requisite for the nature of the rest of the cyclothem. Another minor variant is the passage between chamosite mudstone and bioclastic limestone. The nature of the relationship between these two facies in the facies relationship diagrams is ambiguous. The limestone may occur either before or after

deposition of the chamosite mudstone. The low probability of occurrence of the transition from chamosite mudstone to bioclastic limestone and the higher probability of occurrence of the transition from bioclastic limestone to chamosite mudstone supports the proposed cyclothem. The formal transition is not thought to be a pre-requisite for the nature of the cyclothem. The facies relationship diagram for core CW17 is somewhat different in nature to the other diagrams. The main reason for this is the frequent presence of shale in the CW17 sequence. No major conclusions can be drawn from this diagram since shale does not occur in any of the other diagrams. It is interesting to note, however, that here shale appears to take the place of chamosite mudstone in the ideal Frodingham Ironstone cyclothem. The ideal cyclothem is illustrated in Figure 2.8 together with average unit thicknesses.

2.2.4.ii Lateral relationships within the Frodingham Ironstone: On the basis of the above statistical study of vertical sequences within the Frodingham Ironstone it has been suggested that the ironstone has a cyclic infrastructure. On the basis of Walthers Law the test of the correctness of this suggestion would be the presence of lateral transitions from one lithological type to another in the same order as in the cyclic motif. A field study of the lateral relationships within the pits has been carried out and the results are reported below.

Beds of chamositic chamosite oolite are restricted to Yarborough Pit. No direct transition from this lithology to another has been recorded. However, within the chamosite mudstone of Bed Y9 lenses, less than 15 cm in length, of chamosite ooids or ooimoulds occur. This may represent the beginning of a lateral passage from chamosite

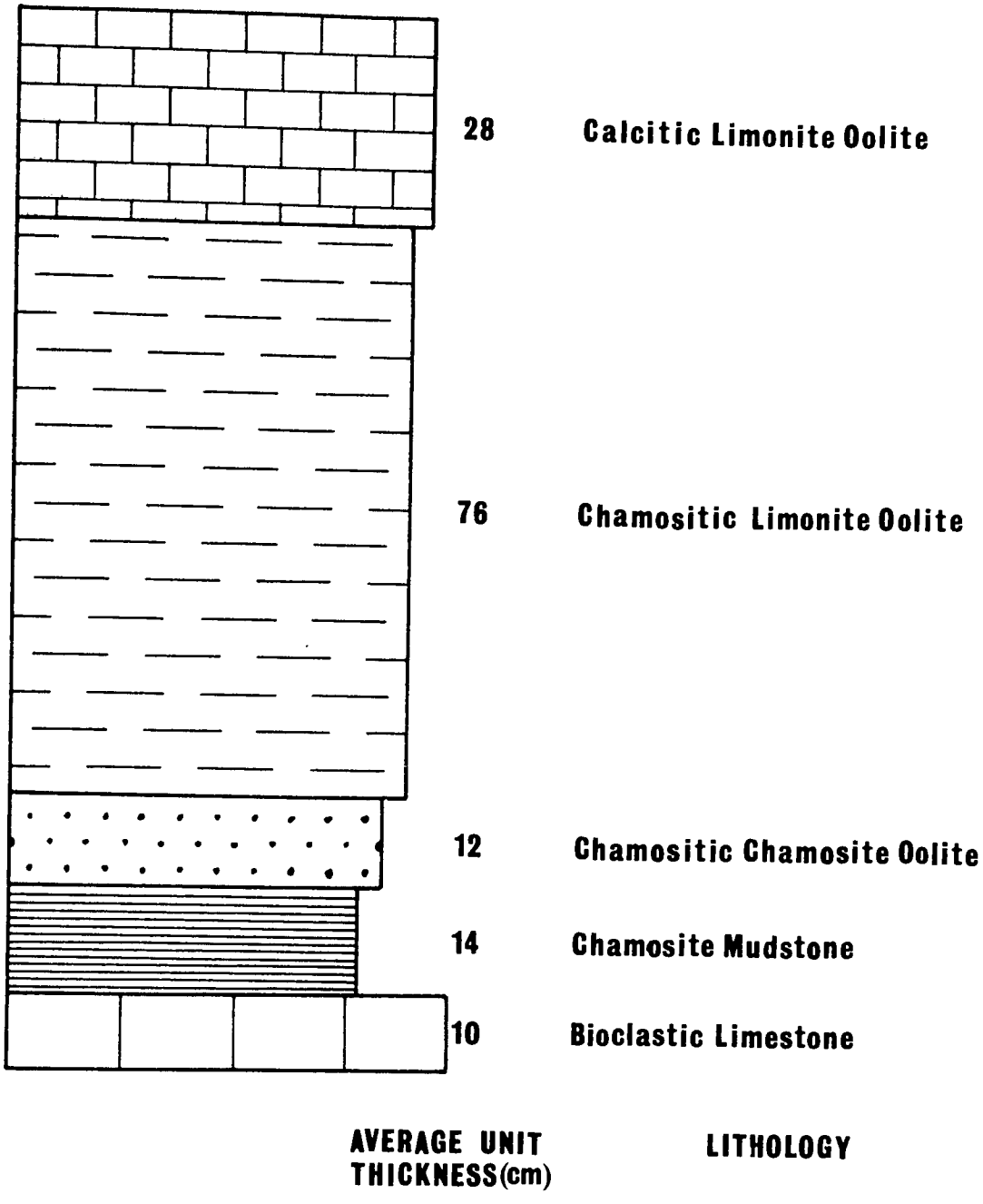

Figure 2.8: Ideal Frodingham Ironstone Cyclothem

Within beds of chamosite mudstone at Yarborough and Winterton Pits a lateral change to chamositic limonite oolites and calcitic limonite oolites can be clearly demonstrated: Bed Y5 at Yarborough Pit is dominantly a chamositic limonite oolite, but contains well defined lenses of chamosite mudstone. Bed WP6 at Winterton Pit is a chamosite mudstone. Limonite ooids occur sparingly to the extent of approximately 2% modally in the lower 18 cm. In the upper 10 cm, however, these are concentrated in thin laminations and lenticular areas, usually less than 15 cm long. Within these areas the ooids may make up 20-30% modally of the lithology which becomes strictly a chamositic limonite oolite. The overall facies remains, however, a chamosite mudstone. The uppermost chamosite mudstone at this locality, WP7, shows such lenses and laminae throughout. It is interesting to note that this bed is overlain by a chamositic limonite oolite. Hallimond (1925) has described this type of chamosite mudstone as being typical of the Frodingham chamosite mudstones.

Lateral transitions from chamosite mudstones to calcitic limonite oolites are abrupt. Bed Y11 at Yarborough Pit was, where first seen, a chamosite mudstone in entirety. Following this bed 2 m to the south, a large (50 cm long) wedge of calcitic limonite oolite appeared. This wedge (Figure 2.9) was characterised by limonite ooids defining foreset lamination. It was surrounded on all sides by chamosite mudstone. A section 5 m to the south shows that chamosite mudstone deposition had ceased entirely by this point; a bed of calcitic limonite oolite having taken its place. The ironstone sequence above and below the calcitic limonite oolite remains unchanged. The nature of this lateral transition suggests that the observed passage results from a dynamic incursion of the calcitic limonite oolite into the area of chamosite mudstone. At

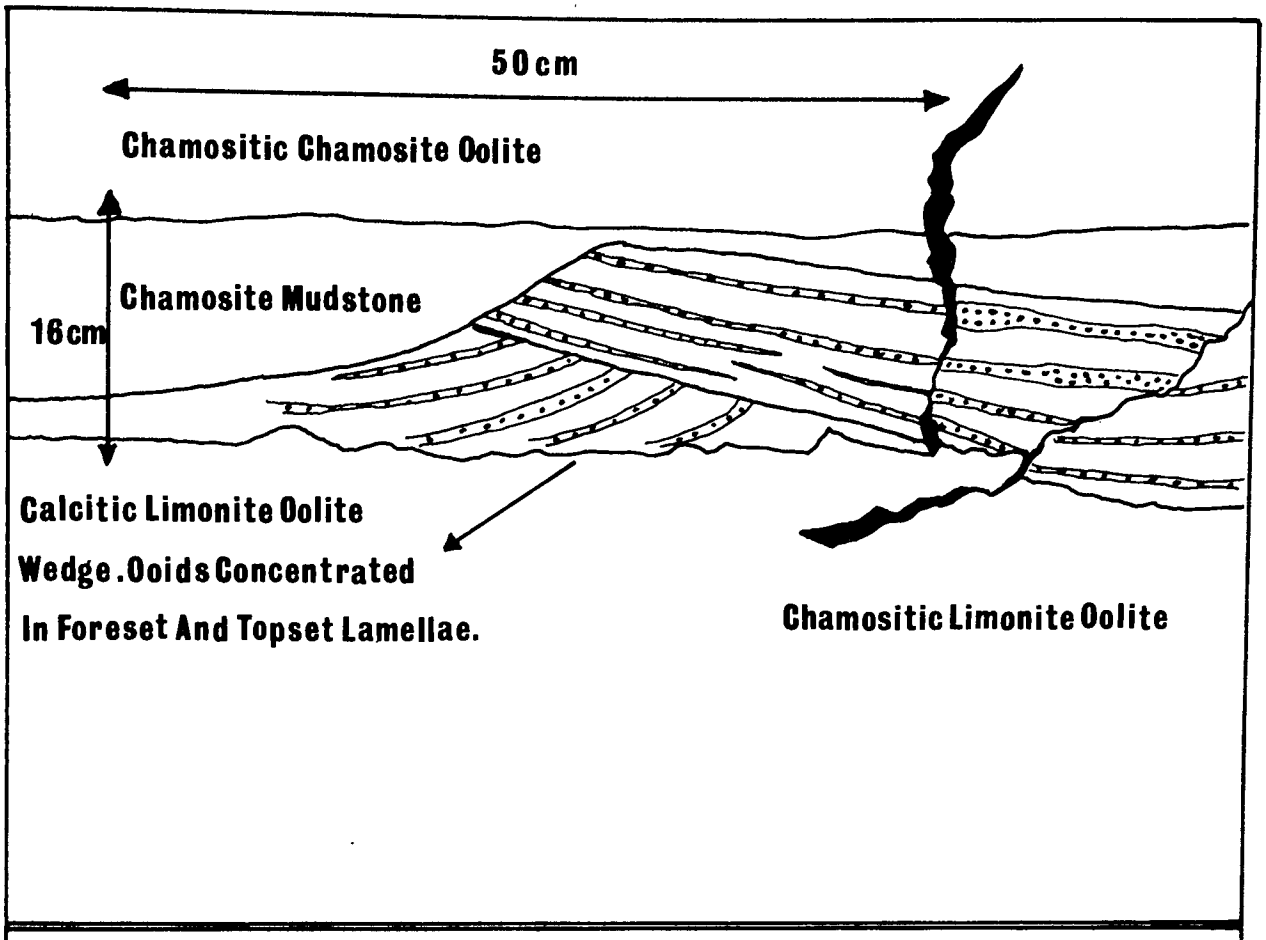

Figure 2.9

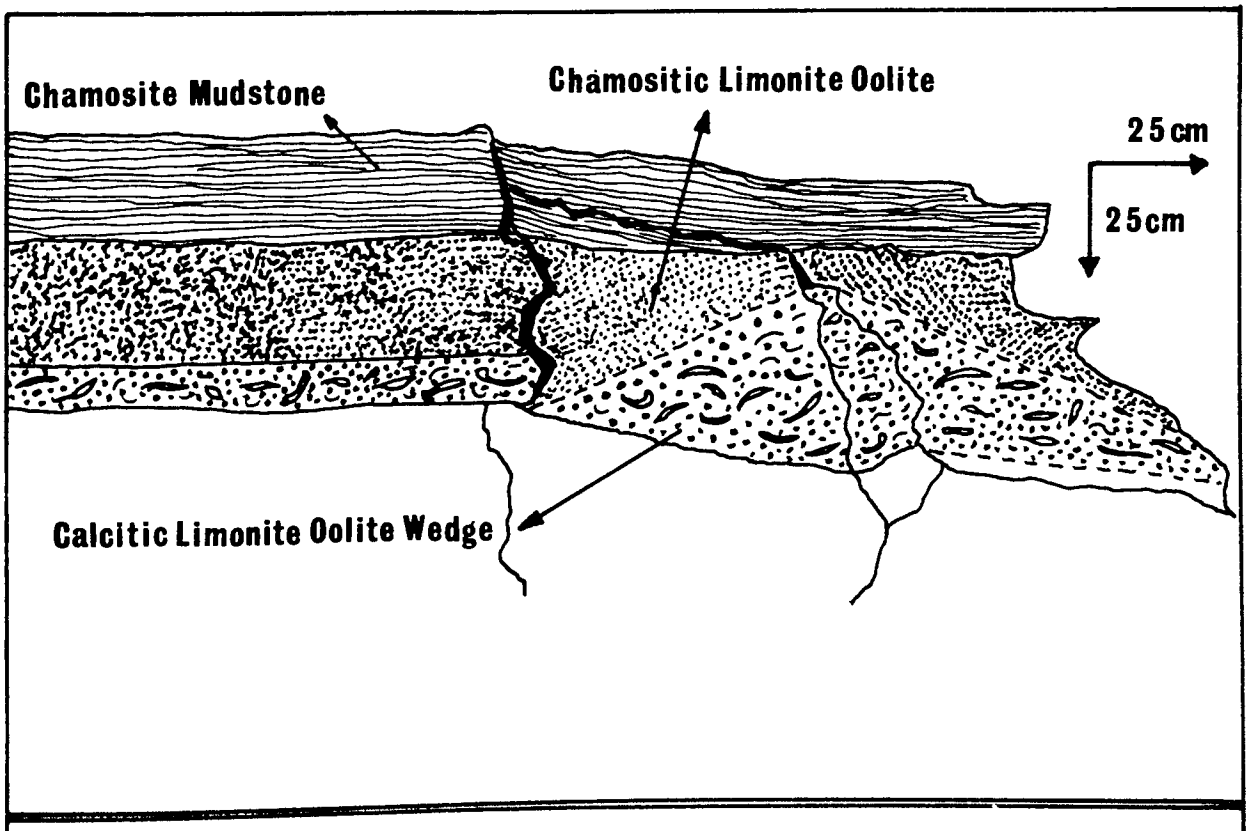

Figure 2.10

Winterton Pit a chamosite mudstone is found to pass laterally and abruptly into a calcitic limonite oolite.

Evidence for lateral transitions from chamositic limonite oolites to calcitic limonite oolites is common at Yarborough, Crosby Warren and Winterton Pits. Bed Y15 at Yarborough Pit, for instance, is characterised by an abundance of approximately 1 m long wedges and lenses of calcitic limonite oolite and bioclastic limestones. Commonly, the calcitic limonite oolites are characterised by limonite ooids concentrated in foreset lamellae. The bioclastic limestones are shell accumulations with few limonite ooids. The nature of these wedges and lenses are suggestive of localised conditions of higher energy winnowing away chamosite mud whilst concentrating the heavier shells and limonite ooids. This may indicate the proximity of more widespread conditions of calcitic limonite oolite deposition. At Crosby Warren, an example of a calcitic limonite oolite wedging out into chamositic limonite oolite was found (Figure 2.10). In Bed WP5 at Winterton Pit, a chamositic limonite oolite, a series of very large lenses of calcitic limonite oolite occur at the same level. These vary in length from 1-6 m, and may reach 1.5 m in thickness.

From the above evidence, it is clear that certain facies pass laterally into others. The criterion to determine the nature of lateral passage is simple; where a lens of one facies is found surrounded by another facies then this is indicative of a passage from the latter to the former. Application of this criterion during the field study has shown that although a particular passage may occur, the reverse does not. The matrix in Figure 2.11 shows the number of different lateral transitions which have been observed, thus summarising and quantifying the above observations.

	1	2	3	5	6	
1	0	5	10	1	0	16
2	0	0	0	0	0	0
3	5	0	0	11	0	16
5	1	0	0	0	0	1
6	1	0	0	0	0	1
	7	5	10	12	0	34

Figure 2.11: Observed Lateral Transitions

	1	2	3	5	6
1	0	0.31	0.62	0.06	0
2	0	0	0	0	0
3	0.31	0	0	0.68	0
5	1.00	0	0	0	0
6	1.00	0	0	0	0

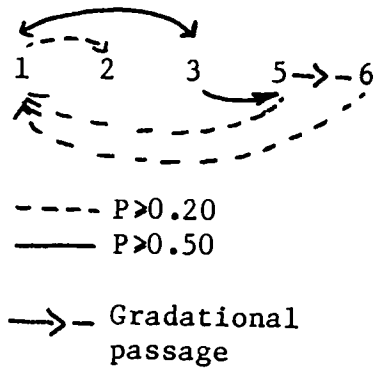

Figure 2.12: Transitional Probability Matrix and Facies Relationship Diagram For Observed Lateral Passages

1: Chamosite mudstone, 2: Chamositic chamosite oolite, 3: Chamositic limonite oolite, 5: Calcitic limonite oolite, 6: Bioclastic limestone, 8: Shale.

Application of the same statistical test used to determine whether the vertical sequences had a random arrangement or not yields a chi-squared value of 3.09. Since this lies outside the 95% confidence level of the chi-squared distribution it can be concluded that the observed lateral transitions are non-random, and that the occurrence of any one facies is dependent on the nature of the nearest different facies at the same horizon. Using the method outlined above a transitional probability matrix for lateral transitions can be constructed and a facies relationship diagram, showing the order of lateral passages, constructed (Figure 2.12).

It is clear from the facies relationship diagram of Figure 2.12 that the ideal sequence of lithologies which would be expected to occur as lateral equivalents, at any given horizon, within the ironstone is as follows: Chamosite mudstone, chamositic limonite oolite, calcitic limonite oolite/bioclastic limestone. No lateral passage between bioclastic limestone and chamosite mudstone has been recorded. The abrupt type of passage which characterises the other lateral transitions between lithologies has not been recognised between calcitic limonite oolite and bioclastic limestone. Since the latter lithological type is the equivalent of the former, but without limonite ooids, a gradational passage might be expected. Thus, these two lithological types may be bracketed together from this point of view. It is interesting to note that the lateral passages recorded between chamosite mudstone and chamositic chamosite oolite show up well on the facies relationship diagram. As has been noted, no other lateral passages from, or to, chamositic chamosite oolite have been recorded. This leads to the isolation of this facies from the others, with the exception of the chamosite mudstone.

The evidence from the field study of the lateral relationships between the component facies of the Frodingham Ironstone, and its statistical analysis, lends a great deal of support to the conclusions of the preceding section. Field evidence shows that lateral transitions occur in the order predicted by the suggested cyclic hypothesis.

2.2.4.iii Amalgamation of the results of vertical and lateral studies: Comparison of the facies analysis diagrams derived from vertical sequences, and the diagram derived by quantifying all the lateral transitions encountered, shows a common sequence of facies in both the vertical and horizontal senses. In both cases, the sequence of lithologies is the same. This sequence is shown diagramatically in Figure 2.13, where the relationship between vertical and horizontal lithological transitions is shown in an ideal way.

The block diagram in Figure 2.13 satisfies all the facies relationships defined from the studies described above. It cannot, however, be held to be representative of the ironstone field as a whole. The reason for this is that the chamositic chamosite oolite has been assumed to have the same quantitative significance as the other lithological types and to have been controlled by the same dynamic sedimentological processes. If this were the case, it would be expected to be more frequent in its occurrence, whereas it is the least common facies in the southern-most pit and is totally absent from the northern-most. The facies relationship diagrams show that at Yarborough Pit, there is a demonstrable vertical and lateral relationship between chamosite mudstone and chamositic chamosite oolite. Although one vertical transition has been recorded from chamositic chamosite oolite to chamositic limonite oolite, the

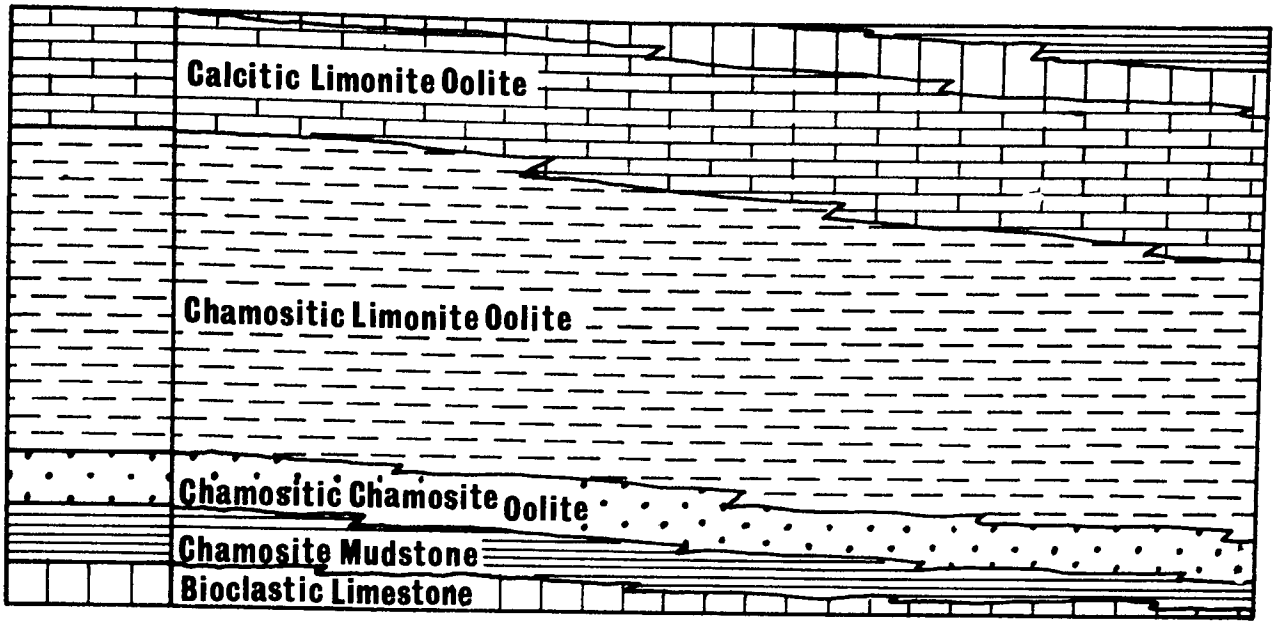

Figure 2.13:Lateral And Vertical Facies Relationships

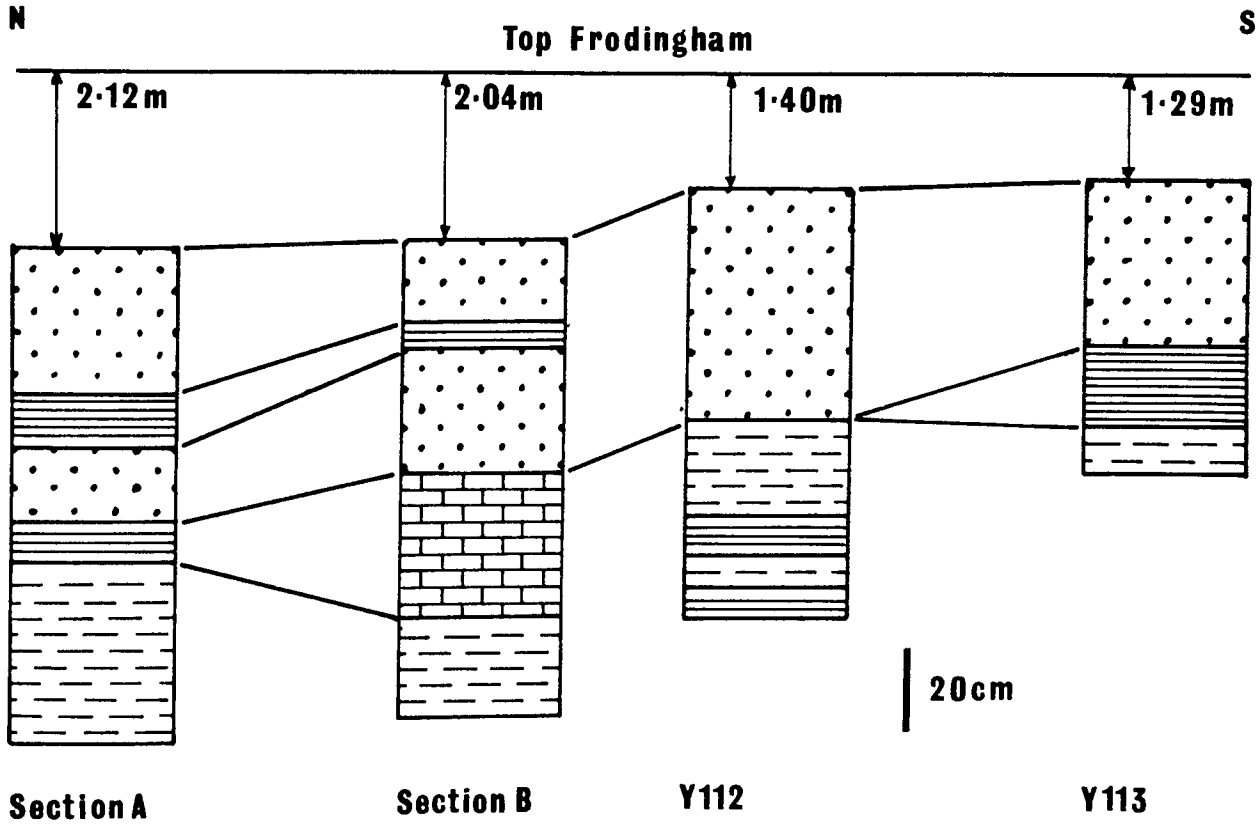

Figure 2.14:Correlation Between Upper Portions Of Yarborough Logs

overall relationship appears to be one of vertical and lateral passage between chamosite mudstone and chamositic chamosite oolite of the form A,B - A,B - A,B ...., within areas of chamosite mud deposition.

Consideration of the sections from Yarborough Pit (Figure 2.5) shows that chamositic chamosite oolite occurs at approximately the same level in all cases. Since the distances between the individual sections are relatively small and the thickness of the chamositic chamosite oolites relatively large, a lithological correlation can be made. These beds are associated with chamosite mudstones. Figure 2.14 shows the relevant portions of the sections and the distances to the top of the Frodingham Ironstone, which is taken to be an isochronous horizon. It is immediately apparent that the sections define a palaeoslope with a dip to the north. The two southern sections of chamositic chamosite oolite occur on a substrate of chamosite mudstone. In contrast, at a lower level on the palaeoslope, the oolites rest on limonite oolites. The presence of chamosite mud dividing the chamositic chamosite oolites of the two northern sections into two separate units suggests the renewal of chamosite mud depositional conditions further down slope at a later stage. Unfortunately, the lack of closely spaced thickness data precludes a more detailed study of thickness variations in this portion of the sequence at Yarborough Pit. Figure 2.15 is a ribbon diagram interpreting the distribution of the chamositic chamosite oolite and chamosite mudstone facies. In Core Y113 the top of the chamositic chamosite oolite - chamosite mudstone is closer to the top of the Frodingham than any of the other sections. From this section the chamositic chamosite oolites thicken towards the site of Core Y112, and thin from the sites of Cores Y112 and Y113 towards

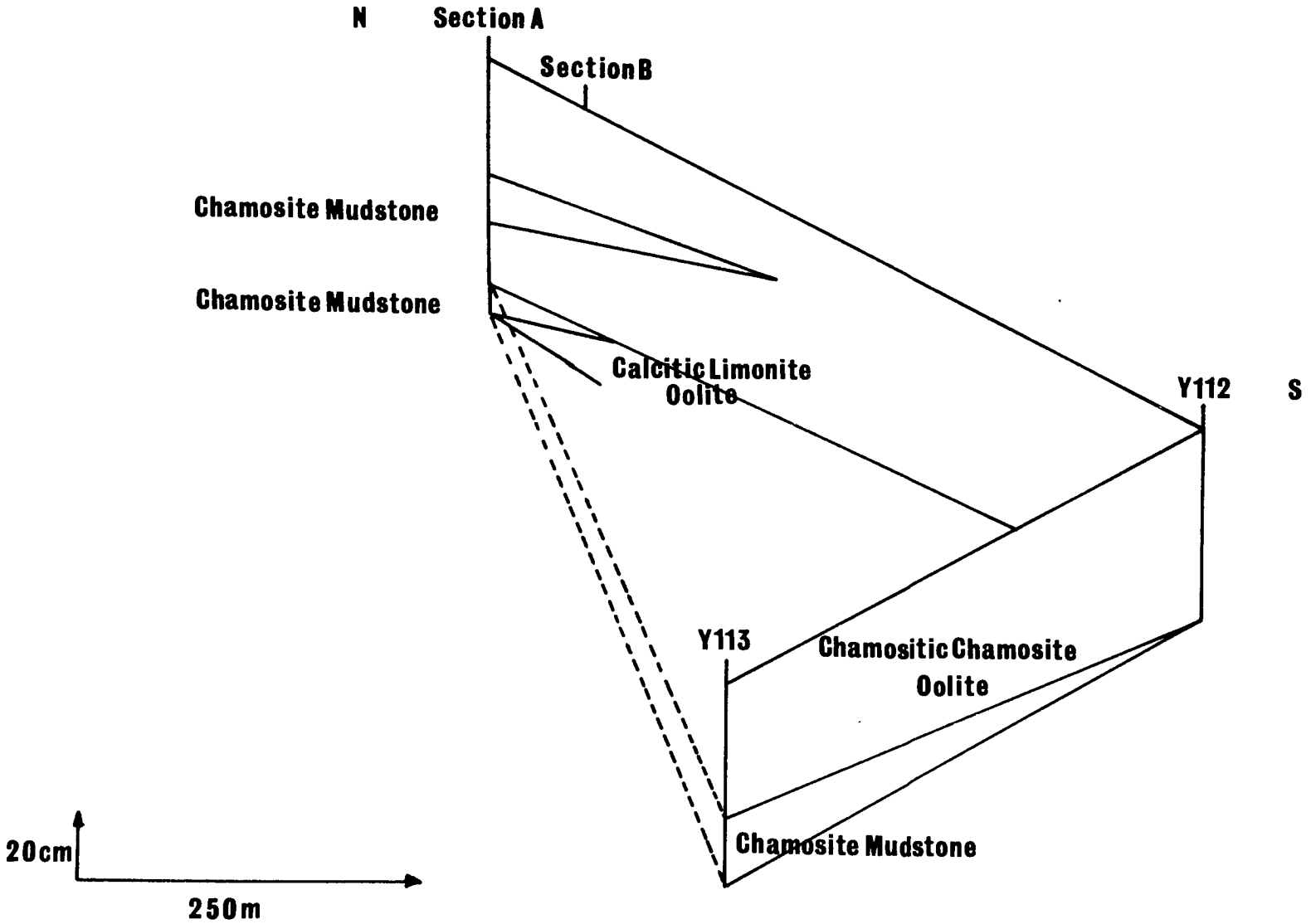

Figure 2.15: Inter-relationships Between Chamosite Oolite And Mud Facies

the northern sections. It would appear that the section derived from Core Y113 represents a close approach to some topographic high on the sea-bed. From a comparatively small thickness over the high, the chamositic chamosite mudstones initially thicken down the slopes of the high and subsequently become thinner with distance from the topographic high. In the immediate vicinity of this feature, deposition of the chamositic chamosite oolites occurred on a carpet of chamosite mud which also thinned around the margins of the high. Thus, in the north, deposition in a marginal area on calcitic limonite oolite and chamositic limonite oolite occurred.

From the above consideration of the nature of the chamositic chamosite oolites in Yarborough Pit, it would appear that in order for such a lithology to develop, some degree of bottom topography was necessary. This suggestion is supported by the work of Knox (1970) and Chowns (1968), who have both suggested shoal areas as a site of chamosite ooid formation, from work on the Winter Gill and Cleveland ironstones, respectively. Further support for the hypothesis comes from elsewhere in the Frodingham Ironstone. No other evidence for a bottom topography has been found; as a result no other examples of a chamositic chamosite oolite are found to occur. By placing the constraint of a bottom topography on the occurrence of this lithology it can be removed from the ideal Frodingham cyclothem as a separate unit, and can be incorporated within the chamosite mudstone. Figure 2.16 is a block diagram relating the vertical and lateral variations after the occurrence of chamositic chamosite oolites have been taken into account. The average unit thicknesses are also shown. Figure 2.17 shows how this model may be applied to the measured sections from the Frodingham

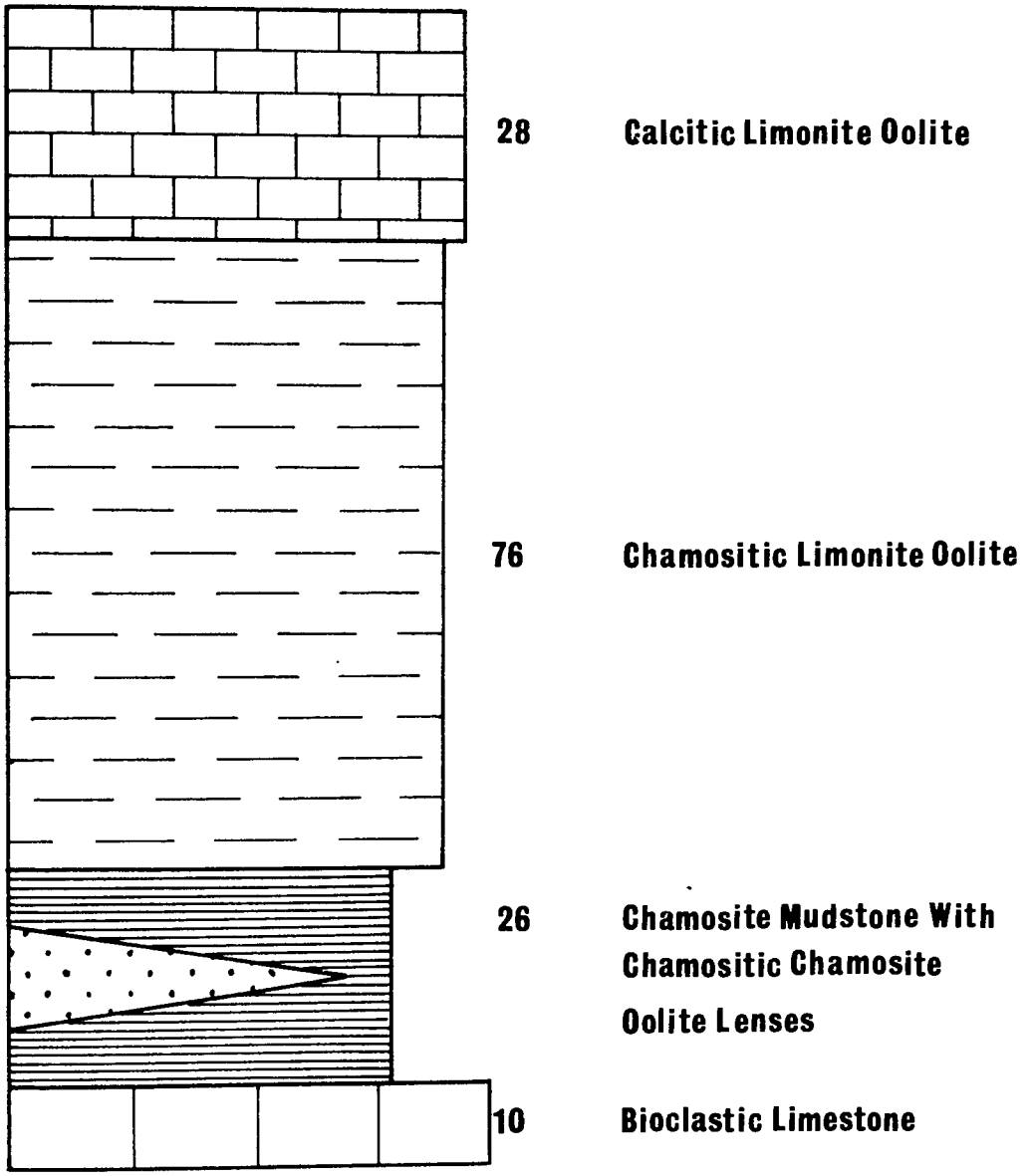

Figure 2.16:Ideal Cyclothem With Chamositic Chamosite Oolite Lenses

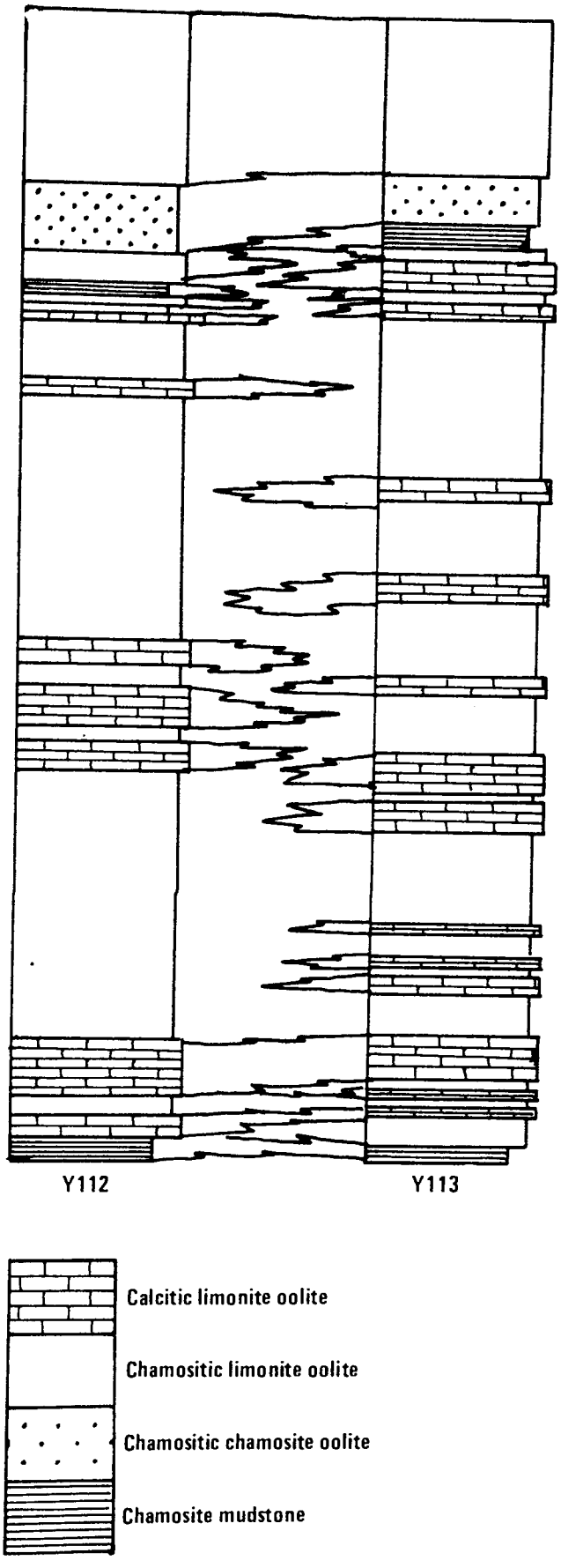

Fig 2.17 Hypothetical facies relationship between cores Y112 and Y113

Ironstone Field. The result is an interdigitating sequence of the major oolitic and mudstone units lapping on and off each other. Broadly, four belts can be defined in this way at both Winterton and Yarborough Pits. With increasing distance from the chamosite mudstone facies, chamositic limonite oolite occurs and is followed by calcitic limonite oolite and then by a bioclastic limestone. Further detailed work would be required to determine whether the extent of these belts is on the scale of the ironstone field or on a more localised scale. The fact that bed to bed correlation between pits is not possible suggests that the latter is more likely to be the case however.

2.2.5 The Nature of the Red Oolites

The lithological description of the Red Oolites sub-divided them into a red limonitic chamosite oolite, a red chamositic limonite oolite, and a red calcitic limonite oolite. Red chamositic chamosite oolites have not been observed in the field. An important feature of the second lithology is the nature of the burrow-infills. In narrow burrows, this is a fine-grained dark-red material, whilst in much wider burrows such material occurs as an outer rim to a central core of chamosite mudstone. Similarly, the fine-grained red material forms large areas of matrix in which much smaller regions of green chamosite mud matrix occurs.The red colouration of the red calcitic limonite oolites is due to the overall salmon-pink colouration of the cementing calcite. This may be patchy in some instances, such as at Winterton Pit, where there is a demonstrable relationship between the development of pink matrix calcite and shells coated with a red fine-grained material rather than authigenic chamosite. The red calcitic limonite oolite

intersected in the Nettleton Core shows that the pink calcite is pervasive throughout. The common factor relating the development of a red colouration in both of these lithologies appears to result from some post-depositional change of the nature of the original chamosite mudstone, whether primary or authigenic. In order for such a change to be related to the salmon pink colour of cementing calcites it must predate the precipitation of this cement.

The overall nature of the beds of red oolites where exposed in the Frodingham Pits show some differences from their non-red counterparts. In place of a sharp, flat bedding plane defining the upper surface of the bed, Beds Y2 and WP9 exhibit somewhat irregular hummocky upper surfaces. The bases of both of these beds are completely flat. The U-shaped burrows of Diplocraterion parallelum (Torell) often extend down from the irregular upper surfaces and are infilled with dark green chamosite mudstone.

The nature of Bed WP2 at Winterton Pit suggests that the creation of red oolites occurred at the time of formation of the Frodingham Ironstone and is not explicable in terms of weathering by later ground-water movement. This bed is 20 cm thick and constructed of calcitic limonite oolite. A band of red calcitic limonite oolite 8 cm thick occurs within the upper half of the bed, with normal calcitic limonite oolite above and below it. The absence of a well defined hummocky upper surface to the red oolite band and the presence of an overlay of calcitic limonite oolite suggests that the conditions of formation of the red oolites were, at this site, rather more transient than in other cases. The argument against ground-water movement being responsible for the red oolites

lies in the fact that two good bedding planes lie above and below the calcitic limonite oolite bed and are separated from the red oolite band by unaltered calcitic limonite oolite. Since a greater amount of groundwater movement would be along the bedding planes, the red oolite would be expected to form at the tops and bottoms of the bed.

Consideration of Figure 2.5 shows that red oolites are found to occur at two levels in the Nettleton Core and in the sections from Yarborough Pit. In Winterton Pit only one red oolite is found to occur near the base of the sequence. Broadly, then, conditions were suitable for red oolite formation at two periods during the formation of the Frodingham Ironstone. The hummocky nature of the surfaces of the beds is suggestive of erosion. The evidence of the chamosite mudstone-filled burrows suggests that following their formation, the external environment changed and this resulted in a mineralogical change in the chamosite. Since chamosite is a mineral containing ferrous iron and the material in thick burrows which margins a chamosite mud core is red, it would seem likely that the mineralogical change resulted from oxidation. Relatively large thicknesses of ironstone beds have been affected in this way. A reasonable suggestion to account for this and for their erosion surfaces would be subaerial exposure. Since this would be expected to occur over wide areas at any one time the appearance of red oolites in the Frodingham Ironstone at approximately the same levels is understandable. The absence of any major conglomerate bands or an accumulated fauna of rolled belemnites and ammonites from these levels indicates that no major erosion occurred during exposure, and that its time span was probably not of significant length relative to the overall depositional span of the Frodingham Ironstone. The pink

colouration of the cementing calcite in the red calcitic limonite oolites can also be explained. Authigenic chamosite formed around allochemical grains prior to exposure might be oxidised and detached and incorporated within the cementing calcite when this precipitated; thus producing a pink colouration to the calcite. Petrographic evidence shows that finely divided goethite is abundant in the cement. The interpretation that can be placed upon the red calcite and chamositic limonite oolites is that their characteristics result from an overprint, due to subaerial exposure, on original chamositic limonite oolites and uncemented calcitic limonite oolites.

2.2.6 Depositional Environment

The Frodingham Ironstone possesses seven different ironstone facies of which five are not the result of diagenetic change. The nature and interelationship of these five facies provides an excellent opportunity for some environmental interpretation to be made. Since there are no present-day analogues of aluminous ironstones this must be carried out using those features of the facies which are in common with Recent sediments. This will provide an environmental framework which is independent of sediment composition.

The ideal Frodingham Ironstone cyclothem is a coarsening-upwards sequence commencing with muds and ending with bioclastic limestones. This reflects an energy spectrum passing from quiet water to energetic conditions. Such a spectrum results in the winnowing of any interstitial mud from the coarser-grained sediments and the breaking of shell material in the more energetic sub-environments.

The chamosite mudstones are laminated and contain abundant quartz. Evidence of biological activity is absent. Laminated bedding is indicative

of the deposition of the component clay platelets from suspension in quiet water. The presence of abundant quartz suggests a strong terrigenous influence on this facies. The marked absence of quartz from any of the other ironstone facies, with the exception of some specimens of chamositic limonite oolite, indicates that this facies was responsible for concentrating any terrigenous material entering the ironstone depositional environment. Oxygen levels at the sediment surface must be held responsible for the absence of fauna. Ooids of either chamosite or limonite are generally absent.

It has been demonstrated that the chamositic chamosite oolite facies represents shoal areas (Figure 2.15). The absence of an in situ fauna is indicative of very low oxygen levels. This is rather strange as shoal areas might be expected to be rather well oxygenated as a result of their topography forming a barrier to moving water. Petrographic evidence indicates that chamosite ooids and chamosite mud were formed at these shoal areas and that they are characterised by abundant organic material.

The chamositic limonite oolite facies exhibits a generally non-quartzose nature. Occasional quartzose specimens have been found. This supports the position of this facies in the Frodingham cyclothem. The facies is characterised by an abundant and varied epifauna and infauna. The common occurrence of Diplocraterion parallelum (Zenker) allows the facies to be placed in the Skolithos (littoral sands) facies of Seilacher (1967) and in the intertidal-shallow subtidal facies of Fursich (1975). Beds of this ironstone facies are usually relatively thick and uniform in nature throughout. Occasional thin beds with lenticular bedding occur, however.

The calcitic limonite oolite facies has an abrupt contact with the chamositic limonite oolite facies and grades into bioclastic limestones. Chamosite mud is entirely absent. This indicates a steep energy gradient bringing about sudden complete winnowing of mud and fragmentation of shelly fauna. Foreset lamination is common in both calcitic limonite oolites and bioclastic limestones and defined by limonite ooid concentrations. These concentrations are often penetrated by short vertical burrows which are also infilled by ooids. This is the only evidence of an in situ fauna. Presumably the higher energy of this facies was unfavourable for colonisation by any shelly fauna.

The red oolites represent periods of widespread exposure of the ironstone. The fact that these horizons can be correlated over large distances suggests that the sea-floor during ironstone deposition had a very low gradient with very little bathymetric variation.

In order to construct an environmental framework it is very important to know the dominant direction of sediment transport. If the ironstone was a clastic deposit the presence of quartz silt in one facies and clay in another would indicate a transport direction from the former (landward) to the latter. The major primary components of the sediment are created within the depositional area. The implication of the restriction of an external terrigenous component to a particular facies must therefore be interpreted with some care. The presence of quartz grains within the chamosite mudstone facies would appear to suggest that this is the most landward facies. Two important related facts argue against this: (a) It has been demonstrated that the chamosite mudstone facies forms the site for the creation of chamosite oolite shoals. These, it could be argued, might protect the mudstone facies

from landward moving currents thereby creating a 'lagoonal'-type environment. The association between chamosite mudstones and chamositic chamosite oolites, however, is by no means ubiquitous. (b) Landward moving currents would be expected to erode the chamosite oolite shoals and transport this material landward. No oolitic phase occurs within the chamosite mudstones but the chamositic limonite oolites, calcitic limonite oolites and bioclastic limestones contain abundant ooids. It would therefore appear that in the ideal lateral sequence of facies the chamosite mudstone facies is the most seaward and the bioclastic limestone facies the most landward. The processes of storms and longshore drift may be invoked to account for the presence of quartz silt within the chamosite mudstone.

It has been noted above that the impossibility of bed to bed correlation between ironstone pits suggests the presence of a complex of similar small depositional areas which give rise to the observed on-lapping and off-lapping sequences. The deeper quieter areas between these would provide an ideal location for the gradual deposition of chamosite mud from suspension and the ponding of quartz silt. Such areas would be characterised by poor circulation giving rise to poor, non-life supporting, oxygen levels. This type of sub-environment might well be termed a clastic trap. It differs from the clastic traps of Hemingway (1951), Huber and Garrels (1953), Knox (1970) and Hallam and Bradshaw (1979) in that it does not occur between land and ironstone depositional sites.

Utilising the sediment-independent parameters defined above, the depositional environment of the ironstone appears to be one which overall shallows shoreward with a concommitant increase in energy. Such broad characteristics are shown by the deposits occurring at the transition between present day beaches and shelves. This environmental

type has been selected for comparison with the Frodingham Ironstone since environmental sub-types which characterise other upward coarsening sequences are absent. Consideration of the literature reporting the nature of Recent beach-shelf transitions shows that the example of the Gulf of Gaeta, Mediterranean Sea, Italy (Reineck and Singh, 1975) is closely similar in sediment-independent features to the Frodingham Ironstone.

The Gulf of Gaeta is situated north of the Gulf of Naples in the Tyrrhenian Sea. It is not affected by tides. The only current activity is provided by storm driven and longshore currents. A detailed description of the sedimentary succession is given by Reineck and Singh (1975). It commences (Figure 2.18) with a thick sequence of bioturbated shelf mud containing intercalations of storm-silt. This is overlain by a fine sand and silt-dominated sequence representing the transition from shelf to beach. Bioturbation, mainly by echinoids, has totally destroyed any original sedimentary lamination. The overlying, Lower, Middle and Upper shoreface units comprise a mixture of fine and medium sands. The latter forms a small component in the Lower unit but increases to approximately 50% of the sediment in the Upper unit. The bedding in these three units comprises gently dipping laminated and foreset laminated sets. Discordances between sets are common. The lamination is characterised by the presence of small vertical burrows. The uppermost portion of the sequence comprises foreshore and sand-dune deposits. From the top of the Upper Shoreface unit to the top of the shelf-mud unit is a water depth which varies from 10 m in the north to 20 m in the south.

The Frodingham Ironstone bears a close resemblance, in sedimentary features, to the Gulf of Gaeta. There is a striking similarity between

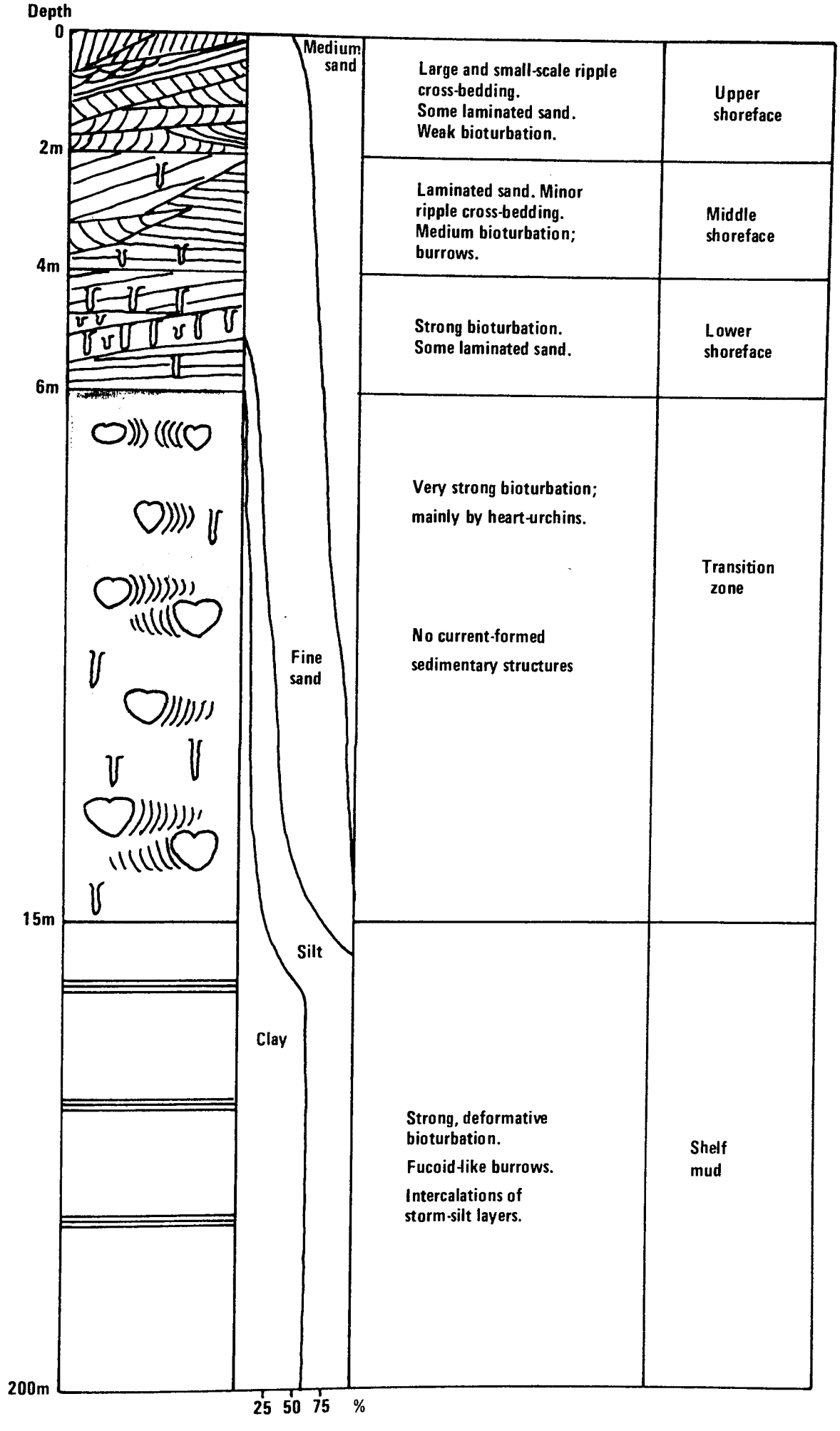

Fig 2.18 The Gulf of Gaeta succession

the sedimentary structures of the Shoreface unit to those of the calcitic limonite oolites and bioclastic limestones. Reineck and Singh (1975) note that shells are transported from the Lower Shoreface towards the Upper Shoreface. The Transition Zone is characterised by abundant bioturbation. Although much of this is due to the burrowing activities of echinoids a shelly infauna also provides a component. This infauna remains as an autochthonous assemblage after death.The Transition Zone is clearly comparable with the chamositic limonite oolite facies. The only major difference between the two sequences occurs between the Shelf-mud and the chamosite mudstone facies. The abundant bioturbation of the former over that of the latter quite possibly reflects its occurrence as a uniform belt parallel to the Italian coast. The occurrence of chamosite mudstone has been discussed. One point that the two have in common, however, is that the coarse component of the Shelf-mud is derived as a result of storm activity. A similar origin for quartz silt in the chamosite mudstones has been suggested. It must not be forgotten that ultimately the Frodingham Ironstone passes laterally into shales and clays of much deeper water facies.

It is concluded that there are similar points in common between the Gulf of Gaeta and Frodingham cyclothem to allow an environmental interpretation of the cyclothem to be made. The chamosite mudstone facies thus represents shelf deposits, chamositic limonite oolites a transition zone from shelf to shoreface, and calcitic limonite oolites and bioclastic limestones shoreface deposits. Since chamositic chamosite oolite shoals occur in association with chamosite mudstones these may be assigned to a shelf environment. Figure 2.19 interprets the graphic logs of the Frodingham Ironstone in these terms. Although thickness data for the Gulf of Gaeta sub-environments are not reported the

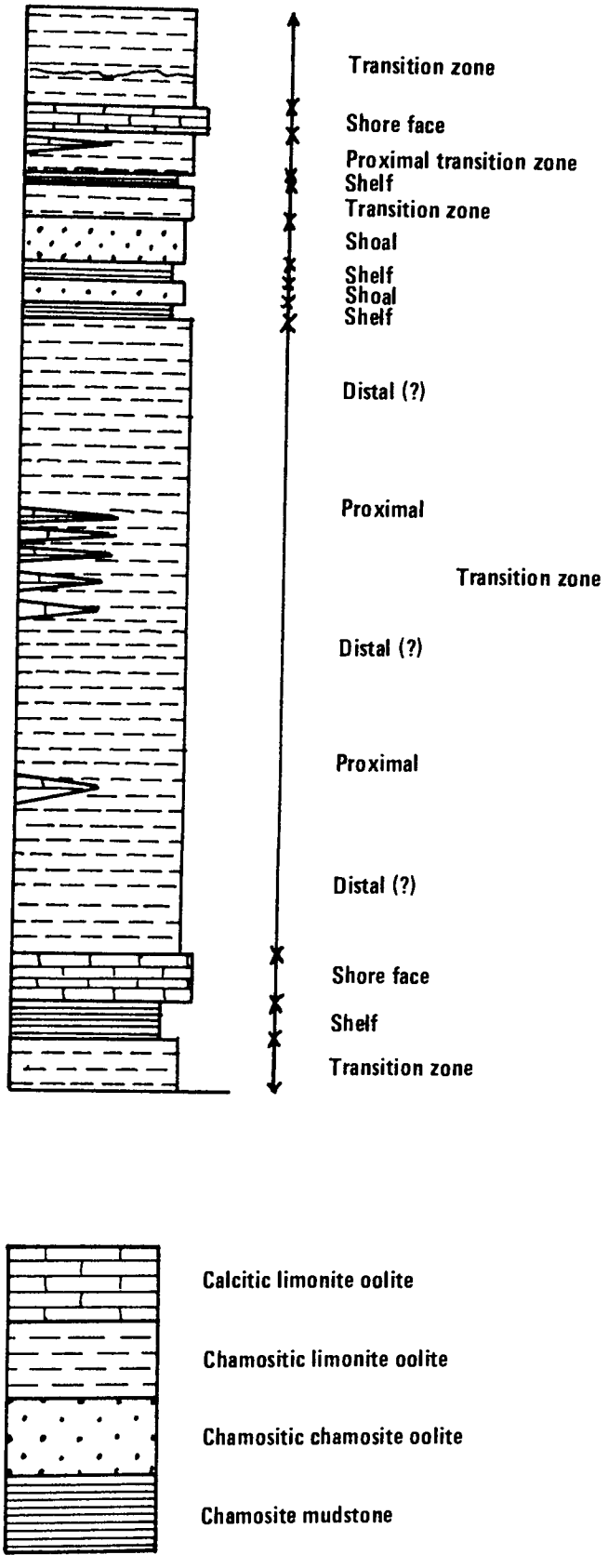

Fig 2.19 Environmental interpretation of the Yarborough Pit Section

difference in water depth between their tops and bottoms gives some guide as to their thickness. These values are given in Figure 2.18. The thickness of the transition unit may thus be estimated at 9 m. Although individual chamositic limonite oolite beds are much thinner than this, net thicknesses, which include calcitic limonite oolite and bioclastic limestone lenses, may reach values of 4-5 m. These values represent post-compactional thicknesses. In general the calcitic limonite oolites and bioclastic limestones are much thinner than the Gulf of Gaeta shoreface facies. The chamosite mudstones are considerably thinner than the shelf facies of the Gulf of Gaeta. With respect to this facies it must be remembered that the thickness of the mud units is controlled by the formation and destruction of chamosite oolite shoals, and that they pass laterally into clays and shales. It would seem likely then that the observed Frodingham Ironstone sequences may represent the transition zone between shoreface and shelf sub-environments. The lateral order of ironstone facies is shown in Figure 2.20, in comparison with a cross-section of the Gulf of Gaeta facies. This indicates the presence of a long-shore bar in the Middle Shoreface unit. Such a feature in the Frodingham Ironstone would be recognised as a thick (probably in excess of 1 m) laterally continuous unit of calcitic limonite oolite and bioclastic limestone. Prograding and retrograding of the facies model in Figure 2.20 would yield the observed sequences. Periodic, storm driven, currents eroding chamosite oolite shoals would provide chamosite ooids, oxidised in the nearer shore areas to limonite, for incorporation in inshore facies. Water depth during Frodingham Ironstone deposition has not been discussed. It is not possible to gain any idea of what this might have been. The depths encountered in the Gulf of Gaeta

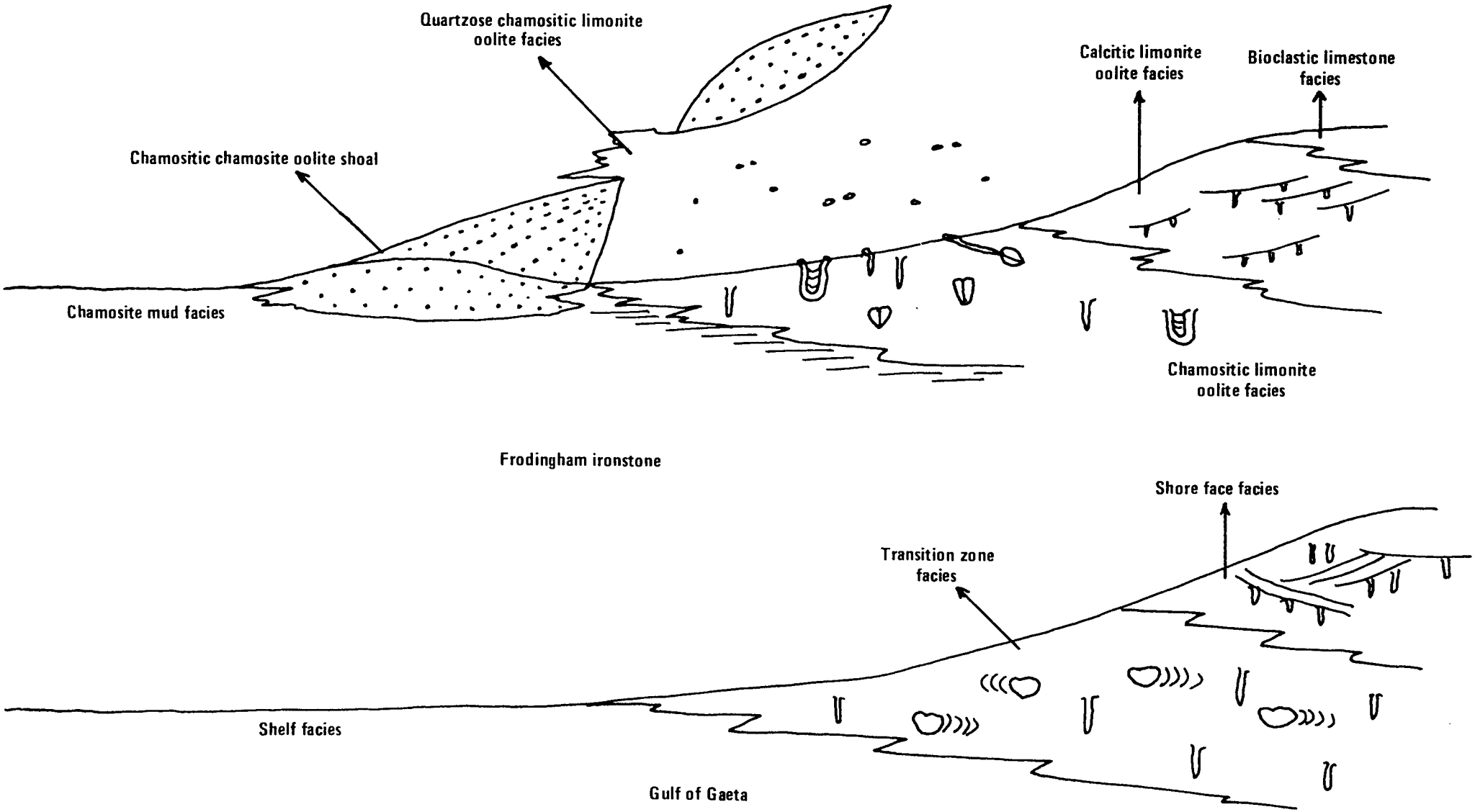

Fig 2.20 Lateral facies relationships between Frodingham facies (Hypothetical) and Gulf of Gaeta facies. Not to scale

are not thought to be so great as to be unrealistic. Depth-related terms such as shelf should be thought of as the deeper depositional areas in context of the Frodingham Ironstone.

2.3 PETROGRAPHY

2.3.1 Goethite Ooids

In all the facies types examined the general nature of the goethite ooids remains the same. This allows a general description of their form and nature to be made. A number of textures are exhibited by these grains which are post-depositional in origin and peculiar to the facies in which they occur. Thus, a general description is given here and the characteristics shown by the ooids in a particular facies separately with the description of that facies.

A variety of colours are shown by the ooids, from a light amber brown to a deep red brown. Occasionally opaque ooids occur. A number of these, however, show a red brown colouration around their margins. The colour differences are shown by micrometer measurement to result from a variation in slide thickness; the lighter and more transparent ooids occurring around the thinner margins, the darker and less transparent in central thicker areas of the slide. In the majority of cases the degree of transparency is sufficient for the internal structure of the ooids to be seen.

The dark body-colour of the ooids results in the masking of any optical characteristics such as pleochroism. There is an important

exception to this, however; between crossed nicols the ooid envelopes show an extinction cross which rotates uniformly with rotation of the stage. Similarly, fragments of ooid envelopes which form ooid cores may also exhibit a fragment of an extinction cross. Ooid core grains with a rectangular form and dark parallel cleavage traces show parallel extinction. These optical characteristics are in keeping with the mineralogy of the ooids being goethite. X-ray powder photography and Mossbauer studies support this identification.

A variety of ooid shapes occur. The most common sectional form is either an oval or an ellipse. Amongst grains with this shape the ratio of the long and short axes varies from as high as 5:1 to 2:1. A long axis size range of 0.10 - 0.60 mm with a mean of approximately 0.35 m has been found. Occasionally, ooids with a circular section occur. These shapes are found entirely in sections cut at right angles to bedding. Sections parallel to bedding show the dominant sectional shape to be circular. Thus the overall form of the ooids is discoidal, as can be seen in hand specimens with the naked eye. The varying ratio of long to short axes is therefore more likely to be apparent rather than actual, resulting from the ooids being sectioned in different orientations. These are illustrated in Figure 2.21.

In addition to the above sectional types a number of more irregular varieties occur. These are broadly divisible into three types, although there may be exceptions; (i) triangular, (ii) trapezoidal, (iii) eccentric. Knox (1970) has described concentric and eccentric chamosite ooids from the Winter Gill Ironstone and has derived certain genetic implications from these shapes. The above subdivision implies no such conotations. A representative selection

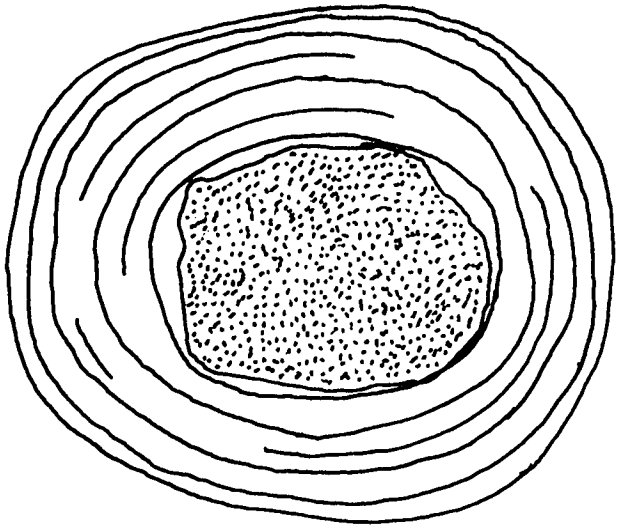

a : Circular Goethite Ooid section. Stippled core. X200

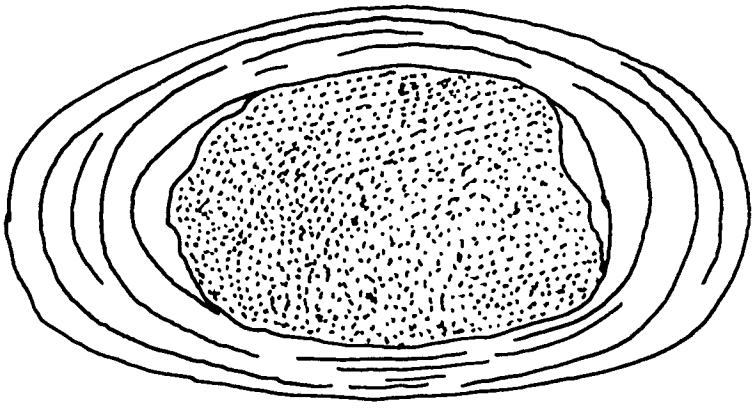

b : Elliptical Goethite Ooid section. Stippled core. X200

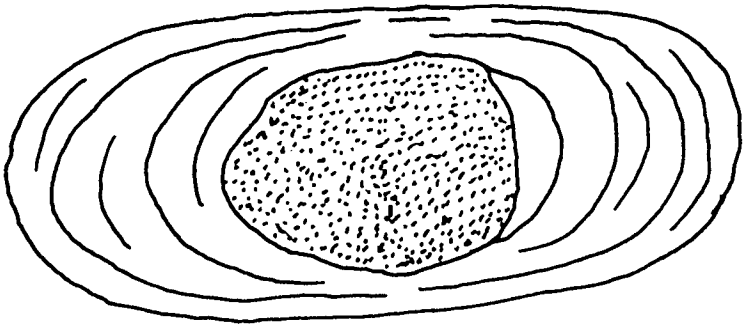

c : Ovate Goethite Ooid section. Stippled core. X200

Fig 2.21 Sketches of Goethite Ooid Sections

of these ooids is shown in Figure 2.22.

The internal structure of the ooids is of a central core grain surrounded by an envelope built up of a series of concordant rings or lamellae. Recognition of the two different components is facilitated by a difference in colour, mineralogy or a clear discontinuity between them. In a number of instances a core grain may appear to be absent. The much greater predominance of ooids with cores suggests that this is probably a result of the sectioning technique exposing only the outer part of the envelope.

The core grains show several different textural and mineralogical forms (Figure 2.23). Of these perhaps core grains formed of various ooid fragments are commonest. These include fragments of ooids that were fractured along the minor axis such that two potential core grains composed of a fragment of both core and envelope were created. A similar type of breakage can also account for core grains which are derived from the ends of ooid long axes. These show the characteristic C-shape of the component rings in this region of the ooid. Portions of ooid envelope which have split off from a parent ooid in the region of the minor axis also form common core-grains. This splitting off may have occurred along a ring contact in which case the inner side of the grain is smooth and slightly curved, or along radial fractures in which case the inner side is ragged and may include a portion of the parent ooid core grain.

A rare type of structured goethite core grain is characterised by a slightly rounded oblong or square shape with black parallel cleavage traces running across it, and parallel to the ooid long axis. In some instances, small'niches' at either end of the traces can be seen (Figure 2.23).

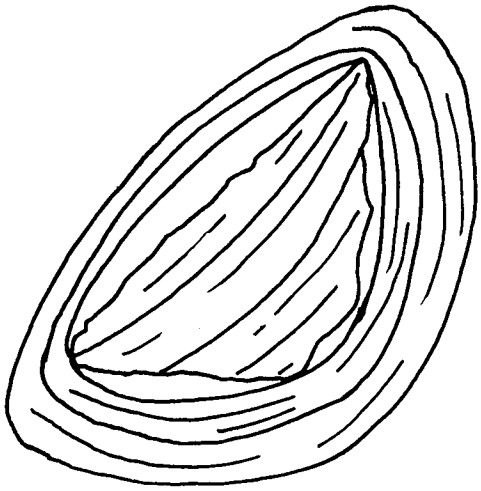

a : Triangular Goethite Ooid section. Ooid fragment core. X150

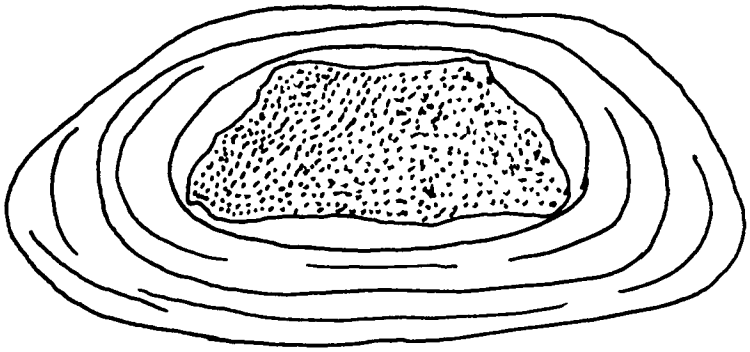

b : Trapezoidal Goethite Ooid section. Stippled core. X200

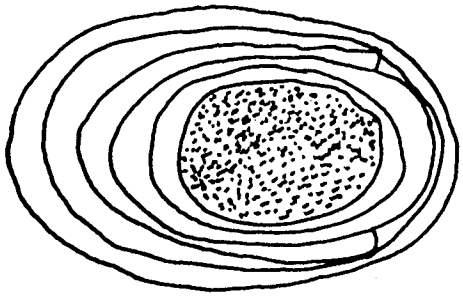

c : Eccentric Goethite Ooid section. Stippled core. X100

Fig 2.22 Sketches of Goethite Ooid Sections

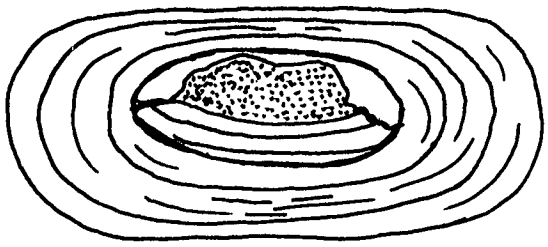

a : Envelope and Core Grain Core
X100

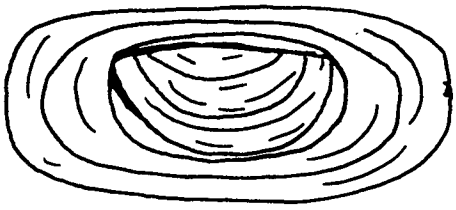

b : End of Envelope Long Axis
Core Grain.
X100

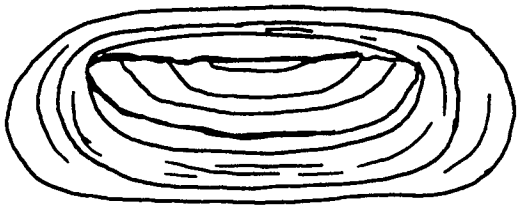

c : End of short Axis Core Grain
X100

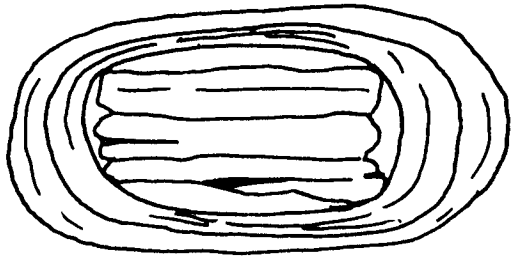

d : Goethite Core Book
X100

Fig 2.23 Sketches of Goethite Ooid Core Grains

In contrast, many core grains of goethite occur which are somewhat irregular and totally structureless. These grains may represent different views of the core grains described above or alternatively they may be grains such as those structureless rounded grains which are present as allochems in their own right. These give no evidence of their origin. Such core grains probably represent a mixture of these two alternatives.

Biogenic material may form the core grains to goethite ooids. The commonest materials of this type are shell fragments. These show signs of a considerable amount of attrition. In the majority of cases they have been subjected to algal boring. The algal tubules that ramify throughout the shell fragments are infilled with fine grained goethite. Complete foram tests are occasionally found as ooid cores. In contrast to the shell fragments they show no signs of either attrition or boring. The chambers are infilled with fine grained goethite. The remaining type of core grain of biogenic origin is represented by the occasional echinoid plate fragment. Such plates have undergone attrition, resulting in rounded shape and in their stereome system being infilled by fine-grained goethite. In all the cases seen, the echinoid plate calcite is of a ferroan composition.

The ooid envelope is constructed of a series of concordant rings. They are characterised individually by a thickness maximum measured along the long axis, and a minimum measured along the short axis (Figure 2.24). This is the case in all ooids with other than circular sections. In this case, however, the rings retain a constant thickness. This indicates that once envelope formation about a central core grain had become established, the addition of successive rings does little to alter the final shape of the ooid from the discoidal form noted above.

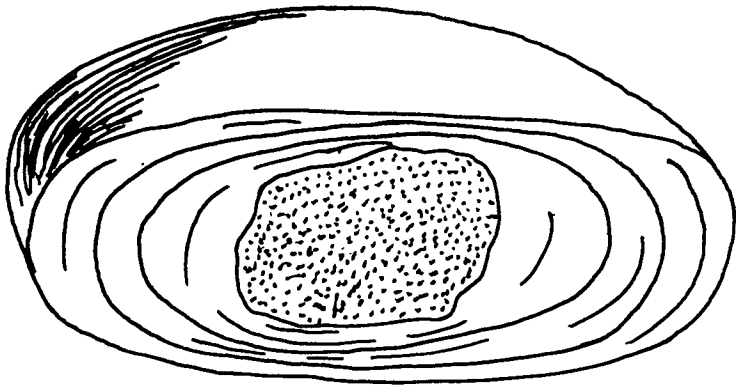

Fig 2.24 Sketch of Ideal Discoidal Frodingham Goethite Ooid

It has also been noted that the ooid envelopes exhibit an extinction cross. Since goethite has parallel extinction, this would suggest that the individual grains of goethite comprising the rings have either a tangential or radial preferred orientation. Unfortunately the deep colouration of the ooids means that an optic sign test to determine which of these is the case is not possible.

Within any given ooid envelope, individual rings are discernable from each other by virtue of colour variations and a thin black line surrounding their outer margins. Such distinction is at an optimum in those portions of the envelope at either end of the long axis. Differentiation of individual rings at either end of the short axis is, however, frequently impossible due to the net envelope thickness reduction in these areas. Indeed, examples of ooids occur in which the envelope thickness in this area is so thin as to be almost absent (Figure 2.25). The vertical and horizontal bars of the extinction cross, corresponding to the short and long ooid axes respectively, show a difference in form corresponding with this observation. The width of the vertical bar spreads out to extinguish a considerable portion of envelope on either side of the short axis, whilst the horizontal bar thickens away from the core extinguishing an isosceles triangle portion of envelope. As would be expected, circular ooid sections do not show such variation. In these cases the characteristics of the long axis area are shown in all orientations of the stage. A variety of envelope thicknesses measured along both long and short axes occur. Generally, the thicker the envelope the more rings comprise it. It does not follow, however, that a thick envelope, measured along the long axis, corresponds to a thick envelope in the region of the short axis.

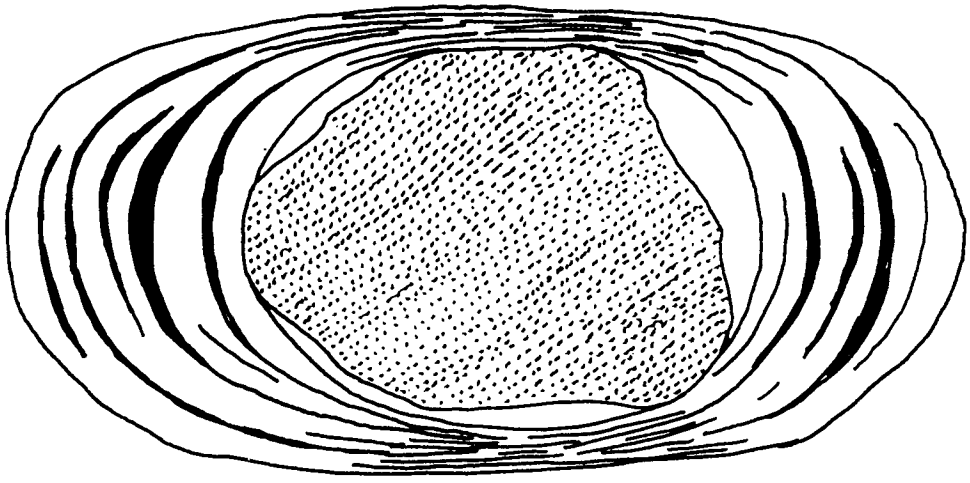

Fig 2.25 Sketch of Ovate Goethite Ooid Section showing the poor degree of resolution of individual rings at either end of the short axis

Consideration of the individual ring thicknesses in any one ooid shows that there is an overall ring thickness increase from those rings immediately around the core grain to the outer rings. In relatively thick envelopes, in the region of the long axis, the outer rings may be ten times thicker than the innermost rings. By no means do all ooid envelopes show such a major thickness variation between rings. The above observation tends to be restricted to those ooids with a thicker envelope.

A number of ooids are characterised by a final ring of goethite which retains a constant thickness around the perimeter of the ooid. In some cases a portion of this ring may be absent, in which case the broken edges of the remainder tend to be rather ragged. For reasons discussed below this final ring is not considered to be an integral part of ooid formation, but to be the oxidation product of an originally authigenic chamosite rim to the ooid.

It has been noted above that five different ooid sectional shapes occur, characterised by a long and short axis. These are ovate, elliptical, triangular, trapezoidal and eccentric. Comparison of the core-grain shape, initial ring form, and net envelope thickness show that the latter three types correspond to early stages in ooid development around core grains with a corresponding shape. Ultimately the first and second sectional types are attained after the addition of a number of rings at a much later date in ooid development. Ovate and elliptical sections do not only occur at such a stage, they may also appear at the initial stages of ooid formation. Their appearance is predicted by core grain sectional shapes which promote the development of such a shape, i.e. ovate, elliptical, rounded squares and oblongs. Figure 2.26 shows

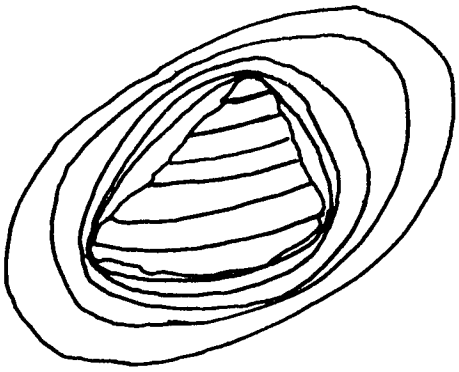

a : Triangular Core Grain

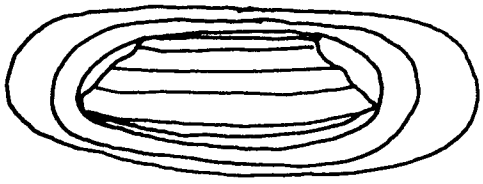

b : Trapezoidal Core Grain

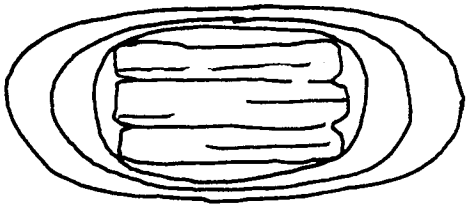

c : Rectangular Goethite Core Book

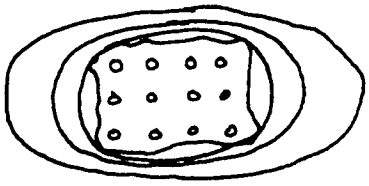

d : Square Echinoid Plate Core Grain

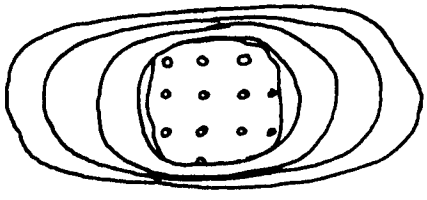

e : Rounded Echinoid Plate Core Grain

Fig 2.26 Core Grain Shapes and successive Envelope Ring Forms Sketches of Goethite Ooids

a representative selection of different ooid core grain shapes and their surrounding envelopes. The development of the various ooid shapes can be traced by a study of successive ooid rings. Ooid ring development commences about a core grain which may be rounded but is more often sub-angular in shape. Two different areas on the core grains have been recognised as controlling the thickness of the initial ring. These are sharp corners or areas with a very small radius of curvature, and straight or gently curving portions of core grain margin, or areas with a large radius of curvature. The initial ring has a minimum or zero thickness over the former areas and thickens to a maximum over the latter areas. The first such ring about any core grain tends to remove all angularities in the initial core grain shape,producing a proto-ooid, the shape of which is closely similar to that of the core grain but rounded. Successive rings follow the same pattern in terms of the controls on ring thickness. Thus, initially, the ooid shape remains broadly similar to that of the core grain. However, since the ooid is increasing in size the areas of originally low radii of curvature gradually increase in this quantity, thereby lessening the shape effect of the core grain. Ultimately this attains the point where, if the core grain was of a triangular, trapezoidal or eccentric shape originally, the shape effect becomes insignificant and ring formation continues to produce an ovate or elliptical shape. The same observations are also true of core grains with rounded or non-rounded square and oblong shapes. In these cases, however, the shape effect is not apparent as the core grain shape promotes the formation of an ovate or elliptical section to the proto-ooid with the deposition of the first ring. In those core grains with ovate or elliptical shapes the above arguments

do not apply as deposition of rings continues as if the core grain were a normal ooid. The importance of the shape effect in the creation of ooids with an ovate or elliptical section follows from the fact that the radius of curvature controls the ooid ring thickness. Small radii of curvature cause a minimum ring growth rate, large radii a maximum growth rate. Thus deposition occurring at two different rates on a square or oblong shaped core grain will result in a rounded grain with a long and a short axis. Thus, ooids with irregular sections are found to correspond to the early cessation of ring formation around similar shaped core grains, and ovate or elliptical grains to early cessation in the case of such ooids with fewer rings. Ooids with ovate and elliptical sections and a thick envelope of many rings can be ascribed to ooid ring formation occurring for a long time.

Comparison of ooids with core grains having a long and a short axis shows that the core grains have a constant orientation with their long axis parallel to that of the ooid envelope. Since core grains would find the more stable orientation on the sea-floor to be with their long axes parallel to bedding it follows that ooid envelope formation also took place in this orientation. In many instances it is found that the distribution of the areas of minimum and maximum radii of curvature on the core grains in this orientation do not correspond to the distribution of ooid envelope thickness maxima and minima. Thus where a core grain has a maximum radius of curvature parallel to its long axis, the ooid envelope is at a minimum normal to this. Therefore it appears that there is a second control on the formation of ooid envelopes required to create the thickness minima and maxima observed in all ooids, and apparently directly related to

dynamic conditions on the sea-bed. It is different from the control described and discussed above since this relates ooid sectional shapes at different times during ooid formation to the shape of the core grain. The nature of the second control cannot be deduced directly from observations of ooids in thin section and is therefore discussed in Chapter 9 under the heading of ooid formation.

Goethite ooids show evidence of a brittle nature. It is common to find ooids with fractures of a straight but rather irregular nature running along the ooid at some point, parallel to either the long or short axes. These may penetrate only a short distance into the envelope or pass all the way across the ooid including the core grain. Radial fractures also occur and tend to be restricted to the envelope. In some instances such radial fractures may be associated with a fracture running along a ring contact. The presence of these incipient fractures (Figure 2.27) in many ooids is the start of their physical break-up which results in the common ooid fragments found in all limonite oolite lithological types with a poorly rounded sub-angular form. On this basis it is logical that the processes of saltation associated with ooid transport are responsible for the initiation and development of ooid break-up.

In contrast to the above discussion some goethite ooids in all limonite oolite facies show that they are capable of undergoing plastic deformation. A selection of such deformation fabrics is shown in Figure 2.28. The distortion is usually of a very simple form involving two ooids in contact. In these situations it is generally found that one ooid is slightly moulded around the more resistant template of the other (Figure 2.28a). More rarely a greater degree of distortion of

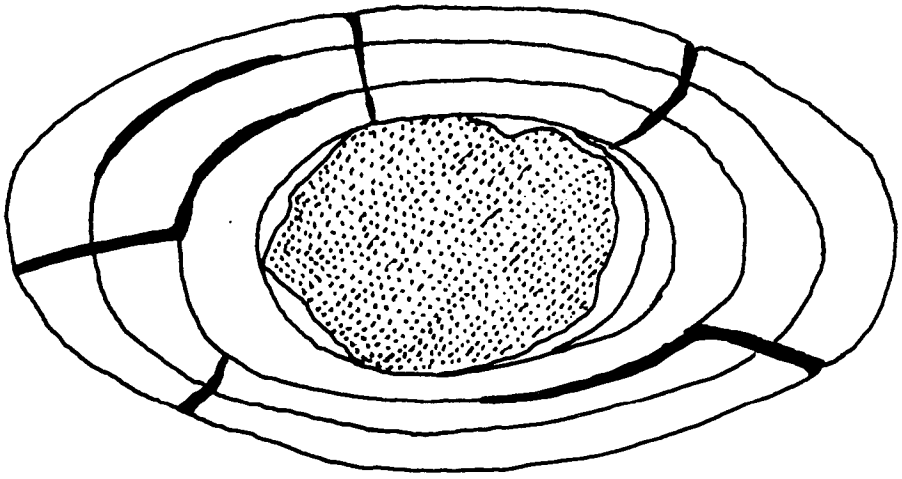

Fig 2.27 Goethite Ooid Exhibiting Radial and Ring Contact Fractures. Stippled Core X150

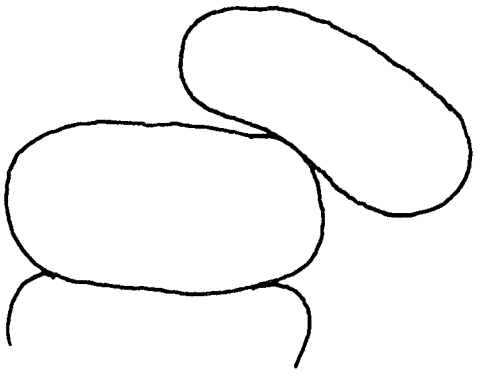

a : Moulding of Ooids
X100

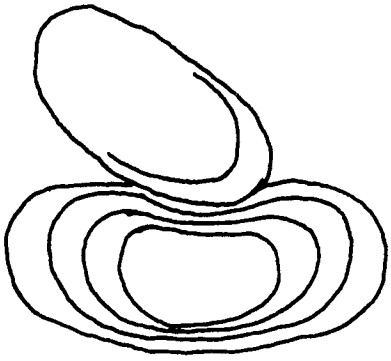

b : Moulding of Ooids creating cuspate contacts and deformed envelopes
X100

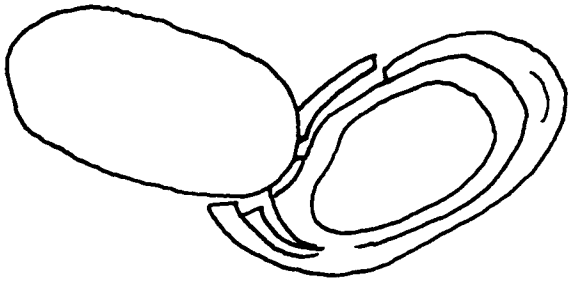

c : Deformation associated with pre-existing fractures
X100

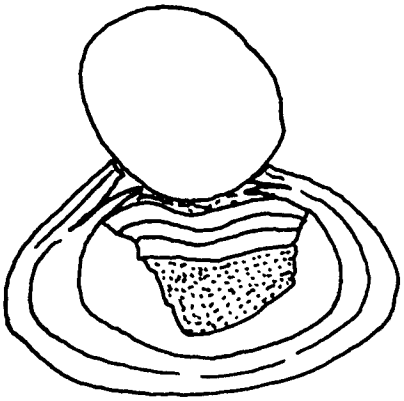

d : Deformation associated with pre-existing fractures and core grain deformation.
X100

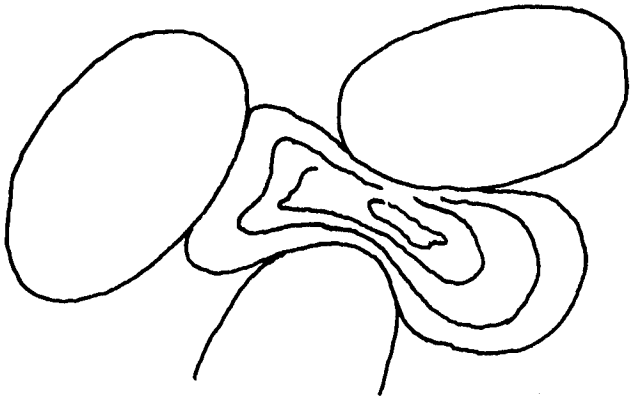

e : 'Squeezing out' of Ooid
X100

Fig 2.28 Sketches of Plastically deformed Goethite Ooids

one or more ooids is encountered. This involves the development of a cuspate area of the distorted ooid (Figure 2.28b) at the contact with either another ooid or some other allochemical grain. This cuspate shape is also shown by the rings within the envelope near the contact. Each of these cusps shows a successively larger radius of curvature with increasing distance from the contact. Pre-existing fractures within the ooid envelope may be exploited by such distortion. Figure 2.28c shows a case where this has led to the removal of one fragment of envelope and as the result of the presence of one such fracture the unwrapping of a portion of ooid envelope. Figure 2.28d shows a similar situation. In this case, however, an initially thin envelope and the presence of radial fractures has resulted in the partial distortion of the ooid core grain. A more extreme type of plastic deformation results in the 'squeezing out' of an ooid from between three other ooids (Figure 2.28e). The nature of this deformation type again involves the ooid envelope interior, individual rings showing a parallel distortion.

Consideration of the orientation of distorted grains shows that in the majority of cases the distorted area e.g. the 'squeezed out' portion of envelope in Figure 2.28e, is parallel or sub-parallel to bedding. This implies a maximum compressional direction normal to bedding. Thus ooid distortion appears to result from a bedding phenomenon. The fact that where distortion of one ooid occurs when it is in contact with another suggests that the former is softer than the latter. The degree of resolution offered by the microscope shows that there is no mineralogical difference between such ooids so this hypothesis is somewhat tenuous. The orientation of a distorting ooid

relative to a distorted ooid shows that the distortion occurs in areas where the ooid envelope has a larger radius of curvature than the contact area of the distorting ooid envelope. Where two ooids are in contact the overburden pressure would be constant. However, its distribution, over the ooid surfaces, differs as a function of their radii of curvature. In ooids where the overburden pressure acts over the envelope surface at either end of the long axis, in cases where the long axis is aligned perpendicular to bedding, the overburden pressure per unit area is high. In ooids oriented with the long axis parallel to bedding the surface area over which the overburden pressure acts is large and thus the overburden pressure per unit area low. Thus where two ooids with these orientations are in contact such that a high overburden pressure per unit area is against a low value per unit area there will be a resultant movement of the former ooid towards the latter such that a contact area over the surface of this ooid is created with an overburden pressure distribution equal to that of the higher value. This argument is supported by the fact that where ooids are in contact over an area where their radii of curvature are apparently equal they show no distortion.

Considered together, all the ooids of any one slide of limonite oolite show a number of depositional textures. The commonest of these is an imbrication. In this a group of ooids are orientated with their long axes parallel and at either a low angle ($>0<30^{o}$) or a high angle ($>60^{o}<90^{o}$) to bedding. The direction of imbrication is not constant throughout the slide. Ooids imbricated in one direction at one level may be immediately succeeded by ooids imbricated in the opposite direction. It is not uncommon for this to occur several times, creating

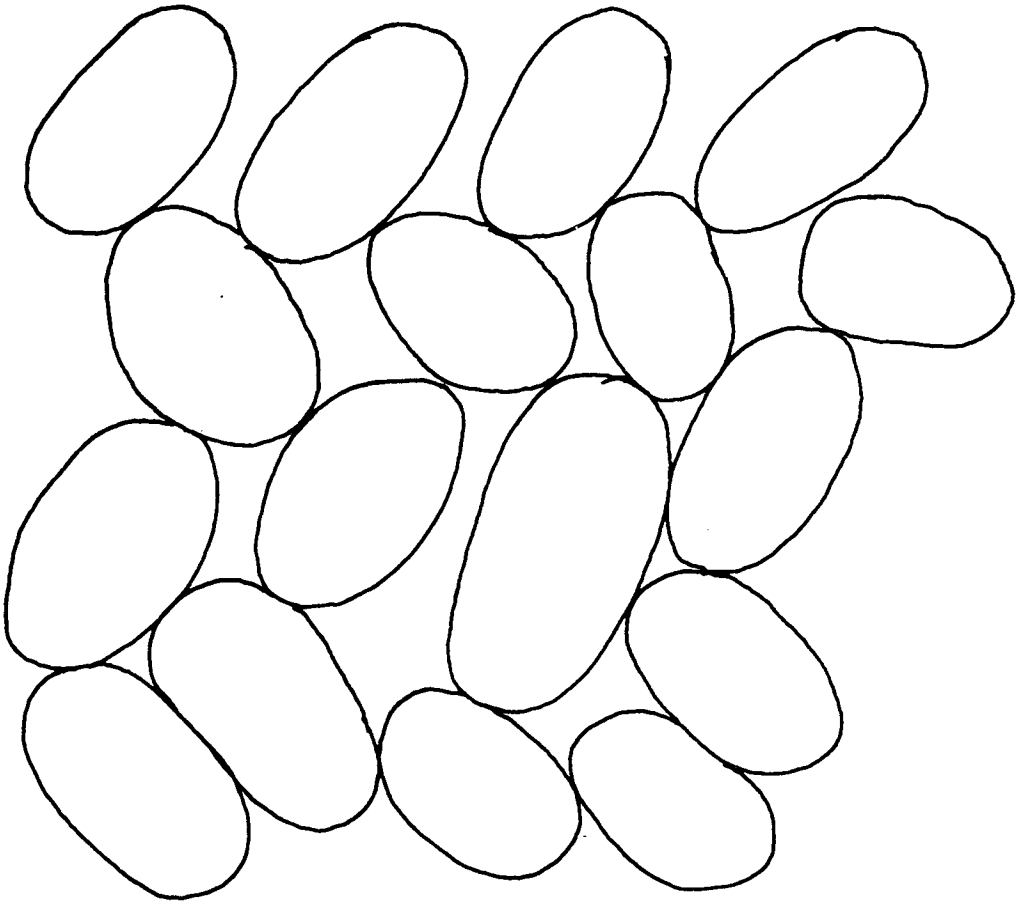

Fig 2.29 Ooid Herringbone imbrication. Common in Calcitic Limonite Oolite X100

a herringbone structure (Figure 2.29). A second depositional texture involves several ooids orientated with their long axes parallel to bedding and piled one upon the other. Where large shell fragments occur ooids tend to be lined up along its edges with their long axes parallel to that of the shell.

2.3.2 Chamosite Mudstone

As a result of field studies three sub-types of chamosite mudstone have been recognised; sub-types (i) and (ii) are soft, fissile dark-green mudstones and sub-type (iii) a hard, poorly fissile bluish grey-green mudstone. Petrographic studies show that the former are quartz-rich with little diagenetic siderite, whereas the latter lacks abundant quartz, but contains in excess of 60% diagenetic siderite.

2.3.2.a Chamosite Mudstone sub-types (i) and (ii): This lithological sub-type (Plate 2.1) is characterised by an abundance of quartz grains distributed throughout depositional chamosite mud. The relative proportions of quartz and chamosite mud are usually approximately 40%:60%, occasionally reaching 50%:50%. Occasional lenticles of chamosite mud, less than 10 cm long, and sub-vertical burrows infilled with chamosite mud may show a much lower proportion of quartz.

2.3.2.a.i Depositional chamosite mud: The depositional fabric of the chamosite mudstone is indicated by a pleochroism between light olive green or brown (W-E) and dark variants of these colours (N-S) and a bulk parallel extinction. The extinction is, however, somewhat spotty.

This indicates that the chamosite mud is composed of individual platelets of clay-grade chamosite with a dominant orientation of the (001) cleavage parallel to bedding.

Within the chamosite mud with the above characteristics, approximately circular and somewhat flattened ovate areas, often with a dark brown rim, occur. These are at most 5.0 mm across. They show a bulk pleochroism and extinction which is at an angle to that of the surrounding mudstone. Such areas may contain a much higher proportion of quartz grains than is usual, together with occassional goethite ooids. Since the flattened areas are flattened parallel to bedding these areas are considered to represent chamosite mud intraclasts analogous to the mud-lumps found in the present-day shallow marine environment. These are often armoured by other clastic grains (Plate 2.2). By the same analogy the higher quartz content of the chamosite intraclasts is thought to be due to their armouring prior to incorporation within the sediment. It is generally the case that chamosite mud intraclasts and goethite ooids occur commonly together at one horizon. This may represent periods of higher than normal current activity ripping up the unconsolidated chamosite mud, and washing some goethite ooids into the area of chamosite mud formation.

A different variety of chamosite also occurs within the chamosite mudstone. This is characterised by a grass-green colouration, and has a slightly lower relief than the above chamosite mud. It shows little to no pleochroism and extinguishes uniformly, albeit slightly spotty, over irregular areas less than 0.05 mm across. The extinction of this type of chamosite is unrelated to the bulk extinction shown by the above type. Its occurrence is restricted to areas containing common quartz grains to which it forms an irregularly developed cement. Where shell

fragments have been fractured following deposition the space between these fragments is infilled by this type of chamosite.

In addition to the above chamosite, which is extremely fine grained, books of chamosite also occur. These are generally less than 0.05 mm in length, measured parallel to the (001) cleavage. Their thickness is usually much less than this, but occasional books with an upper thickness limit of 0.15 mm have been found. Two varieties of chamosite book occur which are distinguished on the basis of their colour; olive green and grass green. The olive green variety is most common (Plate 2.3a) and occurs within areas of primary chamosite mud, in some instances with the (001) cleavage parallel to bedding. The grass-green variety (Plate 2.3b) is rare, and passes with optical continuity into grass-green cement chamosite. This is evidence for the in situ growth of this variety of chamosite book. Further evidence is supplied by occasional grass-green books which are rooted on quartz grains.

2.3.2.a.ii Quartz grains: These detrital components of the sub-lithology are characterised by equant sub-angular, shard-like, and less commonly equant, poorly rounded grain shapes. They have a grain size range of 0.15 - 0.03 mm. These grains are usually very clear with occasional fluid inclusions and pre-existing syntaxial overgrowths. They show a uniform or undulose extinction. The quartz grains are generally randomly oriented, but in some instances they may show a preferred orientation with the long axis oriented parallel to bedding.

2.3.2.a.iii Biogenic material: There is only a small component of biogenic material within the chamosite mudstones and this is entirely fragmentary.

Shell fragments are oriented parallel to bedding. They are often less than 1 mm in length although fragments 1 cm or more long are common. The smaller fragments are rounded and abraded. There is a general absence of ferroan calcite or other material representing original aragonitic shell material; all the shell fragments present being of primary non-ferroan calcite.

The shell material shows replacement by pyrite. This occurs as individual or 'colonies' of pyrite framboids within shell fragments. In other cases, pyrite with massive and euhedral habits forms variable sized irregular areas within shell debris. In some instances shells may be completely replaced. Marcasite is occasionally present within massive pyrite, showing a typical stellate form. Pyrite may also occur as irregular masses within the chamosite mud.

Echinoid debris is scarce. It is represented by plate fragments and spines. These are constructed of ferroan calcite. The stereome systems are infilled by grass-green authigenic chamosite which also forms a thick coating to the plates.

A few foram tests occur within specimens of chamosite mudstone sub-type (i). These are of non-ferroan calcite. The chambers are infilled by authigenic chamosite.

2.3.2.a.iv Siderite: This diagenetic mineral is disseminated throughout the sub-lithology, forming less than 5% of an entire specimen. The mode of occurrence of the siderite is as equant or irregular anhedra less than 0.03 mm across. Some grains may be constructed of three or four mutually interfering anhedra of this type. In areas of chamosite mud from which quartz is absent, siderite forms short trains of anhedra

(Plate 2.4) parallel to bedding. Individual siderite anhedra may be found totally surrounded by grass-green chamosite.

2.3.2.a.v Paragenesis: Very little post-depositional modification has occurred in this sub-lithological type due largely to the absence of an extensive primary porosity. Figure 2.30 shows the order of post-depositional events. The olive green and brown chamosite which has a dominant orientation parallel to bedding, olive green chamosite books, quartz grains, ooids and shell fragments are regarded as the primary components of the sub-lithology.

The first post-depositional change to occur is the precipitation and subsequent growth of siderite anhedra within the depositional chamosite mud. Where such siderite anhedra occur in association with the grass-green chamosite this either totally or partially surrounds them.

On the basis of its inter-relationships with siderite, the formation of grass-green chamosite is the second diagenetic change within the sub-lithology. The phase is identified as being post-depositional in origin on the basis that any pleochroism and its extinction, which is uniform over small (0.05 mm) areas, are not related to the depositional fabric of the rock. Since optically continuous chamosite of this type also surrounds quartz grains it would appear to form a poorly developed cement. Thus, chamosite with these characteristics is considered to be authigenic.

It has been noted that grass-green chamosite books pass with optical continuity into grass-green authigenic chamosite. Such books are occasionally found rooted on quartz grains (Plate 2.3b). In one

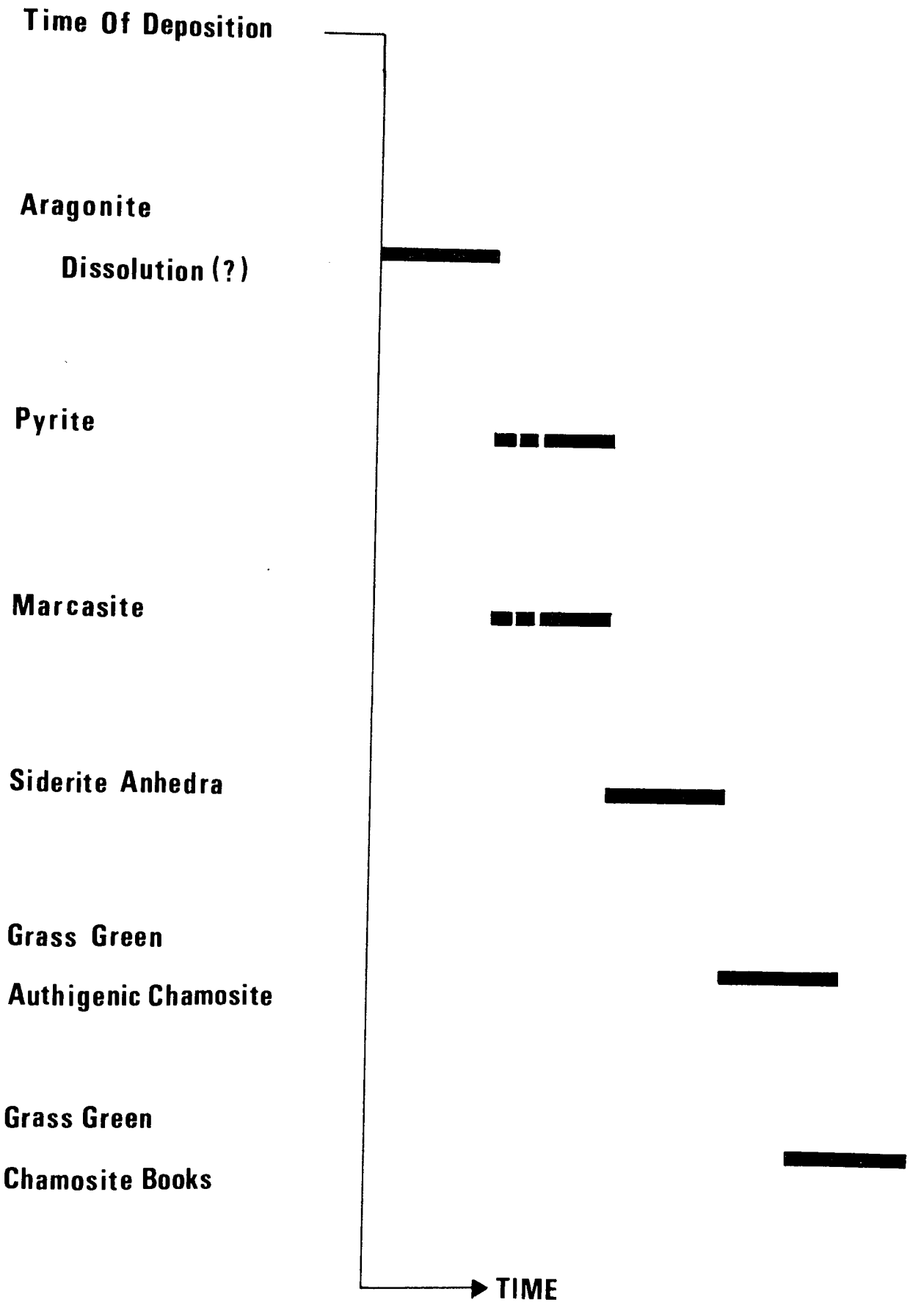

Figure 2.30 : Paragenesis Of Chamosite Mudstone (i,ii)

case a book in this situation passed between two siderite anhedra; the width of the book and the separation between cleavage planes increasing with distance from the quartz and siderite, a 'fanning out' texture suggestive of less restricted growth. This is clear evidence for book development having occurred after siderite precipitation. Thus, the development of chamosite books with these characteristics appears to represent a further stage in chamosite authigenesis. The time and depth of burial required for this is clearly not great as reworking of the chamosite mud would release these books to be incorporated within redeposited chamosite mud as the olive green variety. The change in colour would presumably result from partial oxidation of ferrous iron within the chamosite structure.

Since marcasite in association with pyrite as shell replacement phases are restricted to these grains it is not possible to date the point at which replacement commenced. However, pyrite occurs as irregular masses within the chamosite mud, and has a cross-cutting relationship with respect to it. Since both calcite and chamosite replacement would require a sulphide activity at least locally in excess of dissolved carbonate activity (Curtis and Spears, 1968a) it is suggested that marcasite and pyrite probably predate the precipitation of siderite. No siderite-pyrite textural features have been found.

No evidence of originally aragonite shell debris has been found. If such grains were originally present the secondary porosity resulting from their dissolution must have collapsed before any potential infill could precipitate.

2.3.2.b Chamosite mudstone sub-type (iii): This sub-lithology is characterised by the complete absence of detrital quartz grains. In contrast to sub-types (i) and (ii) siderite is abundant. The relative proportions of siderite and chamosite vary from 75%:25% to 85%:15% (Plate 2.5). In all other respects the two sub-lithologies are precisely the same. It is difficult to see any original depositional fabric, or the relationship between depositional olive green and brown and grass-green authigenic chamosite since these infill the very small areas between siderite grains. Occasional grass-green chamosite books are found passing with optical continuity into authigenic chamosite. Siderite occurs as mutually interfering equant anhedra less than 0.05 mm across, individual anhedra, but dominantly as trains of anhedra parallel to bedding.

The paragenetic sequence for the sub-lithology is the same as that for sub-type (i). Clearly the paragenesis is slightly different with respect to siderite, however, as in this case its precipitation and growth has either been much faster, or prolonged over a much greater length of time.

2.3.3 Chamositic Chamosite Oolite

The allochemical components of this facies comprise chamosite ooids, chamosite pisoliths and shell fragments (Plate 2.6). The characteristic texture in both hand specimen and thin section is the presence of abundant ooimoulds. The major post-depositional changes are the collapse of this secondary porosity and the precipitation of the diagenetic minerals siderite, ferroan dolomite, ferroan calcite, pyrite and authigenic chamosite. The presence of an initial radial-fibrous growth of high-magnesian calcite can be demonstrated.

2.3.3.i Chamosite ooids: In general these allochemical grains, where complete, show all the characteristics of the goethite ooids described above. It should be noted, however, that goethite is completely absent from the ooids. Plate 2.7 shows a typical chamosite ooid.

The ooid chamosite is a yellowish or brownish green in colour. In a large number of cases the internal ooid structure is not easily discernable. The core grains show a darker green or brown rim around their margins. The ring structure of the envelope is clear in a number of cases, but in many ooids individual ring contacts can only be seen in the portion of envelope to either side of the short axis or in the portion to either side of the major axis. Rotation of the microscope stage shows that the ooids show a pleochroic scheme between light variants of the above colours when the ooid axes are parallel to the west-east cross-hair, and dark variants when parallel to the north-south cross-hair. Between crossed polars a positive uniaxial extinction cross is exhibited (Plate 2.8). Thus, since chamosite is length-slow, the ooids are constructed of tangentially oriented platelets of chamosite throughout; the poor development of a ring structure is not a reflection of a poor degree of preferred orientation.

A large number of ooids show the presence of filamentous inclusions. Examples of long and cross-sections are found (Plate 2.9). The former appear tubular, and the latter either circular or ovate. The larger filaments are transparent and of the order of 10 μm in length, and 1 μm across. Many examples are smaller than this and black or brown in colour. Polished sections show that the occurrence of pyrite framboids do not correspond to the occurrence of this material. The filaments are found concentrated along ring contacts rather than

within individual rings. Individual filaments are often found with the long axis subparallel to ring contacts. The possibility that these ooid inclusions are algal borings can be discounted on the basis that these are occasionally found within ooids (Plate 2.10), having dimensions between five and ten times those of the filaments, and on orientation which is perpendicular to the ring or core grain edge.

Occasionally primary chamosite mud is found interstitially to ooids, but having a close relationship to the surrounding ooids (Plate 2.11). Interstitial chamosite having the same characteristics as that of the ooids is found, for instance, in areas A, B and C. It is characterised by the presence of filaments subparallel to the edge of the ooid. These portions of chamosite mud show no evidence of being remnant portions of ooid envelope as no ring structure is seen within them and the edges of the surrounding ooids show that they are discrete bodies. Rotation of the stage between crossed polars shows that the areas A, B and C partake in extinction as the extinction cross rotates past them. Insertion of a mica plate shows that area A is optically contiguous with ooid (1) and areas B and C with ooid (2). This suggests that the chamosite mud is constructed of chamosite platelets with a preferred orientation parallel to that of the platelets in ooid (1), in the case of area A and ooid (2) in the case of areas B and C. This is rather unusual as in the lithologies discussed below chamosite mud is normally found with a bedding parallel or random platelet orientation. The presence of filaments in the chamosite mud areas sub-parallel to the ooid margins suggests that this texture may have important consequences for the origin of chamosite ooids. Due to its textural relationship with chamosite ooids it is designated as primary chamosite mud.

The most characteristic texture of the lithological type, in which chamosite ooids are involved, is the presence of large numbers of ooimoulds. These are generally characterised by an outer wall comprising the outer one or two envelope rings surrounding a secondary porosity (Plate 2.12). The creation of such a secondary porosity presumably results from the removal, in solution, of large amounts of internal ooid chamosite. This dissolution evidently commences at the centre of the ooid as all stages are seen between ooids from which a central portion of the core grain, or all the core grain, is missing and the normal type of ooimould. In some instances dissolution has been concentrated in the central rings of the envelope. In these cases the core grain and the first two or three envelope rings lie at the bottom of an ooimould lined by the outer core or two envelope rings. A number of ooimoulds are characterised by complete outer walls of siderate anhedra (Plate 2.13). These are iron stained. The surrounding cement generations abut against this siderite. Within the siderite wall ghosts of the original ooid outer margin and the first ring contact can be seen. Splinters of the outer chamosite envelope may be partly included within such siderite. It is interesting to note that the solution process which created ooimoulds left occasional foram core grains unaffected.

Chain ooids are occasionally present. Their mode of formation is similar to that suggested for the origin of chain pisoliths by Conley (1977). Chain ooids in this lithological type are made up of two and sometimes three component ooids. Ooids which, on the basis of their form, might once have been a potential 'link' in the chains are common relative to chains. These have flame and long axis faulted flame shapes (Figure 2.31, Plate 2.14). A narrow flame or stretched sigmoidal area

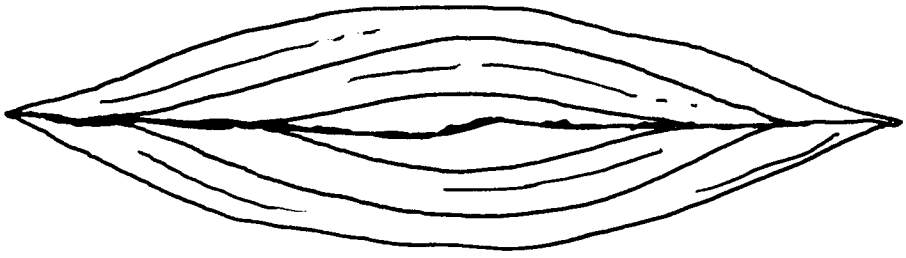

a : Flame Ooid
X100

b : Asymmetrical Long Axis Faulted
Flame Ooid
X100

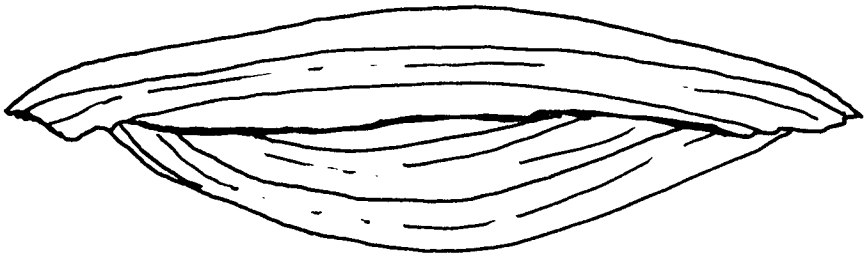

c : Symmetrical Long Axis Faulted
Flame Ooid X100

Fig 2.31 Collapsed Chamosite Ooimoulds

lacking any ooid material or any other infill may divide these grains along the long axis. Alternatively a black suture line may have this function. Rotation of such grains between crossed polars is characterised by the movement of two black lines, parallel to the short axis, in opposing directions along the long axis. The observed features are in keeping with what would be expected if an ooimould with an outer wall of two or three rings collapsed under loading. If the loading is normal to the ooid long axis flame and symmetrical ooids would result. In contrast, a load applied at an angle to the long axis would tend to cause a lateral displacement of the upper ooid envelope as the grain collapsed creating an asymmetrical grain. The faulting accompanying the formation of asymmetrical and symmetrical grains creates a hook at either end of the grain which may link up with a hook on another slightly lower or higher adjacent grain which has undergone a similar deformation (Plate 2.15). The subsequent 'unwrapping' or 'stringing-out' which accompanies the formation of chain ooids in other ironstone lithologies (Chowns, 1968) is absent from these chain textures. It is perhaps significant that such grains often occur immediately beneath shell fragments. The above mode of formation of chain ooids is analogous to the method proposed by Conley (1977) in that it involves pre-existing ooimoulds, but differs in that the final chain ooids are of primary material. Conley attributes chain pisoliths to the collapse of a cement fabric following 'pisomould' formation and subsequent cement precipitation within the secondary porosity.

Bands of collapsed ooimoulds occur parallel to bedding and having a texture which can only be described as an ooimould melange (Plate 2.16). Within this textural type small fragments having an envelope type structure

can be discerned but the dominant trend in the creation of the texture is one of structure destruction by compression. Occasional structureless grains with flame and faulted flame forms may be found. A variety of different colours of chamosite are present but it is impossible to assign any post-compressional origin to any one variety due to the absence of any apparent remnant primary or secondary porosity. A relict porosity is occasionally present. In some specimens this is fringed by an isopachous green chamosite which is restricted to any one pore space, i.e. it is not laterally extensive. There is an absence, however, of any discrete allochemical grains upon which the isopachous chamosite could have been precipitated. This texture is interpreted as representing an isopachous primary porosity lining which was deposited around the ooimoulds prior to their collapse. Due to their uniform thickness such rims might be expected to deform around collapsing ooimoulds rather than to collapse also. It is interesting to note that shell fragments are sparsely distributed in ooid melanges.

2.3.3.ii Pisoliths: These allochemical grains are common in this lithological type. They have an oval sectional shape in the plane of the long and short axes. The grains are well sorted having a mean long axis length of 1 cm and a mean short axis length of 0.5 cm. As with ooids they may be divided into a central core grain surrounded by a layered envelope (Plate 2.17).

In hand specimen the core material is apparently an amorphous limonitic material but in thin section is found to be constructed of ferroan calcite forming a cement to yellowish brown ooids. These have a random orientation with respect to the pisolith envelope. They show occasional rings of normal green chamosite. The uniform extinction of

some such grains and the very poorly developed extinction cross shown by others suggests that some mineralogical change correlating with a randomisation of the ooid microstructure might be associated with their incorporation in the pisolith. Ferroan calcite and siderite show replacive textures with respect to the ooids.

The surrounding envelope is characterised by concordant but botroidal rings which retain a constant width around the pisoliths. The dominant envelope mineralogy is dark green chamosite. Along ring contacts lenses of chamosite containing abundant dark brown and black filamentous material, often subparallel to the lamination, occur. Discontinuous lenses of ferroan calcite and siderite also occur,concordant with the pisolith envelope lamination. Ooids are present in the envelope oriented with their long axes tangential to the envelope rings. It would appear that such grains have been incorporated in the pisolith by accretionary movement of the pisolith. Ooids present in the pisolith envelope have the same characteristics as those in the pisolith core.

2.3.3.iii Biogenic material: This comprises entirely fragmentary bivalve material less than 1 cm in length, occasional echinoid plates and spines, and foram tests. The bivalve material can be divided into a primary non-ferroan group and an original aragonite group which underwent dissolution following burial. Both of these groups are characterised by the presence of complete or partial micrite envelopes.

The non-ferroan calcite shell fragments are all rounded. The original calcite fibre shell structure can be clearly seen. The fragments are characterised by algal bores which may be infilled by either fine-grained goethite or chamosite of a darker green than that of the ooids

(Plate 2.18). It is often found that algal bores infilled by chamosite have a circular area of chamosite approximately 0.05 mm in diameter at their terminations.

Originally aragonitic shell fragments may be recognised by a brownish or pinkish grey micrite envelope, with shell fragment shape, surrounding an infill comprising cement generation minerals (Plate 2.19). In the majority of cases the secondary porosity which followed the aragonite dissolution is rimmed by a radial fibrous growth of siderite. In some instances this is the only infill to the secondary porosity and may be complete or incomplete. In other instances the remaining secondary porosity may be infilled by chamosite of a darker green colour than that of the ooids and showing a spotty extinction.Filamentous inclusions are present within this chamosite arranged in linear and branching colonies. This material may pass laterally into chamosite patches with a circular outline approximately 0.05 mm in diameter. Either ferroan calcite or occasionally non-ferroan dolomite may infill any remaining secondary porosity. Pyrite may be confined to such secondary porosity with a replacive role with respect to the above infilling minerals.

Echinoid plate fragments and spines are scarce. Some plate fragments have evidently been derived from a different depositional area as these are of ferroan calcite with a goethite infill to the stereome system; goethite is an extremely rare mineral in the assemblage of this lithological type. Other echinoid fragments are characterised by a stereome system infill of ferroan calcite and exhibit a syntaxial over-growth of siderite. The presence of a syntaxial overgrowth implies that these fragments were deposited in a relatively 'clean' state in the depositional area of this lithological type.

2.3.3.iv Cement minerals: The minerals which comprise the cement to the above allochemical constituents are siderite, ferroan calcite, ferroan dolomite, non-ferroan dolomite, and pyrite. Since they often exhibit textures in which two or more are enveloped they are discussed together.

The dominant cement mineral is siderite. This infills the interstices between closely packed chamosite ooids and ooimoulds with an inequigranular xenotopic fabric. It may infill the secondary porosity represented by ooimoulds in some instances. Where the interstitial primary pores are slightly larger than normal the siderite may line them with a radial dogs tooth habit. Where primary chamosite mud occurs in contact with siderite a mixed zone of greenish siderite occurs. The remaining primary porosity is infilled by ferroan calcite. In some cases pyrite may have replaced the siderite at the pore margin, in which case this is surrounded by any ferroan calcite present. Siderite and ferroan calcite in the form of single anhedral grains infill any porosity in bands of collapsed ooimoulds. Additionally irregular anhedra of siderite of variable size occur with a deforming role with respect to any two discrete areas of chamosite in that they are pinched in at their contact with the siderite.

Ooimoulds are occasionally infilled or partially infilled by cement minerals. It has been noted that siderite occurs in this role. In addition ferroan calcite may cross-cut the ooimould wall and infill the secondary porosity. Rhombs of ferroan dolomite occur within ooimoulds rooted on their walls (Plate 2.20).

In areas of higher porosity lacking abundant ooids but containing common shell fragments ferroan calcite, ferroan dolomite and siderite form the cement. In such areas ferroan calcite with irregular grain

outlines and containing ferroan dolomite rhombs is concentrated along the edges of non-ferroan calcite shell fragments (Plate 2.21). The outer boundaries of these calcite grains, which run sub-parallel to the shell edge are somewhat ragged. The ferroan dolomite rhombs occur singly and as rhombic intergrowth, with a long axis sub-parallel to the shell fragments, located in the larger calcite grains. An isopachous growth of siderite coats the ferroan calcite-ferroan dolomite intergrowth where large areas of original primary porosity occur (Plate 2.22). Close to the ragged margins of the ferroan calcite the siderite consists of small anhedral grains, but at the edges of the remnant primary porosity is constructed of large euhedral crystals with dogs tooth terminations and lying sub-parallel to the shell margins. In areas of smaller primary pores siderite with an inequigranular xenotopic fabric may completely infill the porosity. In all cases this siderite occurrence is characterised by the presence of ghost prisms with dogs tooth terminations. In the case of isopachous siderite only the termination can be seen 'mounted' on the ferroan calcite grains. Occasionally the ghost prism margins of these terminations can be seen continuing in the ferroan calcite and ferroan dolomite to the shell margin. In pores completely infilled with siderite complete ghosts are seen and the ferroan calcite-ferroan dolomite texture occurs in adjacent pore spaces or partakes in the pore infill.

In areas of secondary porosity, representing dissolved aragonite shell fragments, which has become linked to the rest of the porosity due to the partial or complete absence of a micrite envelope, large ferroan dolomite rhombs, occasional siderite subhedra, and circular patches of dark-green chamosite are set in a matrix of ferroan calcite.

It is evident that some shell fragments were constructed of high-magnesian calcite which underwent solution at a relatively late stage

in the history of evolution of the cement providing magnesium for dolomite formation. These grains are surrounded by the ferroan calcite, ferroan dolomite and siderite generations with the characteristics described above. The secondary porosity created by dissolution of the shell fragment is infilled by non-ferroan dolomite which may penetrate beyond the secondary porosity due to an incomplete micrite or ferroan calcite-ferroan dolomite rim. Such non-ferroan dolomite infills adjacent remnant primary porosity between pore-filling siderite, and secondary porosity represented by ooimoulds and microstylolites. The latter are less than 5 mm in length and cross-cut the pore-filling siderite, ooids and ooimoulds. Where passing through ooids the microstylolites follow ring contacts. There is a small off-set between grains on either side of microstylolite. The non-ferroan dolomite in the above interconnecting textures is in optical continuity. Brownish-yellow laths of organic material are set in the non-ferroan dolomite infill to the original shell fragment.

Ferroan calcite infills the remaining primary porosity, such as that lined by isopachous or dogs tooth siderite, and secondary porosity such as microstylolites.

2.3.3.v Paragenesis: It is evident from the modified nature of many of the primary components of the lithology and the presence of several different cement minerals and textures, that the post-depositional history of this facies is somewhat complex. Figure 2.32 summarises the sequence of events.

The fact that chamosite ooids are found partially surrounded by primary chamosite mud, showing a preferred orientation of the component

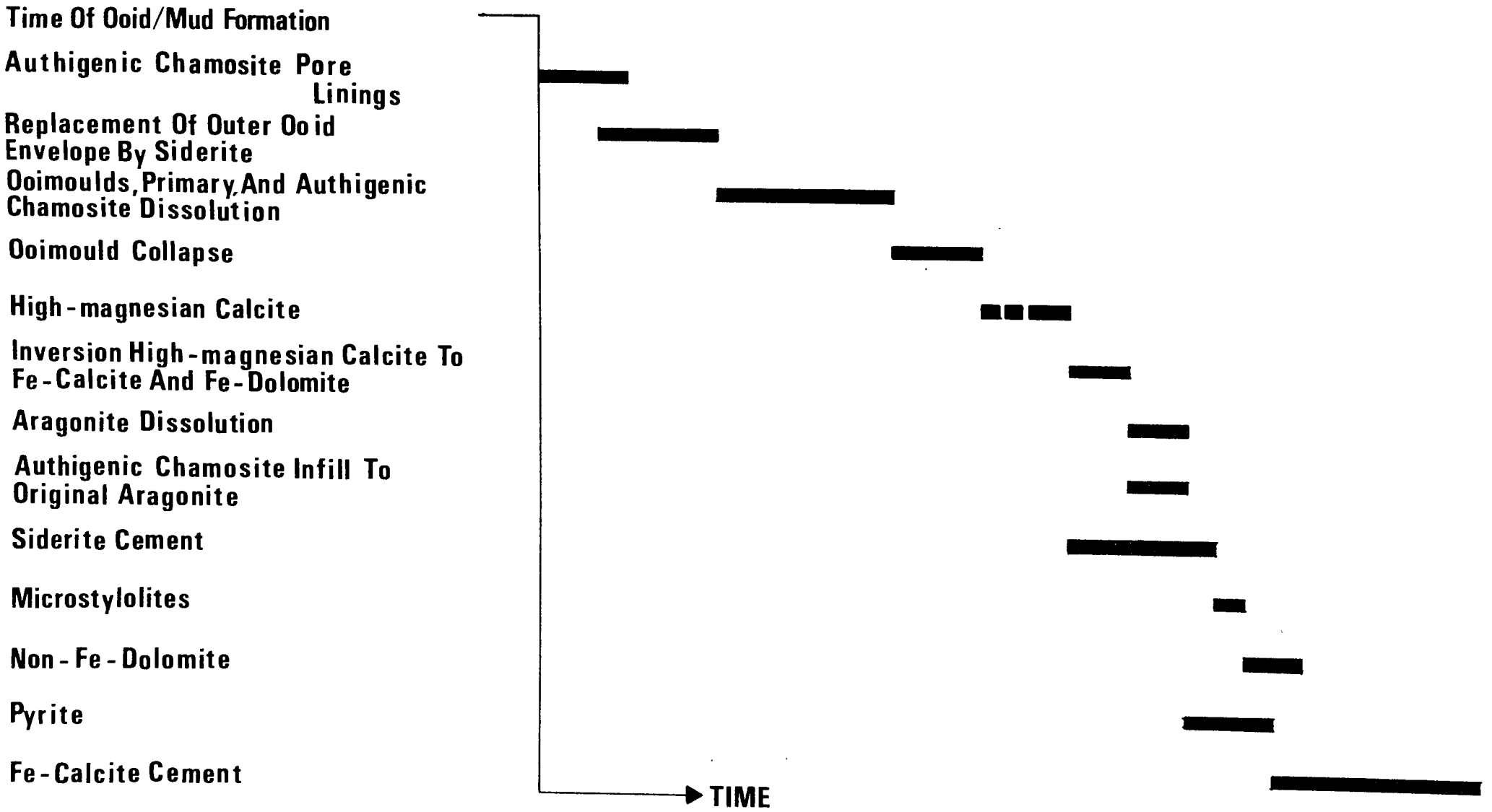

Figure 2.32 : Paragenesis Of The Chamositic Chamosite Oolites

flakes parallel to the ooid margins, suggests that ooid formation, via accretion, may have occurred beneath the sediment surface. The presence of filamentous inclusions concentrated along the ring contacts of ooids and within primary chamosite mud suggests that micro-organisms may have played some role in ooid formation. This proposition is explored in more detail below (Chapter 9). The absence of much of the primary chamosite mud is attributed to its dissolution at the time of formation of the ooimoulds. It is not possible, therefore, to determine what porosity is secondary and what primary.

It has been noted that many ooimoulds are characterised by a fringe of siderite anhedra replacing the outer one or two ooid rings. Ghost ring contacts within these grains and their lack of continuity with the surrounding siderite cement generation indicates that this siderite may represent an earlier generation to that which infills much of the porosity. In order for the outer margins of individual ooid rim siderite grains to correspond to the original ooid boundary it is necessary to invoke some porosity lining or infill predating porosity-infilling siderite. This would form a mould around the chamosite ooids restricting the precipitation of replacive minerals to their original limits. Since textures in which a crescent of siderite grains fringe only the upper portions of ooids are not observed the diagenetic reactions in which chamosite dissolves and siderite is precipitated must be considered to occur more or less simultaneously. This precludes the formation of a void which the remaining ooid fragment could drop to the bottom of. Alternatively, the chamosite and siderite may represent a reactant and a product of a single diagenetic reaction. There is some evidence to suggest that the primary porosity was originally partially infilled by

primary chamosite mud and the remainder fringed by authigenic chamosite: Occasional patches of primary chamosite mud in optical continuity with chamosite ooids occur showing replacement by the porosity-infilling siderite. In areas of chamosite ooid melange complete and fragmentary authigenic chamosite porosity fringes are found which bear no apparent relationship to the surrounding distorted ooids; the creation of such a melange would be expected to reduce porosity to a minimum.

The formation of ooimoulds within original chamosite ooids evidently followed the replacement of the outer ooid rings by siderite. If these two events had been contemporaneous, or at least had some degree of overlap, these ooimoulds which contain no chamosite at all but have a siderite ring replacement would be expected to have been infilled by this siderite generation. Since a number of ooimoulds take the form of ooid-shaped voids surrounded by a remaining portion of envelope chamosite, ooimould formation must have commenced at the ooid centre. It is interesting to note that foram tests are found within ooimoulds. These are clearly the original core grains. Thus, the diagenetic reaction causing the dissolution of ooid chamosite could not have occurred at pH values of less than 7.0. It is likely that the physico-chemical conditions which prevailed at the time of ooimould formation become more uniformly developed throughout the chamositic chamosite oolite facies resulting in the removal of primary chamosite mud and porosity linings of authigenic chamosite. Since these early diagenetic events all have some effect on the authigenic chamosite rims these may represent primary porosity linings within the lithology.

Following the formation of ooimoulds and the complete to partial removal of the primary and pore lining varieties of chamosite a phase of considerable structural modification occurred within the sediment.

This is represented by ooid melange in extreme cases and chain ooids in less extreme cases. The sediment collapse represented by these two textures is probably due to the inability of the allochemical grains remaining, after ooimould formation and the removal of interstial chamosite, to mechanically support the overlying sediment. Evidence in favour of this suggestion is given by chain ooids and collapsed ooimoulds which show a maximum flattening parallel to bedding.

Areas within the chamositic chamosite oolite specimens may contain a relatively high proportion of shell debris. These allochemical components have provided a framework within the sediment which has evidently been capable of supporting the overlying material. It is in such areas that the cement fabrics involving ferroan dolomite, ferroan calcite and siderite occur. These fabrics are characterised by ghosts of dogs tooth crystals perpendicular to shell fragments. On the basis that ferroan dolomite rhombs are found set in ferroan calcite with ragged outer margins and that this association is frequently contiguous with shell fragments it is suggested that the ghost prisms represent an original radial fibrous growth of high-magnesian calcite around the shell fragments (Bathurst, 1975; Lohmann and Meyers, 1977; Richter and Fuchtbauer, 1978). It is not possible to say whether this growth formed in a primary porosity between shell fragments at a time when the primary porosity elsewhere was infilled by primary chamosite mud, or whether it developed after the removal of such mud from between the shell fragments. At some stage after the formation of these radial fibrous growths the high-magnesian calcite became unstable in the prevailing diagenetic environment and inverted to low-magnesian calcite. The ragged nature of the texture is indicative of some degree of dissolution of the soluble high-magnesian calcite prior to or during inversion. Overall, the texture is analogous to microdolomite

inclusions in echinoid plates which have inverted to low-magnesian calcite (Lohmann and Meyers, 1977). By analogy, therefore, it is considered that the texture represents a partially closed system in which the magnesium released by the inversion immediately reprecipitated as ferroan dolomite. It is necessary to postulate a partially closed environment in order to allow the entry of ferrous iron into the system. Significant quantities of ferrous iron in high-magnesian calcite have not been reported from Recent sediments. It should, however, be borne in mind that the post-depositional environment of ironstones would be expected to be rich in dissolved ferrous iron and that, therefore, there is a possibility that the initial high-magnesian calcite precipitates might also have been ferroan. If this were the case then the creation of the texture under discussion could possibly represent a closed system. During dissolution of the high-magnesian calcite siderite precipitated. This follows from the fact that in areas of high porosity where this siderite generation has a botryoidal isopachous nature its contact with the ferroan calcite is characterised by ghost-prism terminations penetrating into it from the ferroan calcite. If the siderite had precipitated after a short interval of time this feature would not be observed. Further evidence for this is provided by siderite containing complete ghost prisms and occurring as porosity infills. In these cases ferroan dolomite rhombs and ferroan calcite occur in adjacent pores but without the presence of ghost prisms. This may be explicable in terms of a non-uniform concentration of ferrous iron which would tend to inhibit the precipitation of carbonate minerals other than siderite when present in sufficient excess. It is interesting to note in this context that the botryoidal form of siderite tends to occur in areas where the only major allochemical component is shell material, whereas

the type containing complete ghost prisms occurs in areas where there is also a high component of chamosite ooids and chain ooids. The precipitation of siderite thus overlaps the dissolution of high-magnesian calcite and the subsequent formation of ferroan dolomite and ferroan calcite.

Siderite containing ghost prisms and infilling pores between allochemical components has an inequigranular xenotopic fabric. Areas containing chamosite ooids and chain ooids as the dominant allochemical component are cemented by siderite with this fabric but lacking ghost prisms. In the absence of any evidence to the contrary it is concluded that all porosity filling siderite in the chamositic chamosite oolites precipitated at the same time.

Dark green blebs of chamosite containing filamentous material occur in that porosity remaining after siderite precipitation. Such material may represent the sub-surface colonisation of the sediment by some micro-organisms.

At some stage after the precipitation of pore-filling siderite and the formation of 'biogenic' chamosite, microstylolites formed within the sediment. This follows from the fact that they cross-cut all allochemical components and cement generations other than non-ferroan dolomite and porosity filling ferroan calcite.

A minor proportion of the porosity remaining after siderite precipitation is infilled by non-ferroan dolomite. The origin of this cement generation is thought to be high-magnesian calcite shell fragments, which did not undergo inversion or dissolution at an earlier stage in the diagenetic history of this facies. This may be a result of the micrite envelope which is found lying within areas of non-ferroan

dolomite. It is difficult to explain why the original high-magnesian calcite was not replaced by dolomite and calcite as in the case of the radial fibrous rims. The answer to this problem is perhaps associated with two different solution processes. Bathurst (1975) notes that shell fragment dissolution, whether aragonite or high-magnesian calcite, when occurring by a solution film process leaves the organic material that lay between individual carbonate layers in situ. The shell fragments in question show such an original orientation of organic lamellae. The more normal mode of epitaxial replacement would be expected in the case of radial fibrous high-magnesian calcite which occurred in a more open system. Due to the very localised nature of the non-ferroan dolomite it is not possible to determine when non-ferroan dolomite precipitation ceased. Since the rims of these areas are not characterised by a ferroan composition it is likely that precipitation halted prior to the precipitation of pore-filling ferroan calcite.

Pyrite occurs with a replacive role to all the preceding diagenetic products and also to chamosite ooids and pisoliths. It occasionally partially infills the primary porosity.

Ferroan calcite infills all the remaining porosity which was not completely sealed when this cement generation was forming.

It is possible to date precisely the point at which aragonite dissolution occurred. All original aragonite shell fragments are characterised by a complete or partial micrite envelope which retained their shape during aragonite dissolution. Since the majority of such secondary pores are lined with siderite of the pore-filling generation, it follows that aragonite dissolution must have overlapped with the precipitation of this cement generation and that infilling commenced soon after. It is interesting to note that dark green chamosite containing

filamentous material is commonly found infilling such secondary porosity and post-dating the pore-filling siderite. This may reflect a preference for organic material, remaining after aragonite dissolution, by the micro-organisms.

2.3.4 Chamositic Limonite Oolite

Three different sub-types of this facies have been recognised on the criteria of chamosite mud matrix colour and ooid form and nature. The Type C ironstone described by Davies and Dixie (1951) corresponds to this category. These authors have not, however, found any such internal variation within the lithology.

2.3.4.a Chamositic limonite oolite sub-type (i): This sub-type (Plate 2.23) is characterised by a dark green chamosite mud matrix and well-formed, polished, goethite ooids. The allochemical components, goethite ooids, intraclasts, quartz grains, biogenic debris and depositional chamosite mud constitute the greater part (modally > 90%) of the rock. The remaining primary porosity is infilled by calcite cement. There is a certain degree of separation between these components in that lenses containing a high proportion of chamosite mud, some intraclasts and many quartz grains are common within regions with a random intermixture of allochems, chamosite mud and sparse cementing calcite. It should be noted that not all the thin sections of this sub-type contain quartz.

2.3.4.a.i Goethite ooids: These allochemical grains show all the characteristics described above.

2.3.4.a.ii Depositional chamosite mud: This material forms 2-5 mm thick lenticles which are usually more than 2 cm long, and often exceed 5 cm. These grade into areas above and below which are characterised by a much higher proportion of the allochemical constituents. In plane polarised light the chamosite mud of the lenticles is an olive-green to olive-brown colour. Rotation of the stage reveals that these are the colours of the 'pleochroic scheme' which varies from the former to the latter for any given area. For this to occur some degree of preferred orientation of the components of the mud is necessary. Between crossed polars the chamosite mud has a grey, green and black speckled aspect. On rotation of the stage many of the 'specks' extinguish individually. The greater proportion, however, extinguish when the cross-hairs are parallel to bedding. This indicates that the chamosite mud is composed of clay-grade particles of chamosite which are generally oriented with (001) parallel to bedding, a typical depositional fabric. The chamosite mud of the allochem-rich areas also shows these characteristics, but has a tendency to be a darker brown in colour in plane polarised light.

Within the lenticular areas, and to a lesser extent in the allochemical-rich portions, rounded areas of chamosite mud with an approximate diameter of 0.5 - 1.5 mm occur, and can be seen to be distinct from the surrounding mud matrix. The edges of these are a brownish olive-green around a core of olive-green chamosite. Rotation of the stage between crossed polars shows that the orientation of the individual flakes in the rims is at an angle to both that of the surrounding chamosite mud and that in the core region of the grain. It is common to find several areas with these characteristics in close proximity. Where they are in contact they show a moulding around each other. Hence these areas of

chamosite mud are considered to represent chamosite mud-lumps or intraclasts analogous to those composed of clay minerals such as illite and montmorillonite found in areas of shallow terrigenous sedimentation at the present time.

2.3.4.a.iii Quartz grains: The chamosite mud of the lenticular areas and the chamosite mud intraclasts contain abundant quartz grains. In contrast very little quartz occurs in the allochem-rich portions of the sub-lithology. The quartz grains are sub-well sorted, having a size range of 0.10 - 0.15 mm. They are generally angular to sub-angular, although a few sub-rounded grains occur. The grain shape is commonly equant, but a number of shard-like grains are found. The quartz is characteristically very clear, lacking any fluid or mineral inclusions. An undulose extinction is observed.

2.3.4.a.iv Intraclasts: Two intraclast types have been recognised; chamosite mud intraclasts described above and intraclasts comprising goethite ooids, shell fragments and quartz grains in a matrix of chamosite mud. These grains are not an important physical constituent of the sub-lithology. They range in size from 1.0 to 3.0 mm.

2.3.4.a.v Biogenic material: These allochemical grains are represented by bivalve debris, echinoid fragments and occasional forams.

The bivalve material present is entirely fragmentary in nature and often has an abraded aspect. Algal borings within the fragments are common and are infilled with the primary chamosite mud of the matrix. An original dichotomy in shell mineralogy can be recognised. Non-ferroan

calcite fragments represent primary shell calcite, whereas ferroan calcite fragments represent primary aragonite shells which have been replaced by calcite subsequent to burial. The former grains often show the lamellar structure of Gryphaea arcuata. The latter are characterised by an inequigranular xenotopic fabric. The individual grains of this fabric type are usually restricted to the original shell boundaries, however, occasional individual grains may transgress this boundary to partake in the calcite cement fabric. Both primary calcite and inverted aragonite shells show thin micrite envelopes.

The echinoid fragments comprise echinoid plates and spines, and crinoid collumnals. All are of ferroan calcite. The stereome systems are infilled with depositional chamosite mud. It is usually the case that syntaxial overgrowths are absent. This is presumably a result of the abundance of primary chamosite mud considerably reducing the nucleation sites for calcium carbonate on the individual echinoid plates.

Forams are sparse and of non-ferroan calcite. Their chambers are infilled by depositional chamosite mud.

2.3.4.a.vi Calcite cement: It has been noted above that primary components comprise, modally, approximately 90% of the sub-lithology. The remaining primary porosity is infilled by ferroan calcite which has an inequigranular xenotopic fabric. The individual grains are less than, or equal to 0.1 mm, in size. This is the case in the normal allochem-rich portions of the sub-lithology. With regard to the chamosite mud lenticles, however, a different situation exists. Normally calcite cement is absent, but where several of the sparse allochems are grouped together they may create an

interstitial space which was not infilled by the chamosite mud. It is found that cement calcite infills these interstices.

2.3.4.a.vii Paragenesis: It is clear from the nature of the textures described above that very little post-depositional modification of the sub-lithology has occurred, the majority of the components being primary in origin. The development of diagenetic minerals is thus restricted to calcite cement and the ferroan calcite of originally aragonite shells. Since the grains of the replacive calcite have been found transgressing the original shell boundary to form part of the cement fabric, it is evident that aragonite dissolution created a secondary porosity which was infilled at the time of ferroan calcite cement precipitation. The secondary porosity would be preserved by the surrounding micrite envelopes.

2.3.4.b Chamositic limonite oolite sub-type (ii): This sub-type of the chamositic limonite oolites is characterised by light-green interstitial chamosite and well-formed, polished goethite ooids (Plate 2.24). The allochemical components comprise goethite ooids, intraclasts, pisolith fragments and biogenic debris. Chamosite mud is the dominant matrix component comprising, modally, 40-60% of the rock. Two different varieties of interstitial chamosite are recognised; olive-green depositional chamosite mud and grass-green authigenic chamosite. The former occurs as occasional small lenticles and patches within the latter. The dominance of the authigenic chamosite results in the light-green colouration of the chamosite matrix seen in hand specimen. These constituents make up approximately 85% modally of the rock. The remaining porosity is infilled by ferroan calcite. Siderite

occurs as a diagenetic mineral in association with ooids and authigenic chamosite.

2.3.4.b.i Goethite ooids: These allochemical grains show all the characteristics described above.

The ooid mineralogy is dominantly goethite. However, within different examples of this sub-type ooid mineralogy varies from being entirely goethite to being a mixture of goethite and chamosite. The chamosite varies in colour from a yellowish-green to a yellowish-brown. The occurrence of such chamosite is restricted to the more central portions of the ooid envelope and core. Thus, cores of structureless chamosite and individual envelope rings of chamosite occur in dominantly goethite ooids (Plate 2.25). The proportion of such chamosite occasionally forms up to 95% of an individual ooid. Ooids containing such chamosite often exhibit structures inexplicable by the physical processes of ooid formation suggested above. Textures that fall under the heading range in scale from a part of a single ring to an entire ooid.

Ooids are present which show an outer goethite rim of several rings around an interior constructed entirely of chamosite (Plate 2.26) and alternate rings of chamosite and goethite in the envelope (Plate 2.27). In these cases it is usual to find that any given ring is composed entirely of chamosite or goethite. In some instances, however, chamosite forms only a part of a ring of goethite. At either end of these chamosite portions there is an apparently ragged junction with the goethite of the remainder of the ring. High power magnification of the chamosite of such partial and complete rings occasionally shows the presence of very small ($\sim$0.01 mm) slivers of goethite lying within the ring chamosite (Plate 2.28). The goethite slivers are oriented with their long axes parallel to the edges of the ring.

Occasional discontinuous rings of opal occur within the envelope.

The textures described above are a function of a dual ooid mineralogy. One texture has been observed which is a result of the creation of space within the ooid by solution or some other process which would allow the removal of a portion of ooid envelope without distorting the remainder. The nature of this texture is such that a portion of the outermost envelope has been removed allowing the inner envelope and core to drop to the bottom of the void thus created (Plate 2.29). The possibility that the original ooid was formed with the core grain very close to the edge of the ooid envelope can be neglected on the basis that: (i) the irregular edges of the core and inner envelope can be matched with the edges of the void within the rest of the ooid, and (ii) the rotation of the extinction cross in the outer, unmoved, portion of envelope is out of phase with that of the cross in the inner, dropped, envelope fragment. The void created within the ooid was subsequently infilled by siderite. A number of ooids show the incipient development of this texture: 'Solution' has removed a portion of envelope at either end of the short axis creating the necessary void within the ooid and leaving a central ooid fragment, but has not proceeded to detach it from the outer portion of envelope at either end of the long axis. Detachment of these grains would allow them to fall to the bottom of the void. It should be noted that in all cases the original ooid shape is retained.

In specimens in which ooids which have undergone partial solution are present, ooids occur commonly which contain anhedral masses of siderite (less than 0.25 mm). Such siderite may constitute up to 75% of the ooid. No distortion of the ooid structure is associated with this

siderite. Often the siderite appears to be iron stained, but high-power microscopy reveals that this is in fact small particles of goethite that have presumably been detached from the ooid envelope. It is likely that such textures are sections of ooids which have undergone partial solution but the sectioning technique has not exposed diagnostic evidence of this.

Ooid distortion textures which result from the precipitation of siderite are not uncommon in either specimens characterised by partial ooid solution or specimens from which this texture is absent. This texture occurs at the edges of ooids and takes the form of the internal ring structure bowing around a siderite grain which has crystallised at the ooid edge (Plate 2.30). These siderite grains are usually less than 0.05 mm in length and are oriented such that their long axis is parallel to the ooid edge. In cases where the ooid was totally surrounded by authigenic chamosite prior to siderite crystallisation the outer edge of the siderite grains corresponds to the shape of the ooid edge at this time. The distortion of the ring structure then becomes explicable in terms of the pressure of crystallisation of siderite as it continued to grow following nucleation at some point along this contact. In a number of instances the outer edge of the siderite does not follow the contour of the original ooid edge but has an irregular outer margin. In all cases this texture shows siderite in contact with the ooid and authigenic chamosite at least over a short distance. Thus it may also have an outer contact with calcite cement. Where such siderite is completely covered by a thin rim of chamosite this may be bowed out from its original position against the ooid. The only instances in which siderite does not distort the ooid structure is when its crystallisation has exploited some pre-existing weakness such as an incipient fracture.

The only other textures in which the goethite ooids are involved are those involving authigenic chamosite. The chamosite is a light grass-green in colour and in any given case exhibits optical continuity under crossed polars. Three different textural forms occur, all closely related.

(i) Chamosite forms rims of uniform thickness (0.015 mm) around individual ooids. The rims are generally complete; totally enclosing the ooid concerned (Plate 2.31).

(ii) Where several ooids displaying textural type (i) occur in very close proximity their chamosite rims coalesce occluding any central pore-space. Thus in the minimum separation area between two ooids there may be a common chamosite rim. This may have a maximum thickness equal to the total thickness of the individual rims and a minimum thickness corresponding to a finite ooid separation. If the separation exceeds the maximum value, then there is no coalescence of the rims. Where three ooids are involved in such mutual rimming the interstitial space is lined entirely by chamosite. In this case, if the ooids are in very close proximity or in contact, the interstitial space may be filled with chamosite.

(iii) Chamosite of the type occurring in the previous two textural types occurs with ooids in a destructive texture. This appears to be intimately associated with incipient structural weaknesses such as fractures within ooids: Ooids showing a fracture parallel to one of the axes have been separated either partially or entirely along the fracture, the space created being infilled by chamosite. In such cases it appears that structural weaknesses have been exploited by precipitating chamosite in preference to its precipitation around the ooid margin. In the

discussion of the general form of goethite ooids (Section 2.3.1) it was noted that radial and ring contact fractures occur. These have also been exploited by chamosite creating an ooid 'explosion texture'. This is characterised (Plate 2.32) by an ooid surrounded in whole or in part by a chamosite rim of a slightly greater thickness than in case (i). Within this rim, splinters of single and several rings thickness occur. By virtue of their smooth long surfaces it appears that they have been removed by exploitation of ring-contact fractures. Similarly, from the fact that either ends of the splinters are irregular and apparently radially distributed with respect to the parent ooid, it is likely that these correspond to original radial fractures. The result of exploitation of radial and ring contact fractures by chamosite results in the removal of fragments of ooid envelope from the parent ooid. Their ultimate distribution in the chamosite rim is such that they show an exploded view of the ooid infrastructure. Hence, if the fragments were pushed back together by the shortest possible route the ooid would be recreated.

It has been noted above that some ooid textures that occur in one set of specimens of the sub-type are sparingly present, or absent from, another set of specimens. The occurrence of these textures are summarised below in Table 2.2.

2.3.4.b.ii Biogenic material: This group of allochemical grains comprises bivalve shell fragments, echinoid plate, spine, and collumnal fragments and foram tests.

The bivalve shells present are all fragmentary. They are usually less than 5 mm in length and oriented with their long axis parallel to

Texture	Specimen Set (i)	Specimen Set (ii)
Partial solution of ooids with siderite infill to voids	Absent	Common
Ooid distortion textures resulting from siderite crystallisation at ooid boundary	Uncommon	Common
Goethite ooid/authigenic chamosite textures	Uncommon	Uncommon

Table 2.2

bedding. As before two types of primary shell material are recognised: (i) primary shell calcite with a non-ferroan composition, and (ii) primary aragonite which has been replaced by ferroan calcite.

The edges of the primary calcite shell fragments show clear evidence of rounding and abrasion. They are often algally bored and the algal tubules infilled with authigenic chamosite or fine-grained goethite. In many instances the original shell structure, such as the lamellar structure of Gryphaea arcuata, can be seen.

The ferroan calcite shell fragments are in all cases surrounded by authigenic chamosite. They are characterised by a replacive fabric of equigranular to inequigranular xenotopic ferroan calcite. In some cases authigenic chamosite is present within the fragment as a continuation of the surrounding chamosite.

The echinoid fragments present vary in abundance. The test material is usually constructed of ferroan calcite. Occasional plates, however, show a compositional zonation from non-ferroan pink calcite in the central areas to blue, ferroan calcite in marginal areas (Plate 2.33). The stereome systems are infilled by authigenic chamosite. In a few instances the infill is of either ferroan calcite, of a similar colour to that of the ferroan calcite cement, or fine grained goethite. In areas where calcite cement occurs in relatively large areas (>0.3 mm) echinoid debris is characterised by the presence of syntaxial overgrowths of ferroan calcite. This is compositionally similar to that of the calcite cement. In contrast, where the echinoid fragments are totally surrounded by authigenic chamosite no syntaxial overgrowth is present. In many cases where a syntaxial overgrowth is present the stereome system is infilled by authigenic chamosite. It is found, however, that

there is no chamosite coating to the edges of the grain. The nature of the stereome system infill does not appear to control the extent of syntaxial overgrowth development. Plates have been observed with a ferroan calcite infill at one end and authigenic chamosite at the other. The syntaxial overgrowth is uniformly developed. The edges of the syntaxial rims have a similar shape to the boundaries of the individual cement calcite crystals with which they are in contact.

Foram tests are occasionally present. They are of non-ferroan calcite. The chambers are infilled by unoriented authigenic chamosite or authigenic chamosite with a radial orientation or entirely by ferroan calcite.

2.3.4.b.iii Chamosite: Two varieties of chamosite occur. The most common type has a grass-green colouration and shows unit extinction (Plate 2.34). The less commonly occurring variety is olive green-brown in colour. It forms lenticular and somewhat irregular patches 2-3 mm across within the grass-green chamosite (Plate 2.34). The lenticular areas lack any allochemical grains. They show a bulk pleochroism when the axis of the lenticle is parallel to the cross hairs and bulk, albeit spotty, extinction when in the same orientation. The similarity of such material to the depositional chamosite mud rich portions of chamositic limonite oolite sub-type (i) suggests that this material is also depositional chamosite mud. Small patches of the grass-green variety occur within it. The boundaries between the two varieties of chamosite are rather irregular and vary from being diffuse to imperceptible. The textures exhibited by the grass-green chamosite with respect to the allochemical grains, described above, suggest that this type of chamosite is entirely authigenic in origin.

The primary chamosite contains common siderite anhedra. These have an equant shape and are approximately 0.03 mm across. Characteristically they occur as trains of individual anhedra one grain thick and of several millimetres length running parallel to the lamination within the chamosite mud. Small, irregular, patches of ferroan calcite are sparsely distributed within this chamosite.

The authigenic chamosite contains frequent areas of lath and polygonal-shaped patches of ferroan calcite and siderite (Plate 2.35). The siderite is either white or greenish. Equant anhedral siderite grains with a white colour, relatively higher relief, and a size of less than 0.03 mm also occur. An important texture involving this type of chamosite, greenish siderite and ferroan calcite occurs at the edges of non-ferroan calcite shell fragments. These are surrounded by a radial fibrous fringe of fine calcite and siderite prisms, each of which appears to be separated by a thin filament of authigenic chamosite (Plate 2.36).

2.3.4.b.iv Calcite cement: This is usually a sparsely distributed component, infilling the remaining primary porosity which was not infilled by the authigenic and primary chamosite. Very locally it may form up to 50% of the non-allochemical components of the sub-lithology. The calcite cement is ferroan in composition. Two generations have been recognised: (i) Prismatic radial fibrous generation. This has only been found associated with primary calcite shell fragments in the localised areas with much calcite cement, noted above. It probably corresponds to the radial fibrous generations found in areas of authigenic chamosite. The prisms are rooted on non-ferroan calcite shell fragments lacking

either a micrite envelope or authigenic chamosite rim. Their terminations are often irregular. A number of adjacent prisms may show a unit extinction. (ii) Inequigranular xenotopic generation. This occurs in the above localised areas and elsewhere in the sub-lithology where the primary porosity had not been completely infilled at the time of its precipitation. It has an inequigranular xenotopic fabric. The individual component calcite crystals have straight boundaries and are usually less than 0.3 mm in size.

2.3.4.b.v Paragenesis: The textural descriptions of the various mineralogical phases given above indicate that following the deposition of the primary components a number of diagenetic changes occurred. These involve not only the precipitation of diagenetic minerals, but also physical and chemical changes within the primary phases. Figure 2.33 shows diagramatically the relative order of these events.

The occurrence of ooids constructed of goethite and chamosite in structurally separated areas suggests that these grains represent ooids undergoing oxidation from chamosite to goethite. The dominant texture of an outer goethite shell to a chamosite interior suggests that oxidation proceeded from the outside and moved inwards. This is the mode of oxidation which would be expected to occur in chamosite ooids being moved around in the marine environment. Those textures which involve alternating chamosite and goethite rings have been accounted for by Davies and Dixie (1951) who suggested that they resulted from fluctuating Eh levels at the site of ooid formation. It is unlikely, however, that Eh fluctuates so rapidly that a ferrous mineral can be formed shortly after a ferric mineral. An alternative

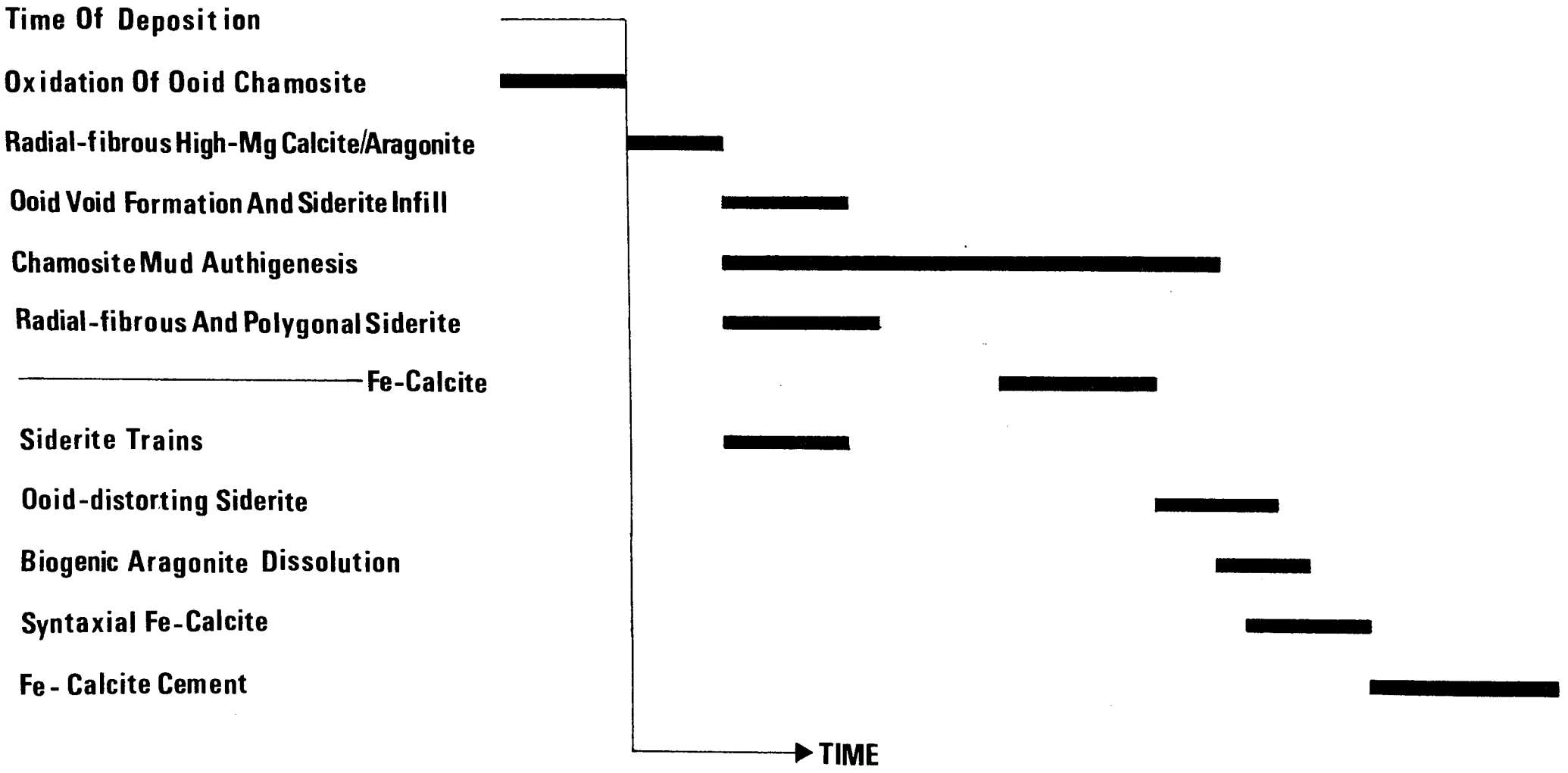

Figure 2.33: Paragenesis Of Chamositic Limonite Oolites ; Sub-type (ii)

hypothesis would be that the ooids were shuttled backwards and forwards between the environment of chamosite formation and the environment of chamosite oxidation. The textures involving splinters of goethite within a chamosite shell may be accounted for by this hypothesis or by oxidation of chamosite within ooids being non-uniform. Logically the formation of chamosite and goethite ooids must result from sea-floor oxidation rather than sub-surface formation of chamosite from goethite. Early diagenetic phases clearly indicate a reducing diagenetic environment.

It is not possible to date the replacement of occasional goethite rings by opal.

Since ooids containing chamosite and goethite rings exhibit textures suggestive of partial solution it follows that the process resulting in these textures post-dates the oxidation of ooid chamosite. In some instances the voids formed by this process have created an opening in the ooid envelope. Many of these are surrounded by authigenic chamosite, but this has not entered the void. Thus the voids were infilled by siderite prior to authigenic chamosite formation.

As authigenic chamosite surrounds ooids containing voids infilled with siderite, this material must post-date the infilling of ooid voids. The origin of the authigenic chamosite is an important aspect of the history of this sub-type. Figure 2.4 shows that in the majority of cases it occurs in the field in association with sub-type (i) chamositic limonite oolites. Its presence in the thin sections of specimens of the sub-type under discussion is ubiquitous. Indeed, if it was not for the textures which suggest an authigenic origin for this chamosite it could be assumed to be depositional chamosite mud. It has been noted above that small areas of depositional chamosite mud occur within the authigenic

chamosite. The two types of chamosite have a diffuse to imperceptible contact. Patches of optically continuous authigenic chamosite are occasionally present within the primary variety. Textural evidence, therefore, suggests that the authigenic chamosite results from in situ recrystallisation of the depositional chamosite. Had the authigenic chamosite been a precipitate from interstitial waters the overall textural type created would be expected to be one of interfering isopachous linings to the pre-existing primary porosity. In those areas of the sub-type where authigenic chamosite forms an isopachous pore-lining it is difficult to escape the conclusion that such chamosite does represent a precipitate from aqueous solution. The presence of solutions bearing the components of chamosite within a sediment with abundant chamosite is by no means inconceivable. Such solutions would occur as thin films around individual chamosite grains but would concentrate in areas of porosity which are now characterised by an isopachous rim of authigenic chamosite. It is often found that the ooids exhibiting an explosion texture are set in such optically continuous isopachous chamosite. The origin of this texture may well be due to chamosite-component-bearing fluids entering such ooids along pre-existing weaknesses such as fractures and ring contacts. Precipitation of chamosite and subsequent crystal growth would break up the ooid and move the fragments towards the surrounding open space. The wedges of authigenic chamosite would form in a similar way. The earliest time at which the recrystallisation of authigenic chamosite could have commenced probably post-dates the ooid dissolution and infilling by siderite.

The onset of recrystallisation and the formation of fluids from which chamosite could precipitate places a lower limit on the time at which echinoid stereome systems could be partially or totally infilled by authigenic chamosite.

The authigenic chamosite contains numerous polygons and laths of ferroan calcite and greenish siderite. These three minerals also occur as radial fibrous growths around shell fragments. These two textural forms are thought to represent different views of the same texture: Radial fibrous textures would be expected to be seen as laths and polygons when seen in cross-section. The fact that occasional radial fibrous textures in which a number of adjacent calcite prisms, not separated by siderite or authigenic chamosite, show a unit extinction suggests that this calcite is replacive in origin. By analogy with Recent carbonate sediments the original radial fibrous fabric would have consisted of either high-magnesian calcite or aragonite. Evidence which would allow the identification of the original phase is not present. It is difficult to understand how a radial fibrous fabric could develop on a shell fragment surrounded by authigenic chamosite, bearing in mind that an authigenic chamosite coating to echinoid fragments prevents the formation of a syntaxial overgrowth. This problem could be overcome if those areas which are characterised by these textures were originally primary pore spaces. If this were the case then the development of radial fibrous textures around shell fragments would be possible. Penecontemporaneous precipitation of authigenic chamosite from interstitial solutions, which would preclude the formation of complete isopachous fabrics, would surround the radial carbonate prisms. In the presence of such a

moulding medium low-magnesian ferroan calcite and siderite could pseudomorph the original prisms of aragonite or high-magnesian calcite on their dissolution. The reasons for the infill of some moulds by calcite and others by siderite is obscure; no mutual textures occur which allow the distinction of the first of these two phases. It would be reasonable to suggest that the greenish colour of the siderite is due to the presence of finely-divided chamosite. Unfortunately, analysis with the electron microprobe has not been able to establish this beyond doubt. If it was the case, however, then finely divided chamosite within siderite would suggest contemporaneous precipitation of the two. Since these grains are pseudomorphs of either aragonite or high-magnesian calcite the dissolution of these phases must have occurred prior to siderite precipitation. Their dissolution would have provided CO_3^{2-} for siderite formation. Unstained thin-sections show that the ferroan calcite which also occurs in this texture is not greenish in colour. The calcite, therefore, represents reprecipitation of CO_3^{2-} either within a microenvironment low in ferrous iron or the later infilling of moulds of the pre-existing carbonate phases in the authigenic chamosite. In either case coprecipitation of authigenic chamosite would not be expected.

Irregular anhedra of siderite occur in a distortive form between ooid and authigenic chamosite contacts. This siderite shows, relatively, a high relief in contrast to the radial fibrous variety within the authigenic chamosite. Similar siderite occurs as equant anhedra within the authigenic chamosite, and singly and in trains within primary chamosite mud. It clearly post-dates the formation of authigenic chamosite, because it is restricted within original ooid contacts. It is

difficult to reconcile the presence of high-relief siderite anhedra within authigenic chamosite with the processes put forward in the preceding paragraph. Since single anhedra of siderite are present within primary chamosite mud at a time prior to its authigenesis it seems reasonable that the equant siderite anhedra seen within authigenic chamosite may have been present at its time of formation, thus representing inclusions. It should be noted that siderite trains only occur in allochemical poor regions of primary chamosite mud. Since all the authigenic chamosite contains a high proportion of allochemical grains trains would not be expected. Thus, the ooid distorting siderite represents a later stage of siderite formation due to the passage of iron bearing fluids along the easiest path represented by ooid-authigenic chamosite contacts. Evidence for this is supported by the distortion of some authigenic chamosite ooid coats by this type of siderite.

The development of syntaxial overgrowth on echinoid plates commences at a time when chamosite authigenesis was finishing. This is indicated by plates containing both calcite and authigenic chamosite stereome system infills. An external overgrowth generally does not occur due to potential calcite nucleation sites being considerably reduced by the presence of authigenic chamosite coats. Such external overgrowths are far better developed in those localised areas where the abundance of authigenic chamosite is much lower than elsewhere. Here, large syntaxial calcite overgrowths extend from echinoid fragments into open space. The growth of such rims continued into the time at which the second calcite generation was forming. Evidence for this comes from the fact that the outer edges of the rims partake in the fabric of this calcite generation. Syntaxial overgrowths are compositionally similar in iron content to this calcite generation.

The prismatic calcite growth is rooted on non-ferroan shell fragments. It is only present in regions lacking a complete infill of authigenic chamosite. The prism terminations are irregular. Since some adjacent prisms show unit extinction it would appear that the ferroan calcite is a replacement of an original prismatic cement generation. By analogy with present day carbonate sediments this may have been either aragonite or high-magnesian calcite. It is not possible to determine when this cement generation formed. The somewhat ragged prism terminations and the absence of their original form as ghosts from the second generation suggests that their replacement by calcite occurred at some stage prior to its crystallisation.

The second calcite generation infills all the remaining primary porosity. It is the last post-depositional diagenetic growth, bringing about the cessation of growth of the preceding syntaxial growths.

In many instances the patches of ferroan calcite within the authigenic chamosite can be demonstrated to be originally aragonitic shell material. This is characterised by a replacive inequigranular xenotopic fabric of ferroan calcite. The dissolution post-dates the chamosite authigenesis. This follows from the fact that the dissolution causes the creation of a secondary porosity. In order to retain the shell shape an external material is required to retain it in the form of a mould. Subsequently calcite precipitation would infill the mould. Since authigenic chamosite is occasionally present within the replacive calcite, it is evident that the secondary porosity developed towards the end of the formation of authigenic chamosite.

It has been noted at various points in the description of the textures within this sub-type that certain textures are present in some specimens, but not in others (Table 2.2). All specimens are characterised

by the presence of an authigenic chamosite matrix. In some cases there is an imperceptible passage from authigenic chamosite, from which some textures are absent, to authigenic chamosite within which they are present. Hence it is not proposed to further sub-divide the sub-type but to consider both specimen types as representing different degrees of diagenetic change within it.

2.3.4.c Chamositic limonite oolite sub-type (iii): This sub-type is characterised by a light-green chamosite interstitial to poorly developed or relict dull ochre coloured goethite ooids.The allochemical components present comprise goethite ooids, intraclasts and biogenic debris. In contrast to sub-types (i) and (ii) primary chamosite mud is apparently absent. The abundance of authigenic chamosite is the cause of the light green chamosite colouration seen in hand specimen. The goethite ooids are replaced by variable amounts of siderite which results in their dull, relict appearance (Plate 2.37). It is extremely difficult to recognise any primary porosity within the sub-lithology.

2.3.4.c.i Goethite ooids: These allochemical grains show all the characteristics described above.

In a number of specimens of the sub-type ooid distortion textures occur. In some cases these can be attributed to loading phenomena, as described above, but the majority are due to the formation of chain ooids. Several different textures that may be ascribed to this mode of ooid distortion have been recognised. All involve a change in the ooid shape and concommitant internal envelope distortion. The least distorted textural type is represented by individual hooked ooids

(Plate 2.38). These are characterised by diametrically opposed hooks formed by the outermost envelope ring. In many cases the creation of these hooks can be seen to have resulted in the fracturing of this ring. This deformation causes an overfolding in the interior rings, the 'axial trace' of which passes through the fracture edge of the outermost ring (Figure 2.34). True chain ooids are common and are constructed of two, three and rarely, four such hooked ooids. The chain linkage between these grains takes the form of the contact between the outer envelope rings of adjacent ooids, providing they face in opposing directions. Thus their 'axial traces' are parallel or become one trace (Figure 2.35, Plate 2.39). In extreme cases the linkage between ooids may become rather long and tortuous (Plate 2.40) and is associated with a marked thinning and increased internal distortion of the ooid. It is interesting to note that in the great majority of cases the linkage occurs between hooks formed in the area of maximum curvature of the ooid; usually at either end of the long axis.

The mode of formation of carbonate chain ooids and pisoliths has been discussed by Cayeux (1935), Carozzi (1961, 1963) and Conley (1977). Two forms of such deformed grains have been recognised; those which retain their original spheroidal shape, but which have either distorted envelopes or displaced nuclei, or both; and those which consist of grains with a modified external shape and distorted internal structure. The ooids described above are clearly representatives of the second group. Carozzi (1961) has attributed such grains to distortion of soft ooids at the time of deposition by 'reciprocal impacts' in a very agitated environment. This cannot be the case in the present situation as the fragile linkages between ooids could not be expected to survive such

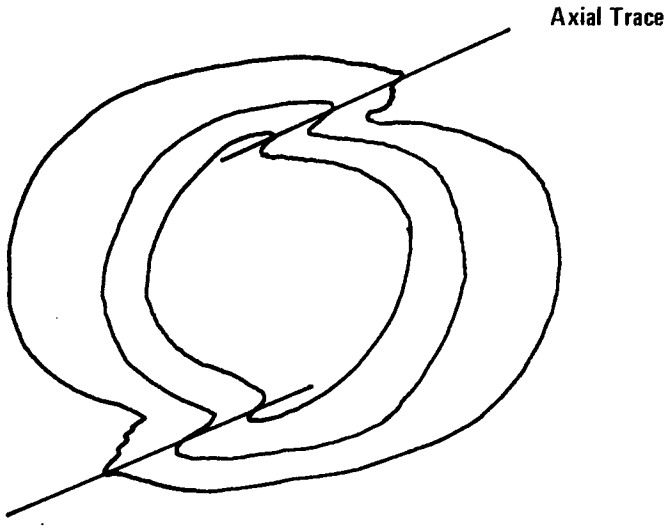

Fig 2.34 Diagrammatic sketch of Hooked Ooid

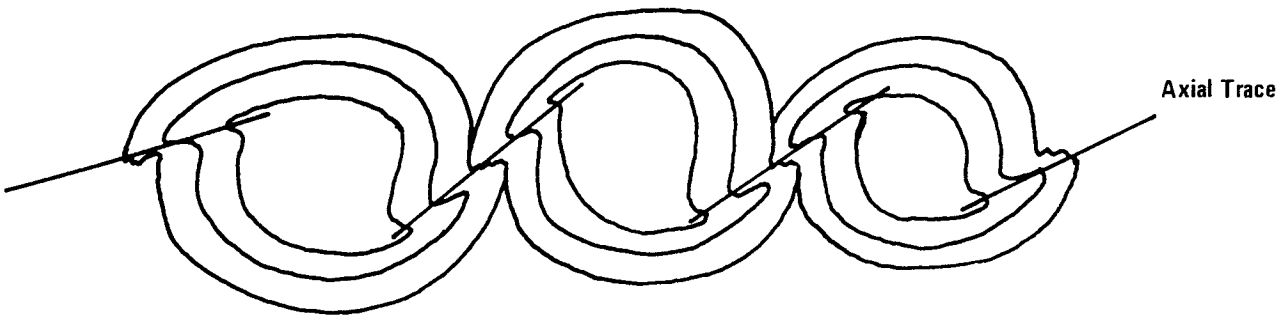

Fig 2.35 Diagrammatic sketch of Chain Hooked Ooids

hydro-dynamic movement. Cayeux (1935) has assumed that this type of chain ooid developed after deposition and partial cementation, but remarked that the cementation processes would be extremely complex and involve large changes in rock volume. Conley (1977) has demonstrated, for the Plattsburg Limestone (Pennsylvanian, Carboniferous), that chain pisoliths of this type are formed as a result of cementation followed by pisolith solution and subsequent cement collapse forming a chain pisolith-shaped secondary porosity which was subsequently infilled.

In the specific example of goethite chain ooids in chamositic limonite oolite sub-type (iii) the model of Conley (1977) cannot be directly applied as internal ooid ring structures are retained thus indicating that ooimould formation did not precede hook and chain formation. The initial hooked ooids might indicate that differential stresses operating in opposite directions on either side of the ooid caused the hook formation, but it is difficult to explain the attendant vertical movement. Alternatively such stresses causing ooids, which were initially in contact, to scrape past each other and in doing so create a mechanical linkage which would be stretched with continuing movement could be postulated. Hooked ooids are occasionally found, however, whose hooks match exactly and are separated by a thin, straight, line passing through the authigenic chamosite cement (Plate 2.41). The chamosite, which is normally in optical continuity over large areas, is not quite in such continuity to either side of the line. It is proposed that chain ooids are formed by the creation of small fractures within the authigenic chamosite cement, at points where it occurs between ooids and is therefore mechanically weaker than elsewhere, and allowing such areas of chamosite to pivot into the ooid envelopes.

It is evidently not a prerequisite for hook formation that chamosite fracturing should only occur between ooids as ooids showing hooks occur with a complete surround of authigenic chamosite and separated by some distance from the nearest ooid. Similarly, it is not a prerequisite that two hooks should be formed on any one ooid; one and three hooks may be found. The movement into the goethite ooids by authigenic chamosite may be explicable in terms of the goethite having a resistance to such deformation less than the causative force. Such entry would result in the apparent fracture of the outer ring and the interior envelope deformation around the authigenic chamosite fragment. The proposed mechanism of chain formation is broadly similar to that of Conley (1977) in that it involves movement of the surrounding cement. Since it involves fracturing of authigenic chamosite the mechanism must post-date authigenic chamosite formation. The causative factor may, therefore, be related to pore pressure variation concentrated along intergrain boundaries at a time of compaction.

As in the case of the ooids of chamositic limonite oolite sub-type (ii) (2.3.4.b.i) ooids consisting of a mixture of chamosite and goethite occur. The two minerals are structurally separated within the confines of the ooid ring structure. These are considered to represent ooids of chamosite undergoing oxidation to goethite at their time of incorporation in the sediment.

In the majority of cases the edges of ooids are seen to be somewhat ragged. In a very few instances this can be seen to be due to solution removing part of the outer envelope and much of the ooid interior, followed by precipitation of siderite within the void. In all other cases the ragged edges can be seen to be due to siderite precipitating at the ooid margin and distorting the ooid envelope by pressure of

crystallisation (Plate 2.42). Where authigenic chamosite forms rims to ooids the siderite occurs between the chamosite and ooids. In the absence of an authigenic chamosite rim the siderite forms equant anhedra penetrating into both the ooid and the surrounding space. These two textures have been described and discussed in the section on chamositic limonite oolite sub-type (ii) (2.3.4.b.i).

A number of specimens are additionally characterised by a slightly different siderite-ooid texture. The nature of the texture is such that a rim of sub-prismatic siderite replaces the outer ooid envelope ring (Plate 2.43). Occasional splinters of goethite are present within the siderite. Where an individual prism passes with optical continuity into the surrounding siderite a thin line ghosts the original ooid edge. In many cases the outer margin of the siderite rim corresponds to the outer ooid boundary. Some ooids may show an inner ring of such siderite. The role of the siderite in this texture is not markedly distortive, indicating a possible phase of ooid solution removing the outer envelope ring contemporaneously with siderite precipitation. Thus ooid void textures are not found.

The only other textures seen in ooids are those which involve authigenic chamosite. These are represented by chamosite wedges explosion textures, and linings to the primary porosity. These have been discussed above.

2.3.4.c.ii Biogenic material: These allochemical grains are sparsely distributed. They include bivalve fragments, echinoid plates and spines and forams.

The bivalve fragments are oriented parallel to bedding and are usually less than 2 cm in length. All the fragments are of non-ferroan

calcite. The smaller shell grains (those less than 0.5 mm) are rounded and algally bored. These are infilled by fine-grained goethite. The long shell fragments have often been broken. The presence of ferroan calcite lamellae within some of these shells implies that they may have been high-magnesian calcite layers within it. Where these have been exposed by shell break-up authigenic chamosite and siderite penetrate a short distance into the lamellae.

Occasional areas of authigenic chamosite and siderite occur with an overall shape similar to that of rounded shell fragments. The authigenic chamosite is a darker green than that which forms the matrix. It is suggested that these areas represent original aragonite shell fragments which underwent dissolution following the authigenesis of the surrounding chamosite. This formed a mould which was later infilled by the darker green authigenic chamosite and siderite.

The echinoid plates and spines present are constructed of either ferroan or non-ferroan calcite. Their stereome systems are infilled by fine-grained goethite, ferroan calcite and authigenic chamosite. Of these infills the last is most common. Syntaxial overgrowths have not been found although in some cases clean-edged echinoid plates occur surrounded by a single non-optically continuous siderite grain.

2.3.4.c.iii Chamosite: No chamosite having the characteristics of depositional chamosite mud has been found; all the chamosite present is apparently authigenic in origin. It is grass green in colour and has unit extinction over variable sized, irregular patches or uniformly across the slide. In the latter case it can be seen to form fringes of radially oriented flakes, with a very faint extinction cross,

around all allochemical grains.

The abundance of authigenic chamosite is found to be variable both within one specimen and between specimens (Plate 2.37). Some have a ubiquitous distribution of chamosite (Plate 2.44) whereas in others the authigenic chamosite forms a low proportion of the cement. In the pore spaces the chamosite may occur in association with abundant 0.05 mm equant siderite anhedra. The two minerals generally form an equal proportion of the cement. Where allochemical grains are close together the authigenic chamosite may line or totally infill the interstitial space. In specimens with a low proportion of chamosite siderite infills the remaining pore spaces and has an inequigranular xenotopic fabric. A dark green authigenic chamosite may occur with abundant equant anhedra of siderite in the centre of pore spaces (Plate 2.45). Irregular and lenticular areas consisting entirely of chamosite and siderite which vary from 25-75% to 5-95% occur. The siderite grains are again equant anhedra and often form trains, usually less than 2 mm long, parallel to bedding.

2.3.4.c.iv Calcite: Ferroan calcite infills the very few remaining primary interstices as individual inequigranular grains.

2.3.4.c.v Cement infill to complete shells: In specimens characterised by a dominantly siderite infill to the pore spaces occasional complete shells or partially open shells containing no allochemical grains or depositional chamosite mud reveal the order of precipitation of the cement minerals. This commences with a prismatic, isopachous, generation of siderite growing at right-angles to the interior shell wall. The

terminations of these grains are perfectly flat. The contact between these prisms and the massive growth of dogs tooth siderite which abuts against them is ironstained. The remaining primary porosity is infilled by ferroan calcite crystals which grow normally to the shell wall. Near the junctions between this cement and the preceding siderite clots of authigenic chamosite occur which contain equant anhedra of siderite.

2.3.4.c.vi Paragenesis: The fact that specimens exhibit different proportions of authigenic chamosite and siderite cement whilst having a number of textures involving allochemical grains in common, suggests that the diagenetic histories of these specimens are slightly different. Thus the following discussion of the paragenesis of this sub-lithology takes account of this feature. Figure 2.36 summarises the order and extent of post-depositional changes within the sub-lithology.

The first change in the nature of the ooids is their oxidation from chamosite to goethite in the marine environment. This has been discussed above (2.3.4.b.v). Although affecting the nature of a mineral already formed the oxidation is a pre-depositional event.

Within the chamosite-dominated cement specimens ooids show textures suggestive of partial dissolution of the interior ooid envelope, followed by void infill by siderite. The same texture has been reported from sub-lithology (ii) (2.3.4.b.i) and the same reasoning for its recognition as the second diagenetic change applies to its occurrence in this sub-lithology.

The ooids of the siderite-dominated cement specimens show an outer fringe of prismatic siderite replacing the outer ooid envelope ring, and occasionally, inner rings. Since this siderite is not distortive with respect to the ooid, it follows that some solution process was operative

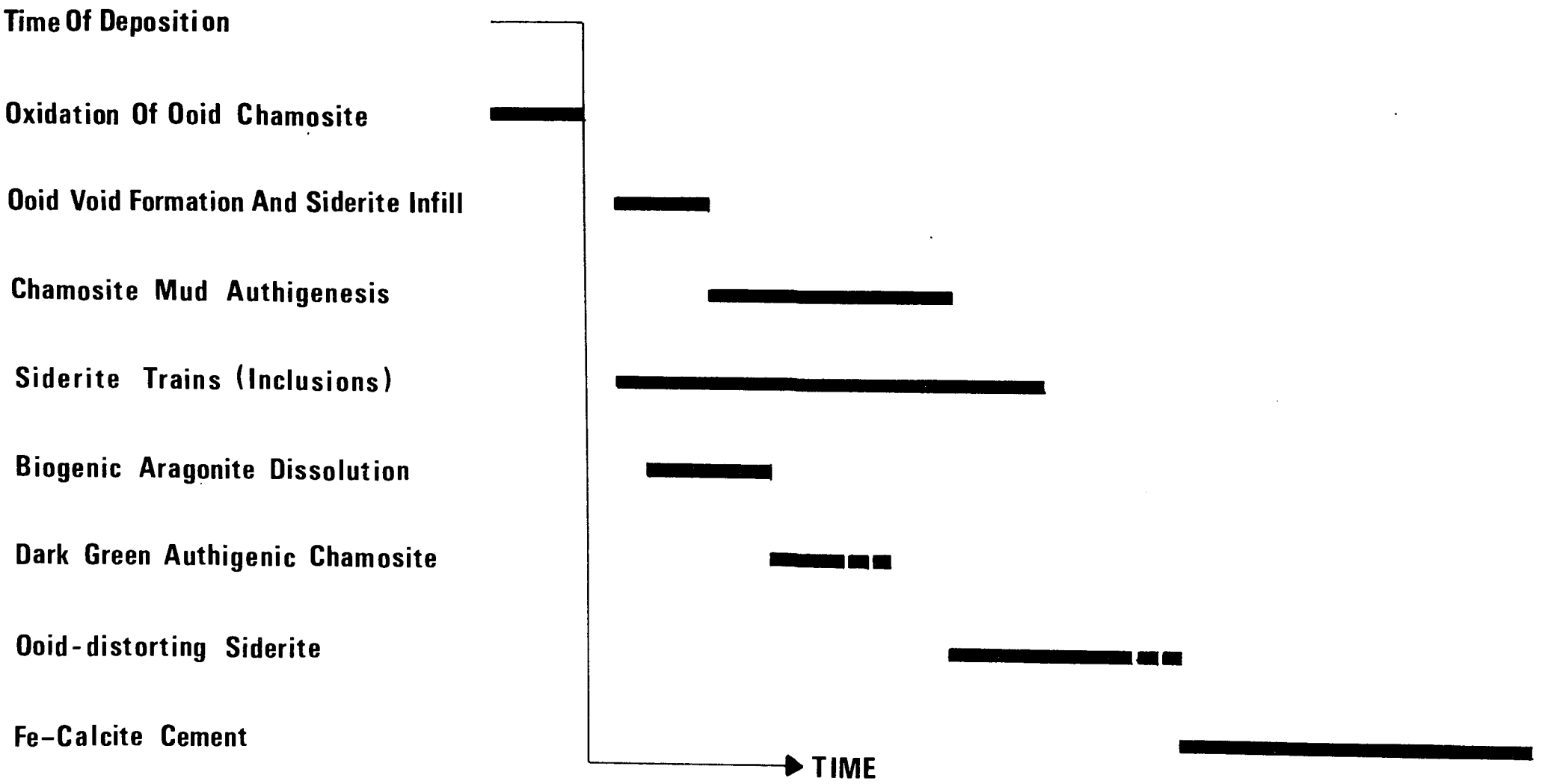

Figure 2.36a: Paragenesis Of Chamosite Cemented Chamositic Limonite Oolites; Sub-type(iii)

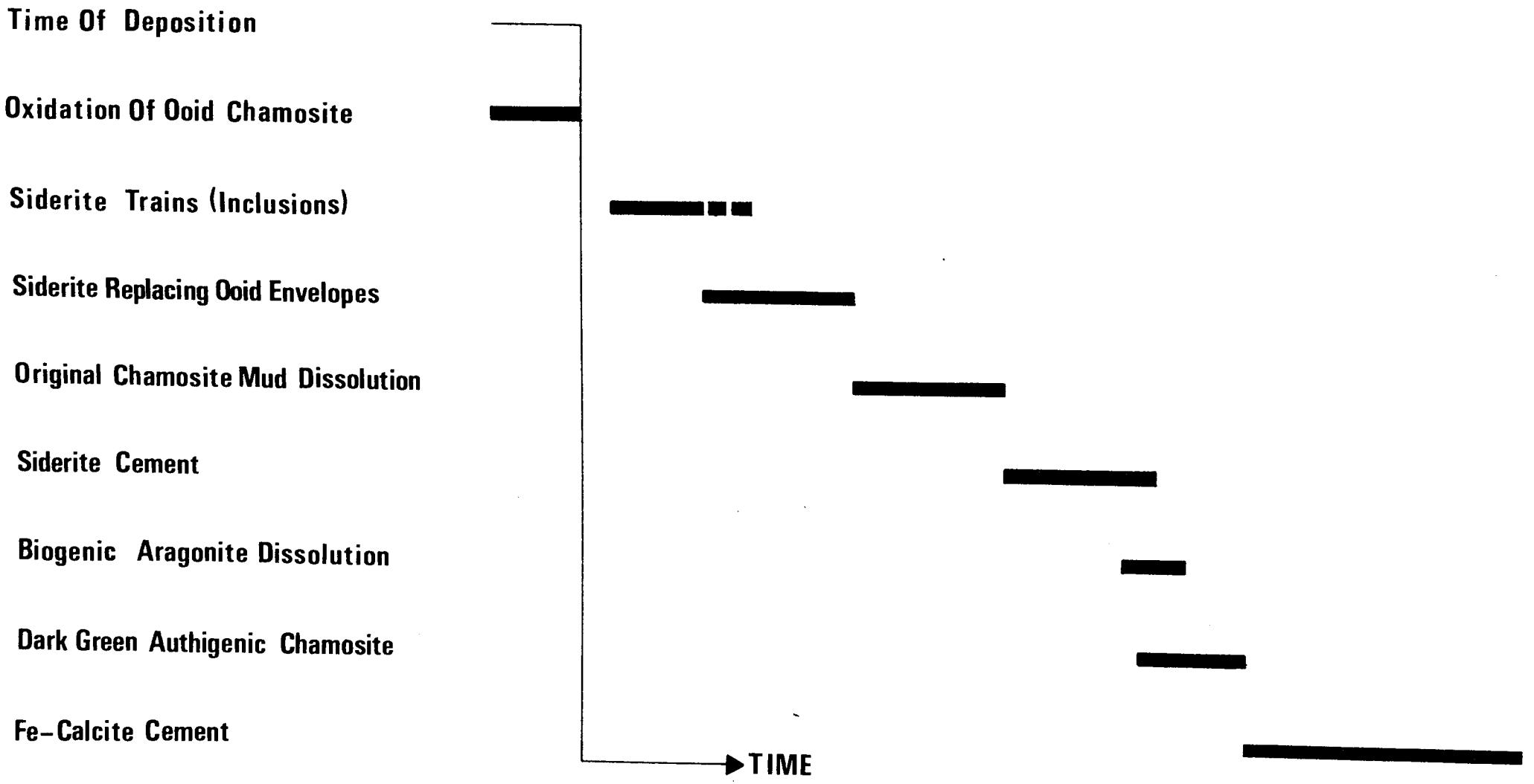

Figure 2.36b: Paragenesis Of Siderite Cemented Chamositic Limonite Oolites Sub-type (iii)

in order to allow such a texture to form. Evidence for the dissolution hypothesis is given by the presence of ooid boundary ghosts within siderite prisms. In order for such siderite fringes to develop, some lining to the pore spaces would be required to retain the ooid grain shape during dissolution of the outer portion of the goethite ooid envelope. Assuming this to have been accomplished siderite crystallisation would have had to proceed as the goethite was removed in order to prevent the remaining portion of the ooid dropping to the bottom of the void created. There is no evidence for the presence of a cement generation in the sub-lithology at this time. Shell cavities are lined with an initial prismatic siderite generation. The terminations to this, which would have been expected to be euhedral, are flat and characterised by a thin brown iron oxide stain at this level. This is indicative of a solution phase following its crystallisation, which might also be responsible for the removal of a porosity lining. Hence the ooid siderite fringes do not appear to represent the second diagenetic event within siderite-dominated matrix specimens, but do represent a phase of ooid dissolution which might correlate with that of the chamosite-dominated cement specimens.

There is good evidence for the authigenic origin of chamosite in the chamosite-dominated cement specimens. Lenticular and irregular patches with few allochemical grains are characterised by trains of siderite anhedra set in authigenic chamosite. This textural form of siderite is found in allochem-poor areas of depositional chamosite mud in other sediments. Similarly, individual siderite anhedra occur in areas of allochem-rich primary chamosite mud. Thus, it would appear that the original matrix was depositional chamosite mud in which siderite with the noted textural forms precipitated prior to the

authigenesis of the chamosite mud. This textural type may be thought of as siderite inclusions. The occasional patches of authigenic chamosite with such siderite anhedra in the siderite-dominated cement specimens can be attributed to the same origin.

The nature of the authigenesis of the depositional chamosite mud has been discussed above in context of the ooid distortion which it causes (2.3.4.b.v). Hence, the wedge, explosion, and isopachous pore-lining textures occurring in the chamosite cemented sub-type developed at the same time as the authigenesis. In addition, the echinoid stereome systems were also infilled by authigenic chamosite at this time.

Following the crystallisation of chamosite within the chamosite-dominated cement specimens, siderite crystallised at ooid margins distorting the interior structure by its pressure of crystallisation. The outer margin of this siderite corresponds to the original contact between the ooid and authigenic chamosite. Thus, in order for the outer margin to be preserved it is necessary for the authigenic chamosite to have crystallised prior to the precipitation of siderite. Presumably, it was easier for siderite to distort the ooid than the surrounding siderite.

In contrast, the main porosity infill to the siderite-dominated cement specimens is siderite. This material surrounds the majority of allochemical grains and patches of authigenic chamosite. It thus post-dates this type of chamosite. In the case of some ooids the siderite may penetrate the envelope causing distortion of the rings. In instances of ooids showing a fringe of siderite prisms replacing the outer ring the pore-filling siderite abuts against the individual prism terminations. Hence the porosity-filling siderite post-dates the prismatic siderite.

Evidence in support of this is supplied by shell infills which show a massive growth of siderite with a dogs tooth habit abutting against an earlier prismatic generation. The centres of pore spaces contain dark-green authigenic chamosite and siderite anhedra. Their position indicates a time of precipitation late in the history of siderite cement precipitation.

The remaining porosity in the case of chamosite-dominated cement specimens is infilled by ferroan calcite which therefore post-dates all the preceding generations.

The proportion of orginally aragonite shells which have undergone dissolution and replacement is low in both cement type specimens. Areas with a shell shape and infilled by dark-green authigenic chamosite and siderite anhedra occur, however, and are thought to represent this replacement. It is not possible to date the point at which aragonite dissolution occurred. The replacement of these shells, however, would require some form of mould, whether a micrite envelope or a pre-existing cement. The former has not been observed. The time at which the secondary porosity resulting from aragonite dissolution was infilled correlates with the later stages of siderite cement precipitation. Pore spaces containing a central infill of a similar material to the aragonite shell replacement occur in the siderite-cemented specimens.

It is clear from the above consideration of the order of textural developments within the sub-lithology that the same broad sequence of events characterises both chamosite and siderite-dominated cement varieties of the sub-lithology. On this basis, then, the two varieties are different variants of sub-lithology (iii). It has been shown in the discussion of sub-lithology (ii) that authigenic chamosite develops from depositional chamosite mud, thus the chamosite-dominated matrix variety

is a further development of this theme. Authigenic chamosite of this type is present within the siderite-dominated cement variety, but is not widely developed. In the discussion of the prismatic siderite replacing the outer ring of ooids it was pointed out that there is some evidence to suggest the dissolution of a porosity lining. A similar texture is encountered between the margins of ooids and their authigenic chamosite surroundings. The prismatic texture is evidently related to this although it is not accompanied by a major distortion in the ooid envelope, in that it occurs as ooid margins. It is suggested that authigenic chamosite formed an initial porosity infill, but was subsequently removed in solution. The change from primary chamosite mud to authigenic chamosite is accompanied by an increase in the importance of siderite evidently reflecting a change in the physico-chemical environment. This might ultimately result in conditions which would promote dissolution of chamosite and increasing precipitation of siderite. This proposition is examined in more depth in Chapter 8.

2.3.5 Sideritic Chamositic Limonite Oolite

This facies is characterised in thin section by a ubiquitous isopachous authigenic chamosite lining of primary pore spaces (Plate 2.46).

2.3.5.i Goethite ooids: These allochemical grains show all the above characteristics. Goethite is the only ooid-forming mineral which has been identified.

The ooids form three textures with authigenic chamosite. Of these, the most characteristic is their surround of isopachous chamosite which lines all the pore-spaces (Plate 2.47). The authigenic chamosite rim is 0.02 mm in width.

The other two textures in which ooids and authigenic chamosite participate are wedge and explosion textures. The nature and proposed method of formation of these textures, at the time of chamosite precipitation, has been discussed above (2.3.4.b.i).

The only other texture in which ooids are involved is formed as a result of the precipitation of siderite at the contact between ooids and authigenic chamosite rims. This is precisely the same texture as has been described from the chamositic limonite oolite sub-types (ii) and (iii) (2.3.4.b.i) above. Again it involves a distortion of the envelope structure around a lenticular siderite grain whose outer margin corresponds to the original outer margin of the ooid. Normally the siderite grains do not penetrate beyond the first or second envelope ring. In some cases, however, they penetrate to the third and fourth rings, in which case the first and second rings are cut off at the boundary of the siderite and are not deformed around it. The proportion of such siderite within ooids is usually less than 15%, but in extreme cases may make up 30% of the ooid.

2.3.5.ii Intraclasts: These allochemical grains comprise irregular, rounded intraclasts of limonitic limonite oolite and structureless grains of goethite. Such allochems have an upper size limit of approximately 0.6 mm. Intraclasts are sparsely distributed throughout the lithological type.

2.3.5.iii Biogenic material: Shell material, echinoid plates and spines, are sparsely distributed. The shell fragments are usually of a similar size to the ooids and are in all cases rounded and abraded. They

commonly show algal borings which are infilled by fine-grained goethite. It is interesting to note that all the shell material is of non-ferroan calcite. There is no evidence of any ferroan calcite representing original aragonite shell material. Echinoid plates and spines are of ferroan calcite and their stereome systems are infilled by authigenic chamosite. No syntaxial overgrowths have been observed.

2.3.5.iv Chamosite: The chamosite present in this lithological type is of a grass-green colouration and optically continuous throughout the slide (Plate 2.47). This, combined with the textures which it is involved in demand that it is authigenic in origin, forming a lining of the primary porosity. The chamosite is in optical continuity throughout the sections examined. The outer margins of the chamosite lining are characterised by a slightly hummocky outline and a greyish-green diffuse aspect.

2.3.5.v. Siderite: This mineral is entirely diagenetic in origin. It occurs with a distortive texture in ooids. In some cases it is found that siderite grains in this role have lifted the surrounding chamosite rim away from the ooid during the course of their growth. This may result in a complete chamosite rim which curves away from the ooid and around the siderite grain, or more commonly a chamosite rim broken at one point and lifted away from the ooid by the continued growth of the siderite through the gap thus created.

Siderite may completely infill the remaining porosity, when it is found surrounded by chamosite with a hummocky and grey-green diffuse appearance. In some specimens, however, it infills the narrower portions

of the porosity thus forming a second, discontinuous rim around it. In some cases it is found that this siderite is responsible for lifting the chamosite rim from around the ooids. If this exposes a distortive siderite grain the contact between the two follows the curve of the original ooid-chamosite contact.

In some areas, such as between shell fragments, and as lenticles less than 5 mm long and parallel to bedding, no allochems occur. These areas are characterised by an intermixture of equant siderite anhedra less than 0.05 mm in size, and grass-green authigenic chamosite in the proportion 75%:25%. The proportion of siderite may be greater than this. Within such areas siderite anhedra often form trains one grain thick and approximately 0.5 mm long.

2.3.5.vi Calcite: Ferroan calcite infills the remaining porosity, providing that siderite has not already done this. The calcite tends to occur as one crystal infilling an interstitial space (Plate 2.46).

2.3.5.vii Paragenesis: The sequence of post-depositional events within this lithological type is very simple, appearing to represent the gradual infill of a primary porosity with relatively little effect on the primary components. Figure 2.37 shows the sequence of post-depositional events.

The development of authigenic chamosite is the first post-depositional event. It should be noted, however, that areas characterised by the absence of allochemical components probably represent small areas of depositional chamosite mud in which siderite anhedra developed before its authigenesis and are now present as inclusion trails. The isopachous chamosite lining is characteristic of precipitation from aqueous solution. Its optical

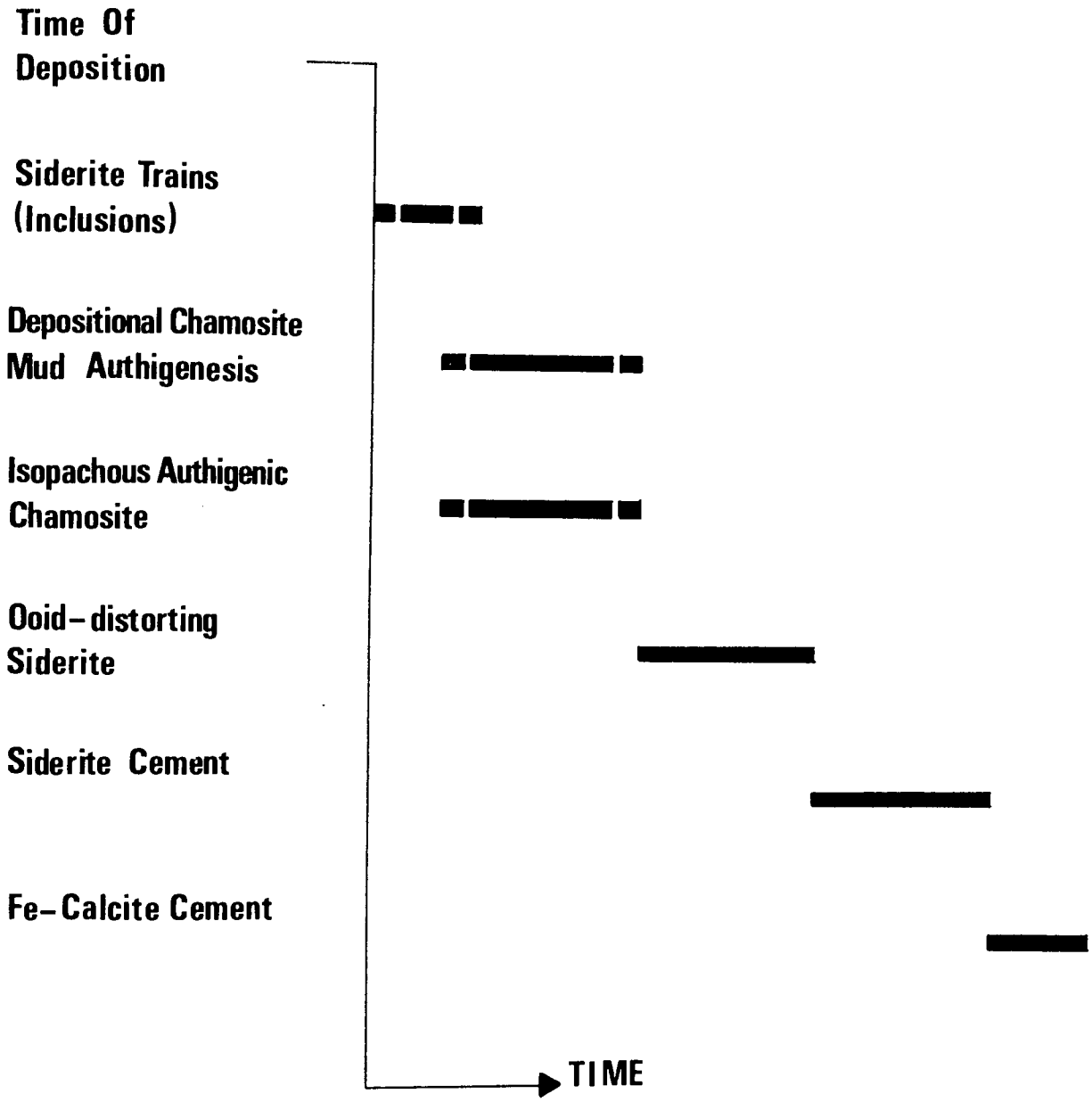

Figure 2.37: Paragenesis Of The Sideritic Chamositic Limonite Oolites

continuity is evidence in support of this. Penetration of aqueous solutions, which would precipitate chamosite, along structural weaknesses in ooids would bring about the formation of the allied wedge and explosion textures.

In order for distortive siderite to occur within ooids with an outer margin corresponding to the original ooid margin, it is necessary that the authigenic chamosite lining should pre-date this in order to retain the ooid shape. Thus siderite precipitation and growth post-dates the development of the chamosite pore linings. The fact that in some cases the siderite cross-cuts the outer ooid rings, indicates that at some stage goethite began to enter solution.

Where a chamosite rim has been lifted from an ooid, exposing a distortive siderite grain, the contact between this and the porosity filling siderite corresponds to the original ooid outline. Thus the porosity filling siderite post-dates the distortive siderite. Since, in all cases, this siderite is surrounded totally or partially by chamosite with a hummocky and grey-green appearance it also post-dates this.

The last diagenetic phase to precipitate is ferroan calcite. This infills the remaining porosity. This clearly post-dates the previous diagenetic phases as individual grains of ferroan calcite abut against or surround these phases.

2.3.6 Calcitic Limonite Oolite

Texturally and mineralogically this facies (Plate 2.48) is the simplest of the true ironstone lithologies occurring in the Frodingham Field. Physically it comprises ooids, intraclasts, shell fragments and cement

The major mineral components are goethite and ferroan calcite. Authigenic chamosite occurs sparingly. Goethite is restricted in its mode of occurrence to ooids and intraclasts, calcite forms the remaining physical components and in addition may occur in intraclasts. This ironstone type corresponds to Type D of Davies and Dixie (1951).

2.3.6.i Goethite ooids: The ooid phase in the calcitic limonite oolite shows all the characteristics described above.

Rarely occurring textures in this oolite, which involve goethite ooids and grass-green authigenic chamosite, are the porosity linings, wedge and explosion textures which have been described and discussed above.

2.3.6.ii Pisoliths: These allochemical grains show elliptical and circular sections. They vary in size from 2-7 mm, measured along the long axis. In form, many are rounded and have missing portions which is suggestive of transport and abrasion. Radial fissures and fractures are commonly found. Mineralogically, pisoliths are composed of goethite, chamosite, siderite and ferroan calcite. In general, goethite is the major mineral.

Some pisoliths have been found in which it is possible to discern the internal structure and mineralogical distribution. As with ooids, these grains can be divided into a core and envelope. The core is usually a totally structureless area of goethite. Occasional ooids may form the core, however, and shell material may also form a core. The surrounding envelope is constructed of a series of rings with a maximum thickness measured along the long axis and a minimum along

the short axis. This is the case in elliptical sections. In circular sections, the rings show a constant thickness. This thickness variation is suggestive of an ellipsoidal shape for the pisoliths, which is borne out by their shape when seen in hand specimen. Unlike the goethite ooids, the individual rings of the envelope are not concordant. Ring contacts are picked out by dark brown goethite, and this shows them to be hummocky or mammilated. This characteristic is most noticeable amongst the central rings. In pisoliths which are not composed entirely of goethite, it is found that some rings are entirely of fine-grained siderite, others of chamosite, and the outer rings of goethite. The chamosite is often an olive-brown in colour and shows a spotted extinction suggestive of a random distribution of individual flakes rather than an optically continuous material. There is no regular alternation of minerals forming each ring. It is interesting to note that other allochemical grains such as shell fragments and small ooids are incorporated within the pisolith envelope. These are oriented with their long axes tangential to the pisolith envelope. The presence of material of this origin and orientation is suggestive of some degree of movement by rolling of the pisolith, during growth stages. The fact that ring contacts are irregular, however, indicates that movement, if any, was spasmodic. If this were not the case, smooth contacts would be expected.

2.3.6.iii Intraclasts: Three intraclast types have been recognised within the calcitic limonite oolites. These allochemical grains are not abundant in the lithology; indeed, they tend to be rather sparsely distributed. This is in contrast to the observations of Davies and Dixie (1951) who

considered that this lithological type was composed dominantly of intraclasts derived by erosion from their ironstone Types A, B and C.

(a) Goethite-matrix intraclasts: Mineralogically these intraclast types are composed entirely of goethite in matrix and ooid phases. Calcite is occasionally present in the form of shell fragments. The matrix is identified as goethite on the basis of its optical similarity to the ooids which it surrounds. Grains of this type are approximately equidimensional and show a grain size variation of 1.0 - 1.5 mm. In shape they are rounded but somewhat irregular. This evidently results from the matrix being more susceptible to attrition than the ooids, for the ooids present form the outstanding areas of intraclast margin whilst the trough areas correspond to intraclast matrix.

(b) Biogenic calcite intraclasts: These are subdivided into intraclasts comprising several grains of the order of 1 mm across. The allochemical component of these consists of rounded bivalve and echinoid fragments. A very thin rim of dark brown goethite separates each grain. The stereome system of the echinoid fragments is infilled by the same material. The bivalve fragments may be non-ferroan in composition or of ferroan calcite, in which case they exhibit a fabric of inequigranular xenotopic calcite crystals. This results from post-depositional aragonite dissolution and replacement.

The latter type of carbonate intraclast is recognised as having been derived from a different area of deposition on the basis of a thin encompassing rim of goethite. There are two possibilities for the nature of this deviation; they were initially part of intraclasts of the former type which were broken down, or that they were removed from their area of deposition in the form which they occur with in this lithological type. Two forms of calcite are represented by these allochems: Non-

ferroan calcite showing primary structure and algal borings infilled with fine-grained goethite, and ferroan calcite which shows neither of these primary structures, but a fabric of inequigranular xenotopic calcite resulting from the post-depositional replacement of aragonite. If these grains were removed singly by erosion from their depositional areas, then the possibility that the goethite rim represents an oxidised rim of authigenic chamosite occurs. The same criteria that were applied to recognise this material in the case of ooids cannot be applied here as it has been shown that rims of authigenic chamosite around shell fragments are not always complete and commonly do not retain a constant thickness.

(c) Chamosite matrix intraclasts: These occur rarely in this lithological type. They comprise allochemical grains represented by complete and fragmentary goethite ooids, shell fragments and fragments of echinoid plates. The matrix is of an olive brown to brown fine-grained chamosite. This identification is made on the basis that occasional patches of fine-grained green chamosite occur which show a grey and white spotted appearance between crossed polars and grade imperceptibly into the more common matrix type which show the same characteristics between crossed polars. Such grains vary in size from 0.3 - 10.0 mm across. The smaller grains tend to be irregular with poorly rounded margins and entirely of chamosite. The larger are elongate to circular in shape and have more or less sharply defined margins. The elongate variety are often oriented with their long axis parallel to bedding. At the time of deposition of these intraclasts in the depositional area of calcitic limonite oolites the chamosite mud was evidently 'sticky'. This follows from the fact that allochemical

grains such as ooids may be found extending from the chamosite mud, but with only a very small contact area with it i.e. these grains adhered to the mud intraclast as it was transported. Small voids within the chamosite mud matrix are infilled by ferroan calcite. Davies and Dixie (1951) reported intraclasts of their Ironstone Types A, B and C to be present. This work can only positively identify intraclasts of Type C of these authors, although no siderite has been found.

2.3.6.iv Biogenic material: A variety of biogenic material occurs within the calcitic limonite oolites. It comprises abundant bivalve fragments and fragments of echinoid spines and plates. Crinoid ossicles, gastropods, belemnites and forams are less common.

Bivalve fragments have a size range of 0.25 - 15.00 mm, measured along their long axes. Occasional complete bivalve shells occur. Those fragments greater than 0.50 mm in length are oriented parallel or subparallel to bedding. Small fragments often show algal borings which may be infilled by fine-grained goethite, or rarely authigenic chamosite. Many shell fragments are surrounded totally, or in part, by a thin micrite envelope. Both calcite and originally aragonite shell fragments are present.

Calcite shell fragments are non-ferroan in composition. Often a fibrous structure to the shells can be seen. A common sectional type of this form is that of Gryphaea arcuata.

Originally aragonite shell fragments are replaced by shell-shaped areas of ferroan calcite which has an inequigranular xenotopic fabric. The mould required to retain the original shell shape was presumably formed by micrite envelopes.

Fragments of echinoid plates and spines are common. They are usually less than 0.5 mm across. Some degree of rounding is exhibited. The stereome system of these fragments is infilled by either fine-grained goethite, light green authigenic chamosite or ferroan calcite. In many cases a syntaxial overgrowth of ferroan-calcite around the echinoid fragment occurs. In cases where stereome systems are partially infilled with goethite or authigenic chamosite the echinoid fragment may be only partially surrounded by a syntaxial rim. In the cases of fragments whose stereome systems are totally blocked up by these two minerals, and which may also coat its outer surfaces, no syntaxial overgrowth is present. This is interesting with respect to the work of Evamy and Shearman (1965, 1969) who showed that growth of syntaxial rims occurred as a result of the calcite of echinoid plates providing nucleation sites for calcite precipitating from pore waters. In the case of echinoid fragments coated with goethite or chamosite such sites would be vastly diminished and nucleation could not occur. Where syntaxial rims are well-developed a partial envelopment of adjacent allochemical grains may occur.

Occasional forams and gastropods occur. The former are of non-ferroan calcite, the latter of ferroan calcite indicating their original aragonitic nature. The chambers of both groups are infilled with either fine-grained goethite, fine-grained chamosite and less commonly calcite cement. Very rarely authigenic chamosite occurs with a radial orientation within the chambers.

2.3.6.v Authigenic chamosite: The occurrence of this mineral and its nature has been discussed above in context of the ooids present. In addition, it is found in association with shell material. Here it is

ubiquitously associated with the ferroan calcite of orginally aragonite shell fragments,forming a complete rim around them. The outer edge may be irregular. The inner margin is usually sharp, corresponding to the original shell boundary. Irregularities in this may be ascribed to the infill of burrows within the fragment. Small siderite prism-shaped grains with a greenish colouration are often present within this authigenic chamosite. It is interesting to note that authigenic chamosite is rarely found in association with primary non-ferroan shell material.

2.3.6.vi Calcite cement: Two generations of calcite cement have been recognised:

'Prismatic'generation: This occurs (Plate 2.49) as growths of sub-prismatic calcite grains perpendicular to, and rooted on, non-ferroan calcite shell fragments. It is usually found where the micrite envelope to the shell is thin or absent. The majority of the prism terminations are irregular. In a number of cases the extinction of any one grain corresponds to the extinction of its neighbours.

Inequigranular xenotopic generation: This corresponds to the greater part of the calcite cement. The larger grains are often found to be syntaxial growths around echinoid fragments. The mutual boundaries between individual grains vary from being approximately planar or slightly rounded in the case of the larger grains, to being slightly serate to diffuse in the case of smaller grains.

2.3.6.vii Paragenesis: The textures described above show that the goethite ooids, pisoliths, intraclasts and calcitic and aragonitic biogenic debris can be defined as the primary constituents of the sediment. The remaining

phases are thus all diagenetic in origin. Consideration of the textures involving these phases allows a paragenetic sequence to be drawn up (Figure 2.38).

The nature of the explosion texture involving goethite ooids and authigenic chamosite indicates that this chamosite was one of the first authigenic minerals to precipitate. This follows from the fact that development of the texture involves a net increase in volume of the grain which does not show interference from other authigenic phases such as the inequigranular xenotopic calcite. Further evidence for the early precipitation of the authigenic chamosite is provided by echinoid fragments which are surrounded entirely or partially by a syntaxial overgrowth of calcite, and whose stereome systems are partly infilled by such chamosite. The precipitation of chamosite appears to have continued until the syntaxial calcite crystallised. This follows from the fact that authigenic chamosite only occurs in the echinoid stereome system, but never around the edges of the grain. As with the occurrence of these textures in other facies it is thought that the chamosite precipitated from aqueous solution.

It is necessary to explain the ubiquitous association of authigenic chamosite with originally aragonitic shell fragments and its absence as a surround to calcite shell fragments. Many calcite shell fragments exhibit a radial fibrous growth of ferroan calcite which shows a relict prismatic structure. By analogy with Recent sediments it seems likely that this type of calcite represents an original radial fibrous growth of high-magnesian calcite which subsequently inverted to low-magnesian ferroan calcite. The presence of such a growth would clearly prevent authigenic chamosite from precipitating on these grains. On this basis, therefore, it may be concluded that an authigenic chamosite rim to

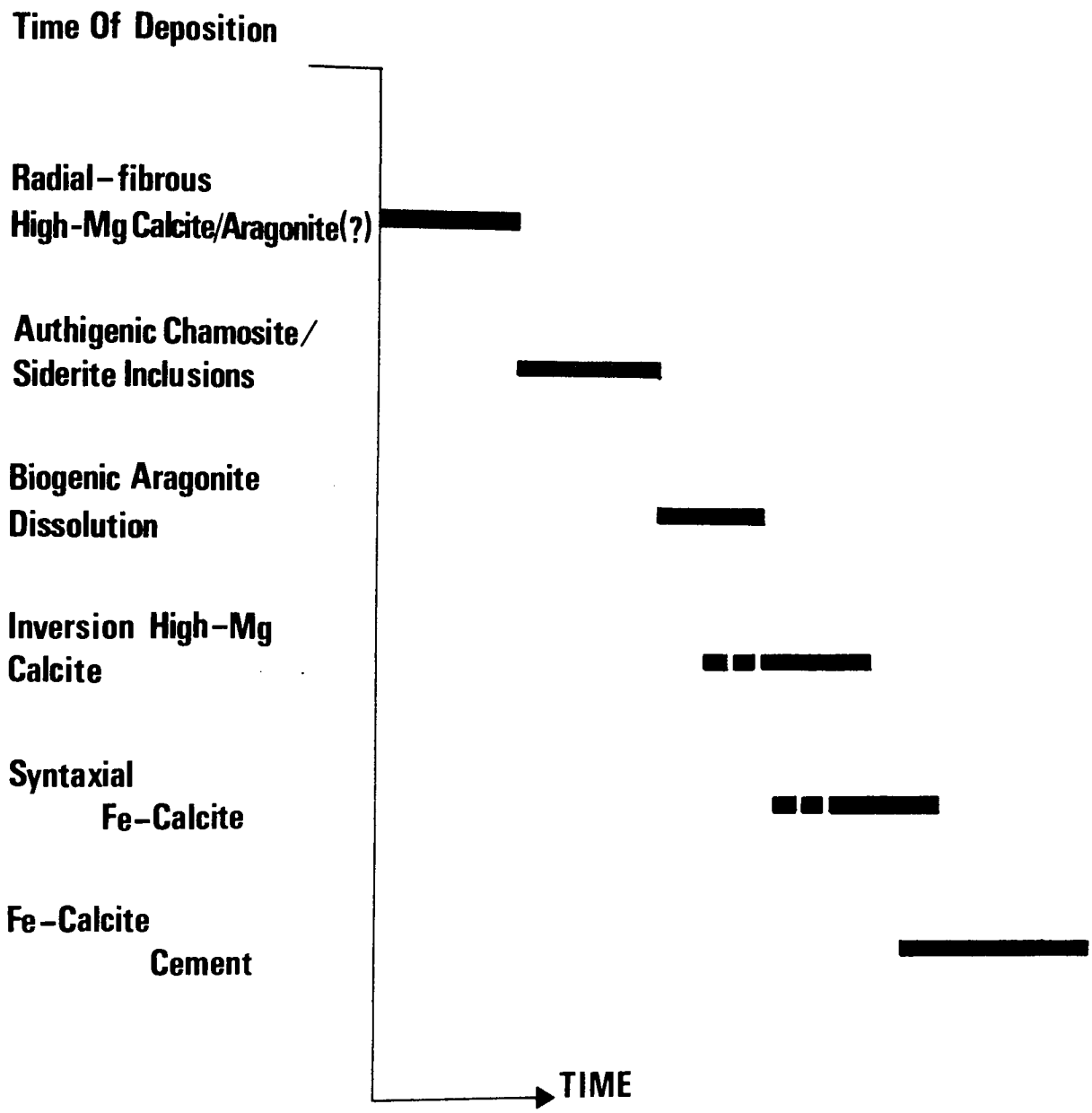

Figure 2.38: Paragenesis Of The Calcitic Limonite Oolites

original aragonite fragments was deposited in the absence of a radial-fibrous generation. This may well reflect the primary shell mineralogy; many Recent calcite shells exhibit an outer coat of high-magnesian calcite whereas aragonite shells do not. Clearly, this is evidence for the above hypothesis; a radial fibrous growth of high-magnesian calcite would be expected on the former shell type but not on the latter. It has been noted that small laths of greenish siderite occur within authigenic chamosite rims to originally aragonite shell fragments. These may represent a very poorly developed aragonite radial fibrous growth to this shell type which was enveloped by authigenic chamosite. Dissolution of the aragonite contemporaneously with the chamosite precipitation would lead to the prism being replaced by siderite, in the presence of abundant ferrous iron, and the inclusion of small particles of authigenic chamosite.

The overgrowths to echinoid fragments indicate that crystallisation of this calcite generation continued until the final consolidation of the lithological type. Evidence for this is given by the nature of the syntaxial overgrowth outer boundaries which are in contact with those of grains of inequigranular xenotopic calcite and very similar to the boundaries between crystals of this calcite.

The first generation of cement calcite comprises the sub-prismatic growths found rooted on non-ferroan calcite shell fragments which lack a micrite envelope. The unit extinction exhibited by a number of these grains and the absence of well-developed prism terminations suggests that the calcite is replacive. The origin of this generation has been discussed above.

The final diagenetic phase is represented by inequigranular xenotopic calcite which infills the remaining voids in the rock, leading to final consolidation. Individual crystals abut against prisms of the earlier sub-prismatic generation thus post-dating this phase.

Some textures allow the dating of the dissolution of aragonitic material. Bathurst (1975) notes that in order for an aragonite shell fragment to be replaced the secondary porosity created by its dissolution must be protected by a micrite envelope. Some shell fragments in the calcitic limonite oolites, that have inverted from aragonite, are found to have such an envelope. Others are surrounded, instead, by a rim of authigenic chamosite. Thus, aragonite shell fragment dissolution and the creation of a secondary porosity post-date the precipitation of an authigenic chamosite coating. The subsequent replacement of the secondary porosity by the ferroan calcite follows this.

2.3.7 Bioclastic Limestone

Petrographically this facies is precisely the same as the calcitic limonite oolites except that the textures involving limonite ooids are absent. Authigenic chamosite is occasionally present.

2.3.8 Red Oolites

The field study has shown the occurrence of red oolites having all the textural characteristics of chamosite mudstones, chamositic limonite oolites and calcitic limonite oolites. Red equivalents of non-red chamosite bearing lithologies contain insignificant quantities of chamosite. They do, however, contain large amounts of fine-grained goethite which, on the basis of its textural forms, represents an

oxidation product of depositional chamosite. Fine-grained goethite having textural forms analogous to authigenic chamosite does not occur. Abundant eye-shaped subhedra of siderite less than 0.03 mm in length characterise the majority of red 'chamosite' mudstone and red oolite sections. Clearly, the importance of these ironstone types is to be found in the nature of their post-depositional mineralogy.

2.3.8.a Red 'chamosite' mudstone: This is constructed of a mixture of approximately 50% fine-grained goethite and approximately 50% eye-shaped siderite subhedra (Plate 2.50). Within this irregular quartz grains, as described above, occur concentrated in burrows and laminations. The goethite is dark brown and exhibits a faint bulk pleochroism, the limits of which occur when bedding is parallel to the north-south and east-west cross-hairs. The siderite subhedra are generally oriented with their long axes parallel to bedding. Although occasional equant siderite anhedra are present trains of the type described above are not present.

Ferroan calcite is sparsely distributed, generally occurring as a cement in quartz-filled burrows and quartzose laminations. It does, however, occur in two minor but important textures with goethite. The first of these is a radial fibrous fabric surrounding the occasional shell fragment and foram test. The individual 'fibres' of calcite are not in contact with each other along their edges, but are separated by a thin wall of goethite. The second is rather more important in context

of the environment which led to the formation of these red ironstone types. Discontinuous stringers of goethite, usually less than 0.2 mm thick, are separated by elongate lenses of ferroan calcite (Plate 2.51), of a similar width. The fabric of this calcite is sub-prismatic in that it comprises a series of sub-parallel calcite crystals with slightly irregular mutual contacts at right angles to the goethite stringers. The boundaries between individual calcite crystals are picked out by a thin goethite layer.

The only other carbonate mineral present is ferroan dolomite. This forms occasional rhombs within the goethite.

It is difficult to establish the precise order of events which led to the formation of red mustones with the above characteristics. The goethite present shows a close textural similarity to the depositional chamosite of chamosite mudstone. It is suggested, therefore, that the goethite represents oxidised depositional chamosite. In chamosite mudstones and chamositic limonite oolites shell fragments and foram shells are surrounded by radial fibrous ferroan calcite, the individual prisms of which may be separated by a filament of authigenic chamosite. Since a similar texture occurs in red 'chamosite' mudstones in which goethite takes the place of chamosite, it follows that such a radial fibrous texture developed prior to chamosite oxidation. The presence of ferroan dolomite rhombs may be related to this texture. If the radial fibrous material was originally high-magnesian calcite its inversion would release magnesium which could subsequently precipitate as dolomite. In the presence of dissolved ferrous iron this would be ferroan in composition. The greater stability of calcite over dolomite would lead to its pseudomorphing

original magnesian calcite. Exposure and dessication of a mud would be expected to bring about shrinkage and hence the development of an internal porosity preferentially parallel to bedding. Lenticular portions of ferroan calcite separating goethite stringers are thought to represent an infill to such a porosity. The normal fabric of porosity filling calcite is inequigranular xenotopic. The fabric of the calcite in this texture is broadly prismatic. The formation of calcite as a result of the upward percolation and evaporation of calcium-bearing interstitial waters in subaerially exposed sediment to form caliche has been documented by Swineford et al (1958). These workers have recorded prismatic calcite of the type described above. In context of the field relationships and mineralogy of the red mudstones it seems likely that such calcite represents subsurface caliche formed during chamosite mudstone exposure. It is not possible to date the time of precipitation of the eye-shaped siderite subhedra or its cessation. They exhibit no evidence of partial oxidation such as iron-staining which might be expected had they been present at the time of subaerial exposure. Thus their precipitation must have occurred at some later date. The remaining porosity, such as that due to the activities of burrowing organisms is infilled by ferroan calcite with an inequigranular xenotopic fabric. Figure 2.39 shows the paragenesis of the various mineral generations present.

2.3.8.b Red 'chamositic' limonite oolite: The textures shown by the matrix of these oolitic types confirm that the fine-grained goethite, which is the dominant matrix mineral, is an oxidation product of pre-existing depositional chamosite. Lenses and burrows containing little allochemical material are characterised by a zonation in which fine-grained goethite forms their outer portions and surrounds a core

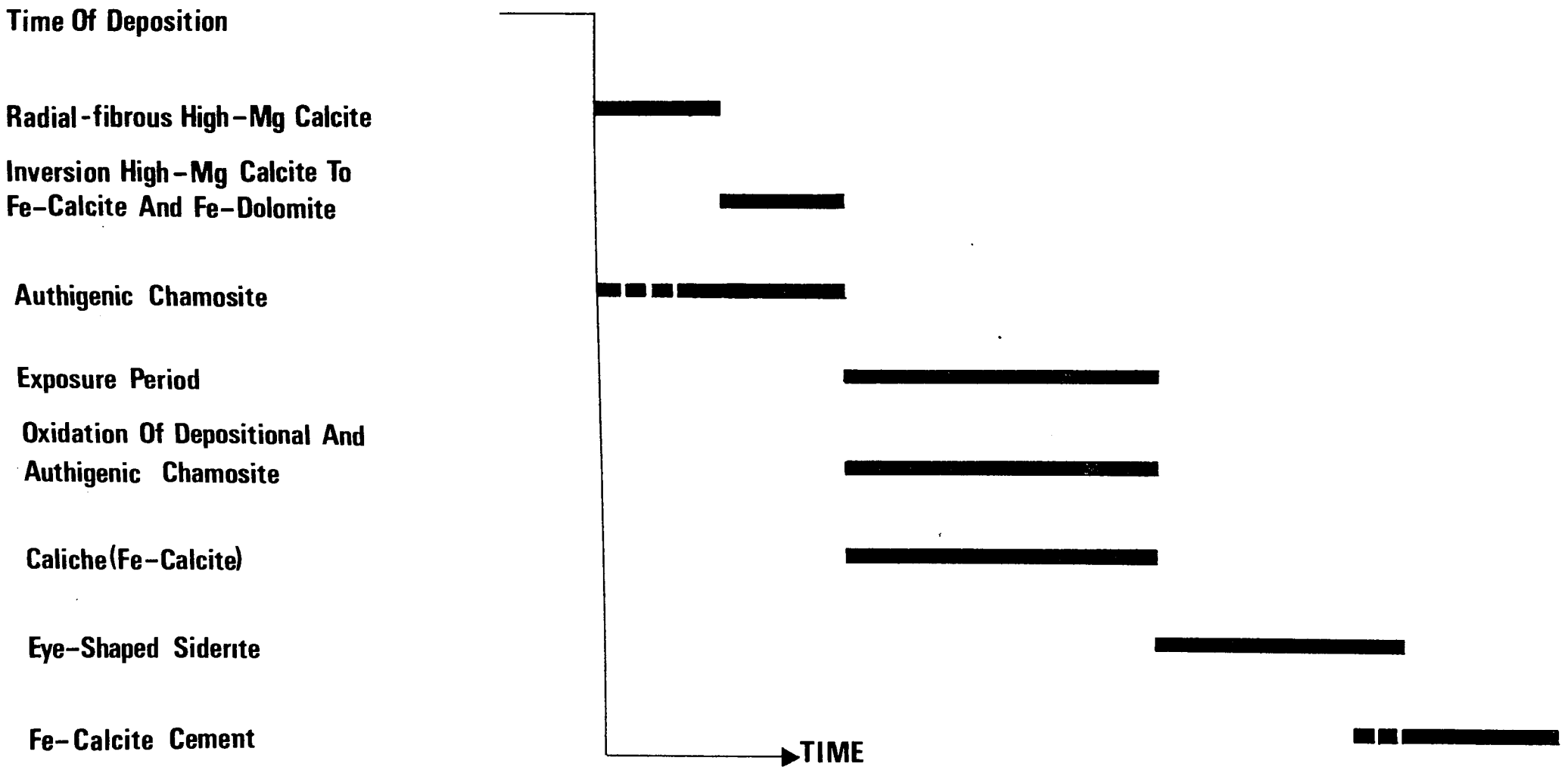

Figure 2.39: Paragenesis Of The Red 'Chamosite' Mudstones

of brownish chamosite. There is a gradational contact between them. Whilst the goethite shows only a very faint bulk pleochroism that of the chamosite is more distinct. In allochem-rich areas (Plate 2.52) goethite is the dominant matrix mineral, chamosite being absent. Both the goethite and chamosite contain abundant eye-shaped siderite subhedra. Fine-grained goethite coats shell fragments and infills echinoid stereome systems.

Ferroan calcite infills the porosity with an inequigranular xenotopic fabric. It is interesting to note that original aragonitic shell fragments, whose margins are defined by a thin line of goethite, have been replaced by ferroan calcite which also has this fabric type and commonly transgresses the original shell boundaries to partake in the cement calcite fabric.

The post-depositional history of the red 'chamositic' limonite oolites is relatively simple. Prior to their exposure authigenic chamosite precipitated around some shell fragments and in the stereome systems of echinoids. Dissolution of aragonite and the creation of a secondary porosity occurred prior to, during,or after exposure. Following exposure all the authigenic chamosite and the depositional chamosite interstial to allochemical grains was oxidised to chamosite. In the cases of chamosite mud lenticles and burrows oxidation was most intense in the outer portions and its effect diminished inwards. Thus an outer zone of goethite followed by a brownish chamosite was created. The chamosite colouration is probably indicative of partial oxidation as chamosite from environments where oxidation was inoperative e.g. chamosite mudstone is green. At some later date eye-shaped siderite subhedra precipitated. For the reasons noted above it is likely that

this occurred after cessation of subaerial exposure. Ferroan calcite infilled the remaining porosity. Since the ferroan calcite aragonite replacement crystals have intercrystalline boundaries with those of the fabric of the ferroan calcite cement its precipitation occurred at the same time. Figure 2.40 indicates the sequence of events in this lithology.

2.3.8.c Red calcitic limonite oolite: Unlike non-red calcitic limonite oolites the cement in these oolitic types is not entirely calcite but consists of a variable intermixture of ferroan calcite, eye-shaped siderite subhedra and fine-grained interstitial goethite (Plate 2.53). The relative proportions of these cement generations vary from 33% calcite, 33% siderite and 33% goethite to 80% siderite and 20% goethite, calcite being absent, to 80% calcite and 20% siderite, from which goethite is absent. The fine-grained interstitial goethite is probably responsible for the pink cement colouration seen in hand specimen.

The characteristic texture found in this lithology involves the distribution of ferroan calcite around goethite ooids. In areas where ferroan calcite is absent from the surrounding cement it is found to occur as a very thin band along the contact points of ooids (Plate 2.54). Occasionally, ferroan calcite may form a thin-non-replacive coating to these grains (Plate 2.54). Where ferroan calcite is present in the bulk of the cement its occurrence at ooid contacts is slightly more extensive, forming a wedge of cement to either side of the contact. The junction of these wedges with the cement is meniscus shaped (Plate 2.54), the meniscus being concave towards the ooid contact. No siderite or goethite is present within such calcite, which are unit grains. Dunham (1971) has

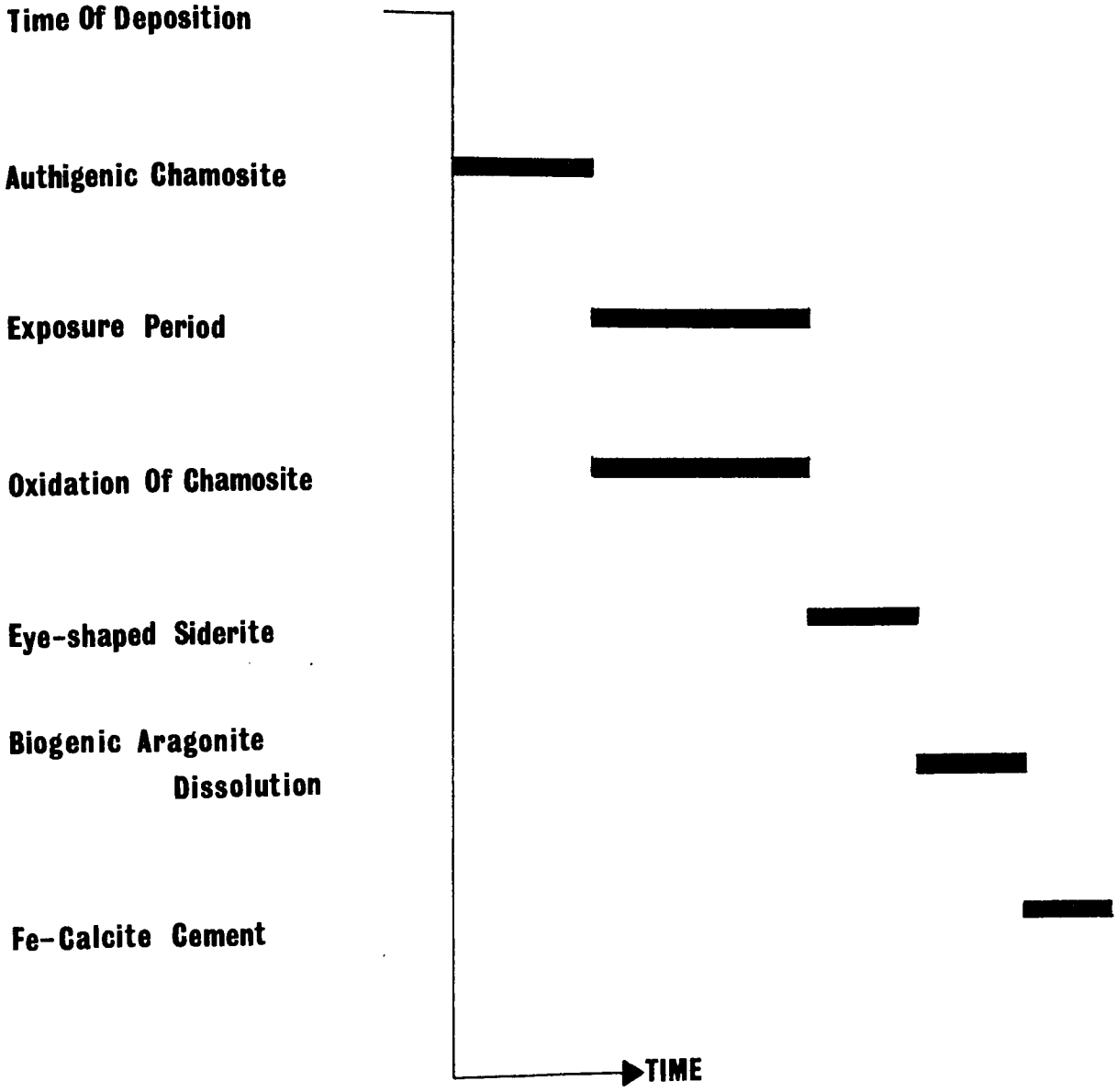

Figure 2.40:Paragenesis Of Red Chamositic Limonite Oolites

proposed that meniscus-shaped pore-cement interfaces are characteristic of precipitation within the vadose zone from water localised around the points of grain contact.

The paragenetic sequence in the red calcitic limonite oolites is very simple. On the basis of the work of Dunham (1971) the meniscus-shaped ferroan calcite is thought to represent the first cement generation, precipitated in the vadose zone at the time of subaerial exposure of the unconsolidated sediment. The precise origin and mineralogical precursor of the fine-grained goethite is unknown, but since it is a ferric mineral it may well have formed during subaerial exposure. Since siderite is a ferrous mineral it is likely that the eye-shaped siderite subhedra precipitated at some time after subaerial exposure. The remaining porosity was infilled by ferroan calcite with an inequigranular xenotopic fabric. Figure 2.41 shows the order of cement mineral precipitation.

2.4 SUMMARY

The Frodingham Ironstone represents a series of facies thought to represent the deposits of the shelf-shore face transition zone. Shoal areas in the deeper areas form the site of chamosite ooid and mud formation. Periodic destruction of these shoals yields ooids and mud for transport. Much of the chamosite mud is transported to deeper areas where it forms a chamosite mudstone facies. Quartz from other sources is also concentrated in this area. The rest of the chamosite mud and the chamosite ooids are transported towards the shore and are separated

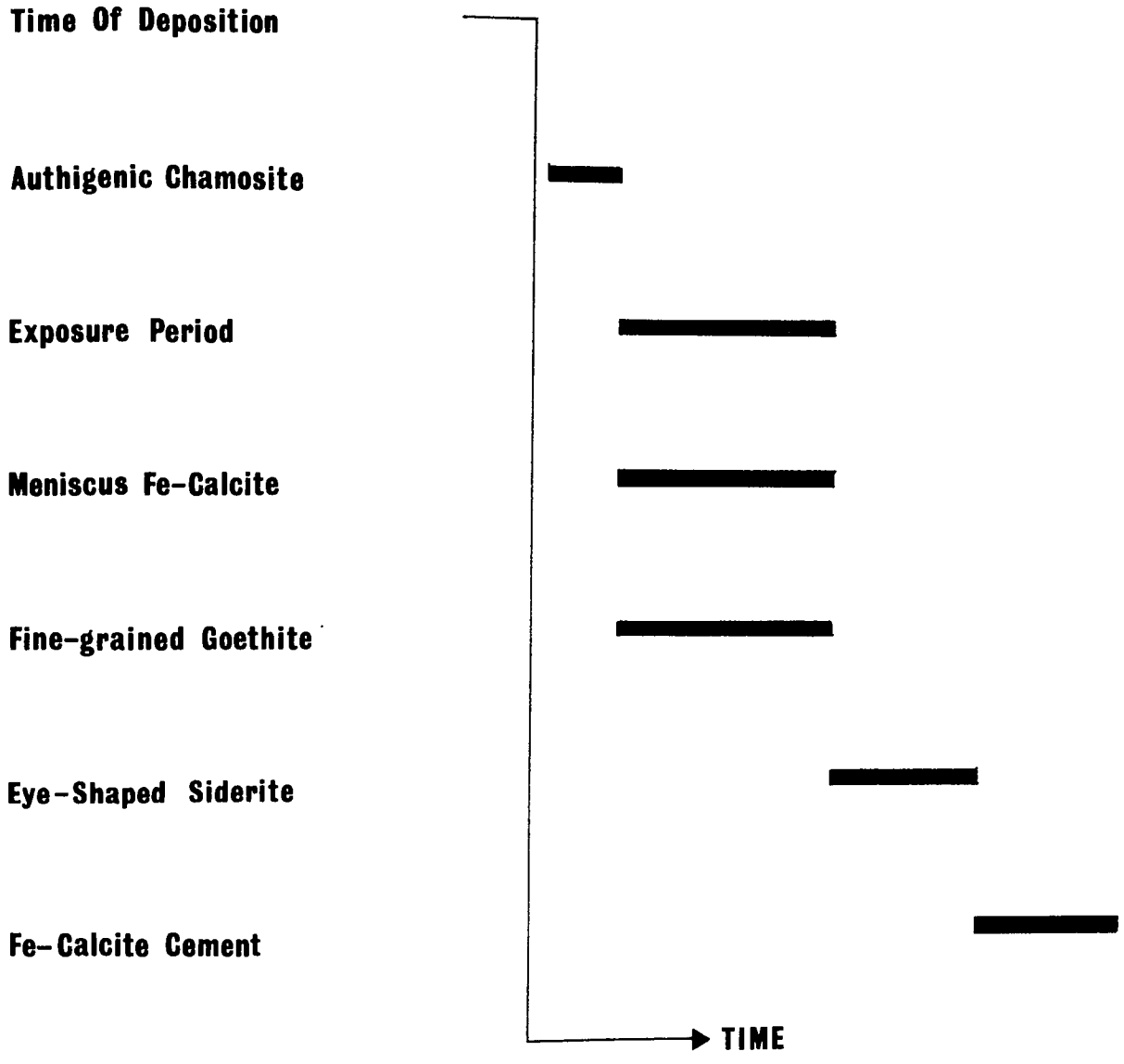

Figure 2.41:Paragenesis Of The Red Calcitic Limonite Oolites

into chamositic limonite oolite, calcitic limonite oolite and bioclastic limestone facies. The transport results in oxidation of the chamosite ooids to goethite. An increasing degree of winnowing with increasing current strength shorewards causes concentration of the chamosite mud within the chamositic limonite oolite facies. This facies is extensively colonised by epifauna and infauna. These provide shell-fragmental material for transport into the facies of calcitic limonite oolites and bioclastic limestones. Twice during the history of the ironstone widespread exposure caused reddening of those facies which were exposed.

The petrography of the ironstone indicates that each depositional facies may be characterised by a diagenetic mineral assemblage and textures formed as a result of burial and cement precipitation. The presence of diagenetic facies; the sideritic chamositic limonite oolites, and red oolites are indicated. In each facies a common trend in the order and chemistry of cement phases is evident. The first phase is the precipitation of authigenic chamosite, the second siderite and the third, ferroan calcite. The first two may overlap to some degree. The petrographic examination of the ooids indicates that they are formed in the shoal areas of chamositic chamosite oolite as chamosite ooids. There is some evidence of micro-organism influence in their formation. Transport and oxidation results in the formation of goethite ooids. Incomplete oxidation forms ooids composed of goethite and chamosite which are restricted to the chamositic limonite oolite facies.

CHAPTER 3

THE MARLSTONE ROCK-BED IRONSTONE

THE MARLSTONE ROCK-BED IRONSTONE

3.1 INTRODUCTION

The Marlstone Rock-bed crops out along the strike of Domerian strata from the Dorset coast in the south to the River Humber in the north-east. It is best known, however, in the Banbury and Leicestershire-Lincolnshire districts where it has been exploited as an iron ore and as a building stone. Figure 3.1 shows the outcrop of the Marlstone Rock-bed.

The Marlstone is approximately restricted to the Spinatum zone of the Domerian (Figure 1.1). In the Stowell Park borehole (Figure 3.1), however, its deposition appears to have commenced in the preceeding Margaritatus zone (Bull. Geol. Surv. G.B., 1956). In the Leicestershire-Lincolnshire district the Marlstone is divisible into an upper ironstone unit and a lower chamositic sandstone unit, the Sandrock. There is a notable thickness variation along the outcrop of the Marlstone: On the Dorset coast it is 0.20 m thick, in Oxfordshire thicknesses of 2.00m have been reported, increasing to 7.00m in the Banbury area and in Leicestershire the Marlstone reaches a thickness of 5.62 m at Tilton. Further north, in Lincolnshire, thicknesses of around 7.50 m occur. In contrast, the time-equivalent strata of Raasay are approximately 42.00 m thick. Thus, the Marlstone Rock-bed represents a period of much reduced deposition in east, central, and southern England during Spinatum times. Hallam (1966) concludes that the Marlstone is a condensed sequence.

The nature of the sequence above and below the Marlstone Rock-bed is fairly well-known. The sediments deposited prior to the Marlstone represent an overall shallowing phase: Mudstones are succeeded by

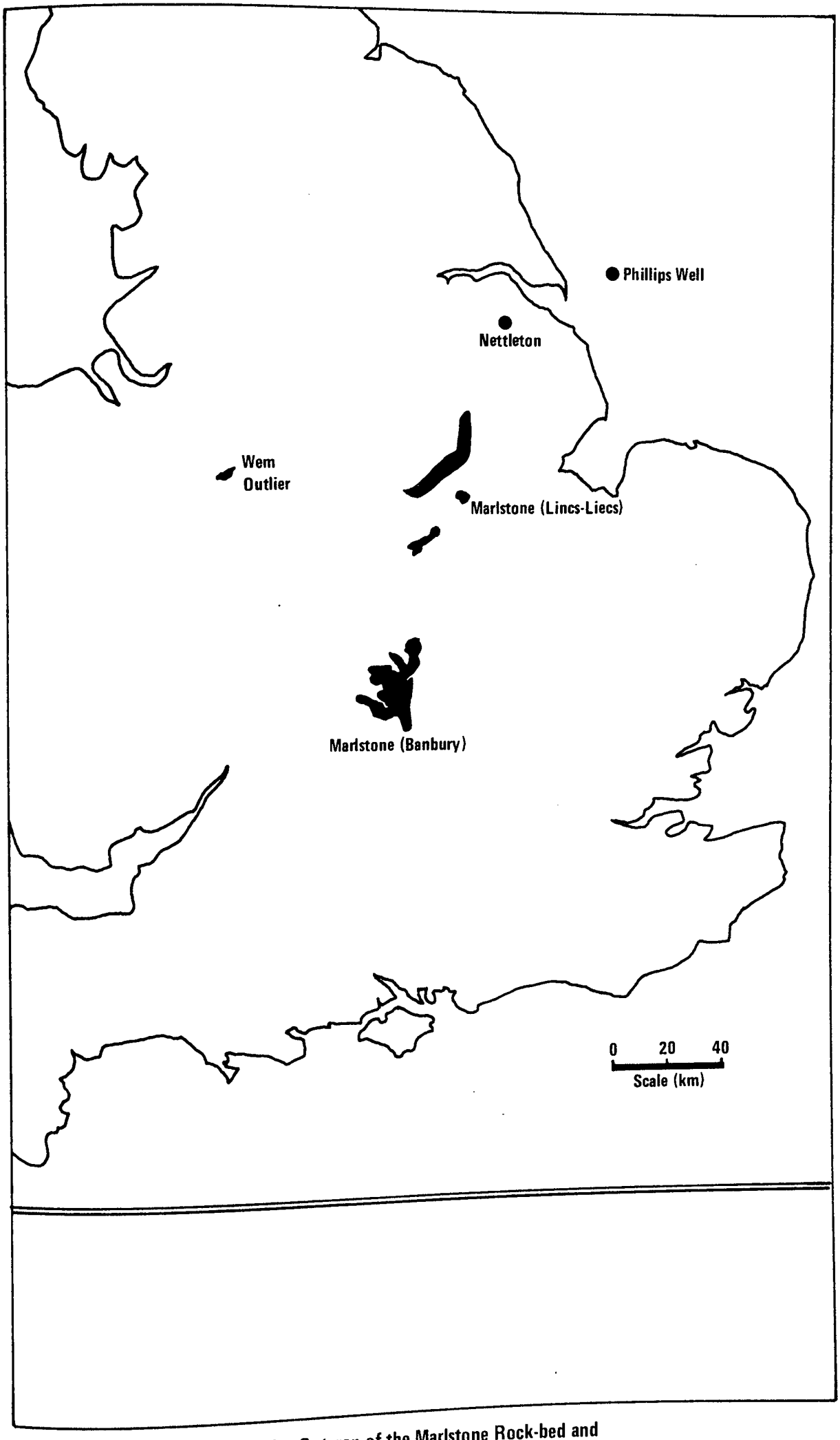

Fig 3.1 Outcrop of the Marlstone Rock-bed and position of The Phillips Well

mudstones and argillaceous limestones, and these by local sandstones such as the Sandrock. A major transgression at the beginning of the Toarcian brought ironstone deposition to an end and saw the commencement of bituminous shale deposition (Hallam and Bradshaw, 1979).

3.2 FORM AND NATURE OF THE IRONSTONE

The Marlstone Rock-bed has been examined at outcrop in the Banbury, Leicestershire, and Lincolnshire districts. In addition it has been studied in the Nettleton Quarry core. Figure 3.2. shows the sites of these localities.

The ironstone has been logged in the greatest detail possible at these locations. This has shown that the Marlstone can be divided into four different facies. Individual graphic logs of the sections examined are presented in Figure 3.3. Due to the distances between localities and the fact that the top and bottom of the Marlstone was rarely seen, a correlation between them has not been attempted.

3.2.1 Thickness Variation

In addition to the field study of the Marlstone Rock-bed a literature survey was carried out in order to collate all the reported thicknesses of the Marlstone and Sandrock with a view to revealing any major thickness trends. These data are presented in Figure 3.4. As expected the data points are distributed along a NNE-SSW line corresponding to the Domerian outcrop. The only exceptions to this are the Wem-Audlem outlier and the North Sea well data.

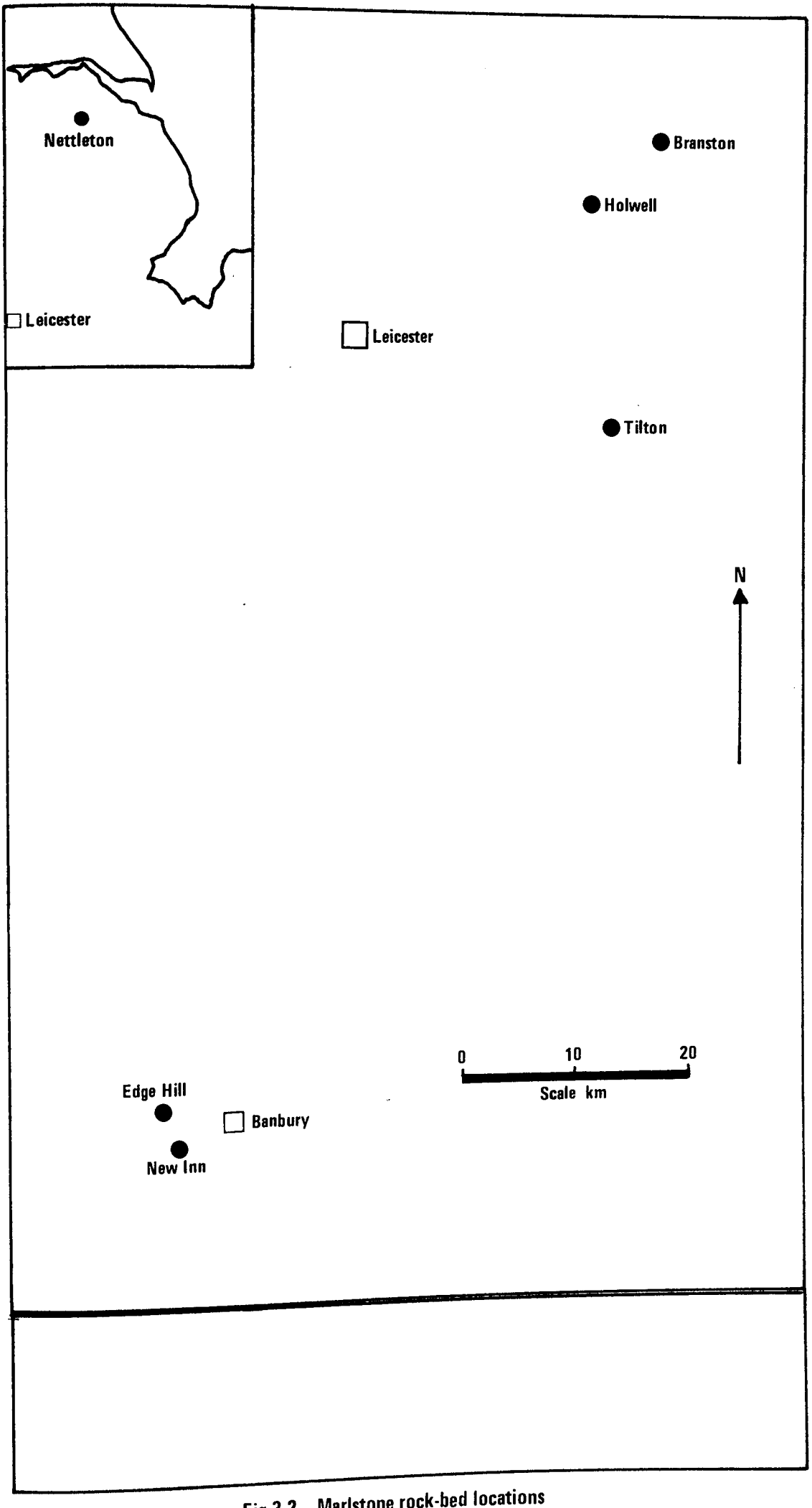

Fig 3.2 Marlstone rock-bed locations

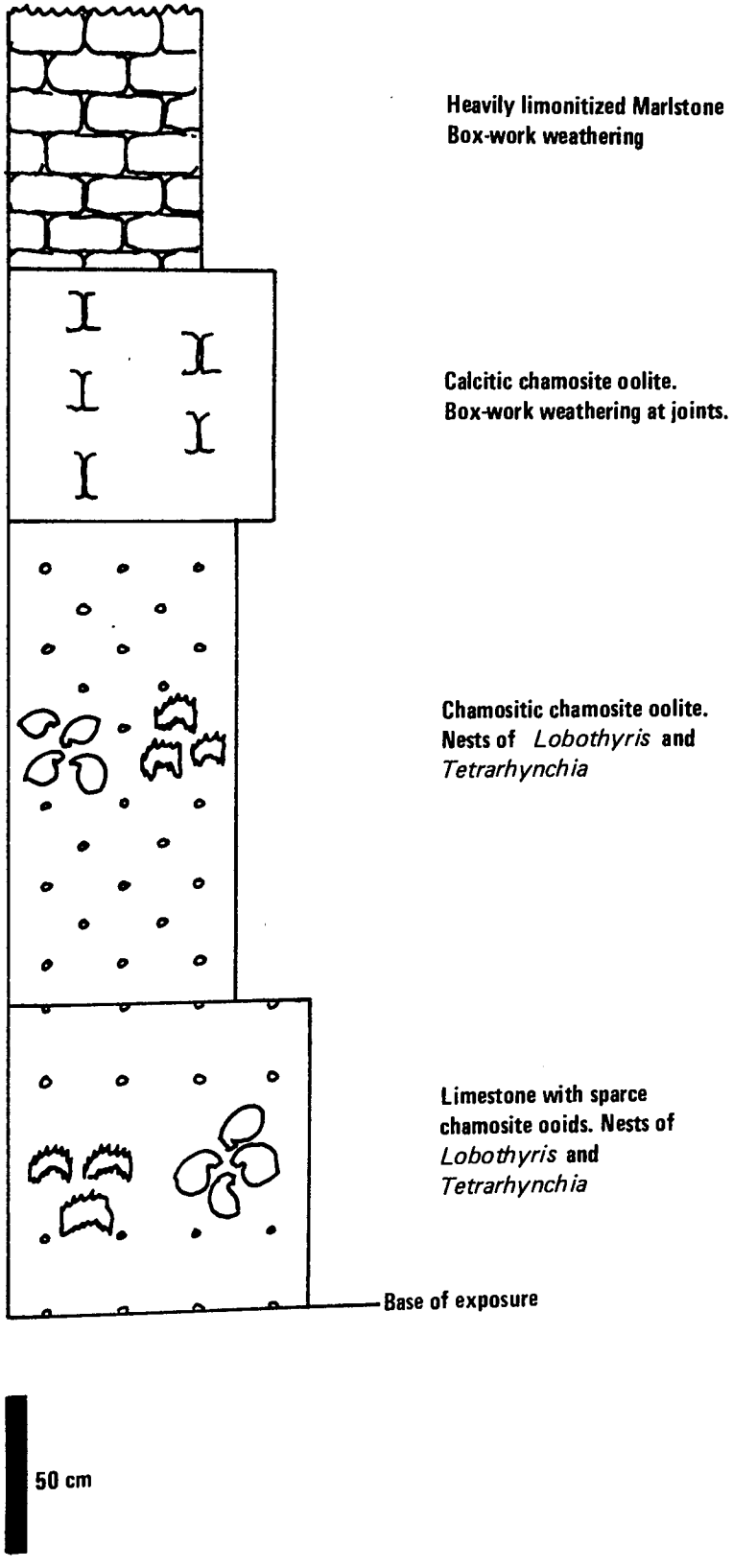

Fig 3.3a Branston Quarry (806, 290)

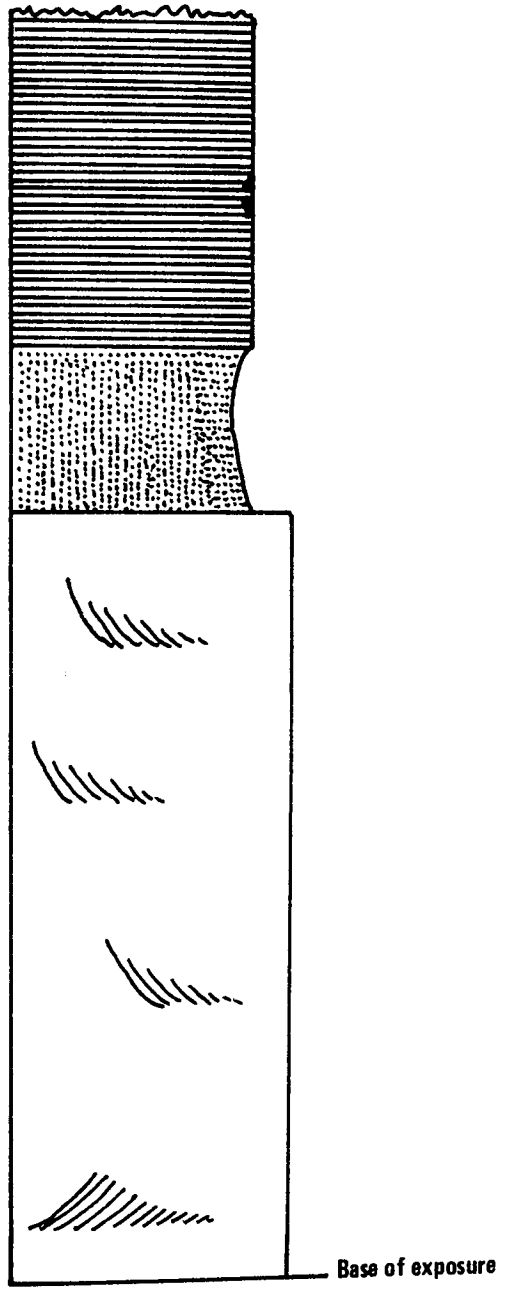

Fig 3.3b Browns Hill Quarry, Holwell (743,237)

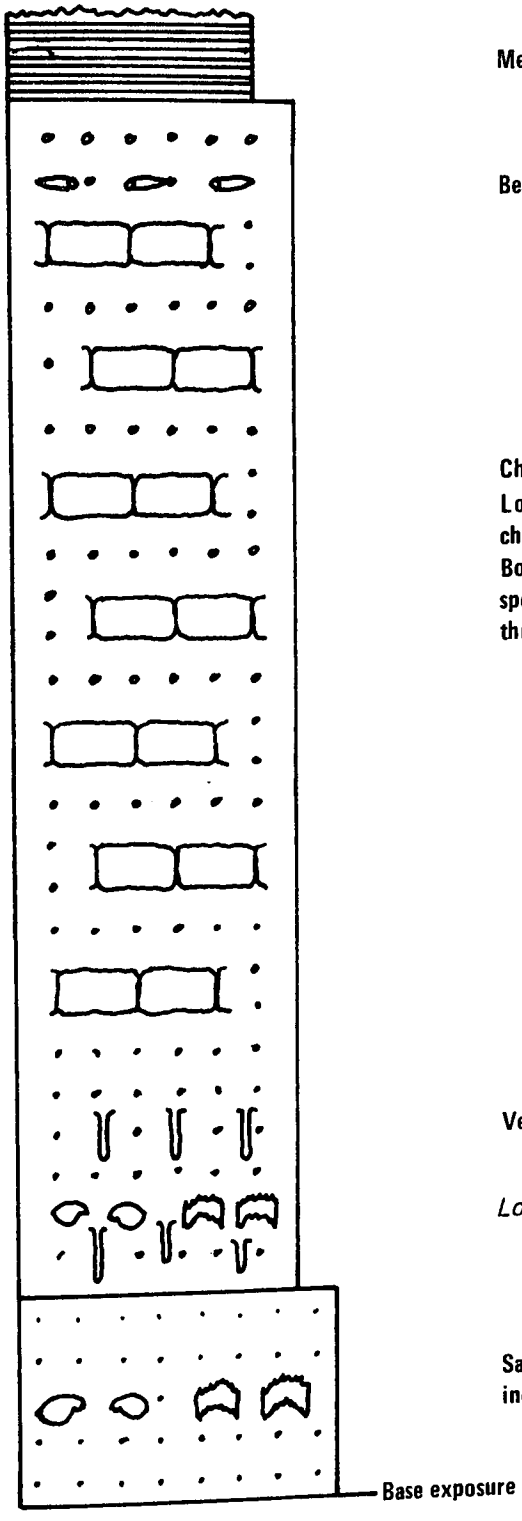

Fig 3.3c Tilton Railway Cutting (761, 057)

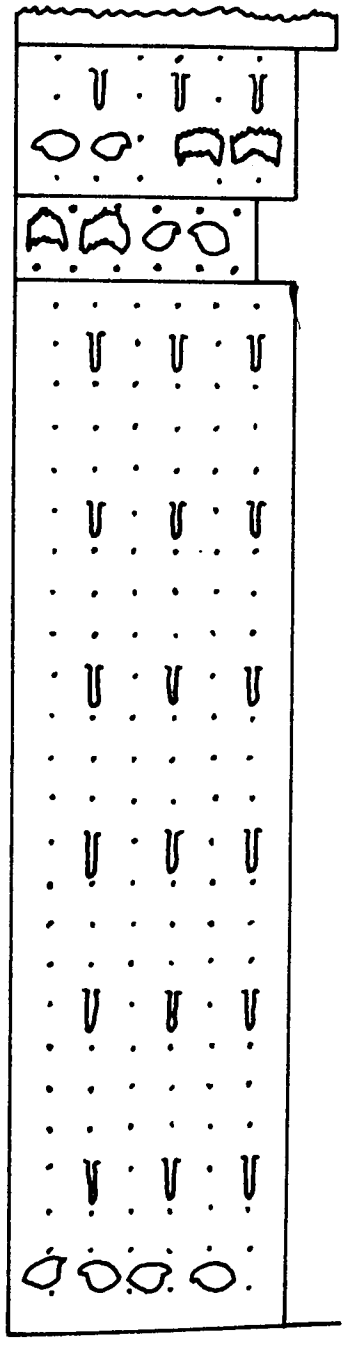

Limestone

Calcitic chamositic chamosite oolite.
Lobothyris and *Tetrarynchia.*
Chamositic chamosite oolite.
Lobothyris and *Tetrarynchia*

Calcitic chamositic chamosite oolite.
Burrows infilled with chamosite ooids common.
Sporadic patches of chamosite mud.
Lobothyris at base of exposure.

Base of exposure

50 cm

Fig 3.3d Ratley Quarry, Edge Hill (372, 471)

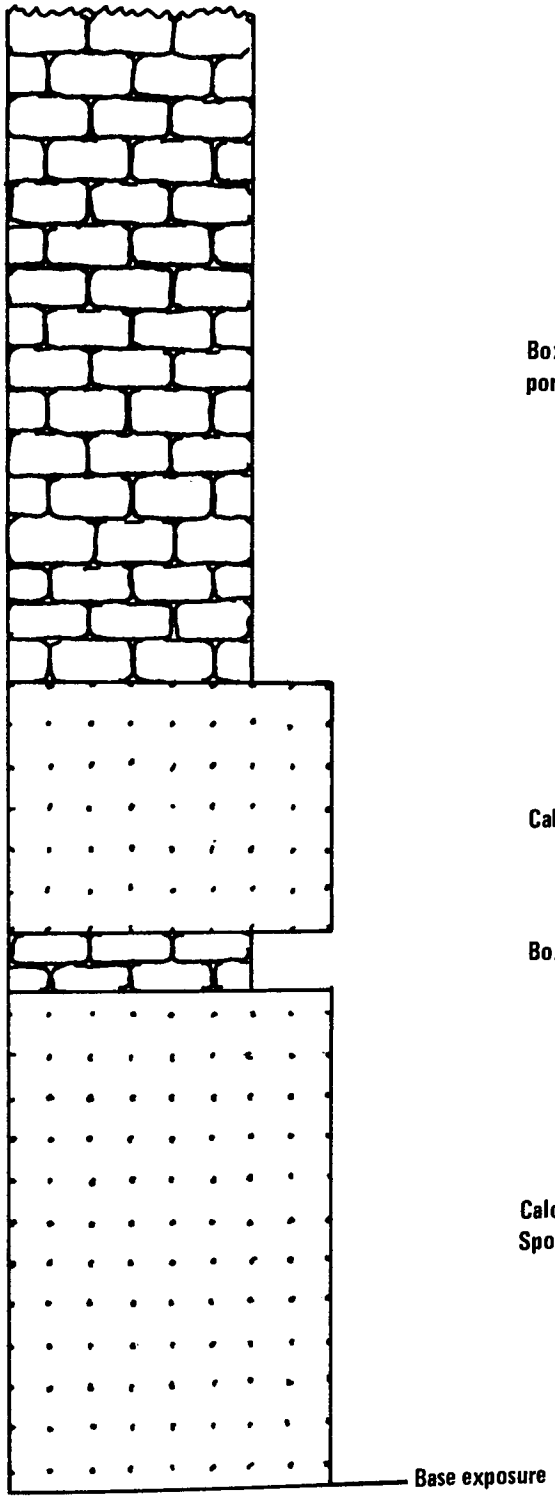

Fig 3.3e New Inn (386, 435)

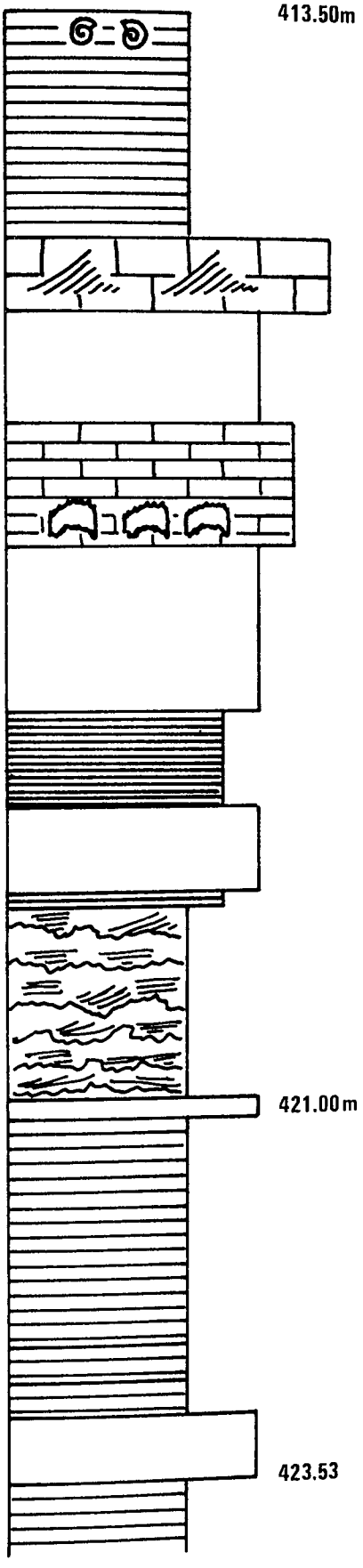

413.50m

Grey-green chamositic (?) micaceous siltstone.
Tiltonoseras sp. at top. Quartzose.

Biosparite with foreset lamellae defined by chamosite ooid concentrations. Quartzose.

Chamositic chamosite oolite.

Calcitic chamosite oolite. Abundant *Lobothyris* and *Tetrarynchia* debris. *Tetrarhynchia* nest at base.

Chamositic chamosite oolite.

Light green chamosite mudstone.

Chamositic chamosite oolite.

Chamosite mudstone.

Grey-green chamositic quartzose siltstone.
Six erosion surfaces.
Plane and foreset lamellae between.

421.00m

Pyritic chamositic chamosite oolite.

Light grey clay.

Light grey-green mudstone.
Grey clay with abundant chamosite ooids.

Chamositic chamosite oolite.

423.53

Light grey massive mudstone

1m

Fig 3.3f Nettleton Marlstone (413.50m – 421.00m)

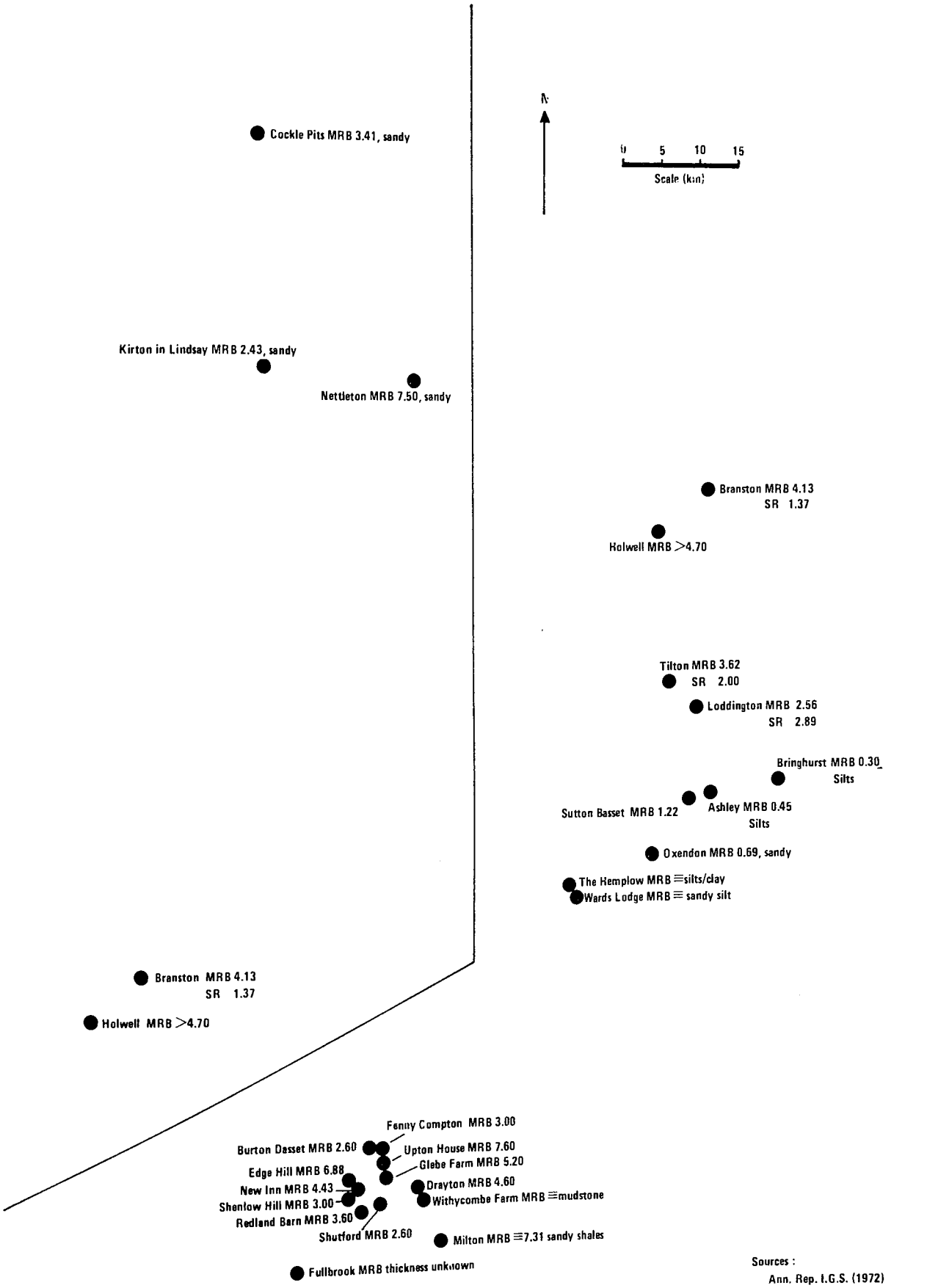

Sources :

Ann. Rep. I.G.S. (1972)
Bull. Geol. Surv. G.B., (1956)
Edmonds and Wilson (1965)
Hallam (1968)
Hollingworth and Taylor (1951)
Howarth and Rawson (1965)
Poole et al. (1968)
Richardson et al. (1946)
Taylor (1949, 1963)
Whitehead et al. (1952)

Fig 3.4 Collated Marlstone Thicknesses

At the most northerly data point, Cockle Pits, the Marlstone is 3.41 m thick and sandy throughout (Ann. Rep. IGS., 1972). Passing south from here it thins to 2.4 m at Warlaby (Bull. Geol. Surv. G.B., 1979) before thickening to 7.50 m at Nettleton. As shown in Figure 3.3 the Nettleton Marlstone comprises a dominantly sandy sequence within which bed of ironstone are present. The type locality for the Marlstone and Sandrock is at Tilton in Leicestershire where these units are 3.62 m and 2.0 m thick, respectively. At Ashley the Marlstone is 0.45 m thick and overlies silts. In the region of Market Harborough the Marlstone passes into thin ironstone bands within clays and locally may be entirely absent the Spinatum zone being represented by silts less than 1.0 m thick, such as at The Hemplow. The Marlstone reappears in the Banbury district where it exhibits thicknesses of 7.0 m such as at Edge Hill. In this area the Marlstone rests on Margaritatus zone clays silts. In the Stowell Park borehole (Bull. Geol. Surv. G.B., 1956) the Marlstone is 1.77 m thick and rests on sands of the Margaritatus zone which may be chamositic and contain beds of ironstone. To the west in the Wem-Audlem outlier of Cheshire Margaritatus zone clays and sands pass up into approximately 3 m of Marlstone. In the North Sea the Phillips 47/15-1 well has intersected 1 m of strata which yields a Domerian microfauna. These strata comprise silty shales passing gradually into siltstone which is overlain by a prominant band of sandstone containing chamosite ooids (Rhys, 1974). Other wells in this area provide similar data.

Unfortunately the distribution of data points does not allow a useful isopachyte map to be constructed. Thus, only a qualitative analysis can be carried out. Passing from Nettleton to The Hemplow the quartz component diminishes in importance from being present

throughout the greater part of the sequence to being restricted to the Sandrock beneath the Marlstone, to being absent. In contrast, the Marlstone or ironstone component increases in importance from occurring as a series of thin, separated beds to forming a thick bed which then thins to nothing. The disappearance of an underlying Sandrock is accompanied by the appearance of Spinatum zone silts on which the Marlstone rests. An interesting feature of the data is that this sediment distribution is mirrored by the sediments to the south west of The Hemplow. Figure 3.5 is a ribbon diagram illustrating this analysis. Hallam (1968) has briefly described this sediment distribution and illustrated it with a kite-diagram (Figure 3.5 inset).

Hallam (1968) considers that the only factor which needs to be invoked to account for the thinning of the Marlstone is condensation. The distribution of spinatum zone sediments reported above, however, suggests that a more involved explanation may be required. The sediments were deposited on the East Midland shelf (Figure 3.6). Their depositional area was limited to the north by the Market Weighton block. Evidence for this is provided by their northward thinning from Nettleton to Worlaby and Cockle Pits. To the east, the edge of the East Midland shelf is formed by the Dowsing fault which is down-thrown to the east. Data from wells between the East Coast and this fault show the presence of a zone of Domerian sediments having the characteristics of those in the Phillips 47/15-1 well (Rhys, 1974). These are of the order of 1 m thick. To the south east and south the London-Brabant massif occurs. The sediments of the Market Harborough area appear to be closest to the most northerly point of the massif. In the west the Pennine block occurs. Palaeogeographical reconstructions of this block vary from it being completely absent during

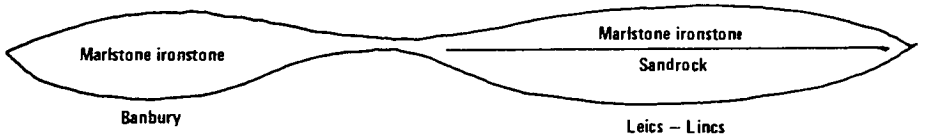

Thickness variation after Hallam (1968)

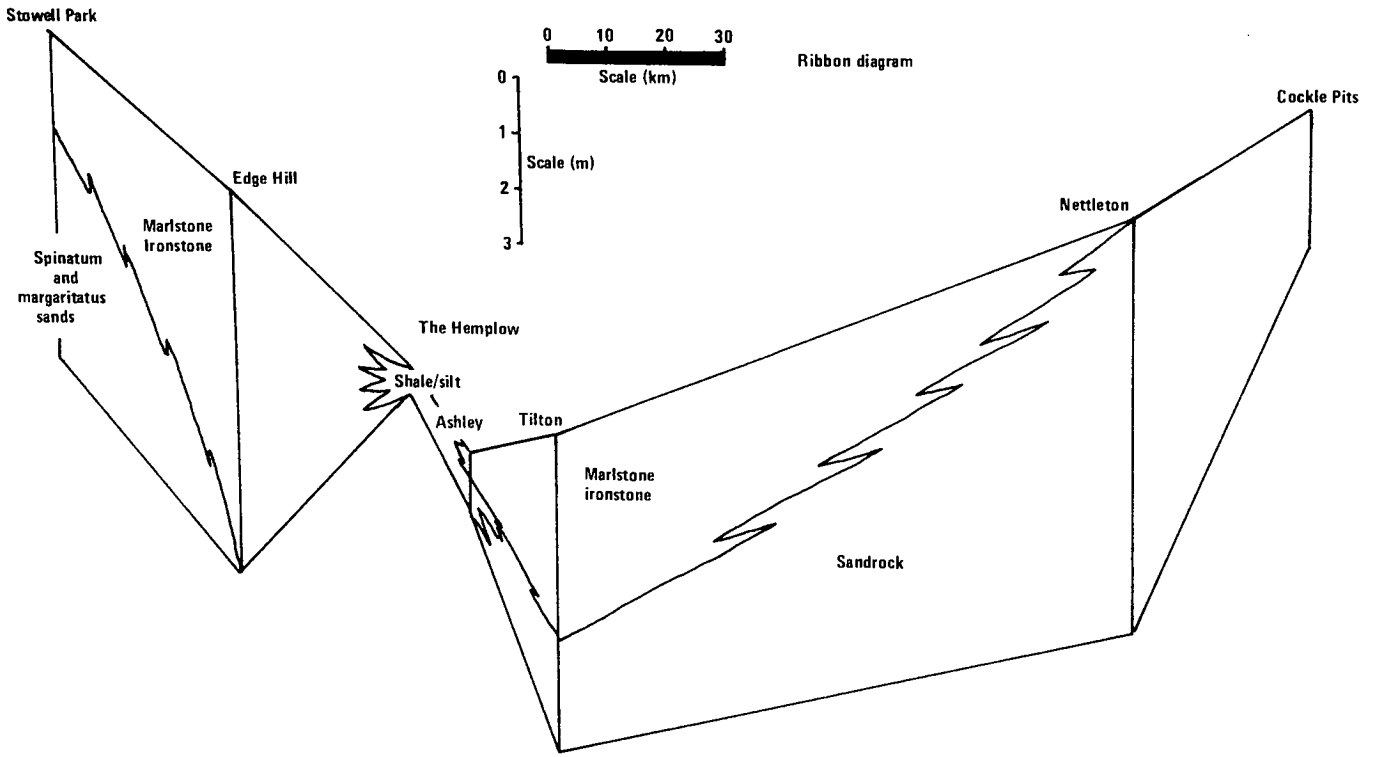

Fig 3.5 Thickness variation in the Marlstone Rock-bed

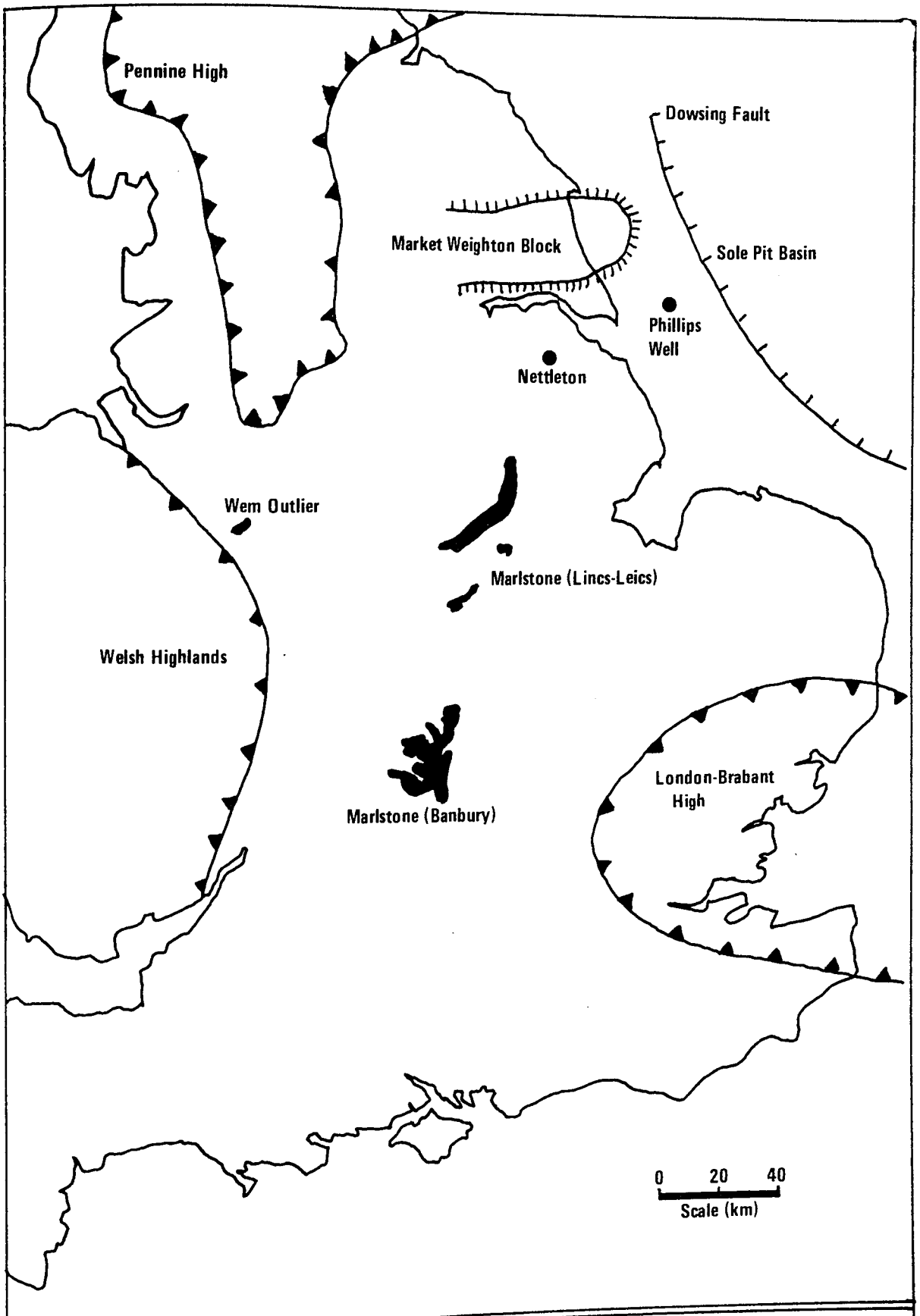

Fig 3.6 Middle Lias Structural Units (Ziegler, 1978; Kent, 1980)

Liassic times (Hallam and Sellwood, 1975) to considering that it was a northerly extension of the London-Brabant massif (Rhys, 1974). The reconstructions of Ziegler (1978) suggest that the Pennine block extended only as far south as the River Humber. The presence of the Marlstone Rock-bed in the Wem-Audlem outlier indicate that this may well have been the case. Thus the Pennine block would appear to have formed a peninsula within the depositional area of the Marlstone. Alternatively the Wem-Audlem outlier might be the only remnant of a depositional area in Cheshire, separated from that of the East Midlands by a Pennine block extending much further to the south. In the absence of any other firm data in addition to that of the Wem-Audlem outlier it is not possible to draw any unambiguous conclusions regarding the eastern limit of the Marlstone depositional area.

A comparision of the Spinatum zone sediment distribution with the known tectonic and physical limits of the depositional area show that there is a noticeable degree of thinning towards these limits. The peripheral areas are characterised by dominantly sandy facies which become much less important in the central areas of the East Midland shelf. In contrast, the ironstone facies become much more important in these central areas. Clearly, therefore, the depositional area exhibits a number of the features of a depositional basin. That part of Figure 3.5 from Cockle Pits to The Hemplow is the type of sediment distribution expected along the axis of a basin, whereas that from Tilton to Stowell Park is what would be expected along a line at right angles to this. The presence of Spinatum silts in the area closest to the London-Brabant massif is difficult to explain in this context. They might represent the fine sediments expected in the deeper portions of a depositional basin, but their location in

an area which was in all probability rather shallow argues against this. A possible explanation might be found in the sediment supply from the London-Brabant massif. It appears, therefore, that the Marlstone Rock-bed and its associated facies were deposited on the East Midlands shelf within an area which might be thought of as a depositional basin. In the absence of more detailed data it is not possible to further refine this model. It is interesting to note, however, that the later Aalenian Northampton Sand Ironstone, which was also deposited on the East Midland shelf, finds a similar sediment distribution with marginal sandy facies in the north and east surrounding centrally situated ironstone facies..

3.2.2 Marlstone Rock-bed Ironstone Facies

The logging of the Marlstone Rock-bed at outcrop and in core has shown that it is divisible into four different facies.

3.2.2.i Sandrock: The term sandrock is a stratigraphic name for the sandstone which occurs beneath the Marlstone Rock-bed in Leicestershire and Lincolnshire. It is a calcite cemented chamositic sandstone. At Tilton the Sandrock is light brown to yellowish grey in colour. It is hard and well indurated. It is a medium grained sandstone in which the component grains are sub-angular and well sorted. Sedimentary structures were not observed at outcrop.

The division between Sandrock and Ironstone cannot be made in the case of the Nettleton core Marlstone where normal ironstone beds occur as beds within a dominantly sandy sequence. In this case the Sandrock type facies is again a calcite cemented chamositic sandstone. The colour varies from a greyish green to a light green, reflecting a

low and a high proportion of chamosite respectively. It is hard and well indurated. The sandrock facies varies from a fine to a medium grained sandstone in which the component quartz grains are subangular and well sorted. Muscovite is common throughout the sandy facies. Lenses of chamosite mudstone are common. They are usually 5 cm in length and 0.5 cm in thickness. These concentrations of chamosite, and those beds containing more chamosite than normal, often show the presence of burrows 1 cm in length and 0.2 cm in diameter. They are either inclined at approximatley 45° to bedding or are horizontal. Quartz grains are concentrated within them. It has not been possible to identify these burrows in terms of ichnogenera but they are referable to the endichnial burrows of Martinsson's (1970) stratonomic classification. Current-generated sedimentary structures are generally absent although at one level in the sequence a series of erosion surfaces, each succeeded by foreset and plane lamination, were encountered. No in situ shelly fauna was found, but fragments of Lobothyris sp. and Tetrarhynchia sp. were recorded at some levels.

3.2.2.ii Chamositic Chamosite Oolites: This is a commonly occurring facies of the Marlstone Rock-bed Ironstone. At some localities it is the only facies present.

The chamosite ooids are characterised by a greenish white to green colouration. In all cases they have a prolate ellipsoidal shape. There is very little variation in ooid size between localities; the ooids generally having a size range of 0.3 - 0.4 mm, measured along the the long axis. The exception to this occurs in the Nettleton core where the ooids have a size range of 0.5 - 0.6 mm. In all cases the ooids are well sorted. They are commmonly oriented

with their long axes subparallel to bedding.

Ooimoulds are common in this facies. They are usually found where the apparently complete ooids have a greenish white colour. The ooimoulds may take the form of a void within an ooid, in which case the chamosite of the remaining ooid envelope is greenish white. In other instances there is no ooid material present and the ooimould is an ooid shaped void within the matrix. This may be either chamosite or cream-coloured siderite. It is generally found that ooimoulds occur together in irregular patches several centimetres across whilst complete ooids cocur together in separate irregular patches.

The dominant matrix mineral is green chamosite mud. In addition to infilling the interstices between ooids it also forms small lenses from which ooids are more or less absent.

There is little evidence of any in situ fauna. Vertical 3-5 cm long burrows occur at some horizons such as close to the base of the Marlstone Rock-bed at Tilton. Although in situ nests of the brachiopods Lobothyris punctata and Tetrarhynchia tetrahedra are common in the Marlstone, none have been found within this facies. Quite often, however, complete individuals do occur and have a geopetal infilling of chamosite ooids. In the case of the Terebratulids this can be demonstrated to have entered the valve through the pedicle opening. Unequivocal evidence for the in situ nature of such individuals e.g. a stable substrate as indicated by nests, is absent.

Wood fragments have been found within this facies at Branston.

3.2.2.iii Calcitic Chamosite Oolite: As with the preceeding facies this facies also commonly occurs within the Marlstone Rock-bed,

and may also be the only facies present at some localities.

The ooids of chamosite are uniformly green in colour. They have prolate ellipsoidal shapes. There is very little variation in ooid size between localities. They are generally well sorted with a size range of 0.3-0.4 mm, measured along the long axis. The ooids are commonly oriented with their long axes subparallel to bedding

Rounded intraclasts of chamosite mud are occasionally found. They are usually less than 1 mm in size.

The cement to these allochemical grains appears to be entirely of calcite but petrographic work reveals the presence of a small amount of siderite cement.

Nests of Lobothyris punctata and Tetrarhynchia tetrahedra are common within this facies. Hallam (1961) has shown that these are in situ life assemblages. From this, it follows that their development occurred during periods of very little sedimentation, on a stable substrate. Their subsequent extinction resulted from a sudden influx of sediment causing their rapid burial (Hallam, 1961; Blake, 1977). The nature of the brachiopod nests suggests, therefore, that they did not develop contemporaneously with the deposition of the calcitic chamosite oolites. Elsewhere within the facies disarticulated values of Pseudopecten sp., Entolium sp., Modiolus scalprum, Oxytoma sp., and Protocardia sp., occur. Evidence of the presence of entirely soft-bodied organisms is provided by common vertical burrows. These are generally characterised by an infill of chamosite ooids.

3.2.2.iv Bioclastic Limestones: This is a rarely occurring facies. It has been found as occasional beds at the top of the Marlstone

Rock-bed sequence in the Nettleton core and forming the upper portion of the sequence at Browns Hill Quarry, Holwell. In the former case it is a shell fragmental limestone exhibiting foreset lamination along which chamosite ooids are concentrated. In the latter case it is a ferruginous shell fragmental limestone. All the shell fragments are comminuted and less than 1 mm in size. Foreset lamination is common. Coarser shell fragments define the individual lamellae.

3.2.3. Inter-relationships between Facies

The broad facies relationships between the Sandrock and Marlstone Rock-bed Ironstone have been discussed above. The fact that any one of the above facies tends to predominate at any one locality and the separation of individual localities rules out any closer study of their inter-relationships.

3.3 PETROGRAPHY

3.3.1 Chamosite Ooids

In all the facies examined the general nature of the chamosite ooids remains the same. This allows a general description of their form and nature. Textures involving chamosite ooids which are restricted to a particular facies are described in the discussion of that facies.

X-ray powder photography of individual ooids confirms that they are constructed of the 7A septechlorite chamosite.

The chamosite ooids (Plate 3.1) show a range of colour shades between the end members grass-green and olive-brown. Any one ooid does not always show the same colour shade throughout its structure. The core-grain may be green and the envelope olive-brown, or vice versa. The individual envelope rings commonly show a different colour shade to that of their neighbours and exhibit a bulk pleochroism. The pleochroic scheme exhibited by individual chamosite books is dark when the (001) cleavage is parallel to north-south, and light when parallel to west-east.

Between crossed-polars the chamosite ooid envelopes exhibit an extinction cross which is pseudo-uniaxial and positive (Plate 3.2). Since chamosite has straight extinction and is length-slow this implies that the component chamosite flakes of the envelope have an orientation in which the (001) cleavage is tangential to the core-grain. The nature of the envelope pleochroism supports this. Direct evidence of the fine structure of chamosite ooid envelopes has been provided by high power transmission electron microscopy (Turner et al., in prep.). This shows that they are constructed of chamosite books or flakes less than 1μ m in size and having a preferred orientation in which the (001) cleavage is tangential to the ooid core-grain.

A variety of ooid shapes occur. The most common sectional form is either an oval or an ellipse. (Figure 3.7). Amongst grains with this shape the ratio of the long and short axes tends to vary from 4:1 to 3:1. Circular ooid sections i.e. those with a ratio of 1:1 are not uncommon (Figure 3.7). A long axis size range of 0.15-0.60 mm with a mean of approximately 0.40 mm has been found. These sectional types reflect the prolate ellipsoidal shape of the ooids seen in

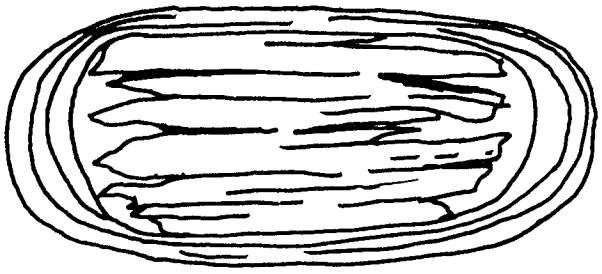

a : Ovate Ooid Section
Chamosite Book Core
X150

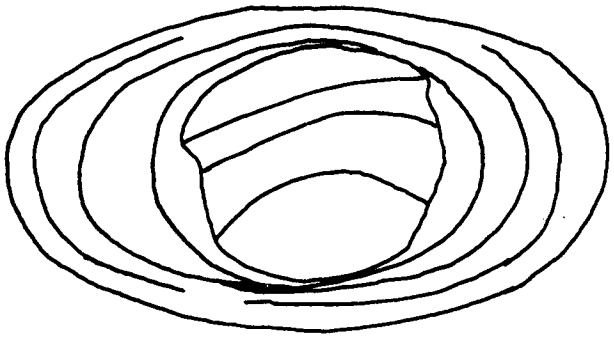

b : Elliptical Ooid Section
Ooid Envelope Fragment
Core
X150

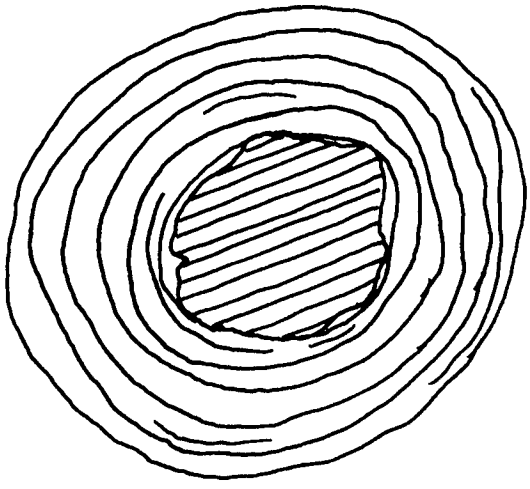

c : Circular Ooid Section
Optically continuous
Chamosite Core Grain
X200

Fig 3.7 Sketches of Chamosite Ooid Sections

hand specimen and with the aid of the scanning electron microscope. The variation in the ratio of long to short axes is therefore more likely to be apparent rather than actual, resulting from the ooids being sectioned in different orientations.

A number of more irregular sectional varieties occur. As in the case of the Frodingham Ironstone these are divisible into three types, although there may be exceptions; (i) triangular, (ii) trapezoidal, (iii) eccentric. A representative selection of these types is illustrated in Figure 3.8.

The internal structure of the ooids is of a central core grain surrounded by an envelope constructed of a series of concordant rings. Recognition of these two structural components is promoted by a difference in colour, mineralogy, or a clear discontinuity between them. In a number of instances a core grain may appear to be absent. The much greater predominance of ooids with cores suggests that this is probably a result of the sectioning technique exposing only the outer part of the envelope.

The ooid core grains are in all cases constructed of chamosite. Fragments of biogenic material of detrital quartz are rarely found as core grains. The core grains are divisible into two groups; those which are chamosite books and those which are fragments of chamosite ooid envelopes. The former are more common than the latter.

Chamosite core books are characterised by a well developed basal (001) cleavage. They commonly have a rounded square or oblong shape (Plate 3.3). This might indicate a period of rounding prior to their incorporation in ooids. A number of books have not undergone such a marked degree of rounding as they retain sharp corners. Many core books exhibit a concertina appearance in which the niches correspond

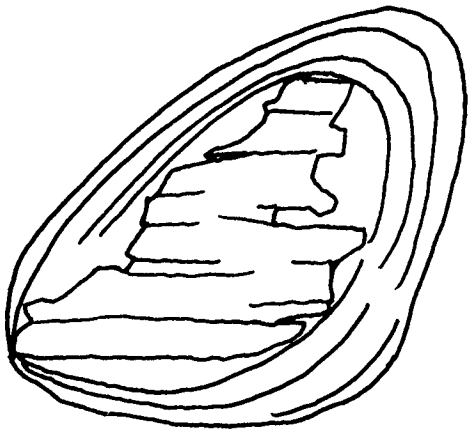

a : Triangular Ooid Section
Chamosite Core Book
X150

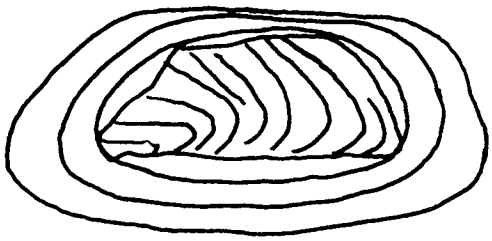

b : Trapezoidal Ooid Section
Ooid Envelope Fragment
Core Grain
X150

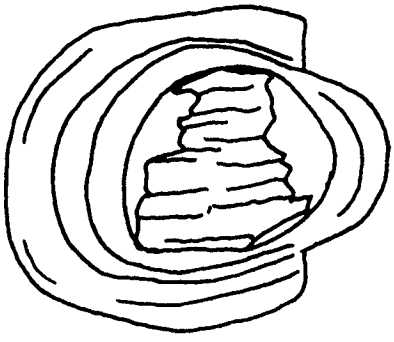

c : Eccentric Ooid Section
Chamosite Core Book
X150

Fig 3.8 Sketches of Chamosite Ooid Sections

to cleavage traces (plate 3.4). This is attributed to attrition of grains being concentrated at points of structural weakness. The colour of the core-books varies between grass-green and olive brown, and is uniform across any given book. They are pleochroic as described above. A number of core-grains, which are optically continuous within the limits of the core, but lacking cleavage traces occur. These are thought to be core books seen in an orientation approximately perpendicular to (001). Characteristically the cleavage traces of a book correspond to its long axis and are parallel to the long axis of the surrounding envelope. Rarely, however, books occur in which the cleavage traces correspond to the short axes of the book and the surrounding envelope. The rarity of this orientation is explicable in terms of mechanical stability of the books during rounding: A book in which the cleavage traces are parallel to its long axis would have a much lower tendency to break up into its component flakes than would a book in which the traces corresponded to the short axis. The relationship between core-grains and their surrounding envelopes is discussed below, but one feature which has an effect on the core books, rather than the envelope, deserves mention here. This is the apparent separation of cleavage flakes by the injection of chamosite along the cleavage traces at the time of formation of the first ring.

The chamosite ooid envelope fragments which form core grains are in all cases rounded but irregular. Thus, triangular, trapezoidal and eccentric core grain shapes are common within this core grain group. (Figure 3.9). The fact that they represent the break-up of ooids and the subsequent rounding of the resultant grains, points to a somewhat energetic environment supplying ooid core material.

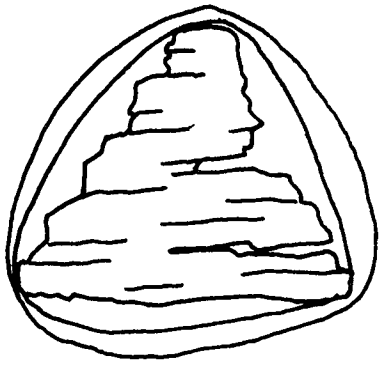

a : Triangular Chamosite Core Book
X100

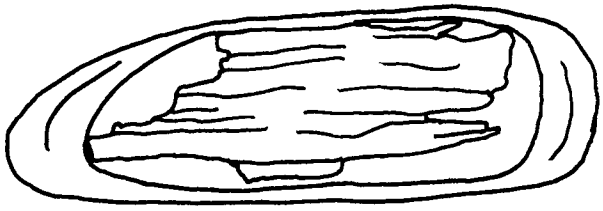

b : Trapezoidal Chamosite
Core Book
X150

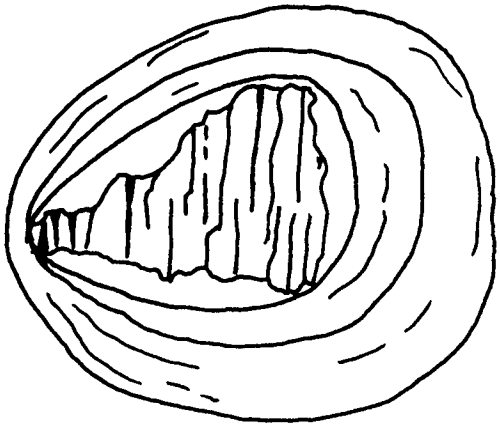

c : Triangular Chamosite
Core Book resulting in
Eccentric Ooid Envelope
X150

Fig 3.9 Sketches of Ooids with Different Shaped Ooid Core Books

This must also apply to the rounded core books. The general orientation of such fragments within on ooid is such that the long axis of the ooid fragment is parallel to that of the surrounding envelope. Such fragments of chamosite ooid envelopes exhibit all the characteristics of a complete envelope.

The ooid envelope is constructed of a series of concordant rings. They are characterised individually by a thickness maximum measured along the long axis, and a minimum measured along the short axis. (Figure 3.10). This is the case in all ooids with non-circular sectional shapes. In the case of circular sections, however, a constant ring thickness variation is retained. This indicates that once envelope formation about a central core grain has become established, the addition of successive rings does little to alter the final shape of the ooid from the prolate ellipsoidal form noted above.

Within any given ooid envelope individual rings are discernable from each other by virtue of colour variations and a thin black line surrounding their outer margins. This distinction is best seen in those portions of the envelope at either end of the long axis. Any differentiation of the rings at either end of the short axis is, however, frequently impossible as a result of the envelope thickness reduction in these areas. The vertical and horizontal bars of the extinction cross, corresponding to the short and long ooid axes respectively, show a difference in form corresponding with this observation. The width of the vertical bar spreads out to extinguish a considerable portion of envelope on either side of the short axis, whilst the horizontal bar thickens away from the core extinguishing a portion of envelope corresponding in shape to an isosceles triangle.

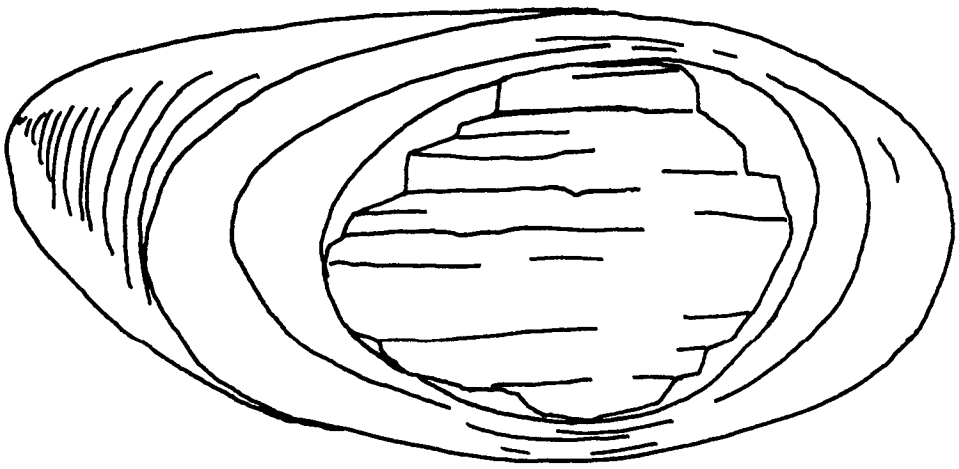

Fig 3.10 Diagrammatic Sketch of Ellipsoidal Chamosite Ooid

As would be expected, circular ooid sections do not show such variation. In these cases the characteristics of the long axis area are shown in all orientations of the stage. A variety of envelope thicknesses measured along both long and short axes occur. Generally, the thicker the envelope the more rings comprise it. It does not follow, however, that a thick envelope, measured along the long axis, corresponds to a thick envelope in the region of the short axis. Consideration of the individual ring thicknesses in any one ooid shows that there is an overall ring thickness increase from those rings immediately around the core grain to the outer rings. In relatively thick envelopes, in the region of the long axis, the outer rings may be ten times thicker than the innermost rings. By no means do all ooid envelopes show such a major thickness variation between rings. The above observation tends to be restricted to those ooids with a thicker envelope.

It has been noted above that six different ooid section types are found. These are ovate, elliptical, circular, triangular, trapezoidal, and eccentric. The examination of a large number of thin sections indicates that the latter three sectional types are a feature of some ooids. i.e. they are not apparent sections resulting from the thin section preparation method. Comparison of the core grain shape, initial ring form, and net envelope thickness show that the latter three types correspond to early stages in ooid development around core grains with a corresponding shape. This leads to the ultimate attainment of the first and second sectional types after the addition of a number of rings at a much later date in ooid development. Ovate and elliptical sections may also appear in the initial stages of ooid formation. Their appearance is predicted

by core grain shapes which promote the development of such a shape i.e. rounded squares and oblongs. Figure 3.11 shows a selection of different ooid core grain shapes and their surrounding envelopes. The development of the various ooid shapes can be traced by a study of successive ooid rings. Ooid ring development commences about a core grain which may be rounded but is more commonly subangular in shape. Two different areas on the core grains control the thickness of the initial ring. These are areas with a very small radius of curvature or corners, and straight or gently curving portions of core grain margin which are areas with a large radius of curvature. The initial ring has a minimum or zero thickness over the former area, thickening to a maximum over the latter. The first ring about any core grain removes all angularities in the initial core grain shape thus producing a proto-ooid whose shape is closely similar to that of the core grain but rounded. Subsequent rings follow the same pattern in terms of the controls on ring thickness. Thus, initially, the ooid shape remains closely similar to that of the core grain. However, since the ooid is increasing in size the areas of originally low radii of curvature gradually increase in this quantity, thereby lessening the core grain shape effect. This ultimately reaches the stage where, in the the cases of triangular, trapezoidal, and eccentric core grains, the shape effect becomes insignificant and ring formation continues to produce an ovate or elliptical shape. The same sequence also occurs in ooids with rounded or non-rounded square or oblong core grains. The shape effect is not apparent in those cases, however, since the core grain shape promotes the formation of an ovate of elliptical section to the proto-ooid with the deposition of the first ring. In the cases of core grains with

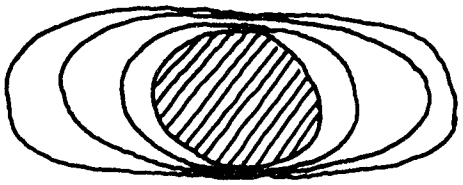

a : Circular, Optically continuous Chamosite Core
X150

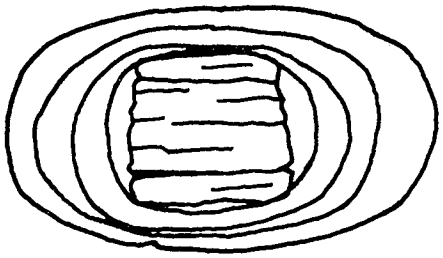

b : Square Chamosite Core Book
X150

c : Oblong Chamosite Core Book
X150

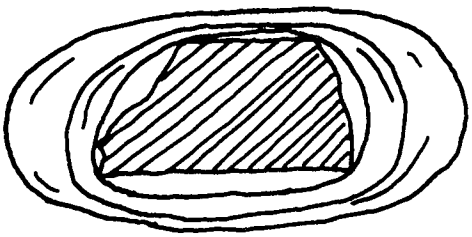

d : Trapezoidal, Optically continuous Chamosite Core.

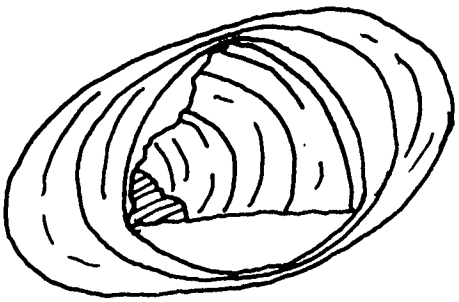

e : Triangular Chamosite Ooid Envelope Fragment Core
X150

Fig 3.11 Chamosite Ooid Core Grains and Successive

ovate or elliptical sections the above arguments do not apply as the depostion of rings proceeds as if the core grain were a normal ooid. The importance of the shape effect in the formation of ooids with ovate or elliptical sections follows from the fact that the ooid ring thickness is controlled by the radius of curvature: Small radii of curvature cause a minimum ring growth rate, large radii a maximum growth rate. Ring deposition occurring at two different rates on a square or oblong shaped core grain will result in a rounded grain with a long and a short axis. Thus, ooids with irregular sections are found to correspond to the early cessation of ring formation around similar shaped core grains, and ovate or elliptical grains to early cessation in the case of such ooids with fewer rings. Ooids with ovate and elliptical sections and a thick envelope of many rings can be ascribed to ooid ring formation occurring for a long time.

Comparison of ooids with core grains having a long and a short axis shows that the core grains have a constant orientation with their long axis subparallel to that of the ooid envelope. Since core grains would find the more stable orientation on the sea floor to be with their long axis parallel to bedding it follows that ooid envelope formation also took place in this orientation. In many instances the distribution of the areas of maximum and minimum radii of curvature on the core grains do not correspond to the distribution of envelope thickness maxima and minima. Thus, where a core grain has a maximum radius of curvature parallel to its long axis, the ooid envelope is at a minimum normal to this. It appears, therefore, that there is a second control on the formation of ooid envelopes required to create the thickness

maxima and minima observed in all ooids, and apparently directly related to dynamic conditions on the sea bed. It is different to the control described and discussed above since this relates ooid sectional shapes at different times during ooid formation to the shape of the core grain. The nature of the second control cannot be resolved directly from observations of ooids in thin section, and is therefore discussed in Chapter 9 under the heading of ooid formation.

A common feature of many chamosite ooids is the presence of black specks and black filamentous inclusions concentrated at ring contacts (Plate 3.5). In some instances these are also concentrated within and at the terminations of cleavage traces in core books. It is interesting to note that they are generally absent from chamosite books occurring without ooid envelopes. They are generally less than 5 μm in length and 1 μm in diameter. Due to their abundance it is usually difficult to resolve their form in any greater detail. This is, however, possible in a few cases. These show that the black spots are cross-sectional views of the filamentous material. This has an overall U-shaped form, the black material forming the walls. It is generally the case that the filamentous material is orientated with the long axis sub-parallel to the ring contacts. These inclusions are often found concentrated preferentially in those areas of the envelope to either side of the ooid long axis. On the basis of its form and the fact that X-ray powder diffraction studies of individual ooids have not revealed the presence of any other minerals but chamosite, calcite, and siderite, this material is considered to represent remnant organic matter. Such inclusions have also been found in chamosite ooids in the Frodingham

and Cleveland Ironstones. Their importance is discussed in Chapter 9 under the heading of ooid formation.

A common feature exhibited by chamosite ooids is a plastic deformation in response to loading in areas where the sediment was originally grain-supported. Three textures occur which are ascribed to such an origin and apparently greater degrees of loading. (i) The first of these is represented by ooid contacts at a point or over small area of envelope surface. In such cases one ooid remains undeformed and occupies a small portion of the space originally occupied by the other. The envelope rings of the latter ooid deform slightly around the envelope of the former. (Figure 3.12a). In some cases the contact between two such ooids is straight and the rings of each envelope have deformed slightly in order to also become straight. (ii) The second ooid deformation texture involves the deformation of a complete ooid rather than a part of an ooid. (Figure 3.12b). Examples of this take the form of one ooid being partially bent, or moulded, around part of an adjacent ooid which usually remains undeformed. (iii) The most extreme form of ooid deformation results in total ooid distortion. (Figure 3.12c). It can be seen to follow on from the previous mode of deformation and results in small patches of ooids which are all moulded around each other to a greater or lesser extent. Within the aggregate thus formed each ooid is severely deformed, a feature which is expressed in the concomitant distortion of the extinction cross. The tangential orientation of envelope platelets may be randomised in some cases, resulting in the absence of an extinction cross. The occurrence of all three textures on the scale of a microscope slide suggests that sediment loading is not the only factor which causes deformation, Since the third

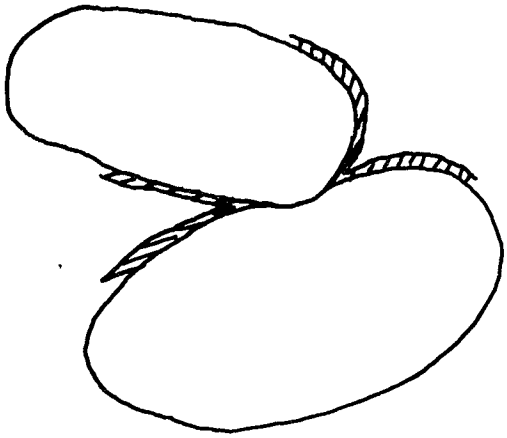

a : Partial Ooid Deformation at Point Contacts.
Hatching = Authigenic Chamosite
X150

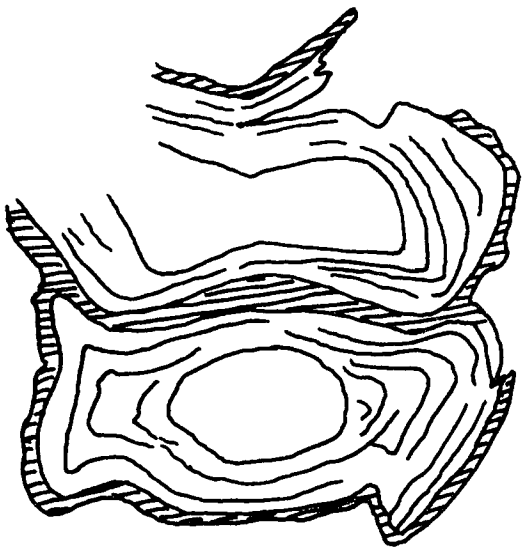

b : Moulding of one Ooid around another
Hatching = Authigenic Chamosite
X150

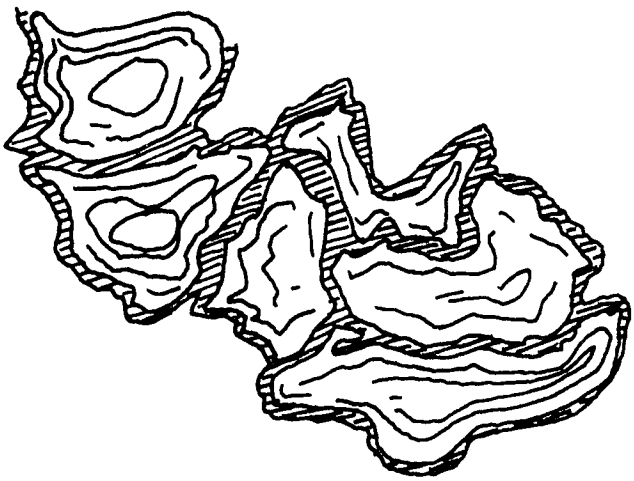

c : Complete Ooid Deformation
Hatching = Authigenic Chamosite

Fig 3.12 Chamosite Ooid Deformation Textures

deformation style evidently involves a higher ooid density than the two others this may also be a controlling factor. The fact that some ooids appear to deform around each other indicates that some ooids might have a greater mechanical strength than others. In those areas where texture (iii) occurs, calcite shell material is generally absent. This would mean that in such areas the sediment was entirely ooid-supported. When the weight of overlying sediment exceeded the mechanical strength of this support the ooids would deform around each other until they again supported the sediment. Deformation types (i) and (ii) are explicable in terms of differential overburden pressure distribution over the surfaces of ooids deposited in contact with each other. This has been discussed with respect to the distortion of goethite ooids in the Frodingham Ironstone (Chapter 2, Section 2.3.1). From this it is concluded that any difference in the mechanical strength of ooids played a minor role in their deformation.

The orientation of chamosite ooids within thin sections of Marlstone Rock-bed Ironstone show no depositionally controlled preferred orientate. The only significant depositional texture exhibited by the ooids is their concentration as burrow infills.

3.3.2. Sandrock

Petrographically this facies is a calcite cemented chamositic quartz arenite. Chamosite is often concentrated as small lenticles of chamosite mudstone less than 5 cm long (Plate 3.6).

3.2.2.i Quartz: These grains comprise the major terrigenous component of the sandrock facies. The modal proportion of quartz varies from 30-50% in the representatives of this facies in the Nettleton core.

In the sandrock of the Tilton sequence quartz has a modal proportion of 15%.

The individual quartz grains are generally subangular with occasional angular and sub-rounded grains. They are commonly square, rectangular, triangular, and ovate in shape. Elongate triangular and rectangular shard-like grains are common and are a characteristic of the sandrock facies. A grain size range of 0.01-0.40 mm had been found in all the specimens examined. In those which represent fine-grained quartz arenites a mean grain size of approximately 0.2 mm is common, and in those which represent medium-grained quartz arenites a mean of approximately 0.3 mm is common.

The quartz grains are in all cases characterised by a very clear nature. Fluid inclusions and rutile are uncommon. There are no syntaxial overgrowths. The majority exhibit a uniform extinction, only a few grains showing an undulose extinction.

3.3.2.ii Chamosite: This mineral occurs dominantly as books. A less major mode of occurrence is as chamosite mud lenticles, burrow infills, and intraclasts. Occasional ooids are present. The proportion of chamosite mud is variable from a mode of less than 5% to as much as 20%. Those specimens of sandrock facies with a green colouration are found to contain such high proportions of chamosite mud.

Chamosite books are an abundant component of the sandrock facies. They are usually absent from the chamosite mud lenticles. These grains are pleochroic varying from a deep green, when the (001) cleavage is parallel to the north-south cross hair, to a yellow-green or straw colour when the cleavage is parallel to west-east. The chamosite books are commonly of the order of 0.35 mm long, measured parallel to

cleavage, and 0.15 mm wide. (Plate 3.7). A number of books reaching 1.0 mm in length but not exceeding 0.10 mm in width occur. These books are characterised by the presence of a well developed basal (001) cleavage. The terminations of the books are either flat or slightly rounded. In general the books of the Nettleton sandrock show no evidence of having undergone rounding or abrasion during their history. It is interesting to note that the niches which characterise the cleavage traces of chamosite ooid core books occurring in chamosite oolites, but without an ooid envelope, are absent from these chamosite books. The chamosite books of the uppermost portion of the sandrock in the Tilton sequence, however, all show signs of rounding. Niches are also present.

The chamosite books in the sandrock facies of the Nettleton core exhibit a number of textures in conjunction with other minerals: Chamosite books maybe totally or partially enclosed the detrital quartz grains. (Plate 3.8). Where two quartz grains occur in close proximity and a chamosite book is sandwiched between, it may diverge and increase its width at either end of the quartz grains. (Plate 3.9). This corresponds to a position at which its boundaries are no longer constrained. Chamosite may occur within a single grain of muscovite. In these cases a thin cleavage flake of chamosite lies parallel to the cleavage of the muscovite. The muscovite does not appear to be constructed of two separate grains sandwiching the chamosite as they are optically contiguous. Thin lenses of siderite and ferroan calcite occur along the cleavage traces of chamosite books.

Where occurring as mud lenticles within the sandrock facies the chamosite has an olive-green or olive-brown colouration. It exhibits a bulk pleochroism with the normal scheme. Between crossed

polars a bulk extinction occurs when the lenticles are in these positions. This chamosite mud thus has a depositional fabric. The lenticles are characterised by the more or less complete absence of quartz grains and chamosite books. They often exhibit burrow cross and long sections which are infilled with small quartz grains, in contrast to their surround. The burrows are usually 1-2 mm wide. The only post-depositional modification shown by these lenticles is the precipitation of siderite which occurs as individual and as trains of equant anhedra parallel to the lenticle axis. These are usually less than 0.05 mm across. The abundance of such siderite is low, but in some instances it may form up to 75% of the lenticle, obscuring the nature of the depositional chamosite.

Olive-green or olive-brown chamosite mud occurs without a depositional fabric as infills to burrows. These occur both sub-parallel, and at a high angle, to bedding. Books of chamosite and quartz grains are absent from them. Equant siderite anhedra are common.

Rounded and slightly irregular intraclasts of olive-green or olive-brown chamosite mud are occasionally found. They show no evidence of a depositional fabric. In contrast to the previous occurrences of chamosite mud chamosite books, ooids, and shell fragments may be included within them. They range in size from 1-12 mm.

Chamosite ooids are found in some specimens of the sandrock facies. They usually occur as rounded fragments but complete ooids are also present. Both of these grain types exhibit the characteristics described above. A number of complete ooids have undergone dissolution creating ooimoulds which are rimmed by the outer two or three envelope rings. In some cases the ooimoulds have subsequently been infilled by

ferroan calcite.

3.3.2.iii Mica: This terrigenous component has only been found in the sandrock facies of the Nettleton core. It is subordinate in abundance to the quartz component and of roughly equal abundance to the chamosite books. It includes both muscovite and biotite, the latter being sparcely distributed. In general the muscovite occurs as long (less than 0.60 mm) thin (0.02-0.04 mm) flakes which are often bent between the other primary components of the facies. The mica exhibits no preferred orientation relative to bedding.

3.3.2.iv Biogenic material: These grains are all fragmentary and constructed of non-ferroan calcite. They are usually of the order of 0.5 mm in size. Bivalve, brachiopod, foram, and echinoid material are all represented. The stereome systems of the echinoid fragments may be infilled by authigenic chamosite or ferroan calcite. The echinoid fragments are commonly surrounded by a syntaxial overgrowth of ferroan calcite.

3.3.2.v Cement: Cements are composed of ferroan dolomite, siderite, and ferroan calcite. Ferroan dolomite occurs as rare individual rhombs within the porosity. Siderite occurs as anhedral masses rooted on the primary grains and partially occluding the porosity. In addition it forms common euhedral rhombs. The remaining porosity is infilled by ferroan calcite with an inequigranular xenotopic texture. In addition this type of calcite occurs as the occasional ragged surround to shell fragments. Within such areas rare prisms of ferroan calcite occur indicating that the surround was originally either a

radial-fibrous growth of high magnesian calcite or aragonite.

3.3.2.vi Paragenesis: The sequence of post-depositional events within the sandrock facies is relatively simple, representing the cementation of a number of primary grains. This sequence of events is illustrated in Figure 3.13.

The chamosite books are characterised by a generally unrounded and non-abraded form in comparison to the books in chamosite oolite facies which have undergone such attrition. Textures in which quartz grains are surrounded by chamosite suggest that the features exhibited by the books result from their formation as a post-depositional mineral within the sandrock facies. The relationship between muscovite and chamosite might suggest that the chamosite books represent altered muscovite. Textures in which muscovite and chamosite are involved are rare, and no textures showing the progressive formation of chamosite from muscovite have been found. Thus it is considered to be more likely that the muscovite formed a convenient site for the nucleation of chamosite. Since lenses of both siderite and ferroan calcite occur along the cleavage traces of chamosite books, the formation of this type of chasmosite must predate the cement generations.

It is not possible to date precisely the point at which authigenic chamosite precipitated within the stereome systems of the echinoid fragments. Obviously it must predate the formation of syntaxial overgrowths to these grains as otherwise the stereome systems would be completely infilled by ferroan calcite. It would be reasonable to suggest that the precipitation of authigenic chamosite may have occurred during the formation of chamosite books.

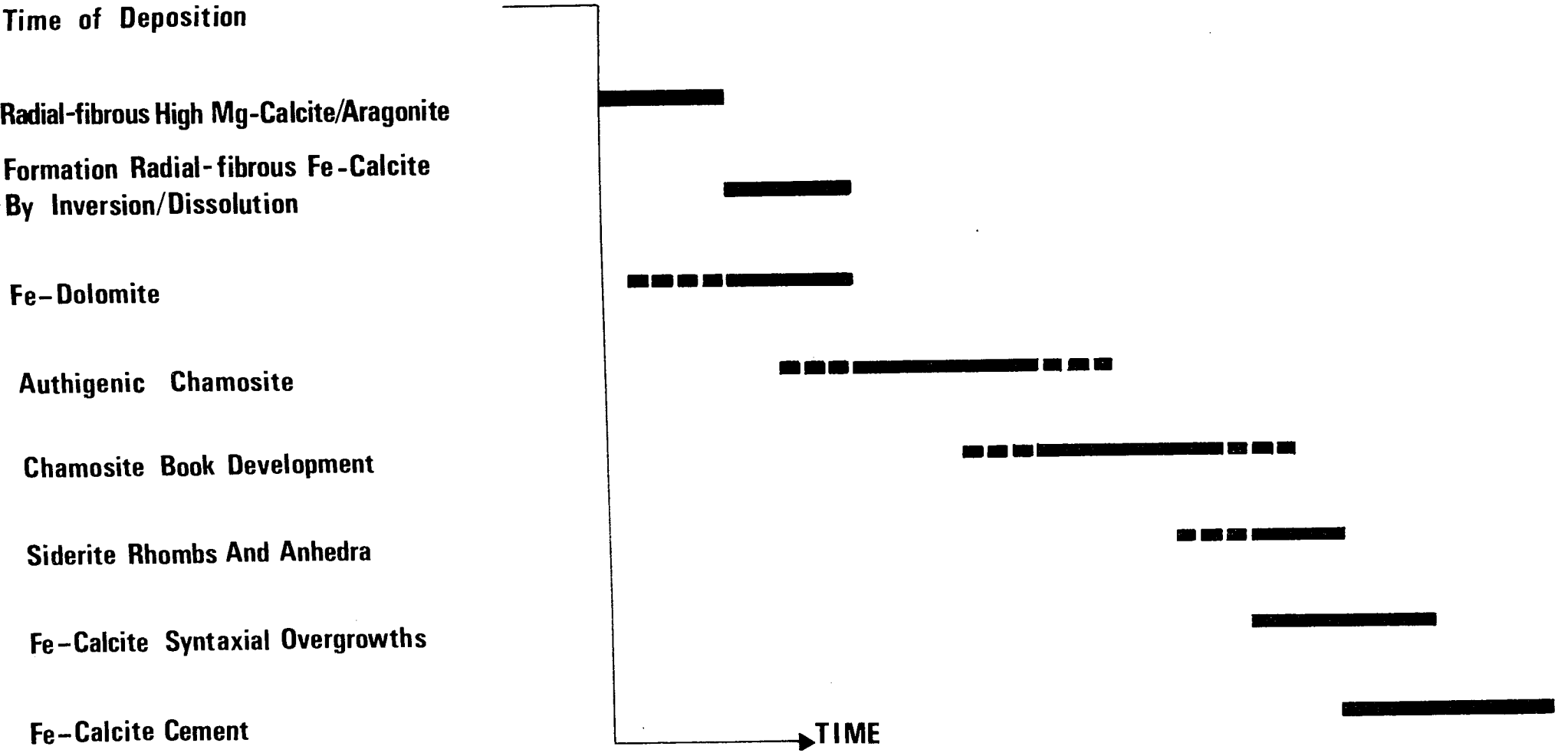

Figure 3.13: Paragenesis Of The Sandrock And Sandrock-Facies

The formation of the cement in the sandrock facies commences with the precipitation of either a high magnesian calcite or aragonite radial fibrous cement around shell fragments. This was subsequently replaced by a ragged surround of ferroan calcite.

Siderite occurs rooted on the primary components of the facies and is surrounded by ferroan calcite. Thus it predates this generation. The point at which it started to precipitate is not possible to date precisely. Since it is found as lenses in chamosite books it must post-date these.

The ferroan calcite syntaxial rims to echinoid fragments partake in the cement fabric. Since they surround fragments with a stereome system infill of ferroan calcite, which is of the same composition as the rims, and authigenic chamosite, the development of syntaxial rims must overlap with the precipitation of authigenic chamosite. The contacts of the rims and surrounding ferroan calcite are of the same type as the boundaries between individual grains of the surrounding calcite. Thus the formation of the syntaxial overgrowths continued until they were impeded by the precipitation of the surrounding inequigranular xenotopic calcite generation.

Since ferroan dolomite occurs in pore spaces with a euhedral form it predates the ferroan calcite cement.

The final cement generation is represented by the inequigranular xenotopic calcite which surrounds all the previous post-deposotional phases.

3.3.3. Chamositic Chamosite Oolite

This facies comprises chamosite ooids, ooimoulds, and occasional shell fragments set in a matrix of green chamosite mud. (Plate 3.10).

Chamosite ooids and ooimoulds constitute, modally, 30-50% of the rock. This facies has not been described in the literature before.

3.3.3.i Chamosite ooids: The chamosite ooids which retain their original nature exhibit all the characteristics described above. The ooids within this facies tend to show very little colour variation between the chamosite of the core grain and that of the surrounding envelope, or between the individual rings of the envelope. (Plate 3.11). They remain a grass-green in colour with the usual pleochroism.

The ooids exhibit a number of textures which result from replacement, dissolution, and distortion.

A number of ooids are characterised by the presence of a complete or incomplete fringe of siderite replacing the outer two or three envelope rings. (Plate 3.12). The innermost siderite is yellow, but passes into white siderite at the ooid margins. The outer boundary of the component siderite grains corresponds to the original boundary of the ooid. The individual siderite grains are generally equant and oriented sub-radially to the ooid margins. Ghost rings contacts may be seen within these grains. Occasional siderite grains penetrate some distance into the ooid envelope and this causes a distortion of the rings immediately round such siderite grains. The overall absence of ooid distortion associated with this texture suggests that it results from progressive dissolution of the chamosite and replacement by siderite. In a few cases replacement of this form has proceeded to a point at which the entire ooid has been replaced by a mosaic of siderite which exhibits a number of ghost rings.

A large number of ooids have undergone dissolution resulting in the formation of ooimoulds. There is no preference shown by this

texture; both normal ooids and those exhibiting replacive siderite rims have been subjected to dissolution. The nature of the ooimoulds resulting takes the form of a void, which is lined by the outer one or two envelope rings, (Plate 3.13) in the case of entirely chamosite ooids, or by the siderite rim in the case of rimmed ooids. These are the ultimate products of ooimould formation. Less commonly, examples in which dissolution has not been complete occur, and these are characterised by a central void representing the site of the original core grain or the core grain and the first one or two ooid rings. Examples of ooimoulds in which one portion of an ooid envelope has been removed in preference to another portion do not occur. The nature of ooimould textures indicate, therefore, that ooid chamosite dissolution commenced in the core region and moved outwards. In chamositic chamosite oolites at Tilton there is an exception to this rule: Chamosite core books occur within the ooimould (Plate 3.14).

The ooid distortion textures present can be ascribed to the distortion of ooimoulds rather than complete grains. All these textures are examples of chain ooids or their component hooked grains. Two forms of chain ooids are present; those which result from the collapse and flattening of ooimoulds, (Plate 3.15), and those which result from small scale mechanical failure of the surrounding chamosite mud and its movement into ooimoulds. (Plate 3.16). The former type is characterised by the absence of a complete replacive siderite rim whereas these may be present in the latter. The formation of these textures has been discussed in Chapter 2, Sections 2.3.3. and 2.3.4.

The only other mineral generation present in association with chamosite ooids is ferroan calcite. This has a replacive and an infilling role. In the former case a range of textures leading to the replacement

of an originally chamosite ooid are encountered. The initial replacive textures take the form of individual rings of chamosite passing laterally into ferroan calcite. Thus crescents of ferroan calcite (Plate 3.17) whose boundaries are ring contacts are found in the ooid envelope at either end of the long axis. A more extensive degree of replacement leads to large portions of the envelope being formed of polygonal masses of ferroan calcite elongated parallel to the ooid margins and with edges parallel to these corresponding to ring contacts. The ultimate expression of this are ooids which are completely replaced by ferroan calcite, (Plate 3.17). The latter two textural types are characterised by the presence of ghost ring contacts and small slivers of chamosite ooid envelope rings lying in their original orientation.

A number of ooimoulds are completely infilled by ferroan calcite. Infilled ooimoulds may be distinguished from replaced ooids by the absence of chamosite slivers and ghost ring contacts. Those ooimoulds which retained a portion of the envelope may exhibit replacement of this in addition to the infill. Chain and hooked ooids resulting from the failure (Plate 3.18) of their surround show clear evidence of the infilling nature of ferroan calcite. In these cases the movement of chamosite mud into the ooimould may move a remnant portion of chamosite envelope away from the original ooid edge. The space created is infilled by ferroan calcite. Both replacive and infilling types of ferroan calcite are of the same generation as the cementing ferroan calcite. This is sometimes found to be in optical continuity with ooimould infills via a fracture in the remaining chamosite envelope or replacive siderite rims. Many ooimoulds have not been infilled at all.

In chamositic chamosite oolites at Tilton ooimould infill often commences with the growth of dog's tooth siderite euhedra. Subsequently, ferroan dolomite may either partially or totally infill the ooimould. In the former case the remaining void is infilled by ferroan calcite.

It has been noted that a number of replaced ooids show the presence of ghost ring-contacts. In many cases these take the form of a thin band of uniform thickness, usually less than 0.05 mm thick, composed of a diffuse buff or brownish grey material, and passing all the way round the original ooid envelope (Plate 3.19). Such bands are also occasionally found in unreplaced chamosite ooid envelopes (Plate 3.19). In addition, ooimoulds which have not been infilled very rarely show the presence of several such bands (Plate 3.19) arranged 'concentrically'. It appears, therefore, that this material is an original component of the chamosite ooid envelopes and inert towards the processes resulting in chamosite dissolution. Close examination indicates that it has no mineralogical nature. Morphologically similar material occurs between the concentric shells of calcite or aragonite in carbonate ooids and is considered to represent mucilaginous envelopes. By analogy with carbonate ooids the above bands are also thought to be mucilaginous envelopes formed during chamosite ooid envelope formation.

3.3.3.ii Chamosite mud: This forms the dominant matrix mineral in the chamositic chamosite oolites of the Nettleton core. It has a grass to olive green colour. Two texturally different types occur. These are (i) lenticles of various sizes which are parallel to bedding and devoid of any allochemical component, and (ii) mud which is interstitial to allochems.

The lenticle- forming chamosite mud exhibits a bulk pleochroism and straight extinction. This type of chamosite mud therefore has a depositional fabric. Chamosite books and occasional muscovite and biotite flakes occur within the lenticles. The chamosite books vary in length from 0.03-0.10 mm. Their widths are variable resulting in long, thin or equidimensional books. They show no preferred orientation relative to the lenticle axis. Those features, such as rounded ends and niches at either end of cleavage traces, which are taken to be indicative of abrasion and rounding are absent. Some books appear to have a gradational contact with the surrounding chamosite mud. Black, tubule-like grains less than 0.01 mm in length are scattered throughout the mud. They are similar in form to many of the organic inclusions within the chamosite ooids and thus may also be organic in origin (Plate 3.20). The only post-depositional changes shown by this type of chamosite mud are represented by the precipitation of individual siderite anhedra and pyrite euhedra and subhedra. The siderite is sometimes found as lenses along the cleavage traces of chamosite books.

The chamosite mud which occurs interstitially to chamosite ooids, their replaced equivalents, and other allochemical grains does not show a depositional fabric. Rotation between crossed-polars shows that the chamosite mud immediately surrounding chamosite ooids undergoes extinction as the extinction cross passes through the adjacent ooid envelope. The fabric of this mud therefore appears to be a tangential arrangement of chamosite platelets around ooids. This is confirmed by the positive sign of the interstitial chamosite mud extinction cross. The black organic inclusions found within the chamosite mud lenticles are also present within this interstitial

mud. Chamosite books, muscovite, and biotite are only present occasionally. The precipitation of siderite and pyrite again represent the only general post-depositional change within this type of chamosite mud.

3.3.3.iii Biogenic material: This is all fragmentary and is usually less than 5 mm across. It comprises bivalve, brachiopod, gastropod, echinoid, and foram remains. The primary shell mineralogy of these groups is non-ferroan calcite, with the exception of some bivalves and all the gastropod material which was aragonite. Originally aragonite shell material has all undergone dissolution and subsequent replacement by siderite and ferroan calcite.

The fragments of non-ferroan calcite bivalves and brachiopods are commonly bored and the borings infilled by optically continuous authigenic chamosite. Micrite envelopes are occasionally present. Amongst the brachiopods, fragments of the impunctate rhynchonellids can be recognised by the absence of punctata and the zig-zag shape of the shell section. Fragments of terebratulids may be recognised by the presence of punctata which are infilled by either authigenic chamosite or ferroan calcite.

Originally aragonite shell material is recognised on the basis of its gross morphology and the presence of micrite or authigenic chamosite infilled burrows within the replacing medium. More or less complete gastropod sections are clearly recognisable by their chamber structure. The original aragonite fragments are all surrounded by chamosite mud. Their dissolution was followed by the crystallisation of dog's tooth siderite around the edges of the secondary porosity. This siderite is usually white at the edge of the porosity

and yellow at its prism terminations, In a number of cases this material has been fragmented and moved to the middle of the secondary pores, together with pre-existing micrite or authigenic chamosite infilled burrows in the original shell fragment (Plate 3.21). Allochemical components that were distributed around the edges of the original grain also enter this porosity at this point. The secondary porosity that remains is infilled by one of more grains of ferroan calcite or ferroan dolomite. The gastropod shells are surrounded externally by chamosite mud and their chambers are lined by inequigranular xenotopic curved siderite crystals. The original aragonite has been replaced by ferroan calcite. Individual chambers are infilled by chamosite with a sponge-like texture. All the chamosite in any one chamber extinguishes at the same time. The chamosite passes into a finely divided brownish material which does not show any mineralogical character. This lines the pores of the chamosite sponges. It is very similar to the material which occurs in ooids as muculaginous envelopes and hence is thought to have an organic origin. The pores of the sponge are infilled by siderite of the same type which occurs as chamber linings.

Echinoid fragments are occasionally present and constructed of ferroan calcite. Their stereome systems are infilled by authigenic chamosite. Syntaxial overgrowths are absent.

Foram tests are constructed of non-ferroan calcite. Their chambers may be infilled by authigenic chamosite.

3.3.3.iv Cement minerals: Locally within specimens of chamositic chamosite oolites the original depositional or primary chamosite mud does not occur. In these areas authigenic chamosite and siderite occur

as cement minerals.

Authigenic chamosite occurs as a complete or discontinuous isopachous pore lining less than 0.10 mm thick. The grains surrounded by this type of chamosite include complete chamosite ooids, ooids replaced by siderite and ferroan calcite and hooked and chain ooids constructed of these minerals.

The greater part of the remaining porosity is infilled by curved crystals of siderite. These have often mutually interfered during growth resulting in a typical drusy fabric. This is the case in the chamositic chamosite oolites of the Nettleton core. More generally, however, such as at Tilton, this siderite generation takes the form of a dog's tooth lining to the porosity, the remaining porosity being infilled by inequigranular xenotopic siderite.

Any remaining porosity is infilled by ferroan calcite.

3.3.3.v Paragenesis: The large number of textures and mineral generations which occur in this facies indicate that a considerable amount of post-depositional modification has occurred. This involves not only the dissolution and precipitation of mineral species but also a degree of structural reorganisation. The sequence of diagenetic events is shown in Figure 3.14. This sequence is characteristic of the chamositic chamosite oolites; lenses of chamosite mud within this facies exhibit a rather more simple series of changes. These are outlined separately.

The first post-depositioanl mineral generation, occurring throughout the facies, is the yellow/white siderite generation. This forms replacive rims to chamosite ooids. The fact that very little envelope distortion accompanies this texture and that it contains

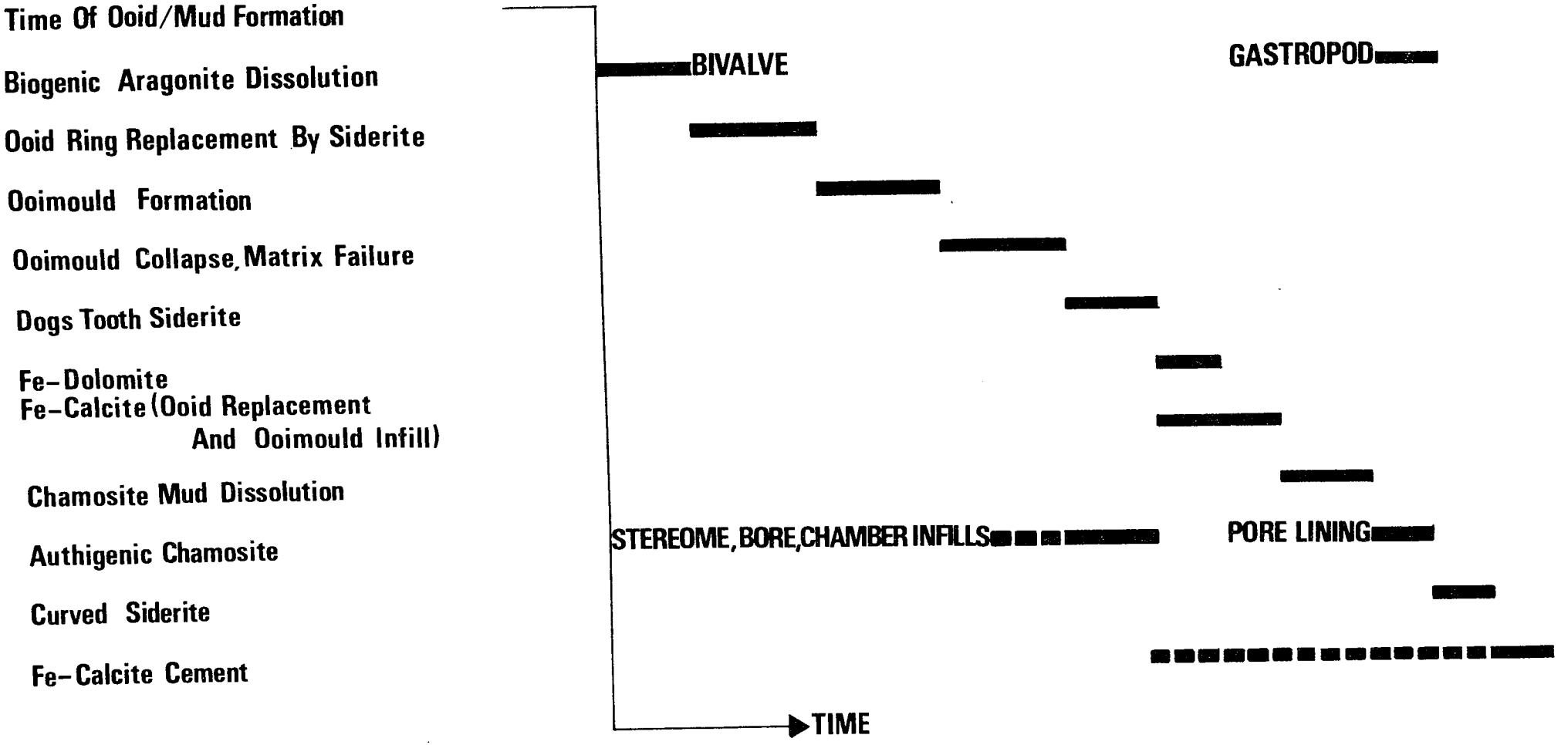

Figure 3.14: Paragenesis Of The Chamositic Chamosite Oolites

ghost ring contacts implies that it represents a chamosite dissolution - siderite precipitation reaction. Since the outer edges of the siderite rims correspond to the original ooid edge it may be concluded that the surrounding chamosite mud had no role in this reaction. In addition this type of siderite forms dog's tooth linings to original aragonitic shell fragments. This clearly indicates that the dissolution of aragonite occurred prior to the precipitation of yellow/white siderite. The secondary porosity formed as a result of this dissolution was retained by the surrounding chamosite mud which formed a mould around the original fragment. The aragonite dissolution had no effect on pre-existing micrite and authigenic chamosite infilled borings which remained intact. The yellow/white siderite therefore crystallised to either side of such apophyses. It should be noted that the relationship between this siderite generation and original aragonite shell fragments is restricted to aragonitic bivalve fragments.

The formation of ooimoulds follows the precipitation of yellow/white siderite. This follows from the fact that ooimoulds with a lining composed solely of this siderite occur. Such linings contain ghost ring contacts. In general there is a complete spectrum of ooimould textures from almost complete chamosite ooids from which part or all of the core is missing to ooimoulds lined by the outer one of two envelope rings or the above noted replacive siderite. In all instances where a portion of the chamosite ooid envelope remains, the ring which surrounds the ooimould is more or less complete. It is a common occurrence in some specimens of this facies that the core book remains within the ooimould and shows no sign of dissolution. These textures indicate that the solution of the chamosite ooids commenced in the core region and proceeded outwards into the envelope

where individual rings were removed one after the other. The rate of this dissolution reaction may be variable. This is suggested by those ooimoulds where core books of chamosite remain unaltered. In these cases the reaction may well have been catalysed by the small size of individual envelope chamosite flakes and was not sufficiently vigorous to dissolve the larger books. An alternative explanation might involve a difference in the porosity between the ooid envelopes and the core books. A porosity would be required for fluid movement.

The presence of an outer, replacive siderite rim to chamosite ooids evidently strengthens subsequently formed ooimoulds as these show little sign of distortion. They remain as a secondary porosity which may be later infilled. Ooimoulds without or with an incomplete siderite rim are commonly found to have collapsed. The collapse removes the secondary porosity entirely or partially. Any remaining porosity is later infilled. Thus, the formation of hooked and chain ooids by ooimould collapse and the small scale mechanical failure of the matrix chamosite mud, resulting in hooked and chain ooimould formation precedes porosity-infilling mineral generations.

Ooimoulds which do not collapse may be successively infilled by siderite, ferroan dolomite, and ferroan calcite. These generations completely infill ooimoulds. Usually, the only infilling generation is ferroan calcite. Since these generations also occur within partially collapsed ooimoulds, hooked, and chain ooids their precipitation post-dates this point in the post-depositional history of the facies. The ferroan calcite which infills ooids may also replace any remaining chamosite. This generation of ferroan calcite also infills the secondary porosity represented by originally aragonite shell fragments. Its precipitation commences at the

edges of the secondary porosity and moves inwards. This is indicated by the fact that the original secondary porosity lining of yellow/white siderite has been fractured and moved towards the centre of the pores and is entirely surrounded by ferroan calcite. In addition to the movement of the siderite lining micrite lined and authigenic chamosite infilled borings are also detached from the edge of the secondary porosity and shifted towards its centre.

Echinoid plate stereome systems, borings in both primary calcite and original aragonite shell fragments, and the chambers of forams are infilled by optically continuous authigenic chamosite. It is not possible to unequivocally conclude at what time this chamosite precipitated as all these grains are surrounded by primary or depositional chamosite; authigenic chamosite does not occur as a pore lining. It is possible to conclude, however, that it precipitated prior to the ferroan calcite secondary porosity infill. This is indicated by authigenic chamosite infilled borings, lying within replaced aragonitic shell fragments, but detached from their edges. It would have been necessary for those borings to have been in contact with the surrounding chamosite mud at the time at which they were infilled. It is reasonsable to assume that the surrounding chamosite mud would have supplied the iron, aluminium, and silica required for the precipitate of authigenic chamosite.

The textures representing the above sequence of events are present in small areas lacking a primary or depositional chamosite mud matrix e.g. the Nettleton core, or over much more extensive areas without such a matrix e.g. the Tilton section material. This indicates that following these post-depositional changes a phase of dissolution of the chamosite mud, interstitial to the allochemical

components, occurred. This created another secondary porosity. The grains within this were subsequently surrounded by an isopachous pore-lining of authigenic chamosite. Much of the remaining secondary porosity was infilled by siderite. The individual siderite crystals nucleated on the authigenic chamosite lining and subsequent growth occurred either normal, or at an angle to the pore walls, thus creating dog's tooth or curved dog's tooth type-grains. Continued growth brought about their mutual interference, causing the development of a drusy fabric in the central areas of the porosity. Any remaining porosity was subsequently infilled by ferroan calcite.

Originally aragonite gastropod shells underwent solution and replacement during this secondary porosity infilling stage. Their external shape was moulded by the surrounding chamosite mud. The walls of their chambers formed nucleation sites for siderite of the type described in the previous paragraph. The siderite lining thus formed an inner mould. Dissolution of the aragonite followed and was replaced by ferroan calcite with an inequigranular xenotopic fabric. It is not possible to correlate this with the final ferroan calcite infill of the secondary porosity resulting from chamosite mud dissolution. The siderite of the chamber lining type also infilled the pores in the sponge-like biogenic chamosite.

Lenticles of depositional chamosite mud exhibit very little post-depositional modification. Chamosite books exhibiting no signs of attrition are common. This is difficult to correlate with their occurrence. The fact that some of these books show gradational contacts with the surrounding chamosite mud suggests that they are post-depositional in origin. This is supported by books showing a small degree of optical continuity with the surrounding mud.

Siderite is the only other authigenic mineral. It occurs as individual anhedra and as lenticular patches localised along chamosite book. cleavage traces. The siderite therefore post-dates the formation of chamosite books. Pyrite occurs within the chamosite mud as anhedral masses which cross-cut the depositional fabric of the mud. Thus, the pyrite has a replacive role with respect to the chamosite mud. No textures involving pyrite and siderite or chamosite books have been found. Due to this it is not possible to relate the formation of pyrite to the formation of these mineral generations.

3.3.4 Calcitic Chamosite Oolite:

This facies is characterised by chamosite ooids, chamosite mud intraclasts, and complete and fragmentary biogenic material set in a calcite cement (Plate 3.3.2). Ooids are often preferentially concentrated in burrows. The ooids generally make up 5-20% of the rock. Hallimond (1925) has briefly described specimens of this facies from the Banbury district and termed the lithology 'Greenstone'. Dunham (in Whitehead et al., 1952) considered the facies at Banbury to be a sideritic chamositic chamosite limestone and that in Leicestershire - Lincolnshire to be a sideritic chamositic limestone. Neither of these workers have provided detailed textural descriptions or post-depositional histories of the facies.

3.3.4.i Chamosite ooids: The chamosite ooids exhibit all the features described above. In contrast to the ooids of the chamositic chamosite oolite facies, the ooids of this facies exhibit a wide variation in the colour of their envelope rings. Thus, a grass-green envelope ring may be found adjacent to an olive-brown ring. Such a colour

variation accentuates the internal structure of the ooids. In general, the ooids of this facies have remained unchanged by depositional processes.

In areas of high ooid concentrations authigenic chamosite, grass-green in colour, is common. It forms rims to ooids which are usually less than 0.05 mm in width and have slightly ragged outer edges (Plate 3.23). If shell fragments are present these also exhibit a coating of authigenic chamosite. Two adjacent ooids, with authigenic chamosite rims, often show coalescence of their rims where they are in closest proximity to each other. The separation between the ooids in these areas is generally less than twice the width of an authigenic chamosite rim. The authigenic chamosite may thus form isopachous pore linings in areas of high ooid concentrations. In areas where ooids are severely distorted authigenic chamosite occurs as a distorted zone between ooids. Complete or incomplete rims of authigenic chamosite may occur around individual ooids in areas of low ooid concentrations. Very rarely authigenic chamosite occurs as an interior lining to ooimoulds. The fact that this type of chamosite occurs in association with textures which are clearly of post-depositional origin, and in some cases post-dates them, implies that its identification as a diagenetic mineral is correct. This is supported by the delicate nature of many of these textures which would not have survived in the depositional environment.

Textures are present which indicate that local diagenetic modification of chamosite ooids did occur. Ooimoulds are rare but represent the first stage in one type of such modification. They comprise the outer one or two envelope rings of an ooid surrounding a central void. As before the individual rings are complete. In some

cases complete dissolution of the ooid occurred. The secondary porosity thus created was preserved by a pre-existing rim of authigenic chamosite of the type described above. Ooimoulds may remain empty but they are often infilled by one or more diagenetic generations. The first such generation is authigenic chamosite. This lines the secondary porosity and is again grass-green in colour with a ragged outer boundary. The occurrence of this type of infill is extremely uncommon. More commonly found are siderite infills (Plate 3.24). Siderite may only form a lining to the ooimould or it may completely infill it. In the former case it takes the form of dog's tooth crystals rooted on the wall of the ooimould. In the latter case a single crystal or a mosaic of several grains infill the ooid. Ferroan calcite is the only other ooimould infilling generation. It occurs as one or two grains completely infilling ooimoulds. These may cross cut the ooimould walls to partake in the cement fabric (Plate 3.25). Dunham (in Whitehead el al., 1952) has reported this textural type. Authigenic chamosite and dog's tooth siderite crystals may also occur in ooimoulds infilled by ferroan calcite and are totally surrounded by it.

The second type of diagenetic modification exhibited by chamosite ooids is their replacement by ferroan calcite. The initial stages of this replacement are represented by lenticular shaped areas of ferroan calcite occurring within individual rings and parallel to ring contacts. Crescents of such replacive ferroan calcite often occur in the envelope at either end of the long axis (Plate 3.26). A greater degree of replacement leads to similar shaped portions of ferroan calcite occupying two or three rings width. Ultimately the ooids are completely replaced by ferroan calcite. This usually includes the ooid core grain.

Ghost ring contacts are often seen within this calcite. In addition, ring-shaped bands of a buff or black colouration and having no mineralogical characteristics sometimes occur within the calcite. These are precisely the same as those which are found in ooimoulds, infilled ooimoulds, and replaced ooids within the chamositic chamosite oolites. In some instances splinters of envelope chamosite occur within the ferroan calcite and retain their original orientation within the ooid. Ooimoulds which had a relatively thick envelope remaining and which were infilled by ferroan calcite may show such splinters of chamosite within the calcite indicating that ooid replacement was associated with the ooid infill. The presence of dog's tooth siderite within the ooimould demonstrates that this texture does not represent ooid replacement commencing within the core grain. The ferroan calcite of replaced ooids is of one or two grains which may partake in the cement fabric.

3.3.4.ii Chamosite books: These grains are common within the facies. They are usually less than 0.4 mm in length. The (001) cleavage traces are well defined and are generally parallel to the long axis of the book. In all cases the books have undergone a degree of attrition resulting in the rounding of corners. This results in a series of book shapes from rounded squares and oblongs to ellipses. Although niches are present at either ends of the cleavage traces they are not at all well developed in comparison to those of core books. The colour of the chamosite books is variable but in all cases lies in the browner range of chamosite colours. In areas of high ooid concentrations where authigenic chamosite is common

individual chamosite books are also coated by authigenic chamosite. Books may exhibit replacement by ferroan calcite (Plate 3.27).

3.3.4.iii Intraclasts: These allochemical grains are generally ovate in shape and have a size range of 0.15-6.00 mm, measured along their long axis. The smaller intraclasts are often found to have very irregular forms. The ovate intraclasts show a clear preferred orientation with their major axes being aligned parallel to bedding. It is generally the case that intraclasts tend to well define particular horizons within a slide, although individual intraclasts occur elsewhere. The average size of the former is generally greater than that of the latter.

Mineralogically the intraclasts are composed of dark green to olive green chamosite, siderite, and subordinate ferroan calcite (Plate 3.28). Polished sections show the presence of framboidal pyrite. The chamosite is present as small platelets in a random orientation; under crossed polars platelets extinguish individually giving the intraclast a spotted appearance. Complete and fragmentary ooids are occasionally present within the intraclasts. Siderite occurs as euhedral rhombs and anhedral masses less than 0.05 mm in size. The ferroan calcite infills any porosity within the intraclasts. In addition to the above occurrences of siderite and ferroan calcite. these minerals occur as an infill to rectangular and rounded voids, less than 2 mm in size, set within the intraclasts. These are lined by white or ironstained siderite dog's teeth and infilled by ferroan calcite. This texture occurs with exactly the same form in the chamositic chamosite oolites where it was concluded to represent the infill to a secondary porosity resulting from the dissolution

of aragonite shell fragments. Such intraclasts are clearly derived from areas of chamositic chamosite oolite formation. Rounded and rectangular shaped intraclasts composed of siderite and ferroan calcite also occur. The siderite is distributed around the edges of the grains as dog's teeth which point towards the centre of the grain. Ferroan calcite forms the central areas. This type of intraclast clearly represents the end product of continued abrasion of intraclasts which were originally of the type described above.

3.3.4.iv Biogenic material: The remaining allochemical grains comprise fragments of originally aragonite and calcite bivalves, brachiopod material, echinoid spines and plates, and forams. All the macrofauna is fragmentary and has undergone some degree of abrasion. Although there are exceptions this material is less than 1 mm in size.

The bivalves and brachiopods which had a primary calcite shell mineralogy are often surrounded by a micrite envelope. Amongst the brachiopods fragments of impunctate rhynchonellids can be recognised by their zig-zag cross section. Fragments of terebratulids may be distinguished by the presence of punctata infilled by ferraon calcite. Authigenic chamosite rims to these types of shell fragments are rare.

Original aragonite bivalve debris is characterised by shell-fragment shaped areas surrounded by a rim of authigenic chamosite and infilled by ferroan calcite. Euhedral rhombs of siderite are often mounted on the authigenic chamosite and penetrate both the secondary porosity resulting from the aragonite dissolution and the surrounding primary porosity (Plate 3.29). Authigenic chamosite and euhedral siderite also occur as incomplete rims.

The echinoid fragments are generally constructed of ferroan calcite. Occasional plates show a central non-ferroan calcite core and an outer rim of ferroan calcite. The echinoid stereome systems are often infilled by dusty ferroan calcite. In some instances the infill is of authigenic chamosite. Some echinoid plates are characterised by an initial syntaxial overgrowth of siderite (Plate 3.30). This is seen as a series of siderite rhombs mounted on an echinoid plate and having a preferred orientation in which the rhomb long axes are subparallel. At the centre of each rhomb a small dusty area may occur indicating the position of a stereome system pore. In some cases spots of ferroan calcite occur within the siderite indicating an earlier stereome system infill. The siderite euhedra may be sufficiently closely spaced or have grown to sufficient size to mutally interfere during subsequent growth. All echinoid plates are surrounded by a syntaxial rim of ferroan calcite whose outer edge partakes in the cement fabric.

The forams present are composed of non-ferroan calcite. Their chambers are infilled by ferroan calcite cement.

3.3.4.v. Cement minerals: Dog's tooth siderite euhedra occur rooted on chamosite mud intraclasts and growing perpendicular to them.

Ferroan calcite forms the cement to the above allochemical constituents. Two generations have been recognised. The first of these is a ragged radial fibrous growth (Plate 3.31) found rooted on non-ferroan calcite shell fragments. A complete surround does not occur. The remaining porosity is infilled by ferroan calcite with an inequigranular xenotopic fabric. This passes with optical continuity into the secondary porosity of original aragonite fragments and ooimoulds.

3.3.4.vi Paragenesis: The above textures indicate a relatively simple post-depositional history for the calcitic chamosite oolite facies. The sequence of events is shown in Figure 3.15.

Textural evidence, which has been discussed above, indicates that the grass-green, uniform thickness coating to many allochemical grains is post-depositional in origin. The occurrence of distorted authigenic chamosite between distorted chamosite ooids and the fact that it is either cross-cut or surrounded by other diagenetic mineral generations indicates that it was apparently the first post-depositional mineral to precipitate. Its occurrence as an isopachous lining to the primary porosity is suggestive of precipitation from aqueous solution.

Following the precipitation of authigenic chamosite, ooids in areas of high ooid concentration were distorted in, presumably, response to increased sediment loading. This resulted in the deformation of the interstitial authigenic chamosite. It is interesting to note that the distortion involved entire ooids and was not preceeded by the formation of ooimoulds. Textures such as chain and hooked ooids are therefore absent.

Since ooimoulds occur, albeit rarely, and do not show textures indicative of deformation, it follows that their formation post-dates the structural reorganisation of the oolite in response to loading. As before, the remnant portions of the ooids indicate that chamosite dissolution commenced in the centre of the ooid and moved outwards. The end product of the dissolution process is indicated by ooid-shaped rims of authigenic chamosite surrounding a secondary porosity containing no original chamosite. The presence of occasional authigenic chamosite inner linings to ooimoulds

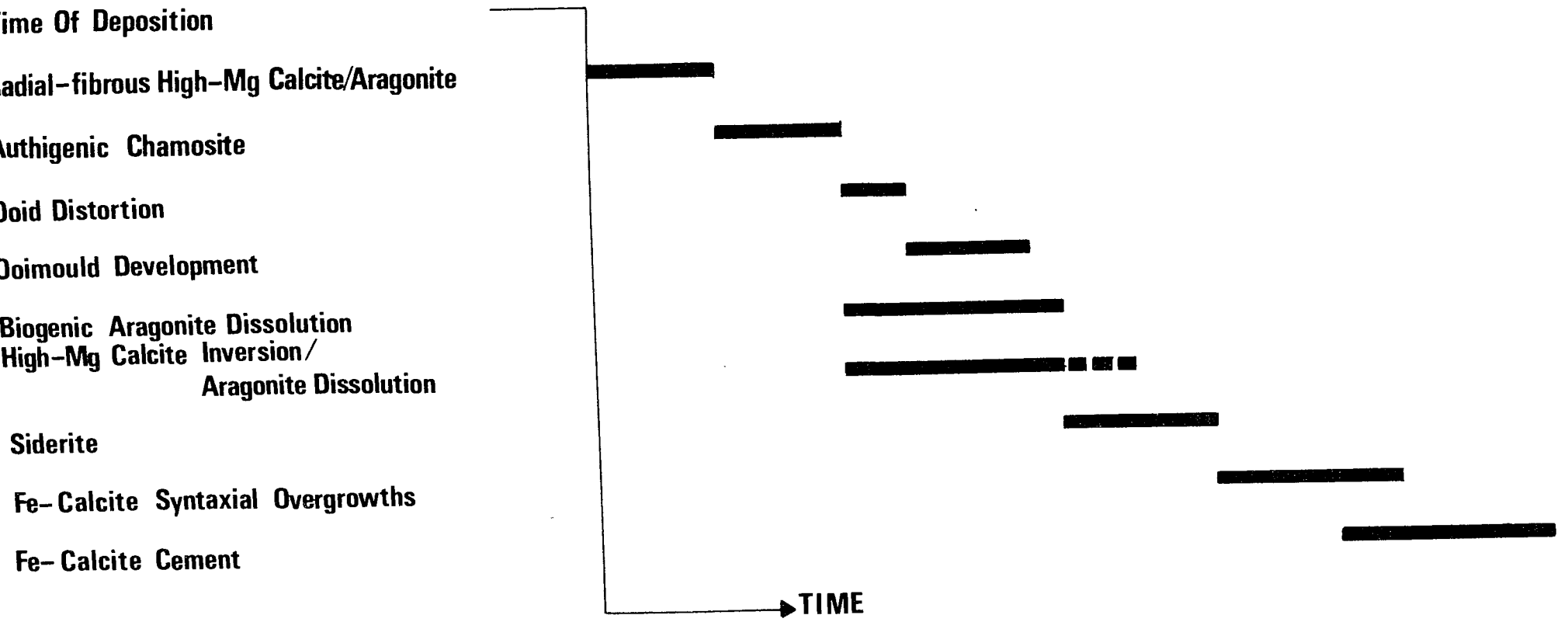

Figure 3.15: Paragenesis Of The Calcitic Chamosite Oolites

indicates that ooimould formation overlapped slightly with the formation of authigenic chamosite. The secondary porosity resulting from ooimould formation provided regions within which later diagenetic mineral generations could precipitate.

The time at which many of the originally aragonitic shell fragments began to dissolve post-dates the precipitation of the authigenic chamosite. This follows from the fact that these were rimmed by authigenic chamosite which acted as a mould to the secondary porosity resulting from aragonite dissolution. In many cases this mould was not complete; as a result the secondary porosity was not retained. That porosity which was retained formed areas of precipitation for later diagenetic generations.

Siderite occurs throughout the facies as a white dog's tooth phase which participates in a number of textures. Its occurrence as a lining to ooimoulds and penetrating the secondary porosity of originally aragonitic shell fragments indicates that it immediately post-dates the creation of these secondary porosities. Its occurrence as a syntaxial overgrowth on echinoid plates indicates that it pre-dates the formation of ferroan calcite overgrowths. This can be deduced from the cross-sectional interpretation of this texture (Evamy and Shearman, 1965, 1969), shown in Figure 3.16. In order for siderite to usually only contain the dusty inclusions which represent stereome pores and be surrounded by syntaxial ferroan calcite the siderite must be the first syntaxial generation. The syntaxial overgrowth of siderite represents an initial lining to the primary porosity. Another example of this type of lining is represented by dog's tooth siderite rooted on chamosite mud intraclasts and growing into the surrounding

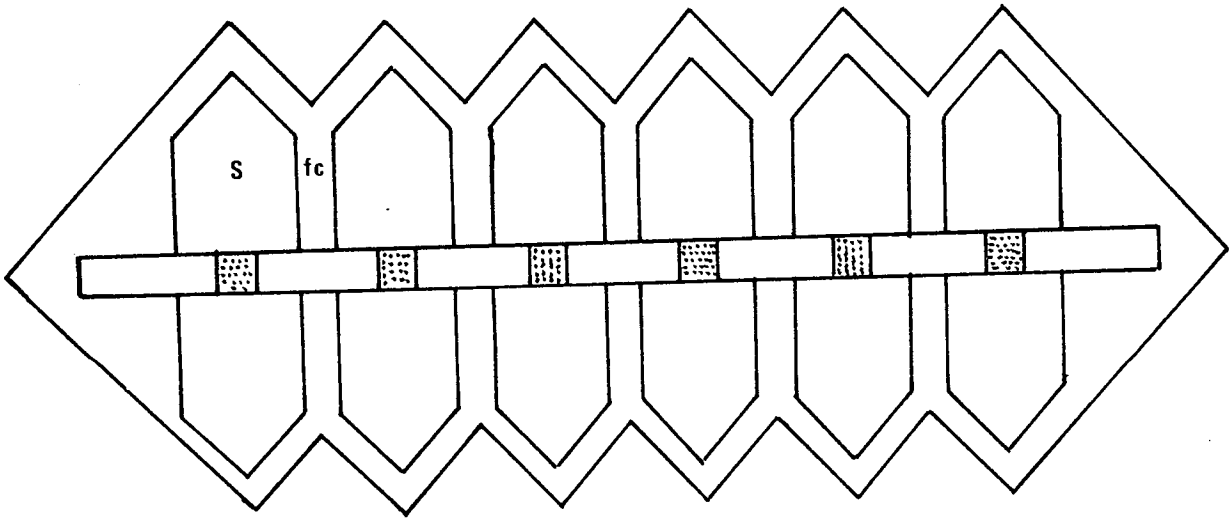

Fig 3.16 Interpretation of Echinoid Plate Overgrowths

Stippling ; dusty inclusions in stereome pores in horizontal echinoid plate. Prismatic crystals mounted on echinoid plate ; siderite(s) surrounding overgrowth ferroan calcite (fc).

porosity. The precipitation of siderite evidently came to a rapid close as it never forms a cement mosaic indicating continued and interfering growth. The very occasional exceptions to this are represented by ooimoulds completely infilled by a siderite mosaic. This would be expected as ooimoulds are small volumes which would be quickly infilled.

Following the cessation of siderite precipitation ferroan calcite began to precipitate. This commenced with the nucleation of ferroan calcite on echinoid plates and the subsequent development of ferroan calcite syntaxial overgrowths. Since the edges of echinoid syntaxial overgrowths interfere with the cement calcite their growth was brought to a close during the precipitation of this generation.

The first cement generation takes the form of ragged radial fibrous growths of ferroan calcite rooted on shell fragments. The ragged edges of this texture and the poor development of internal prism boundaries suggests that it represents an early growth of either high magnesian calcite or aragonite which has subsequently been replaced by ferroan calcite, rather than representing a prismatic generation of ferroan calcite precipitated at this point in the evolution of the facies. The ragged edges of this texture are suggestive of a phase of dissolution prior to replacement. This texture is only found in association with non-ferroan calcite shell fragments. These are very rarely rimmed by authigeneic chamosite. It is therefore concluded that the radial fibrous cement crystallised before the precipitation of authigenic chamosite and nucleated on the calcite shell fragments. This would have prevented authigenic chamosite from forming a rim around these grains. It is not possible to date the point at which the replacement occurred.

It must post-date the precipitation of authigenic chamosite. This follows from the fact that many of the radial fibrous fringes have been completely removed by dissolution. Had this occurred before precipitation of authigenic chamosite ceased the exposed shell fragments would have obtained chamosite rims.

The final cement generation is represented by the inequigranular xenotopic ferroan calcite. This infills all the remaining porosity and surrounds all the previous diagenetic mineral generations. The fact that the ferroan calcite which replaces chamosite ooids may partake in the cement fabric indicates that the replacement occurred during the precipitation of this cement generation.

3.3.5. Bioclastic Limestone

This facies has been briefly described by Hallimond (1925) who referred to it as 'Limy Stone'. Little can be added to his description of it as a rock containing many clean shell fragments, subordinate chamosite ooids, and occasional siderite and calcite intraclasts set in a calcite cement. Originally aragonite shell fragments are absent. The siderite and calcite intraclasts are characterised by an outer zone of dog's tooth siderite surrounding a core of ferroan calcite. The origin of these grains has been discussed above. Authigenic chamosite and siderite are absent. Ragged radial fibrous growths of ferroan calcite rooted on calcite shell fragments occur. These represent either replaced high-magnesian calcite or aragonite. Echinoid fragments are constructed of ferroan calcite and exhibit syntaxial overgrowths of ferroan calcite. The dominant cement mineral is ferroan calcite which has an inequigranular xenotopic fabric and infills the porosity. The paragenesis of the diagenetic minerals

present in this facies is precisely the same as that for the calcitic chamosite oolite facies.

3.4. SUMMARY

The Marlstone Rock-bed Ironstone was deposited in a depositional basin in association with sandstones which form the sandrock facies.

The sandrock and three ironstone facies can be characterised by their depositional and diagenetic mineral assemblages. There is evidence to suggest that chamosite ooids formed in the chamositic chamosite oolite facies. Erosion of these facies yielded ooids and chamosite mudstone intraclasts which could be incorporated in the calcitic chamosite oolite and bioclastic limestone facies. The presence of these phases in the sandrock facies indicates contemporaneous deposition of the sandrock and ironstone facies. The abundance of authigenic chamosite books in the sandrock facies suggests that reworking of this facies may have yielded chamosite books for incorporation in the ironstone facies.

CHAPTER 4

THE CLEVELAND IRONSTONE FORMATION

THE CLEVELAND IRONSTONE

4.1 INTRODUCTION

The Cleveland Ironstone occurs in the Cleveland district of the North Riding of Yorkshire (Figure 4.1). It is best exposed on the coast from Saltburn to Sandsend, a distance of approximately 50 km. Due to minor folding it appears in the cliffs at the northern end of Robin Hood's Bay. Inland the ironstone is exposed along an escarpment which runs 30 km in a south-easterly direction from Saltburn to Roseberry Topping. From here it passes south to Kildale, 8 km away. Due to the Upsall Fault the ironstone sequence is repeated to the north giving rise to Eston, Upleatham, and Hob Hills. In addition, the Cleveland Ironstone is found in a number of the deeply incised dales of the North Yorkshire Moors National Park. The ironstone was exploited as an economic iron ore from 1848 to 1964. Due to the mode of occurrence of the ironstone adit and shaft mining methods were utilised. Although the field is now defunct it is not worked out; Whitehead et al. (1952) estimate that 232 million tons of iron ore remain.

The Cleveland Ironstone occurs as a series of named seams separated by shales and siltstones. Thus, in accordance with current stratigraphic methods, this sequence is termed the Cleveland Ironstone Formation. Figure 4.2 shows the detailed stratigraphy of the Domerian and Whitbian of the Yorkshire coast around Whitby, based on the work of Howarth (1955), 1962, 1973, 1978), Chowns (1968), and Bradshaw et al (1980). It can be seen that deposition of the Formation commenced in Margaritatus zone times, and continued until the start of Whitbian Tenuicostatum zone deposition. The Formation thus occupies the greater part of the

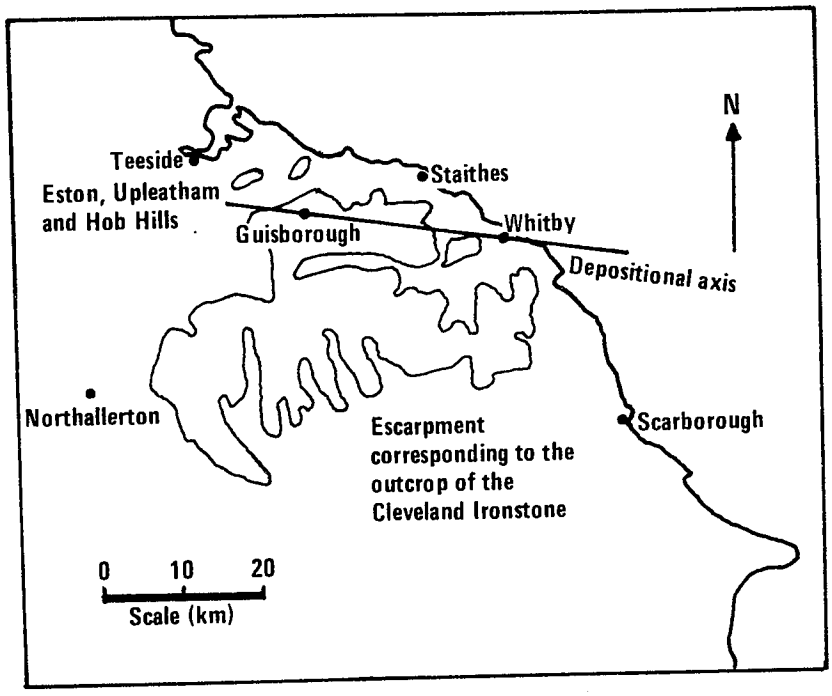

Fig 4.1 Location map of the Cleveland Ironstone formation

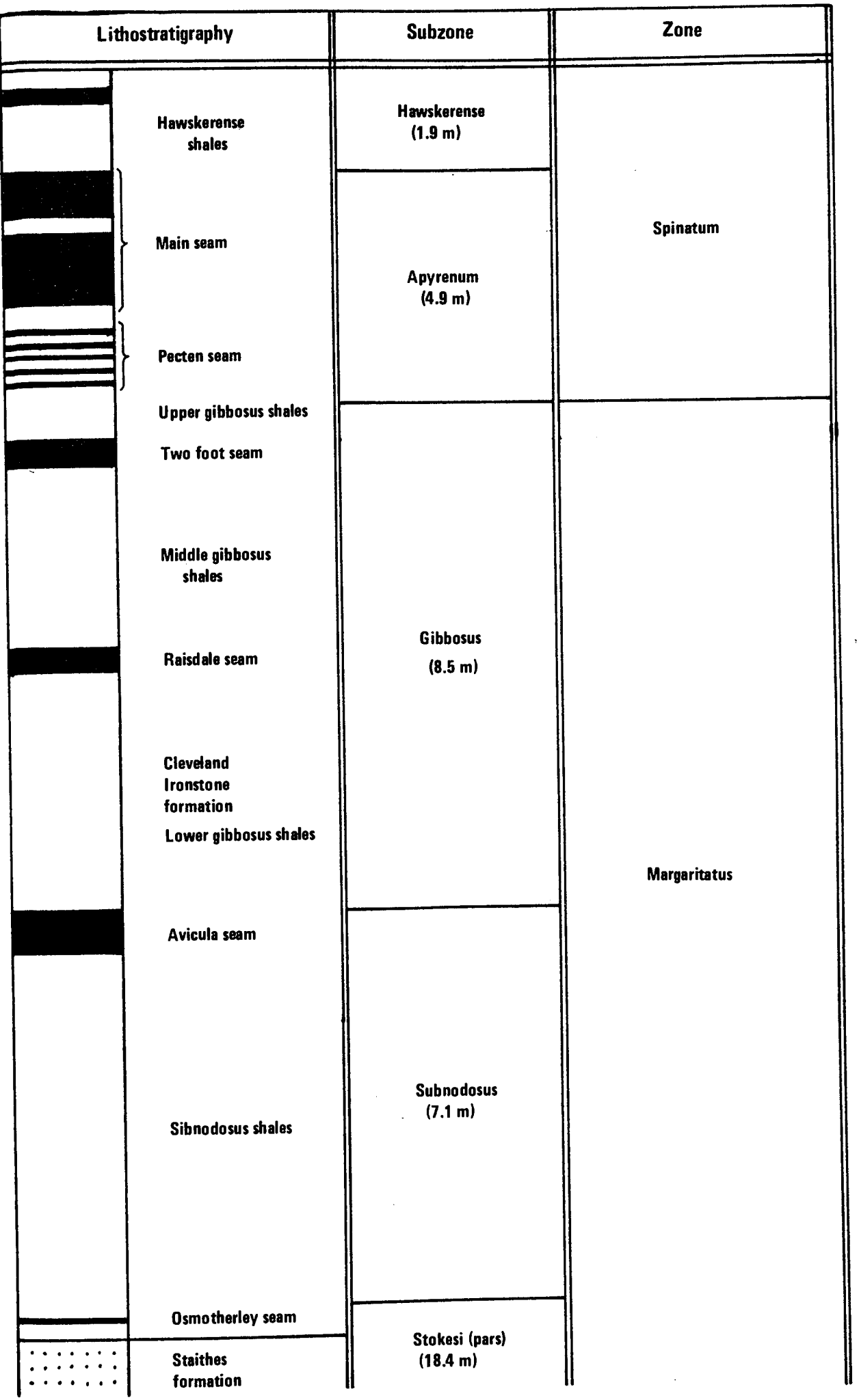

Fig 4.2 Stratigraphy of the Cleveland Ironstone Formation

Domerian strata. It is interesting to note that the Spinatum zone position of the Ironstone Formation is time-equivalent to the Marlstone Rock-bed; conditions favourable to ironstone formation evidently prevailed over a large part of eastern England at this time.

Chowns (1968) has shown that the Cleveland Ironstone Formation occupies a depositional trough within which its maximum thickness occurs along a WNW-ESE axis, running from Guisborough to Whitby (Figure 4.1). At Brackenberry Wyke, 1.5 km south-east of Staithes, the Cleveland Ironstone Formation is approximately 23 m thick. From this area the Formation initially retains its thickness and then thins out in a south-westerly direction. 18 km to the south-east, at Hawsker Bottoms, the Formation is approximately 19 m thick but the ironstone seams are much thinner or absent (Chowns, 1968). In Raasay the Domerian is represented by 75 m of sandstone and it would appear, therefore, that the Cleveland Ironstone Formation is a condensed sequence. This is in keeping with the suggestion of Hallam and Bradshaw (1979) that oolitic ironstones are diagnostic of the minima of regressive phases.

The sequence beneath the Cleveland Ironstone Formation is well-known. The Sinemurian and most of the Carixian comprise a sequence of dark grey finely-laminated or silty shales and fine-grained sandstones. These pass up into the Staithes Formation. This appears in the Davoei zone of the Carixian (Figure 4.2). Its deposition continued until near the end of Domerian Stokesi zone times. The Staithes Formation is made up of medium-grained micaceous sandstones which exhibit current and interference ripple marks, plane bedding, and trough cross-bedding. A benthonic fauna of many different bivalve species, gastropods and brachiopods has been reported. Bioturbation is abundant. Hemmingway

(In Rayner and Hemmingway, 1974) considers the Staithes Formation to represent a shallow marine inshore, or possibly intertidal, environment. The upward passage from argillaceous to sandy, shallow water sediments is clearly indicative of an overall shallowing episode (Hallam, 1978) prior to the deposition of the Cleveland Ironstone Formation.

The Cleveland Ironstone Formation is overlain by the Whitbian Grey Shales which comprise pale grey, silty, pyritic shales. These are overlain by finely-laminated dark brown bituminous shales; the Jet Rock. This succession clearly indicates a period of deepening resulting from the major marine transgression at the end of Domerian times (Hallam, 1978) which terminated deposition of the Cleveland Ironstone Formation.

4.2 FORM AND NATURE OF THE IRONSTONE

The Cleveland Ironstone Formation has been examined at outcrop on the coast and inland. Figure 4.3 shows the sites of the localities visited. Detailed logging of the ironstone sequence exposed at each was carried out. Individual graphic logs of the sections examined are presented in Figure 4.4. The sequence of ironstone seams was established as a result of widespread mining activities in the Cleveland district. This, and the work of Hawarth (1955) and Chowns (1968) (Figure 4.2) has allowed the identification of individual ironstone seams and shale and silt units on a lithostratigraphic basis. Using this approach correlations between the localities visited have been carried out and are presented in Figure 4.13.

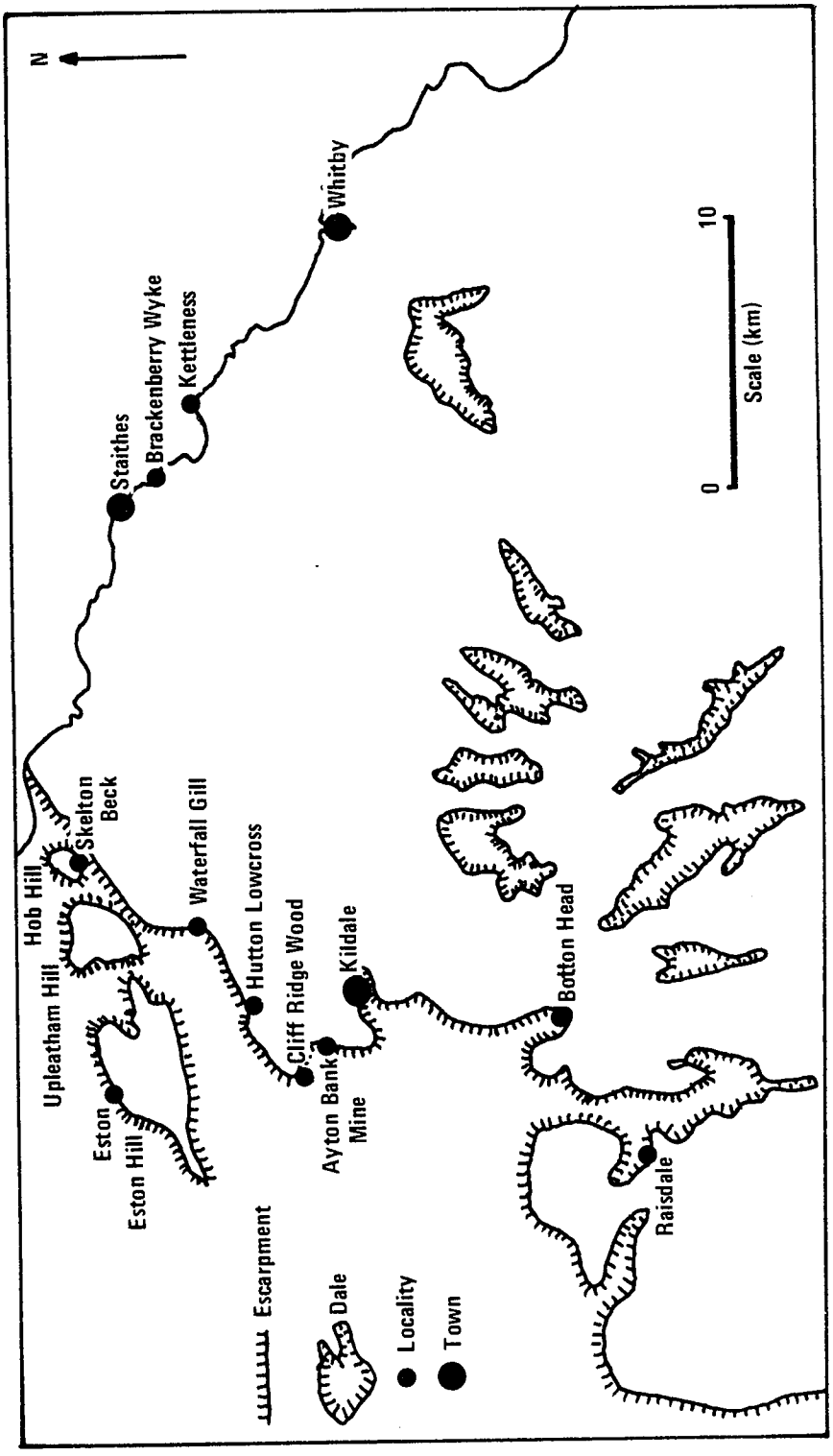

Fig 4.3 Sites of localities in the Cleveland Ironstone Formation

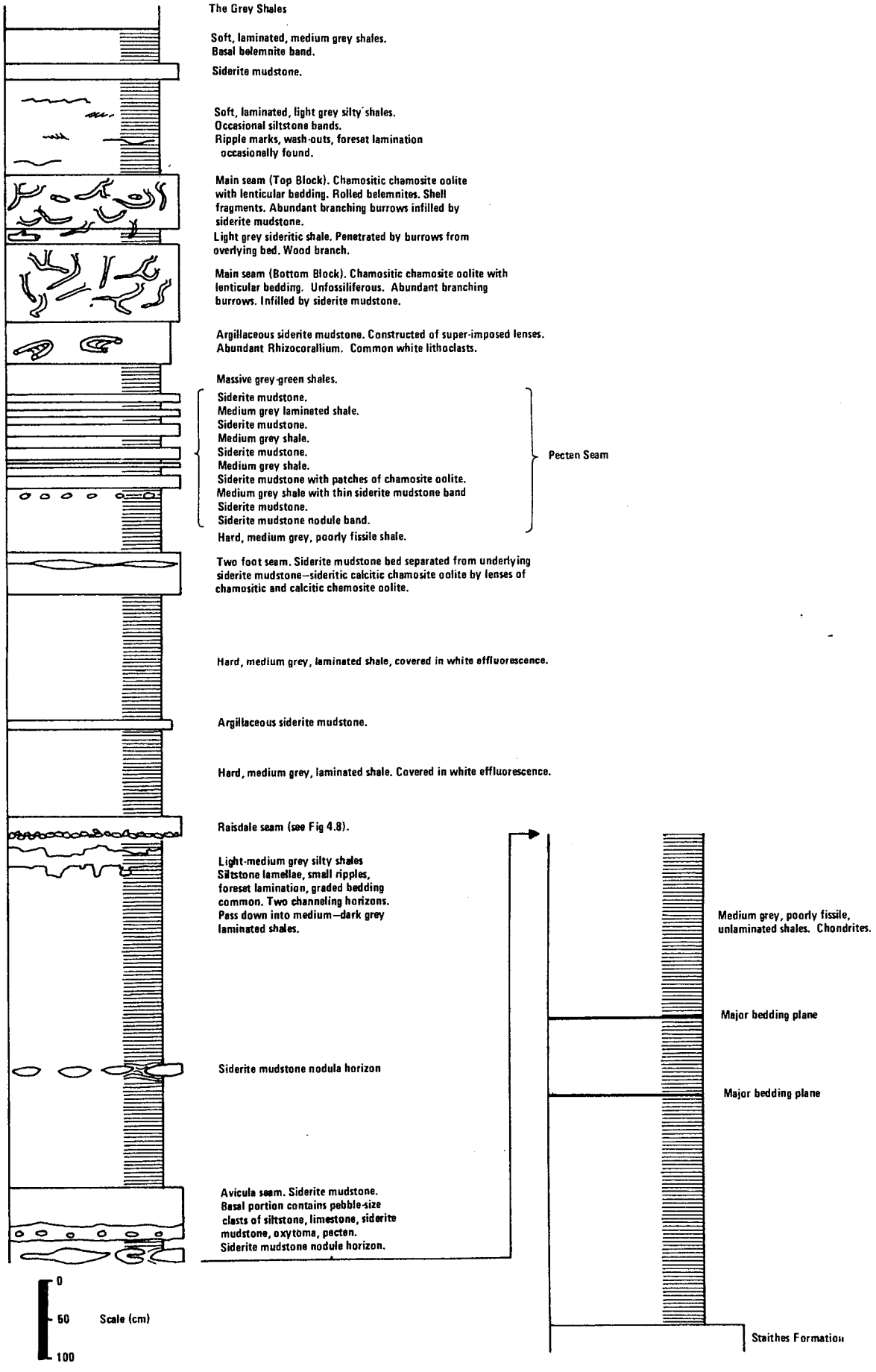

Fig 4.4a The Cleveland Ironstone Formation at Brackenberry Wyke

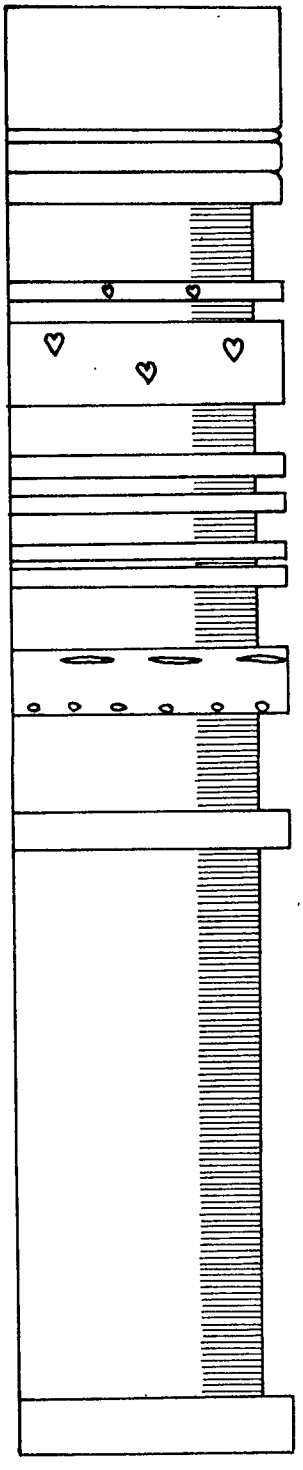

Main seam (Top Block). Overlain by 2 m scree in which paper shales outcrop.
Siderite mudstone with many ooimoulds.

Shale band
Shale band
Shale band

Hard, dark grey, poorly laminated shale

Siderite mudstone. Ooimoulds common. Gresslya.

Main seam (Bottom Block).
Siderite mudstone. Abundant ooimoulds. Gresslya common.
Rhizocorallium common in basal 10 cm.

Hard, dark grey, poorly laminated shale.

Siderite mudstone. Many ooimoulds.
Dark grey shale.
Siderite mudstone. Many ooimoulds.
Dark grey shale
Siderite mudstone. Many ooimoulds
Dark grey shale
Siderite mudstone. Many ooimoulds
} Pecten Seam

Hard, dark green shale

Two Foot Seam. Upper 10 cm siderite mudstone with siderite mudstone nodules. Lower 46 cm chamositic chamosite oolite with oolite clasts at base.

Dark grey, poorly laminated shales.

Raisdale Seam. Siderite mudstone.
Common ooimoulds.

Dark grey, well laminated shales.

Avicula Seam. Siderite mudstone

0
50 Scale (cm)
100

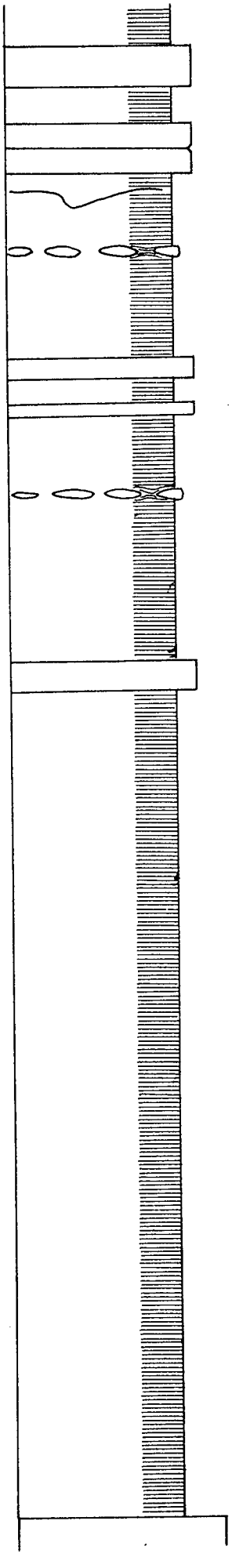

Medium grey, fissile paper shales

Main seam. Siderite mudstone with numerous ooimoulds.

Dark green, poorly fissile shales.

Pecten seam. Siderite mudstone with numerous ooimoulds.
Shale parting.
Two Foot Seam. Siderite mudstone with numerous ooimoulds.

Medium grey, poorly fissile, laminated shales.
Channeling horizon 25 cm from top of unit.

Siderite mudstone nodule horizon.

Raisdale seam. Siderite mudstone with numerous ooimoulds.

Medium grey, fissile, laminated shale.

Avicula seam: Hard, splintery siderite mudstone.

Medium grey silty shales. Silt lamellae pick out small wash-outs and ripples.

Siderite mudstone nodule horizon.

Siderite mudstone with abundant white ooids. Silt lamellae. Pecten, Chlamys, Oxytoma.

Medium grey unlaminated shales.

0
50 Scale (cm)
100

Staithes Formation

Fig 4.4c The Cleveland Ironstone Formation at Raisdale

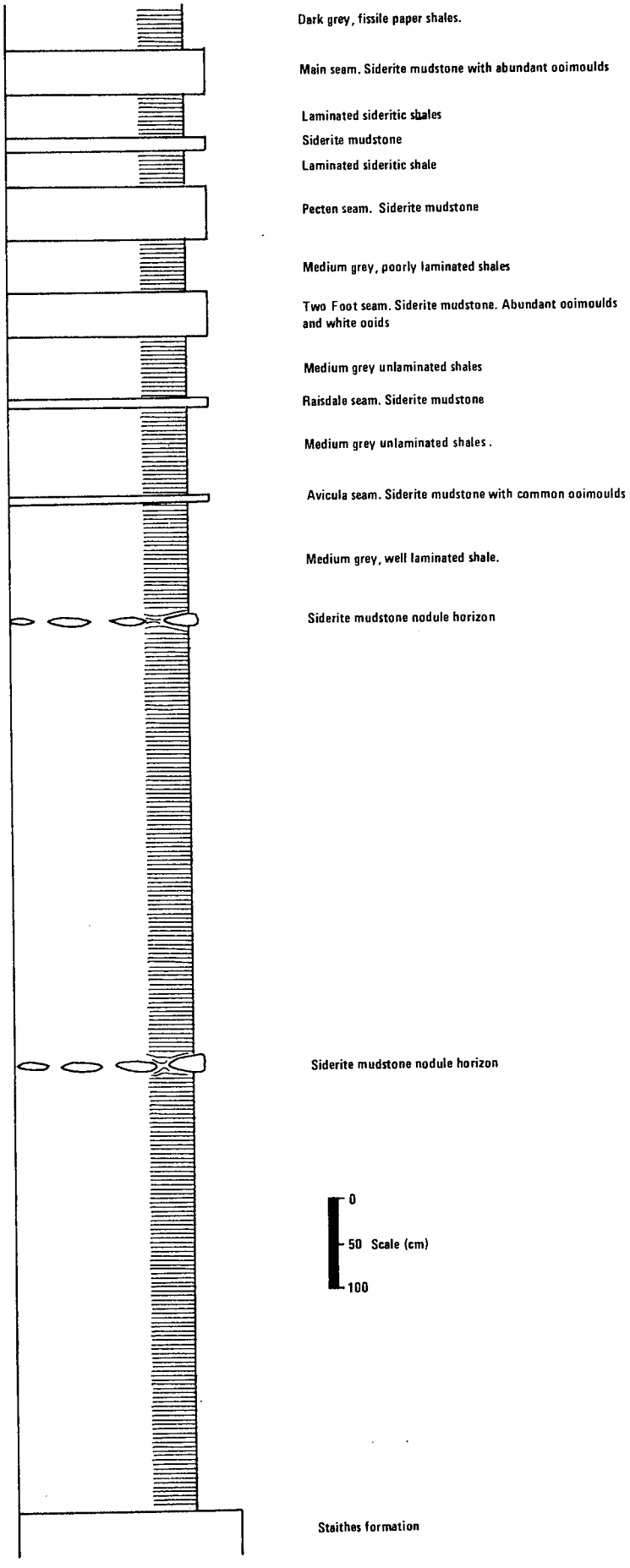

Fig 4.4d The Cleveland Ironstone Formation at Botton Head, Greenhow Moor

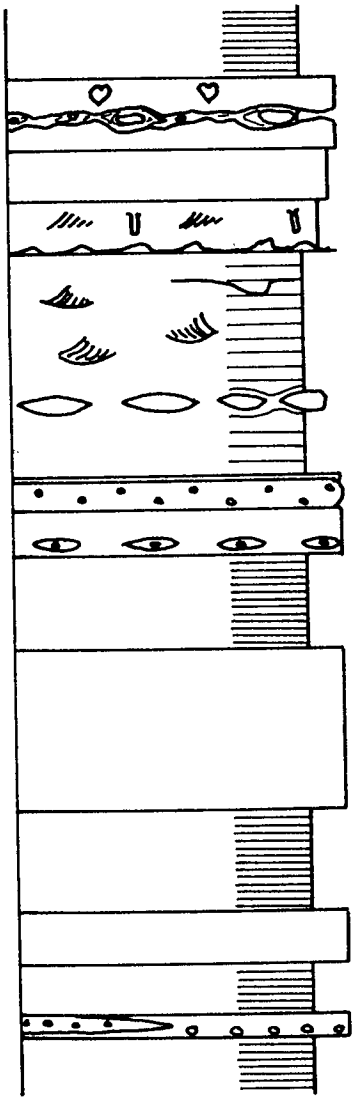

Dark grey, well laminated shales.

Siderite mudstone with irregular base. Gresslya, contorted shale with siderite mudstone nodules.

Bioturbated sandy siltstone.
Grey siltstone, sandy wedges. Chondrites abundant.
Hard siltstone band with rippled surface.

Light-medium grey silty shales. Shale is well laminated and contains silt lamellae and concave downwards laminated wedges. Occasional channels.

Siderite mudstone nodule horizon.

Medium grey poorly laminated shale

Main seam (Top Block). 5 cm siderite mudstone overlies 17 cm chamositic chamosite oolite. Remainder siderite mudstone with basal pods of chamositic chamosite oolite.

Medium grey shales.

Main seam (Bottom Block). Hard siderite mudstone with small lenses of chamosite mudstone.

Medium grey unlaminated shale.

Pecten seam. Siderite mudstone.

Medium grey unlaminated shales.

Two foot seam. Siderite mudstone with lenses of chamositic chamosite oolite. Clasts of bioclastic limestone at base.

0
50 Scale (cm)
100

Fig 4.4e The Cleveland Ironstone formation at Kettleness

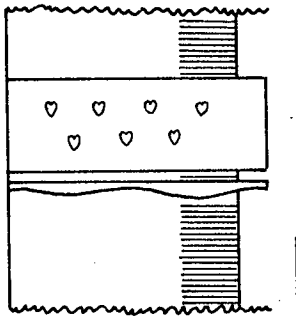

Top Exposure

Hard, dark green chamosite mudstone with dull yellow chamosite ooids and ooimoulds.

Main seam (Bottom Block). Siderite mudstone with abundant Gresslya in life position.

Hard, dark grey shale.
Siderite mudstone.

Dark grey fissile shales.

Base Exposure

Fig 4.4f The main seam exposure at Waterfall Gill

A steep bank representing the Top Block occurs above the exposure.

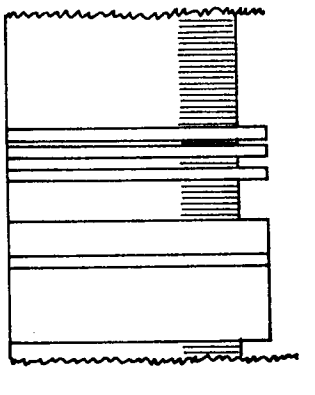

Top Exposure

Dark grey unlaminated shales

Siderite mudstone
Siderite mudstone
Siderite mudstone
Dark grey shales
Dark grey shales
} Pecten Seam

Dark grey unlaminated shale

Siderite mudstone
Chamosite mudstone
Siderite mudstone with chamosite mudstone patches.
} Two Foot seam

Dark grey shale.
Base Exposure.

Fig 4.4g The Pecten and Two Foot seam exposed at Hutton Lowcross

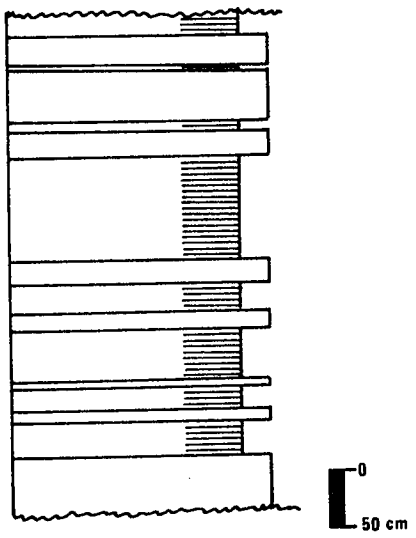

Top exposure
Earthy shales

Main seam (Bottom Block). Siderite Mudstone with ooimoulds split by two shale partings.

Dark grey poorly laminated shales. Abundant Rhizocorallium.

Siderite mudstone
Dark grey shale
Siderite mudstone

Dark grey shale
Siderite mudstone
Dark grey shale
Siderite mudstone
Dark grey shale
} Pecten Seam

Two Foot seam.Siderite mudstone with patches of chamosite and white ooids.

Fig 4.4h The Main Seam, Pecten Seam, and Two Foot Seam at Ayton Banks Mine

A steep bank representing the Top Block occurs above the exposure

Unillustrated Sections :

Skelton Beck : Main Seam; unsplit. 2.40m brittle sideritic chamositic chamosite oolite. Top and bottom of seam not seen.

Eston Hill : Main Seam; unsplit. 1.16m brittle sideritic chamositic chamosite oolite. Top and bottom of seam not seen.

4.2.1 The Cleveland Ironstone Formation, Field Characteristics

Since the Cleveland Ironstone Formation is an alternating sequence of ironstone and shale-silt the nature of each unit should be considered directly in context of the units above and below rather than as a representative of a facies type. Four complete sections of the Cleveland Ironstone Formation have been examined and of these only the Brackenberry Wyke succession reveals detailed information regarding the nature of individual units. The Kettleness succession reveals a similar amount of detail for those units above the base of the Two Foot Seam. This is a result of the fact that they are both coastal exposures. The characteristics of these successions are therefore described below and compared with other successions.

4.2.2 subnodosus Shales

These rest directly on the Staithes Formation. Chowns (1968) has recorded a thin ironstone seam, the Osmotherly Seam, at this junction. The unit comprises light, medium, and dark grey shales. Any original lamination has been destroyed by the ichnogenera Chondrites. This trace fossil indicates bathymetric levels deeper than the deep subtidal (Fursich, 1970). Pyrite is abundant as anhedral masses, and small cubes. Approximately 3 m from the base a major bedding plane occurs which can be traced in the cliff-face from Staithes to the point at which it runs onto the wave-cut platform at Brackenberry Wyke. A similar bedding plane occurs approximately 1 m above it. These probably represent periods of non-deposition during which the original mud underwent a certain amount of consolidation. A fauna of Pseudopecten sp; Entolium sp; Gresslya sp; Oxytoma sp, and belemnites was found.

The top of the subnodosus shales is characterised by a band of siderite mudstone nodules. These are lenticular in cross-section and circular in plan. They are generally less than 1 m in diameter. Occasional irregular nodules representing the coalescence of two adjacent nodules during growth also occur. Small round nodules less than 10 cm across are present between, above, and below the larger nodules. Chowns (1968) has identified laminated calcareous mudstone pebbles and cobbles amongst these and has concluded that they represent a hiatus in deposition. The bedding of the enveloping shales is contorted around the larger nodules. The degree of distortion diminishes with distance from the nodules until no sign of distortion remains. It is often found that the nodules enclose bivalve accumulations. The distortion of the shales indicates that the nodules are diagenetic accumulations. The association of the nodules with organic remains suggests that the decay of this material created a chemical environment favourable to siderite precipitation (Curtis and Spears, 1968a).

4.2.3 The Avicula Seam

This ironstone unit comprises a thin lower bed with an undulating upper surface, separated from a thick upper bed by a shale parting. The shale parting retains a constant thickness which results in an undulating base to the upper bed. At Cliff Ridge Wood, Botton Head, and Raisdale the Avicula Seam is represented by a single bed.

The lower bed is constructed of siderite mudstone. Occasional pendants extend a short distance into the underlying shales. The bedding of the shales in contact with such pendants is contorted around them. Within the main body of the bed clasts of siderite mudstone, less than 10 cm across, occur. The undulations of the upper surface of the bed do not appear to correspond to any current-generated sedimentary structure.

They are more suggestive of a lateral coalescence between large lenticulate siderite mudstone nodules during growth. This conclusion is supported by the presence of shale-distorting pendants. The clasts therefore represent a conglomerate deposited during a depositional hiatus and subsequently included within a bed of siderite mudstone. Chowns (1968) has demonstrated the association of large siderite mudstone accumulations with pauses in deposition in the subnodosus shales. The original nature of the individual clasts is unknown. They may be siderite mudstone derived by erosion from elsewhere, or eroded clasts of some mudrock, sideritised during the formation of this bed.

The thick upper bed is dominantly siderite mudstone. Grey ooids of siderite and white calcite ooids are disseminated throughout and may also occur in small pockets less than 5 cm across. The ooids are prolate ellipsoidal in shape, with long axes generally less than 0.4 mm in length. Petrographic work shows that they were originally chamosite ooids. The undulose nature of the base of this bed indicates that the siderite mudstone formed diagenetically but after the formation of the underlying siderite mudstone bed. This follows from the fact that the two beds do not coalesce, always being separated by the shale parting, and that the undulations of the base of the upper bed match exactly those of the top of the lower bed. The bed contains many large epifaunal bivalves such as Pseudopecten sp. An infauna of Gresslya sp., and Pleuromya sp. has been found.

The Avicula Seam at Cliff Ridge Wood is little different in nature to the upper bed at Brackenberry Wyke. At Raisdale, however, it contains a higher proportion of white ooids and patches of chamosite ooids. It is characterised at this locality by the presence of 1 mm thick silt lamellae. The Seam at Botton Head is much thinner than at any of the previous localities and is characterized by the presence of common ooimoulds.

4.2.4 Lower gibbosus Shales

This unit is divisible into two portions, a lower non-silty portion approximately 35cm thick, and an upper silty portion characterised by many current-generated sedimentary structures. This division can only be seen in the wave-smoothed cliffs at Brackenberry Wyke. The unit as a whole is unfossiliferous and completely lacks any bioturbation structures.

The lower non-silty portion is constructed of medium to dark grey laminated shales. Approximately 1.5 m from the base of the unit a horizon of siderite mudstone nodules occurs. The bedding and lamination of the enveloping shales is distorted around individual nodules.

The base of the upper portion of the unit is defined by the appearance of clean white silt lamellae which alternate with medium to dark grey shale lamellae in a series of small, fining upwards layers. Intervening lamellae of light grey silty shale also occur. The silt laminations are often continuous over distances of several metres. It is not unusual, however, to find small silt wedges and lenticles less than 5 cm in length and 1 cm in height set within shale. Any lamination which occurs within these silt bodies is either parallel or at a slight angle to the lamination of the adjacent shale. Occasional cross-sections of symmetrical silt ripples are seen. At the boundaries between shale and silt lamellae the silt may have foundered into the underlying shale giving rise to shale flame structures, ball and pillow structures, and small silt pseudonodules. These structures are indicative of rapid silt deposition. Approximately 0.5cm and 0.15cm below the top of the unit horizons characterised by abundant channeling occur. These horizons can be traced continuously along the cliff face at Brackenberry Wyke. Where exposed on the wave-cut platform individual channels can be seen in plan view over distances of less than

2-3 m. Their paths are slightly sinuous and have a west-east orientation. Individual channels are usually less than 15 cm wide and rarely more than 10 cm deep. Channel profiles are characterised by a generally asymmetrical form with a gently sloping point and a steep cut side. Both channel sides often exhibit a blocky irregular profile superimposed on this general form (Figure 4.5). In some instances the blocky profile has been slightly rounded by water flow (Figure 4.6). Occasional channels have a symmetrical cross-section characterised by an oversteepening of the banks (Figure 4.7) which results from current scour. Penecontemporaneous faults in channel banks lead to slumping of the banks into the channels. The interchannel areas have a generally smooth topography broken by small rounded rectangular troughs less than 1 cm in depth. The channel infills comprise an alternating sequence of shale and silt lamellae which may be interrupted by silty shale lamellae. The sediment infill to channels often represents a fining-upwards sequence in which the initial infill is almost entirely silt with few shale lamellae and passes up into shale with few or no silt lamellae. Channel infills may also be entirely silt, silty shale, shale, or a regular alternation of the three. The channel infills exhibit two different orientations. The commonest lamellae orientation is horizontal (Figure 4.6). Less commonly the lamellae are curved and asymmetrical in profile (Figure 4.5). No channel lag deposits have been encountered but Chowns (1968) reports shell fragment accumulations from the bottoms of these channels. Both channeling horizons represent erosive phases during the deposition of the unit. The later phase evidently removed a considerable amount of material as it often descends to the level of the earlier phase, incising its channels on those of this phase (Figures 4,5, 4.6, 4.7).

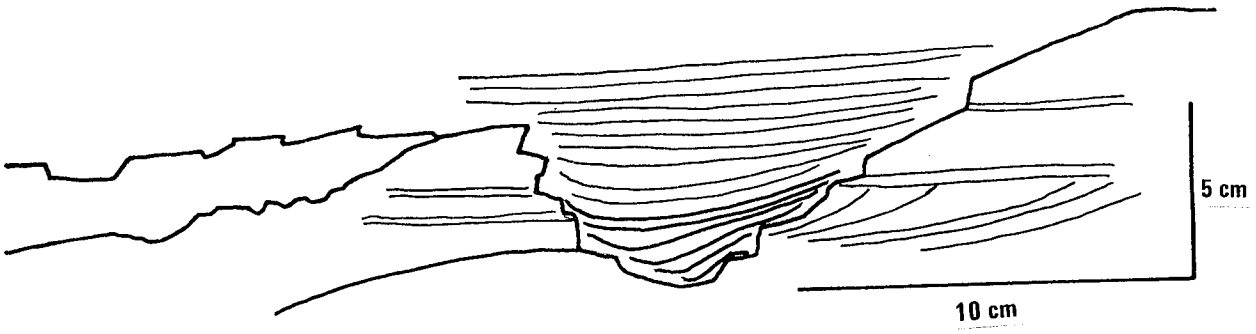

Fig 4.5 Blocky Channel Sides;Upper Channel; Channelling Phase II, Channelling Phase I; Lower Channel. Fine Lines Shale, Thick Lines Silt. (Note curved lamination)

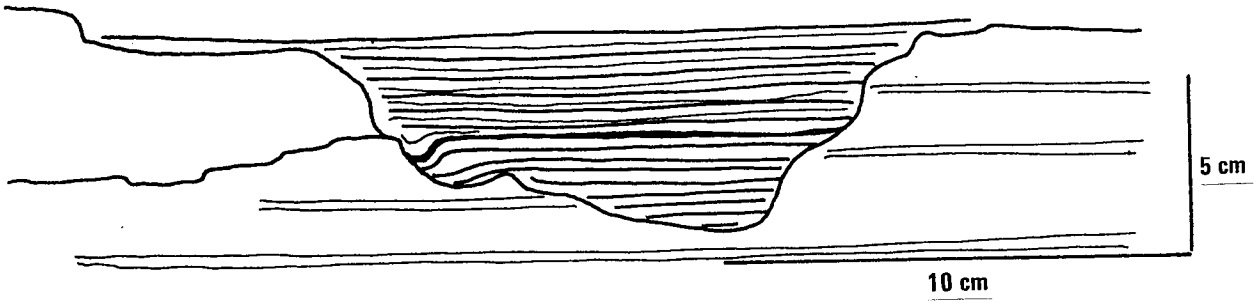

Fig 4.6 Rounded Channel Sides. Two Channelling Phases Horizontal Lamination (Silt and Shale as before)

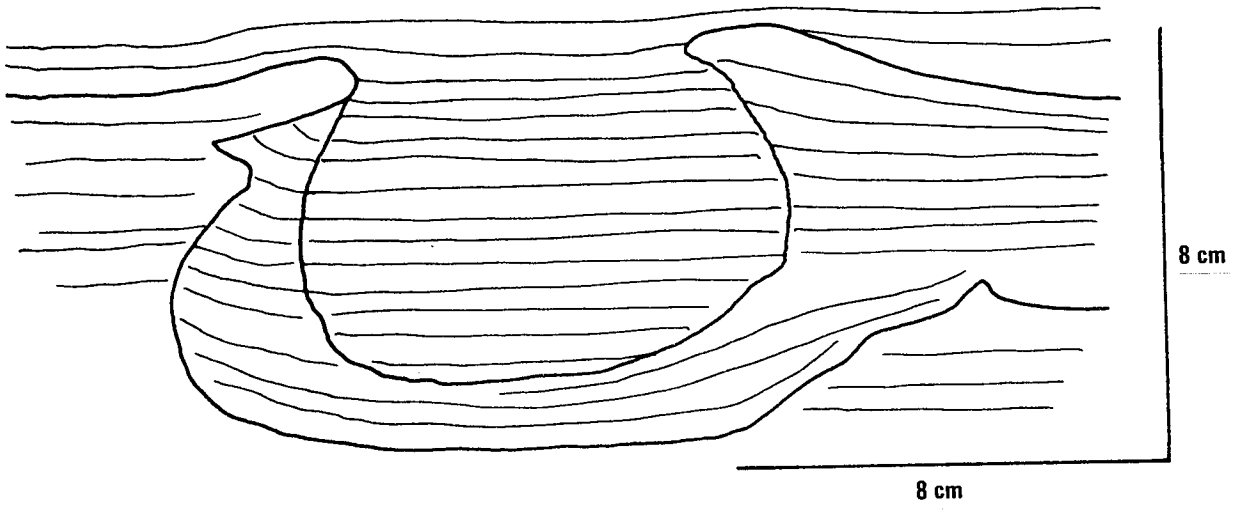

Fig 4.7 Oversteepened Channel Sides. Two Channelling Phases Laminated Shales

The abundant sedimentary features within the lower gibbosus shales provide an opportunity to establish the possible nature of the depositional environment existing prior to the deposition of the overlying Raisdale Seam. Greensmith et al (1980) have carried out a detailed examination of the unit where it is exposed at Brackenberry Wyke and Hawsker Bottoms. They consider that it represents a prodelta or open shelf setting in which the upward fining units represent the deposits of submarine sheet flows Contemporaneous scour and fill resulted in the formation of channels. Present day deposits of this type described from the Niger and Mississippi deltas (Hayes, 1967; Allen, 1970; Coleman et al, 1970; Gould, 1970) exhibit closely similar sedimentary features to those of this unit. The cause of these sheet flows is by analogy, suggested to be either storms or powerful onshore and offshore currents.

4.2.5 The Raisdale Seam

This ironstone unit directly overlies the lower gibbosus shales. It comprises a single but lithologically variable deposit. Chowns (1968) has recorded a belemnite bed at the base of the seam at many localities, and considers that this represents a hiatus in deposition occurring before deposition of the ironstone unit.

On the wave-smoothed surfaces of the Raisdale Seam at Brackenberry Wyke the nature and distribution of the component ironstone lithologies can be clearly seen. Overall the seam is divisible into three layers (Figure 4.8). The lowermost 5 cm is constructed of many 'clasts" of calcitic chamosite oolite. As a result, the base of the unit is somewhat irregular. The component chamosite ooids are prolate ellipsoidal in shape and have a size range of approximately 0.2-0.5 mm, measured along the long axis. They are dark grass-green in colour. It is interesting to

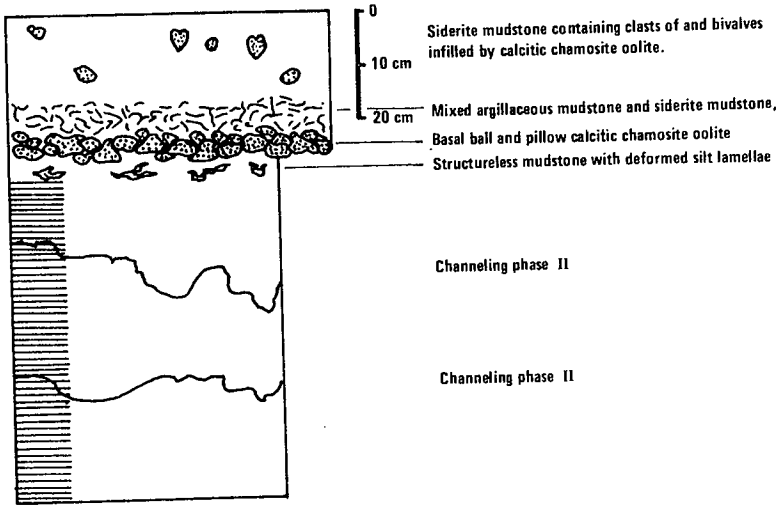

Fig 4.8 Detailed Log of the Raisdale Seam and underlying shales at Brackenberry Wyke

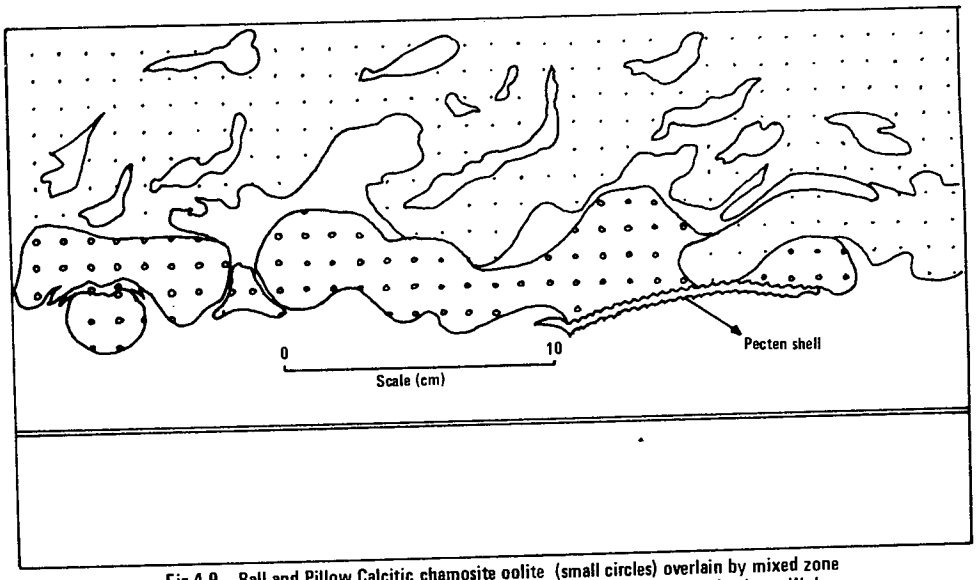

Fig 4.9 Ball and Pillow Calcitic chamosite oolite (small circles) overlain by mixed zone of Argillaceous mudstone (blank) and Siderite mudstone (spotted) Brackenberry Wyke

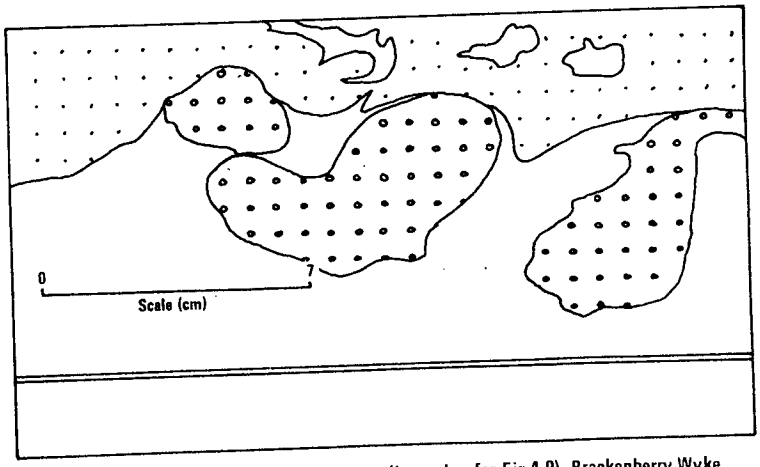

Fig 4.10 Argillaceous mudstone flames. (Legend as for Fig 4.9) Brackenberry Wyke

note that these are the only allochemical grains present within the 'clasts'; shell fragments are absent. Calcite forms the cement to the ooids. The 'clasts' vary in size from 2-20 cm. They exhibit a variety of shapes from circular to elongate (Figure 4.9). The elongate types are either rounded at each end and have an overall ovate shape or are characterised by a lumpy nodular appearance (Figure 4.9). Close examination of the contact between this unit and the underlying shales shows that the 'clasts' are commonly surrounded by mudstone which passes up from the underlying unit. Many of the 'clasts' are only partially surrounded by the mudstone which, in these instances, has a flame structure (Figure 4.10). The irregular shape of the 'clasts' and their relationship with the underlying shale indicates that the lower 5 cm of the ironstone is not conglomeratic but comprises a complex ball and pillow structure with widespread pseudonodule formation. Evidence in support of this is provided by occasional belemnites whose alvaeoli are infilled by calcitic chamosite oolite and lie a few centimetres beneath the base of the ironstone. Since these do not exhibit evidence of attrition they cannot have been washed into the area of shale and silt deposition. They must therefore have sunk through the shale, when it was a semi-liquid mud, from the overlying chamosite oolite. The general nature of the upper portion of the Lower gibbosus Shales has been described above. The top 5 cm of this unit, however, is rather different. It is a band of dark grey mudstone which lacks both lamination and fissility. This material passes up into the oolite as flames. Elongate patches of light grey silty shale 5-10 cm in length are common within this band. They are often parallel to bedding but also commonly exhibit deformation. This band is thought to have originally been no different to the underlying shales and silts, the light

grey elongate portions representing original silt lenticles. Its loss of internal structure would have occurred when the mud became thixotropic at the time of formation of the chamosite oolite ball and pillow structures.

Above the lower chamosite oolite layer a 5 cm mixed zone occurs. This mixed zone comprises many irregular patches of medium grey mudstone set in a pinkish brown weathering siderite mudstone (Figure 4.9). The mudstone is structureless and forms 50-60% of the zone. The contacts between the mudstone and the siderite mudstone are often diffuse. The irregular patches of mudstone are not thought to represent traces of burrowing activity as they exhibit no evidence of the structural organization characteristic of trace fauna. The origin of the mixing may be related to the formation of the chamosite oolite ball and pillow structures. Occasional mudstone flames pass up into this zone changing colour from dark to medium grey as they do so.

The remaining 16 cm of the Raisdale Seam is a hard grey siderite mudstone containing white ooids. These have the same form as the component chamosite ooids of the lower calcitic chamosite oolite. Petrographic work shows that they were chamosite ooids which have been replaced by calcite. Also present in this portion of the Seam are the burrowing bivalves. Pleuromya sp., and Gresslya sp. These are usually found in their life position and are infilled by calcitic chamosite oolite. Presumably these burrowers lived within chamosite oolite which infilled them following their death and decomposition. The infilling oolite would thus be protected from diagenetic changes by the shell walls.

Where exposed at Cliff Ridge Wood and Raisdale the Raisdale Seam is a siderite mudstone containing small concentrations of chamosite ooids, ooids replaced by calcite, ooimoulds, and irregular patches of chamosite mud.

The basal ball and pillow and pseudonodule structures are absent from these exposures. At Botton Head the seam is entirely a siderite mudstone; no ooid-forming phase is present.

The presence of ball and pillow and pseudonodule structures, together with the nature of the immediately underlying mudstones indicates that, at Brackenberry Wyke, the Raisdale Seam was deposited rapidly as a chamosite oolite on water-logged muds. The unconsolidated oolite formed a stable substrate which was colonized by burrowing bivalves. These were later infilled by the oolite. The bulk of the chamosite oolite was later replaced diagenetically by siderite mudstone. Evidence in support of this is provided by the chamosite oolite filled bivalves which are surrounded by this material. The mixed zone may be explicable in this context as chamosite oolite pseudonodules and ball and pillow structures which have been replaced wholesale by siderite mudstone leaving only the intervening mudstone. If this is the case then it is necessary to explain the absence of such replacement from the lowermost ball and pillow and pseudonodule structures. The answer to this is unknown. The fact, however, that siderite mudstone is found in contact with chamosite oolite pseudonodules and in some instances occurs at this horizon with a pseudonodule-like form (Figure 4.9) suggests that the lower layer of chamosite oolite was in the process of being replaced by siderite mudstone when this reaction stopped. The presence of chamosite ooids, ooimoulds, and chamosite mud at other localities, set within siderite mudstone suggests that sideritisation of original chamosite is a widespread feature of the Raisdale Seam.

4.2.6 Middle gibbosus Shales

This unit comprises a sequence of pyritic dark grey laminated shales. They are unfossiliferous. Approximately 1 m from the base of the unit a thin argillaceoussiderite mudstone band occurs. The shales are generally coated by a white effluorescence which is indicative of their pyritic nature.

Inland exposures vary little in nature from those at Brackenberry Wyke. The only exception to this is the Middle gibbosus sequence at Raisdale where channels occur approximately 2 m from the base of the unit and 0.3 m from the top. These probably represent submerged features as the shales remain unchanged in nature throughout the sequence.

4.2.7 The Two Foot Seam

This ironstone unit overlies the Middle gibbosus Shales. Its contact with this unit is always sharp. Concentrations of belemnites and clasts of limestone have been found in the basal position of the unit. This supports Chowns (1968) conclusion that the base of the unit corresponds to a depositional hiatus. This worker has also recorded siltstone clasts at the base of the ironstone.

At Brackenberry Wyke the Two Foot Seam is a distinctive unit constructed of two beds which are lithologically dissimilar and separated by a marked parting. The parting corresponds to a horizon of thin discontinuous ironstone lenticles.

The lower portion of the Seam is a chamositic chamosite ooilite. The chamosite ooids are whitish green in colour and have discoidal shape. They have a size range of 0.3-0.4 mm, measured along the long axis. The ooids are set in a dull whitish green chamosite mud matrix. Within the oolite

irregular but rounded lenses of buff siderite mudstone occur. They are variable in size often reaching a length of 10 cm. Islands of chamositic chamosite oolite may occur within these lenses. White ooids with the same form as the chamosite ooids are occasionally found with the lenses. Petrographic work shows that these were originally chamosite ooids which have been replaced by calcite. The proportion of siderite mudstone is variable along the outcrop of the bed. Thus at some places it forms lenses whereas at others it forms the bulk of the bed and contains patches of chamositic chamosite oolite. The base of the bed is characterised by the presence of common belemnites.

The two ironstone beds are separated by a marked parting. Along this parting lenticles of chamositic chamosite oolite occur. These vary in length from a few centimetres to a maximum of one metre. They are never more than 5 cm in thickness. The presence of this oolite appears to correspond to very slight undulations in the surface of the underlying bed.

The upper bed has a slightly undulose base corresponding to the presence of chamositic chamosite oolite lenses below. It is a buff to light grey siderite mudstone. Ooids of whitish green chamosite and chamosite ooids replaced by calcite are scattered throughout the bed.

At Kettleness the Two Foot Seam is much reduced in thickness in comparison with both Brackenberry Wyke and inland exposures. It is divisible into two portions. The lower portion is constructed of greenish grey chamositic shales which surround 2-3 cm clasts of bioclastic limestone. These appear to be slightly imbricate. The upper portion is a siderite mudstone which passes laterally into lenses of chamositic chamosite oolite.

Inland exposures bear a much closer resemblance to the Two Foot Seam at Brackenberry Wyke than to its exposure at Kettleness. At Cliff Ridge Wood the Seam is divisible into an upper siderite mudstone bed and a lower, much thicker, bed of chamositic chamosite oolite. This bed contains many shell fragments and is characterised by a basal layer of chamositic chamosite oolite intraclasts. At Raisdale and Botton Head the Seam comprises one bed of siderite mudstone within which chamosite ooids replaced by calcite and ooimoulds are abundant. In the case of Botton Head the ooid phase often appears to be concentrated in burrows.

The fact that many exposures exhibit basal concentrations of clasts, intraclasts, or belemnites indicates that a phase of widespread erosion and non-deposition occurred following the cessation of Middle gibbosus Shale deposition but prior to ironstone deposition. The lithological character of the Seam clearly suggests that it was deposited as a chamositic chamosite oolite which subsequently underwent varying degrees of replacement by siderite mudstone. The presence of a major parting between an upper and lower bed at Brackenberry Wyke and Cliff Ridge Wood together with a slightly undulose top to the lower bed indicates the possibility of an erosive phase occurring in the eastern area of deposition. This might be responsible for the reduced thickness of the Two Foot Seam at Kettleness. Following this erosive phase further deposition of chamosite oolites occurred. Such deposition may only have been minor, resulting in the infilling of undulations in the erosion surface, or may have been of greater importance creating a thicker bed of chamosite oolite. If the latter possibility is correct then a further phase of erosion would be necessary in order to reduce the chamosite oolite bed to a laterally discontinuous lenticulate carpet. This explanation seems the more likely

because the former would have resulted in a flat-topped lenticulate deposit. The presence of an oolitic phase in the upper bed indicates that this was deposited as a chamosite oolite and subsequently replaced by siderite mudstone. Deposition and replacement continued uninterrupted in the western area as indicated by the exposures at Botton Head and Raisdale. At Brackenberry Wyke and Cliff Ridge Wood replacement of the lower bed by siderite mudstone was evidently interrupted and stopped by erosion. Following deposition of the upper bed of oolite this bed was completely replaced by siderite mudstone. The presence of an unreplaced lenticulate deposit between the two beds indicates that this replacement did not extend beyond the base of the upper bed. This might be due to cementation sealing off the porosity in the lenticulate oolite prior to deposition of the upper bed.

4.2.8 Upper gibbosus Shales

This shale unit occupies the remainder of the Margaritatus zone. It varies considerably in thickness throughout the Cleveland Ironstone Field. Chowns (1968) has attributed this to widespread erosion of the shales at the end of Margaritatus zone times.

At Brackenberry Wyke the unit comprises a sequence of dark grey poorly laminated fissile pyritic shales. They are unfossilferous.

The Upper gibbosus Shales at Kettleness, Cliff Ridge Wood, and Botton Head are similar to those at Brackenberry Wyke. At Cliff Ridge Wood Rhizocorallium occurs. The shales are absent from the Raisdale succession.

4.2.9 The Pecten Seams

The base of this unit marks the base of the Spinatum zone and the base of the apyrenum sub-zone (Chowns, 1968). Howarth (1958), however, has placed this boundary at the top of the Two Foot Seam. It is generally an alternating sequence of thin ironstone and shale beds. This distinctive character lead to its use as a marker horizon by the mining industry. Chowns (1968) has subdivided the seam into three units, the Top Unit, The Eston Shell Beds, and the Grosmont Pecten Unit (Table 4.1). The criteria used for this tripartite division is the presence or absence of a shelly fauna and a minor disconformity between the Grosmont Pecten Unit and the Eston Shell Beds. During the field study of the Cleveland

	Top Unit:	Two or three beds of siderite mudstone with intervening sideritic chamositic shales. Unfossiliferous.
Upper Pecten Seam		
	Eston Shell Beds:	Shelly siderite and chamosite mudstone and shales. Very fossiliferous.
	Grosmont Pecten Unit:	Fossiliferous siderite mudstones and sideritic chamositic shales similar to Eston Shell Beds but separated by a minor disconformity. Very fossiliferous.
Lower Pecten Seam		

Table 4.1 Subdivision of the Pecten Seam by Chowns (1968)

Ironstone it has been found that the number of ironstone beds is variable from locality to locality and that at some locations the ironstone beds are indistinguishable from the intervening shales. The faunal abundance varies considerably. During the course of the field study it was found preferable to consider the Seam as one unit rather than three.

At Brackenberry Wyke the base of the Pecten Seam is recognised by the appearance of hard medium grey laminated poorly fissile sideritic shales. 20 cm above the base of this shale bed a siderite mudstone nodule horizon occurs. The individual nodules are often as long as 40 cm. Due to the sideritic nature of the enveloping shales it is not possible to determine whether their bedding and lamination has been distorted by nodule growth. As a whole the Pecten Seam comprises a sequence of six shale beds of subequal thickness separated by six ironstone beds of subequal thickenss. The shales are all similar in nature to the basal shale bed. They often contain belemnites and shell fragments. The intervening ironstone beds are all constructed of siderite mudstone. Occasional patches of chamosite ooids occur within them. They are generally unfossiliferous.

At Cliff Ridge Wood the Pecten Seam is made up of four shale beds separated by four ironstone beds. The shales are dark green in colour and are sideritic. They are not laminated. The intervening ironstones are again constructed of siderite mudstone and are characterised by the presence of abundant ooimoulds.

In contrast, the Pecten Seam at Kettleness, Raisdale, and Botton Head is represented by a thick bed of siderite mudstone containing occasional white ooids. As before these are found to be chamosite ooids replaced by calcite. In the case of Raisdale, the Pecten Seam lies directly above the Two Foot Seam. The two are separated by a thin shale parting.

The alternating nature of the Seam at Brackenberry Wyke, Cliff Ridge Wood, and other exposures (Figure 4.4) in the northern area, with the exception of Kettleness, suggest that depositional conditions were fluctuating in this area during Pecten Seam deposition. In the southern area deposition was continuous resulting in a single ironstone unit.

This distribution is illustrated in Figure 4.11. From this it can be seen that the area in which the Seam is split corresponds to the area of maximum deposition (Chowns, 1968). In contrast, the marginal areas correspond to the locations at which the Seam is unsplit. The Kettleness Pecten Seam may thus represent a northerly margin to the depositional area. It is concluded, therefore, that fluctuating water levels in the centre of the depositional basin gave rise to an alternating sequence of shale and ironstone. In marginal areas ironstone deposition continued uninterrupted yielding a thinner but continuous ironstone bed. The presence of an ooid-forming phase in the siderite mudstones of the unit suggests that they were deposited as some form of chamosite oolite which was subsequently replaced by siderite mudstone.

4.2.10 The Black Hard

The Black Hard is a unit of shale which separates the Pecten Seam from the overlying non-oolitic portion of the Main Seam. The name derives from the mining terminology of the Skelton Mining Royalties. It should be noted that the older literature may use the term in the sense of the Upleatham mines which includes all the strata between the Pecten Seam and the oolitic portion of the Main Seam.

At Brackenberry Wyke the Black Hard is a unit of hard chamositic sideritic dark greyish green shales. X-ray diffraction studies have confirmed the presence of chamosite and siderite. They lack any original lamination and are only poorly fissile. They are unfossiliferous. Where seen at other localities, both on the coast and inland, the Black Hard retains these characteristics.

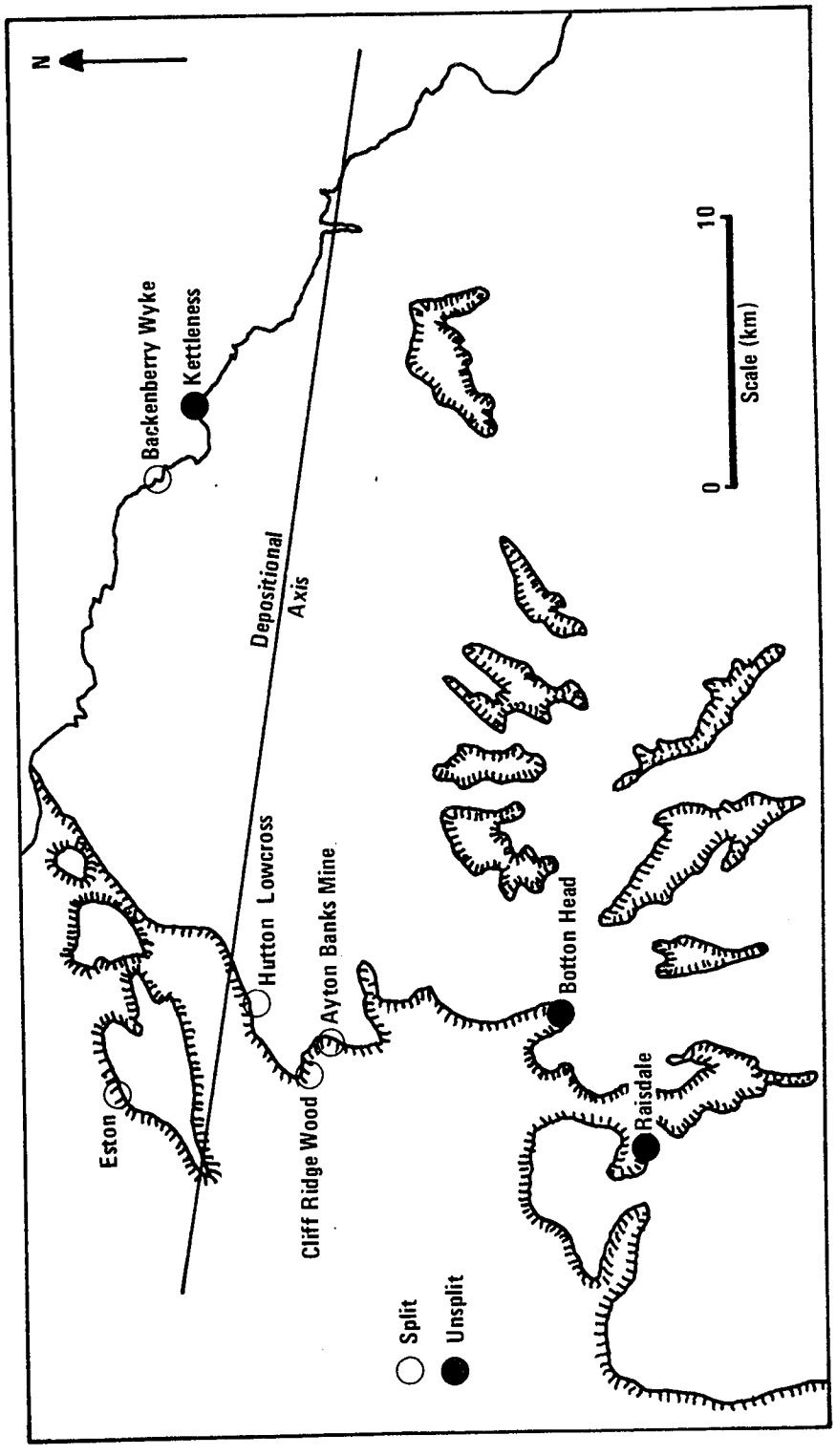

Fig 4.11 Localities at which the Pecten Seam is split and unsplit

4.2.11 The Main Seam

Ironstone mining in the Cleveland Ironstone Field primarily exploited the Main Seam. As a result its nature is well-known throughout the Field. It is composed of four lithologically distinct beds which are named according to mining terminology (Table 4.2). The top of the Main Seam

Top Block	: Chamosite oolite passing laterally into siderite mudstone.
Middle Dogger Band	: Siderite mudstone passing laterally into shales.
Bottom Block	: Chamosite oolite passing laterally into siderite mudstone.
Blue Mottle	: Argillaceous siderite mudstone.

Table 4.2 Lithological subdivision of the Main Seam

corresponds to the top of the apyrenum subzone (Howarth, 1958; Chowns, 1968).

At Brackenberry Wyke the Blue Mottle comprises an argillaceous siderite mudstone. It is characterised by abundant horizontal sinusoidal burrows of the ichnogenera Rhizocorallium jenense (Zenker). These indicate a shallow sub-tidal bathymetric level (Fürsich, 1975). These are infilled by siderite mudstone. The nature of the weathering surfaces reveal that the bed is constructed of many superimposed lenses generally less than 20 cm in length and 10 cm in height. Weathering processes are thus concentrated at the contacts between individual lenses with the result that they are hollowed out. White prolate ellipsoidal ooids are common throughout the Blue Mottle. Petrographic work shows that these are chamosite ooids which have been replaced by calcite. Angular white grains with a size range of 0.5-2.5 mm are scattered throughout the bed. They

occasionally cluster together forming a mosaic. In some instances a reversed graded bedding may be seen in such mosaics. Thin sections of these grains reveal that they are lithic fragments of devitrified volcanic glass containing angular quartz grains and small flakes of mica. No shelly fauna has been found.

A well developed bedding plane separates the Blue Mottle from the overlying Bottom Block . This is a bed constructed of lenticles of chamositic chamosite oolite. It is characterised by abundant ramifying burrows less than 0.5 cm in diameter and infilled by light grey to buff siderite mudstone. The abundance of these burrows often produces irregular lenses constructed almost entirely of siderite mudstone and with very little interstital oolite. The chamositic chamosite oolite is constructed of dark grass-green chamosite ooids with a prolate ellipsoidal shape and a size range of 0.3-0.5 mm, measured along the long axis, set in a matrix of dark green chamosite mud. Lithic fragments of the type described above are present. The only shelly fauna present within the oolite are abraded belemnites and bivalve fragments.

The Middle Dogger Band is represented at Brackenberry Wyke by a bed of heavily weathered sideritic shale.

The Top Block is very similar in nature to the Bottom Block. It is interesting to note that burrows at the base of this bed penetrate into the underlying shales. Since these burrows are of the same type that ramify throughout the bed it would appear that deposition of the Top Block commenced almost as soon as that of the underlying shale finished. In addition to the lenses of chamositic chamosite oolite, occasional lenses of sideritic calcitic chamosite oolite occur. These differ from the chamositic variety in that all the chamosite mud has been winnowed away

leaving a chamosite oolite which has been cemented by a cream coloured siderite and white calcite.

At Kettleness the Main Seam sequence differs only in the nature of the Top and Bottom Blocks. The Bottom Block is a hard splintary siderite mudstone containing 2 cm thick lenses of chamosite mudstone. The ooid phase present comprises chamosite ooids replaced by white calcite. The Top Block is also a siderite mudstone containing white ooids. A bed of chamositic chamosite oolite occurs within it, however, and the basal portion contains pods of this material.

The Main Seam at Cliff Ridge Wood exhibits a similar sequence to that of Brackenberry Wyke. The Top and Bottom Blocks, however, are split into several beds which, in the case of the Top Block, are separated by thin shales. Both Blocks are constructed mainly of siderite mudstone containing many yellowish green chamosite ooids and ooimoulds. The Bottom Block exhibits the only exception to this which is the presence of a bed of lenticulate-bedded chamosite mudstone. Burrowing bivalves such as Gresslya sp. and Pleuromya sp. are common in both Top and Bottom Blocks. The Middle Dogger Band is much thicker than at either Brackenberry Wyke or Kettleness and also differs from these sequences in that a 15 cm siderite mudstone bed occurs within the Band containing the burrowing bivalves Gresslya sp. and Pleuromya sp.

At Botton Head and Raisdale the Main Seam is represented by a single ironstone bed constructed mainly of siderite mudstone. At other inland exposures those parts of the Main Seam ironstone beds which can be seen are either sideritic chamosite oolites such as at Eston Hill and Skelton Beck or siderite mudstones such as at Waterfall Gill and Ayton Banks Mine (Figure 4.4). The sideritic chamosite oolites comprise prolate

ellipsoidal 0.3 mm long yellowish green ooids set in a yellowish brown crystalline siderite. Irregular patches of siderite mudstone occur within this ironstone lithology and may contain yellow-green chamosite ooids and ooimoulds.

There is a clear variation in the nature of the Main Seam throughout the Cleveland Ironstone Field (Figure 4.12). It has a maximum thickness and is unsplit in the most northerly exposures e.g. Eston Hill and Skelton Beck. Passing ESE from this area the seam is split initially by a siderite mudstone (Whitehead et al, 1952), the Middle Dogger Band, which diminishes thickness as a central shale horizon appears and gradually thickens. In exposures of the Seam at Brackenberry Wyke and Kettleness the siderite mudstone is completely absent. This variation in the nature of the material between the Top and Bottom Blocks is not as simple at it would appear as at Cliff Ridge Wood the shale is itself split by a 15 cm siderite mudstone bed containing burrowing bivalves. (Chowns 1968) has shown that the Main Seam passes laterally into sideritic and normal shales at Hawsker Bottoms. In the western portion of the Ironstone Field the Seam is thinned and is unsplit. Chowns (1968) considers that the thickness maxima in the northern portion of the Ironstone Field represents an oolite shoal with an axis trending approximately west-east. By analogy with present-day carbonate shoals Chowns (1968) has proposed that the lateral equivalents of the Main Seam represent various off-shoal facies. Petrographic work which is discussed below suggests that the Eston Hill, Skelton Beck, and Cliff Ridge Wood area is one in which chamosite ooids were formed whereas the Staithes and Kettleness area represents an area of both chamosite ooid formation and chamosite oolite deposition. The widespread replacement of the Main Seam by siderite

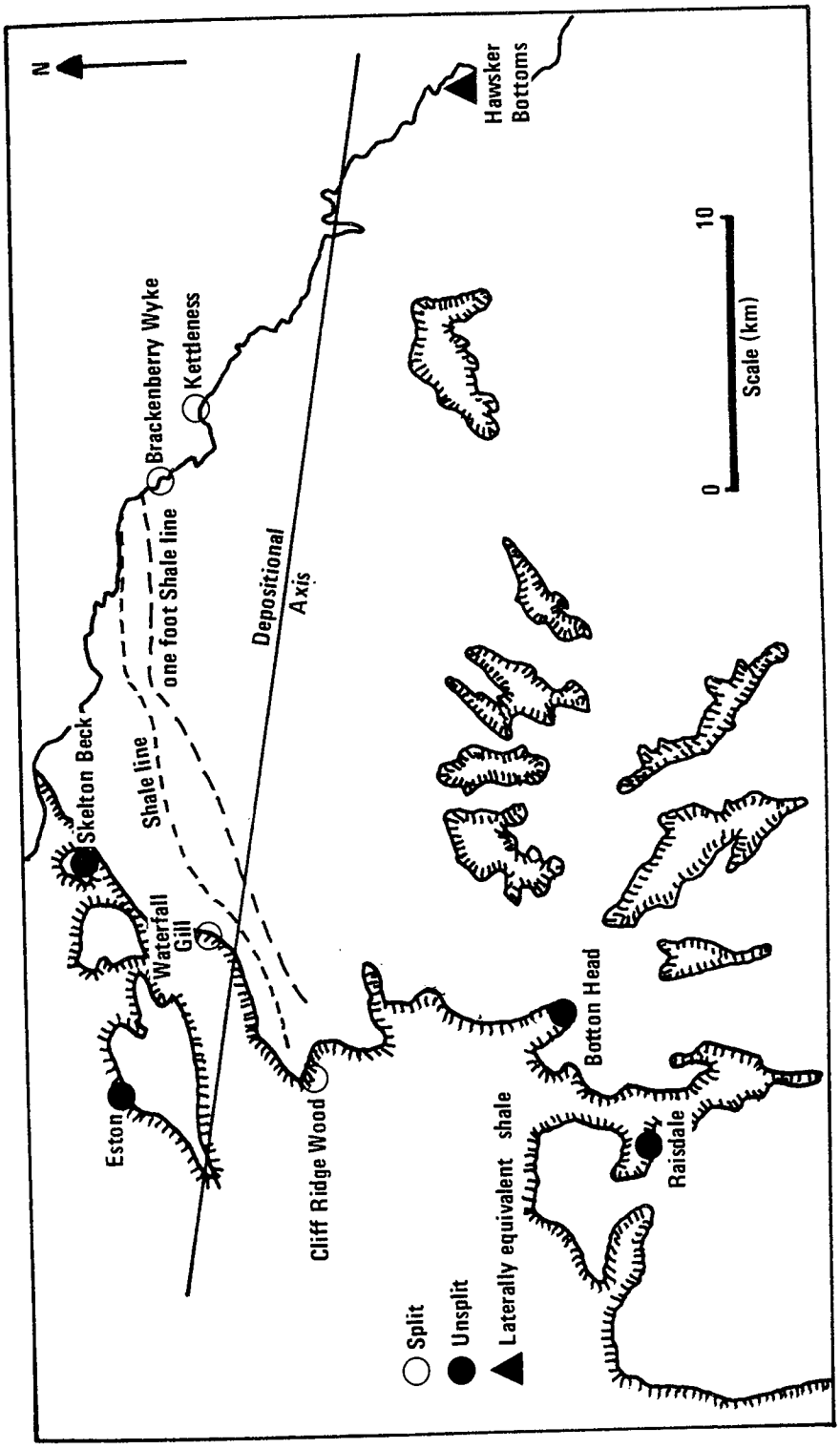

Fig 4.12 Localities at which the MainSeam is split and unsplit

mudstone makes the task of separating individual off-shoal ironstone facies very difficult, if not impossible. The nature of the Main Seam throughout the depositional basin suggests that the oolite shoal thins towards the margins of the basin and also along the axial portion. Thinning in the axial region was evidently accompanied by one period of rapid basinal subsidence in order to bring about the creation of a Top and Bottom Block. This is analogous to the splitting of coal seams in the Westphalian. The occurrence of deeper water in the Hawsker Bottoms area favoured the deposition of shale rather than ironstone.

4.2.12 hawskerense Shales

The top of the Main Seam defines the top of the apyrenum sub-zone and the base of the overlying hawskerense sub-zone. This is the uppermost sub-zone of the Spinatum zone.

The nature of the hawskerense Shales can be clearly seen in the wave-smoothed cliffs at Brackenberry Wyke and Kettleness. The unit exhibits an upward passage from medium grey silty shales to siltstone to a sandy siltstone. At Kettleness this sequence is capped by a siderite mudstone bed. At Brackenberry Wyke this bed occurs at a level of 50 cm below the top of the hawskerense Shales. The difference in level of this bed can be accounted for by erosion accompanying the transgression which swept across Europe at the end of the Domerian period. The paper shales of the basal member of the succeeding Whitbian Grey Shales; the Sulphur Band lie above the hawskerense Shales at Brackenberry Wyke and above the siderite mudstone bed at Kettleness.

The overall nature of the hawskerense Shale unit is indicative of a shallowing episode leading to the deposition of the siderite mudstone. The lower silty shales are characterised by thin (usually less than 2 cm thick) upward fining layers from silt to shale. Small lenticulate wedges of clean silt exhibiting topset and foreset lamination are common. Occasional channels occur. A 2 cm thick resistant quartzose silt with rippled top band separates this bed from the overlying siltstone. The siltstone is light grey in colour and laminated. The lamellae take the form of white quartzose silt lamellae alternating with silt lamellae. Occasional lenticulate wedges of white quartzose silt with foreset lamination are present. The ichnogenera Chondrites sp. occurs throughout the bed. The overlying sandy siltstone forms a massive bed in which little original sedimentary lamination remains due to its bioturbated nature. A horizon of small irregular siderite mudstone nodules separates the sandy siltstone from the overlying siderite mudstone bed. The base of this bed is slightly irregular such that it parallels the underlying nodules. The burrowing bivalves Gresslya sp. and Pleuromya sp. are common within the siderite mudstone orientated in their life position. They are infilled by this material. At Brackenberry Wyke medium grey laminated silty shales succeed the siderite mudstone bed.

The hawskerense Shale unit is absent at Raisdale and Botton Head.

The nature of the hawskerense Shales which underlie the siderite mudstone bed at Brackenberry Wyke and Kettleness is very similar to that of the Lower gibbosus Shales. They are therefore interpreted as submarine sheet flow deposits in a prodelta or open shelf setting. The abundance of Chondrites supports this. Fürsich (1975) considers that this trace fossil represents a bathymetric level deeper than the deep subtidal levels.

4.2.13 Deposition of the Cleveland Ironstone Formation

The nature, environment and lateral variation of the various shale and ironstone units which comprise the Formation are tabulated in Table 4.3.

It is clear that within the Cleveland Ironstone Formation there is an alteration between facies deposited between extremes of bathymetric levels; deeper than the deep subtidal and shallow ironstone facies. Examples of the types of deposit represented by the hawskerense and Lower gibbosus Shales are reported by Hayes (1967) from the Gulf of Mexico and Howard and Reineck (1972) from the Georgia coast where they occur in water depths of 2-10 m. The shallow subtidal environment of deposition of the Blue Mottle and the upward shallowing sequences represented by the lower portion of the hawskerense and lower gibbosus units clearly indicates that deposition of ironstone was preceeded by a shallowing phase. The bathymetric levels encountered prior to ironstone suggest that these might be shore-face deposits. The Cleveland Ironstone Formation therefore appears to represent a series of upward shallowing cycles culminating in ironstone deposition. It is difficult to escape the conclusion that ironstone deposition was interrupted by basinal subsidence creating deeper water unfavourable to ironstone formation (Chowns, 1968; Kimberley, 1979). Subsequent infilling of the basin by fine-grained clastic material would bring about shallowing until depths favourable to ironstone formation were reached.

The relationship between depth and ironstone formation naturally implies that individual ironstone units may be diachronous, marginal areas in the basin attaining favourable depths prior to more central areas. Stratgraphic work (Chowns, 1968) indicates that if this is the case then diachronism of the Formation units must be on the scale of

Unit	Lithology	Environment	Lateral Variation
hawskerense Shales.	Upward passage from silty shale to siltstone to sandy siltstone.	Open shelf, pro-delta. Deep subtidal.	Restricted areal extent due to transgression at the end of the Domerion.
Main Seam	Chamosite oolites	Shore face (?) Shallow subtidal or shallower.	One unit in marginal areas. Split by shale in central areas. Lateral passage into shales.
Blue Mottle	Argillaceous siderite mudstone	Shallow subtidal	
Black Hard	Chamositic sideritic shale	Deep water	No major variation.
Pecten Seam	Siderite mudstone	Indeterminate	One unit in marginal areas. Split by shale in central areas.
Upper gibbosus Shales	Shale	Deep water	Variable thickness due to erosion at end of Margaritatus times.
Two Foot Seam	Chamosite oolites and siderite mudstones.	Indeterminate	One seam of variable thickness.
Middle gibbosus Shales	Laminated shale	Deep water	Variable thickness
Raisdale Seam	Chamosite oolites and siderite mudstones.	Shallower than deep subtidal.	One seam of variable thickness.
Lower gibbosus Shales	Dark shale passing up into silty shale and silts.	Deep water shallowing to open shelf or prodelta deep subtidal.	Thin in marginal areas, thick in central areas.
Avicula Seam	Siderite mudstone	Indeterminate	One seam of variable thickness.
Subnodosus Shales	Grey shales	Deeper than deep subtidal	Apparent uniform thickness.

Table 4.3 : Lithology, Environment of deposition and lateral variation of the units of the Cleveland Ironstone Formation

the time represented by an ammonite subzone. The Raisdale Seam, a calcitic chamosite oolite deposited rapidly on water-logged silts and clays, indicates the diachronism may occur, ie. It would have been necessary for the chamosite ooids to have been formed elsewhere and transported to Brackenberry Wyke en masse as the Raisdale Seam at this locality does not represent a site of chamosite ooid formation. In the case of the Main and Pecten Seams diachronism is suggested by the continuous, thick, nature of these units in marginal areas and their lateral passage into a series of two or more thinner seams, split by shales, and ultimately into shales in the case of the Main Seam, with increasing proximity to the basinal axis and hence also increasing depth.

The field study has allowed the recognition of five ironstone lithologies; siderite mudstone with or without an ooid phase, chamositic chamosite oolites, sideritic chamosite oolites, sideritic calcitic chamosite oolites, and calcitic chamosite oolites. Throughout the Ironstone Field individual seams show varying degrees of siderite mudstone replacement with the result that it is impossible to determine the spatial variation of any primary ironstone facies. The petrography of these lithologies is described and discussed below.

The overall thickness variation of the Cleveland Ironstone Formation has been elucidated by Chowns (1968). He has shown that it occupies a depositional basin with an axial zone extending ESE from Guisborough to near Whitby. This corresponds to the underlying Carboniferous Cleveland Gulf. That portion of the sequence from the top of the Pecten Seam to the base of the Formation finds a maximum thickness in the axial zone and thins towards the margins (Figure 4.13a). Widespread erosion

resulting from crustal movement at the end of Margaritatus times brought about the formation of an intraformational uncomformity. Subsequent Main Seam and hawskerense Shale deposition occurred within the same basin with the same thickness variation as the pre-uncomformity sediments. The findings of the field study support the conclusions of Chowns (1968). Figure 4.13b shows a section approximately normal to the basin axis but further south than that of Chowns (1968) section (Figure 4.13a).

4.3 PETROGRAPHY OF THE CLEVELAND IRONSTONE FORMATION IRONSTONE LITHOLOGIES

The field study of the Cleveland Ironstone Formation has led to the recognition of five distinct ironstone lithologies. These are summarised in Table 4.4. Hallimond (1925), Dunham (in Whitehead et al, 1952), and Chowns (1968) have reported on the petrographic character of specimens from various ironstone seams. Only Chowns (1968) has discussed the possible diagenetic history of the ironstones but only in terms of early and late diagenesis. Diagenetic changes occurring specifically in lithological types are not recognised. The petrography and paragenesis of the ironstone lithological types are described and discussed below. As before, the nature of the chamosite ooids is discussed separately and any variation characteristic of a particular lithology discussed where appropriate.

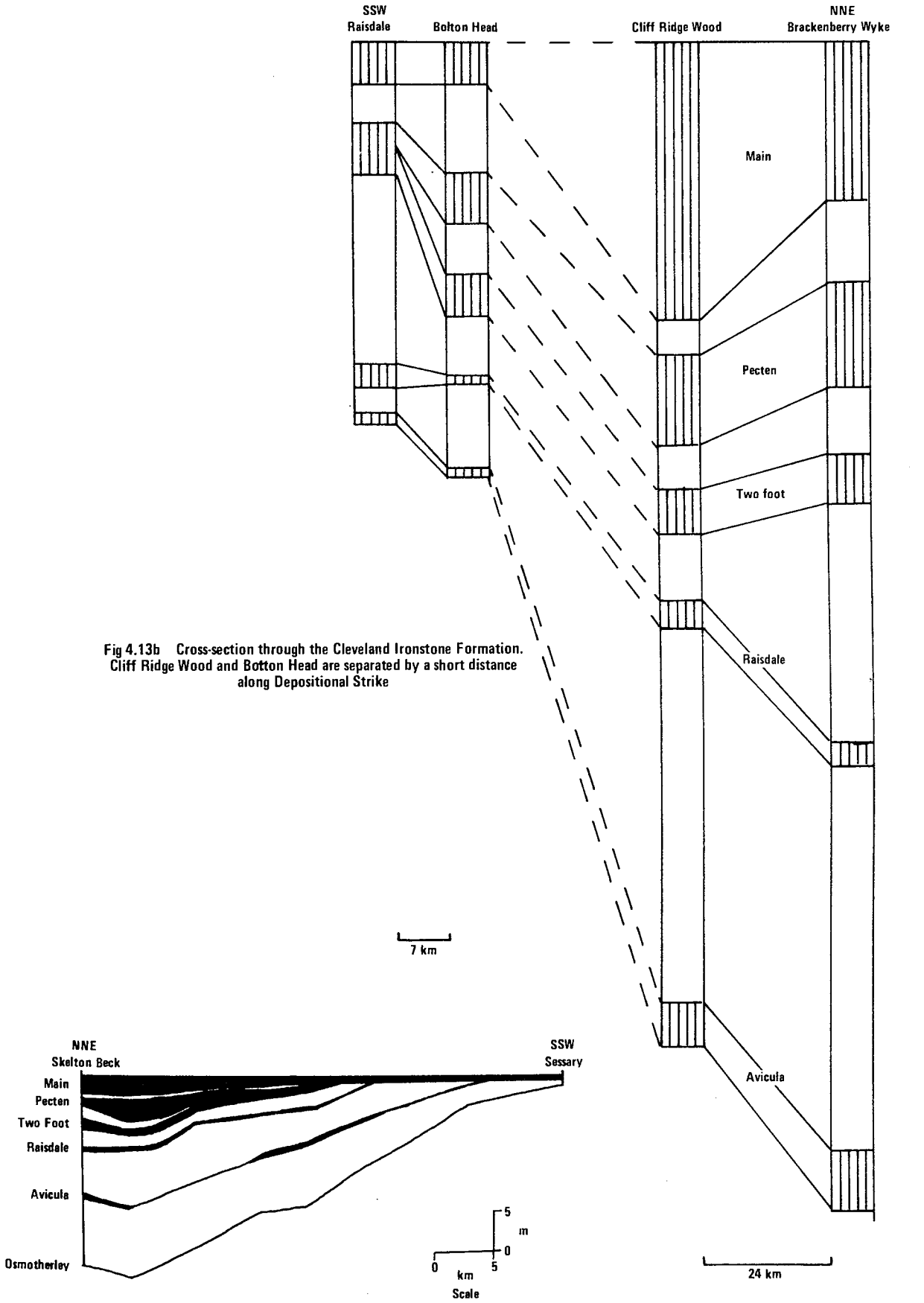

Fig 4.13b Cross-section through the Cleveland Ironstone Formation. Cliff Ridge Wood and Botton Head are separated by a short distance along Depositional Strike

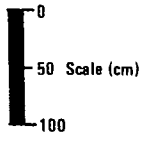

Fig 4.13a Chowns (1968) section of The Cleveland Ironstone Formation

Locality	Chamositic chamosite oolite	Calcitic sideritic chamosite oolite	Sideritic chamosite oolite	Calcitic chamosits oolite	Siderite mudstone
Brackenberry Wyke	T(I), MS(B) (T)	MS (T)		R	A,R,T(u), P
Kettleness	T(I), MS (B)				T,P, MS(B), MS(T)
Cliff Ridge Wood	T(I), MS (B)				A,R, T(u), P,MS(B) MS(T)
Botton Head					A, R, T, P, MS
Raisdale					A, R, T, P, MS
Eston Hill			MS (T)		
Skelton Beck			MS (T)		
Ayton Banks Mine					MS (T)
Waterfall Gill					MS (B)

A : Avicula Seam; R : Raisdale Seam ; T : Two Foot Seam [u : upper, l : lower]; P : Pecten Seam; MS : Main Seam [T : Top Block; B : Bottom Block]

Table 4.4 Distribution of ironstone lithologies

4.3.1 Chamosite Ooids

These allochemical grains exhibit all the characteristics shown by the chamosite ooids of the Marlstone Rock-bed Ironstone (Chapter 3, Section 3.3.1). Several features, however, are not in common with the Marlstone ooids. Perhaps the most important of these is that chamosite ooids of the Cleveland Ironstone exhibit a uniform grass-green colouration. Colour differences between the individual ooid envelope rings and between the envelope and core-grains are absent (Plate 4.1). This makes the distinction of these structural units somewhat difficult. In general, however, thin black lines mark the boundaries between such units. This does not indicate a difference in ooid infrastructure as ooid envelopes exhibit a positive pseudouniaxial extinction cross between crossed polars (Plate 4.1b). Individual envelope rings tend to be slightly thicker than those of Marlstone ooids indicating more rapid accretion and less abrasion. Overall the rings are characterised by a greater proportion of organic concentrations which are seen as thin, slightly irregular, rings or crescents concordant with the enclosing envelope rings (Plate 4.2). Such material also occurs within the niches of core-books and along cleavage traces. An interesting feature of Cleveland core-books in comparison to those of the Marlstone is that they do not commonly show rounding and concertina features considered to be indicative of seafloor abrasion in the case of this ironstone (Plate 4.3). The brown shades of green found as core-book colours in the Marlstone are also absent from Cleveland core-books, these being entirely grass-green. In this context it is interesting to note that where envelope fragments occur as core-grains they do not show a great degree of rounding.

4.3.2 Chamositic Chamosite Oolites

This lithological type comprises ellipsoidal chamosite ooids set in a matrix of chamosite mud. Frequently, but on a scale of 10-15 cm this type of oolite passes laterally and vertically into an oolite comprising white ooids set in a chamosite mud matrix. The latter oolite type often passes laterally into siderite mudstone which may or may not exhibit an oolitic phase. Both oolitic ironstone types are penetrated by burrows infilled by siderite mudstone.

4.3.2i Chamosite ooids: These allochemical grains have all the features described above. A variety of textural forms are shown by chamosite ooids which results in a low abundance of 'normal' ooids. As noted above mineralogical variation within this phase is also common.

Evidence of chamosite ooid dissolution is provided by the presence of common ooimoulds. Externally these show the normal ooid form. Internally, however, variable amounts of chamosite have been removed, leaving only the outer few envelope rings intact. The edge of any one ooimould generally corresponds to the ring contact of the innermost envelope ring. In some instances the process of ooimould formation has proceeded to completion, with the result that the original ooid is entirely absent being now represented by a secondary porosity retained by the chamosite mud matrix.

Ooid distortion textures are common and may be subdivided into three types: (i) Ooimould collapse, (ii) failure of chamosite mud matrix, and (iii) distortion of complete ooids.

(i) Distortion due to ooimould collapse (Plate 4.4) creates distorted flame-shaped ooids. These occur individually and as chains. Three types of flame-shaped ooids are found (Figure 4.14); those with no hooks at

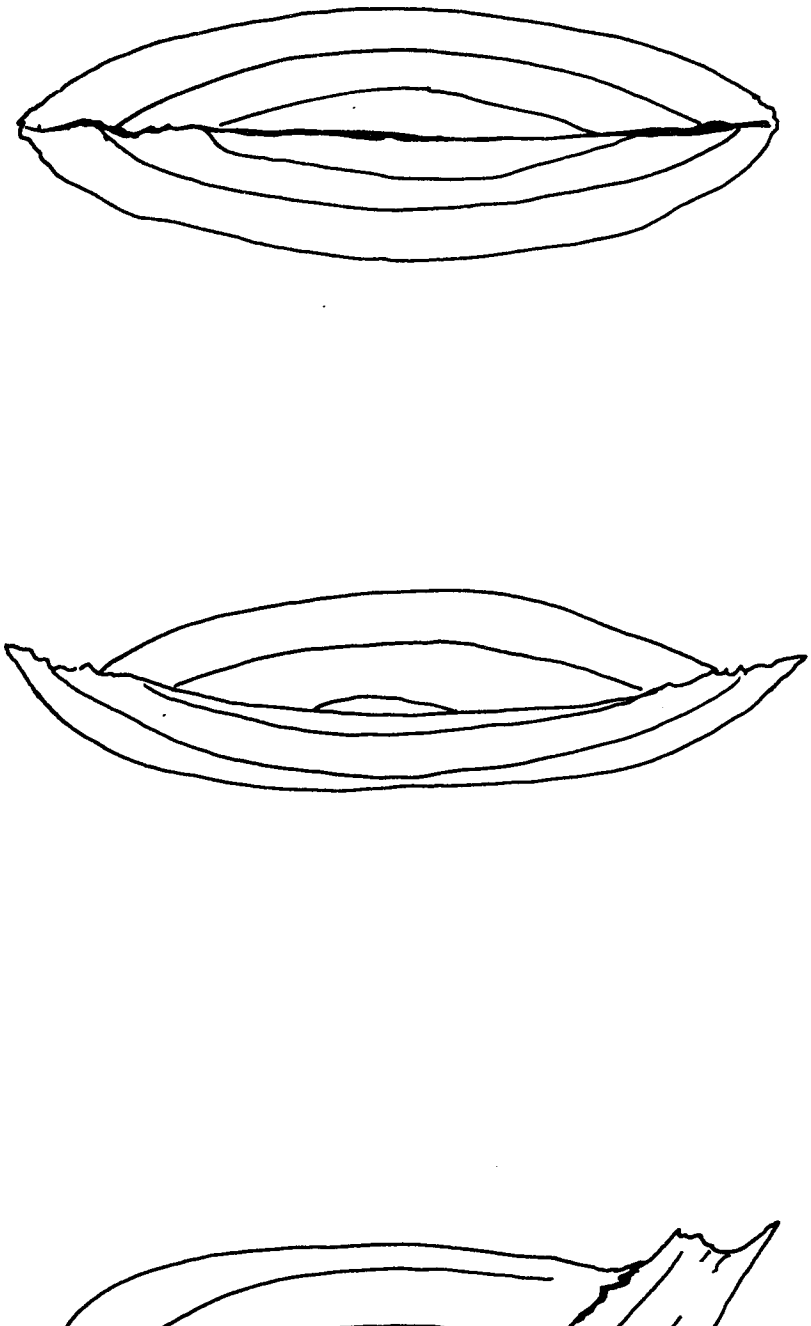

Fig 4.14 Flame-shaped Ooids resulting from Ooimould collapse x 200

either end, those with hooks pointing in the same direction, and those with hooks pointing in opposing directions. Compression of the original ooimould causes fracturing of the remnant portion of an envelope and the formation of ragged fracture surfaces. Subsequent movement of the two portions towards each other, as a function of compression, brings about the development of the first two flame ooid types; if an element of lateral motion is developed the third type forms. Ooimoulds originally in close proximity, and perhaps touching, would promote the formation of chains of flame ooids on collapse. In some instances complete ooimould collapse has not occurred and a flame-shaped central ooimould remains.

(ii) Small scale mechanical failure of the chamosite mud matrix surrounding ooimoulds creates hooked and chain ooids comprising two or more hooked ooids. These are easily distinguishable from the hooked ooids of type (i) deformation: They lack the distinctive flame-shape, and the ends of individual hooks abut sharply against the chamosite mud matrix in contrast to the rather ragged contact found in the case of flame ooids. Sharp black lines are occasionally found extending from the hooks of these ooids into the chamosite mud matrix. It is easy to see that a slight degree of rotation of the failed matrix into the space represented by an ooimould would create a hook. Evidence that this type of motion occurs is provided by the remnants of ooid envelopes which are bent back at an angle into the ooimould. Rotation of a portion of failed chamosite mud matrix lying between two ooimoulds, away from one and towards the other,

would bring about the formation of chain ooids of this type. It is clear that hook and chain ooid formation by this process would not bring about complete collapse of an ooimould. The fact that a large proportion of the secondary porosity represented by ooimoulds is preserved in textures of this type supports this. Hook and chain ooids formed by the same type of matrix failure have been described in Chapter 3, and for 'pisomoulds' and chain pisoliths by Conley (1977).

(iii) Deformation textures involving hooked and chain ooids, but which cannot be related to a pre-existing ooimould generation, are common. Ooids of this type have been referred to as spastoliths (Plate 4.5) by Rastall and Hemmingway (1940) and Chowns (1968). The formation of such a fabric appears to have a progressive form related to bedding and relative burial depth: Individual spastoliths may occur in association with other ooid deformation textures. Immediately below these numerous spastoliths may occur showing mutual boundary textures. Ooimould deformation textures present in this lower area are generally entirely of type (i) and have proceeded to a more advanced degree i.e. complete flattening. Individual spastoliths exhibit irregular shapes which can only be attributable to drawing-out and compressional processes. The ooid envelope ring structure generally runs parallel to such irregularities in the external shape. If deformation of the ooid has occurred such that a process has been drawn out at a high angle to the rest of the ooid then it is common to find irregular incipient fractures in the ooid envelope in this area. In areas of many spastoliths deformation of the original ooid is extreme and generally takes the form of a flattening of the ooid creating a spastolith with a long axis parallel to bedding. Due to the creation of many spastoliths in these areas mutual boundary textures occur

and take the form of the deformation of one elongate spastolith around another. This may result in the creation of spastoliths with hooks and chain spastoliths. An important feature in the formation of such spastoliths is the complete disruption of the original envelope structure. Only discrete fragments with a ring structure are found. This enables the distinction of spastoliths from flattened ooimoulds which exhibit a good ring structure and extinction cross. It is interesting to note that the formation of spastoliths does not affect the form of original core books. Although an envelope surrounding a book may be drawn out to form a spastolith core-book remains undeformed, acting as a rigid body. The nature of the processes which result in the formation of spastoliths are rather difficult to establish as the surrounding chamosite mud matrix appears to be no different than it is in areas where spastoliths are not found. Their mutual moulding textures and their association with flattened flame ooids clearly indicates a post-depositional time of formation. The association of spastoliths with distorted ooids resulting from chamosite mud matrix movement suggests that they may also result from such movement.

Variation in the mineralogy of the ooid phase occurs as a result of the infilling of ooimoulds. Siderite and ferroan calcite are the usual infilling generations and are discussed below. Kaolinite occurs as an occasional infill. This is seen as an irregular mosaic of equant kaolinite crystals which either partially or totally infill the ooimould.

4.3.2ii Chamosite mud matrix: This is characterised by a grass-green colouration. It is constructed of irregular chamosite grains approximately 0.02 mm in size which exhibit a unit extinction (Plate 4.6). Those grains of chamosite which immediately surround complete, undeformed ooids

extinguish at the same time as the adjacent ooid envelope extinguishes. It is difficult to distinguish the actual nature of the component chamosite grains due to the abundance of siderite anhedra in the matrix. Small organic inclusions, approximately 0.5-1.0 μm in length and with circular cross-sections occur with a variable abundance in the chamosite mud. These are morphologically similar to algal filaments.

4.3.2iii Intraclasts and lithic clasts: There is a generally low abundance of fragments of ironstone contemporaneously eroded and redeposited. In comparison to other ironstones the abundance of lithic clasts is high, although these are only represented in the occasional sample.

Intraclasts comprise irregular sub-angular and sub-rounded fragments of chamositic chamosite oolite identical to the surrounding oolite. Such grains are generally less than 0.5 mm in size.

Lithic clasts are represented by pinkish buff devitrified glass containing angular quartz grains and small mica flakes (Plate 4.7). The clasts have irregular shapes and are sub-angular. Grain sizes less than 0.5 mm are encountered. It is interesting to note that the quartz grains appear to be identical to those encountered as occasional ooid core-grains in the Cleveland Ironstone ooids, within the Sandrock and sandrock facies of the Marlstone Rock-bed, and within the chamosite mudstone and chamositic limonite oolite facies of the Frodingham Ironstone.

4.3.2 iv Biogenic material: This is sparcely distributed and is entirely fragmentary in nature. An upper grain size limit for the long axes of shell fragments of 0.5 mm is found. The material may be subdivided into

calcite and originally aragonite bivalve fragments, originally aragonite gastropod remains, and calcite echinoid plates.

The calcitic bivalve fragments are non-ferroan in composition and exhibit an original shell structure. The originally aragonitic fragments have undergone dissolution and are now seen as shell-shaped areas of inequigranular xenotopic ferroan calcite. The originally aragonite gastropod fragments are also replaced by ferroan calcite.

Echinoid plates are found to be constructed of ferroan calcite. The stereome systems of these fragments are infilled by siderite. Both carbonate generations are in optical continuity.

4.3.2v Cement generation minerals: The only cementing minerals present are two generations of siderite and ferroan calcite. The ferroan calcite generation can be related to the formation of occasional stylolites.

A commonly occurring type of siderite, which is associated only with the chamosite mud matrix, is found as 1-2 μm equant anhedra. These are golden brown in colour. An individual grain of this type may surround a single algal filament-like inclusion.

Larger equant anhedra (0.03 mm) of white siderite are abundant within the chamosite mud matrix. They characteristically form trains of anhedra of ten or more grains length (Plate 4.8). There is no apparent preferred orientation for the trains although in lenticulate areas of chamosite mudstone they tend to run parallel to the lenticle axis. A number of trains which are constructed of two trains, one upon the other, occur. In some instances these are found to run through the chamosite mud matrix and abut against the fracture surface of an ooimould which is undergoing type (ii) deformation. These are found to sometimes pass laterally into stylolites (Plate 4.9). A similar texture is exhibited by one anhedra thick chains which run through the matrix until their path is interrupted by an

allochemical grain. At this point their orientation changes and they pass around the grain forming either a complete or incomplete rind (Plate 4.9 and 4.10).

The majority of allochemical grains exhibit a siderite anhedra rind whether they be complete ooids, ooimoulds, deformed ooids, shell fragments, intraclasts or lithic clasts. Individual anhedra which partake in this fabric type are neither distortive or replacive. The only exceptions to this are occasional chamosite ooids which show distortion of envelope rings around larger than normal siderite anhedra.

Ferroan calcite occurs as an inequigranular xenotopic mosaic infilling ooimoulds, chain ooimoulds (Plate 4.11), and originally aragonitic shell fragments. Optical continuity between ferroan calcite infills to two such grains which are in contact indicates that these infills do not represent separate ferroan calcite generations. Many ooids and ooimoulds exhibit irregular fragments of chamosite ooid envelopes totally surrounded by ferroan calcite but retaining their original orientation (Plate 4.12). Similarly occasional ooid mucilaginous envelopes occur in their original positions and are surrounded by ferroan calcite. These two textural types indicate that such calcite is replacive with respect to chamosite. Where occurring with kaolinite as an ooimould infill ferroan calcite may totally or partially surround the grains of this mineral. Ooimould infills are constructed of three or less grains of ferroan calcite.

Siderite and ferroan calcite occur together as an infill to stylolites (Plate 4.9). Stylolites take the form of veins less than 1 cm in length and 0.07 mm in width which cross-cut both matrix chamosite and ooid phases. It should be noted that they always cross-cut ooids which show evidence of the type (ii) deformation described above. A slight displacement of ooids and ooimoulds cut by stylolites is often demonstrable. Where stylolites cross-cut three or more very closely spaced ooimoulds some degree of disruption is common. This takes the form of islands of chamosite mud, originally interstitial to the ooimoulds and therefore being coated

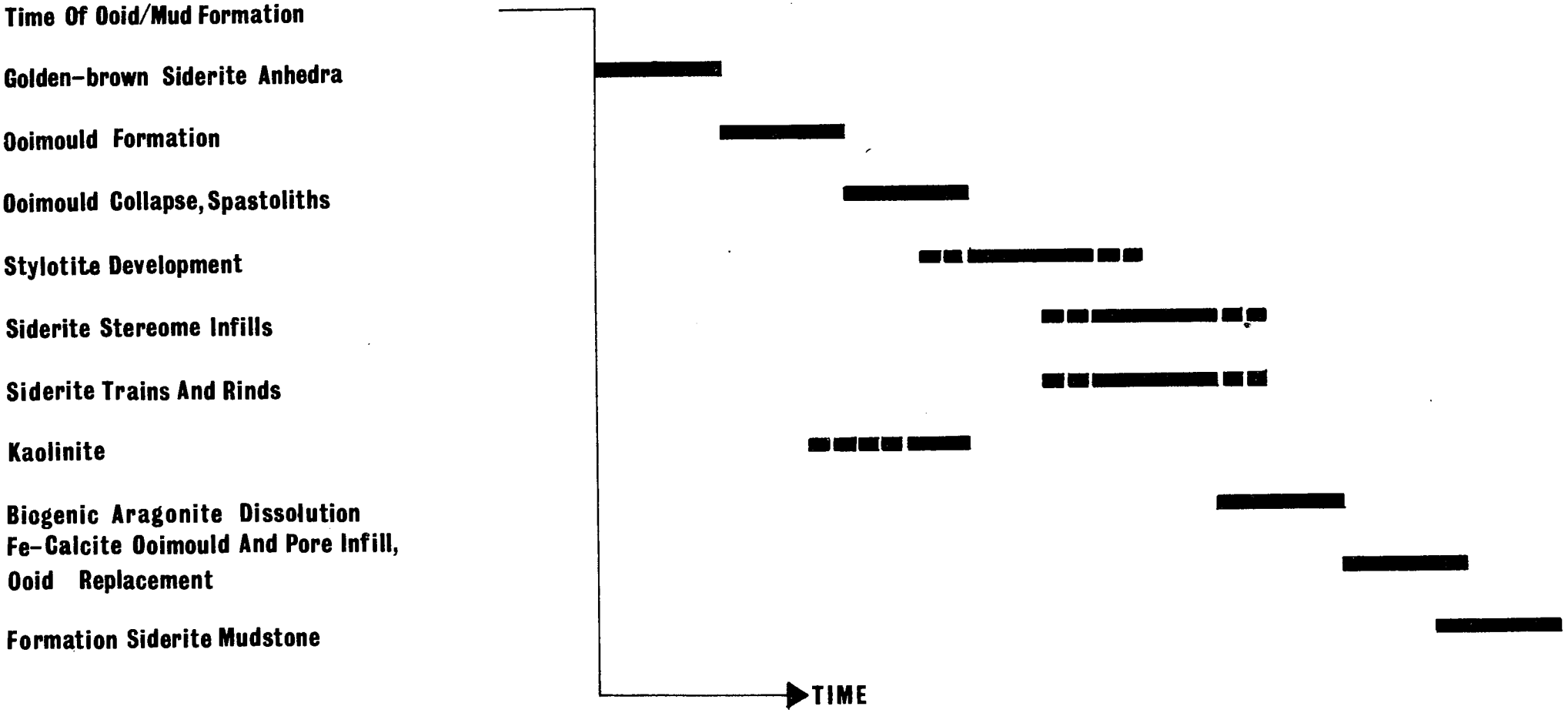

Figure 4.15:Paragenesis Of The Chamositic Chamosite Oolites

entirely or partially with a rind of siderite anhedra, displaced from their original position and set within the ooimould and stylolite ferroan calcite infill. Where having a true vein-like form stylolites are lined by equant siderite anhedra and infilled by inequigranular xenotopic ferroan calcite.

4.3.2vi Paragenesis: The textural types and cement mineral generations described above indicate a post-depositional history for the lithology involving dissolution, structural reorganisation, and the precipitation of cement minerals. This sequence of events is shown in Figure 4.15.

Since the chamosite ooids and chamosite mud are affected by all the subsequent diagenetic changes it is concluded that these represent the initial components of the lithology. Biogenic material and lithic clasts are also included in this bracket as they have obviously been included in the sediment. The chamosite mud is characterised by a more or less complete absence of any depositional fabric. The unit extinction of component grains suggest that it may be authigenic in nature. If this is the case, however, the stereome systems of echinoid fragments would be expected to be infilled with authigenic chamosite. There is no evident primary porosity between ooids or other grains which could form a site for the deposition of isopachous pore-linings. Textures indicative of extensive removal of chamosite mud are absent. The tendency of chamosite mud surrounding chamosite ooids to extinguish with the extinction of the chamosite ooid envelope suggests some degree of orientation of the chamosite mud parallel to the tangential orientation of the component envelope flakes.

It is not possible to date unequivocally the time at which the golden brown siderite anhedra precipitated. The fact that many of these anhedra surround algal material whereas the later coarse white siderite does not suggest that the golden brown siderite may pre-date the white siderite.

Since the collapse of ooimoulds to form flame ooids and the mechanical failure of the chamosite mud matrix requires the presence of space within ooids it follows that the formation of ooimoulds must predate such structural change. The variety of ooimould types which occur from ooids with a small central secondary porosity to ooimoulds from which all the chamosite is absent, suggests that the dissolution process commenced in the ooid core and moved outwards. This is supported by the commonly occurring ooimoulds which retain, intact, their original outer two or three envelope rings. Dissolution therefore appears to move from ring to ring rather than being concentrated at just one place.

Ooid distortion textures (flame ooids, matrix failure, and spastoliths) are cross-cut by all the subsequent products of diagenetic changes. Chowns (1968), although not differentiating between deformed ooids, notes that spastoliths appear to form prior to cementation. The mode of deformation of ooids and ooimoulds has been discussed above. Those ooimoulds which have been deformed as a result of small scale mechanical failure of the chamosite mud matrix are related to thin black lines in the matrix, representing failure surfaces, and stylolites.

The great majority of all allochemical phases are surrounded by a thin siderite rind of equant anhedra which pass laterally into trains in the chamosite mud matrix. Since deformed grains also exhibit such rinds it follows that precipitation of this siderite generation follows ooid and ooimould deformation.

Echinoid plate stereome systems are infilled by white siderite rather than ferroan calcite. It seems likely that the precipitation of this siderite occurred contemporaneously with the precipitation of other white siderite textural varieties.

The time at which stylolites develop is somewhat problematical. They appear to correspond to the failure surfaces of the chamosite mud matrix. All gradations of stylolites occur from relatively thick varieties lined by equant anhedra of siderite and infilled by ferroan calcite to thin types represented by two layers of equant siderite anhedra. The former may pass laterally into the latter. Stylolites are pressure solution phenonoma resulting from overburden stress (Bathurst, 1975). Their relationship to failure surfaces suggest that these fractures formed sites at which pressure solution of chamosite could occur. They are lined, however, by siderite trains which would indicate that their formation pre-dates this cement generation. The larger stylolites (infilled by ferroan calcite) often appear to mechanically disrupt the fine interstitial features between ooids resulting in the removal of such fragments which are coated with siderite anhedra to a new location. The presence of such siderite on these fragments suggests that stylolite formation occurred after siderite precipitation Since such fabrics are only associated with stylolites infilled by ferroan calcite the passage of diagenetic fluids and the precipitation of this cement may be responsible for this type of fragmentation. If the formation of stylolites pre-dates the siderite precipitation, and since they correspond to chamosite mud matrix failure surfaces are these failure surfaces or incipient stylolites? If the latter was the case then the solution leading to ooimould formation might also be expected to occur in the mud matrix. It is interesting to note that this period corresponds broadly with the deformation of ooids and ooimoulds which is considered to represent the compaction of the sediment under overburden stress. The siderite rinds which surround allochems are neither distortive with respect to allochemical phases, where this would be possible, or the chamosite mud matrix. The

The fact that they occur as linings to stylolites suggests that their fabric may be an open-space fabric. If this is the case then solution of chamosite mud around allochemical phases may represent a form of stylolite laterally continuous with other 'normal' stylolites. Evidence in support of this suggestion derives from other ironstone lithologies where stylolites are apparently absent and any siderite which occurs with a rind-like form is restricted to chamosite or goethite ooids and is demonstrably replacive or distortive.

Kaolinite occurs as ooimould infills. Since its mode of occurrence is restricted to ooimoulds its time of formation can only be considered relative to ooimould formation and any other ooimould-infilling phase. There are three possibilities which might explain its presence: (i) Chamosite has a similar structure to kaolinite (Brindley, 1949; Brindley, 1951). Leaching of iron from chamosite during ooimould formation might lead to the formation of kaolinite. (ii) Direct precipitation of kaolinite as an authigenic mineral phase. (iii) Diagenetic breakdown of feldspar. The leaching of chamosite to form kaolinite would be expected to be an in situ process leading to the pseudomorphing of original chamosite by kaolinite. Kaolinite occurring in envelope areas should therefore exhibit an extinction cross. This is not observed. On this basis, possibility (i) is rejected and allows kaolinite to be classed as an ooimould infill rather than a chamosite replacement. If kaolinite was precipitated from solution it might be expected to form very coarse euhedral crystals in ooimoulds and also to occur as stylolite infills. Neither of these textural types occur. Chowns (1968) considers, from the occurrence of kaolinite as occasional originally aragonite shell infills and septarian crack infills in ooids, that this is the origin of the

kaolinite. The presence of lithic clasts and ooid core-grains of quartz, of the type included within the clasts, indicates the possibility that lithic clasts or feldspar might have formed ooid core-grains. Ooimould formation might have promoted 'weathering' of such core-grains and hence the formation of kaolinite. It is not possible to judge which of these two processes is responsible for the occurrence of kaolinite Since incomplete ooimould infills of kaolinite are either partially or totally surrounded by ferroan calcite its precipitation pre-dates this cement generation.

Originally aragonitic shells are represented by shell-shaped areas of ferroan calcite and are surrounded by equant anhedra of siderite. Where the original shell and an entirely or partially ferroan calcite infilled ooid occur with a tangential contact area, indicative of an original, depositional contact, both are surrounded by a continuous rim of siderite and infilled by optically continuous ferroan calcite. This indicates that dissolution of the aragonite did not occur until after precipitation of the siderite i.e. The siderite is not a secondary porosity lining to the original aragonite shell. This secondary porosity was subsequently infilled by ferroan calcite.

Ferroan calcite infills all the secondary porosity, there being no evident primary porosity. The relationship between fragments of chamosite within ooimoulds and the infilling ferroan calcite suggests that the influx of ferroan calcite precipitating fluids promoted a second phase of chamosite dissolution. Ferroan calcite precipitation was contemporaneous with this in order to retain ooid fragments in their original orientations. Such fragments do not occur as geopetal deposits.

It was noted in the introduction to this section that chamositic chamosite oolite with green chamosite ooids passes into a chamositic oolite in which the ooid phase comprises white ooids. It is found that there is a petrographic gradation between these two lithologies. The former is characterised by abundant chamosite ooids, the latter by abundant ooids replaced by ferroan calcite and exhibiting a siderite rind.

4.3.3 Sideritic Chamosite Oolites

This lithological type comprises ellipsoidal greenish white ooids set in a dominantly crystalline siderite matrix (Plate 4.13). Chamosite mud is often present as a matrix mineral. The lithology passes vertically and laterally into siderite mudstone in which an ooid phase may or may not be present.

4.3.3i Chamosite ooids: These exhibit all the characteristics described above. They differ, however, in that they are greyish yellow or yellowish green in colour. X-ray data confirms their identification as chamosite. A further difference exhibited by these ooids is the abundance of a dark-brown to black diffuse material in the ooid envelopes (Plate 4.14). This does not have any mineralogical characteristics.

The dark-brown to black diffuse material noted above occurs in ooid envelopes as discrete rings from which chamosite appears to be absent. This mode of occurrence may take the form of a complete ring or the corresponding ring crescents at either end of the ooid long axis. A second common occurrence of this material is as irregular regions within the ooid envelope, masking the original chamosite and envelope structure but passing laterally into a normal ooid envelope. Such material is also found in ooid core-grains. It may totally or partially 'pseudomorph' core-books. In cases where the core-grain is an ooid envelope fragment its

occurrence is that which is found in ooid envelopes. The rings the material forms in these grains do not continue into the surrounding envelope. The petrographic evidence suggests that this dark-brown to black material is not a result of some diagenetic reaction but is a feature of ooid formation. Similar features occur in carbonate ooids where they are observed as micritisation destroying the original ooid shell lamination, and with which boring algae may be associated (Shearman et al, 1970). By analogy this diffuse material is thought to result from the activities of boring algae. Its colouration may represent the remains of such organisms. Due to the masking effect of this diffuse material it is not always possible to determine optically whether the bored chamosite is oriented or unoriented. In cases where this is possible the envelope to either side of the organic material exhibits an extinction cross suggesting that ooid ring destruction by an alternative process of template-collapse, which also involves boring algae (Shearman et al., 1970), did not occur as this would result in the loss of an extinction cross.

The formation of ooimoulds in this lithology is not uncommon. As in other lithologies much of the ooid interior is removed leaving the outer two or three rings intact. Ooimoulds representing total removal of the grain are rather more frequent than in other lithologies.

Ooid distortion, whether due to ooimould deformation or the formation of spatoliths, is rare. That which does occur is due to the flattening of ooimoulds creating flame-shaped ooimoulds and chain ooids. Complete flattening of such distorted grains yields laminated chamosite strips. The extinction of these grains is divided into two bars perpendicular to the grain long axis and which pass in opposite directions along the grain with rotation. This supports the suggestion that such grains are flattened flame ooids and indicates that the lamination is the original envelope

structure which has also been flattened. Flattened ooids occasionally occur with either end in contact with a normal chamosite ooid. This texture was considered by Chowns (1968) to represent the unwrapping of an ooid.

Ferroan dolomite and siderite occur as replacements to the outer one, two, or three rings of normal ooids, ooimoulds, and distorted ooids (Plate 4.15). It should be noted that these two carbonates do not occur together in such replacement textures. The texture takes the form of a rim of equant carbonate anhedra in the outer portion of the ooid envelope. Their outermost boundary corresponds to the original outer boundary of the ooid. A ghost ring contact may be observed if the carbonate grains transgress the first envelope ring. Individual ferroan dolomite grains occurring in this texture may exhibit euhedral rhombic terminations within the ooid. Ferroan dolomite rhombs occurring within ooimoulds are considered to represent a different view of this texture. Some ooimoulds from which chamosite is absent are lined by this textural variety of siderite and ferroan dolomite.

4.3.3ii Chamosite mud: Yellowish brown to yellowish green chamosite mud occurs as irregular, variable size, patches of matrix and as burrow infills. It is characterised by a spotty appearance. This is due to the abundance of small (less than 5 μm) circular, ovate and rod-like sections of black inclusions which are nearly always surrounded by a rim of siderite (Plate 4.16). Due to these inclusions it is very difficult, if not impossible, to distinguish any fabric in the chamosite mud. Individual areas of chamosite, however, exhibit a unit extinction and there is a tendency for chamosite mud surrounding chamosite ooids to extinguish with the rotation of the ooid extinction cross.

4.3.3iii Intraclasts: Occasional intraclasts of chamositic chamosite oolite occur. These comprise chamosite ooids set in a chamosite mud. They are irregular in shape and are either sub-angular or sub-rounded. They are generally less than 0.5 mm in size.

4.3.3iv Biogenic material: This is restricted to rounded shell fragments of non-ferroan calcite which may be almost entirely micritised and originally aragonitic grains. The latter are recognised by their shell fragment-like shapes which are lined by siderite dogs teeth or ferroan dolomite rhombs. They are not completely infilled.

Fragments of fossil wood are not uncommon. These are rounded grains of a yellow colour showing black organic laminations.

4.3.3v Cement minerals: Siderite and ferroan dolomite (Plate 4.17) are the only cement minerals present. They do not occur together as a cement to the above phases. Both exhibit an inequigramular xenotopic fabric. At the margins to ooids individual cement crystals may penetrate the envelope, cross-cutting the ring structure. In the case of a ferroan dolomite cement such crystals exhibit euhedral rhombic terminations. Occasional complete ooids may contain dolomite rhombs which have a cross-cutting relationship with respect to the structure. This is considered to represent a different view of the same texture. Where surrounding ooids with carbonate rim replacements the carbonate ring and cement are in optical continuity, providing that they are the same carbonate mineral. A ghost ooid rim separates the composite grain thus formed into the two generations that it represents.

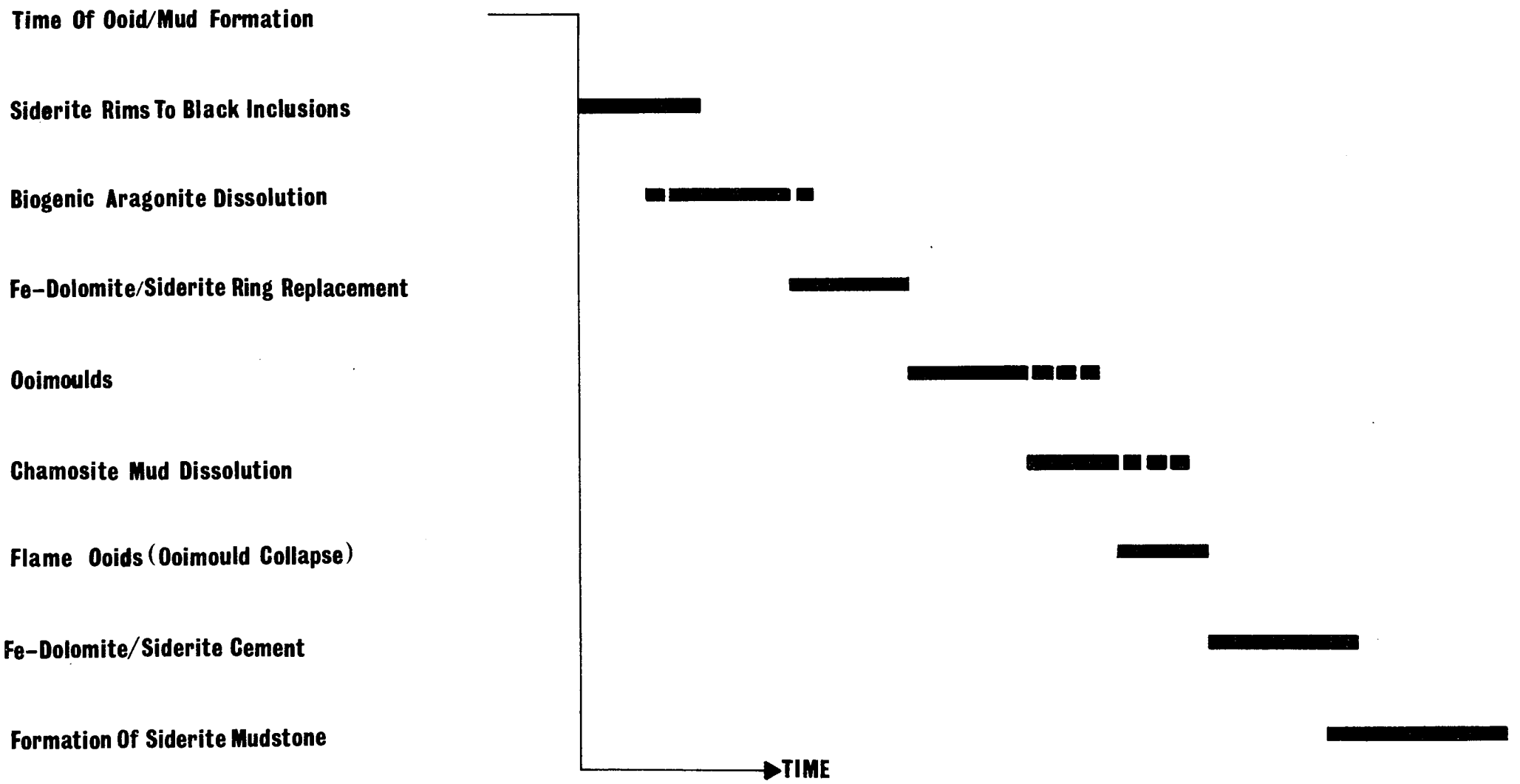

Figure 4.16: Paragenesis Of The Sideritic Chamosite Oolites

4.3.3vi Paragenesis: The above textures indicate a post-depositional history for the lithology involving dissolution, some degree of structural reorganisation, and the precipitation of cement. The order of events is outlined in Figure 4.16.

Chamosite mud, chamosite ooids, intraclasts and biogenic material represent the primary components of this lithology, being affected by all diagenetic generations. The absence of a depositional fabric to the chamosite mud and its unit extinction, combined with its relationship to the chamosite ooids suggests that it may have some authigenic character. In this context, the presence of small black inclusions, which have not been recorded from depositional chamosite mud in other lithologies, similar to those considered to be of micro-organism origin in chamosite ooids may be important.

It is not possible to date unequivocally the point at which the siderite surrounds to the black inclusions in the chamosite mud precipitated. It is interesting to hypothesise, however, that if the inclusions were of organic material their decay would yield locally high concentrations of CO_2 in a geochemical environment rich in dissolved ferrous iron, which would be conducive to the precipitation of siderite.

Replacive rims of siderite and ferroan dolomite occur around normal ooids, ooimoulds with a remnant envelope, ooimoulds from which all original chamosite has been removed, and flame-shaped ooids. In order for ooimoulds with no remaining chamosite to exhibit such a texture replacement by siderite and ferroan dolomite must have occurred prior to ooimould formation.

The nature of ooimoulds indicates that ooid dissolution commenced in the core and moved outwards.

In general, flame-shaped ooimoulds, which result from the deformation of ooimoulds, do not exhibit replacive rims of carbonate phases. In order for such rims to occur in this lithology, therefore, ooimould formation and deformation must overlap with the development of rim replacements. It is not possible to determine at what stage these three processes ceased relative to each other.

Ooids with replacive outer rims of siderite and ferroan dolomite occur in both areas of chamosite matrix and areas of siderite or ferroan dolomite cement. In the latter areas the outer edge of the replacive carbonate corresponds to the edge of the original ooid and abuts against the surrounding carbonate cement. In order for this feature to occur some pre-cement phase would be necessary to form a mould around the ooid. The occurrence of this texture in the areas of chamosite mud matrix suggests that this was the moulding medium and was subsequently removed by dissolution.

Further evidence for a phase of chamosite mud dissolution is provided by shell shaped areas lined by siderite or ferroan dolomite and occurring in areas of carbonate cement. These represent originally aragonite shell fragments. In order for their form to be retained some moulding medium would have been required to have been present from their time of deposition to their dissolution. Following the aragonite dissolution siderite dogs teeth and ferroan dolomite rhombs precipitated as a lining to the mould and rooted on the walls of the mould. It is likely that these carbonate phases are equivalent to the ooid rim replacement carbonates. The only potential moulding medium present in the lithology which could have been present at the time the shells were incorporated in the sediment is the chamosite mud. Thus, following ooid rim replacement and aragonite dissolution the original chamosite mud underwent dissolution.

The secondary porosity resulting from the dissolution of the chamosite mud was infilled by the cement generations of ferroan dolomite and siderite.

It is interesting to note that the initial nucleation sites for these generations were formed by the rim replacement carbonates. Thus, the two generations may be found in optical continuity but separated by a line representing the original ooid margin. Where replacive rims to the ooids are absent deformation of the ooids due to the pressure of crystallisation of the cement grains occurred. The clear separation of siderite and ferroan dolomite indicates that although they are contemporaneous cement generations they are geochemically incompatible.

4.3.4 Calcitic Sideritic Chamosite Oolites

These oolites are characterised by green ellipsoidal chamosite ooids set in a calcite and siderite cement (Plate 4.18). Chamosite mud is absent. Lateral and vertical passages into siderite mudstone with or without an ooid phase occur.

4.3.4i Chamosite ooids: These have all the characteristics described above. They are grass-green in colour. Filamentous inclusions are common. Ooid deformation is a frequently occurring feature. Due to the fact that oolites of this type are grain supported the deformation can be ascribed entirely to loading. It takes the form of those moulding textures described from the Marlstone Rock-bed (Chapter 3, Section 3.3.1). The most frequently occurring of these is tangential touch which in this lithology might be termed pressure welding; the original contact points are impossible to see. Complete ooid deformation results in the distortion of one or more chamosite ooids around their neighbours. Due to the pressure welding effect it is not possible to see original boundaries. The deformed ooid is generally only recognisable as an ooid on the basis of any remnant ring structure.

Ooimould formation in this lithology is rare. Examples of ooimoulds include both undeformed and deformed ooids. As before, the result of ooimould formation is an ooid in which the outer two or three envelope rings surround a central ooid. No distorted ooimoulds occur. Siderite and ferroan calcite cements form ooimould infills and are non-replacive.

Replacement of the chamosite of complete ooids is a very commonly occurring feature (Plate 4.19). The replacing mineral is siderite. It usually occurs as greenish-white equant anhedra less than 0.05 mm in size. The replacement is associated with distortion of the ooid envelope. The abundance of siderite varies from one or two grains to almost complete replacement. The degree of ooid distortion increases with the number of such grains. In cases where a great many are present the original ooid structure is totally destroyed resulting in the absence of an extinction cross.

4.3.4ii Biogenic material: This comprises the fragmentary remains of originally aragonite and calcite bivalve fragments and echinoid plates. Their grain size is generally less than 1 mm.

Calcite shell fragments are non-ferroan in composition. They are often bored. These may be infilled by authigenic chamosite. An occasionally occurring texture which is found in association with such shell fragments is a layer of radial fibrous ferroan calcite located between the shell and a rim of authigenic chamosite. The contact with the authigenic chamosite is characteristically zig-zag in nature. This texture is interpreted as the remains of a high-magnesian calcite or aragonite radial fibrous fringe to the shell fragment which was subsequently surrounded by authigenic chamosite.

Originally aragonite shell fragments are recognised by analogy with a similar texture in the Marlstone Rock-bed (Chapter 3). Shell shaped

areas of one or two grains of ferroan calcite are surrounded completely or partially by a coat of authigenic chamosite. Siderite rhombs may be rooted on the coating growing into both the original shell void and the surrounding pore space.

Echinoid plates are constructed of ferroan calcite. Occasional compositionally zone plates have been found showing a ferroan calcite margin to a non-ferroan calcite core. The stereome system is infilled by authigenic chamosite. Very few plates are surrounded by syntaxial overgrowths of ferroan calcite.

4.3.4iii Authigenic chamosite: Authigenic chamosite occurs in elongate areas approximately 1 mm across and with lengths of the order of 5 mm. These areas are considered to represent sections of burrows. Any fabric to the chamosite infill of these burrows is obscured by the presence of abundant golden brown siderite sub-hedra and anhedra. The chamosite grains occurring between the siderite have a unit extinction. Occasional black inclusions similar to those reported from the previous Cleveland Ironstone lithologies are found within the chamosite and also within the siderite grains.

Authigenic chamosite also forms a lining to the primary porosity of the lithology. It occurs as an isopachous lining to interstices between ooids, being distinguishable from them by a slightly darker green colouration. This lining is difficult to discern in many instances due to the fact that it has been deformed with the chamosite ooids. Its relationship with respect to biogenic material has already been noted.

4.3.4iv Cement minerals: Siderite infills many of the smaller (less than 0.2 mm) pore spaces. It occurs as rhombs rooted on the authigenic chamosite rims to originally aragonite shell fragments. In large pore spaces siderite may occur as dogs teeth or anhedra lining the pore and

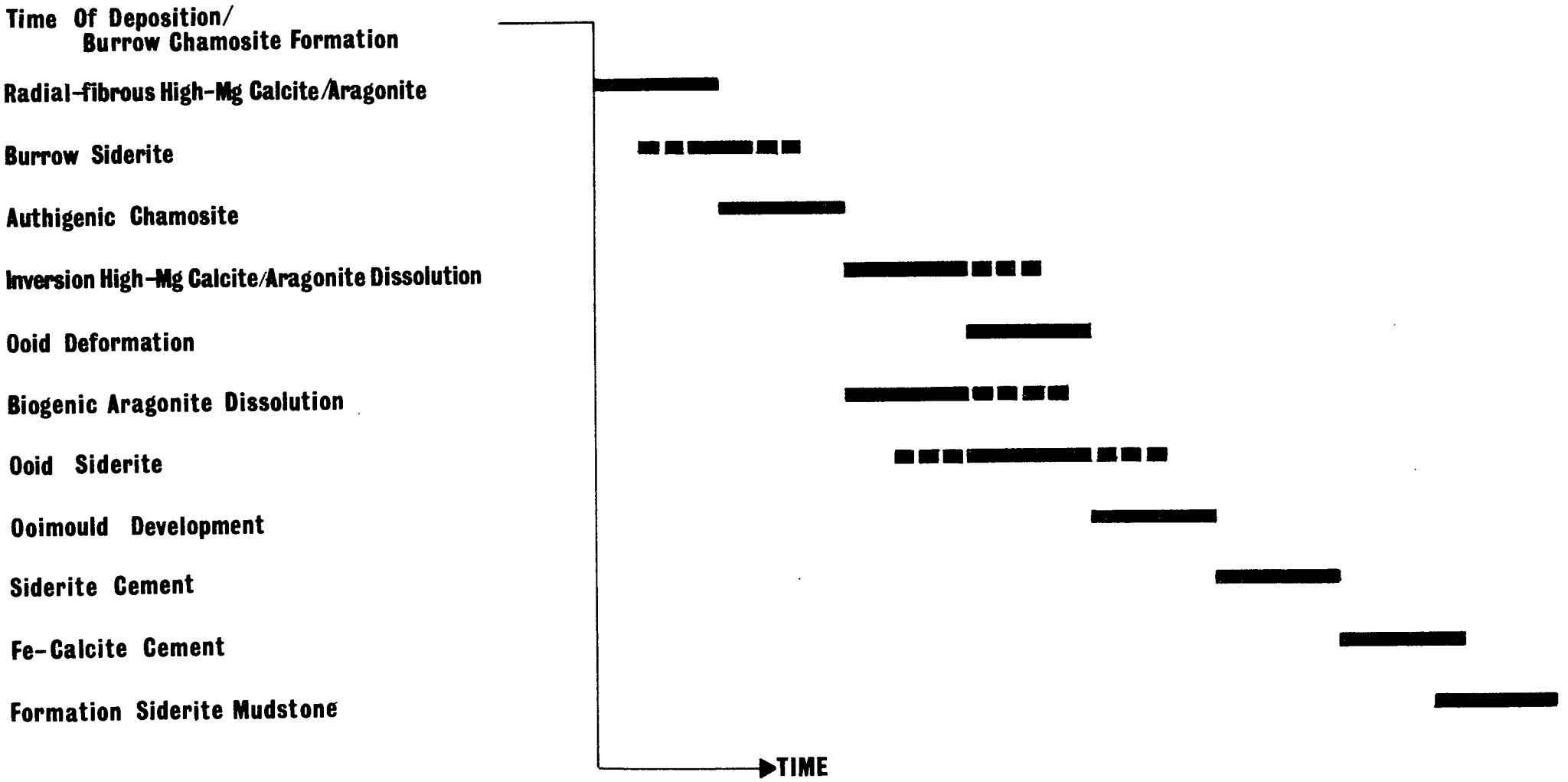

Figure 4.17:Paragenesis Of The Calcitic Sideritic Chamosite Oolites

The pore space remaining after siderite precipitation is infilled by individual grains of ferroan calcite. This cement mineral also infills the secondary porosity represented by originally aragonite shell fragments.

4.3.4v Paragenesis: The above textures indicate a relatively simple sequence of post depositional events mainly involving the precipitation of various cement phases. The sequence of events is indicated in Figure 4.17.

Since chamosite ooids exhibit deformation features which have been ascribed to loading of an unconsolidated sediment they are considered, together with biogenic material, to represent the primary components of the lithology.

The unit extinction of the burrow-infilling chamosite mud suggests that it has some authigenic character. The similarity (black inclusions, golden-brown siderite sub-hedra and anhedra) between this material and that which has been demonstrated to be a primary chamosite mud in the sideritic chamosite oolites may be an in situ burrow infill formed by the same processes.

Radial fibrous ferroan calcite representing a similar fabric of originally either high-magnesian calcite or aragonite occurs between shell fragments and authigenic chamosite pore-linings. Since authigenic chamosite is cross-cut by later pore-filling minerals or deformed by compaction processes it follows that this carbonate generation was the first diagenetic mineral to be precipitated and was followed by authigenic chamosite (pore-lining). The isopachous fabric of the pore-lining chamosite is indicative of precipitation from solution.

The fact that authigenic chamosite pore-linings are distorted together with the chamosite ooids indicates that sediment compaction did not occur until after this phase was precipitated.

It is not possible to date the time at which the siderite anhedra occurring within chamosite ooids precipitated. If, however, it precipitated before ooid deformation it might be expected to give some mechanical strength to the ooids, making them more resistant to deformation. Deformed ooids do not appear to be any different in their replacive siderite content to relatively undeformed ooids. If this siderite precipitated after ooimould formation these would be expected to be infilled by greenish siderite rather than the cement variety.

Although ooimoulds occur in deformed ooids these are not of the flame type which would indicate ooimould formation prior to deformation. The time of formation of ooimoulds is thus considered to post-date ooid deformation.

Following ooid deformation siderite precipitated as a cement partially filling the larger pore-spaces and totally occluding the smaller pores.

The fact that ferroan calcite infills all the primary and secondary porositiy within the lithology and surrounds totally or partially all other mineral generations indicates that it is the final diagenetic precipitate.

In order for originally aragonite shells to be preserved as a replacement by ferroan calcite some mould is required to retain the shape of these grains on their dissolution. Since all shell-shaped areas, infilled by ferroan calcite, are surrounded by authigenic chamosite it would appear that this mineral provided a suitable moulding medium. Siderite rhombs are rooted on authigenic chamosite in this role and grow into the original shell space. These textures indicate, therefore, that aragonite dissolution occurred between authigenic chamosite and siderite precipitation.

4.3.5 Calcitic Chamosite Oolites:

These oolites are identical to the calcitic sideritic chamosite oolites except that the proportion of siderite cement is much reduced or may be

It is not possible to date the time at which the siderite anhedra occurring within chamosite ooids precipitated. If, however, it precipitated before ooid deformation it might be expected to give some mechanical strength to the ooids, making them more resistant to deformation. Deformed ooids do not appear to be any different in their replacive siderite content to relatively undeformed ooids. If this siderite precipitated after ooimould formation these would be expected to be infilled by greenish siderite rather than the cement variety.

Although ooimoulds occur in deformed ooids these are not of the flame type which would indicate ooimould formation prior to deformation. The time of formation of ooimoulds is thus considered to post-date ooid deformation.

Following ooid deformation siderite precipitated as a cement partially filling the larger pore-spaces and totally occluding the smaller pores.

The fact that ferroan calcite infills all the primary and secondary porositiy within the lithology and surrounds totally or partially all other mineral generations indicates that it is the final diagenetic precipitate.

In order for originally aragonite shells to be preserved as a replacement by ferroan calcite some mould is required to retain the shape of these grains on their dissolution. Since all shell-shaped areas, infilled by ferroan calcite, are surrounded by authigenic chamosite it would appear that this mineral provided a suitable moulding medium. Siderite rhombs are rooted on authigenic chamosite in this role and grow into the original shell space. These textures indicate, therefore, that aragonite dissolution occurred between authigenic chamosite and siderite precipitation.

4.3.5 Calcitic Chamosite Oolites:

These oolites are identical to the calcitic sideritic chamosite oolites except that the proportion of siderite cement is much reduced or may be

4.3.6 Siderite Mudstones

This is the most frequently occurring lithology in the Cleveland Ironstone Field. It is a fine grained grey rock within which an ooid phase may be present (Plate 4.21). The vertical and lateral passages from other lithologies into irregular patches of siderite mudstone and siderite mudstone beds indicate the replacive nature of the siderite mudstone.

4.3.6i Ooids: When present this allochemical phase is sparcely distributed. It comprises ooids similar in shape and size to the chamosite ooids of other lithologies. The original chamositic nature of these grains is indicated by occasional ooimoulds which retain the outer two or three chamosite envelope rings. Generally, however, the ooids exhibit a replacement by one or two grains of ferroan calcite. They may be characterised by an outer fringe of siderite anhedra. Ooid deformation textures such as hooked and chain ooids of the flame type may be present and are entirely replaced by ferroan calcite and siderite.

4.3.6ii Biogenic material: This material is sparcely distributed and fragmentary in nature. Calcite bivalve fragments of non-ferroan calcite and originally aragonite shell fragments, represented by shell fragment shaped areas of ferroan calcite, can be recognised.

4.3.6iii Siderite mud: This is strictly a cement generation developed by replacement of pre-existing phases. It has an equigranular xenotopic fabric in which the individual crystals are less than 0.05 mm in size (Plate 4.21). In slides in which siderite mudstone and chamositic chamosite oolites occur a gredational passage from the chamosite mud

of the latter to the siderite mudstone occurs. The nature of the passage is seen as a gradual increase in the numbers of siderite anhedra present in the chamosite mud until the chamosite mud is totally absent as an interstitial component to these grains.

4.3.6iv Paragenesis: The replacive nature of siderite mudstone has been concluded from field petrographic evidence. The fact that the siderite mudstone lithology encludes textures seen in lithologies such as the chamositic chamosite oolites, and that the chamosite mud of such lithologies is replaced by equigranular xenotopic siderite suggests that the replacement may be added as a final event at the bottom of the paragenesis of this lithology. Thus, ooid textures seen within the siderite mudstones may be regarded as inclusions. Since all lithologies exhibit replacement by siderite mudstone, on the basis of field evidence, such late-stage replacement must be added as a final event in the paragenesis of all the Cleveland Ironstone ironstone lithologies.

The absence of ghost textures and many deformed chamosite ooids from the siderite mudstones indicates that replacement of chamosite phases by siderite mudstone was neither a dissolution-precipitation nor a pressure of crystallisation process. Thus, dissolution of these phases must have occurred slightly prior to the precipitation of siderite in the space occupied by them. Since ooids which were replaced or infilled by carbonate phases, in the lithology undergoing replacement by siderite mudstone, do not show any indication of dissolution it follows that the pore fluids at the time of siderite mudstone formation were saturated with respect to siderite and ferroan calcite.

4.4 SUMMARY

The Cleveland Ironstone Formation occurs at the minima of a regressive event. It was deposited within a depositional basin in which water depths fluctuated as a result of subsidence and deposition. This gave rise to an alternating sequence of shales and ironstone. The shales may be interpreted as open-shelf or slightly deeper deposits, whereas the ironstones are considered to represent shallower deposits. The Blue Mottle which underlies the Main Seam may represent shallow subtidal bathymetric levels in which case the ironstones may represent beach-face sediments.

Five different ironstone lithologies have been recognised and are well characterised by their diagenetic mineral assemblages. There is good evidence to suggest that the chamosite mud occurring in the sideritic chamosite oolites is an original component. The absence of any depositional fabric indicates that it was not deposited from suspension. The abundance of material similar to algal filaments within it suggests that it may be a primary chamosite mud. Its similarity to the chamosite mud matrix of the chamositic chamosite oolites suggests that this too is primary. Thus the sideritic chamosite oolites represent the product of diagenetic change within the chamositic chamosite oolites. In all respects, except that the chamosite mud has undergone some dissolution, these two lithologies are identical. Calcitic sideritic chamosite oolites and calcitic chamosite oolites differ only in their relative proportions of siderite cement. Both are characterised by the absence of any depositional chamosite mud and a clean, winnowed nature. It is concluded that these oolites represent ooids removed from a site of ooid formation, perhaps the chamositic chamosite oolites, transported and redeposited. There

is no possibility that any original abundant chamosite mud has been removed by dissolution from these two lithologies as textures where this does occur are absent. The replacement of all original oolite facies by siderite mudstone is a late diagenetic event. It obscures the nature of the original lithology. Thus, facies interpretations in the context of the entire Field are very difficult.

CHAPTER 5

GEOCHEMICAL VARIATION IN THE FRODINGHAM, MARLSTONE ROCK-BED AND CLEVELAND IRONSTONES

5.1 INTRODUCTION

The field and laboratory investigations of the Frodingham, Marlstone Rock-bed, and Cleveland Ironstones have lead to the recognition of a number of distinctive facies. Some of these occur in all three ironstones, some are restricted to only one. Since each facies is characterised by the presence of a specific mineral assemblage, they should also have characteristic chemical compositions. The proportion of a given mineral present in any given facies may be variable between different specimens of that facies. This would be expected to be reflected in a range of analyses for any given facies. In order to assess to what extent individual facies types may be compared and contrasted on the basis of their chemical constitution bulk rock geochemical analysis of a large selection of specimens has been carried out.

James (1954) proposed that, with respect to silicate ironstones, an ironstone should be considered to contain more than 15 wt% iron. This was later amended to embrace all sedimentary ironstones (James, 1966). Following an investigation of the Lake Superior silicate ironstones he proposed that such ironstones could be considered in terms of genetically related facies; sulphide, silicate, oxide, and carbonate, on the basis of the dominant, depositional or primary, iron-bearing mineral (James, 1954). A consideration of a number of bulk rock analyses of various ironstone types in context of their mineral assemblages allowed James (1966) to extend this hypothesis to aluminous ironstones. Whilst being a valuable method of classifying ironstones in terms of their mineralogy and chemistry there is no evidence, with respect to the ironstones under consideration, that such facies reflect the geochemical environment of deposition.

Wilson (1952) has briefly reviewed the chemical constitution of the major British aluminous ironstones and has divided them into three main classes:

(1) Unweathered ferrous ores in which the iron-bearing minerals are siderite and chamosite.

(2) Unweathered ferroso-ferric ores in which limonite and exceptionally magnetite are present in addition to siderite and chamosite.

(3) The weathered ferric ores in which limonite is the predominant iron-bearing mineral and ferrous compounds are virtually absent.

This three-fold classification embraces the Marlstone Rock-bed and Cleveland Ironstones in (1) and the Frodingham Ironstone in (2). Present-day weathering of any of the three yields an ironstone of type (3).

To-date, the consideration of bulk-rock analyses in conjunction with their mineral assemblages has provided little useful information which would aid a better understanding of aluminous ironstones. Although a number of authors (Hallimond, 1925; Taylor, 1949; Whitehead et al., 1952) report analyses of individual ironstones these are quoted as an indication of ironstone ore quality, variability in the constitution of the ore, or ore variation within the ironstone field.

5.2 ANALYTICAL METHODS

The petrography of the three ironstones shows that chamosite, goethite, siderite, ferroan calcite, ferroan dolomite, and quartz are present within them. Specimens were therefore analysed for Fe, Si, Al, Ca, Mg, Mn, Na, and K.

Powdered ironstone specimens were obtained by initial crushing in a jaw-crusher and subsequent grinding in a Tema mill. Non-ferrous equipment was used in order to avoid contamination.

In order to carry out analyses aqueous solutions were required. Since dissolution methods using hydrofluoric acid often leave an insoluble residue of clay minerals the lithium metaborate fusion method was employed (Van Loon and Parissis, 1969), and this is as follows: 0.20 g of powdered ironstone were mixed with 1.40 g of lithium metaborate. The mixture was placed in a graphite crucible preignited in a furnace by heating at 950 C for 30 minutes, and heated in a furnace at 900 C for 15 minutes. The resulting melt was poured into a plastic beaker containing approximately 100 cm^3 of dilute (1:24) nitric acid and stirred with a magnetic stirrer until dissolution was complete. The solution was poured into a 250 cm^3 plastic volumetric flask. The beaker and stirrer were washed with 1:24 nitric acid and the washings added to the flask. The solution was made up to 250 cm^3 with 1:24 nitric acid and transferred, after shaking well, to a plastic specimen bottle. It should be noted that plastic apparatus was used in preference to glass as this often adsorps metal at its surface. In addition to preparing solutions of ironstone samples a standard (Ardnamurchan dolerite) solution and a blank (lithium metaborate only) solution were made up with each batch of ironstone solutions.

Analysis of the specimen, standard, and blank solutions, for the elements noted above, was carried out using a Perkin-Elmer 260 atomic absorption spectrophotometer. A problem arises when analysing solutions comprising mixtures of elements in that interference effects occur between them which lead to low values for particular elements. Van Loon and Parissis (1969) have attempted to overcome this problem by the

addition of 'spikes'. A modified method of 'spiking' was used in analysis. The standard solution was important in this context as XRF analyses of the rock were available, thus allowing a comparison of results obtained by the two analytical methods. Suffice to say that in all cases A.A. analyses yielded results to within 1 wt% of the XRF analyses. The standard conditions and 'spikes' used in analysis of the elements are given in Table 5.1. A blank solution was analysed in order to establish that the lithium metaborate did not contain any impurities which would produce misleading results for the ironstone analyses. In all cases the elements under consideration were below the detection limit of the machine when the blank was analysed. Table 5.2 reports the results of the analysis of the ironstone specimens.

5.3 COMPUTATION OF RESULTS

Analysis of ironstone solutions by atomic absorption yielded elementa- concentrations measured as parts per million. In order to express these as weight per cent oxides the following calculation was carried out:

$$\text{Wt\% oxide} = \frac{\text{ppm} \times 100 \times \text{Autodilution factor} \times k}{1000 \times \text{Wt. initial specimen} \times 4}$$

The autodilution factor is an experimental value resulting from any dilution of the specimen which was necessary in order to yield an elemental concentration lying between the two callibrating solutions. K is equal to the molecular weight of an elemental oxide divided

Table 5.1 - Standard Conditions and spikes used in A.A. Analysis

Element	Flame	Calibrating solutions (ppm)	Spikes
Si	Nitrous Oxide-Acetylene	50.0, 5.0 Silicon	-
Fe	Air-Acetylene	5.0, 1.0 $Fe(NO_3)_2$	Calibrating solutions and sample dilutions in 1:24 HNO_3.
Ca	Air-Acetylene	5.0, 0.2 $Ca(NO_3)_2$	Calibrating solutions contain liBo, $LaCl_2$. Sample solutions also contain $LaCl_2$.
Mg	Nitrous Oxide-Acetylene	0.5, 0.1 $Mg(NO_3)_2$	Calibrating solutions and sample dilutions in 1:24 HNO_3.
Al	Nitrous Oxide-Acetylene	50.0, 5.0, $Al(NO_3)_3$	KCl added to calibrating sample solutions. Calibrating solutions and sample dilultions in 1:24 HNO_3.
Mn	Air-Acetylene	1.0, 0.1 $Mn(NO_3)_2$	-
Na	Air-Acetylene	1.0, 0.1 $NaNO_3$	-
K	Air-Acetylene	1.0, 0.1 KNO_3	-

Wt% Oxide	A13	Y9	W103	A118	Y10	CW5	CW7(R)	CW2	A104	N2(R)	A94	CW1	W53
SiO_2	21.50	14.48	34.85	44.68	11.04	20.30	13.48	2.86	7.00	33.72	7.06	3.06	2.32
Fe_2O_3	21.60	30.12	14.17	18.03	31.17	27.42	39.56	25.08	29.87	24.35	40.30	23.01	20.44
CaO	15.64	14.24	16.24	6.55	15.03	8.43	8.38	31.18	26.74	9.04	17.22	41.08	47.09
MgO	2.81	3.20	2.25	2.09	3.44	3.70	2.22	0.86	1.53	1.25	1.48	0.75	1.12
Al_2O_3	5.49	5.47	6.60	5.57	3.67	5.37	4.13	1.36	2.14	8.42	2.68	1.42	1.06
MnO	0.50	0.81	0.24	0.10	2.31	1.27	0.79	2.40	1.42	0.13	1.01	1.53	1.15
Na_2O	1.33	0.25	0.14	0.28	0.11	0.14	0.10	0.19	0.10	0.53	0.07	0.08	0.07
K_2O	0.87	0.39	0.76	0.96	0.07	0.39	0.32	0.03	0.17	0.35	0.11	0.03	0.10
%Fe	16.08	-	10.56	13.46	-	20.42	29.48	18.70	22.27	-	30.03	17.13	15.23

	Chamositic Limonite Oolite Sub-type (iii)	Calcitic Limonite Oolite									Sideritic Chamositic (Calcitic) Limonite Oolite	
Wt % Oxide	CW3	A46	A35	A69	CW4	W15	A57	A7(R)	N3(R)	RCOWP1(R)	RCOWP2(R)	A27	CW8
SiO_2	5.52	5.34	5.17	3.37	3.36	3.45	1.16	12.72	5.02	2.73	2.78	4.21	2.90
Fe_2O_3	38.85	45.85	26.49	29.44	28.23	36.95	19.33	42.04	34.99	31.60	38.34	41.45	25.77
CaO	15.54	10.60	31.21	30.35	31.85	26.24	46.97	9.64	15.62	33.56	22.23	12.76	32.08
MgO	1.73	1.71	1.50	0.90	1.47	1.16	0.94	1.95	2.50	1.30	1.03	2.22	0.72
Al_2O_3	2.38	2.39	1.76	1.44	1.75	1.86	0.62	3.77	2.06	1.56	1.91	1.70	1.31
MnO	1.71	1.23	0.83	1.61	2.36	0.71	1.64	0.71	0.19	3.16	1.28	2.99	0.75
Na_2O	0.08	0.09	0.07	0.08	0.07	0.07	0.07	0.10	0.42	0.08	0.06	0.07	0.08
K_2O	0.07	0.06	0.05	0.06	0.10	0.07	0.01	0.22	0.06	0.07	0.04	0.05	0.04
%Fe	28.96	34.10	19.76	21.95	21.02	27.56	14.41	31.37	-	-	-	15.46	19.20

Table 5.2a - Bulk Rock Analyses For The Frodingham Ironstone

						Oolite		Oolite Sub-type (i)			Oolite Sub-type (ii)		
Wt% Oxide	A13	Y9	W103	A118	Y10	CW5	CW7(R)	CW2	A104	N2(R)	A94	CW1	W53
SiO_2	21.50	14.48	34.85	44.68	11.04	20.30	13.48	2.86	7.00	33.72	7.06	3.06	2.32
Fe_2O_3	21.60	30.12	14.17	18.03	31.17	27.42	39.56	25.08	29.87	24.35	40.30	23.01	20.44
CaO	15.64	14.24	16.24	6.55	15.03	8.43	8.38	31.18	26.74	9.04	17.22	41.08	47.09
MgO	2.81	3.20	2.25	2.09	3.44	3.70	2.22	0.86	1.53	1.25	1.48	0.75	1.12
Al_2O_3	5.49	5.47	6.60	5.57	3.67	5.37	4.13	1.36	2.14	8.42	2.68	1.42	1.06
MnO	0.50	0.81	0.24	0.10	2.31	1.27	0.79	2.40	1.42	0.13	1.01	1.53	1.15
Na_2O	1.33	0.25	0.14	0.28	0.11	0.14	0.10	0.19	0.10	0.53	0.07	0.08	0.07
K_2O	0.87	0.39	0.76	0.96	0.07	0.39	0.32	0.03	0.17	0.35	0.11	0.03	0.10
%Fe	16.08	-	10.56	13.46	-	20.42	29.48	18.70	22.27	-	30.03	17.13	15.23

	Chamositic Limonite Oolite Sub-type (iii)		Calcitic Limonite Oolite									Sideritic Chamositic (Calcitic) Limonite Oolite	
Wt % Oxide	CW3	A46	A35	A69	CW4	W15	A57	A7(R)	N3(R)	RCOWP1(R)	RCOWP2(R)	A27	CW8
SiO_2	5.52	5.34	5.17	3.37	3.36	3.45	1.16	12.72	5.02	2.73	2.78	4.21	2.90
Fe_2O_3	38.85	45.85	26.49	29.44	28.23	36.95	19.33	42.04	34.99	31.60	38.34	41.45	25.77
CaO	15.54	10.60	31.21	30.35	31.85	26.24	46.97	9.64	15.62	33.56	22.23	12.76	32.08
MgO	1.73	1.71	1.50	0.90	1.47	1.16	0.94	1.95	2.50	1.30	1.03	2.22	0.72
Al_2O_3	2.38	2.39	1.76	1.44	1.75	1.86	0.62	3.77	2.06	1.56	1.91	1.70	1.31
MnO	1.71	1.23	0.83	1.61	2.36	0.71	1.64	0.71	0.19	3.16	1.28	2.99	0.75
Na_2O	0.08	0.09	0.07	0.08	0.07	0.07	0.07	0.10	0.42	0.08	0.06	0.07	0.08
K_2O	0.07	0.06	0.05	0.06	0.10	0.07	0.01	0.22	0.06	0.07	0.04	0.05	0.04
%Fe	28.96	34.10	19.76	21.95	21.02	27.56	14.41	31.37	-	-	-	15.46	19.20

Table 5.2a - Bulk Rock Analyses For The Frodingham Ironstone

	Calcitic Chamosite Oolite	Bioclastic Limestone		Green Silt
Wt % Oxide	A18	CW6	W104	N1
SiO_z	5.46	2.11	2.79	69.69
Fe_2O_3	16.86	14.32	4.35	5.78
CaO	38.69	54.21	55.37	3.29
MgO	2.16	1.81	1.06	1.501
Al_2O_5	1.83	0.55	0.48	8.03
MnO	1.29	1.20	0.81	0.08
Na_2O	0.10	0.10	0.05	0.259
K_2O	0.09	0.03	0.09	0.58
% Fe	12.58	10.67	3.25	-

(R): Red Oolitic Equivalent.

Locations.

A : Core Y112, Yarborough Pit.

W : Core W145, Winterton Pit.

CW : Core CW17, Crosby Warren Pit.

Y : Logged Quarry Section, Yarborough Pit.

N : Nettleton Core.

Table 5.2a - Continued

Core Y112				Core Y113			
Section length (cm)	Wt % Fe	CaO	Insolubles	Section length (cm)	Wt %FeO	CaO	Insolubles
0-30	32.1	4.5	23.0	0-30	30.9	6.2	21.9
30-60	31.2	6.5	21.6	30-60	32.0	6.5	21.6
60-90	30.7	11.5	17.0	60-90	27.3	15.8	16.0
90-120	26.6	12.1	22.9	90-120	27.4	9.1	25.7
120-150	22.4	11.4	28.8	120-150	22.2	11.9	23.9
150-180	23.4	17.8	11.5	150-180	21.2	21.7	8.3
180-210	27.3	15.5	7.3	180-210	18.4	15.0	29.1
210-240	27.5	12.8	16.4	210-240	21.8	23.5	10.7
240-270	30.0	17.4	6.3	240-270	27.0	23.5	5.2
270-300	24.9	25.0	4.1	270-300	31.4	12.5	8.2
300-330	23.1	24.1	8.2	300-330	37.6	7.8	7.2
330-360	21.7	30.0	4.1	330-360	34.0	14.0	6.3
360-390	37.1	11.3	5.8	360-390	30.1	19.6	4.6
390-420	29.0	21.0	3.9	390-420	27.1	23.4	4.0
420-450	36.6	11.2	4.7	420-450	39.8	8.1	6.5
450-480	43.3	6.0	5.9	450-480	35.7	13.7	4.4
480-510	21.7	28.6	3.7	480-510	18.3	31.4	5.7
510-540	25.2	21.8	8.9	510-540	22.7	24.8	9.1
540-570	15.9	36.3	3.5	540-570	15.7	35.9	3.3
570-600	16.6	35.7	2.8	570-600	24.7	23.4	5.7
600-630	27.7	19.8	6.0	600-630	22.2	26.2	6.0
630-660	16.0	34.4	4.1	630-660	17.9	29.4	6.0
660-690	20.2	29.2	5.0	660-690	16.8	30.9	6.0
690-720	16.6	30.0	4.6	690-720	18.6	31.3	3.5
720-750	18.7	29.9	3.1	720-750	24.1	25.8	6.0
750-780	22.4	26.7	6.3	750-780	23.5	18.4	14.6
780-810	27.6	17.4	11.9	780-810	16.7	33.8	4.5
810-840	26.0	21.8	6.3	810-840	20.4	27.6	8.5
840-870	25.2	24.5	6.1	840-870	18.5	26.2	13.5
870-900	20.5	20.8	17.2	870-900	19.8	28.8	6.2
900-930	18.2	32.8	3.3	900-930	17.5	30.7	7.9
930-960	21.6	24.6	9.2				

Table 5.2b - B.S.C. Bulk Rock Analyses For Cores

Core W145

Section length (cm)	Wt % Fe	SiO_2	Al_2O_3	MgO	CaO
0-30	32.0	11.3	6.60	3.75	7.8
30-60	28.1	5.7	3.60	2.60	17.9
60-90	20.7	3.5	2.25	1.30	29.4
90-120	30.3	7.7	4.60	3.10	12.9
120-150	20.5	5.4	3.00	1.85	26.7
150-180	24.5	8.3	4.85	2.25	20.3
180-210	21.5	6.9	4.35	1.90	24.6
210-240	26.2	6.1	3.75	1.90	21.5
240-270	15.7	4.5	2.90	1.45	32.8
270-300	18.0	3.6	2.10	2.20	29.7
300-330	26.4	4.5	3.20	2.30	20.7
330-360	22.5	3.7	2.85	1.50	27.1
360-390	15.2	3.3	2.00	1.50	34.2
390-420	13.1	3.1	1.95	1.30	36.4
420-450	14.2	4.7	3.20	1.50	33.3
450-480	22.4	24.8	10.40	2.80	9.2
480-510	23.1	7.8	4.55	1.95	22.4
510-540	18.7	9.9	5.05	2.00	25.6
540-570	23.8	5.2	3.65	1.75	24.8
570-600	14.8	7.8	3.85	1.40	32.1
600-630	9.3	21.6	8.00	1.95	25.8

Core CW17

Section length (cm)	Wt % Fe	SiO_2	Al_2O_3	MgO	CaO
0-30	30.2	15.3	6.75	3.20	8.5
30-60	21.6	14.6	6.05	3.15	16.8
60-90	16.9	3.7	2.25	1.30	33.4
90-120	22.4	6.3	3.70	2.00	25.6
120-150	21.9	22.3	8.40	2.35	14.1
150-180	30.4	19.1	8.45	3.40	6.5
180-210	23.0	15.9	7.60	2.40	16.3
210-240	20.9	7.2	3.95	2.10	24.3
240-270	31.8	5.2	3.45	2.00	17.3
270-300	25.8	4.2	2.85	1.65	24.5
300-330	28.7	5.0	3.25	2.10	19.3
330-360	34.4	5.5	3.95	2.00	14.0
360-390	40.1	5.5	4.05	2.30	7.2
390-420	33.9	3.8	2.55	2.00	16.4
420-450	16.7	2.3	1.25	1.35	34.6
450-480	15.1	3.0	1.70	1.15	35.7
480-510	23.2	4.2	2.75	2.05	24.1
510-540	32.5	7.6	5.15	2.95	11.1
540-570	13.1	3.4	2.20	1.35	36.6
570-600	15.9	4.2	2.95	1.70	32.2
600-630	18.3	6.4	4.10	2.85	23.5
630-660	14.8	3.4	2.15	1.95	32.2
660-690	18.9	3.5	2.55	1.45	30.7
690-720	19.4	3.7	2.55	1.30	31.4
720-750	17.5	3.7	2.50	1.30	32.3
750-780	18.1	3.5	2.45	1.15	32.8
780-810	19.4	7.2	5.00	1.55	27.9
810-840	22.7	10.6	6.90	2.10	21.6
840-870	20.7	9.6	6.25	2.15	23.7
870-900	17.2	10.4	4.65	1.55	28.0
900-930	15.6	27.0	7.85	2.30	15.8
930-960					

Table 5.2b - Continued

	Chamositic Chamosite Oolites						Siderite Mudstone	Calcitic Chamosite Oolite	Pyritic Chamositic Chamosite Oolite
Wt % Oxide	T1	T2	T3	B3	B5	N7	N4	E1	N5
SiO_2	10.91	12.04	26.40	9.67	9.30	12.92	24.08	6.07	8.93
Fe_2O_3	31.98	29.59	18.56	30.19	28.86	36.27	31.41	22.10	11.16
CaO	7.66	14.27	11.23	11.74	10.35	9.12	4.29	28.15	4.22
MgO	4.17	2.14	2.05	2.34	2.73	2.75	4.15	1.77	0.81
Al_2O_3	5.49	5.69	4.46	4.75	4.16	6.23	8.27	2.36	3.70
MnO	0.24	0.16	0.15	0.21	0.24	0.22	0.26	0.31	0.04
Na_2O	0.09	0.15	0.29	0.09	0.09	0.54	0.30	0.06	0.74
K_2O	0.30	0.07	0.36	0.02	0.07	0.19	0.41	0.01	0.15

Sandrock

Wt % Oxide	N6	N8	N9	N10	N11	T4
SiO_2	57.80	33.36	35.36	17.45	34.77	16.12
Fe_2O_3	17.50	18.54	8.65	8.94	10.22	5.69
CaO	10.88	14.88	25.69	36.98	17.00	45.04
MgO	1.35	2.84	1.04	1.20	1.55	0.92
Al_2O_3	6.16	4.28	2.53	3.28	4.50	1.88
MnO	0.10	0.17	0.14	0.13	0.15	0.15
Na_2O	1.02	0.59	0.55	0.21	4.5	0.26
K_2O	1.79	0.98	0.54	0.35	0.15	0.21

Locations:

T : Tilton Railway Cutting.

B : Branston Quarry.

N : Nettleton Core.

E : Edge Hill Quarry.

Table 5.2c - Bulk Rock Analyses For The Marlstone Rock-bed

	Chamositic Chamosite Oolite			Siderite Chamosite Oolites			Chamosite Oolite	Siderite Mudstone Replacing Chamosite Oolite						Replacing Sideritic Chamosite Oolite	
Wt % Oxide	TB2	TB3	K4	BB1	BB3	CR7	CR13	K6	C1	C2	C6	C19	BB2	W16	SB3	E3
SiO_2	12.80	14.70	15.15	15.73	16.59	19.32	18.06	17.97	12.11	7.95	10.41	12.59	7.98	8.16	9.14	9.66
Fe_2O_3	32.65	30.73	31.48	32.21	33.44	36.98	42.74	25.33	33.65	37.16	38.49	42.97	39.28	39.26	44.90	44.27
CaO	8.03	5.91	8.64	2.16	1.44	4.64	2.91	13.06	8.07	8.44	6.90	3.69	2.72	9.72	5.28	4.86
MgO	3.97	3.70	3.30	4.27	3.86	4.17	3.41	2.72	3.29	3.88	4.63	4.15	3.89	3.72	3.78	4.55
Al_2O_3	7.43	7.87	6.94	9.68	12.09	10.15	11.42	5.58	10.19	5.67	6.26	6.94	6.23	4.15	6.47	4.90
MnO	0.47	0.38	0.37	0.18	0.19	0.58	0.51	0.48	0.38	0.53	0.32	0.35	0.62	0.54	0.23	0.41
Na_2O	0.35	0.54	0.43	0.91	0.78	0.03	0.20	0.78	0.48	0.29	0.42	0.44	0.45	0.47	0.27	0.09
K_2O	0.71	0.90	0.17	1.07	1.08	0.21	0.03	0.20	0.22	0.28	0.43	0.96	0.44	0.07	0.01	0.15

Siderite Mudstone

Wt % Oxide	C3	C4	C5	C7	C23	C24	C25	C26	C27	G4	A3	R5	GM3
SiO_2	8.86	13.60	15.11	12.48	11.35	11.87	16.80	16.52	9.85	12.15	11.20	7.91	9.00
Fe_2O_3	34.54	35.72	34.77	35.30	35.28	31.13	34.42	31.56	42.14	40.25	40.60	45.17	44.56
CaO	7.02	6.78	6.82	7.23	7.33	9.12	4.87	5.79	3.55	3.86	2.85	5.04	6.06
MgO	5.05	4.61	4.15	4.76	3.37	3.44	3.75	3.34	4.64	6.26	4.07	4.98	4.78
Al_2O_3	5.31	8.41	8.24	6.85	5.43	4.70	7.36	7.15	3.02	3.99	3.80	2.47	2.96
MnO	0.61	0.30	0.32	0.29	0.44	0.46	0.41	0.38	0.54	0.56	0.32	0.46	0.40
Na_2O	0.42	0.58	0.27	0.27	0.41	0.53	0.58	0.40	0.27	0.39	0.31	0.24	0.10
K_2O	0.32	0.51	0.63	0.05	0.67	0.63	0.84	0.93	0.49	0.15	0.17	0.06	0.13

Locations

TB: Top Block, Main Seam, Brackenberry Wyke.
BB: Bottom Block, Main Seam, Brackenberry Wyke
C : Seams below the Main Seam, Brackenberry Wyke; see Figure 5.9.
K : Top Block, Main Seam, Kettleness.
CR: Main Seam, Top Block (CR13), Bottom Block (CR7), Cliff Ridge Wood.
W : Bottom Block, Main Seam, Waterfall Gill
SB: Main Seam, Skelton Beck.
E : Main Seam, Eston Hill
G : Main Seam, Glaisdale.
A : Main Seam, Ayton Banks Mine.
R : Main Seam, Raisdale.
GM: Main Seam, Botton Head (Greenhow Moor).

Table 5.2d - Bulk Rock Analyses For The Cleveland Ironstone

by the atomic weight of the same element and is a constant for any given element.

5.3.1 Cluster Analysis

It has been suggested that individual facies may be characterised by a range of analyses (Section 5.1). It would not be correct to look at the analyses for a given facies and take the highest and lowest values of specific oxides as geochemical parameters defining that facies. The above suggestion would then become an assumption. The correct approach is to consider how similar different analyses are and compare this with the facies which they represent. The ideal tool for such a study is cluster analysis.

The results reported in Table 5.2 represent a matrix of m observations for n samples. This allows the construction of two other symmetrical matrices; an n x n matrix and an m x m matrix. Since the similarities and dissimilarities between samples (Q-mode) and between elements (R-mode) are being considered the cells in the symmetrical matrices must contain some numerical evaluation of this. Two measures of similarity are in common useage; a correlation coefficient and a distance coefficient. The former is calculated in the normal way and is restricted between the limits of +. The latter is calculated from;

$$d_{ij} = \sqrt{\Sigma \frac{\sum_{k=1}^{m} (X_{ik} - X_{jk})^2}{m}}$$

where X_{ik} denotes the K^{th} variable measured on object i and X_{jk} is the K^{th} variable measured on object j.m variables are measured in all,

and d_{ij} is the distance between object i and object j. The values obtained for d_{ij} are not restricted between any limits. A good degree of similarity is indicated by high correlation coefficients and low distance coefficients whereas a poor degree of similarity is reflected by low and high values respectively.

A graphical assessment of similarity and dissimilarity may be made using dendrograms. These allow the clustering of observations in a hierarchy such that those with mutual high similarities are grouped together forming a series of first-order clusters which may be linked together as second-order clusters by virtue of mutual similarity values. In the context of dendrograms the nature of the evaluation of similarity between observations is important. If a correlation coefficient is used although it is accurate at the first-order level thereafter clusters are treated as single observations and thus their correlations with other observations represent averages. This introduces a distortion in the nature of the dendrogram. The distance coefficient is not restricted to the range $\pm$ 1 and thus produces a more useful dendrogram if a few observations are very dissimilar from another (Davis, 1973). This follows from the fact that in computing this coefficient all observations are standardised. A measure of the distortion in dendrograms is given by the cophenetic correlation coefficient. If a cophenetic coefficient of less than 0.8 occurs then severe distortion amongst the higher order clusters is indicated. It is generally found that distance correlation coefficient matrices yield good results with cophenetic coefficients in excess of 0.8.

The cluster analysis computer program of Davies (1973) has been used to carry out cluster analysis of the ironstone sample analyses.

The results are discussed on the following page.

5.4 GEOCHEMICAL VARIATION IN THE FRODINGHAM IRONSTONE

5.4.1 Core Analyses

In addition to providing four ironstone cores the British Steel Corporation have also supplied the results of the analysis of every 30 cm section of core. Figure 5.1 illustrates the geochemical variation within the cores based on the B.S.C. analytical results obtained during this work. It should be noted that the percentage of iron present is used rather than the Fe_2O_3 percentage and that in the cases of cores Y112 and Y113 SiO_2, Al_2O_3, MgO, and any other components are expressed as insolubles by B.S.C.

It is immediately apparent that there is a marked antipathetic variation between Fe and CaO whereas there is a a parallel variation between SiO_2, Al_2O_3, and MgO). A clear antipathetic variation also occurs between CaO and SiO_2, Al_2O_3, and MgO. The relationship between iron variation and variation in SiO_2, Al_2O_3, and MgO is less clear. In some instances it appears to be antipathetic, in others parallel.

The causative factor in this geochemical variation is quite clearly related to mineralogy and mineral abundance. Chamosite contains Fe, Si, Al, and Mg. The parallel variation between SiO_2, Al_2O_3, and MgO are clearly due to variations in the abundance of chamosite. The presence of quartz in chamosite mudstones will create a further increase in the level of SiO_2. Higher values occur where thicker units of chamosite mudstone,

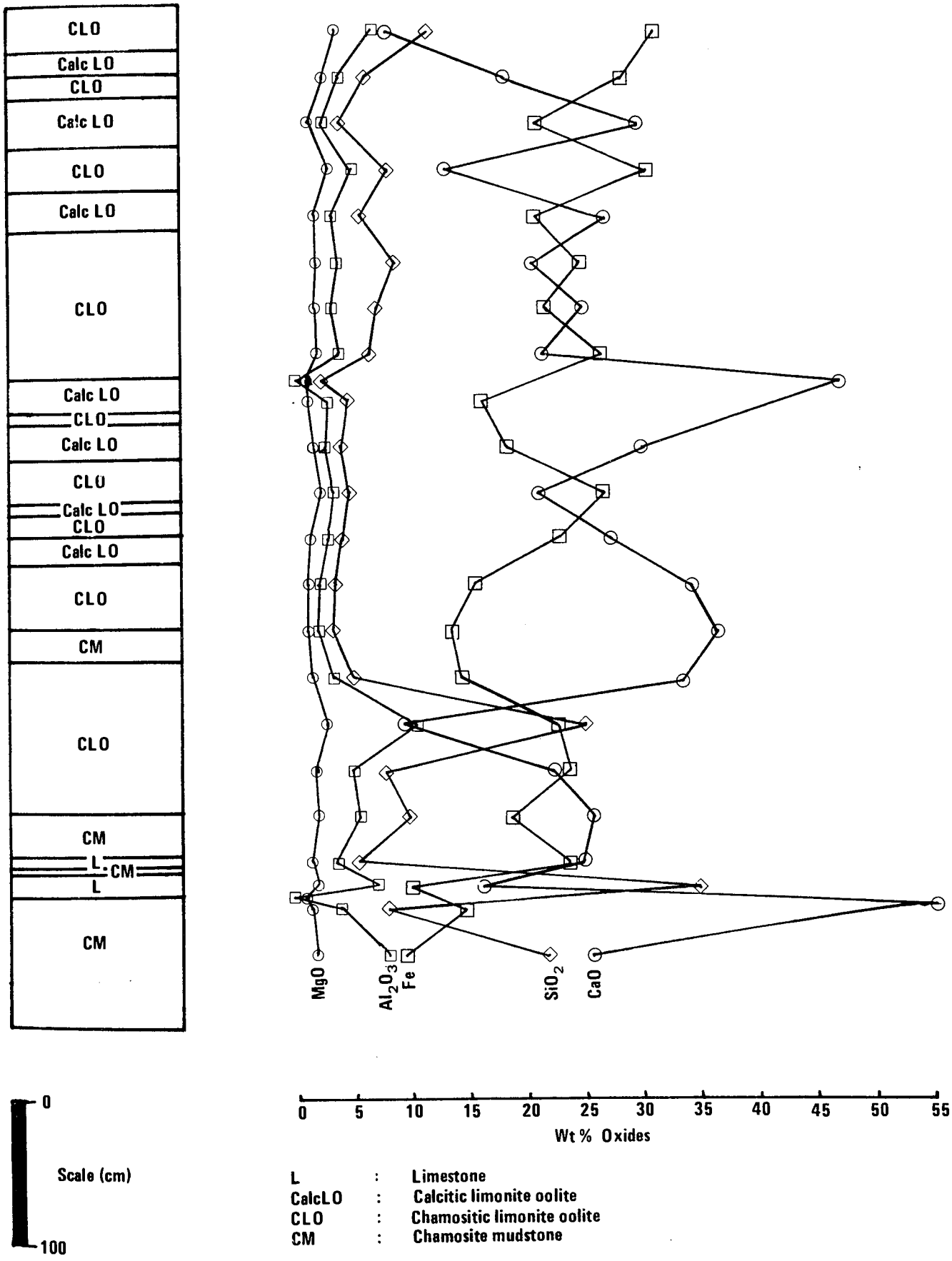

Fig 5.1a Geochemical variation in Core W145

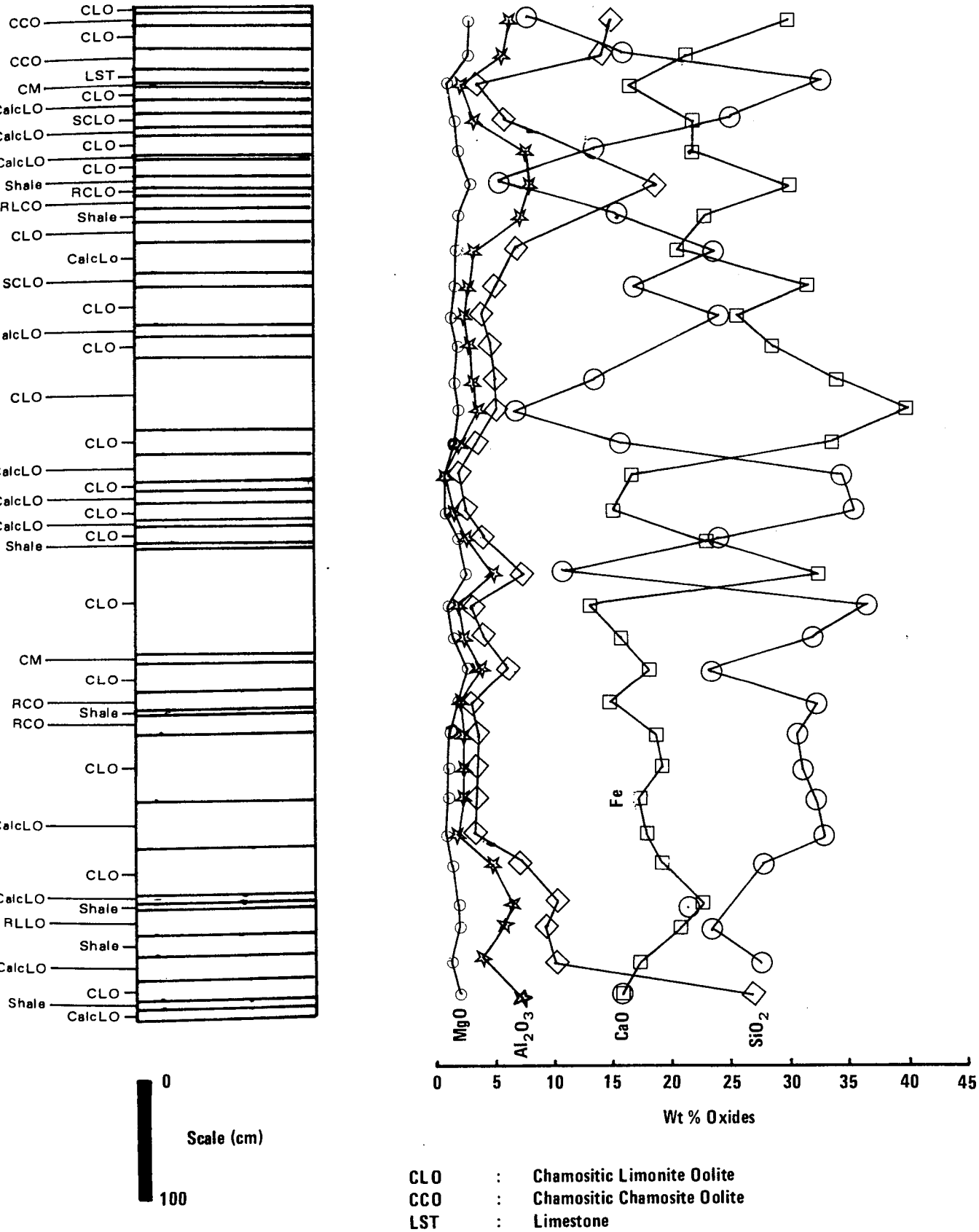

CLO	:	Chamositic Limonite Oolite
CCO	:	Chamositic Chamosite Oolite
LST	:	Limestone
CM	:	Chamosite Mudstone
CalcLO	:	Calcitic Limonite Oolite
SCLO	:	Sideritic Chamositic Limonite Oolite
R	:	Red Equivalent
L	:	Limonitic Chamosite or Limonite Oolite

Fig 5.1b Geochemical variation in Core CW 17

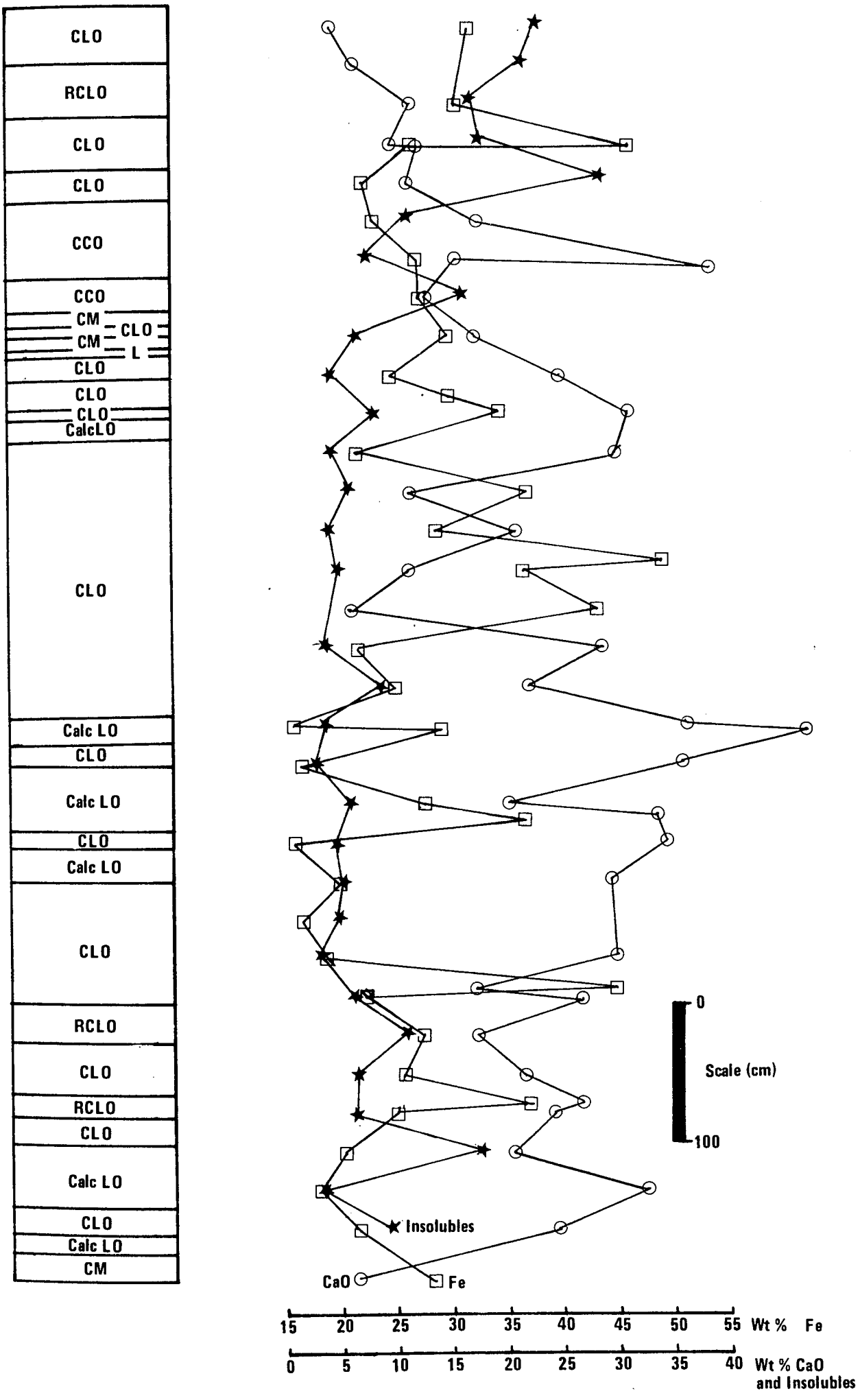

Fig 5.1c Geochemical Variation in Core Y112. (See Figures 5.1a and b, for Legend

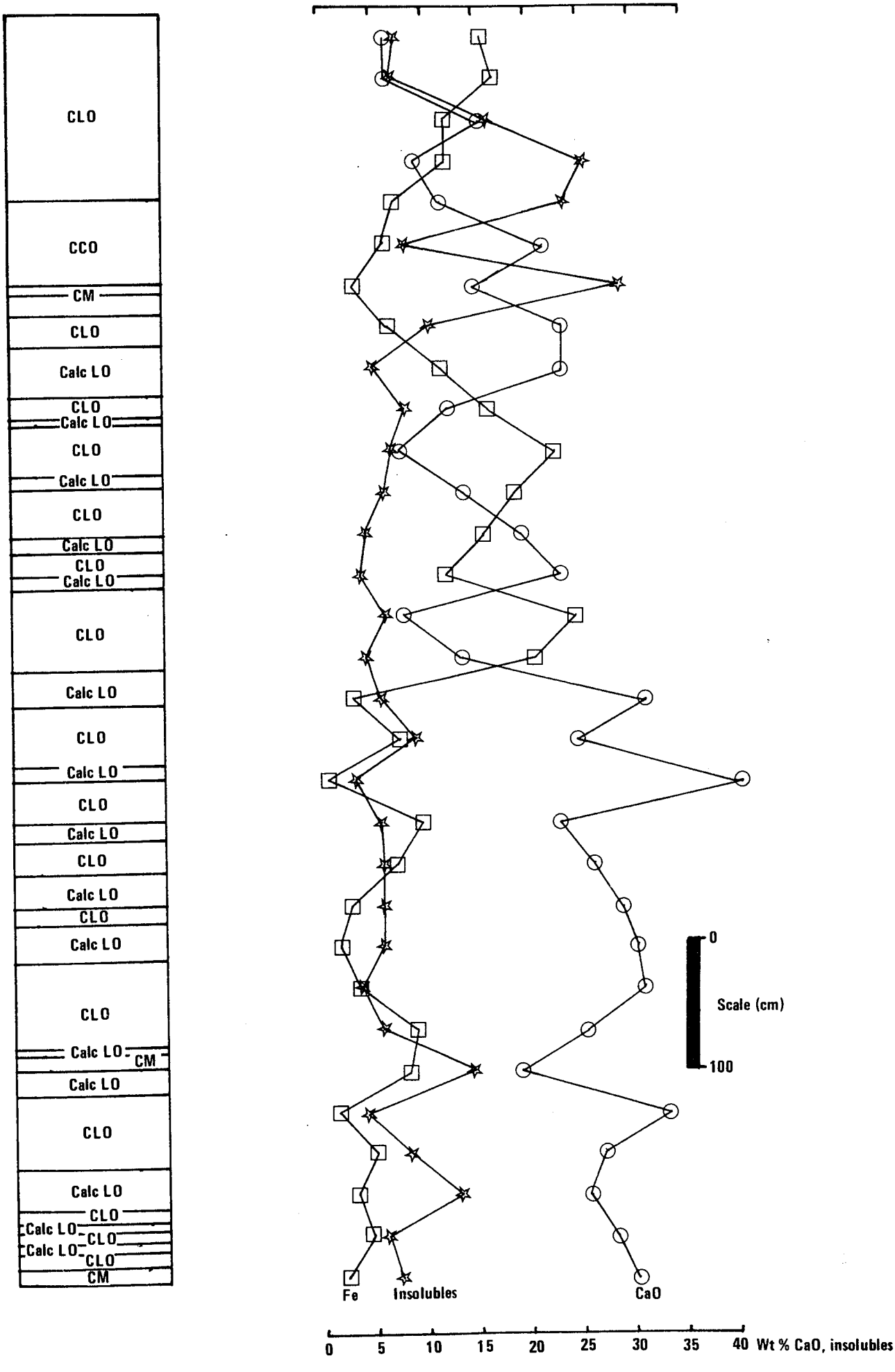

Fig 5.1d Geochemical variation in Core Y113
(See Figures 5.1a and b, for Legend)

chamositic chamosite oolite, and chamositic limonite oolite occur. At these horizons the level of CaO drops indicating the low abundance of calcite cement. Conversely, where beds of calcitic limonite oolite and bioclastic limestone occur the proportion of CaO increases showing up the abundance of calcite as cement and shell material. Iron occurs within chamosite and goethite. The relative abundance of these two minerals therefore controls the proportion of iron present. Where chamositic limonite oolites occur both minerals are abundant resulting in high iron levels. In contrast, beds of chamosite mudstone and chamositic chamosite oolite contain only chamosite which results in a diminution of iron. Iron is present as goethite in calcitic limonite oolites and bioclastic limestones. Although iron is plotted as Fe rather than Fe_2O_3 reference to Table 5.2 shows that specimens corresponding to these lithologies exhibit an excess of CaO over Fe_2O_3, as suggested by the plots. This reflects the abundance of calcite as cement and shell material relative to goethite. It should be noted that these variations do not reflect bed-to-bed variation but give an average value for all the beds present in one 30 cm segment. This is obviously weighted in favour of the dominant facies and minerals. The analyses produced during this work were of much smaller segments of rock and may be taken as 'point analyses'. They clearly indicate the overall geochemical variation more precisely.

5.4.2 Cluster Analysis

Plotting of analytical data derived from cores shows a variation which is attributed to the nature of the component facies. Cluster analysis may be able to allow a further differentiation between facies on a geochemical

basis. Dendrograms for the analyses of Frodingham Ironstone samples given in Table 5.2 are presented in Figures 5.2 and 5.4. They show the similarities between samples using the correlation coefficient and distance coefficient. This type of clustering may be referred to as Q-mode.

The sample correlation coefficient (Figure 5.2.i) dendrogram indicates a number of low-order clusters of samples. These correspond, in general, to the low-order clusters exhibited by the sample distance coefficient (Figure 5.2.ii) dendrogram. These clusters are as follows and are discussed with respect to Figure 5.2.ii.

Although lacking very low distance coefficients samples N1, N2, W103, and A118 form a cluster which is extremely dissimilar to any other cluster. These samples comprise different lithologies but have one feature in common. This is the presence of abundant detrital quartz.

Samples of CW3, A94, and A27 contain abundant authigenic chamosite and siderite. N3 is linked to the cluster of these three but is dissimilar to them in that chamosite is more or less absent but siderite is abundant. A46 is a chamositic limonite oolite sub-type III specimen containing authigenic chamosite and siderite. The reasons for its dissimilarity with the other members of the cluster are unknown but may be related to a low siderite content which does not characterise the other samples.

The red oolites CW7 and A7, and the chamositic limonite oolite sub-type (i) sample A1 are characterised by a matrix of goethite and brownish chamosite which contains a little siderite. They are linked at a relatively high level to the previous cluster.

Y10, Y9, CW5, and A13 are made up of dominantly chamosite phases with subordinate siderite. Unlike the previous two clusters they lack any goethite ooids. It is difficult to understand the cause of the

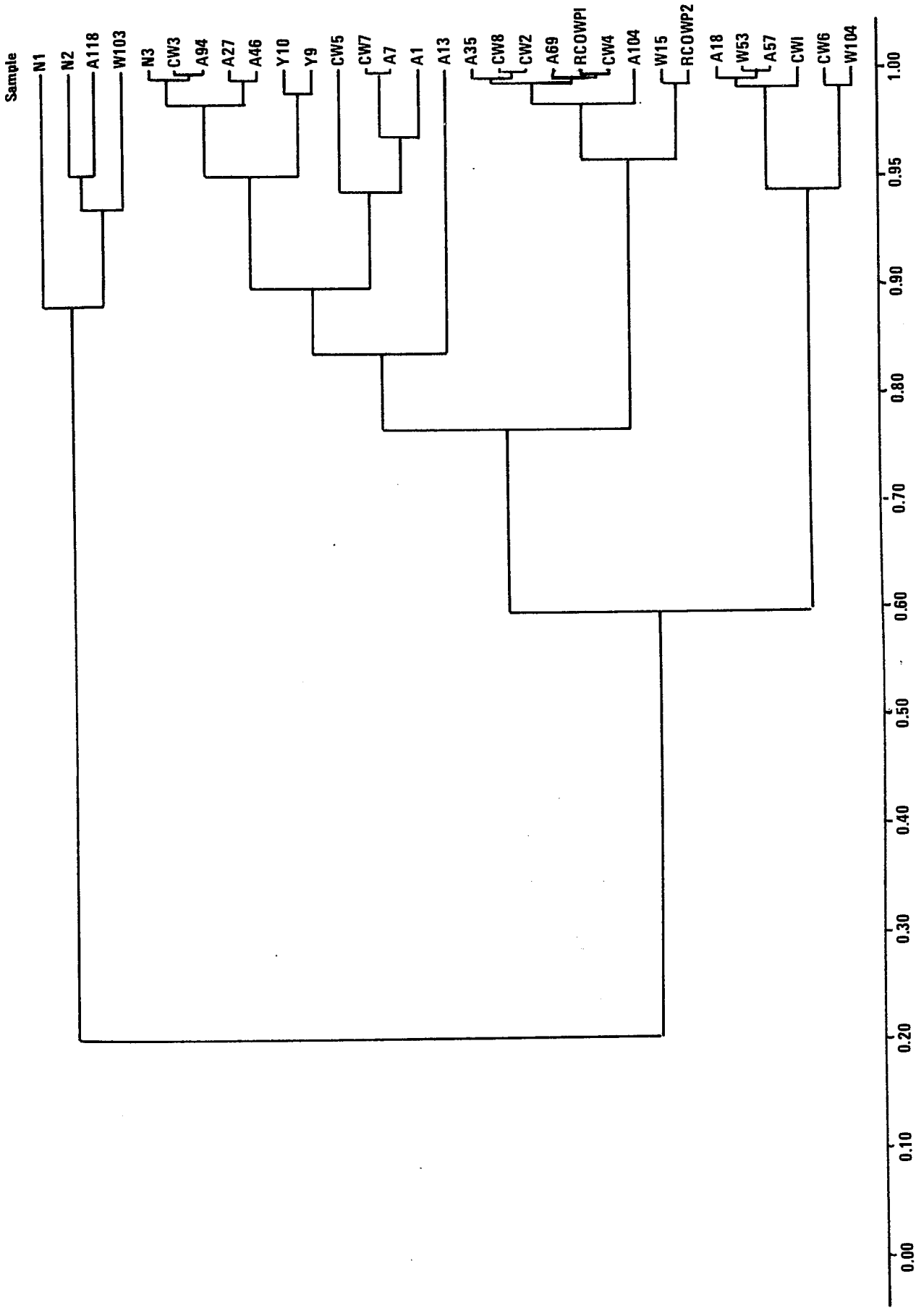

Fig 5.2 i Q–mode variation between samples. Frodingham

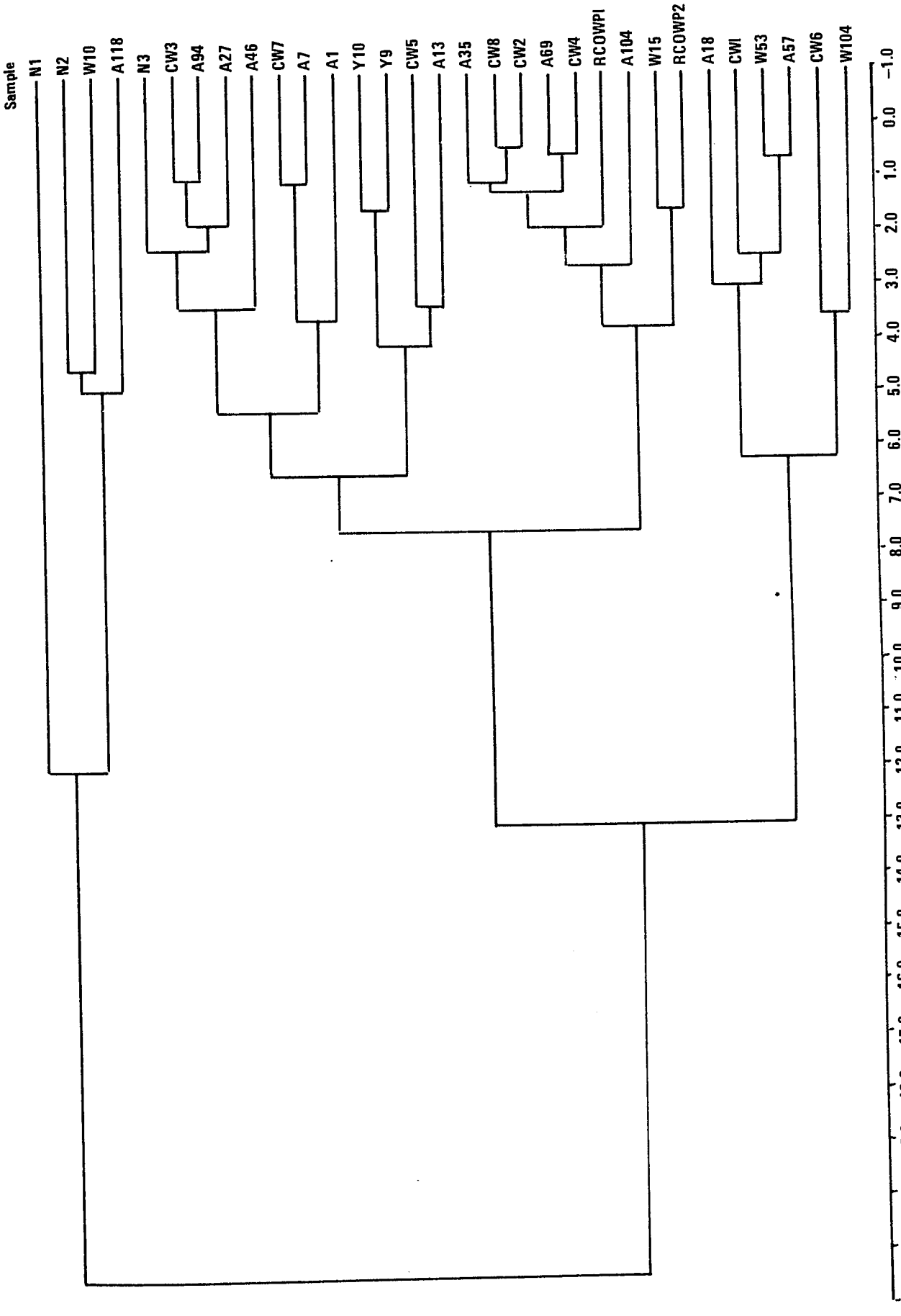

Fig 5.2 ii Q–mode variation between samples. Frodingham

dissimilarity between Y10 and Y9 and CW5 and A13 which lead to their linkage at a relatively high level. The cause of this may be a very small component of quartz silt in A13.

Samples of A35, CW8, CW2, A69, CW4, RCOWP1, A104, W15, and RCOWP2 represent lithological types in which goethite ooids are set in a matrix of chamosite and cemented by ferroan calcite. It is interesting to note the absence of chamositic limonite sub-type (ii) and (iii) representatives in which ferroan calcite is not a major component.

The penultimate cluster is formed by samples A18, CW1, W53, and A57. All are characterised by a high calcite content which is due to calcite cement and shell material in varying proportions with respect to each other.

The limestones CW6 and W104 form the final cluster.

It is concluded that the six clusters represent groups of samples containing high proportions of quartz, siderite and chamosite, chamosite, chamosite, chamosite and ferroan calcite, calcite, and ferroan calcite with very low proportions of chamosite and goethite, respectively. The justification for these clusters is found in a comparison of how dissimilar they are to each other: The limestones and calcite-rich clusters are linked by virtue of their mutually high calcite content. Due to their mutually high chamosite contents the chamosite-rich and chamosite and siderite-rich specimens are linked. Again as a result of chamosite contents these two clusters are linked with the chamosite and ferroan calcite cluster at a higher level. Of these three major clusters the calcite-rich and chamosite-rich clusters are linked. The most dissimilar cluster i.e. that characterised by the presence of quartz is finally linked with the calcite and chamosite cluster which is non-quartzose.

Since the cluster analysis was carried out using chemical analyses as data and the resulting clusters can be interpreted mineralogically it seems that the original premise that different facies can be characterised by their chemistry is correct. However, it is not possible to make a direct comparison between facies and clusters. For example, it has not been possible to separate the chamositic limonite oolite sub-types (ii) and (iii) and the sideritic (calcitic) chamositic limonite oolites or the non-quartzose chamosite mudstones and chamositic chamosite oolites in terms of their bulk chemical composition. The abundance of shell material in some samples which would otherwise be incorporated in other clusters leads to their inclusion in the calcite-cement rich cluster. An attempt to place chemical limits on the clusters is given in Figure 5.3. This has been done by taking the highest and lowest values for the oxides comprising the samples in the clusters and plotting these as variation bars for each oxide.

The similarity shown by oxides is illustrated by the correlation coefficient and distance coefficient dendrograms in Figure 5.4. Such clustering is termed R-mode. The former dendrogram (Figure 5.4.i) suggests a similar variation in SiO_2 and Al_2O_3 by virtue of the fact that they have a high correlation coefficient. The latter dendrogram (Figure 5.4.ii) indicates a clearer picture of the similarity between oxides. MgO, MnO, Na_2O, K_2O, and Al_2O_3 are all linked in a cluster with low distance coefficients which suggests a similar variation between them. SiO_2 is linked to this cluster at a low level (high distance coefficient) indicating some dissimilarity in the variation of this oxide with respect to the others. Fe_2O_3 and CaO are very dissimilar in their variation. The high distance coefficient at which SiO_2 and the other oxides are linked to Fe_2O_3 and CaO indicates marked dissimilarity in

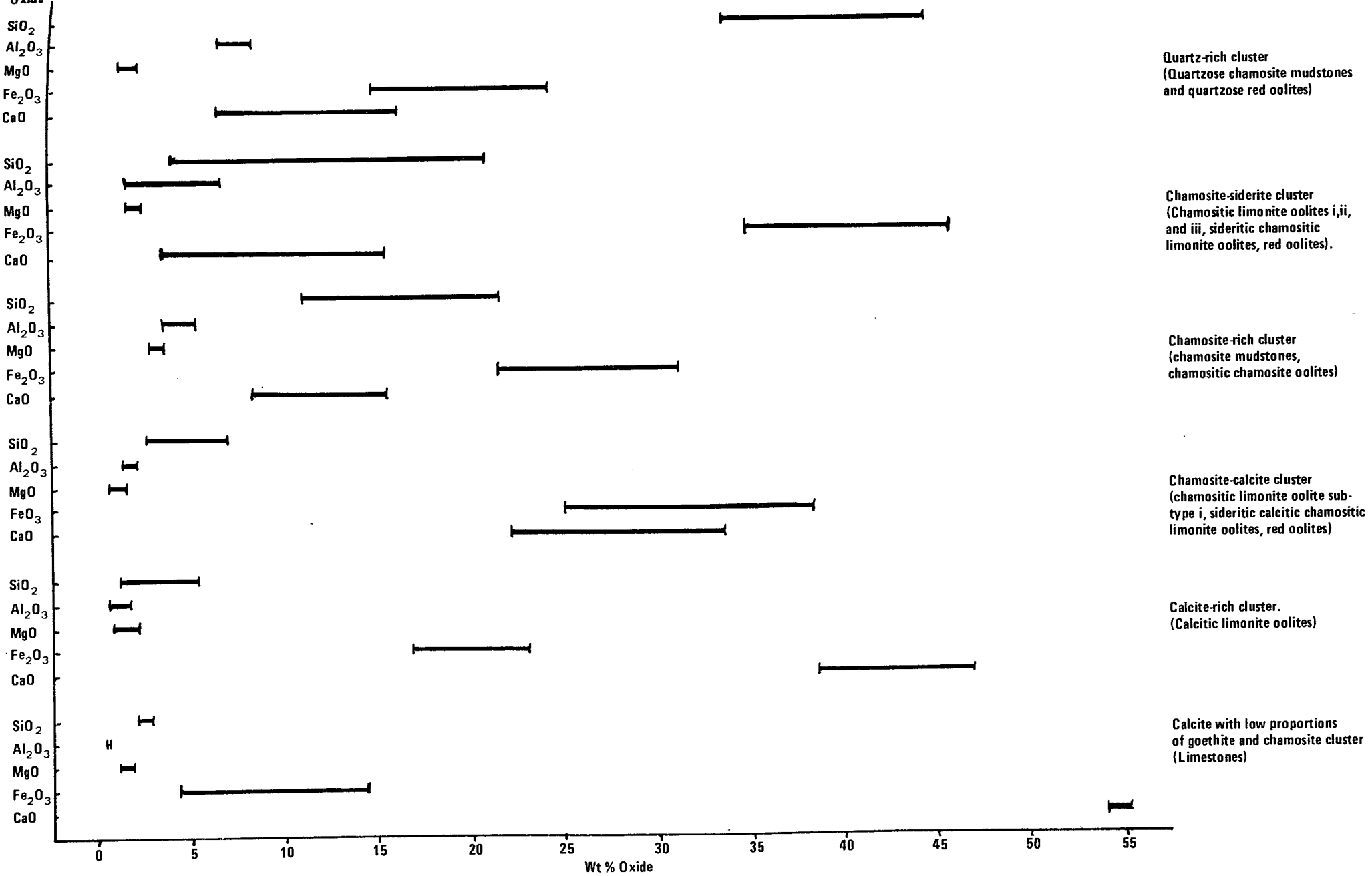

Fig 5.3 Chemical ranges represented by clusters

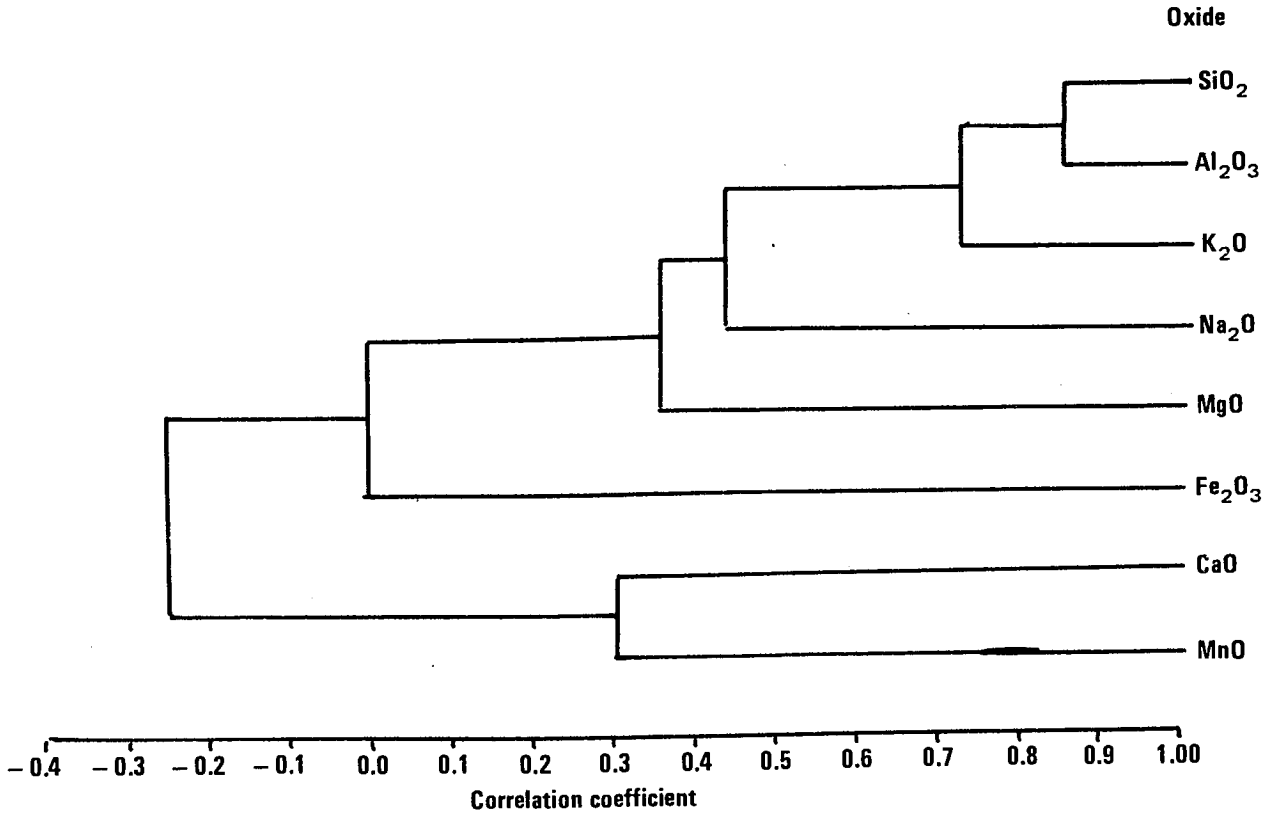

Fig 5.4.i R–mode variation between oxides. Frodingham

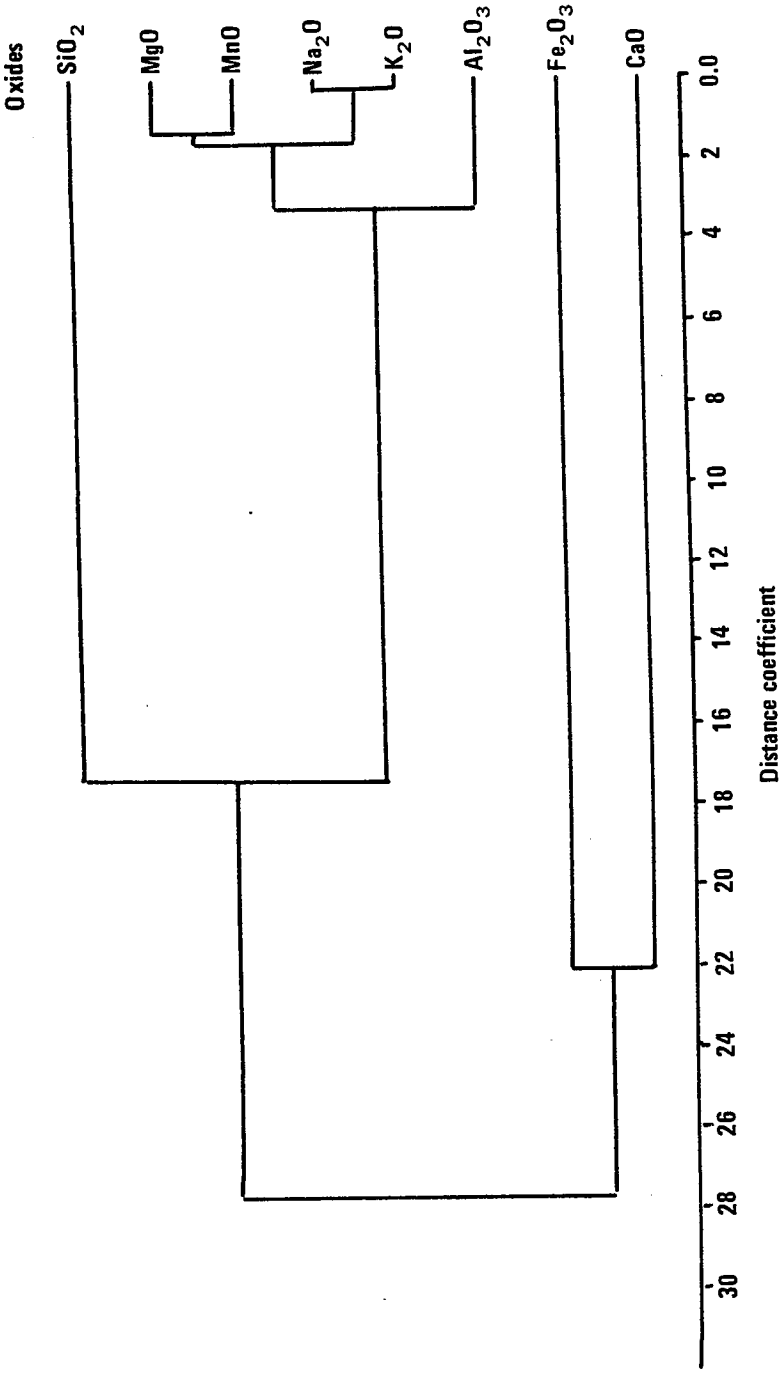

Fig 5.4ii R–mode variation between oxides. Frodingham

the variation between these two clusters. It is very interesting to compare this variation between oxides with what is observed when analyses are plotted as a function of depth (Figure 5.2): SiO_2, Al_2O_3, and MgO are parallel and antipathetic with respect to CaO. This is supported by the dissimilarity between these oxides. An antipathetic relationship between Fe_2O_3 and CaO was also observed and is also supported by the results of cluster analysis. The relationship between Fe_2O_3 and the other oxides was not entirely clear from Figure 5.2. The distance coefficient dendrogram rather suggests a variation similar to that of CaO i.e. antipathetic. The dissimilar variation between SiO_2 and MgO, MnO, Na_2O, K_2O, and Al_2O was not observable in Figure 5.2. This dissimilarity may well reflect the presence of SiO_2 as quartz in addition to chamosite in some samples.

5.5 GEOCHEMICAL VARIATION IN THE MARLSTONE ROCK-BED IRONSTONE

5.5.1 Core and Section Analyses

The analyses of samples of the Marlstone Rock-bed derived from the Tilton railway cutting exposure and the Nettleton core are plotted in Figure 5.5 as a function of depth. The variation in the chemical composition of the Marlstone is not as clear as that of the Frodingham Ironstone. A parallel variation between MgO and Al_2O_3 is again found. SiO_2, CaO, and Fe_2O_3 all exhibit a variation which approaches an antipathetic character.

The variation in composition exhibited by the Marlstone is

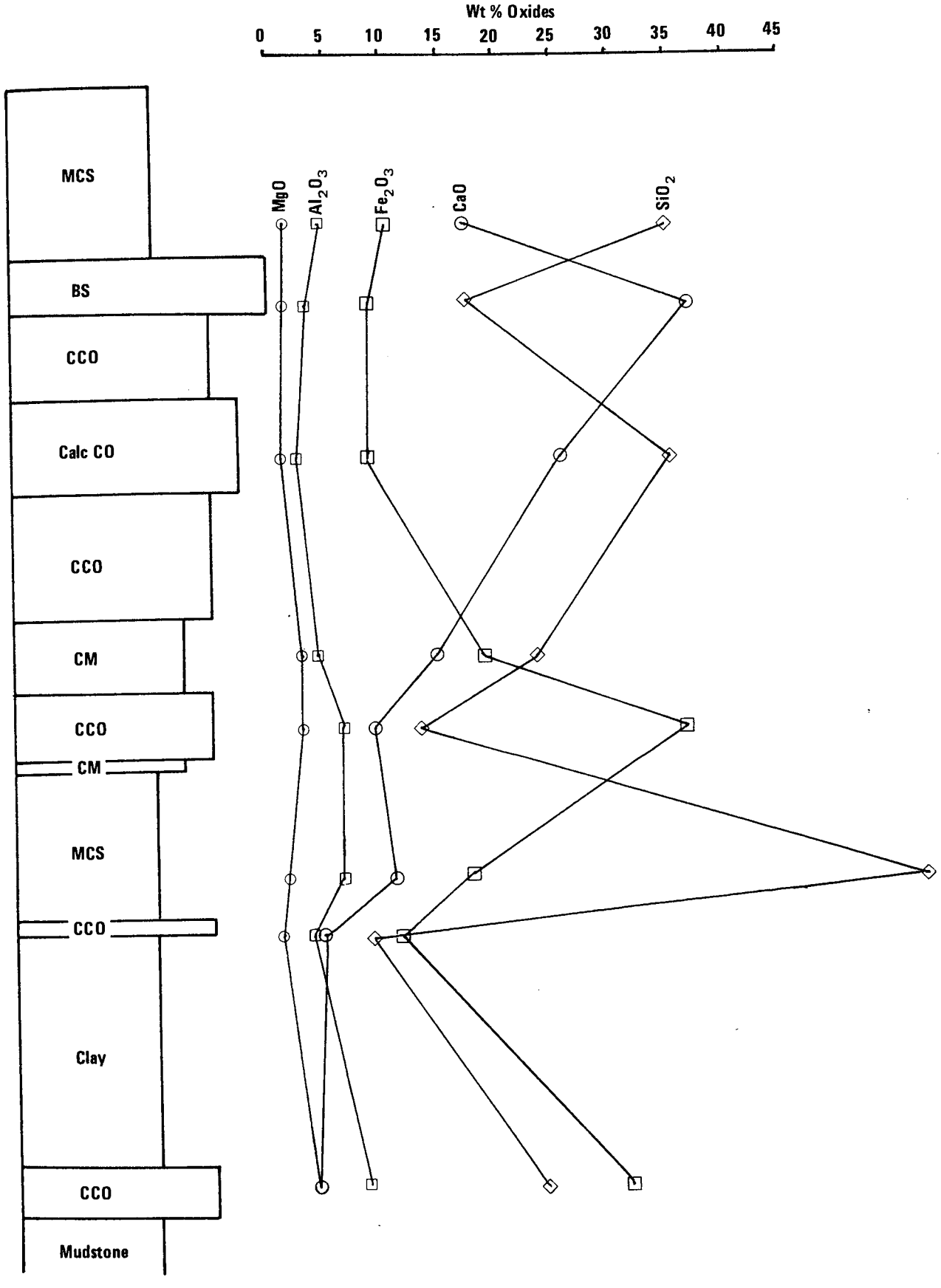

Fig 5.5a Geochemical variation in The Nettleton Core

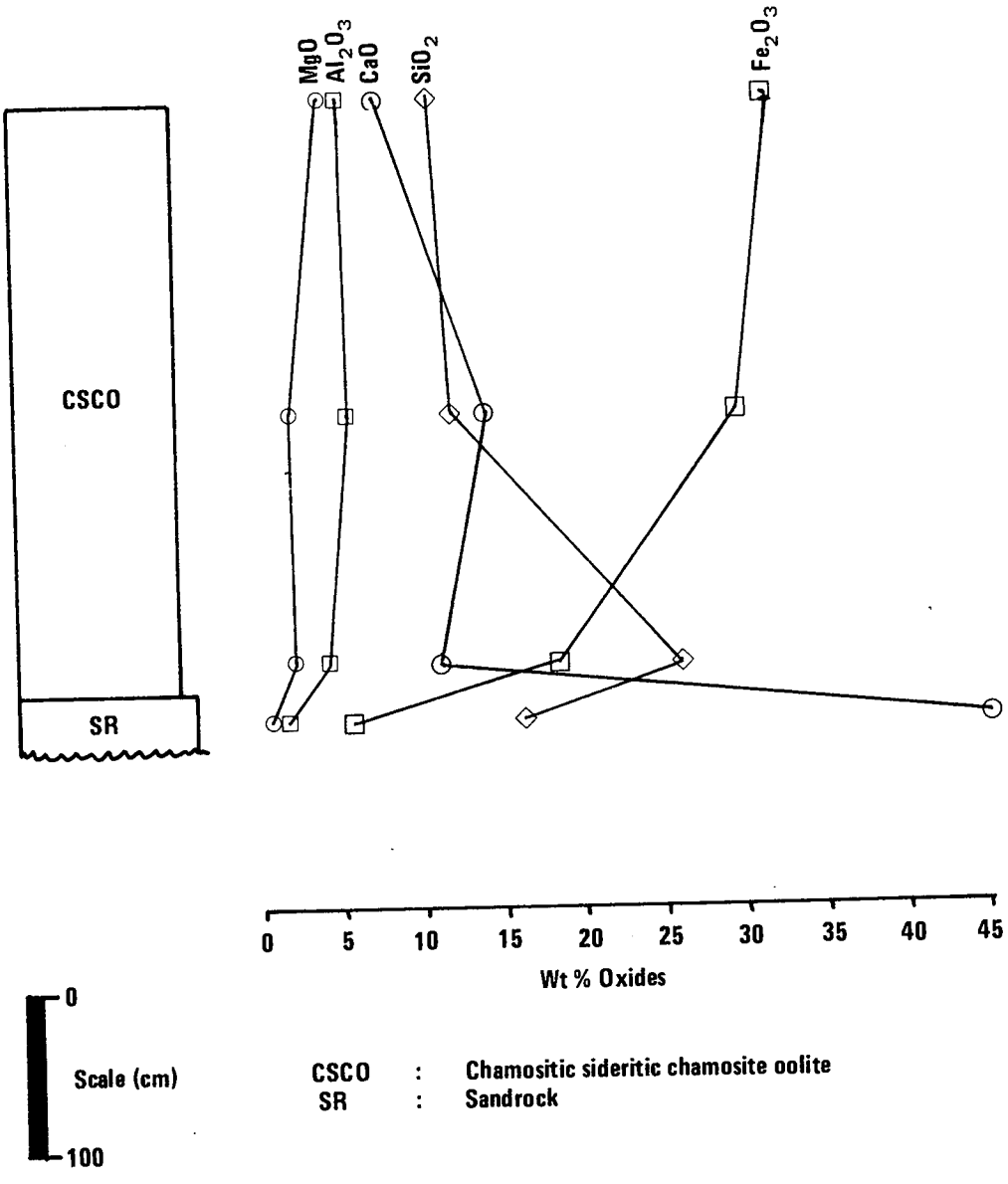

Fig 5.5b Geochemical variation in The Tilton Railway Cutting

apparently a result of its mineralogy and the relative abundance of these components. If the MgO and Al_2O_3 are assumed to represent the concentration of Mg and Al in chamosite then a parallel variation is easily explicable. The variation in SiO_2 results from the relative abundance of detrital quartz and chamosite. In the case of the Tilton analyses SiO_2 retains an initially constant proportion of the ironstone and is restricted to chamosite. At the base of the ironstone sequence, however, it increases to a much greater value which is due to the presence of quartz in this portion of the sequence. In the Nettleton core high SiO_2 values correspond to beds in which both chamosite and quartz are present and low values to beds in which only chamosite is present. The occurrence of micas in the Nettleton core add another source, albeit some what minor, of SiO_2. As in the case of SiO_2, CaO owes its variationto two major forms of occurrence; as calcite cement and as shell material. Petrographic evidence shows the former to be somewhat variable as a proportion of the rock as a whole. In the case of the Tilton Sandrock, for instance, it is much more abundant than the allochemical components which it cements, thus leading to a high CaO level in this sample. In contrast, the abundance of allochems in the Nettleton sandrock facies lead to a low proportion of CaO in these samples. In lithologies such as biosparites where chamosite and quartz are reduced in abundance CaO is very high. Fe_2O_3 is distributed between chamosite and siderite as Fe^{2+} and Fe^{3+}. The variation in the abundance of these minerals thus controls the level of Fe_2O_3. Where all other components are reduced in importance such as in chamositic chamosite oolites and siderite mudstones Fe_2O_3 is the major chemical constituent of the rock.

5.5.2 Cluster Analysis

It is difficult to differentiate clearly between different lithological types of Marlstone by a qualitative approach. Cluster analysis allows a clear distinction to be made by geochemical parameters.

Q-mode dendrograms (Figure 5.6) which cluster samples according to both correlation and distance coefficients show well defined clustering of ironstone samples and sandrock facies samples. The relationship between samples is shown up well by the distance coefficient dendrogram (Figure 5.6.ii). Samples N7, T1, T2, B3, and B5 are all siderite-rich chamositic chamosite oolites. They therefore cluster together at low coefficients. Similarly, samples N8, T3, N9, N11 all cluster together. These are sandrock facies specimens characterised by the presence of quartz in varying proportions. N10 and T4 are sandrock facies samples which have a high calcite content. This is evidently responsible for their separation from the other sandrock facies material. Four samples are somewhat dissimilar to those which form these three clusters. N4 is a siderite mudstone from which quartz is absent and contains chamosite and goethite ooids. Its sideritic nature leads to its linkage with the chamositic chamosite oolite cluster. Sample N5 is composed dominantly of pyrite and contains some chamositic chamosite oolite material and siderite. Thus, it is clustered with the chamosite-rich cluster but at a distance coefficient reflecting its dissimilarity with these samples. E1 does not contain quartz but is calcite-rich. This dissimilarity results in its clustering, at a high distance coefficient, with the calcite-rich but quartz-bearing samples T4 and N10. Since the sandrock facies cluster represents samples containing chamosite and siderite they are less dissimilar to the chamositic chamosite oolite cluster than the calcite-rich cluster. Thus these two clusters are

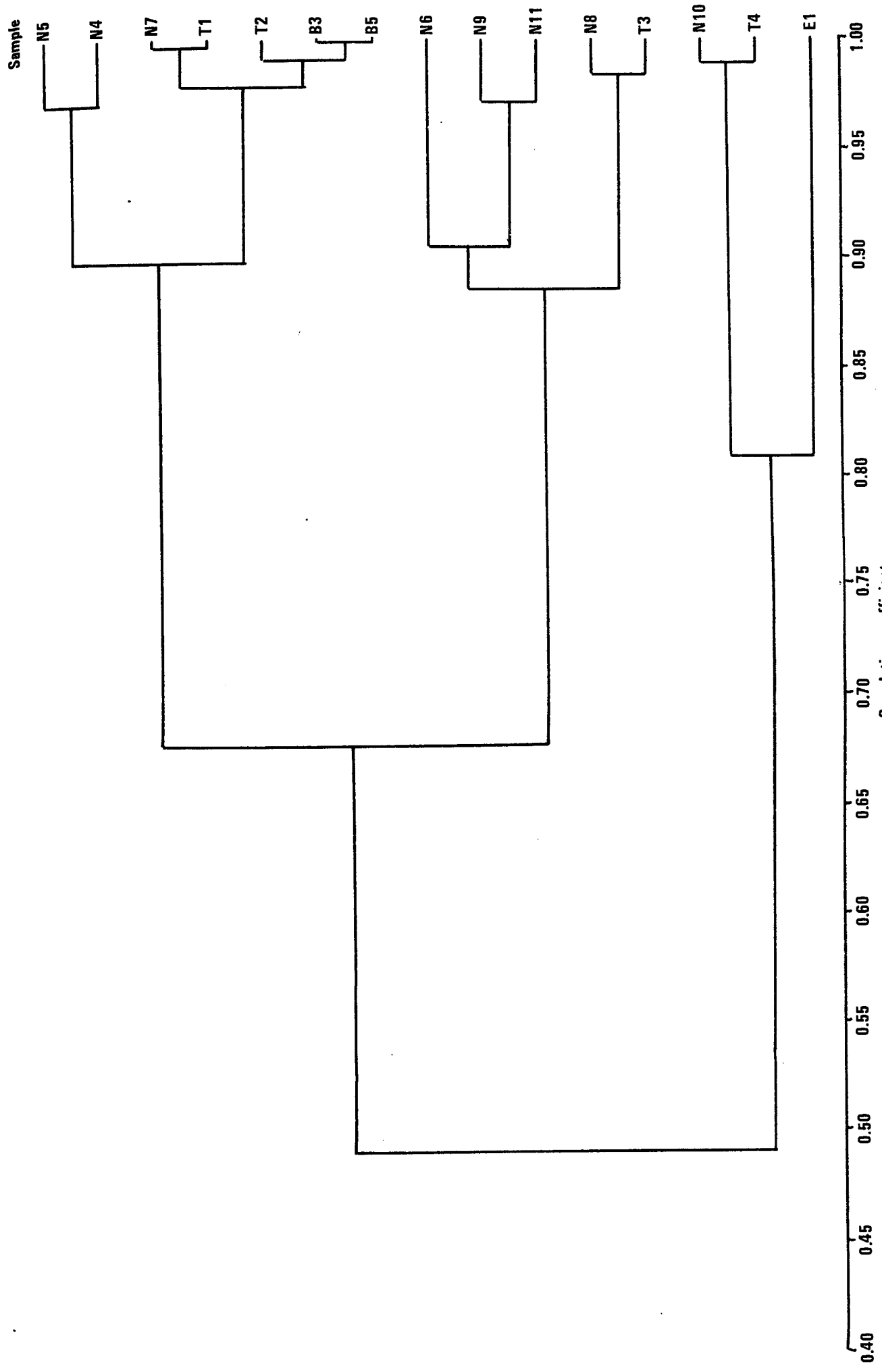

Fig 5.6 i Q–mode variation between samples Marlstone Rock-bed

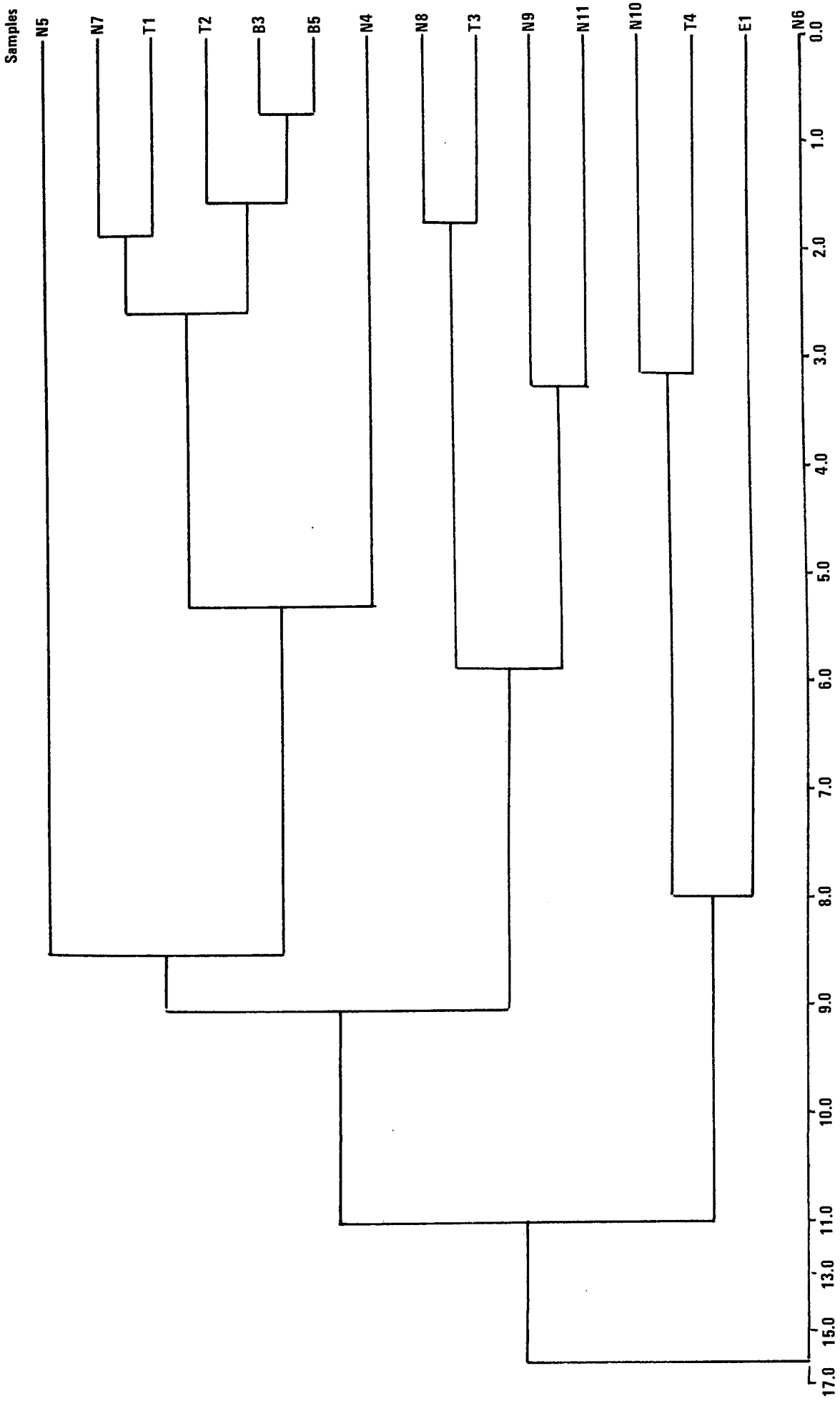

Fig 5.6 ii Q–mode variation between samples. Marlstone Rock-bed

linked and form a cluster which is linked with the calcite-rich cluster. The one sample which is not involved in any of these clusters is N6. Since it is linked at a very high distance coefficient to the other samples it is extremely dissimilar. This may reflect its high mica content in comparision to other sandrock samples.

Since cluster analysis of samples was performed on analytical data and the results can be explained on a mineralogical basis it is concluded that different lithological types may be characterised by a range of analyses. This is illustrated in Figure 5.7. It should be noted that although the chamositic chamosite oolite and sandrock facies are clearly separated, the calcitic chamosite oolite facies is most similar to calcite-rich sandrock facies specimens. In order to further resolve this and obtain some idea of the chemical ranges exhibited by this facies more analyses would be required.

The similarity and dissimilarity between the variation in oxides is shown by the correlation and distance coefficient dendrograms in Figure 5.8. High correlation coefficients (Figure 5.8.i) suggest a similar variation between SiO_2, K_2O, and Na_2O and between Fe_2O_3, MgO, and Al_2O_3. The variation in CaO is dissimilar to both of these clusters. Bearing in mind that micas and feldspars occur in sandrock specimens the first of these clusters might be attributed to these minerals. The second cluster may well be attributed to the widespread presence of chamosite. A clear picture is obtained from an examination of the distance coefficient dendrogram (Figure 5.8.ii). SiO_2, CaO, and Fe_2O_3 are clustered at high distance coefficients indicative of a dissimilar variation. This is supported by the variation in these oxides when considered as a function of depth (Figure 5.5). MnO, Na_2O, and K_2O have very low distance coefficients which suggest a

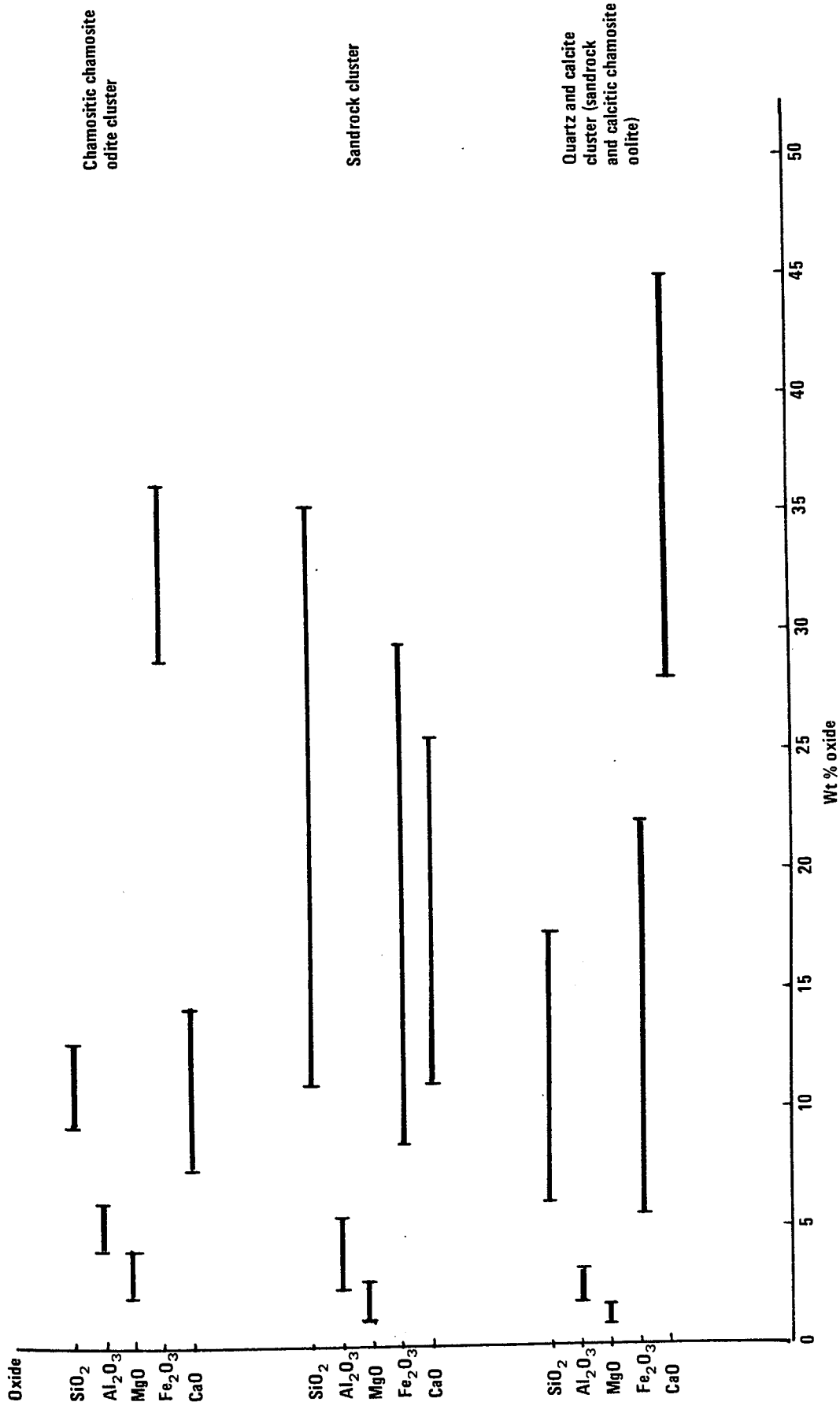

Fig 5.7 Geochemical variation of clusters

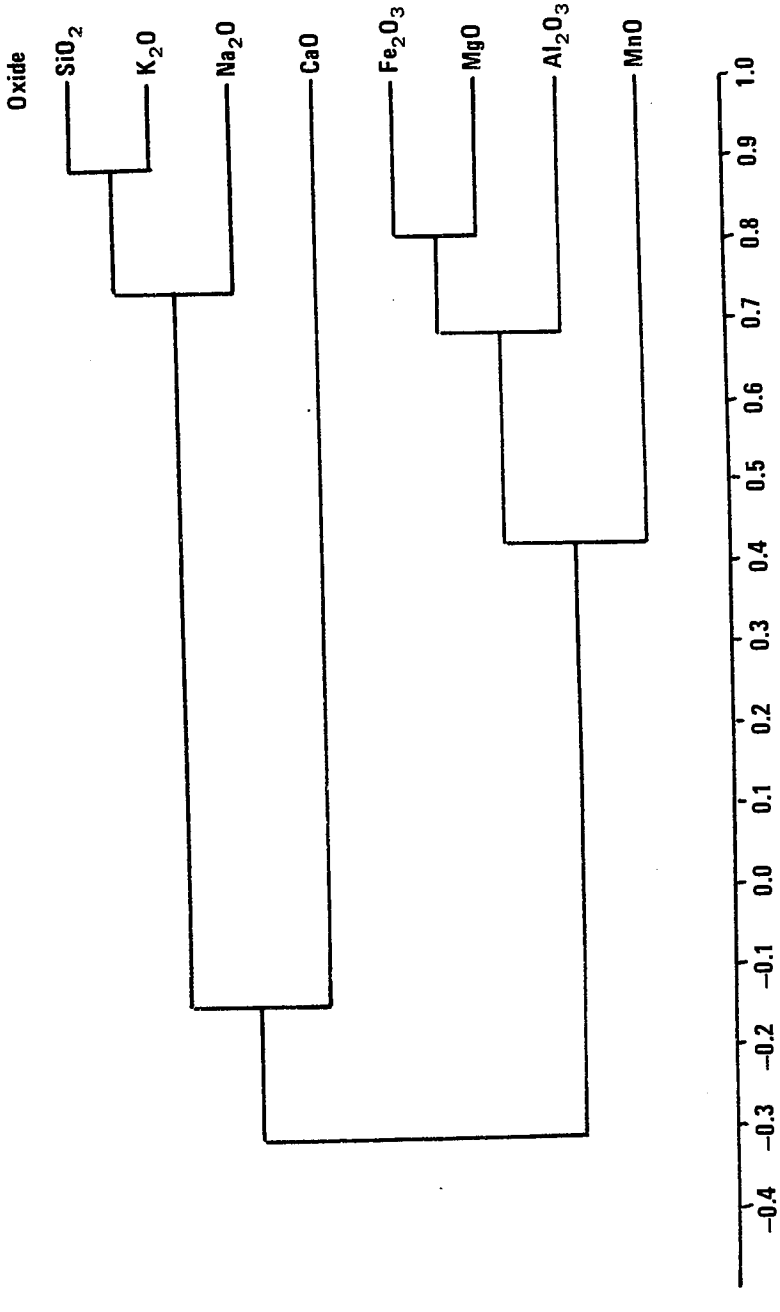

Fig 5.8 i R–mode variation between oxides. Marlstone Rock-bed

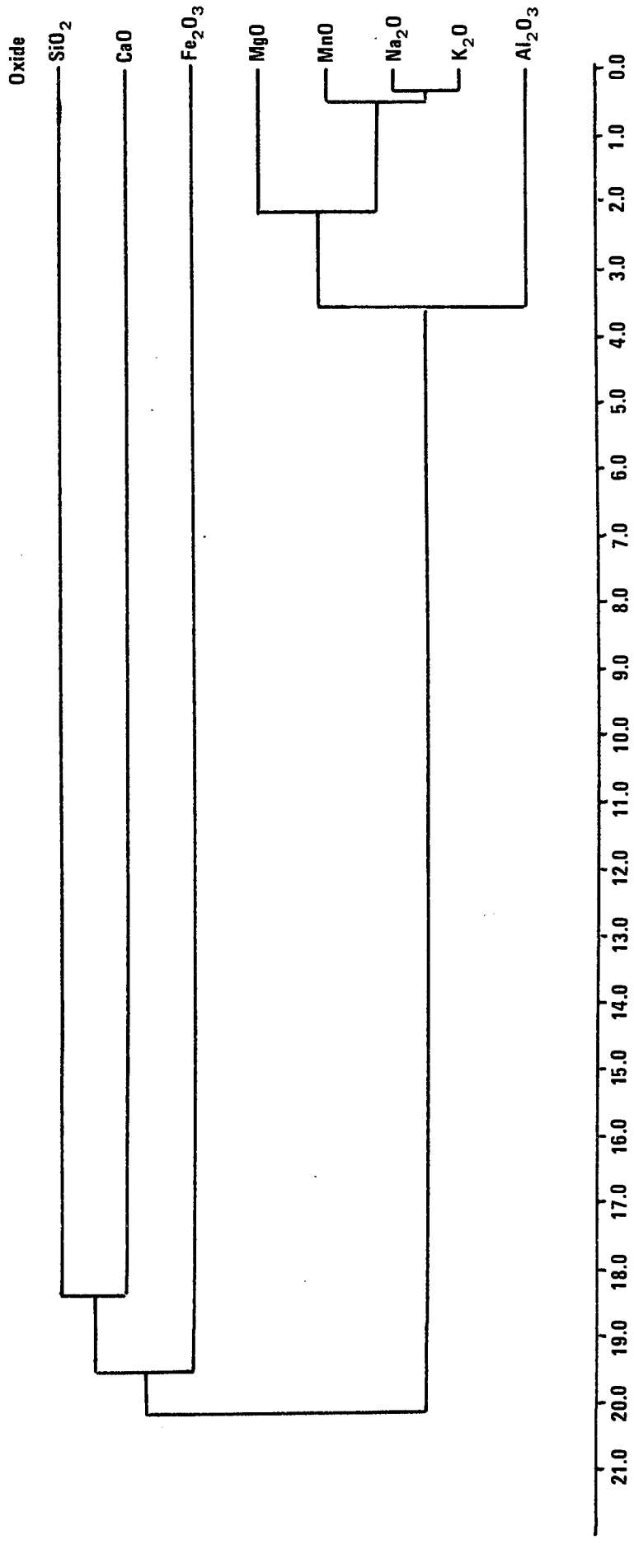

Fig 5.8 ii R–mode variation between oxides. Marlstone Rock-bed

similar variation. This would be expected, bearing in mind the presence of micas and feldspars. MgO and Al_2O_3, although being related to each other and to the MnO, Na_2O, and K_2O cluster exhibit a degree of clustering which suggests that their variation is not entirely similar. Again this is attributable to their presence in micas, feldspars and also in chamosite. The variation between these oxides and SiO_2, CaO, and Fe_2O_3 is very dissimilar, a fact bourne out by their mutual variation relative to depth (Figure 5.5).

5.6 GEOCHEMICAL VARIATION IN THE CLEVELAND IRONSTONE

5.6.1 Section Analysis

The variation in the geochemical composition of the Cleveland Ironstone at Brackenberry Wyke is plotted in Figure 5.9. Analyses of the shales have been carried out by Catt et al. (1971) and these are also plotted.

The alternating ironstone and shale sequence is reflected clearly in the geochemical variation: The ironstones contain relatively low proportions of SiO_2, Al_2O_3, and MgO, and relatively high proportions of Fe_2O_3 and CaO. In contrast the shales contain relatively high proportions of SiO_2 and Al_2O_3, and low proportions of Fe_2O_3, CaO, and MgO. This results in the antipathetic variation which is observed and corresponds to the alternation of shale and ironstone.

The variation within the ironstones is not entirely clear. The Raisdale Seam comprises a siderite mudstone which passes down into a calcitic chamosite oolite. This is reflected in the parallel variation between SiO_2, Al_2O_3, and MgO which increase from the top of the bed to

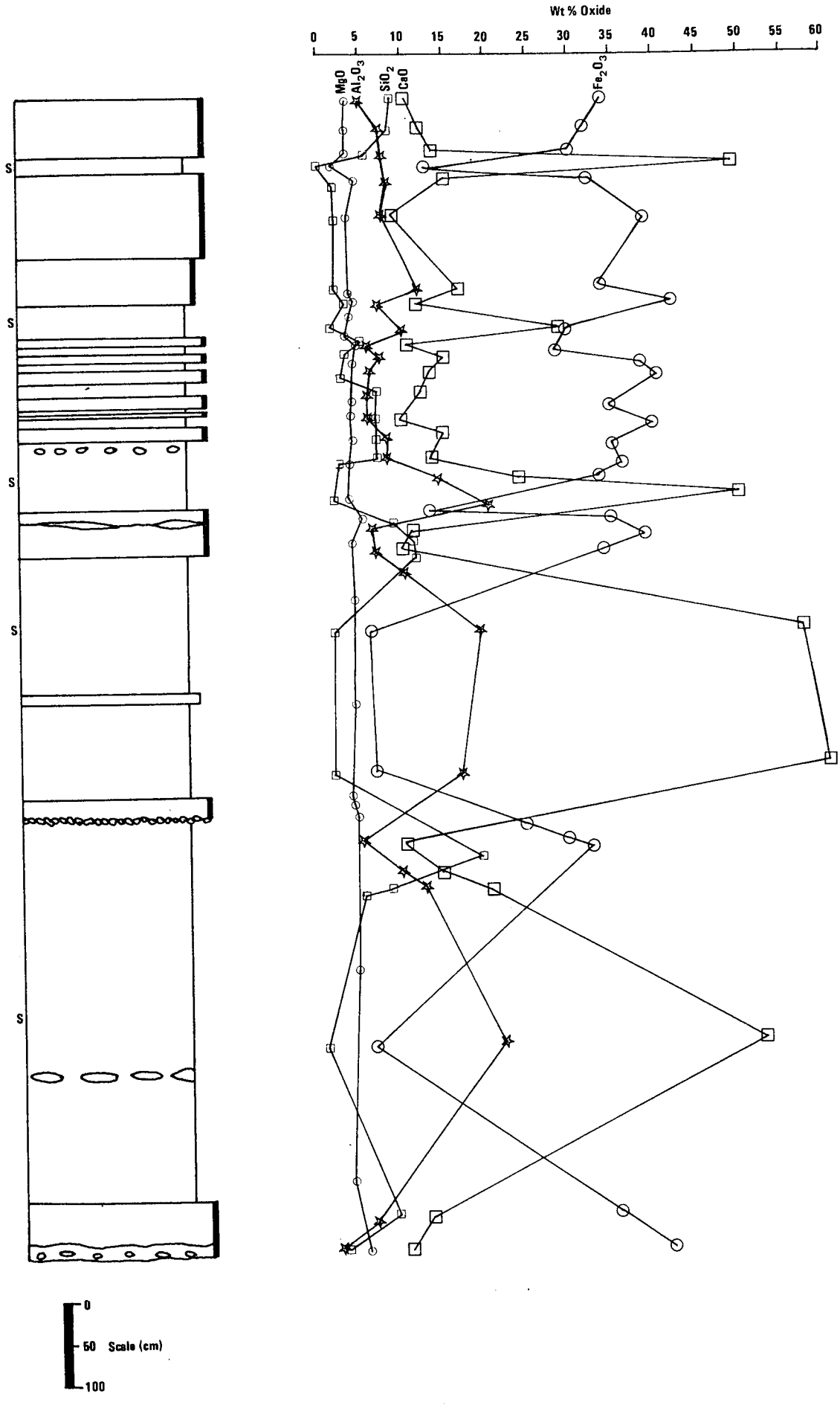

Fig 5.9 Geochemical variation in The Cleveland Ironstone Formation at Brackenberry Wyke

the base. The change in CaO is opposite to this and may reflect the increasing abundance of chamosite over calcite. Similar variations between these oxides occur in the Main Seam, the Two Foot Seam, and the Avicula Seam. The nature of the variation of MgO and CaO is a little different in some places within these seams as they exhibit an opposite trend to that expected on the basis of their trend in the Raisdale Seam. The variation in Fe_2O_3 is due to the relative abundance of siderite and chamosite in any one sample. No clear, repetitive, variation is observed.

5.6.2 Cluster Analysis

There is some suggestion that the geochemical variation within ironstones is a function of the relative abundance of different minerals. This should be reflected in the clustering of samples. In order to obtain a clear picture of the nature of the geochemical variation cluster analyses of oxides must be examined.

Correlation and distance coefficient dendrograms in which samples are clustered are presented in Figure 5.10. The dendrogram using correlation coefficients (Figure 5.10.i) does not show any significant arrangement of samples at the first-order clustering level. There is a tendency for lithologically similar samples to be paired off. A similar situation occurs in the distance coefficient dendrogram (Figure 5.10.ii) but there is a much more clearly defined clustering between samples. Several groups are apparent:

Samples TB1, C3, C7 and C23 are all siderite mudstones. A linkage between this cluster and samples C2, W16, and C6, which are siderite mudstones containing small amounts of chamosite oolite occurs at a low coefficient.

The chamositic chamosite oolites, TB2, K4, and TB3 are clustered

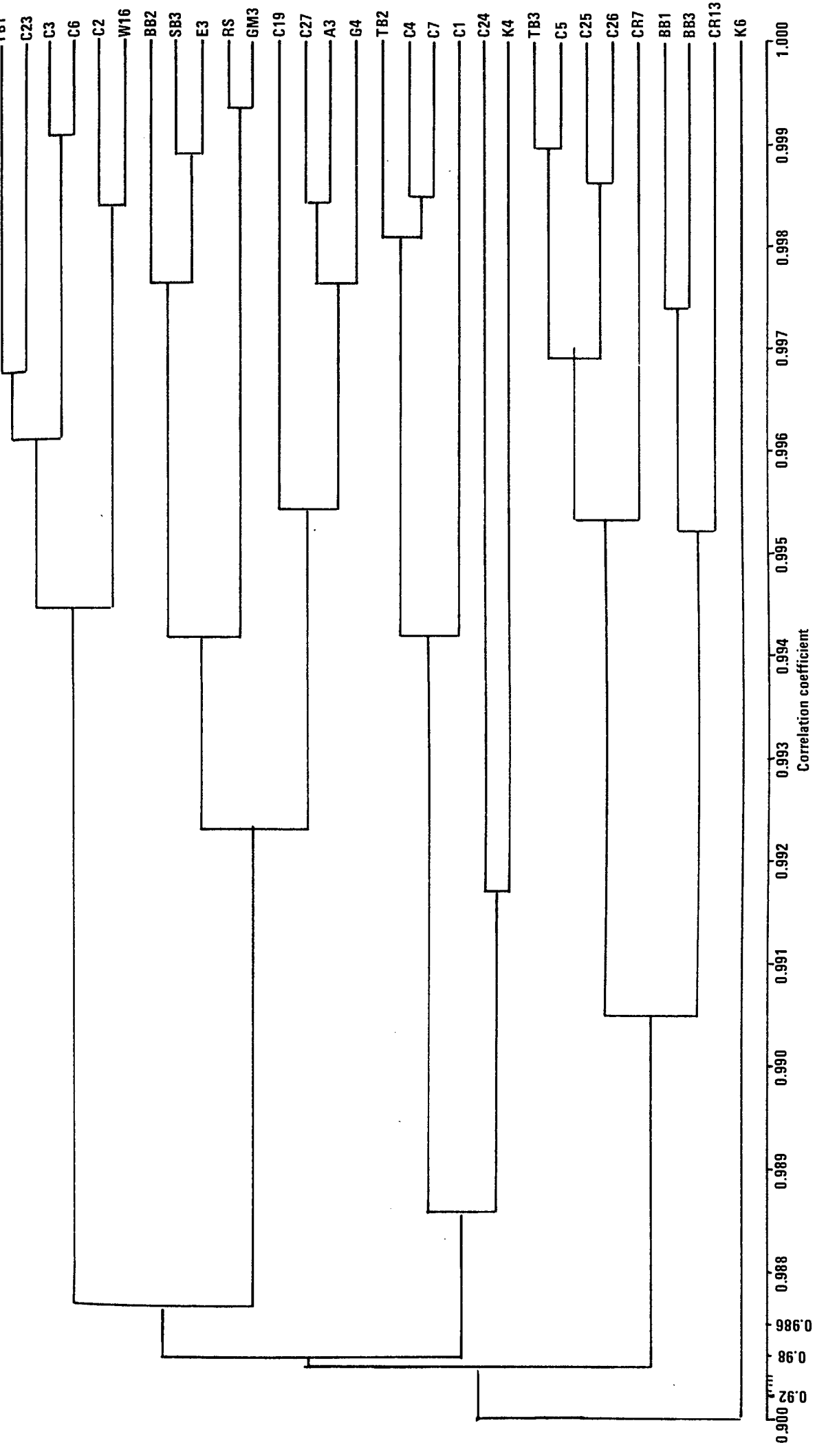

Fig 5.10 i Q–mode variation between samples. Cleveland

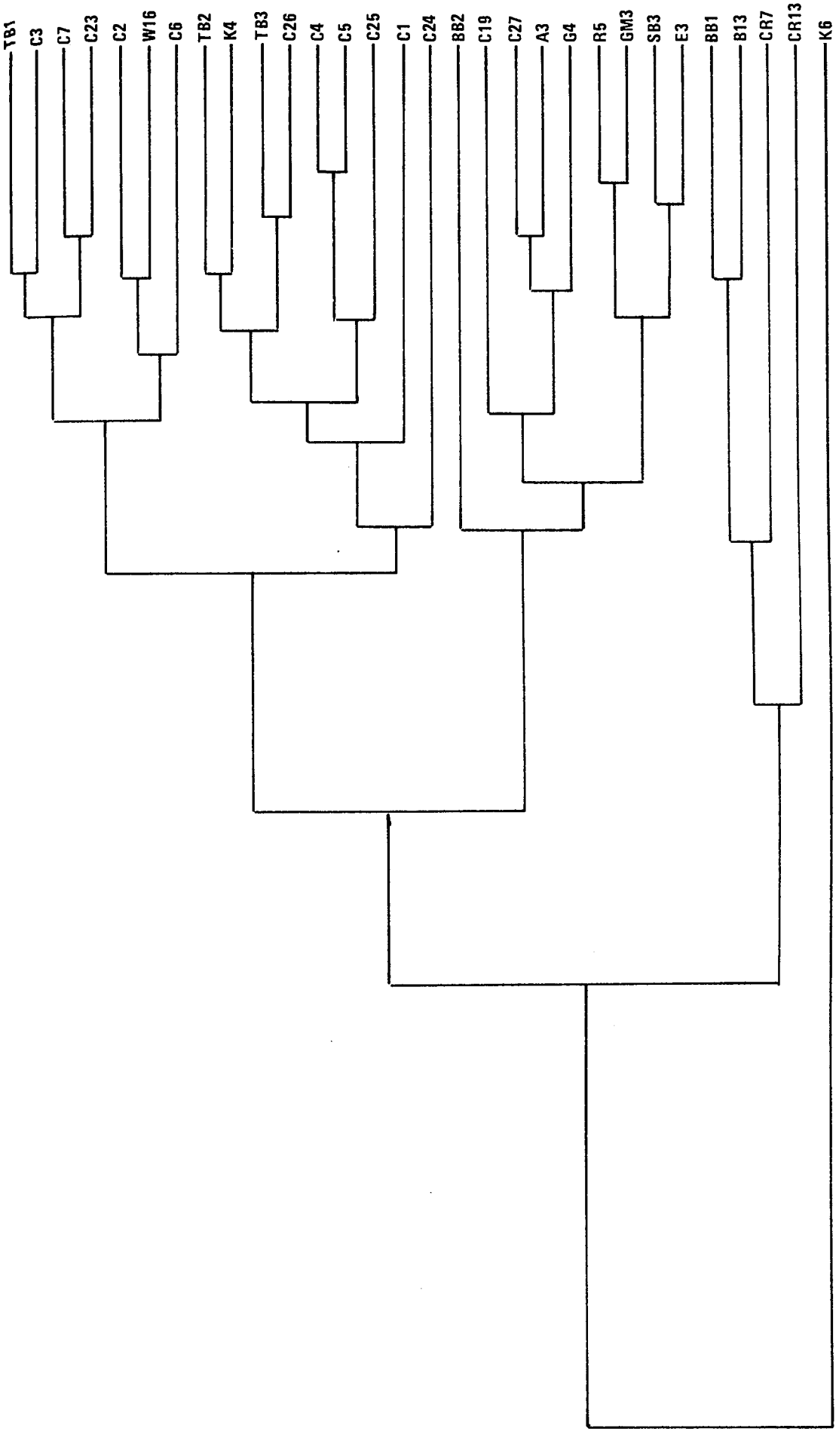

Fig 5.10 ii Q–mode variation between samples. Cleveland

with C26. The inclusion of C26 within this group is strange as it appeared to be a siderite mudstone devoid of any chamosite. Reference to Table 5.2, however shows a close similarity in the compositions of all four specimens. The presence of siderite mudstone filled burrows in TB2, K4, and TB3 results in their clustering with siderite mudstones.

C4, C5, and C25 are all siderite mudstones. There is a high degree of similarity between these samples and the preceding chamositic chamosite oolite cluster.

Sample C1 is linked with a good degree of similarity to the two previous clusters. This is presumably a result of the fact that it consisted of a chamositic chamosite oolite containing large, irregular, patches of replacive siderite mudstone.

It is diffcult to understand the very similar nature of samples BB2, C19, C27, A3, G4, R5, GM3, SB3, and E3 since they represent four different lithological types which would be expected to cluster with similar lithologies elsewhere. The answer to this problem is to be found in Table 5.2. In general their analyses show slightly higher Fe_2O_3 and slightly lower SiO_2 levels than are found in other samples.

The cluster represented by BB1, BB3, CR7, and CR13 represents the sideritic chamosite oolites in which variable proportions of chamosite occur. This leads to some dissimilarlity between the members of the cluster.

The abundance of calcite in sample K6 and the more or less complete absence of siderite results in the dissimilar nature of this sample with respect to the others.

From interpretation of the clusters it is clear that samples which did not exhibit replacement by microcrystalline siderite mudstone and those which did form separate clusters. In the former group individual

clusters can be explained mineralogically, therefore indicating that their mineral assemblages represent different geochemical ranges. In the latter group a mineralogical explanation for clusters can also be invoked although clusters contain samples of different lithologies and more than one siderite mudstone cluster occurs. All the samples in this group exhibit replacement by siderite mudstone. It is possible, therefore that these clusters represent different stages in the formation of siderite mudstone from other lithologies. Figure 5.11 illustrates the compositional ranges of the clusters. Those clusters representing unreplaced lithologies are placed at the top of the diagram, those representing partial replacement in the middle, and those which have been completely replaced at the bottom. Although the chemical variation between the chamositic chamosite oolites, sideritic chamosite oolites, and calcitic chamosite oolites and between the various siderite mudstone clusters is not great there is a noticable difference between the unreplaced and replaced groups. This is a lower SiO_2 and Al_2O_3 level in the siderite mudstones than in the unreplaced lithologies. Since chamosite is the mineral replaced by siderite mudstone such a difference would be expected. Fe_2O_3 remains similar in both groups, as would also be expected

The dendrograms from which the nature of the variation between the component oxides may be derived are shown in Figure 5.12. The correlation coefficient dendrogram (Figure 5.12.i) suggests a similar variation between SiO_2 and Al_2O_3, Na_2O and K_2O, and Fe_2O_3 and MgO. In contrast, the distance coefficient dendrogram (Figure 5.12.ii) indicates that there is a similar variation between CaO, MgO, and Al_2O_3, and between MnO, Na_2O, and K_2O, and that the variation between these clusters is somewhat similar. SiO_2, however, does not show a similar variation to

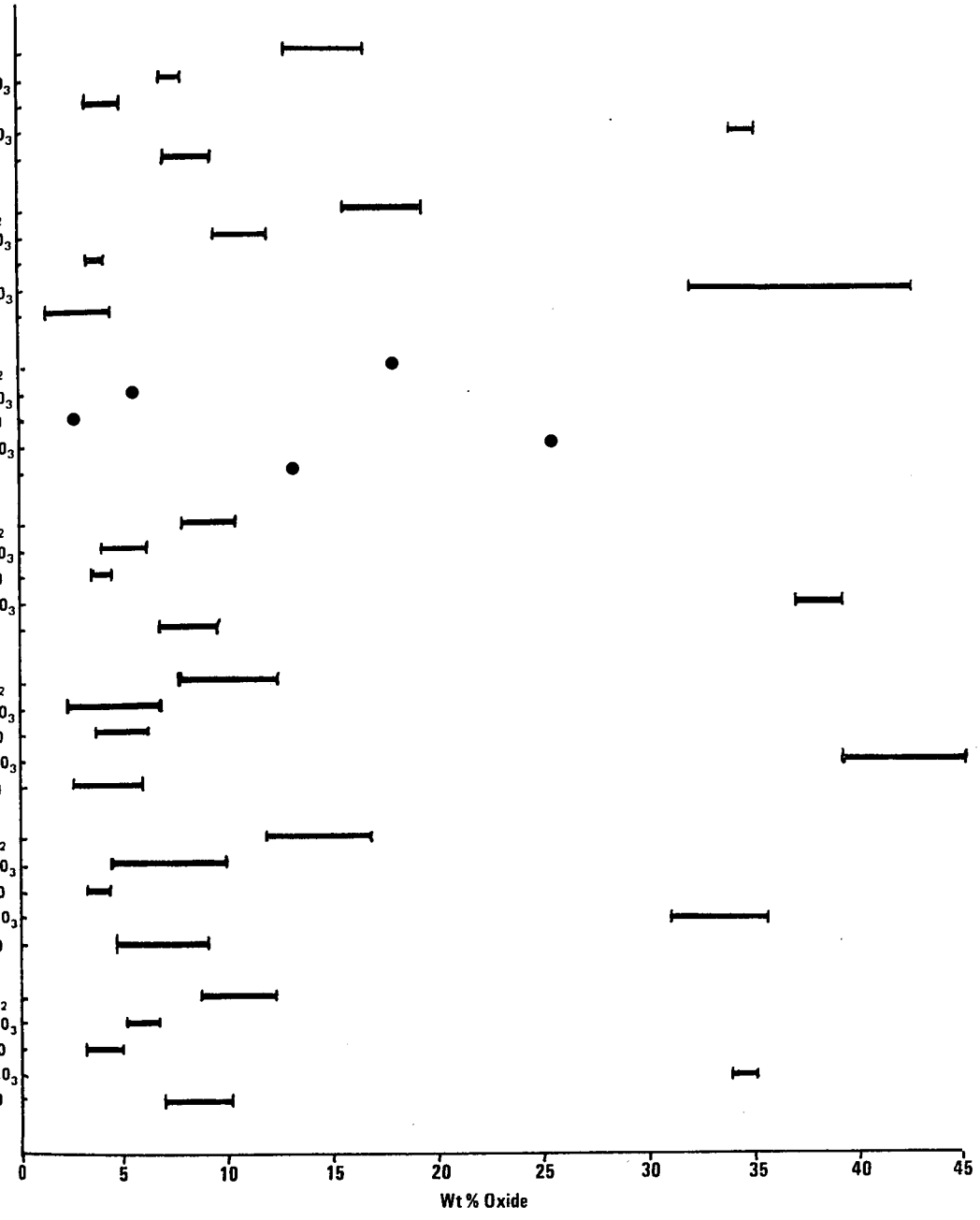

Cluster

Chamositic chamosite oolites (TB2, K4, TB3 ; C26 included as member of this cluster).

Sideritic chamosite oolites (BB1, BB3, CR7,CR13)

Calcitic chamosite oolite (K6)

Siderite mudstones containing chamosite oolite (C2, W16, C6)

Siderite mudstones containing chamositic chamosite oolite. Chamosite oolite and sideritic chamosite oolite (BB2, C19, C27, A3, G4 R5, GM3, SB3, E3)

Siderite mudstone with a little chamosite oolite (C4, C5, C25, C1, C24)

Siderite mudstones (T1, C3, C7, C23)

Fig 5.11

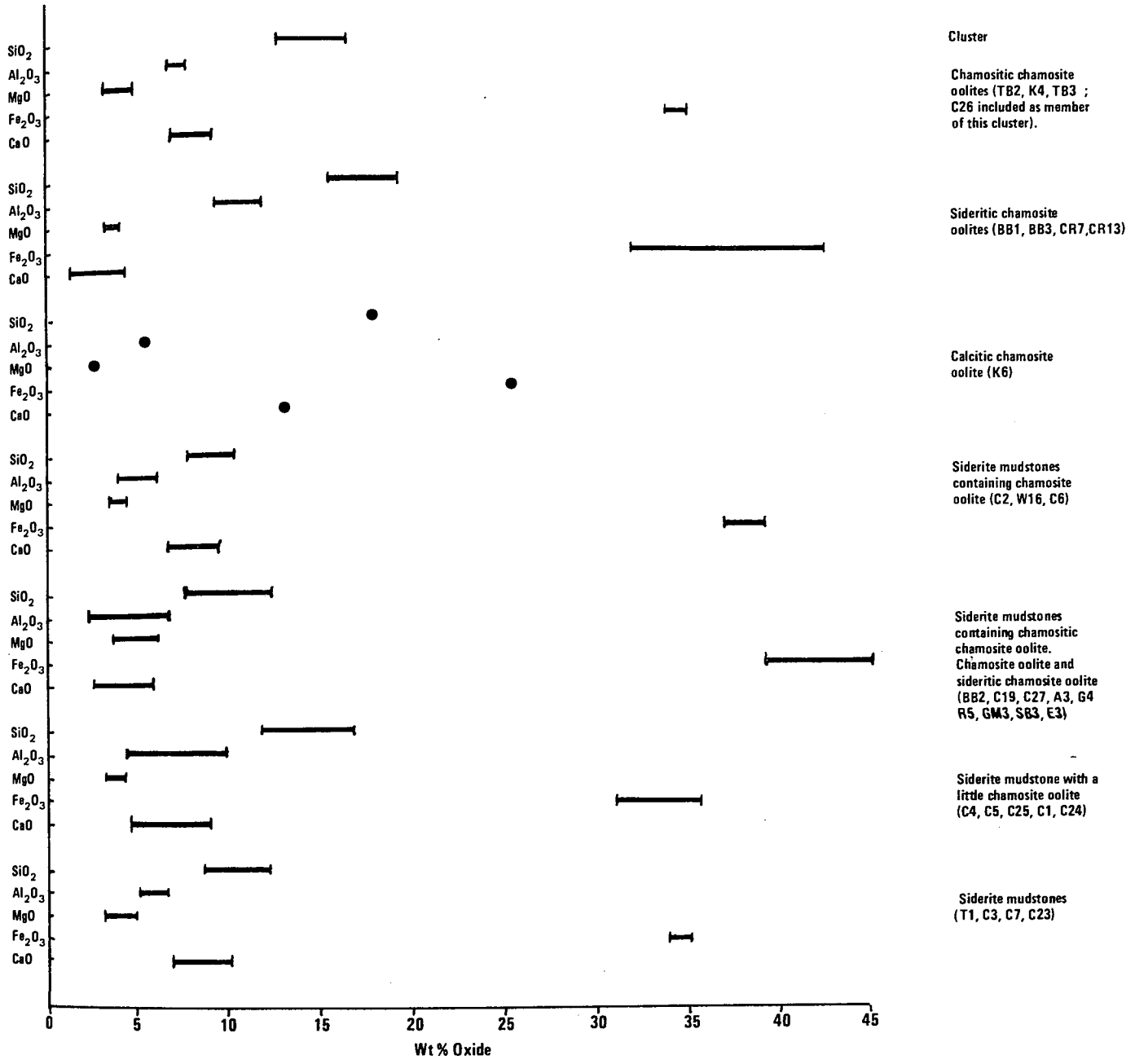
Cluster
SiO2
Al2O3
MgO
Fe2O3
CaO
Chamositic chamosite oolites (TB2, K4, TB3 ; C26 included as member of this cluster).
Sideritic chamosite oolites (BB1, BB3, CR7,CR13)
Calcitic chamosite oolite (K6)
Siderite mudstones containing chamosite oolite (C2, W16, C6)
Siderite mudstones containing chamositic chamosite oolite. Chamosite oolite and sideritic chamosite oolite (BB2, C19, C27, A3, G4 R5, GM3, SB3, E3)
Siderite mudstone with a little chamosite oolite (C4, C5, C25, C1, C24)
Siderite mudstones (T1, C3, C7, C23)
0
5
10
15
20
25
30
35
40
45
Wt % Oxide

Fig 5.11

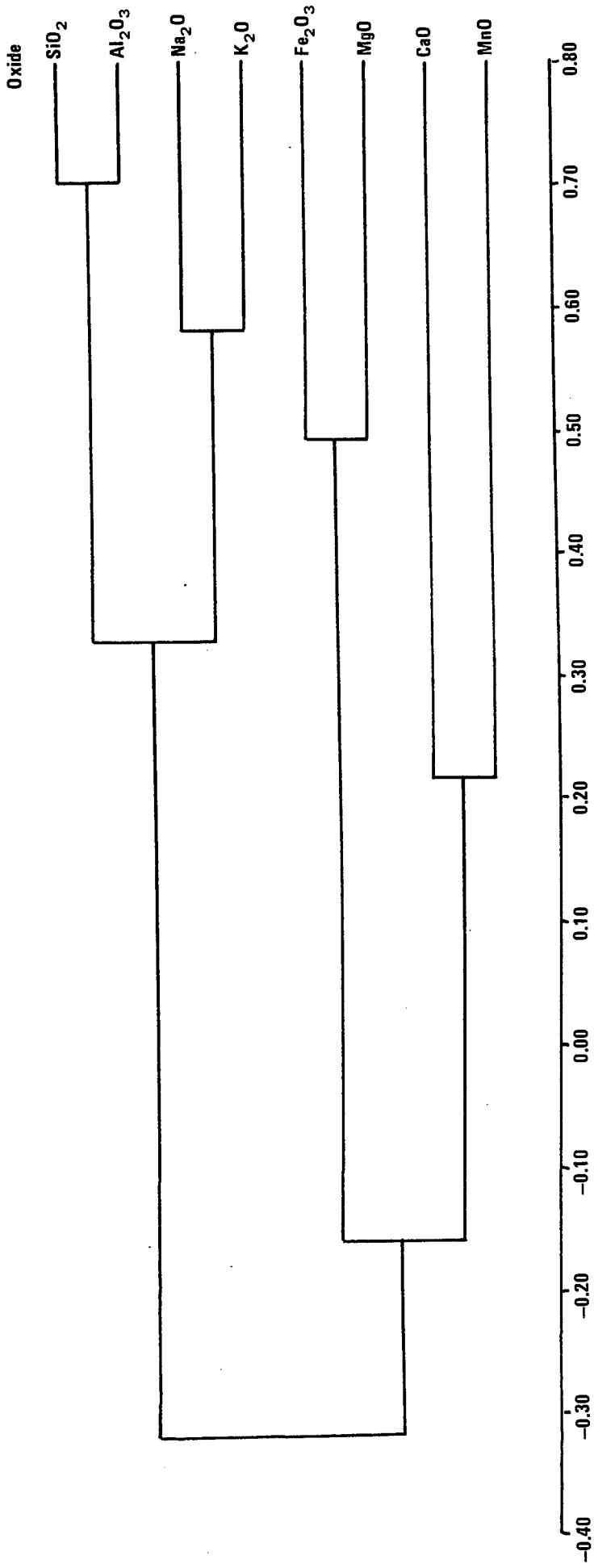

Fig 5.12 i R–mode variation between oxides. Cleveland

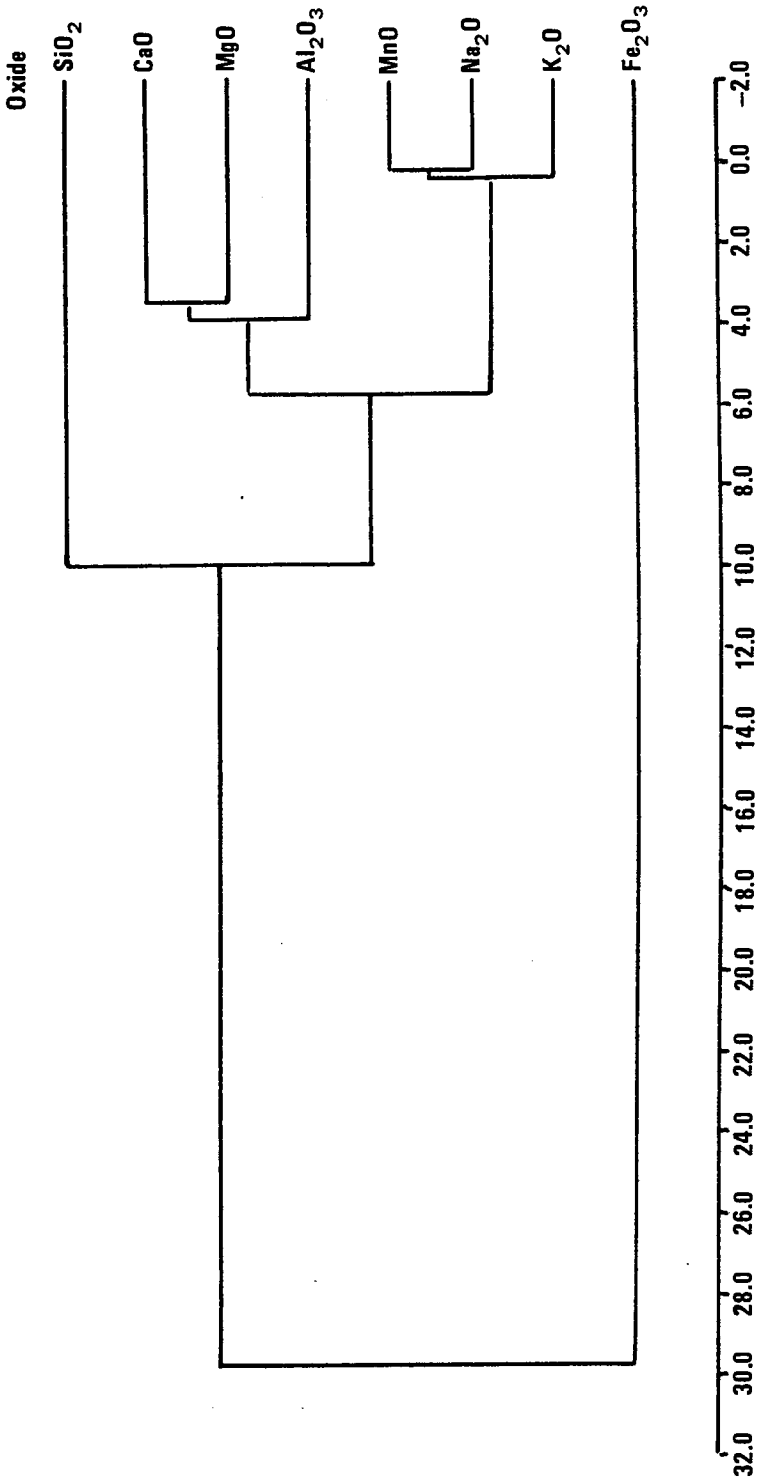

Fig 5.12 ii R–mode variation between oxides. Cleveland

these and Fe_2O_3 has an entirely dissimilar variation. In the case of the Marlstone MgO, MnO, Na_2O, K_2O, and Al_2O_3 also showed a similar variation which was attributed to the presence of micas and feldspars. The presence of kaolinite and lithoclasts of igneous material in the Cleveland Ironstone may, therefore, be the cause of the similar variation between these oxides. SiO_2 is present dominantly as chamosite which also contains Al_2O_3 and MgO and as a result shows a slightly similar variation to these oxides. Fe_2O_3 is present mainly as siderite and as subordinate chamosite which leads to a very dissimilar variation with respect to the other oxides. It is interesting to note the absence of a dissimilar variation between Fe_2O_3 and CaO reflected as a single cluster. This evidently results from the reduced importance of calcite as a cement mineral in the Cleveland Ironstone.

5.7 GEOCHEMICAL VARIATION BETWEEN LIASSIC IRONSTONES

The geochemical variation within individual ironstones has been discussed above. The Frodingham Ironstone and Marlstone Rock-bed ironstones appear to be similar whereas the Cleveland Ironstone is slightly different due to the abundance of siderite mudstone. It remains to assess the precise differences and similarities between the fields.

5.7.1 Sample Variation

The easiest way to obtain an overall view of any variation in the geochemistry of samples from the three ironstones is to plot their analyses on a triangular diagram (Figure 5.13). The apices of the diagram are chosen to be CaO, Fe_2O_3, and SiO_2, Al_2O_3, MgO, MnO, Na_2O,

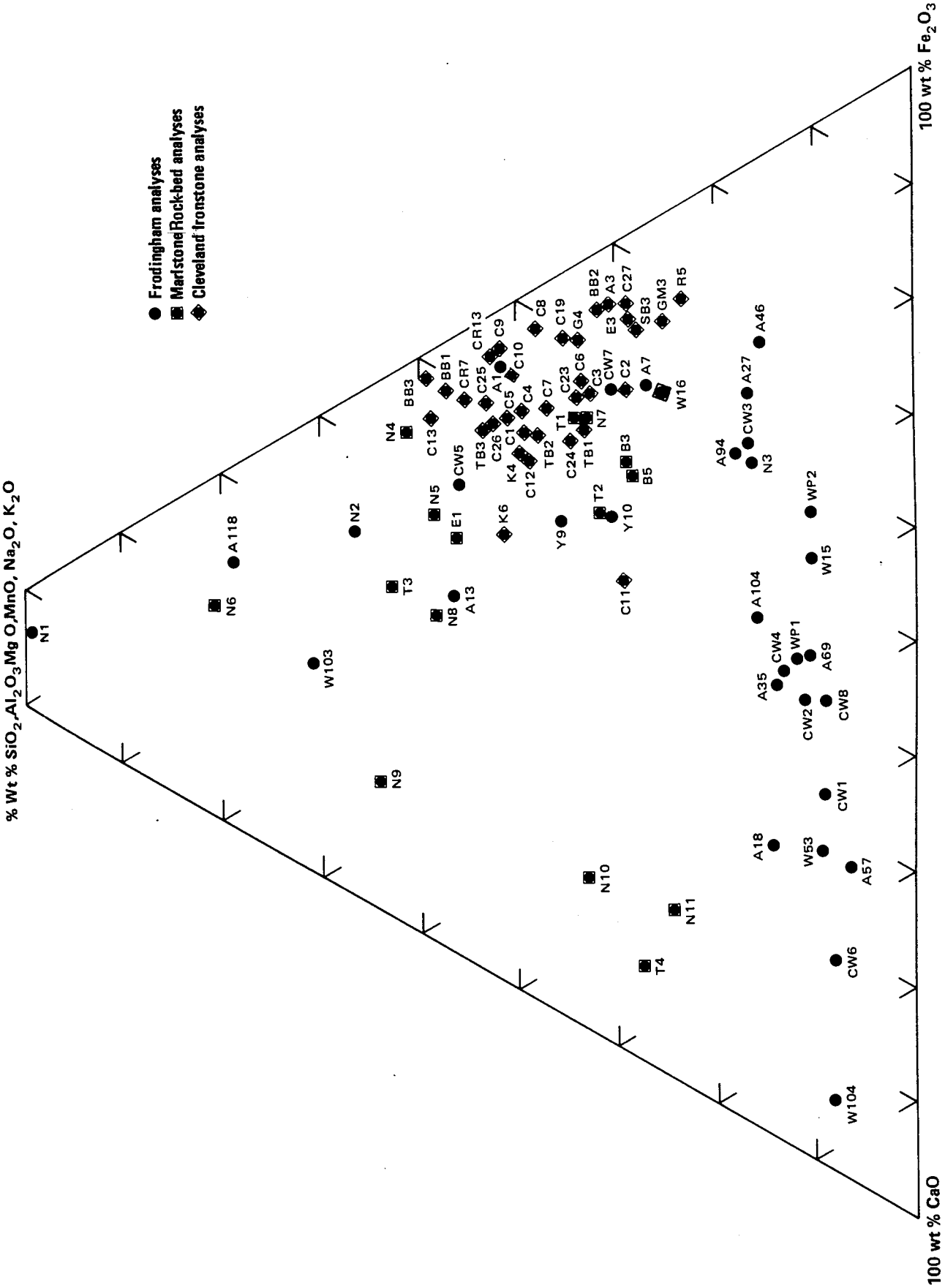

Fig 5.13 Triangular plot of bulk rock analyses of the Liassic Ironstones

and K_2O as CaO, Fe_2O_3, and SiO_2 are the most abundant oxides in any given analysis. The other oxides are included with SiO_2 as they are suspected to be present within in silicates. As would be expected the Frodingham samples do not form a group but more of a trend from Sio_2-rich to Fe_2O_3-rich to CaO-rich samples. In contrast, the samples from the other two fields are grouped. The Cleveland samples form a well-defined group representing relatively high Fe_2O_3 and low CaO and SiO_2 levels. The ironstone samples from the Marlstone are grouped close to the Cleveland material but tend to be slightly richer in SiO_2. As would be expected the sandrock facies samples form a separate group at relatively high CaO and low Fe_2O_3 values. The Cleveland and Marlstone ironstone samples occur in the area of the chamositic chamosite oolite and chamosite-rich limonite oolite portion of the Frodingham 'trend'. There is, therefore, a clear difference in the overall geochemistry of the ironstone fields.

In order to further investigate the geochemical differences between the ironstones and to try to obtain some idea of the causative factors cluster analysis of all the samples was carried out. Since distance coefficient dendrograms have provided the most useful data in the preceding sections only this dendrogram type is considered (Figure 5.14). Nearly all the Cleveland Ironstone samples are clustered together in the same cluster arrays that were obtained before. The only major difference is the presence of the chamositic chamosite oolites N7 and T1 (Marlstone Rock-bed) and the red oolites CW7 and A7 (Frodingham) in two siderite mudstone clusters. Lithologically they are completely dissimilar. Consideration of Table 5.2, however, shows that they have very similar analyses. The Frodingham Ironstone samples retain their original clusters but are expanded by the inclusion of Marlstone samples with similar

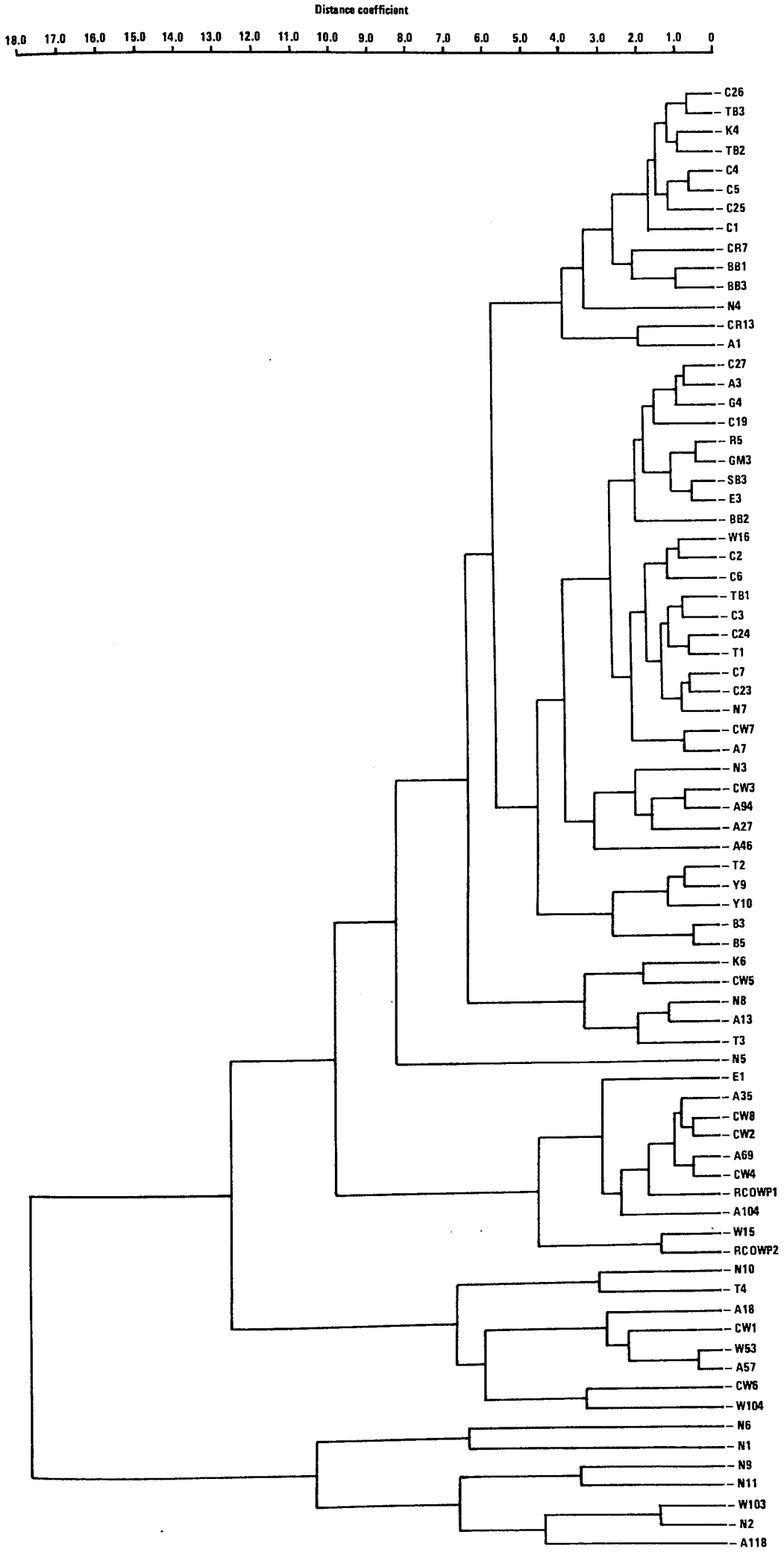

Fig 5.14 Q–mode variation between all samples

lithological characteristics. Thus, in the cluster representing chamositic chamosite oolites and chamosite mudstones the Marlstone representatives of this cluster are included. In the discussion of this cluster (5.4.2) the two-fold separation of the cluster was not clear. The presence of the slightly quartzose specimens N8 and T3 in the A13 and CW5 cluster suggests that the separation may result from this. The Cleveland sample K6 is also included in the cluster. It is lithologically dissimilar but has a similar chemistry. The Marlstone samples N10 and T4 are similar to the calcite cemented and limestone clusters of the Frodingham Ironstone but are separated as a result of their slightly quartzose nature. Samples N6, N9, and N11 (Marlstone) and W103, N2, and A118, (Frodingham) are presented as being dissimilar to all the other samples and having a dissimilar character to each other. This is presumably a result of their mica, quartz, and chamosite-rich natures.

Since the Cleveland samples are linked initially in a way similar to their clustering when considered individually, it is concluded that geochemically the Cleveland Field differs markedly from the Frodingham and Marlstone Fields whose samples cluster together and are, therefore, concluded to be geochemically similar.

5.7.2 Oxide Variation

From the distance coefficient dendrogram representing the variation between the analyses of all the ironstone samples (Figure 5.15) the overall variation between oxides can be assessed. This indicates that MgO, MnO, Na_2O, K_2O, and Al_2O_3 exhibit a similar variation. SiO_2, CaO, abd Fe_2O_3 vary in a way which is dissimilar to each other and to the MgO cluster. As has been discussed above such a variation reflects the

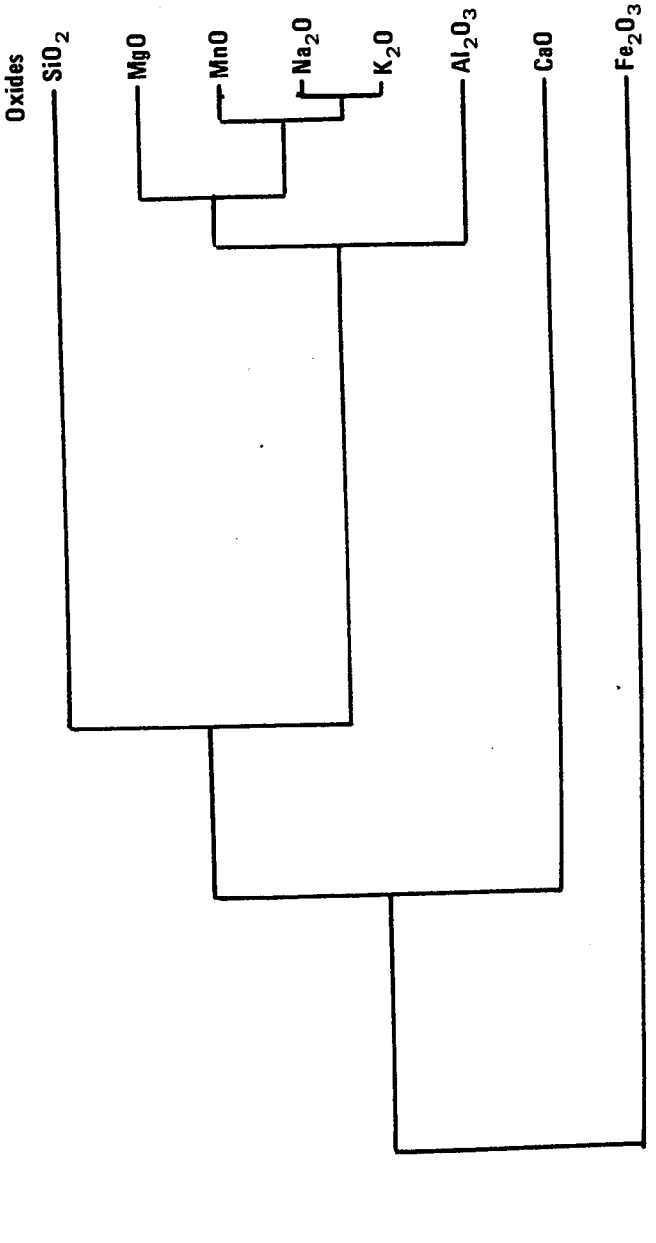

Fig 5.15 R–mode variation between oxides. All samples.

relative abundances of chamosite, siderite, calcite and other non-iron-bearing silicates.

5.8 CONCLUSIONS

A number of conclusions can be drawn from the geochemical study of the three ironstones. These are as follows:

(1) All three ironstones are geochemically distinct. The Frodingham Ironstone represents a geochemical trend. The Marlstone Rock-bed is represented by relatively SiO_2 and Fe_2O_3 rich ironstone facies and relatively SiO_2 and CaO rich sandrock facies. The Cleveland Ironstone, in comparison, is richer than the Marlstone Rock-bed.

The trend exhibited by the Frodingham Ironstone is a natural reflection of the relationships between facies. The ideal lateral order of depositional facies in this ironstone is chamosite mudstone and chamositic oolite - chamositic limonite oolite - calcitic limonite oolite - bioclastic limestone. This is shown up in the trend of specimens from these lithologies from high SiO_2 and Fe_2O_3 levels to high CaO and Fe_2O_3 levels. The absence of goethite from Marlstone Rock-bed samples results in similar Fe_2O_3 and SiO_2 levels to the Frodingham Ironstone for the chamosite-rich ironstone facies . The relative abundance of calcite, reflected as CaO, allows the calcitic facies to be differentiated from the non-calcitic chamositic facies. There is very little geochemical variation between different facies of the Cleveland Ironstone. For the siderite mudstones this is understandable since the siderite is replacive and the process of replacement would be expected to be uniform over large areas as suggested by the lateral extent of siderite mudstone

ironstones. The non-replaced Cleveland lithologies, with the exception of the calcitic chamosite oolites all contain an abundance of siderite as an early diagenetic mineral. This might be expected to result in analyses similar to those of the siderite mudstones. This is supported by the fact that the calcitic chamosite oolites, which do not contain siderite, are lower in Fe_2O_3 and higher in SiO_2 and CaO, and that the unreplaced lithologies tend to exhibit slightly higher Al_2O_3 and SiO_2 levels.

(2) The analyses of material from the Frodingham and Marlstone Ironstones can be divided into a number of clusters which are geochemically and mineralogically distinct. These correspond to the ironstone facies recognised by field and petrographic studies. A fine degree of resolution of individual facies is not, however, possible. The premise that these facies would be expected to have different chemical natures is thus confirmed. By taking the highest and lowest values for the component oxides in the members of the clusters it is possible to obtain some idea of the chemical ranges they represent. Standard deviations and means have not been quoted to express this as the clusters comprise a small number of samples each and thus these statistical values would not be meaningful.

(3) The Cleveland Ironstone is characterised by a number of clusters, some of which are mineralogically distinct. They do not, however, correspond to a marked difference between the compositional ranges of the clusters. Unreplaced lithologies, as a group, can be differentiated from replaced lithologies.

(4) Cluster analysis of the component oxides shows generally that SiO_2, Fe_2O_3 and CaO have very dissimilar trends. This is clearly supported by the variation between these oxides, when considered as

a function of depth and as lithology, which is seen to be mutually antipathetic. Such a consideration also shows that SiO_2, Al_2O_3, and MgO are parallel. This is not always borne out by the results of cluster analyses due to the fact that any one oxide may be present in more than one mineral. This results in the variation determined by cluster analysis being an average of the variation for the oxide in each of its parent minerals.

The method of cluster analysis is clearly a useful tool in establishing similarities between groups of observations. Two points have arisen from its use in this study. Firstly, it provides good results for observations which yield clusters of notably different characteristics. However, where observations are only slightly different dissimilar clusters are produced containing members which on a less rigorous classification scheme would be considered to be one group. Care must therefore be taken in interpreting the results of cluster analysis and this must be carried out utilising data obtained from other studies e.g. petrography. Secondly, in other commonly used statistical studies tests which provide some level of significance for results are utilised. No such tests have, as yet, been devised for cluster analysis. This arises from the fact that an n-dimensional distribution of data is considered in cluster analysis whereas other statistical studies consider two or three-dimensional data distributions. Thus, it is not possible to ascertain just how significant a linkage between clusters is i.e. what degree of similarity or dissimilarity does it imply? Use of the correlation coefficient dendrograms might provide this type of information but for reasons given above would be somewhat dubious. The clusters must be judged objectively according to the known features of the data.

It will have been noted that the role of MnO, K_2O, and Na_2O in the geochemistry of the ironstones has been given little attention. This is due to the fact that they comprise a very small part of any one ironstone analysis and that their variation appears to be random. The cluster analyses always show a very similar variation between them which might indicate an origin in some terrigenous mineral such as mica or feldspar or, as in the case of the Cleveland Ironstone, igneous lithoclasts.

CHAPTER 6

THE MINERALOGICAL NATURE OF CHAMOSITE: X-RAY, ELECTRON PROBE MICROANALYSIS AND MÖSSBAUER STUDIES

THE MINERALOGICAL NATURE OF CHAMOSITE: X-RAY, ELECTRON PROBE MICROANALYSIS AND MÖSSBAUER STUDIES

6.1 INTRODUCTION

The petrographic studies of various ironstone lithological types have shown that several different textural and mineralogical forms of chamosite occur. These may be subdivided into those which are found as primary but allochthonous grains and those which are essentially autochthonous together with those which are the products of diagenetic reactions. In general the colour of these phases corresponds to the two divisions; the first group chamosites are brown shades of green whereas the latter group occurs as grass-green phases. In the Frodingham Ironstone, allochthonous goethite ooids are considered to represent the oxidised equivalents of chamosite ooids. Since the only major difference between these phases is transportation in an energetic, and presumably oxidising, environment, it follows that the observed colour variation and the occurrence of goethite ooids may reflect a progresive oxidation of chamosite. A similar transformation from green to red chamosite is indicated by compositionally zoned burrows of chamosite mudstone occurring at horizons of subaerial exposure in the Frodingham Ironstone. The nature of this zonation is as a central core of dark green chamosite mudstone surrounded by a rim of red mudstone.

Clay minerals often exhibit some degree of authigenesis with depth of burial such as in the formation of mixed-layer montmorillonite-illite from montmorillonite, and the appearance of very late stage kaolinite and dickite. Since chamosite is a clay mineral, it may also exhibit authigenic changes with depth. Authigenic chamosite books have been observed within

chamosite mudstone specimens from the Frodingham Ironstone and also in specimens of the Sandrock and sandrock facies of the Marlstone Rock-bed.

In order to investigate the nature of chamosite oxidation and the possibility of chamosite burial-authigenesis, X-ray diffraction, electron probe microanalysis and Mössbauer spectroscopy studies of a number of specimens have been carried out. The results of these studies are reported and discussed below.

6.1.1 Nomenclature

The mineral chamosite was first observed by Berthier (1820) and named for its site of occurrence in Chamoson, France. Zalinski (1904) provided the first complete description of chamosite. Hallimond (1925) identified chamosite as a major component of the British Jurassic Ironstones and classified it as a chlorite, although noting that it was well separated in composition from other chlorite species. It was not until the work of Engelhardt (1942), Orcel et al (1949) and Brindley (1949) that the mineralogical nature of chamosite was revealed. These authors showed that the Chamoson chamosite was a true chlorite with a 14 Å basal spacing whereas the ironstone chamosites were septechlorites with a 7 Å basal spacing. A problem in nomenclature therefore exists. Following the proposal of Orcel et al (1949) the Nomenclature Committee of the Clay Minerals Society (Bailey et al, 1971) have proposed that the name chamosite should be restricted to the 14 Å variety and that the 7 Å material should be termed berthierine. A number of authors, however, suggest, on the basis of relative abundance, that the name chamosite

should be retained for the 7 Å material, distinguishing it by some structure-related prefix such as 'septe' (Nelson and Roy, 1958) or 'ortho' (Novak et al, 1964). The nomenclature problem has recently been discussed by Bailey (1980) from the structural aspect. He considers that the name chamosite has priority for 2:1 chlorite which is similar in composition to the 1:1 Fe-rich layer silicate commonly occurring in ironstones and which contains appreciable tetrahedral Al. The name berthierine has priority for the latter silicate type (Bailey, 1980). As yet, however, no general agreement has been reached. In this work the 7 Å mineral is referred to as chamosite.

6.2 X-RAY DIFFRACTION STUDIES

6.2.1 The Crystal Structure of Chamosite

The crystal structure of chamosite has been elucidated by Brindley (1949, 1951) who showed it to have a kaolin-type structure characterised by a 7 Å basal ($\underline{d}_{001}$) spacing. In the absence of individual chamosite crystals, the research leading to this conclusion was carried out on chamosite concentrates from laterite and ironstone deposits. Of these specimens, the laterite yielded the most useful X-ray data which was therefore used in the determination of the chamosite unit-cell. Brindley (1949, 1951) concluded that two unit-cells are possible; a monoclinic cell and an orthohexagonal cell. The X-ray data used indicated that both cell types occur. Brindley (1949) notes that the X-ray data for this and other chamosite specimens shows that, of the two structural forms only the orthohexagonal variety occurs alone and that other specimens may comprise equal amounts of the two forms, or approximately

two parts of the orthohexagonal form to one part of the monoclinic form. Consideration of the method by which the two unit cell types are stacked led to the conclusion that they are intergrowths (Brindley, 1951).

The nature of disorder in the chamosite structure, expressed as a variation in the intensity of the series of lines, has been examined by Brindley and Youell (1953) and Youell (1955) using ironstone chamosite specimens. The most extreme disorder is indicated by the complete absence of the (20 ℓ) lines. This type of order/disorder variation is absent from lateritic chamosites (Youell, 1955). In the most disordered chamosites only those lines common to both orthohexagonal and monoclinic cells are present. Youell (1955) considered this to represent the intermediate cell state, the occurrence of which correlates with the chamosite composition and the nature of associated minerals.

6.2.2 Sample Preparation and X-Ray Procedures

In order to obtain good X-ray data for chamosite, concentrates of the mineral were prepared from various specimens. In the majority of cases this was easily accomplished using a vibrating engraving tool to further concentrate chamosite already concentrated by sedimentary processes in lenticles and burrows. The concentrates were ground to a powder with an agate pestle and mortar. In some cases this method of concentration was impossible. Where this was the case, individual grains were isolated using a microscope mounted indentation tool.

In common with current clay mineralogy methods, unoriented and oriented mounts of bulk concentrates were prepared for X-ray diffraction studies. Unoriented mounts were prepared by packing a portion of the concentrate on a glass slide and soaking it in acetone to produce a cohesive specimen. Oriented mounts were prepared by sucking a suspension of the concentrate in

distilled water through an unglazed porcelain tile at a pressure of 15-20 psi. The specimen was then placed in a dessicator to dry at room temperature for 24 hours. Where bulk concentrates could not be obtained the individual grain concentrates were bound together in a small ball with rubber solution glue and mounted on the end of a glass fibre for powder photography.

X-ray diffractograms of the unoriented and oriented mounts were obtained using iron-filtered CoKα radiation. A scan speed of $\frac{1}{2}^{o}$ 2θ minute^{-1} was used in all cases. The time constant and counts per second controls were adjusted for each specimen to give minimum noise and the greatest amplitude for the 001 chamosite peak. Unoriented diffractograms were produced for the range 3-75° 2θ and oriented diffractograms for the range 3-33° 2θ. A diffractogram of a blank tile was run in order to assess the contribution of the tile to the oriented specimen diffractograms. X-ray powder photographs of the individual grain mounts were obtained using a Debye-Scherrer camera with fine collimators and iron-filtered CoKα radiation. An exposure time of 3 hours was found to yield the best results.

6.2.3 Results

Indexing of unoriented diffractograms and X-ray photographs in the normal way indicated that the samples consist of chamosite with siderite, calcite, quartz, muscovite and biotite in various proportions. Quartz is absent from the individual grain concentrates. Muscovite and biotite are only present in the Sandrock specimens T4 and N6. Table 6.1 summarises the chamosite X-ray data derived from these samples. It should be noted that as the 02* peak is used to calculate cell parameters, its position was measured with a rule in order to remove any inaccuracy in the printed diffractogram grid and relative to the quartz 101 peak. This allows the $\underline{d}_{02}$* value to be quoted to three significant figures.

Specimen	001 d(Å)	I	02* (wrt Q101) d(Å)	I	– d(Å)	I	021 d(Å)	I	002 d(Å)	I	– d(Å)	I	200 d(Å)	I	201 d(Å)	I	202 d(Å)	I	060 d(Å)	I	Oriented wrt Q101	001 d(Å)	I	002 d(Å)	I
B17	7.06	100	4.629	13	4.23	5			3.54	62			2.68	18	2.50	17	2.14	29	1.554		FRODINGHAM IRONSTONE	7.136	100	8.553	49
B18	7.02	100	4.615	26	4.22	3			3.53	54			2.69	2	2.51	13	2.09	6	1.556			7.132	100	3.547	37
B20	7.11	100	4.645	16					3.55	52	3.05	7	2.69	14	2.52	4	2.14	54	1.555			7.141	100	3.560	55
B22	7.09	100	4.490	11	4.32	3			3.58	40			2.78	69	2.48	14	2.14	7	1.556			7.166	100	3.553	35
B23	7.09	100	4.508	15	4.32	9			3.53	56	3.02	36	2.70	11	2.55	16	2.12	41	1.557			7.151	100	3.545	40
B24	7.09	100	4.629	7	4.32	18			3.54	70	3.02	12	2.79	37					1.556			7.141	100	3.554	45
W118	7.13	100	4.523	5			3.88	5	3.55	52			2.69	30	2.51	37			1.554			7.107	100	3.574	72
W122	7.09	100	4.477	9					3.52	55			2.70	9	2.44	32	2.12	10	1.553			6.954	100	3.406	41
Y1	7.16	100	4.703	8					3.56	56			2.71	18	2.53	14	2.153	17	1.553			7.122	100	3.680	19
Y78	7.12	100	4.643	4					3.54	43			2.70	19					1.555			7.117	100	3.545	18
Y3	7.06	100	4.477	10					3.53	74			2.71	18	2.52	23	2.15	8	1.555			7.092	100	3.540	38
N3	7.06	100	4.453	54					3.55	96			2.69	68								7.231	100	3.559	88
R1	7.08	100	4.600	21			3.91	7	3.54	50			2.70	20	2.50	31	2.13	22	1.551			7.050	100	3.520	30
C14	6.99	100	4.580	2	4.30	11			3.53	27	3.01	8	2.65	7	2.54	15	2.12	16	1.545		CLEVELAND IRONSTONE	7.176	100	3.541	27
BB3	6.94	100	4.578	16					3.49	56			2.78	18					1.553			7.292	100	3.571	42
BBII	6.99	100	4.596	5					3.49	60			2.77	26	2.49	7	2.12	18	1.551			7.141	100	3.549	54
R2	7.09	100	4.660	13			3.89	6	3.51	63			2.69	15	2.51	20	2.14	20	1.552			7.080	100	8.520	40
N7 ooids	7.16	100	4.693	26					3.65	48	3.03	37	2.71	13	2.54	56	2.15	44	1.561			7.112	100	3.670	27
N7 mud	7.02	100	4.650	16					3.52	43	3.01	15	2.68	10	2.52	39	2.14	26	1.558			7.117	100	3.680	40
B1e	7.22	10	4.69						3.48	2															
T1e	7.17	7	4.70						3.56	4															
EH1e	7.18	8	4.62						3.61	7											MARLSTONE ROCK-BED	X-ray photographs			
T2b	7.22	7	4.70	Diffuse band					3.58	6	3.06	4	2.71	3	2.52	3	2.16	3	1.540	1					
T3b	7.23	4	4.71				3.87	2	3.57	2	3.04	1													
T4b	7.16	3	4.67						3.52	3															
W6	7.02	100	4.596	3	4.28	14			3.54	88			2.70	9	2.55	18	2.16	19	1.558			7.250	100	3.533	38
T4	7.08	100	4.470	9	4.62				3.51	55			2.67	5					1.557			7.129	100	3.537	67

e: Ooid envelope grain concentrate

b: Ooid core book grain concentrate

02*: A 2-dimensional diffraction band equivalent to 020.

060 intensities are not given as a low cps setting was used to reveal the position of this peak.

I: Intensity calculated as I/I_{100}

I_{100} corresponds to the most intense peak for chamosite i.e. (001)

Table 6.1. X-ray diffraction data for chamosite

Oriented sample diffractograms were used in order to accurately determine the chamosite basal spacings; $\underline{d}_{001}$ and $\underline{d}_{002}$. These are quoted separately in Table 6.1. The positions of the 001 and 002 peaks were measured with a rule relative to the quartz 101 peak in order to preclude any inaccuracy which might result from using the printed grid to determine their positions.

Brindley (1949, 1951) has shown that chamosite specimens may be constructed of orthohexagonal or intergrown orthohexagonal and monoclinic unit cells. Table 6.2 gives the calculated $\underline{d}$-spacing and intensities for (hkl) planes resulting from individual monoclinic and orthohexagonal unit cells for the $\underline{d}$-spacing range over which chamosite peaks were observed. A comparison between the X-ray data given in Table 6.1 and the calculated data in Table 6.2 indicates that the samples under consideration are characterised by an orthohexagonal unit cell. Brindley (1951) notes that the presence of the 2.40 Å peak is a reliable indication of the presence of a monoclinic cell. This is absent.

6.2.3.i Non-stratigraphically controlled variation: Variation in the structure of clay minerals is often indicated by a variation in their $\underline{d}_{001}$ and $\underline{d}_{002}$ values. Reference to Table 6.1 shows that there is some variation exhibited by the oriented chamosite data. It is necessary to establish whether this variation is real, i.e. resulting from structural variation, or a random variation resulting from experimental techniques. Figure 6.1 is a graph of $\underline{d}_{001}$ plotted against $\underline{d}_{002}$. The distribution of the points clearly tends towards a linear plot rather than a random distribution. If this distribution indeed reflects a significant variation in the chamosite structure a similar variation should be shown by the unit cell parameters of the individual specimens. Table 6.3 shows these parameters. They have been calculated using the method of Brindley (1951). The b-parameter is twice the $\underline{d}_{020}$ or $\underline{d}_{02*}$ value as obtained from unoriented

Monoclinic (hkl)	d	Intensity	Orthohexagonal (hkl)	d	Intensity
001	7.026	70	001	7.026	70
020	4.657	7	020	4.657	21
110	4.559	14			
$11\bar{1}$	4.274	11			
021	3.880	8	021	3.880	25
002	3.513	38)	002	3.513	38
111	3.492	6)			
$11\bar{2}$	3.132	4			
022	2.804	3	022	2.804	7
$20\bar{1}$	2.679	13)	200	2.688	8
130	2.669	19)			
			201	2.511	88
$20\bar{2}$	2.405	27)			
131	2.396	55)			
201	2.271	4)			
$13\bar{2}$	2.270	9)			
			041	2.210	2
			202	2.135	48

Table 6.2. Calculated d-spacings and intensities for (hkl) planes of the monoclinic and orthohexagonal unit cells of chamosite (Brindley, 1951).

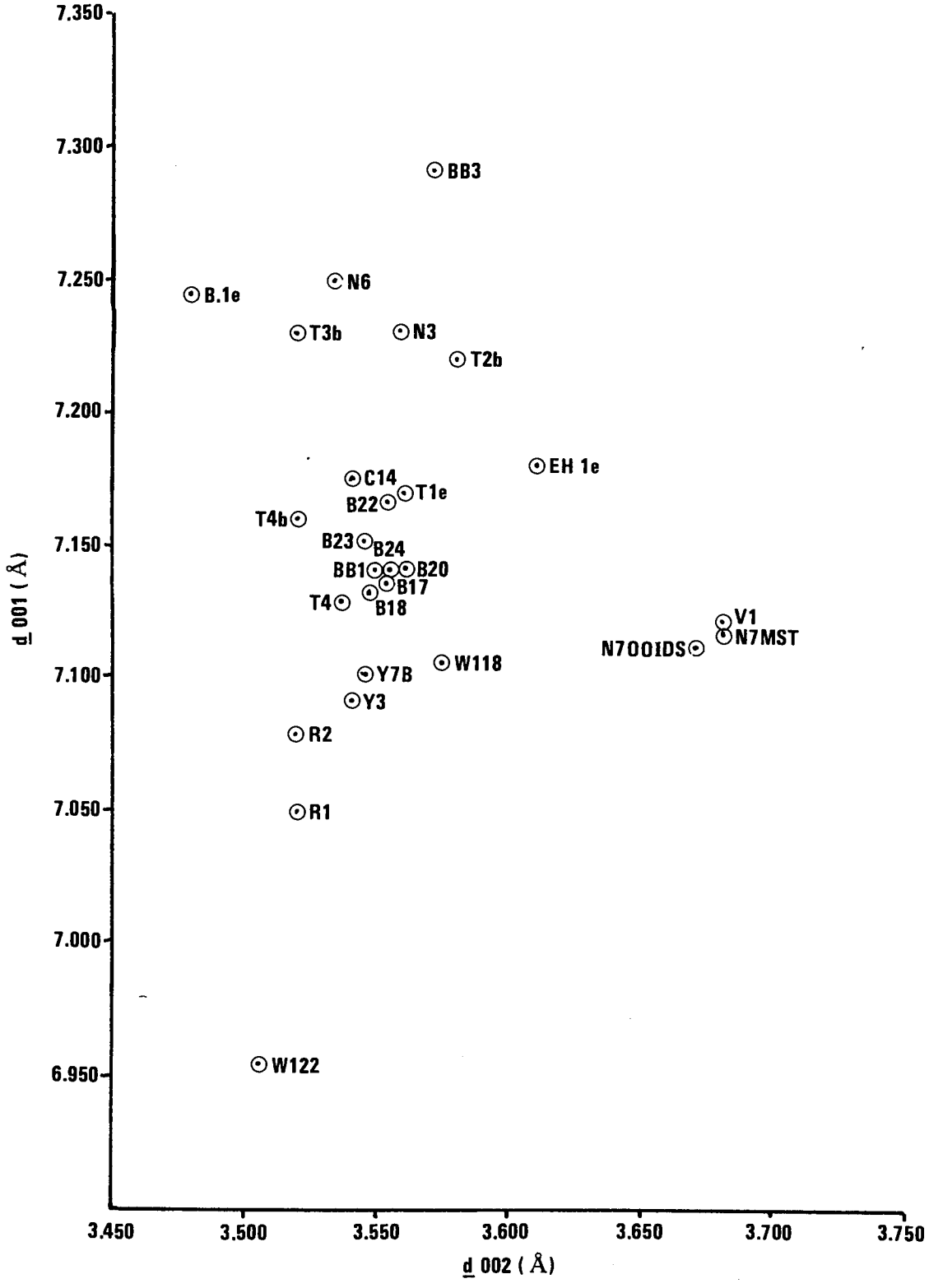

Fig 6.1 : d 001 v d 002 for oriented diffractograms and X-ray photographs

specimen diffractograms. The a-parameter is derived from the b-parameter by dividing this figure by $\sqrt{3}$ (=1.732). The c-parameter is twice the d_{002} spacing recorded from oriented diffractograms. It should be noted that since the a-parameter is related to the b-parameter by a constant it is only necessary to consider any cell parameter variation in terms of b and c-parameters. Derivation of the cell parameters from two different diffractograms removes any possibility of a linear inaccuracy due to measuring all the peak positions from one diffractogram. In Figure 6.2 the b-parameter is plotted against the c-parameter. A significant linear variation is again revealed. Some idea of the direction of the variation has been given by determining the statistical line of best-fit to these points using the regression coefficient method (Davies, 1973). A positive sample correlation coefficient of 0.500, determined by the method of Davies (1973), confirms that there is a degree of linear dependence between the a, b and c cell parameters.

Having established that some systemic variation in the chamosite cell parameters occurs,it is necessary to determine what causes this variation. Evidence from field and petrographic studies yields a good control on the nature of the chamosite specimens under consideration. Table 6.4 summarises the source and nature of these specimens. Those specimens which have remained in situ since formation (autochthonous; coded Aut) are differentiated from those which have undergone transport during their history (allochthonous; coded All), and these are distinguished from those which have been exposed (coded Exp) regardless of their prior history. Several specimens do not fall clearly into any one of these categories. These are placed in the most appropriate approximate category (thus coded Aut$\sim$ or All$\sim$). Each of the data

Specimen	b-parameter (Å)	a-parameter (Å)	c-parameter (Å)
B17	9.258	5.345	7.106
B18	9.230	5.329	7.094
B20	9.290	5.363	7.120
B22	8.980	5.184	7.106
B23	9.016	5.205	7.090
B24	9.258	5.345	7.108
N118	9.046	5.222	7.148
W122	8.954	5.169	7.012
Y1	9.406	5.430	7.360
Y7B	9.286	5.361	7.090
Y3	8.954	5.169	7.080
N3	8.906	5.142	7.118
R1	9.200	5.311	7.040
C14	9.160	5.288	7.082
BB3	9.156	5.286	7.142
BBII	9.192	5.307	7.098
R2	9.320	5.381	7.040
N7 ooids	9.386	5.419	7.340
N7 mud	9.300	5.369	7.360
B1e	9.380	5.415	6.960
T1e	9.400	5.427	7.120
EH1e	9.240	5.334	7.220
T26	9.400	5.427	7.160
T3b	9.420	5.438	7.140
T4b	9.340	5.392	7.040
N6	9.192	5.307	7.066
T4	9.240	5.334	7.074

Table 6.3. Cell parameters for chamosite specimens

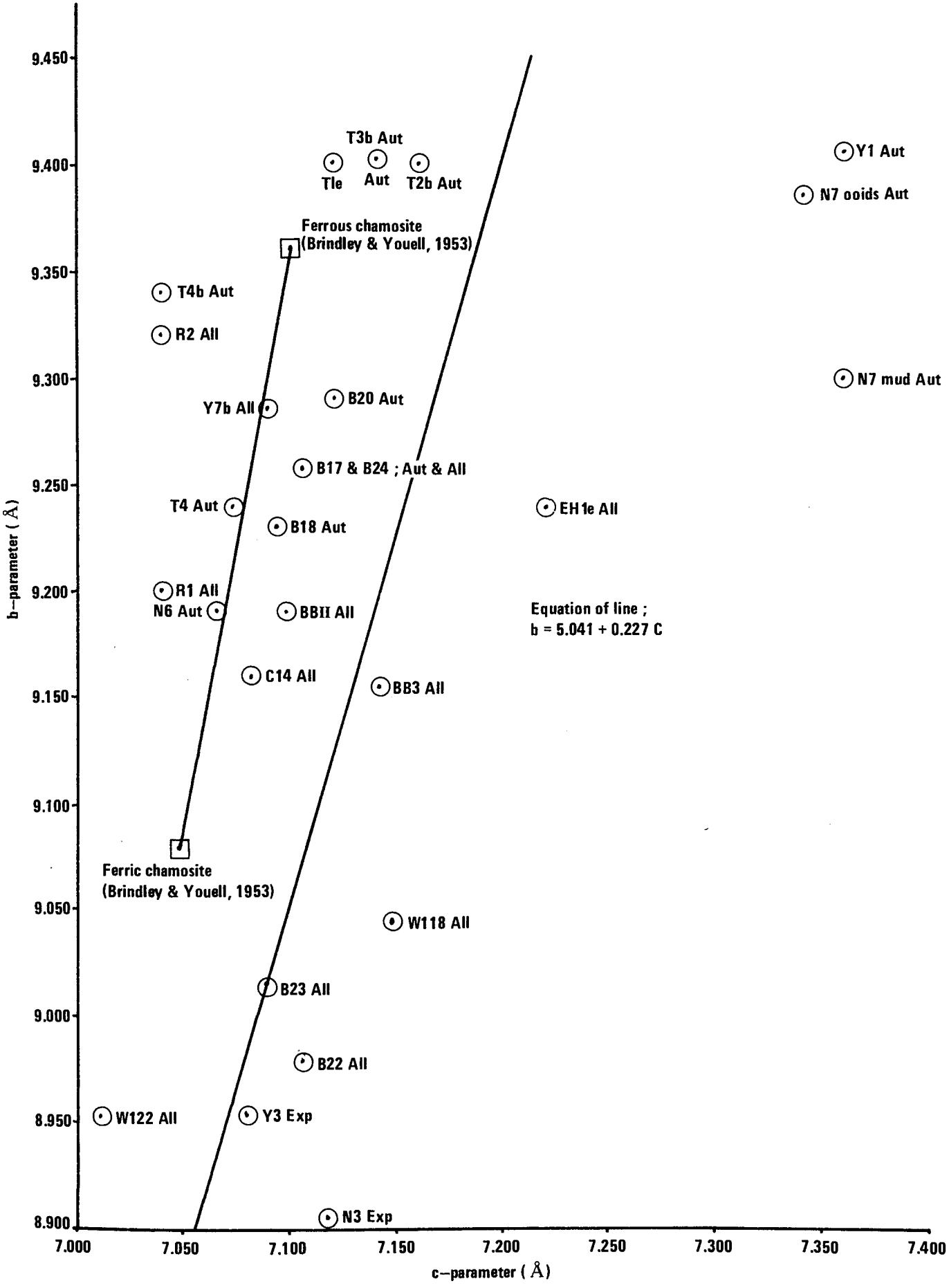

Fig 6.2 b–parameter v c–parameter (for specimen codes see text)

Specimen	Source	Nature	Code
B17	Chamositic chamosite oolites; primary.	Olive green. All chamosite autochthonous	Aut
B18	Chamositic chamosite oolites; primary.	Dark grass green. All chamosite autochthonous.	Aut
B20	Chamositic chamosite oolites; primary.	Olive green. All chamosite autochthonous.	Aut
B22	Depositional chamosite mudstone	Dark grass green. No ooids. Chamosite allochthonous.	All
B23	Depositional chamosite mudstone	Dark grass green. No ooids. Chamosite allochthonous.	All
B24	Depositional chamosite mudstone	Dark grass green. No ooids. Chamosite allochthonous.	All
W118	Depositional chamosite mudstone	Olive green. No ooids. Chamosite allochthonous.	All
W112	Depositional chamosite mudstone	Olive green. No ooids. Chamosite allochthonous.	All
Y1	Chamosite mud from chamositic limonite oolite sub-type ii	Grass green. Large but variable proportion of authigenic chamosite.	Aut∿
Y7B	Chamosite mud from burrow infill in chamositic limonite oolite sub-type ii	Olive brown. Chamosite allochthonous.	All
Y3	Exposed chamosite mudstone	Red brown	Exp
N3	Exposed chamosite mudstone	Red brown	Exp
R1	Chamositic chamosite oolite; primary.	Olive green ooids. Allochthonous.	All
C14	Chamositic chamosite oolite; depositional	Grey-green. Ooids of chamosite allochthonous.	All

Table 6.4. Source and nature of X-ray specimens

Table 6.4 - Continued

Specimen	Source	Nature	Code
BB3	Chamositic chamosite oolite; depositional	Dark grass green. Ooids of chamosite allochthonous	All
BBII	Chamositic chamosite oolite; depositional	Olive green. Ooids of chamosite allochthonous.	All
R2	Chamosite mudstone; depositional	Olive green. No ooids. Allochthonous	All
N7 ooids	Primary chamosite ooids; primary	Light grass green. Ooids autochthonous	Aut
N7 mud	Primary chamosite mud; primary	Light grass green. No ooids. Autochthonous.	Aut
T1e	Chamosite ooid envelope; primary	Grass green. Ooid autochthonous	Aut
EH1e	Chamosite ooid envelope; depositional	Grass green. Ooid allochthonous.	All
T2b	Chamosite ooid core book; primary	Grass green	Aut
T3b	Chamosite ooid core book; primary	Grass green	Aut
T4b	Chamosite ooid core book; primary	Grass green	Aut
N6	Sandrock	Grey. Unabraded chamosite books.	Aut
T4	Sandrock	Greenish grey. Unabraded chamosite books.	Aut

points in Figure 6.2 is coded according to this scheme. It is immediately apparent that there is a well-defined gradation, with increasing cell parameters, from exposed specimens to allochthonous specimens to a mixed region of allochthonous and autochthonous material to an area of dominantly autochthonous specimens. This grouping corresponds roughly to the degree of transport and subaerial exposure which the specimens may have undergone during their history and may therefore reflect an oxidation of chamosite.

Brindley and Youell (1953) report the nature of ferrous and ferric varieties of chamosite. These authors produced ferric chamosite from the ferrous variety by heating a pure ferrous chamosite. Determination of the cell parameters, based on an orthohexagonal cell, showed that formation of ferric chamosite from ferrous chamosite produced a contraction in the cell parameters. The a and b-parameters contracted by 3%, the c-parameter by 0.75%. The cell parameters of the two varieties are plotted on Figure 6.2. It is interesting to note that a line joining these two points lies sub-parallel to the line of best-fit. Analytical data for the chamosite specimens considered here is discussed below but Mössbauer data furnishes important information relevant to this discussion. This is summarised in Table 6.5. Comparison of these data with Figure 6.2 shows that those specimens with smaller cell parameters are higher in ferric iron and lower in ferrous iron that those with larger cell parameters. It appears, therefore, that the observed cell parameter variation in chamosite results from an environmentally induced FeIII:FeII variation.

Specimen	FeIII : FeII
B17	1 : 12.603
B20	1 : 9.084
B22	1 : 4.367
B23	1 : 3.195
W122	1 : 1.197

Table 6.5. FeIII : FeII ratios of selected specimens

The sources of the various chamosite specimens are in agreement with the suggestion that environmental oxidation brings about a diminution in the cell parameters of chamosite. Specimens N7 ooids and N7 mud are derived from a chamositic chamosite oolite which is considered from petrographic work to represent a site of chamosite ooid formation. No evidence of an energetic environment was associated with this bed. A similar statement can be made with respect to specimens B17, B18 and B20. Specimens BBII, BB3 and C14 are derived from chamosite oolites which represent beds created by the deposition of chamosite ooids transported away from their site of formation. Specimens W118, B23, B22 and W122 all represent the redeposition of chamosite derived from elsewhere. Finally, specimens Y3 and N3 are derived from exposed horizons.

It has been noted above that there appears to be a correlation between the colour of a phase and its source; the lighter green varieties being autochthonous, the phases coloured brown shades of green being allochthonous. Comparison of the colours of the X-ray specimens given in Table 6.4 and their positions in Figure 6.2 supports

this observation. The large cell parameter specimens are grass green and the small cell parameter specimens olive brown, olive green or red brown.

Brindley and Youell (1953) and Youell (1955) discuss the nature of the (20ℓ) series of peaks. The production of ferric chamosite from ferrous chamosite (Brindley and Youell, 1953) brings about a diminution in the intensities of the (201) and (202) lines. Youell (1955) considers that the diminution of these intensities is indicative of random a/3 displacements in the chamosite structure bringing about disorder and may be correlated with composition and associated mineralogy. If,as suggested by this worker, the appearance of random a/3 displacements is due, in part, to a reduction in the mean octahedral ionic radius resulting from an increase in the ferric iron content, then this should be observable in the (201) and (202) peak intensities of the chamosite data reported here. This is analysed graphically in Figures 6.3a and 6.3b. It is clear that although a range of intensities occurs, including zero values, significant trends correlating with that of Figure 6.2 are not observed. The other possibilities suggested by Youell (1955) which might bring about intensity variations of this type are compositional variations in components other than iron and the presence or absence of associated minerals such as siderite and kaolinite. Analytical data reported below indicate that there is very little variation in the composition of these chamosite specimens. As noted above, siderite is present in all cases. Youell (1955) notes that ordered chamosite is invariably accompanied by siderite. This is supported by the presence of the (201) series of peaks in the majority of cases reported here. Disordered chamosites, however, are invariably accompanied by kaolinite. This association is characterised by higher than normal Al^{3+} levels in the octahedral sites of such chamosite

this observation. The large cell parameter specimens are grass green and the small cell parameter specimens olive brown, olive green or red brown.

Brindley and Youell (1953) and Youell (1955) discuss the nature of the (20ℓ) series of peaks. The production of ferric chamosite from ferrous chamosite (Brindley and Youell, 1953) brings about a diminution in the intensities of the (201) and (202) lines. Youell (1955) considers that the diminution of these intensities is indicative of random a/3 displacements in the chamosite structure bringing about disorder and may be correlated with composition and associated mineralogy. If,as suggested by this worker, the appearance of random a/3 displacements is due, in part, to a reduction in the mean octahedral ionic radius resulting from an increase in the ferric iron content, then this should be observable in the (201) and (202) peak intensities of the chamosite data reported here. This is analysed graphically in Figures 6.3a and 6.3b. It is clear that although a range of intensities occurs, including zero values, significant trends correlating with that of Figure 6.2 are not observed. The other possibilities suggested by Youell (1955) which might bring about intensity variations of this type are compositional variations in components other than iron and the presence or absence of associated minerals such as siderite and kaolinite. Analytical data reported below indicate that there is very little variation in the composition of these chamosite specimens. As noted above, siderite is present in all cases. Youell (1955) notes that ordered chamosite is invariably accompanied by siderite. This is supported by the presence of the (201) series of peaks in the majority of cases reported here. Disordered chamosites, however, are invariably accompanied by kaolinite. This association is characterised by higher than normal Al^{3+} levels in the octahedral sites of such chamosite

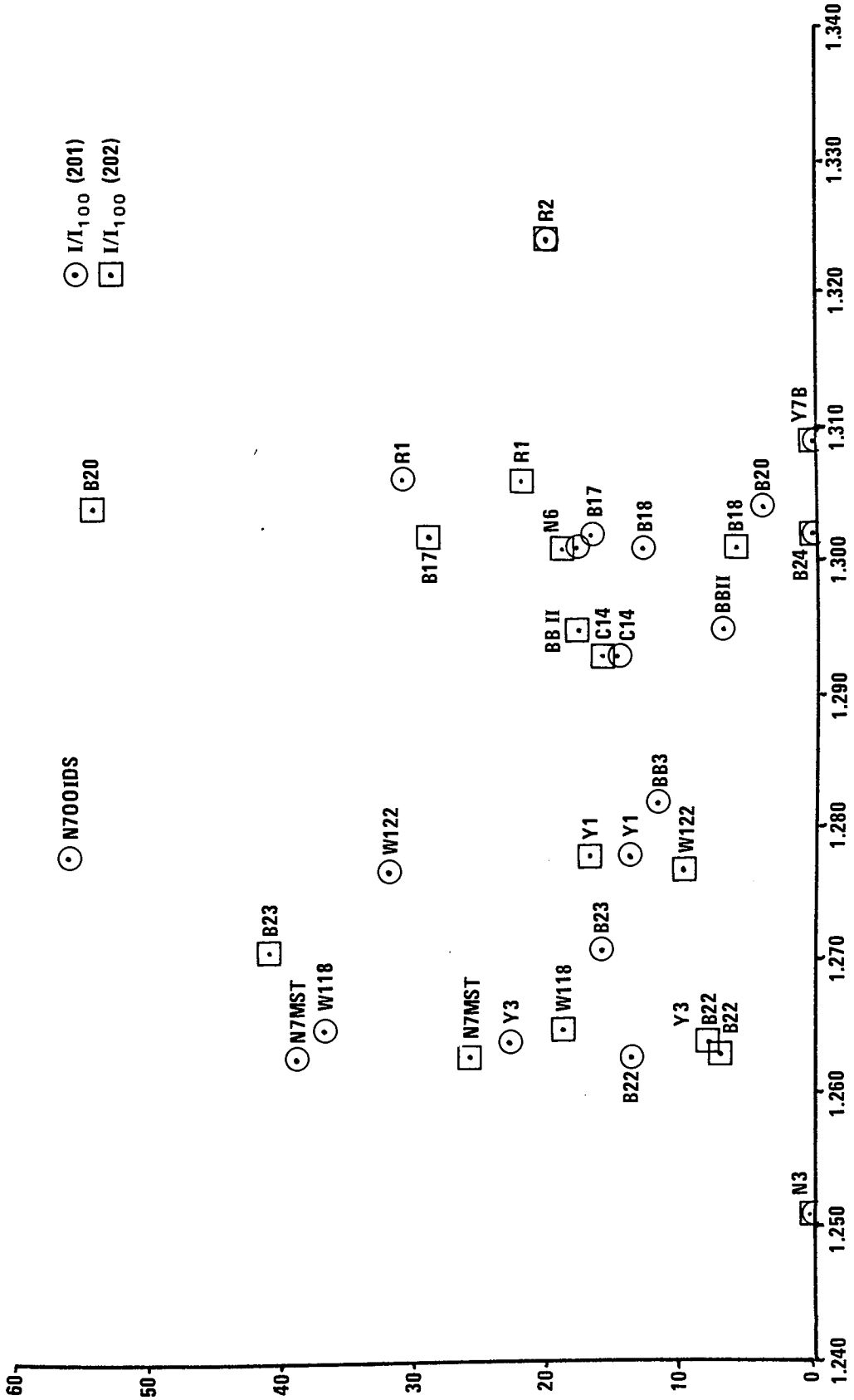

Fig 6.3a Intensity of (201) and (202) peaks relative to cell-parameters

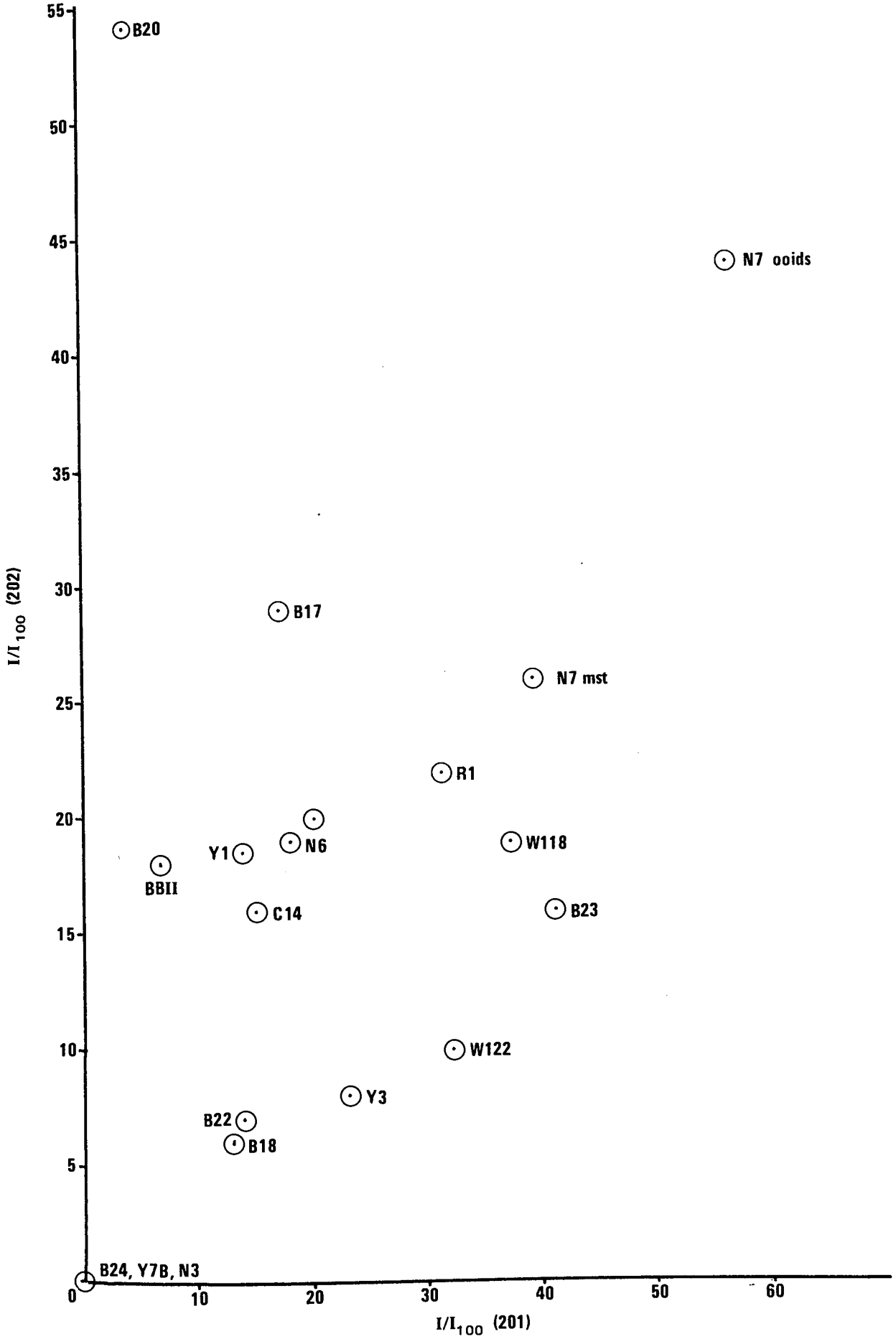

Fig 6.3b (202) intensities v (201) intensities

specimens. No kaolinite has been identified from X-ray diffractograms. Bearing in mind that kaolinite has a monoclinic unit cell in which a/3 displacements occur and the suggestion of Taylor (1949) that kaolinite present in the Northampton Sand Ironstone represents a diagenetically leached chamosite, it seems likely that disordered chamosites represent only partially leached chamosite.

6.2.3.ii Stratigraphically controlled variation: Chamosite occurs as well-formed books, usually less than 0.5 mm in size, and in ooids and mudstones in which the component chamosite flakes are of the clay grade size. Chamosite books have been observed in optical continuity with authigenic, structureless, chamosite in chamosite mudstones and forming textures suggestive of an authigenic origin in the Sandrock facies of the Marlstone Rock-bed. The fact that abraded books also occur in chamosite mudstones and that Marlstone Rock-bed ooids often exhibit core books suggests that the formation of authigenic chamosite books is an early authigenic feature of these sediments. Thus any authigenic change from chamosite mud material to structureless authigenic chamosite to structured authigenic chamosite books may be observable in X-ray diffraction data gathered from specimens representing small differences in burial depth.

Specimens B17 - B24 are derived from a bed of chamositic chamosite oolite and an underlying bed of chamosite mudstone. The chamositic chamosite oolite bed represents a site of ooid formation i.e. formation of clay-grade chamosite. The b- and c-cell parameters for these specimens are plotted against depth from the top of the oolite bed in Figure 6.4. The cell parameters for specimens from this bed show

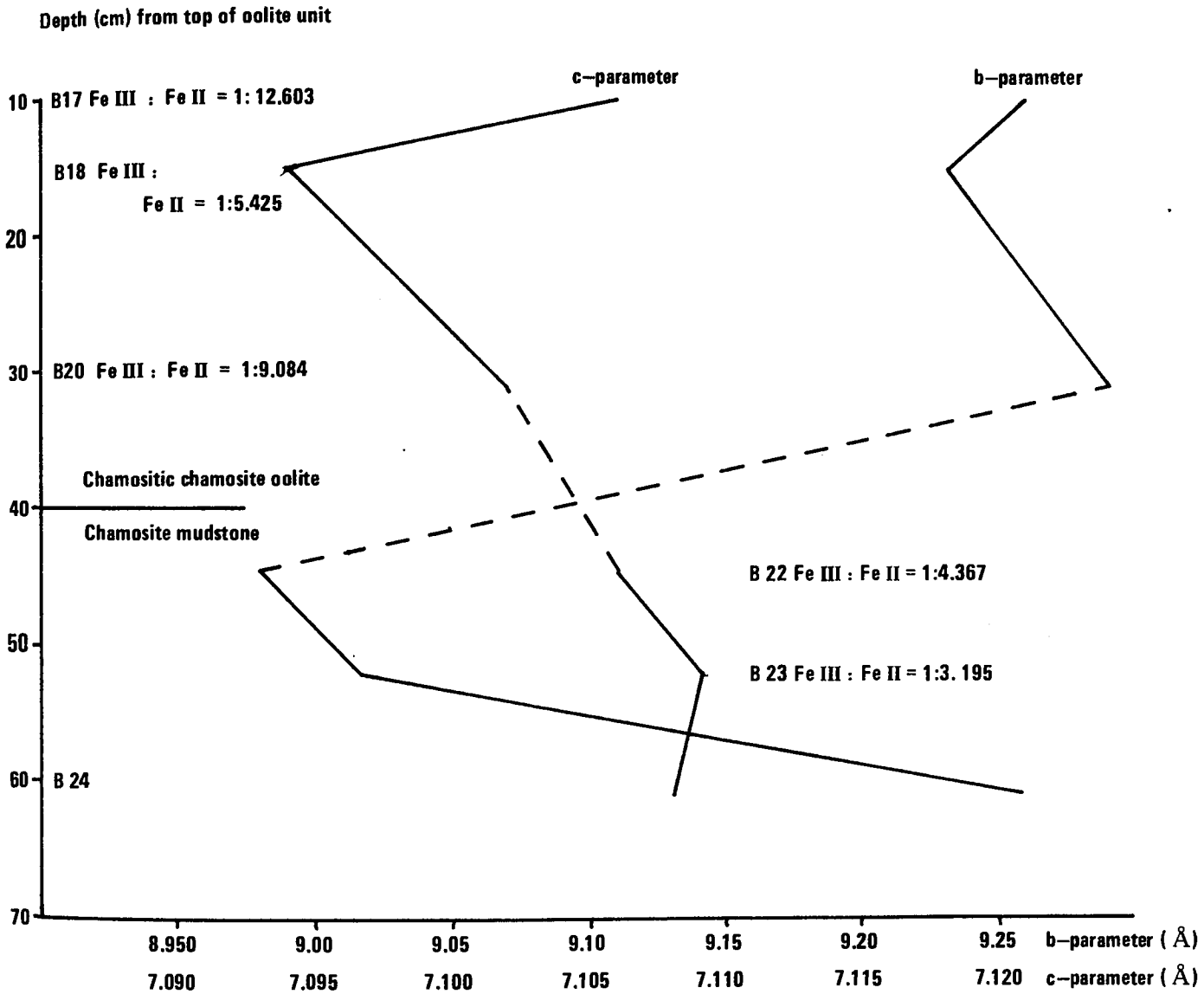

Fig 6.4 Variation in b and c-cell parameters of specimens B17–B24 with depth

a parallel variation. The most important variation occurs in the underlying bed in which the c-cell parameter remains approximately constant but following an initial decrease the b-cell parameter gradually increases with depth. In the sedimentological model of the Frodingham Ironstone (Chapter 2) chamosite mudstones were considered to have been derived from chamositic chamosite oolites as a result of erosion, winnowing, transport and redeposition. This would indicate the possibility of oxidation of the chamosite mud bringing about an increase in ferric iron and hence a decrease in the cell parameters. Ferric iron: ferrous iron ratios indicated in Figure 6.4 show that this is indeed the case. The increase in the b-parameter shown by the deepest data point suggests a decrease in the ferric iron content of this sample. It is not possible to say whether this represents a true authigenic change in the chamosite mud or is a reflection of less intense oxidation during transport. It is interesting to note, however, that in Figure 6.2 a line joining specimens B22, B23 and B24 trends towards the larger cell parameter sizes.

Specimens W118 and W122 are derived from a chamosite mudstone sequence. The former lies 30 cm above the latter. The b- and c-cell parameters for these specimens decrease from W118 to W122 indicating a ferric iron increase with depth. This is the opposite trend to that found between specimens B22 and B24.

From the X-ray data for chamosite specimens considered as a function of depth it is very difficult to unravel what represents a burial authigenic change and what represents environmental oxidation of chamosite. Petrographic evidence shows that chamosite books are formed by authigenic processes and perhaps in specimen B22 there is a suggestion of this.

6.2.3.iii The effect of heating: Brindley and Youell (1953) report the laboratory formation of ferric chamosite from ferrous chamosite by heating. The ferric variety exhibits a smaller unit cell than the ferrous type. Since it has been suggested above that natural chamosites exhibit a range of cell parameters reflecting the degree of environmental oxidation which they have undergone, a contraction of their cell parameters would be expected as a result of laboratory oxidation by heating. Since the work of Brindley and Youell (1953) was based on one specimen additional evidence in support of their conclusions is required.

Unoriented and oriented mounts of four chamosite specimens were heated in a furnace for 2 hours at 400 C in air. These were the experimental conditions used by Brindley and Youell (1953). Diffractograms were then prepared using the same conditions described above. Indexing of the unoriented and oriented diffractograms yielded the chamosite data shown in Table 6.6. Comparison of these results with those reported for ferric chamosite by Brindley and Youell (1953) (Table 6.6) shows that all four yielded the peaks characteristic of ferric chamosite. Comparison of the sample peaks with those for the same sample at room temperature (Table 6.1) shows a change in the (001), (02*) and (002) peak positions, but little noticeable change in the positions of the (201) series. The one exception to this is sample W122 which did not change. The cell parameters of the heated specimens show a contraction with respect to their room temperature values (Table 6.7), again with the exception of W122. The cell parameters for the four specimens are plotted graphically in Figure 6.5. In addition, the cell parameters reported by Brindley and Youell (1953) for ferric chamosite are also plotted. In order to give some

Specimen	001		02*		002		200		201		202		Oriented mounts: 001		002	
	d(Å)	I	d	I	d	I	d	I	d	I	d	I	d	I	d	I
Brindley and Youell (1953)	7.05	S	4.535	M	3.520	S	2.622	M	2.460	MS	2.103	M	X-ray photograph			
B17	7.23	100	4.528	75	3.530	98	2.620	23	2.450	37	2.09	30	7.044	100	3.493	51
W118	7.07	100	4.470	89	3.50	90	2.62	13	2.45	66	2.09	13	7.191	100	3.543	76
W122	As for RT (Table 6.1)															
N7 ooids	7.03	100	4.512	68	3.51	87	2.61	32	2.45	77	2.10	32	7.078	100	3.535	28

02*: 2 dimensional diffraction band

$I = I/I_{100} = I/I_{001}$

S = Strong

M = Medium

W = Weak

Table 6.6. X-ray data for chamosite specimens heated at 400 C for 2 hours

Specimen	b-Parameter (Å)		a-Parameter (Å)		c-Parameter (Å)		Cell contraction: b and a-Parameters	Cell contraction: c-Parameter
	RT	400 C	RT	400 C	RT	400 C		
Brindley and Youell (1953)	9.360	9.080	5.404	5.244	7.100	7.048	3.000%	0.750%
B17	9.258	9.056	5.345	5.228	7.106	6.986	2.181%	1.688%
W118	9.046	8.940	5.222	5.161	7.148	7.086	1.171%	0.867%
W122	As for RT; no cell contraction (Table 6.3)							
N7 ooids	9.386	9.024	5.419	5.210	7.340	7.070	3.856%	3.678%

RT Room Temperature

Table 6.7. Cell parameters and cell contraction after heating

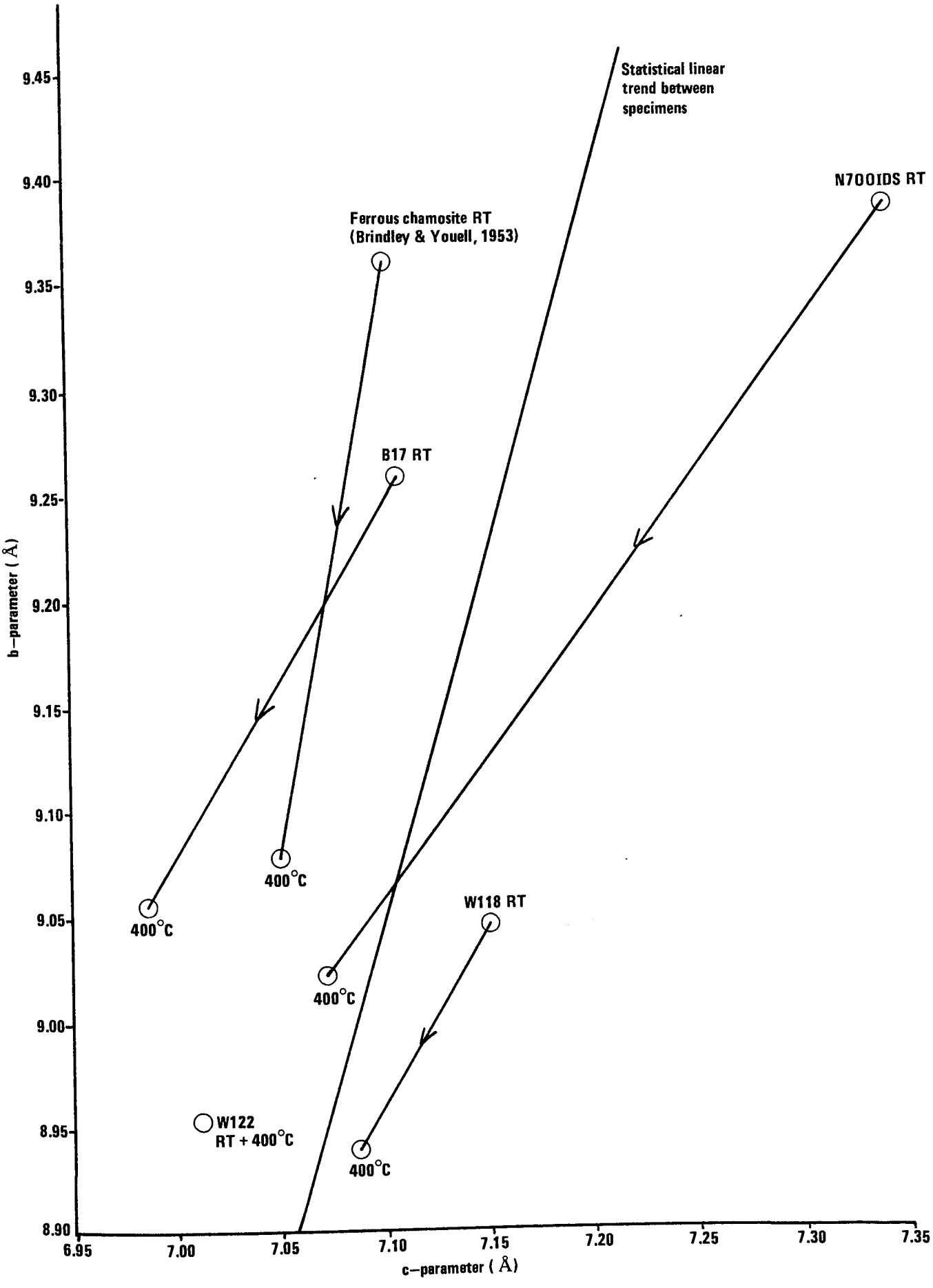

Fig 6.5 Graphical plot of unit cell variation after heating at 400 C for 2 hours

indication of the cell parameter trend of natural specimens the statistical line of best-fit from Figure 6.2 is plotted.

The results of heating given in Tables 6.6 and 6.7 and shown in Figure 6.5 give clear confirmation of the results reported by Brindley and Youell (1953). The most important feature of the oxidation is that the ferric chamosites thus produced cluster in the low cell parameter area of the graph, regardless of their original cell parameters. It is interesting to note that W122 lies in this area; the sample which did not change on oxidation. This might be related to its initially high Fe^{3+} content (Table 6.5). The overall trend from room temperature to 400 C cell parameters is sub-parallel to the line of best-fit, thus indicating that the sample variation leading to this line is due to oxidation. In this context it is interesting to note that N3 and Y3 which are considered to represent the greatest degree of natural oxidation due to exposure lie in the low cell parameter area.

6.3 ELECTRON PROBE MICROANALYSIS

6.3.1 Previous Analyses of Chamosite

Wet chemical analyses of chamosite concentrates from various sources have been reported by Hallimond (1925, 1939), Taylor (1949), Brindley (1951), Whitehead et al (1952) and Brindley and Youell (1953). These workers have all noted that although concentrates were used it was more or less impossible to remove impurities such as calcite, siderite and pyrite. The presence of these minerals causes inaccuracies in the results. The

published analyses of chamosite specimens indicate that iron, silicon, aluminium and magnesium are quantitatively the most important elements present in chamosite. Titanium, manganese and phosphorus have occasionally been reported (Hallimond, 1939; Taylor, 1949) but represent less than one weight per cent of the sample.

6.3.2 Analysis

In order to overcome the problems of purity in samples electron probe microanalysis of the iron, aluminium, silicon and magnesium in various chamosite phases was carried out. Analysis of manganese, titanium, sodium, potassium and phosphorus was carried out on some phases but their values were below the background level. Polished sections of ironstone lithologies from all three ironstone deposits were used. Areas for analysis were selected under a reflecting microscope and ringed with a marker pen. The sections were then coated with carbon to prevent charging of the specimen in the electron beam.

A Cambridge Microscan V Electron Probe Microanalyser was used for analysis. An accelerating voltage of 15 kV was used for all analyses. The crystals and spectrometer angles used in obtaining individual elemental analyses are given in Table 6.8.

Analyses were performed in the following way. A polished standard containing the element to be analysed was placed under the electron beam and a clean area for analysis selected using the reflecting optical microscope system mounted in the instrument. The spectrometer was tuned such that a maximum count-rate was obtained for that element being analysed. Four peak counts were then measured each over a counting time of 10 seconds. The spectrometer was then adjusted so that background

Element	Spectrometer Bragg Angle	Crystal	Standard	Wt % Element
Fe	57° 29'	LiF	Fe (element)	100.00
Si	31° 40'	RAP	Wollastonite	24.00
Al	37° 14'	RAP	Corundum	52.93
Mg	44° 30'	RAP	Periclase	60.31

LiF = Lithium fluoride

RAP = Rubidium acid phthalate

Table 6.8. Spectrometer angles, crystals and standard used in Electron Probe Microanalysis

counts could be recorded. With the spectrometer set at the angle used in recording peak counts from the standard, five peak and five background counts for a selected area of the specimen were then obtained in the same way. The standards used are listed in Table 6.8.

The counts for standards and samples were converted into weight per cent oxides using a computer program written by Dr. J. R. Ashworth. This corrected the results for dead-time, absorption, characteristic fluorescence, continuum fluorescence, backscattering and stopping power. The nature of these corrections is discussed in detail by Reed (1975). The weight per cent values of the elements in the standards used are also given in Table 6.8. Since chamosite is a hydrous mineral and the weight percent (OH) cannot be directly measured by the electron micro-probe this value is also estimated by the computer program on the basis of the ideal chamosite formula $(Fe, Mg, Al)_3(Si,Al)_2O_5(OH)_4$ (Brindley, 1951), and the measured weight percentages of Fe, Si, Al and Mg.

6.3.3 Results

When calculated as weight percent oxides, the component elements of chamosite should total 100%, taking (OH) into account. Individual analysis totals were, however, in all cases low, varying from a total of 50 weight per-cent oxides to 85 weight percent oxides. Occasional totals in excess of this were obtained. Repeated analyses of particular phases for elements in sufficient quantity to make up the excess. Scanning electron micro-scopy and transmission electron microscopy indicate that chamosite ooids in particular, and other chamosite phases to a lesser extent, are porous on a scale of less than 1 μm. Since the micro-probe electron beam has a diameter of 1 μm when focussed at the specimen surface, surficial

irregularities due to a porosity would result in a scattering of the generated X-rays (Reed, 1975). This, in turn, leads to low analytical totals. Defocussing of the microprobe beam failed to overcome this problem.

Recalculation of analytical results to a total of 100 weight percent yields results which are comparable to reported chamosite analyses. Recalculation assumes that the 'lost' counts are proportional to those which have been recorded in the same ratio for all elements analysed. This is not necessarily the case when analyses of a rough surface are being considered. An arbitary value for initial analytical totals of 80 weight percent has been chosen as the cut-off value below which recalculation would not yield meaningful results. As a result, no Cleveland chamosite analyses are reported. These gave analytical totals which were persistently less than 60 weight percent. Those totals greater than 80 weight percent are given in Table 6.9. Iron is calculated as FeO since, on the basis of Mössbauer work, it seems likely that chamosite was formed as a more or less entirely ferrous mineral. For comparison purposes, chamosite analyses by other workers are also reported.

The recalculated results are plotted on a triangular diagram with FeO, SiO_2 and Al_2O_3 as its apices (Figure 6.6). It is immediately apparent that, although there is no chemical distinction between textural varieties of chamosite, chamosite specimens from the Frodingham and Marlstone Rock-bed Ironstones have distinctly different compositions. Both have similar Al_2O_3 concentrations whereas the Marlstone chamosites are higher in FeO and lower in SiO_2 than the Frodingham chamosites. Both

Frodingham Ironstone

Wt % Oxide	(1)	(2)	(3)	(4)	(5)	(6)	(7)	(8)
SiO_2	27.739	28.995	30.184	29.381	29.534	28.700	28.956	28.843
Al_2O_3	14.981	16.115	16.739	16.443	15.618	15.947	15.728	16.215
FeO	41.175	41.462	37.985	39.097	41.342	40.155	41.621	40.001
MgO	5.445	2.711	4.142	4.221	2.772	4.423	2.994	4.153
H_2O	10.657	10.716	10.948	10.855	10.731	10.765	10.698	10.784

	(9)	(10)
SiO_2	29.035	28.045
Al_2O_3	14.833	16.113
FeO	40.664	39.702
MgO	4.097	5.371
H_2O	10.697	10.766

Brindley (1951)

SiO_2	24.90
Al_2O_3	15.60
FeO	35.0
Fe_2O_3	7.2
MgO	4.6
H_2O	12.30

(1)-(4) Chamosite ooid envelope; (5)-(6) Depositional chamosite mud; (7)-(10) Authigenic chamosite

Marlstone Rock-bed

Wt % Oxide	(1)	(2)	(3)	(4)	(5)	(6)	(7)	(8)
SiO_2	24.979	26.331	24.820	25.050	26.176	25.678	23.477	25.302
Al_2O_3	17.634	18.142	18.325	17.059	17.093	16.425	17.738	16.987
FeO	45.234	43.474	45.109	45.299	45.862	42.733	47.006	46.037
MgO	1.745	1.496	1.326	2.116	0.393	4.699	1.516	1.308
H_2O	10.405	10.619	10.420	10.474	10.474	10.473	10.261	10.364

	(9)	(10)	(11)	(12)	(13)	(14)	(15)
SiO_2	25.477	24.741	24.703	24.537	24.716	21.687	25.571
Al_2O_3	18.366	16.311	16.560	14.197	16.703	14.795	15.884
FeO	43.958	46.867	46.396	46.962	46.474	49.835	47.481
MgO	1.692	1.604	1.866	3.107	1.631	3.206	0.588
H_2O	10.502	10.474	10.473	10.474	10.473	10.473	10.474

(1)-(6) Chamosite core books; (7)-(15) Chamosite ooid envelopes

Table 6.9. Electron Probe Microanalyses of chamosite phases. Recalculated to 100 wt %.

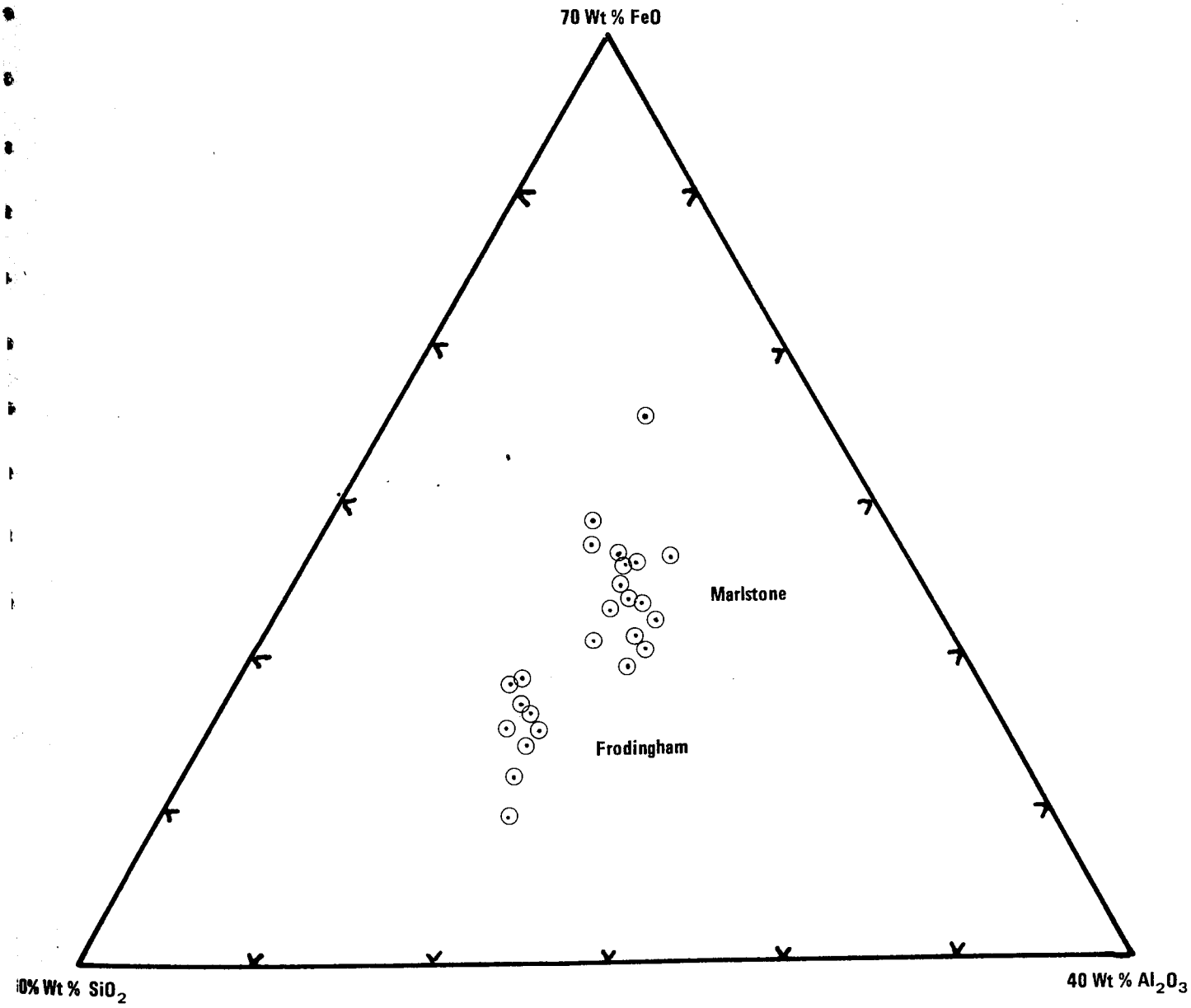

Fig 6.6 : Triangular plot of analyses of Frodingham and Marlstone Chamosite phases

groups of analyses suggest a trend from FeO-rich to SiO_2-rich types which corresponds to increasing Al_2O_3 concentrations.

6.4 MÖSSBAUER SPECTRA STUDIES

6.4.1 Production of Spectra

The decay of the radioisotope Co^{57} results in the formation of the stable isotope Fe^{57}. The decay releases gamma radiation of various energies as the decaying Co^{57} atoms pass through various excited states of Fe^{57}. The 14.4 KeV radiation emitted when the first excited state of Fe^{57} passes to the ground state of Fe^{57} is used in the Mössbauer experiment. This radiation is emitted without recoil, i.e. loss of energy in the atomic framework, and may be absorbed resonantly without recoil by Fe^{57} atoms in a solid absorber such as a mineral. Since Fe^{57} has an approximately 2% natural abundance, the Mössbauer effect can be utilised in understanding features of minerals containing iron which cannot be resolved by other methods. This is because the precise energy at which absorption occurs and the nature of the absorption is dependent on the environment of the Fe^{57} nucleus and hence the oxidation state, coordination etc., of iron in the mineral.

In order to study absorption effects a range of energies must be provided by the experimental system. The schematics of the system are illustrated in Figure 6.7. The source is vibrated, thus producing a range of velocities by the Doppler effect. The mineral absorber is mounted in front of the

source and a γ-ray detector lies on the other side. As the source is swept through a range of velocities the counts recorded by the detector pass into a range of counting cells in the multichannel analyser. The spectrum which is produced by the system is a plot of gamma-ray energies expressed as source velocity (mms-1) against absorption.

In the work reported here, a Co^{57} source in a palladium matrix was used. The samples used were taken from the material prepared for X-ray study with the exception of sample EH ooids which was obtained by concentrating a large number of ooids from a Marlstone hand specimen and crushing them in an agate pestle and mortar. Each sample was set in a hole of 2 cm diameter cut in a piece of card. It was retained by sticky tape on one side and aluminium foil sealed to the card with vacuum grease on the other. Mössbauer spectra were obtained using a conventional constant acceleration spectrometer (Harwell Scientific Services). The spectra were accumulated over a counting time of 24 hours at room temperature and iron foil was used to calibrate the spectrometer.

6.4.2 Interpretation of Spectra

Four examples of the chamosite spectra obtained are shown in Figure 6.8. It is immediately apparent that the initial, unresolved spectra are rather complicated. The spectra that result from Fe^{57} nuclei in different electronic environments are well known. If the environment is spherically symmetrical one peak is obtained the position of which will probably be displaced from the zero point (0.0 mm sec^{-1}) on the scale taken here as the centre of gravity of an iron foil spectrum. This displacement (in mm sec^{-1}) is the isomer shift. Non-spherically symmetrical sites or distorted coordination sites result in a split in the excited state

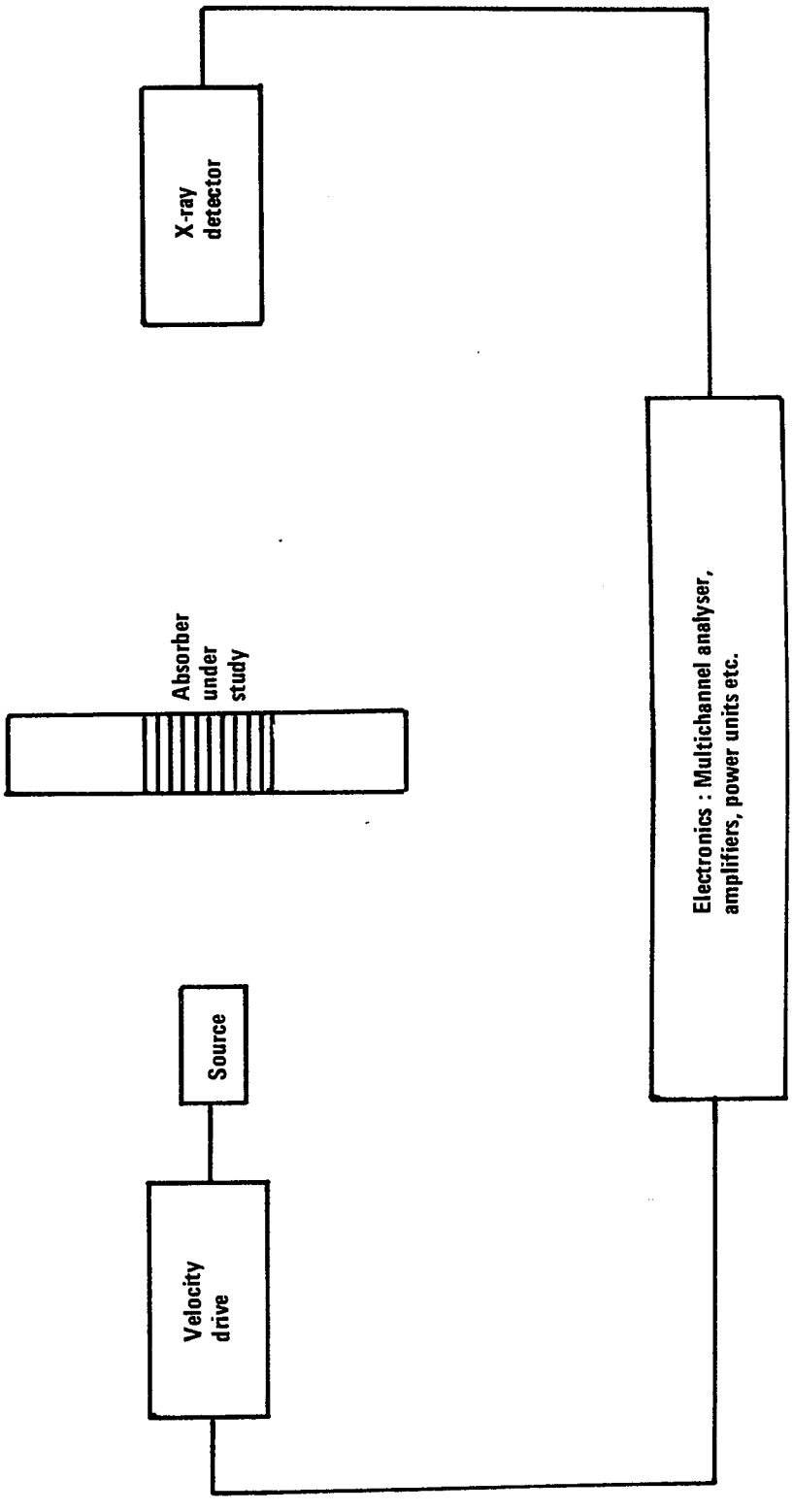

Fig 6.7 Mossbauer Apparatus (Schematic). (Vaughan and Craig, 1978)

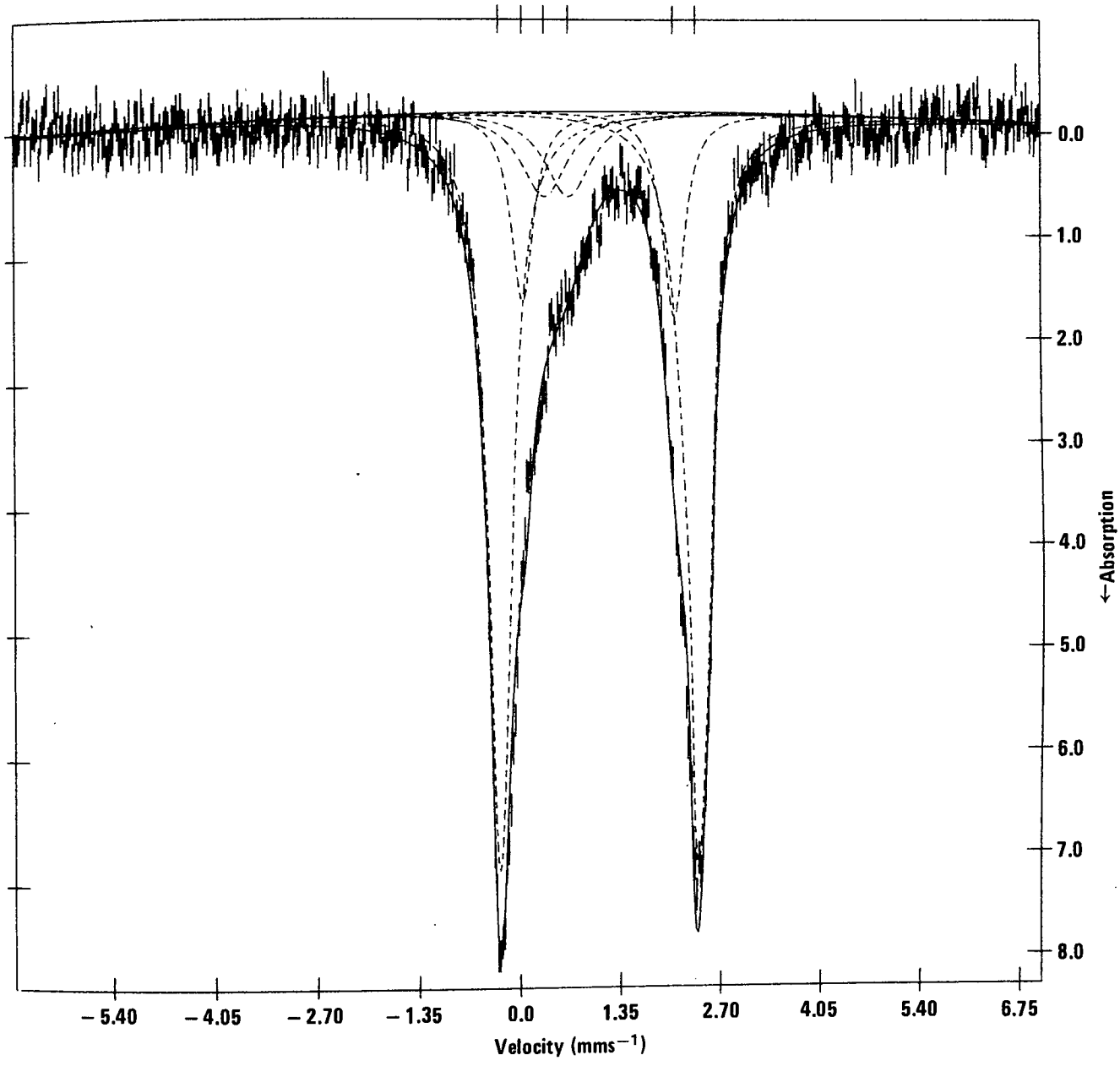

Fig 6.8a Specimen B18; M1 > M2

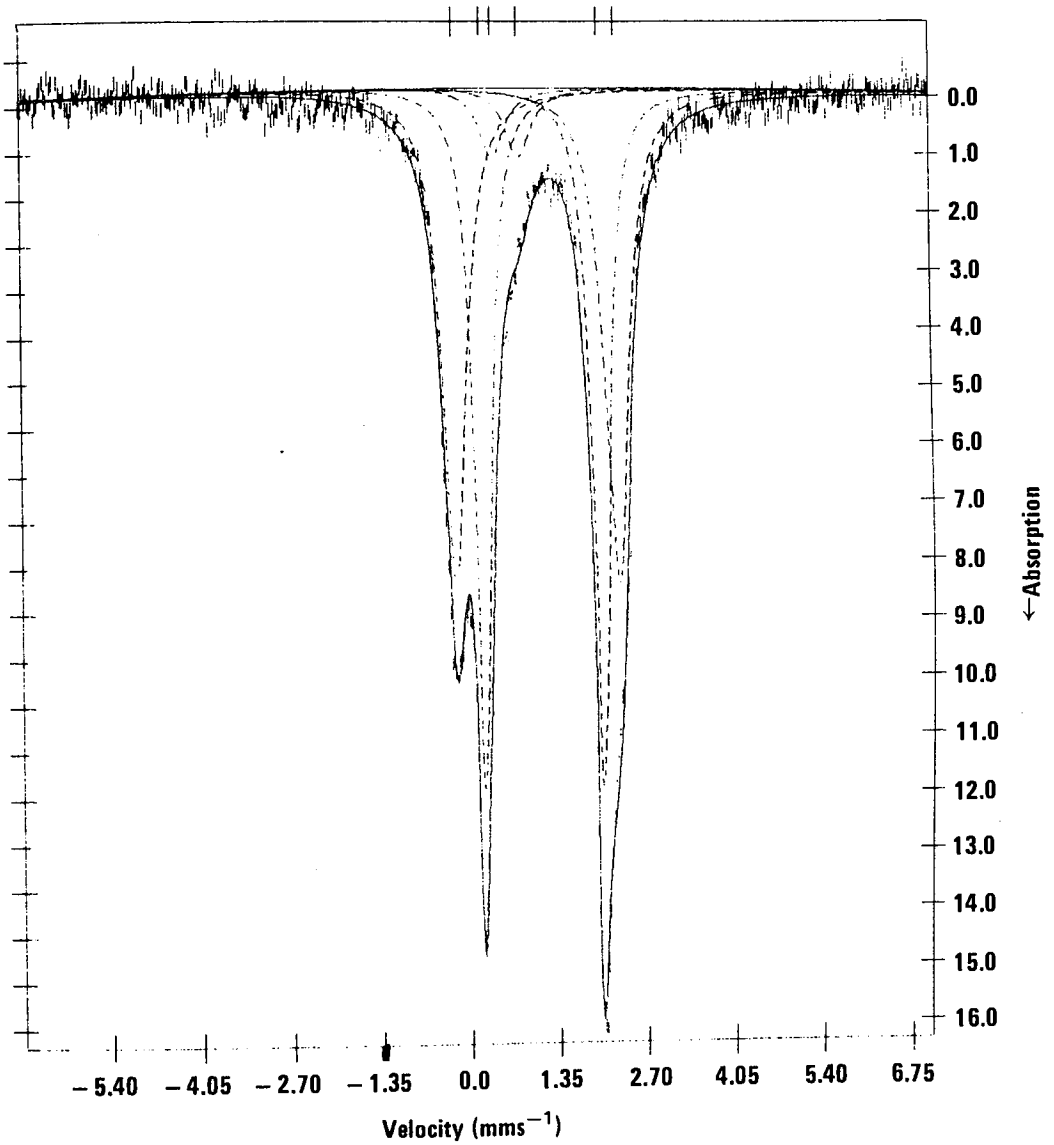

Fig 6.8b Specimen B17; M2 > M1

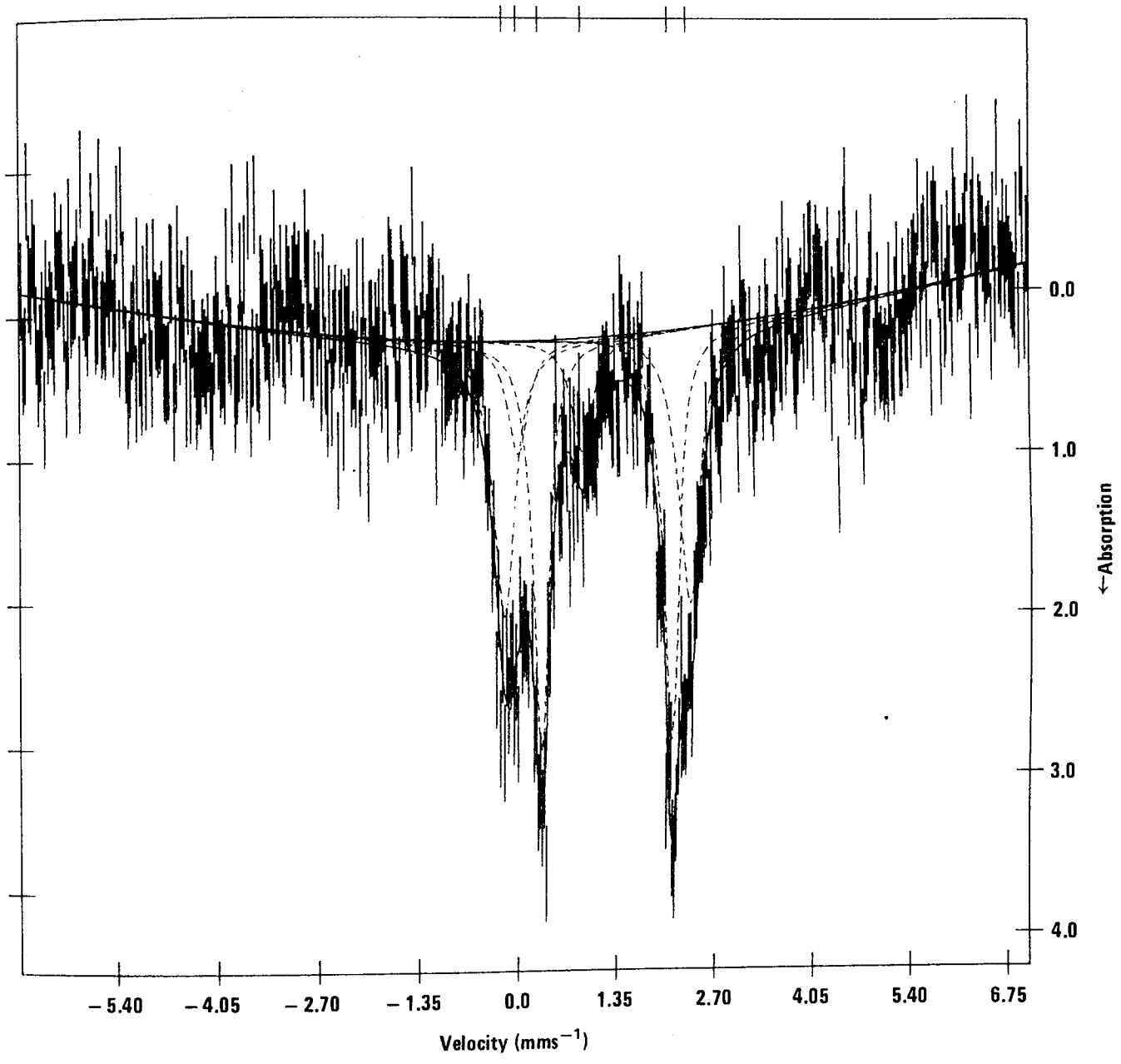

Fig 6.8c Specimen Y3; M2 > M1

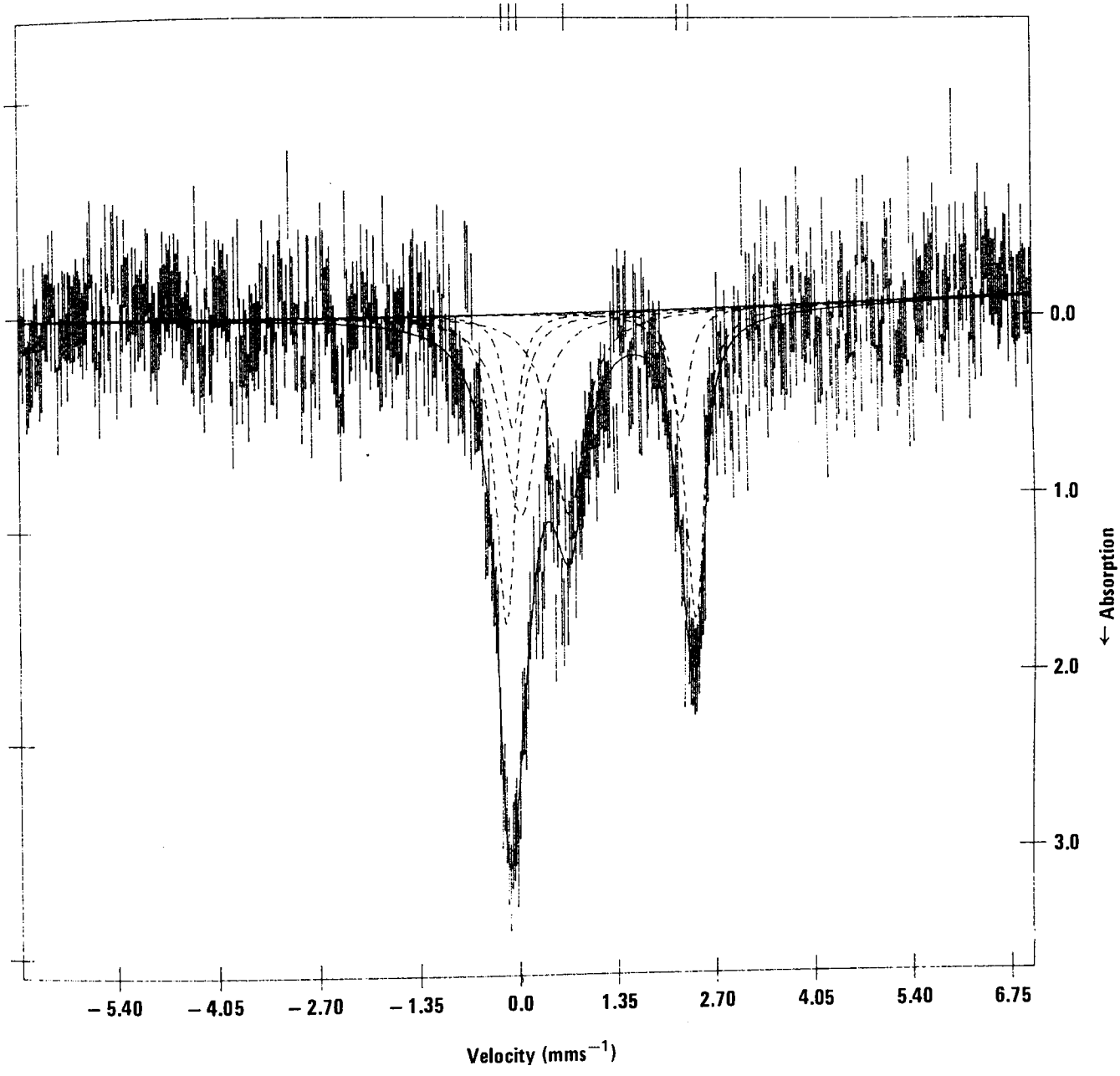

Fig 6.8d Specimen W122; M1 > M2

energy level which produces a two peak spectrum. The separation between peaks is termed the quadrupole splitting and the distance of their mid-point from 0.0 mms^{-1} is again the isomer shift. Magnetic ordering of Fe^{57} atoms produces further splitting in the energy levels which then results in a six peak spectrum. Such spectra are characteristic of goethite, magnetite and haematite. The presence of Fe^{57} nuclei in more than one type of site will clearly cause a multiplication of the peaks observed. The chamosite spectra are not characteristic of magnetically ordered material but show evidence of two or more sites characterised by quadrupole splitting.

In order to analyse the experimentally determined spectra, computer fitting is necessary. A program based on that written by Stone (in Bancroft et al, 1967) was used to fit Lorentzian curves to the spectra. These curves are used since Mössbauer peaks are essentially Lorentzian in shape. The method of resolving the component peaks involves fitting pairs of peaks or doublets with various constraints to the spectra. The constraints retain the peaks of a doublet to be equal in intensity, half-widths (width at half peak amplitude) and position relative to their mid-point. These constraints are required as the two peaks of a doublet should be mirror images for a randomly oriented powder sample. The computer program computes the resultant curve to the fitted doublets and makes adjustments to these doublets in order to obtain a line of best-fit to the spectra. The best-fit is attained when the χ^2 value approaches the number of degrees of freedom. χ^2 is the sum of the squares of the deviations from the line of best-fit divided by the variance of a single channel which is a constant for any given spectrum. The number of degrees of freedom

is the total number of counting channels used in the computation less the number of constraints less one.

Computer processing of the chamosite spectra showed that each is composed of two large doublets and one small doublet (Figure 6.8). The quadrupole splitting, isomer shift and half-width values which define each of these doublets in each sample are reported in Table 6.10. The χ^2 value and the number of degrees of freedom for each sample are also given. The χ^2 values are rather higher than the number of degrees of freedom. There are three possible reasons for this: a) The samples represent different textural phases of chamosite such as authigenic and depositional chamosite which might have slightly different Mössbauer spectra, b) it is impossible to fit one Lorentzian peak to two very similar Lorentzian peaks (Bancroft et al, 1967), and c) impurities such as ferroan calcite, siderite and pyrite, although forming a low proportion of the sample, as indicated by microscopic examination, would contribute to the overall spectra due to their iron content. It is not possible to resolve components which form less than 5% of the total spectrum (Bancroft et al, 1967). For comparison purposes, the data published by Yershova et al (1975) and Goodman and Bain (1978) are included in Table 6.10.

In addition to providing information on structural sites, Mössbauer spectra can be used for site population studies. This is due to the fact that the sum of the areas of the component peaks of a doublet is approximately equal to the number of iron atoms present in the site represented by the doublet. Bancroft (1973) has discussed the assumptions and sources of error made in estimating iron from component Lorentzian peaks and concludes that for spectra in which the standard deviation in the peak

areas is less than 10%, the iron content of different sites in a given sample can be obtained to an accuracy ± 5% better than other determinative methods. Table 6.11 gives the areas for the three doublets recorded from each specimen, the Fe^{3+}:Fe^{2+} ratios for the spectra and the standard deviations in the peak areas.

6.4.3 Results

The identification of three doublets in each chamosite spectrum indicates that iron is present in three different forms (sites and/or oxidation states) in the mineral. Bancroft (1973) has summarised diagramatically the data for ferrous and ferric iron in different site coordination in silicate minerals. These diagrams have been adapted to show isomer shift values relative to an iron foil standard and are shown in Figure 6.9 with the ranges of the chamosite data for the three different doublets. Bancroft et al (1967) note that the isomer shift data are most useful for the identification of Fe^{2+}, Fe^{3+} and structural positions as they cluster in distinct groups as opposed to the data for quadrupole splitting. From Figure 6.9 it can be seen that doublets 1 and 2 correspond to isomer shift values for Fe^{2+} in octahedral coordination and that doublet 3 matches almost exactly the range of values for Fe^{3+} in the same coordination. Brindley (1951) has suggested that Fe^{2+} and Fe^{3+} occur in octahedral coordination in chamosite. The results of Mössbauer spectroscopy suggest that at least two octahedral sites, M1 and M2 characterise chamosite, thus supporting the work of Brindley (1951). The number of possible sites for iron is restricted to two, corresponding to the two ferrous doublets M1 and M2. Ferric iron presumably substitutes for ferrous iron in either M1 or M2. These results agree with the conclusions of Yershova et al (1975) which were based on lateritic chamosite material.

Specimen	Quadrupole splitting			Isomer shift			Half-Widths			Degrees of freedom	χ^2
Doublet:	1 (M1)	2 (M2)	3 (Fe^{3+})	1	2	3	1	2	3		
FRODINGHAM											
B17	2.389	1.735	0.390	0.985	1.069	0.568	0.417	0.282	0.460	497	638.80
B18	2.574	1.973	0.312	1.043	1.049	0.509	0.356	0.346	0.731	499	691.22
B20	2.345	1.727	0.260	1.063	1.173	0.579	0.271	0.434	0.554	496	813.09
B22	2.365	1.712	0.260	1.060	1.168	0.524	0.431	0.233	0.770	496	893.00
B23	2.430	1.711	0.652	1.065	1.176	0.328	0.385	0.279	0.419	496	535.62
Y1	2.538	1.890	0.405	1.083	1.106	0.587	0.353	0.378	0.747	497	969.86
Y7B	2.268	1.863	0.108	1.082	1.057	0.333	0.259	0.535	0.183	499	755.15
W122	2.565	2.295	0.646	1.066	1.187	0.439	0.321	0.291	0.551	498	508.82
Y3	2.533	1.775	0.883	0.931	1.212	0.297	0.352	0.254	0.339	495	565.09
CLEVELAND											
C14	2.600	2.097	0.520	1.081	1.062	0.322	0.288	0.304	0.522	500	695.36
BB3	2.430	1.880	0.407	1.079	1.051	0.310	0.279	0.350	0.505	500	660.54
MARLSTONE											
N7 mst	2.499	1.862	0.343	1.123	1.216	0.552	0.485	0.356	0.475	244	660.54
EH ooids	2.410	1.710	0.671	1.079	1.095	0.560	0.300	0.302	0.650	243	323.86
Yershova et al (1975)	2.620	2.270	0.810	1.060	1.090	0.140	0.200	0.200	0.200		
Goodman and Bain (1978)	2.71	2.42	0.61	1.13	1.12	0.37	0.28	0.39	0.41		

Table 6.10. Mössbauer data for chamosite

Specimen	Doublet 1 (M1)	SD (%)	Doublet 2 (M2)	SD (%)	Doublet 3 (Fe^{3+})	SD (%)	$Fe^{3+}:Fe^{2+}$
B17	47.70	0.75	45.230	0.80	7.35	1.60	1:12.603
B18	67.93	1.30	16.50	0.93	15.56	1.80	1:5.425
B20	3.12	1.30	79.17	0.93	17.69	3.20	1:9.084
B22	53.25	0.80	28.11	1.08	18.63	1.65	1:4.367
B23	41.86	0.90	23.83	1.12	34.30	0.80	1:3.195
Y1	51.84	1.10	22.24	0.99	25.91	2.0	1:2.085
Y7B	23.93	0.98	68.72	1.09	7.34	1.50	1:12.619
W122	40.91	0.86	13.58	0.90	45.50	1.71	1:1.197
Y3	16.04	0.75	43.54	0.92	16.04	1.70	1:5.230
C14	73.22	0.85	14.78	4.5	11.99	3.24	1:7.337
BB3	70.69	0.77	15.45	1.10	11.80	2.13	1:7.300
N7 mst	53.88	0.89	34.95	1.20	11.16	0.99	1:7.955
EH ooids	43.90	2.70	24.40	1.50	31.68	1.62	1:2.156

Table 6.11. Site population data

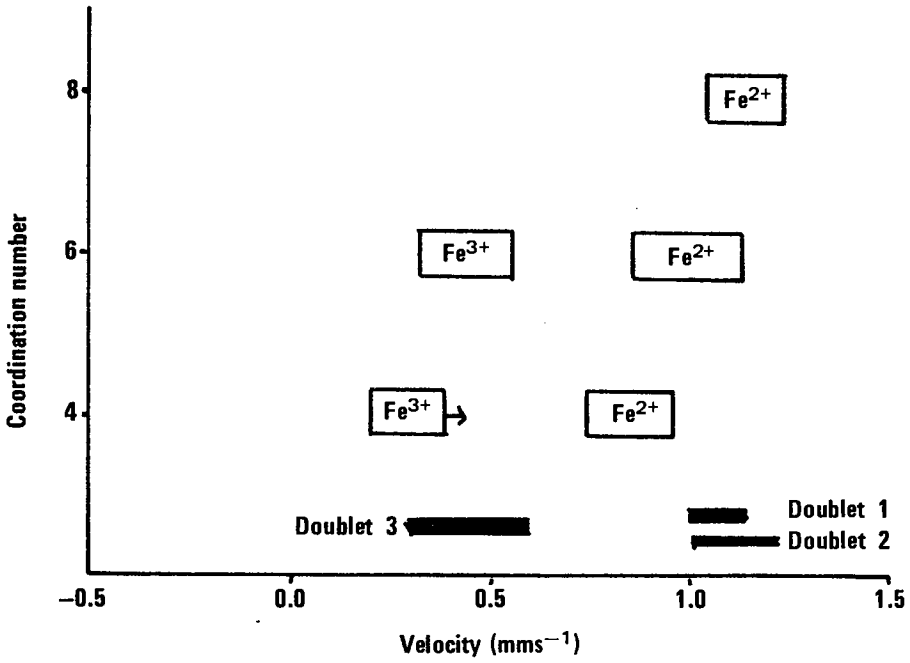

Isomer shift for Fe^{2+} and Fe^{3+} in 4,6, and 8 coordination

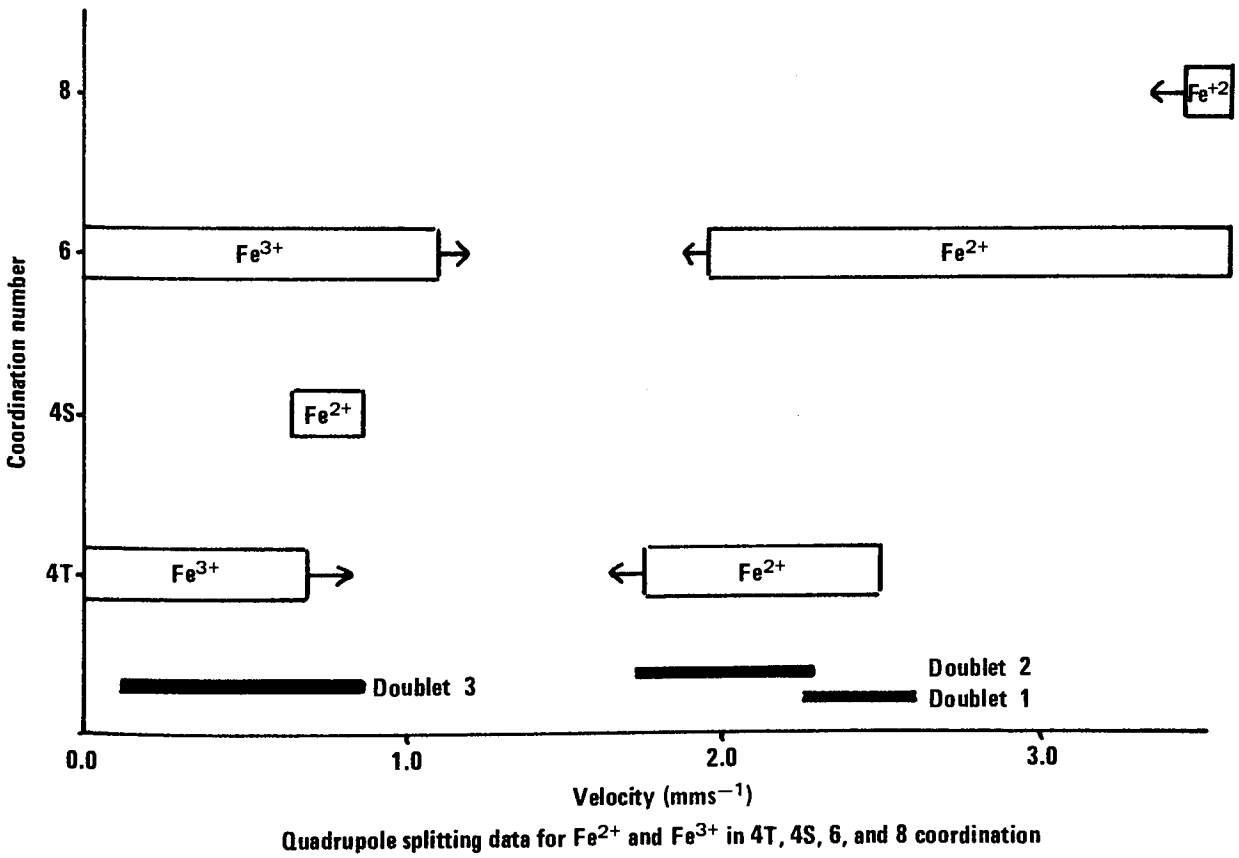

Quadrupole splitting data for Fe^{2+} and Fe^{3+} in 4T, 4S, 6, and 8 coordination

Fig 6.9 Isomer shift and quadrupole splitting data for Fe^{2+}, Fe^{3+} in different coordination sites and in chamosite. Adapted from Bancroft (1973). Arrows indicate that values outside boxes have been observed.

Consideration of the amount of iron in each site (Table 6.11) shows that the samples may be subdivided into chamosites in which Fe^{2+} (M1) is greater than Fe^{2+} (M2) and those in which Fe^{2+} (M2) is greater than Fe^{2+} (M1). One sample (B17) represents a point half-way between these alternatives as approximately equal amounts of iron are present in both M1 and M2. In comparison to the Fe^{2+} content of M1 and M2 Fe^{3+} does not show any noticeable variation. When the Fe^{3+}:total Fe^{2+} ratio is considered, however, it is immediately apparent that the former group (M1 > M2) is characterised by ratios from 1:1.197 to 1:7.955 and the latter group (M2 > M1) by ratios from 1:9.084 to 1:12.603. If it is assumed that chamosite was formed initially as a more or less entirely ferrous compound and was subsequently transported in an oxidising environment, a certain amount of ferrous iron would be oxidised to ferric iron. The most Fe^{2+} rich group has an intense inner ferrous doublet whereas the group with higher Fe^{3+} has an intense outer ferrous doublet and a relatively more intense ferric doublet. It seems difficult to escape the conclusion that under conditions of environmental oxidation, ferrous iron in the M2 octahedral site is most easily oxidised to ferric iron. It follows from this that much of the Fe^{3+} would be located in the M2 site. Oxidation of Fe^{2+} in the M1 site might be expected to occur yielding Fe^{3+} in the M1 site also. It was not possible to resolve the ferric doublet into two component doublets. This would suggest that any Fe^{3+} in the M1 site contributed less than 5% to the entire spectrum.

Bancroft (1973) has shown that in minerals containing Fe^{3+} in octahedral sites, the quadrupole splitting is due entirely to the distortion of the sites from octahedral symmetry. Thus, as Fe^{3+}

increases, the distortion and hence the quadrupole splitting increase. Figure 6.10 plots quadrupole splitting for Fe^{3+} against the Fe^{3+}:Fe^{2+} ratio. A very small octahedral distortion due to the absence of Fe^{3+} and the presence of Fe^{2+} results in a large quadrupole splitting but this diminishes as the content of Fe^{3+}, and hence the site distortion, increases. The quadrupole splitting for M1 and M2 is therefore also plotted on Figure 6.10. It is clear that as the Fe^{3+} content increases (Figure 6.10) so does the quadrupole splitting for the ferric doublet. The M2 quadrupole splitting shows a degree of variation which perhaps suggests a decrease in this value with increasing Fe^{3+}. The M1 quadrupole splitting values are scattered to either side of a constant mean value. If M2 Fe^{2+} was being oxidised to Fe^{3+} this is the variation which would be expected. The absence of any variation with Fe^{3+} in the M1 values tends to support the suggestion of only a very minor amount of oxidation possibly occurring in this site.

Yershova et al (1975) discuss the Mössbauer spectra obtained for chamosite at room temperature and after heating to 350 C and 400 C. The room temperature spectrum was characterised by an intense M1 doublet, a less intense M2 doublet and an Fe^{3+} doublet. The 350 C spectrum indicated that the oxidation brought about by heating caused a diminution in the intensity of M1, so that M2 became the most intense Fe^{2+} doublet, and an increase in the intensity of the Fe^{3+} doublet. The 400 C spectrum comprised two Fe^{3+} doublets whose areas were in the same proportions as the Fe^{2+} populations at room temperature. These results led Yershova et al (1975) to conclude that Fe^{2+} in M1 was more easily oxidised than the Fe^{2+} in M2. This is an interesting result since under conditions of environmental oxidation M2 Fe^{2+} appears to be more easily oxidised. There is one exception to

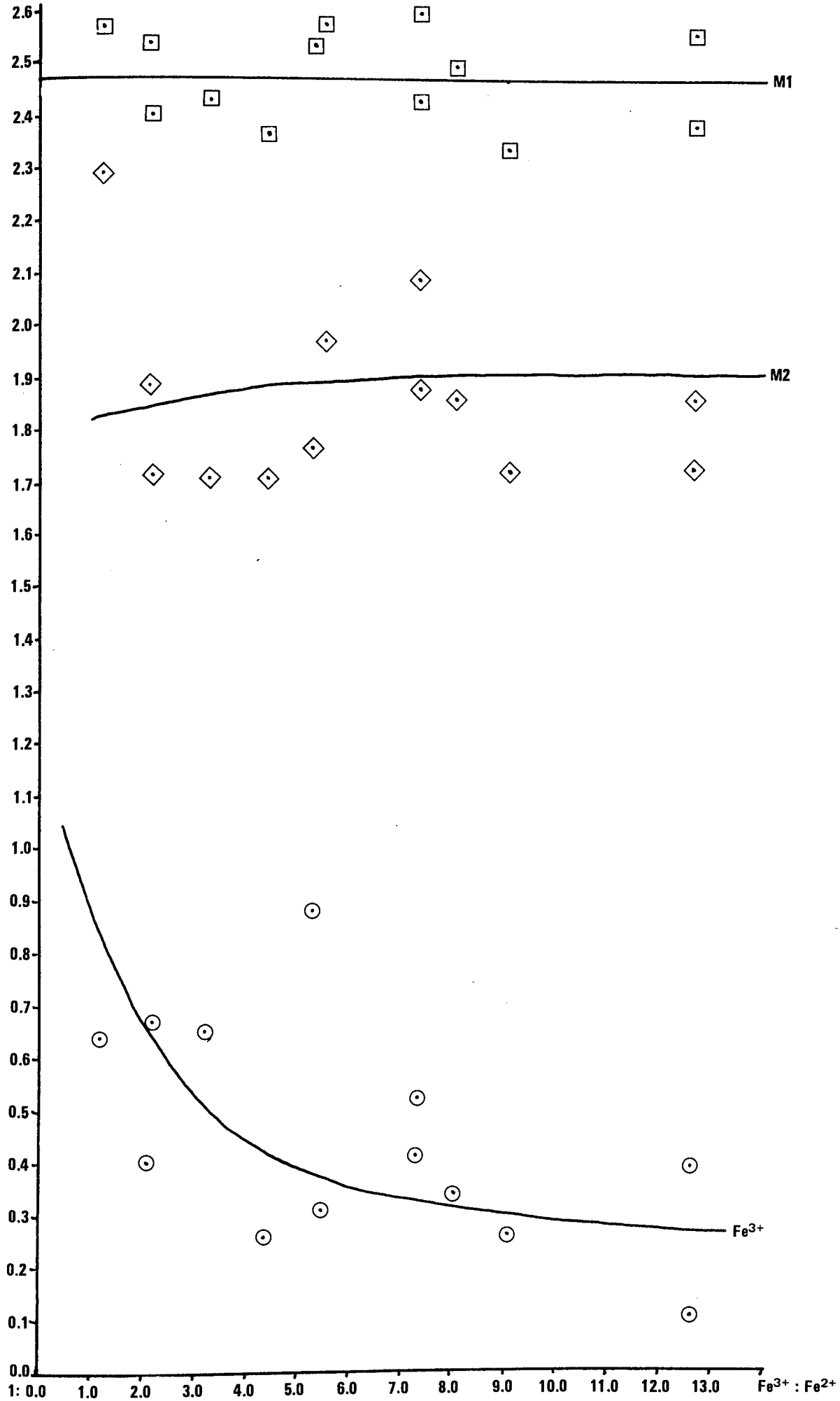

Fig 6.10 Quadrupole splitting v Fe^{3+} : Fe^{2+}

Lines indicate approximate trends in quadrupole splitting

the data in Table 6.10 and Table 6.11. This is that of sample Y3, a red chamosite mudstone. The ferrous iron populations are greater for M2 than M1 and yet the specimen has a ratio of 1:5.23 for Fe^{3+}:Fe^{2+}. This is a rather strange combination of site populations in comparison to those of either group M1 > M2 or M2 > M1. The populations for this sample do, however, compare with those reported by Yershova et al (1975) for chamosite of the type M1 > M2 after heating at 350 C. It is not suggested that Y3 was heated to this temperature, but it is thought to differ from the other samples in the way that it was oxidised. Y3 was collected from a red oolite horizon thought to represent a period of subaerial exposure whereas the others were collected from entirely marine deposits. The major difference between the samples, then, is that Y3 was oxidised in an essentially dry environment whereas the others underwent oxidation in oxygenated water. It is concluded, therefore, that the nature of the oxidising environment may play an important role in determining whether oxidation of M1 or M2 Fe^{2+} occurs. A selection of different chamosite spectra is given in Figure 6.8.

6.5 CONSIDERATION OF X-RAY, ELECTRON PROBE MICROANALYSIS AND MÖSSBAUER DATA

6.5.1 X-ray and Mössbauer Data

It was concluded in Section 6.2 that the variations in cell parameters appear to result from the degree of oxidation which the chamosite specimens have undergone. The Fe^{3+}:Fe^{2+} ratios of specimens for which Mössbauer spectra were prepared indicate, with the exception of

specimen Y1, that large cell parameters correspond to low Fe^{3+} material and small cell parameters to high Fe^{3+} material. Specimen Y1 is excluded from the following discussion as it appears to be anomalous with respect to the rest of the data.

The Mössbauer data show a considerable variation in the Fe^{3+} quadrupole splitting values. It seems likely that this might be related to variation in chamosite cell parameters, as quadrupole splitting, in this instance, is related to a distortion of the octahedral sites. A plot of c-parameters against Fe^{3+}:Fe^{2+} and quadrupole splitting values for Fe^{3+} (Figure 6.11) shows that there is no variation as a function of the iron content of the samples. A plot of the b-parameters against the iron-dependent values (Figure 6.12) shows a spread of data points in two opposing directions: as the Fe^{3+}:Fe^{2+} ratio becomes more Fe^{2+}-rich, the b-cell parameter increases, and as the quadrupole splitting value increases, the b-parameter diminishes. Since the quadrupole splitting increases with Fe^{3+} and the high Fe^{3+}:Fe^{2+} ratios lie to the left of the diagram these two variations are the same. They indicate that as the Fe^{3+} increases, the distortion of the octahedral sites increases, and as a result the b-cell parameter diminishes. Brindley and Youell (1953) have suggested a structure for chamosite which is illustrated In Figure 6.13. Since the b-cell parameter contracts markedly with increasing Fe^{3+}, whereas the c-cell parameter remains approximately constant, it is evident that the site distortion has its greatest effect between the octahedral sites (Figure 6.13), presumably bringing about a bond-length contraction. The more Fe^{3+} within the octahedral sites the greater the bond length contraction will be, and hence the smaller the b-parameter.

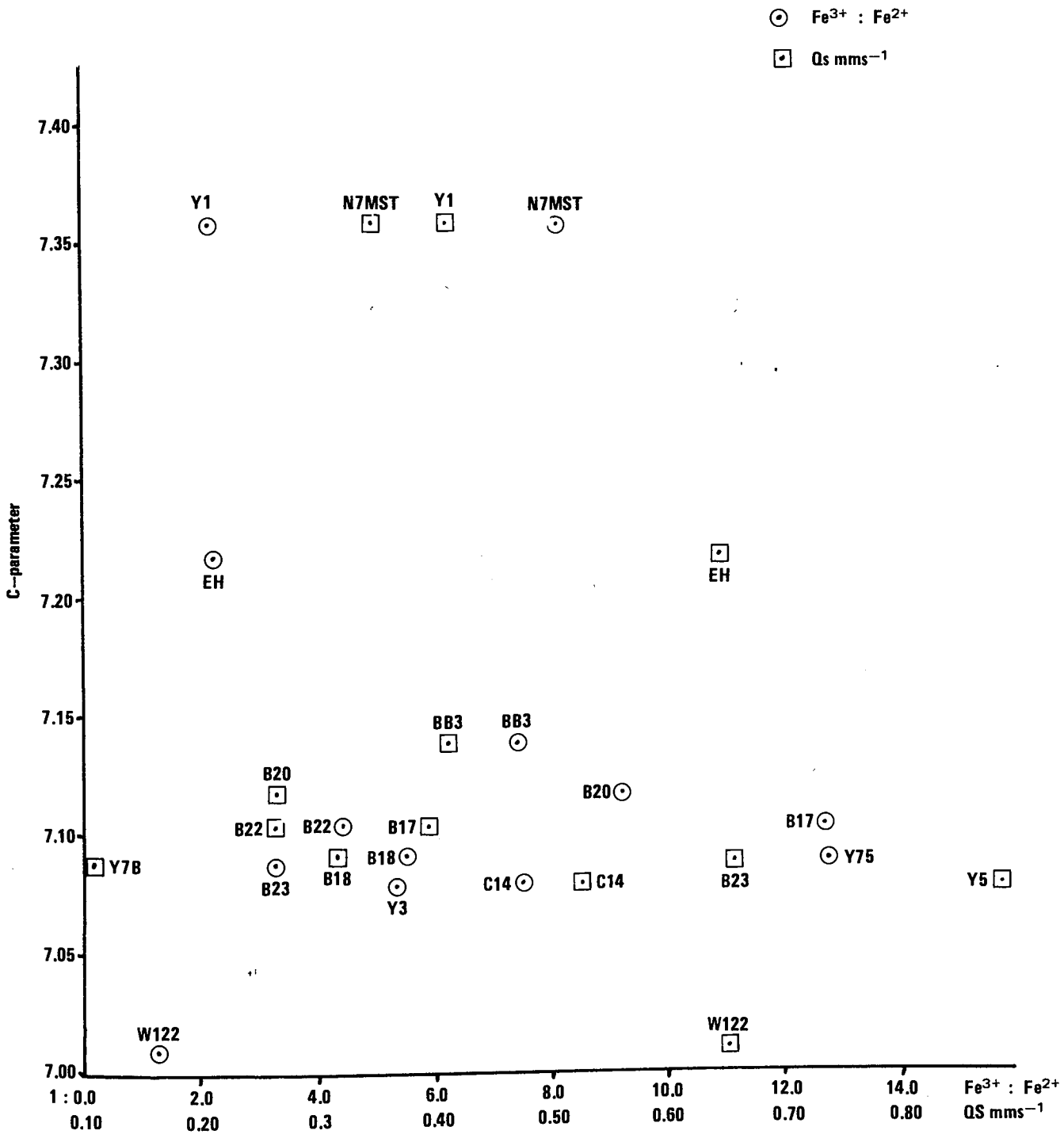

Fig 6.11 C–parameters v Fe^{3+} : Fe^{2+} and quadrupole-splitting values

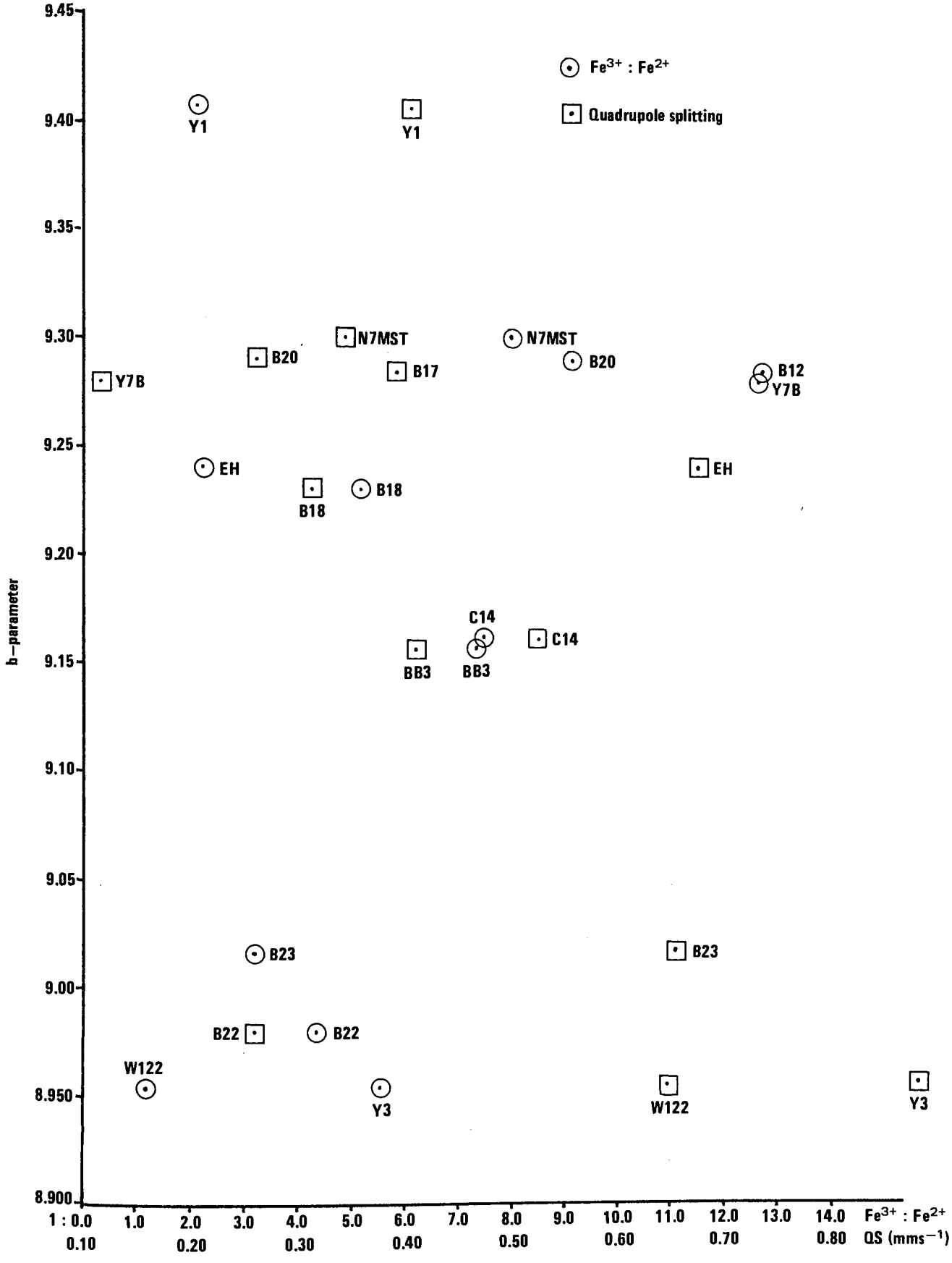

Fig 6.12 b–parameter v Fe^{3+} : Fe^{2+} and quadrupole splitting values

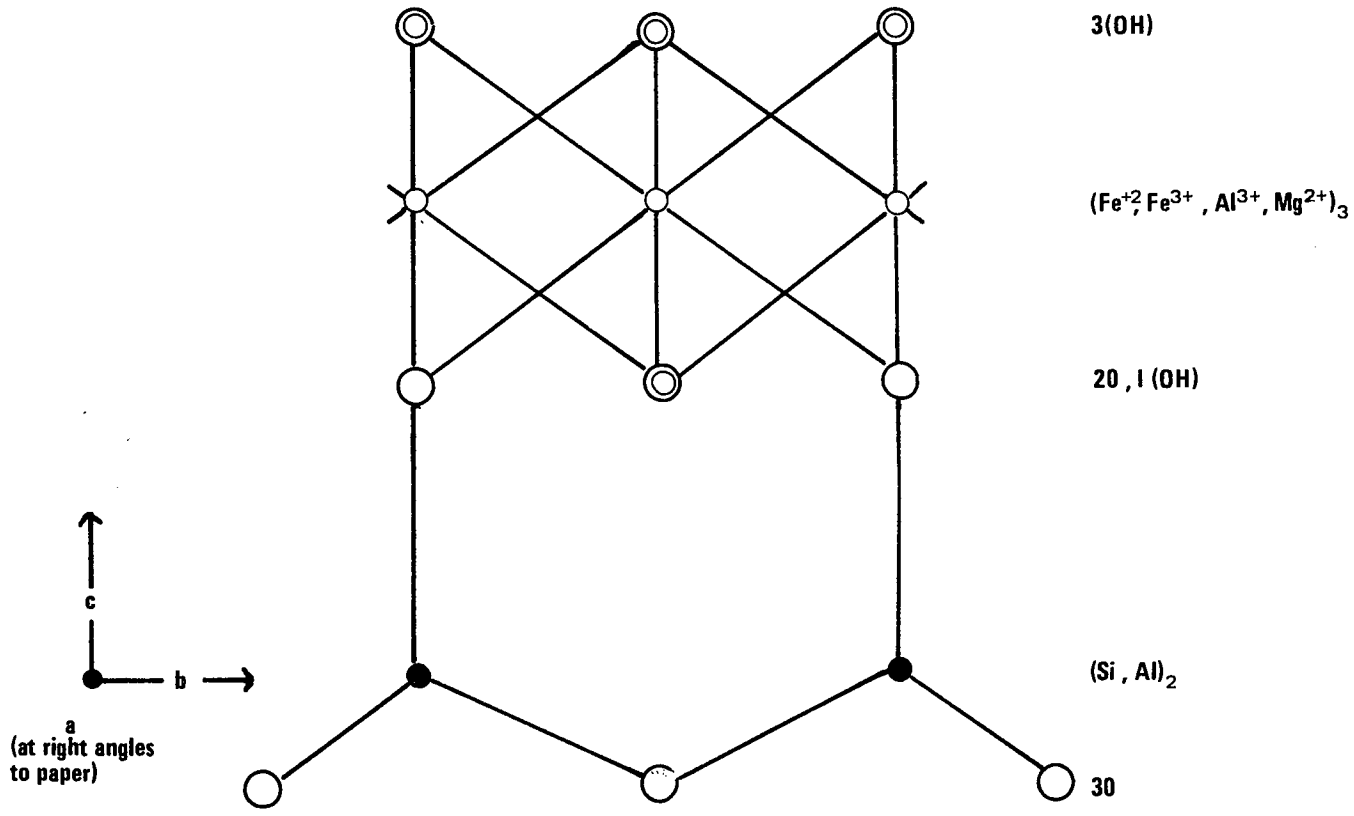

Fig 6.13 Proposed chamosite structure (Brindley & Youell, 1953)

A feature of the X-ray data is the c-parameter separation of the Marlstone data points and specimen Y1 from the Frodingham and Cleveland data. It was noted in the electron probe microanalysis discussion that the Marlstone chamosites are richer in SiO_2 than the Frodingham material and that both contain similar levels of Al_2O_3. The SiO_2 must all be located in the tetrahedral sites, thus the octahedral sites will be higher in Al_2O_3 in Marlstone chamosite than in Frodingham chamosite. The presence of relatively more Al^{3+} in the octahedral sites must, therefore, be a causative factor in creating c-cell parameters greater than those observed in the Frodingham and Cleveland specimens. By analogy with the site distortion caused by the presence of Fe^{3+}, Al^{3+}, which has an ionic radius of 0.57 Å in comparison to 0.67 Å for Fe^{3+}, would be expected to bring about a similar distortion. Clearly, the effects of oxidation of ferrous iron to ferric iron on the octahedral sites will be overprinted on the Al^{3+} distortion.

6.6 CONCLUSIONS

A number of conclusions may be drawn regarding the mineralogy of chamosite. These are as follows:

(1) Electron probe microanalysis indicates that chamosite specimens from the Marlstone Rock-bed Ironstone contain more SiO_2 than those of the Frodingham Ironstone. The FeO and Al_2O_3 content of chamosite from these deposits is similar but each deposit shows a variation from FeO-rich to Al_2O_3-rich varieties. There is no apparent differentiation in

FeO and Al_2O_3 between different structural varieties of chamosite, i.e. ooid envelopes, core books, depositional chamosite mud and authigenic chamosite pore-linings. Due to the poor quality of E.P.M.A. analytical results it has not been thought worthwhile to compare these data with Mössbauer data and obtain structural formulae for the different chamosite phases in which total iron was distributed between FeO and Fe_2O_3.

(2) Studies of Mössbauer spectra of chamosite show that there is a variation between Fe^{2+}-rich and Fe^{3+}-rich varieties. Chamosite specimens derived from chamositic chamosite oolites, which are thought to represent the site of chamosite ooid formation, exhibit M2 sites with Fe^{2+} populations greater than those in the M1 site. A small amount of Fe^{3+} is present. Subsequent oxidation in the aqueous environment results in the oxidation of M2 Fe^{2+} to Fe^{3+} which will be retained in the M2 site. The relative intensity of M1 Fe^{2+} doublets therefore increases. The production of M2 Fe^{3+} causes a distortion of the octahedral site. Increasing M2 Fe^{3+} populations and decreasing M2 Fe^{2+} populations reflect this in an increase and a decrease in quadrupole splitting values for these ions. Heating chamosite results in the oxidation of M1 Fe^{2+} to M1 Fe^{3+} (Yershova et al, 1975). A similar process i.e. dry, subaerial oxidation is thought to result in the type of spectra shown by Y3.

(3) X-ray data for chamosite specimens from different sources show a variation in the b-cell parameter relative to the c-cell parameter. Considered in context of the nature of the chamosite sources, some Fe^{3+}: Fe^{2+} ratios, and the evidence of heating, it appears that this variation represents a cell contraction due to environmental oxidation of Fe^{2+} to

Fe^{3+}. When these conclusions are considered in context of the results of Mössbauer spectroscopy, however, it becomes apparent that two groups of X-ray data are present; the Frodingham and Cleveland group and the Marlstone group. The variation in the b-parameter of both groups was attributed to a distortion of the octahedral sites due to the presence of varying amounts of Fe^{3+}. The c-parameters of each group were approximately constant but noticeably different for each group. This is attributed to the larger proportion of SiO_2 in the Marlstone which in turn causes an increase in Al_2O_3 in the octahedral sites. It is concluded that, providing the chemistry of a particular sample is known, calculation of the b-parameter will give an estimation of the amount of Fe^{3+} present. This, in turn, is related to the degree of environmental oxidation which the chamosite specimen has undergone. The variation in cell parameters is not, therefore, considered to represent order-disorder due to the presence of orthohexagonal and monoclinic cells (Brindley, 1951; Youell, 1955).

(4) The effect of the heating of chamosite on X-ray and Mössbauer data has been considered as this represents an alternative method of oxidation. Brindley and Youell (1953) showed that after heating at 400 C the cell parameters of the initial chamosite were reduced. A similar study resulted in the same conclusions except that one sample which was already extremely rich in Fe^{3+} (W122) did not change. Brindley and Youell (1953) concluded that the heating not only oxidised the Fe^{2+} present to Fe^{3+} but also dehydrated the mineral so that the (OH) group concentration was reduced from four to one per unit cell. Yershova et al (1975) discussed Mössbauer spectra for chamosite heated to 350 C and 400 C.

They concluded that M1 Fe^{2+} was initially oxidised and that in the interval 350 C - 400 C the M2 Fe^{2+} was oxidised. This created a two doublet spectrum of M1 Fe^{3+} and M2 Fe^{3+}. Clearly, the ferric chamosite formed by heating at 400 C is very different in nature from normal room temperature chamosite and should be considered as an artificial mineral. Brindley (1951) concluded that it was possible for chamosite to have two end-member structural formulae; $Fe_3^{2+}Si_2O_5(OH)_4$ and $Fe_2^{3+}Si_2O_5(OH)_4$. Since the Mössbauer spectra of chamosite heated at 350 C and chamosite oxidised by subaerial exposure have similar spectra to unheated chamosite it is thought likely that the ferric chamosite formula of Brindley (1951) is the correct formula for chamosite oxidised under these conditions. Chamosite with a high proportion of Fe^{3+} in either M1 or M2 would be expected to be more stable under fairly rigorous oxidation conditions i.e. heating at 400 C. This may explain why the cell parameters of W122 (Fe^{3+}:Fe^{2+} = 1:1.197) did not change on heating.

CHAPTER 7

PALAEOMAGNETIC STUDIES OF THE FRODINGHAM, MARLSTONE ROCK-BED AND CLEVELAND IRONSTONES

PALAEOMAGNETIC STUDIES OF THE FRODINGHAM, MARLSTONE ROCK-BED AND CLEVELAND IRONSTONES

7.1 INTRODUCTION

Sediments which are iron-rich might be expected to contain magnetic minerals such as magnetite or haematite as either detrital or diagenetic phases. The presence of magnetic minerals would result in the sediment having a measureable magnetic character. Since such magnetic minerals record the nature of the earth's magnetic field at the time of their deposition (depositional remanent magnetism) or at the time of their formation as diagenetic phases within the sediment (chemical remnant magnetism) measurement of the magnetic parameters of ironstones should yield some idea of the nature of the ambient field at their time of formation. In petrographic studies of the ironstones no magnetic phases, with the exception of goethite, were identified. Magnetic minerals have a minimum size below which a magnetic remanent is not retained. This is known as the superparamagnetic region. For magnetite this is a grain diameter less than 10^{-5} cm and for haematite is less than 10^{-3} cm. If these minerals were present and carrying a remanent magnetism they would not necessarily be seen with a microscope. Thus, consideration of the magnetic properties of ironstones may allow the identification of minerals not previously encountered. A study of the palaeomagnetism of the three ironstones has therefore been carried out to determine (a) whether ironstones carry magnetic mineral phases, and (b) if such phases are present whether they will allow the nature of the earths magnetic field at the time of their formation to be deduced.

7.2 SAMPLE COLLECTION, PREPARATION, MEASUREMENT, AND DEMAGNETISATION

7.2.1 Sample Collection

In order to carry out the laboratory measurement of the magnetic properties of ironstones it is necessary to use samples which are oriented with respect to geographic north. Oriented samples were therefore collected at a series of vertically separated sites from the Frodingham Ironstone (Winterton Pit), Marlstone Rock-bed Ironstone (Ratley Quarry, Edge Hill), and the Cleveland Ironstone at Brackenberry Wyke. Figure 7.1 shows the positions of these sites at each location. Vertically separated samples were collected in order that any change in the earths field during ironstone formation could be recognised.

Each sample was oriented in situ and then removed. A tripod was used to carry out sample orientation. This is illustrated in Figure 7.2. The tripod was placed on the top of the sample and moved until the spirit level parallel to two of its legs indicated that a line drawn between these two legs was horizontal. Such a line was drawn. It is termed a fiducial line and corresponds to a strike line. If the surface of the sample is a bedding plane then it corresponds to the tectonic strike. The position of the third leg gave the dip direction which may correspond to the tectonic dip. The amount of dip was obtained by rotating the upper portion of the tripod table about the hinge, and therefore parallel to strike, until the dip spirit level indicated that the table was horizontal. The dip value was then read off the protractor and recorded. The position of the third leg was marked. Ticks were marked along the fiducial line on the down dip side such that they pointed to the northerly end of the line. The direction of the fiducial line was measured using a magnetic compass and recorded. The specimen was then removed using a brass chisel.

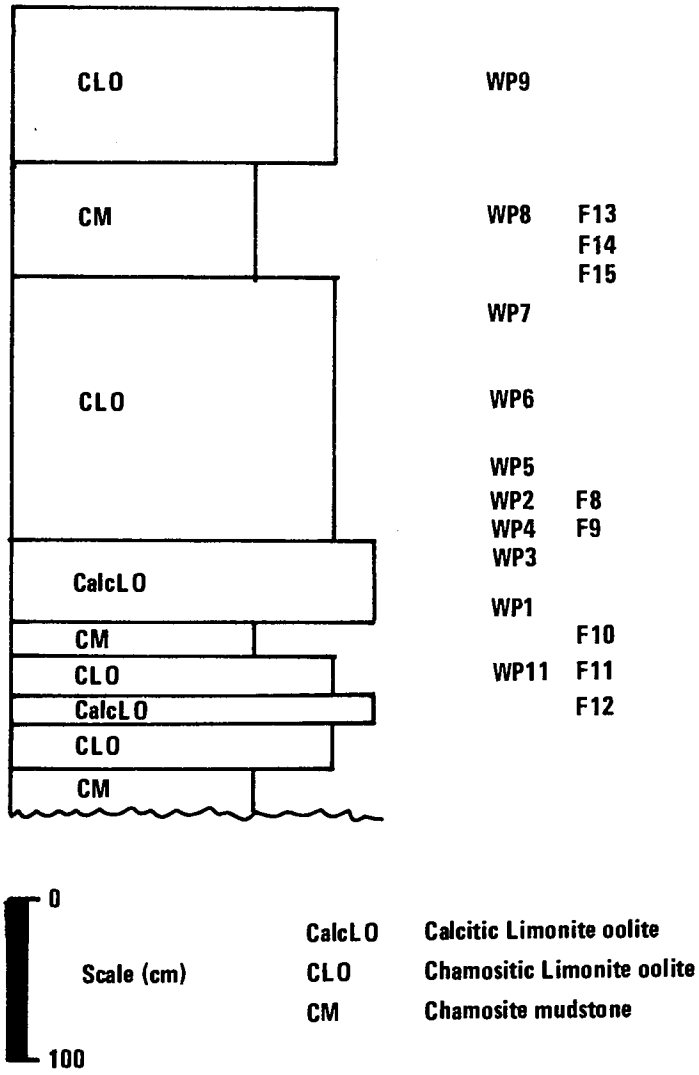

Fig 7.1a Palaeomagnetic sites in the Frodingham Ironstone at Winterton Pit

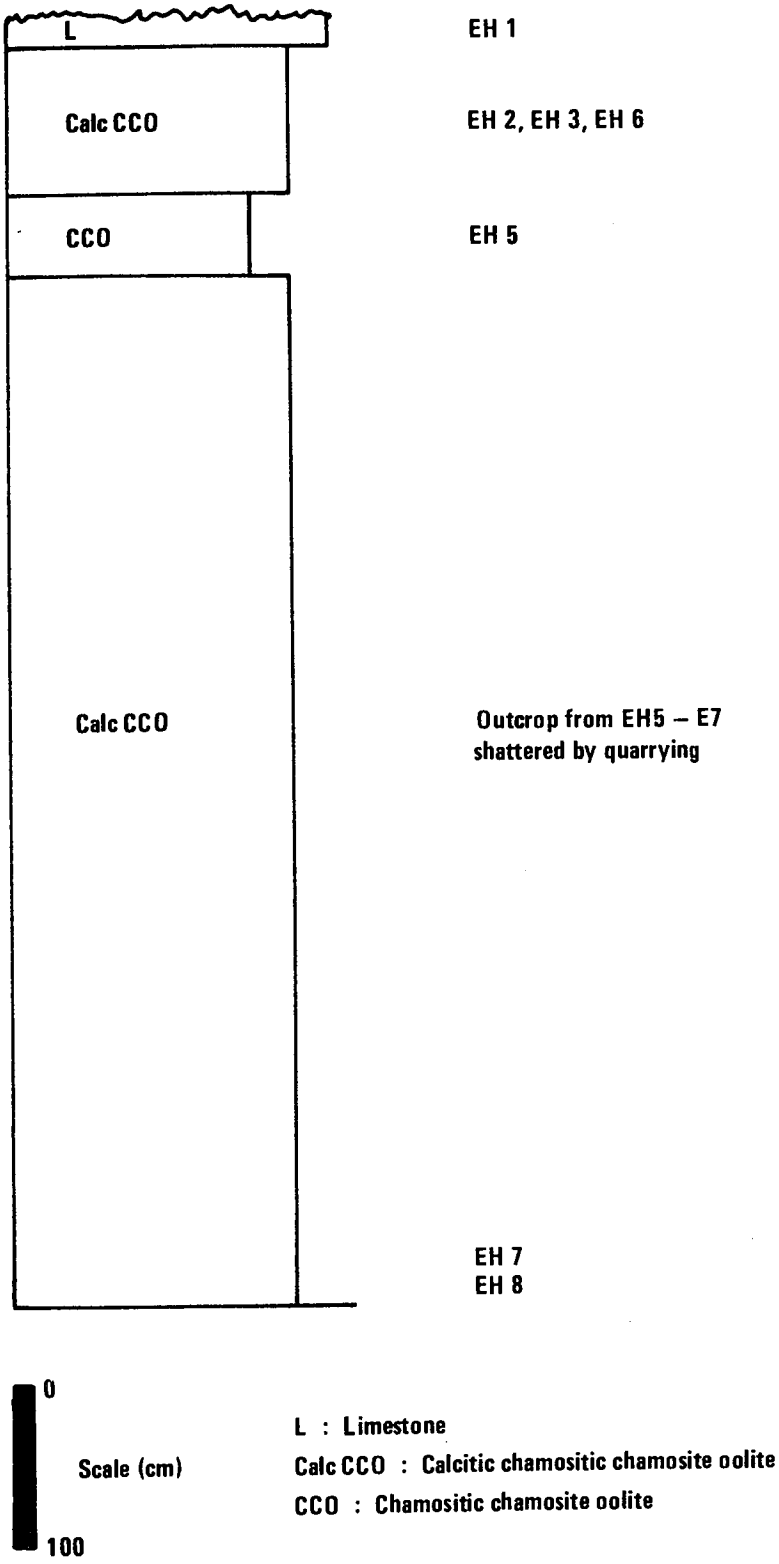

Fig 7.1b Palaemagnetic sites in the Marlstone Rock-bed at Edge Hill

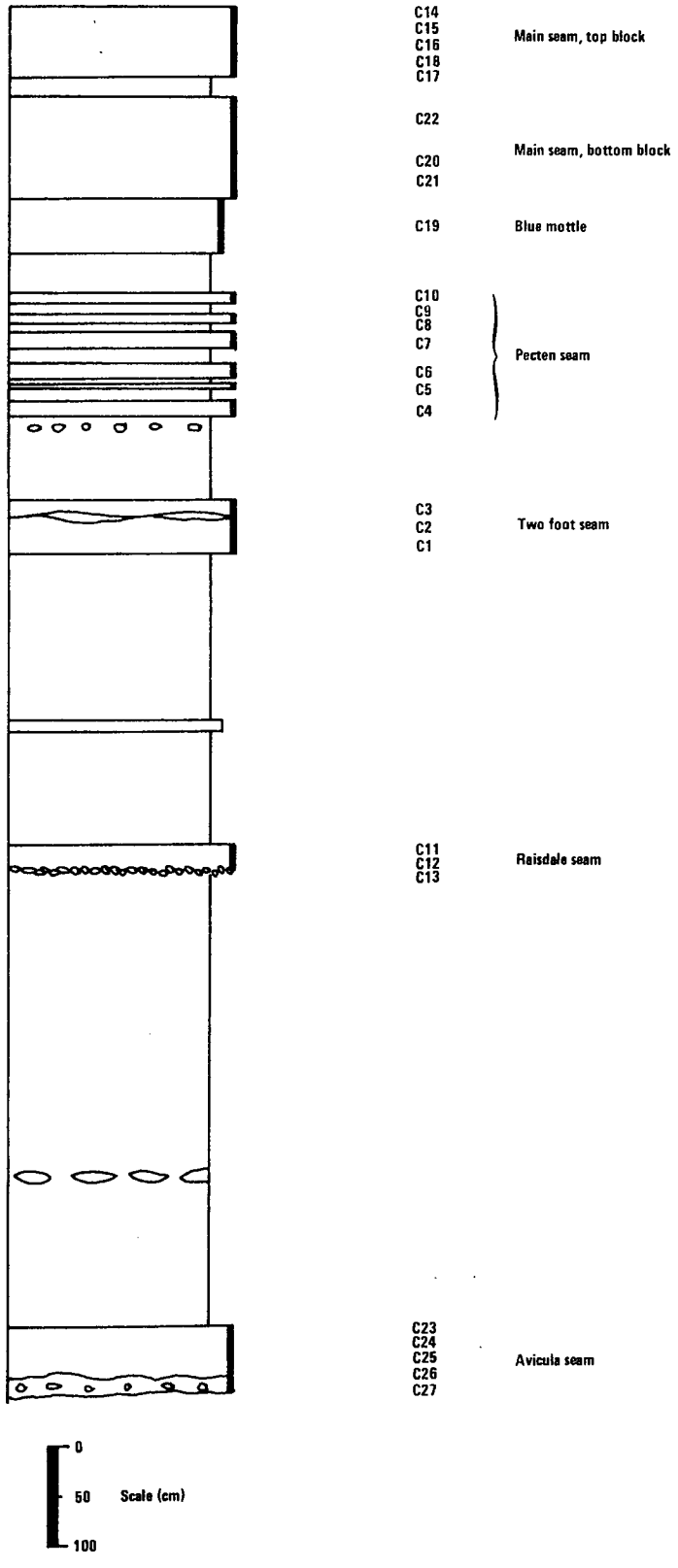

Fig 7.1c Palaeomagnetic sites in the Cleveland Ironstone formation at Brackenberry Wyke

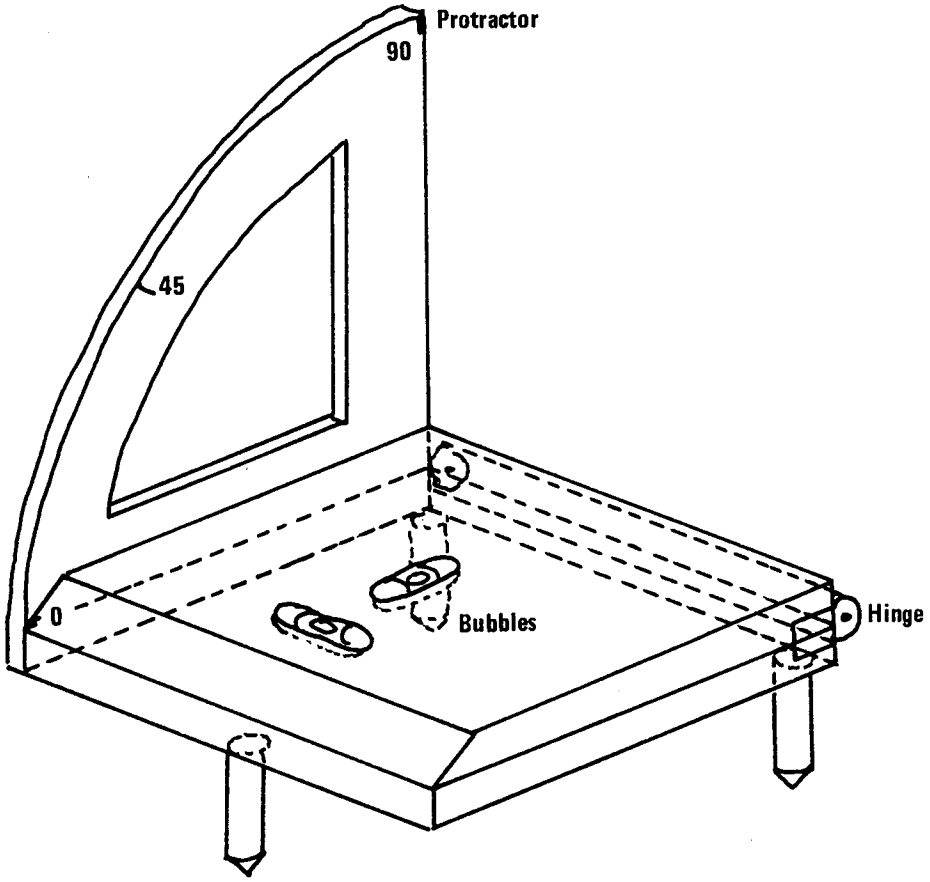

Fig 7.2 Tripod (not to scale)

7.2.2 Sample Preparation

Cylindrical specimens were required for laboratory measurement. These were drilled out of the hand specimens with a water-lubricated, 2.54 cm diameter, hollow drill piece mounted on a pillar drill. The cutting edge of the piece was constructed of diamond-impregnated phosphor-bronze. In order to retain the sample orientation the hand specimen was locked onto a table which was mounted on the drill table with a universal joint connection. The specimen table was adjusted until the surface of the specimen was horizontal. Six cores were then drilled out perpendicular to the specimen surface and having fiducial line across their tops. The cores were removed from the hand specimens by snapping them off with a brass chisel. A fiducial line was drawn on either side of the cores corresponding to the fiducial lines on their tops. They were then trimmed into 2.54 cm lengths with a diamond-impregnated brass circular saw. They were labelled and fiducial lines on their top surfaces drawn.

7.2.3 Sample Measurement

The magnetic properties, declination, inclination, and intensity, of each 2.54 cm core were measured using a Digico spinner magnetometer. These values were determined by the computer attached to the magneto-meter as a result of spinning the specimen in six different orientations. Figure 7.3. is a schematic diagram of the spinner magnetometer. Each spin induces an alternating e.m.f. in the pick-up coils, the amplitude of which depends on the component of magnetisation along the axis of spin and perpendicular to the coil axes. The phase of the direction of this component is measured relative to the fiducial mark on the rotating

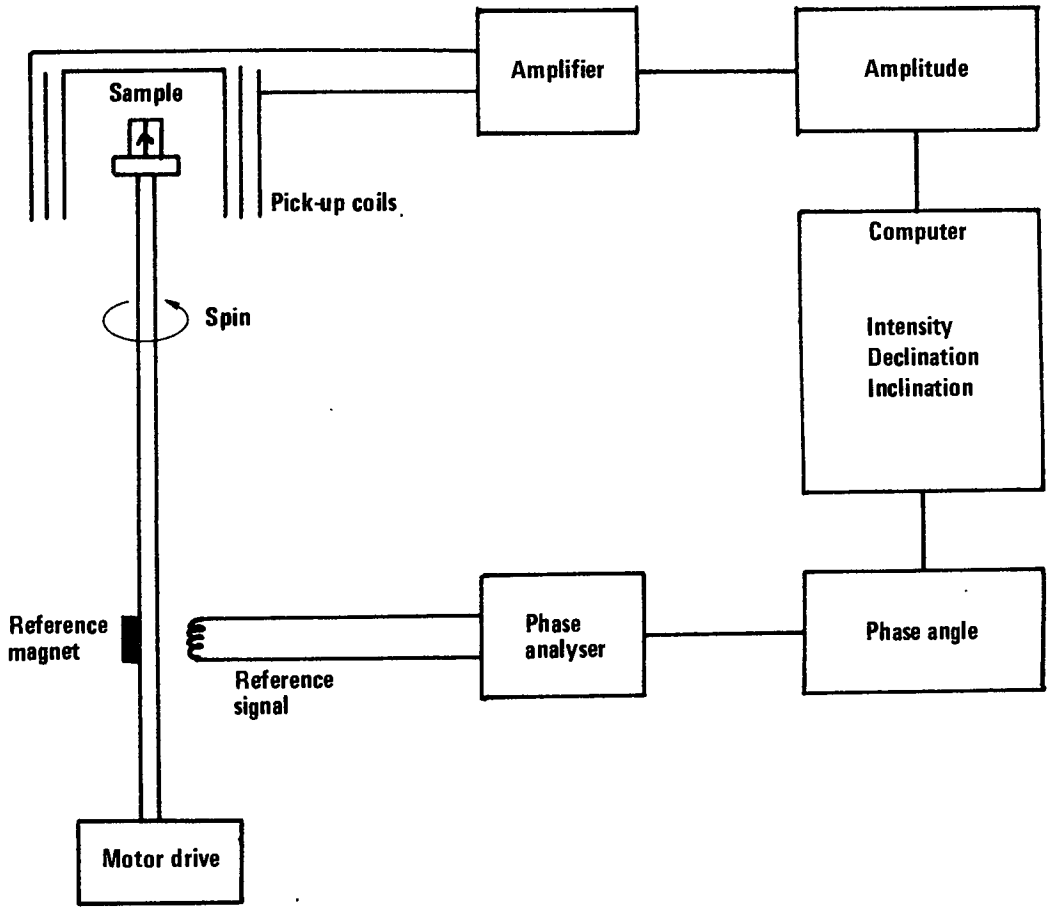

Fig 7.3 Schematic diagram of Spinner Magnetometer

head. In order to obtain correct values for the specimens it was necessary to calibrate the magnetometer after every six specimen measurements with a standard of known intensity. The three magnetic properties define a vector which is the observed magnetism of the core or natural remnant magnetism. Since the cores are oriented the declination value represents the deviation of the specimen from geographic north, the inclination its deviation from the horizontal, and the intensity is its quantity measured in electromagnetic units (micro Gauss).

A correction was applied to all the samples which used their orientation data and their tectonic dip and strike in order to return them to their position at the time of formation. In order to average out errors due to sampling and preparation the mean of six cores representing any given site was calculated by the computer. The calculation also gave a statistical parameter; the cone of confidence, within which lay 99% of the measurement. Table 7.1 give the corrected natural remanence values for all the sites which were measured and their cones of confidence. It should be noted that for a number of hand specimens, each representing one site, the cores which were drilled each provided more than one 2.54 cm long core on trimming. Thus, from each hand specimen several subsites were obtained. These are anotated A, B, C etc. with increasing depth from the hand specimen surface.

7.2.4 Thermal demagnetisation

The natural remanent magnetism incorporates any magnetism obtained by the specimen after its formation as well as the original magnetism. Such later components are generally 'soft' in comparison

Site/subsite (six specimens per site/subsite	Intensity range (micro Gauss)	Inclination (°)	Declination (°)	Cone of confidence
WP1A	3.020-1.902	43.2	70.9	7.6
WP1B	1.512-0.651	37.6	71.8	7.7
WP1C	1.794-0.722	20.0	67.0	7.9
WP1D	0.916-0.474	22.4	68.6	6.5
WP2A	4.078-2.041	239.8	61.7	11.4
WP2B	1.271-1.797	238.2	64.6	9.8
WP3A	2.685-1.399	27.4	73.5	6.7
WP3B	3.230-1.818	358.1	77.1	8.8
WP3C	2.033-0.839	138.2	83.8	15.8
WP4A	4.074-1.350	148.6	69.1	10.5
WP4B	3.001-2.266	153.2	75.8	9.5
WP4C	3.084-2.337	140.2	73.6	15.1
WP4D	2.503-1.334	94.1	66.8	13.9
WP5A	3.030-1.715	176.4	57.2	20.7
WP5B	3.290-1.930	90.1	78.2	4.9
WP5C	2.378-1.476	164.0	74.3	7.2
WP5D	2.337-2.008	121.9	81.9	10.4
WP6A	8.074-5.250	160.0	40.9	4.9
WP6B	6.978-5.397	152.6	43.0	6.0
WP6C	7.317-5.077	151.8	42.7	6.1
WP6D	7.929-5.565	147.5	41.3	11.3
WP7A	12.905-8.266	101.8	68.4	12.6
WP7B	9.260-8.189	122.4	66.6	8.2
WP8A	3.79-2.142	185.2	49.4	25.1
WP8B	4.133-2.691	161.0	64.6	10.4
WP8C	4.859-2.706	157.2	58.2	12.1
WP8D	4.197-2.803	132.8	69.1	18.3
WP11A	9.640-7.066	125.2	61.5	7.0
WP11B	6.346-4.676	111.9	61.1	8.6
WP11C	4.336-3.341	121.4	62.0	10.5
WP16A	6.519-1.787	88.2	78.2	12.7
WP16B	8.321-3.680	93.6	82.0	15.3
WP16C	7.873-3.120	87.4	83.5	15.1
WP16D	8.828-5.552	13.0	79.0	24.9
F8A	9.718-6.662	127.2	81.5	3.5
F9A	2.189-1.755	131.4	78.8	9.2
F9B	3.488-1.445	87.2	81.0	9.7
F10A	5.144-2.739	142.5	79.1	10.7
F10B	2.619-1.656	158.8	79.6	7.3
F11A	8.206-5.822	190.6	62.1	4.7
F11B	5.497-3.322	177.0	69.3	6.3
F11C	4.615-3.565	164.2	73.8	4.7
F11D	4.163-3.317	157.2	72.1	9.0
F12A	13.470-12.251	152.6	73.6	3.9
F13A	7.469-5.218	66.6	74.8	3.0
F13B	5.548-3.488	115.7	73.9	5.6
F13C	3.682-1.676	157.7	52.2	13.2
F14A	13.456-6.186	117.6	76.3	12.6
F14B	7.687-1.171	85.8	65.9	6.5
F15A	12.128-0.568	326.7	84.9	4.4
F15B	4.699-2.807	321.0	83.7	5.3

Table 7.1a - Frodingham Ironstone NRM Measurements

Site/subsite (six specimens per site/subsite	Intensity Range (micro Gauss)	Inclination (°)	Declination (°)	Cone of confidence
EH1A	2.871-1.399	54.9	70.6	3.4
EH1B	1.755-0.267	22.0	70.1	10.5
EH2A	0.704-0.239	4.2	50.0	>90.0
EH2B	0.761-0.167	213.4	45.9	76.5
EH3A	4.031-1.565	318.0	73.0	5.9
EH3B	6.968-0.159	330.1	64.0	26.1
EH3C	5.422-0.102	335.8	55.5	20.6
EH3D	1.107-0.133	320.4	67.3	42.3
EH5A	2.436-1.714	5.9	65.7	5.3
EH5B	1.807-1.422	358.6	64.7	6.4
EH5C	1.603-0.913	353.4	65.0	11.4
EH6A	0.662-0.171	12.3	67.7	19.6
EH8A	1.957-0.640	16.4	65.4	5.9
EH8B	0.461-0.318	16.3	63.2	8.7
EH8C	0.477-0.265	28.9	59.6	12.3

Table 7.1b - Marlstone Rock-bed NRM Measurements

Site/subsite (six specimens per site/subsite	Intensity range (micro Gauss)	Inclination (°)	Declination (°)	Cone of confidence
C1A	0.632-0.103	220.0	-13.6	88.7
C1B	0.353-0.082	292.8	54.5	69.0
C1C	0.548-0.170	280.5	52.0	19.8
C1D	0.153-0.057	292.2	53.6	34.6
C2A	0.157-0.102	152.5	5.9	27.0
C2B	0.156-0.098	171.1	12.8	30.5
C2C	0.308-0.225	156.2	31.4	22.7
C3A	0.227-0.082	185.4	46.4	31.5
C3B	0.131-0.096	206.5	37.8	17.0
C3C	0.099-0.068	210.6	53.5	27.3
C3D	0.243-0.098	201.5	45.6	32.8
C4A	0.359-0.231	287.7	48.6	36.2
C4B	0.371-0.215	301.1	57.7	34.0
C4C	0.419-0.277	305.1	53.1	4.5
C4D	0.521-0.328	310.8	53.8	33.8
C5A	0.296-0.191	329.8	26.0	41.2
C5B	0.244-0.125	9.8	32.1	11.1
C6A	0.193-0.125	317.4	67.9	36.1
C6B	0.202-0.124	297.1	63.6	22.0
C6C	0.205-0.137	291.8	72.9	18.2
C7A	0.164-0.085	327.4	36.1	33.6
C7B	0.159-0.114	346.2	35.1	21.3
C7C	0.166-0.600	338.9	42.1	26.8
C7D	0.162-0.630	350.3	57.5	32.8
C8A	0.182-0.199	324.9	41.5	27.5
C8B	0.181-0.103	343.6	41.9	16.1
C8C	0.304-0.095	329.5	33.6	19.2
C8D	0.219-0.099	338.7	49.3	16.8
C9A	0.343-0.275	274.0	65.8	14.2
C9B	0.415-0.247	306.6	67.3	13.2
C9C	0.394-0.312	301.5	66.5	14.2
C10A	0.289-0.209	334.8	65.6	13.4
C10B	0.265-0.203	345.6	63.0	6.6
C11A	4.840-0.092	16.1	84.4	15.1
C11B	0.115-0.091	148.0	77.2	16.3
C11C	0.098-0.065	161.9	59.5	21.9
C11D	0.153-0.110	150.8	38.6	22.0

Table 7.1c - Cleveland Ironstone NRM Measurements

Site/subsite (six specimens per site/subsite	Intensity range (micro Gauss)	Inclination (°)	Declination (°)	Cone of confidence
C12A	0.315-0.072	91.7	48.2	39.7
C12B	0.118-0.063	121.0	47.1	21.8
C12C	0.137-0.074	129.3	68.6	14.4
C13A	1.513-0.149	34.3	68.3	14.4
C13B	0.201-0.083	50.3	64.9	10.4
C13C	0.311-0.161	59.8	65.6	14.1
C14A	0.273-0.169	109.9	42.6	30.9
C14B	0.371-0.156	119.0	29.5	25.5
C14C	0.377-0.090	128.1	33.0	11.3
C15A	0.253-0.123	343.6	5.3	11.9
C15B	0.157-0.062	336.7	-5.6	19.4
C15C	0.261-0.190	335.1	-12.5	29.4
C15D	0.243-0.186	352.4	7.7	17.9
C16A	0.530-0.185	326.7	77.2	20.9
C16B	0.328-0.144	308.4	76.7	15.6
C16C	0.308-0.113	242.1	63.4	59.4
C17A	0.270-0.185	315.7	69.5	14.4
C17B	0.169-0.117	300.3	59.2	14.8
C17C	0.206-0.144	267.2	71.7	21.4
C17D	0.170-0.115	247.9	73.5	17.3
C18A	0.458-0.295	23.0	54.4	17.1
C18B	0.366-0.248	36.8	60.6	9.5
C19A	0.123-0.074	159.5	70.1	28.5
C19B	0.158-0.116	199.4	59.4	22.7
C19C	0.185-0.079	156.7	75.4	31.6
C19D	0.133-0.101	219.2	75.3	27.2
C20A	0.511-0.429	314.6	62.7	12.3
C20B	0.529-0.395	311.2	64.0	9.9
C20C	0.428-0.277	301.7	66.4	5.3
C21A	0.458-0.328	313.6	60.9	6.0
C21B	0.381-0.289	311.6	65.7	8.8
C21C	0.621-0.199	310.9	63.6	7.7
C22A	0.421-0.303	331.7	69.1	6.8
C22B	0.327-0.249	348.3	68.1	7.3
C22C	0.282-0.254	336.2	68.5	6.8
C23A	0.180-0.063	250.2	35.0	46.9
C24A	0.071-0.062	103.4	47.4	24.6
C24B	0.068-0.062	91.6	15.3	60.8
C25A	0.077-0.065	189.1	80.1	37.4
C25B	0.083-0.070	136.2	65.7	
C26A	0.350-0.237	300.5	44.7	7.5
C27A	0.436-0.117	199.9	40.8	39.0
C27B	1.076-0.216	200.0	75.8	10.6
C27C	0.587-0.154	243.2	58.1	20.9
C27D	0.354-0.180	241.6	50.3	18.2

to those obtained at the time of formation and may be removed by thermal or alternating demagnetisation. Only thermal demagnetisation has been used in this work. The underlying principle of this is that specimens are heated to a known temperature and then allowed to cool in 'field free' magnetic space. In this way components carried by phases with lower blocking temperatures are removed and with progressive temperature increments the components carried by higher blocking temperature phases are gradually revealed.

In general, the higher the temperature required to remove the magnetisation of a specimen the more stable that magnetisation is. Irving and Opdyke (1965) have related the components of magnetisation to the temperatures at which they may be removed. Two types of components are recognised; those which are thermally discrete components whose declination, inclination, and intensity remain unchanged until the carriers of this magnetisation become non-magnetic at their Curie temperatures, and thermally distributed components whose properties are defined by a series of blocking temperatures. On cooling from a high temperature spontaneous magnetisation appears at the Curie point, Tc, and this assumes an equilbrium in the presence of any applied field. Grains of different volumes each have differing blocking temperatures, T_B. As the temperature drops below Tc and passes through each T_B, the relaxation time of these grains increases very quickly. Any equilibrium magnetisation becomes frozen in and subsequent changes in the field direction at temperatures less than T_B are ineffectual in changing the direction of magnetisation. It is necessary to remove the viscous components of magnetisation in order to study any original component of

Site/subsite	Inclination(°)	Declination(°)	Cone of confidence
WP1A	353.4	69.7	4.1
WP1B	2.4	66.2	2.4
WP1C	8.5	69.8	7.3
WP1D	0.8	65.9	5.4
WP2A	340.2	64.6	4.7
WP3A	338.9	72.1	6.7
WP3B	334.4	76.0	10.9
WP3C	339.5	81.4	12.5
WP4A	21.1	60.8	2.2
WP4B	20.5	60.8	4.2
WP4C	22.5	62.7	4.6
WP4D	45.3	60.6	4.1
WP5A	36.6	59.8	3.9
WP5B	29.9	59.7	1.7
WP5C	36.2	57.1	7.3
WP5D	30.0	59.1	6.6
WP6A	5.8	12.4	17.6
WP6B	58.8	34.3	10.4
WP6C	39.4	30.4	11.9
WP7A	44.9	55.0	26.4
WP8A	47.0	67.3	5.4
WP8B	36.7	60.9	8.0
WP8C	33.8	59.6	3.6
WP8D	34.3	58.8	9.7
WP11A	13.7	54.3	16.7
WP11B	4.7	57.8	13.1
WP16B	15.2	84.3	14.0
WP16C	355.0	78.6	12.8
WP16D	349.1	73.8	5.6
F8A	207.5	86.6	3.2
F9A	270.9	71.0	5.8
F9B	267.3	75.7	10.2
F10A	154.7	76.0	11.1
F10B	87.8	74.4	3.0
F14B	31.8	66.4	10.6
F15A	128.1	57.5	43.1
F13A	60.3	75.0	2.5
F13B	60.3	71.8	6.5
F13C	87.8	75.5	9.7
F14A	31.9	73.5	13.8

Table 7.2 - NRM values of Frodingham Ironstone site after bulk thermal demagnetisation

magnetisation. Viscous remanence is carried by smaller than single domain size magnetic particles. McElhinny (1978) notes that such particles have blocking temperatures which correspond to relaxation times of the order of 100 seconds. Thus heating of specimens in field free space followed by cooling results in the loss of viscous remnance since there is no magnetic field to be retained by the viscous remnance carriers.

In order to determine the temperature at which all the low stability remnance had been removed from specimens pilot studies were carried out on a selection of specimens from each field. They were heated in a furnace in field free space to successively higher temperatures. After each temperature increment, which was usually either 50 C or 100 C, they were cooled and their magnetic properties measured. The results were plotted on stereograms. A stable magnetisation was assumed to be represented by a cluster of points for any one specimen lying close together and therefore representing a magnetisation resistant to heating. Bulk demagnetisation of all the specimens was then carried out at this temperature in field free space and was followed by remeasurement after cooling. Table 7.2 gives the declination, inclination, and intensity, corrected as before, of the stable samples after heating. Only the Frodingham Ironstone yielded a stable magnetisation, thus only these samples underwent bulk demagnetisation.

7.3 RESULTS

7.3.1 The Frodingham Ironstone

The mean of the natural remanence measurements made on the Frodingham Ironstone specimens are plotted as stereographic projections on a Wulff net in Figure 7.4. They are all normal i.e. with positive dips in the northern hemisphere and cluster around the centre of the stereogram.

Thermal demagnetisation pilot studies indicated that a stable declination, inclination, and intensity was obtained at temperatures between 250 and 300 C (Figure 7.5). Bulk demagnetisation of all the Frodingham samples was therefore carried out at 275 C. The demagnetised specimens are plotted as the means of sites in Figure 7.6. Again they cluster in the centre of the stereogram and are all normal.

In order to determine whether the distribution of demagnetised specimens corresponded to a remnance obtained at the time of formation of the Frodingham Ironstone the Digico computer was used to calculate a palaeopole position from this data. The mean of the demagnetised site means was calculated first and this had a cone of confidence of 5.5. The palaeopole position calculated from this mean yielded a latitude of 77.8° and a longtitude of 78.2° for the pole. This value is comparable to Lower and Middle Jurassic palaeopole positions Europe (McElhinny and Cowley, 1980). The latter data are plotted stereographically with the position of the Sinemurian pole determined from the Frodingham Ironstone in Figure 7.7.

In order to obtain some idea of what magnetic minerals are present

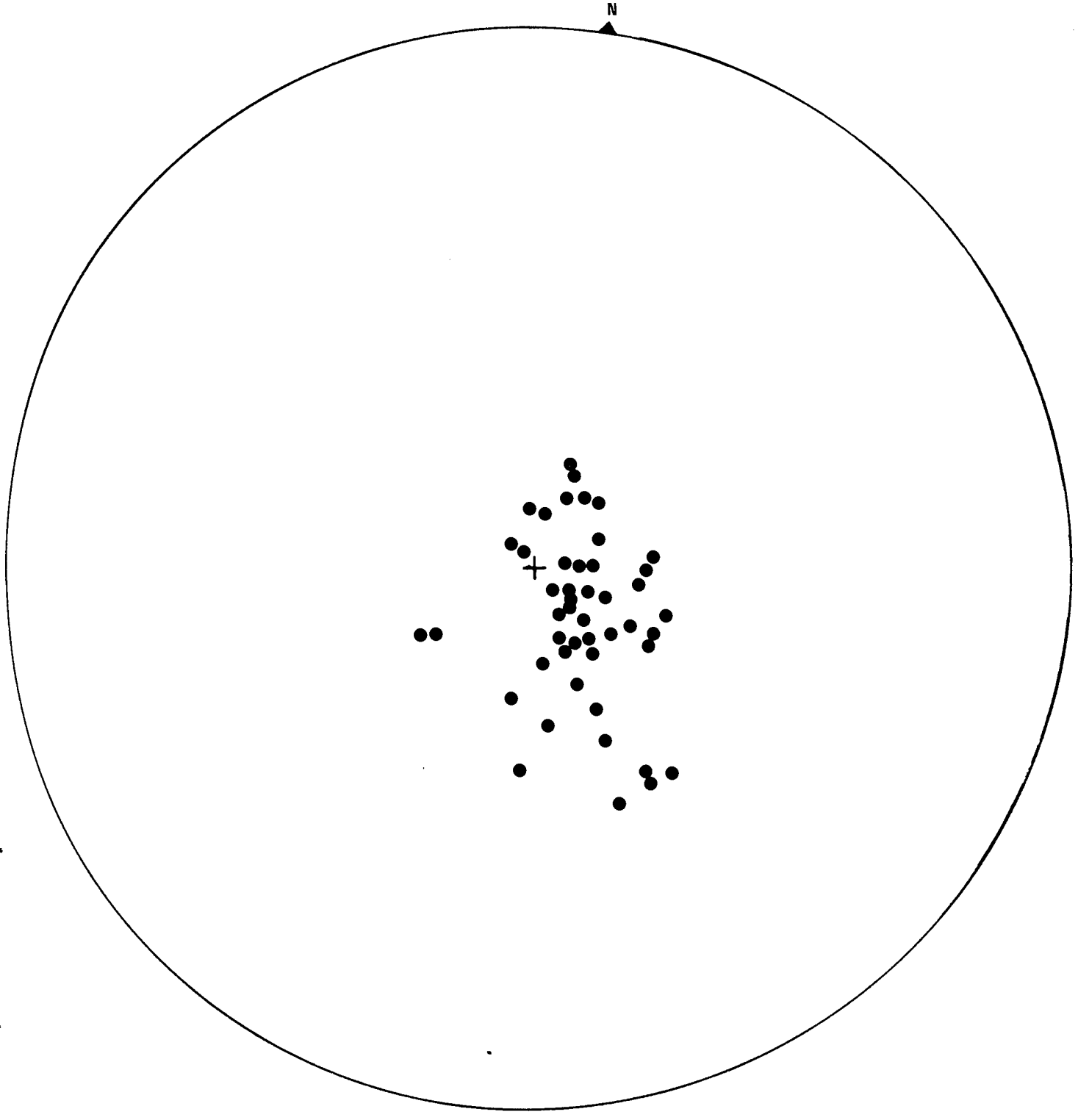

Fig 7.4 Stereographic projection of mean NRM values for Sites in the Frodingham Ironstone

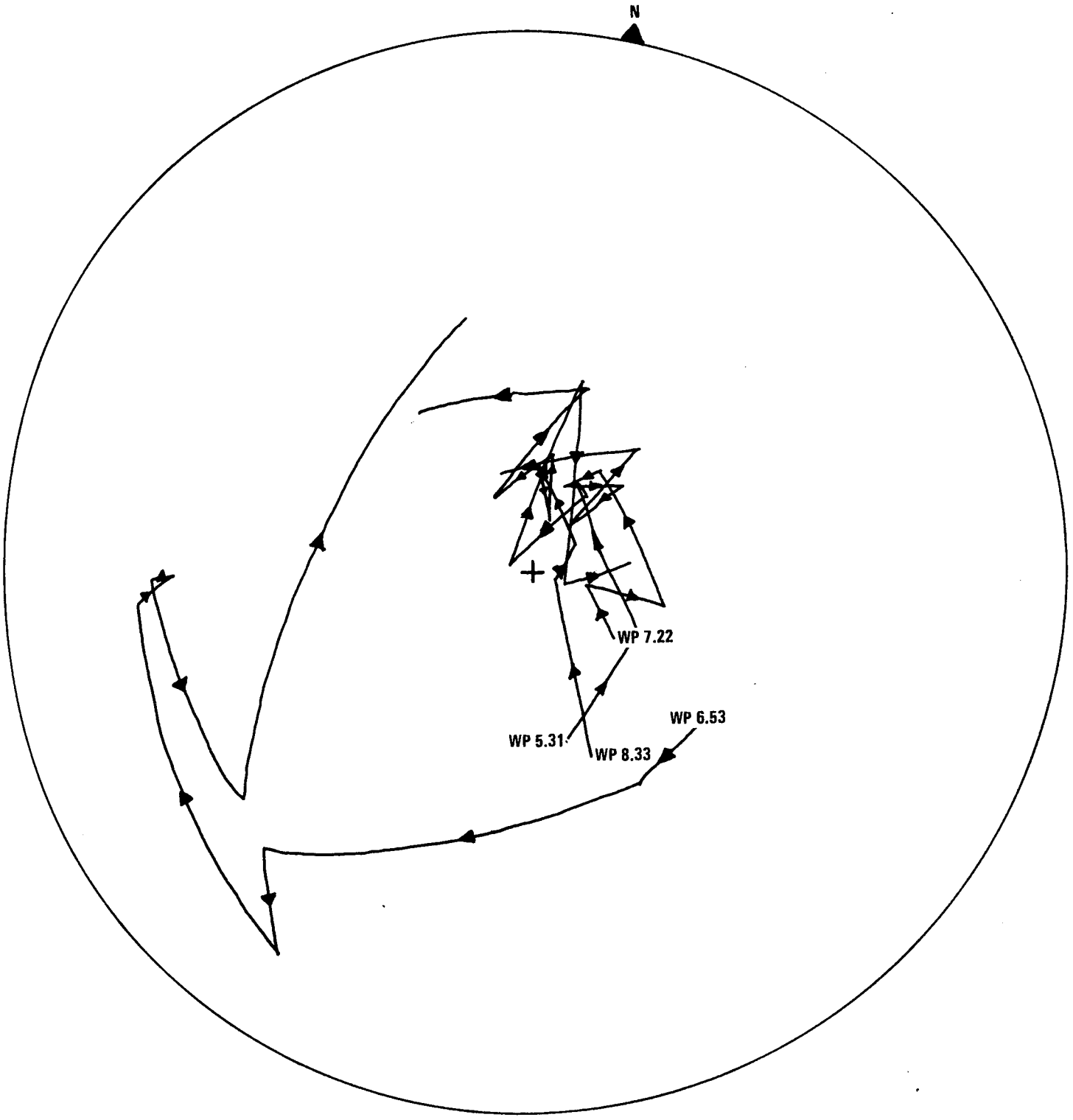

Fig 7.5 Thermal demagnetization Pilot Study. Frodingham Ironstone. Temperature progression; Room temperature, 100C, 200C, 250C, 300C, 350C, 400C, 450C, 550C

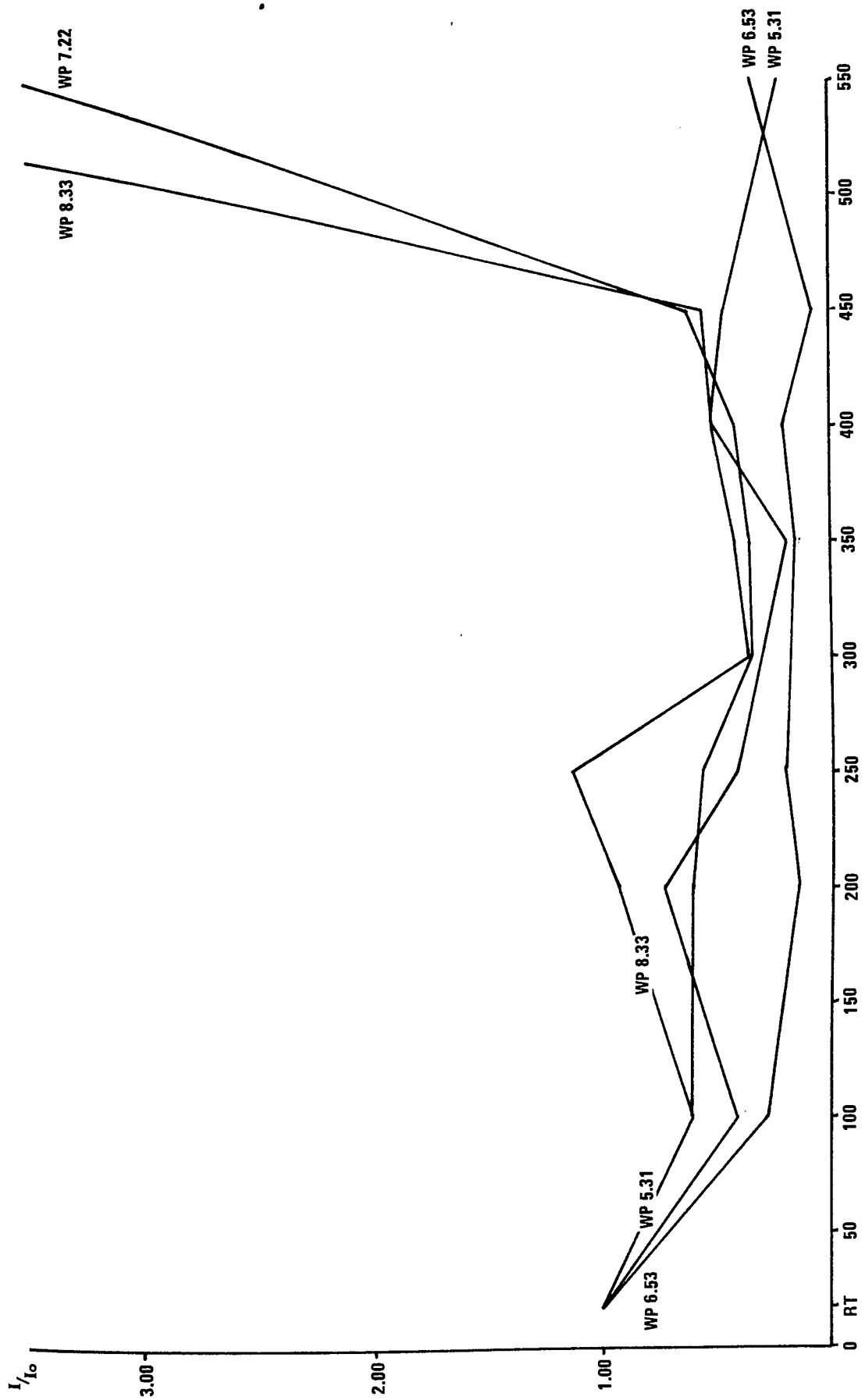

Fig 7.5 Intensity variation with temperature

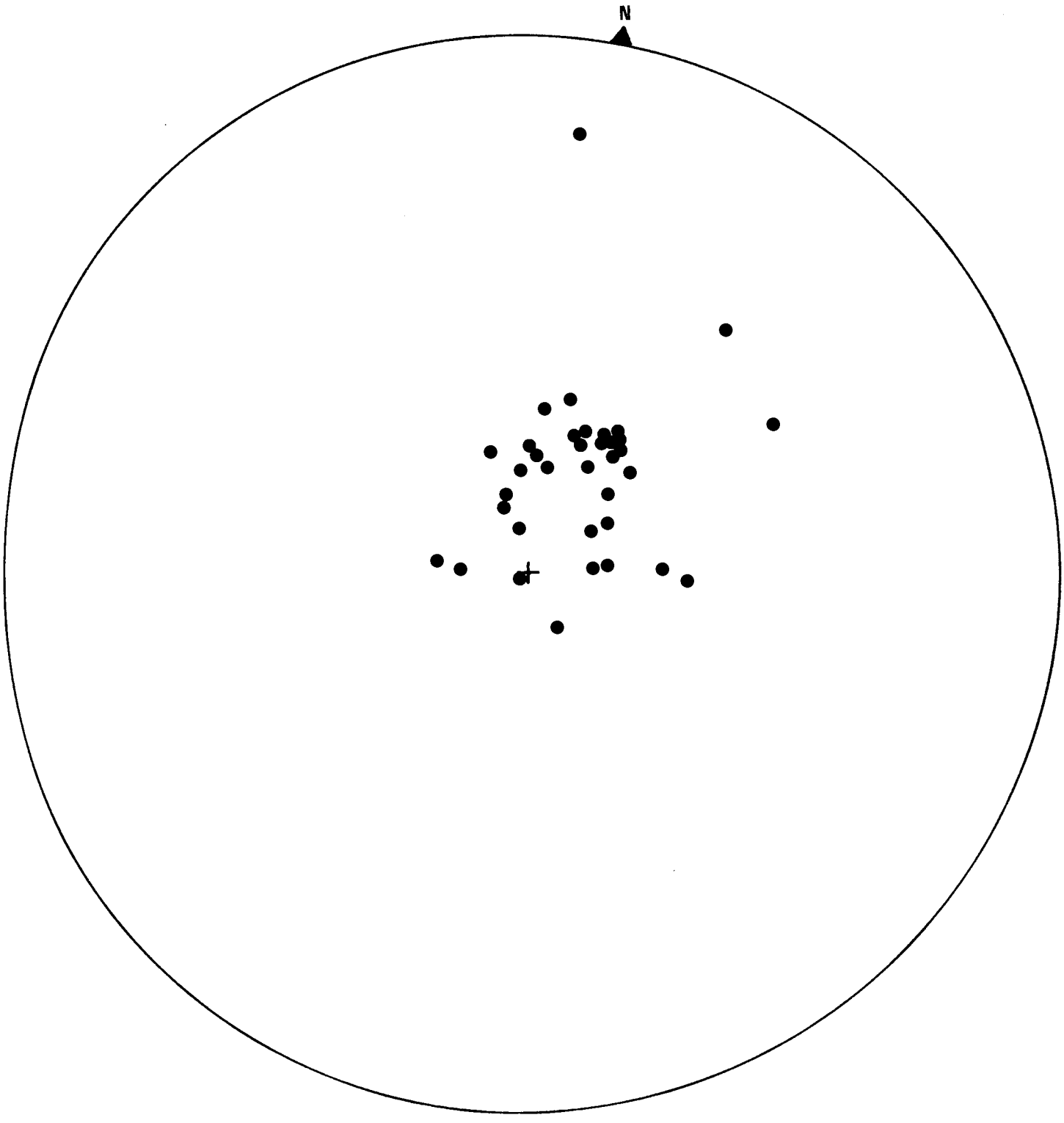

Fig 7.6 Stereographic projection of mean values for sites in the Frodingham Ironstone after thermal demagnetization at 275C. The cone of confidence is $\ll$15.0 for all sites

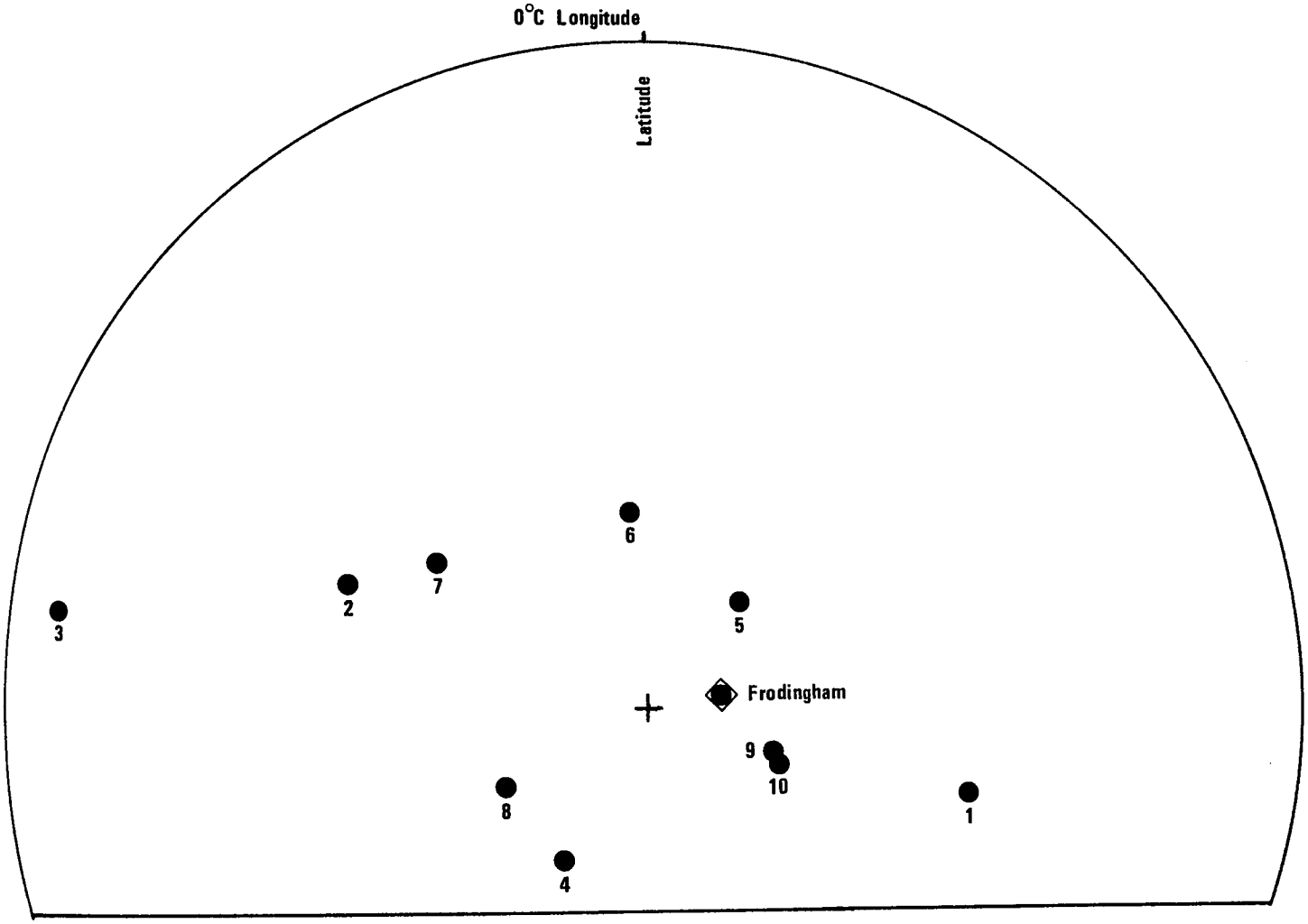

Fig 7.7 Middle and Lower Jurassic Pole positions (McElhinney and Cowley, 1980)

10	Summerville Formation, cleanest samples, Utah, USA.	Middle Jurossic
9	Summerville Formation, all samples	
8	Intrusive Rocks, Nigeria	
7	Tasmanian Dolerite, Australia (S.Pole)	
6	Tasmanian Dolerite	
5	Recrystallized limestones, Morocco	Lower Jurossic
4	Limestones, Midelt, Morocco	
3	Imiter Massif, Morocco	
2	Umbrian Sequence, Italy. Toarcian–Aalenian	
1	Red limestones, Osterhorn Mountains, Austria	

in the Frodingham Ironstone an isothermal remanent magnetism (IRM) curve was determined for two specimens. This was carried out by magnetising the specimens in successively higher fields for one minute with a Franz separator and measuring the induced magnetism after each increment. The results obtained are plotted as the intensity of the IRM against the applied field in Figure 7.8. In neither case is there any indication of saturation. The three most commonly occurring magnetic minerals are magnetite, haematite, and goethite. Of these, magnetite attains a saturation level by the time and applied field value of 3kOe has been reached whereas haematite and goethite do not saturate until applied fields have been raised to 20-30 kOe (McElhinny, 1973). It seems likely, therefore, that in view of the abundance of goethite in the Frodingham Ironstone this mineral is the major remanent magnetism carrier.

7.3.2 The Marlstone Rock-bed And Cleveland Ironstones

The mean natural remanent magnetism for each site in these ironstones is plotted stereographically in Figures 7.9 and 7.10. A considerable spread of results is obtained in both cases, but which tend to cluster close to the earth's present field.

Thermal demagnetisation pilot studies of both ironstones did not indicate the presence of any stable direction of magnetisation. The variation in declination and inclination is shown in Figures 7.11 and 7.12. The progressive increase in the distance between successively higher temperature declinations and inclinations is suggestive of a considerable viscous component of magnetisation. The intensity variation with temperature (Figures 7.11 and 7.12) often shows an initial drop

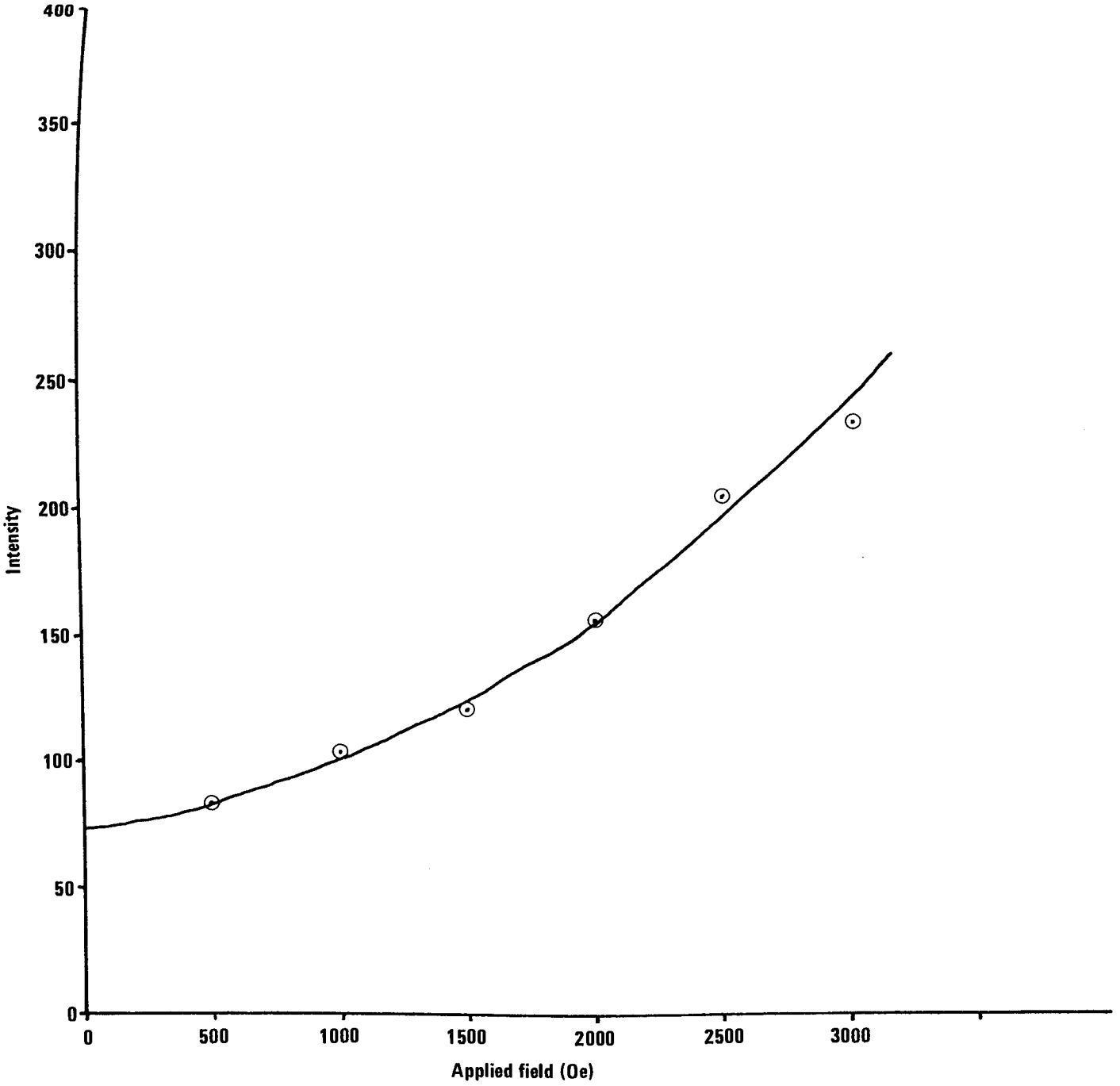

Fig 7.8a IRM curve for sample WP 3.41

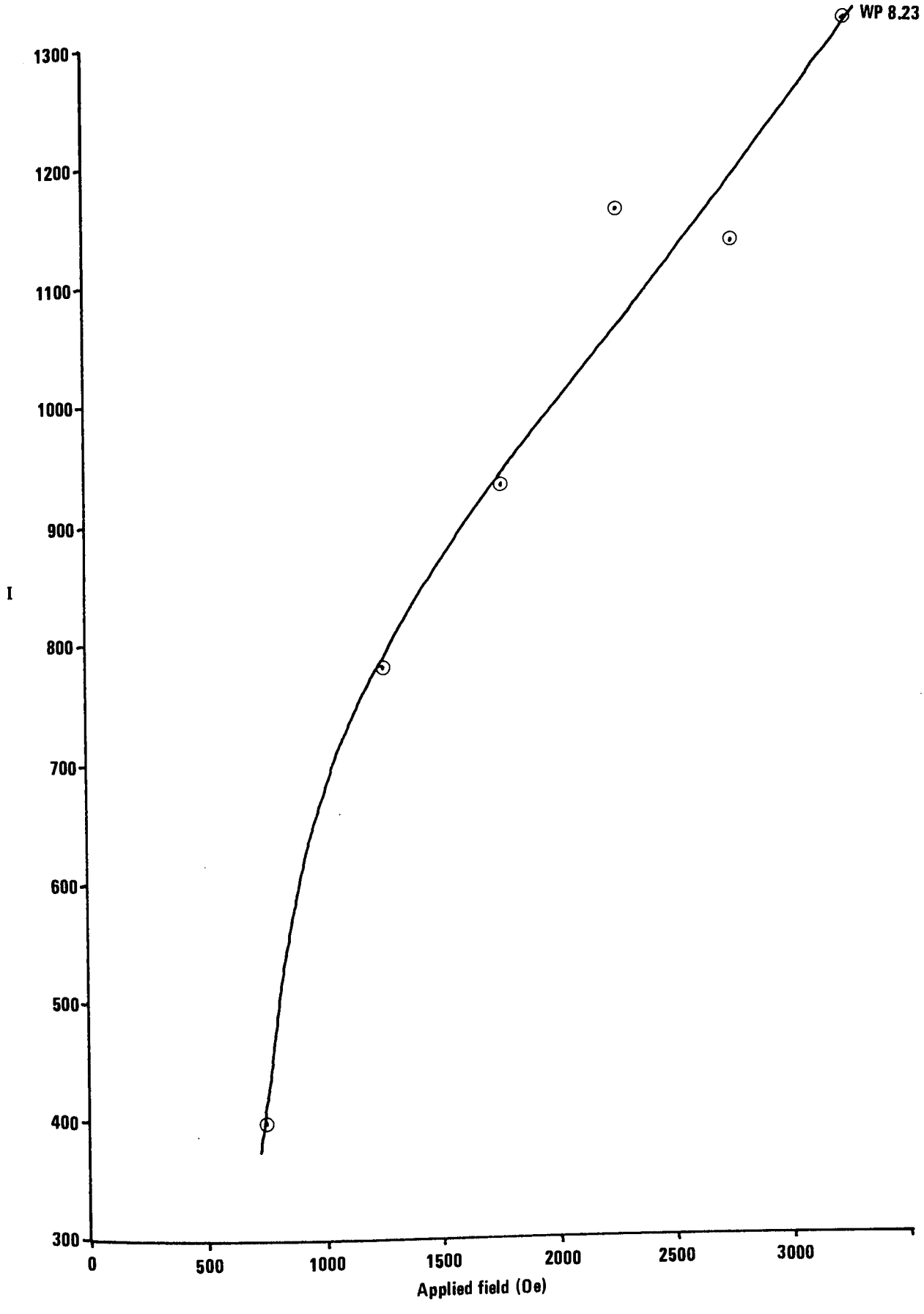

Fig 7.8b IRM curve for sample WP 8.33

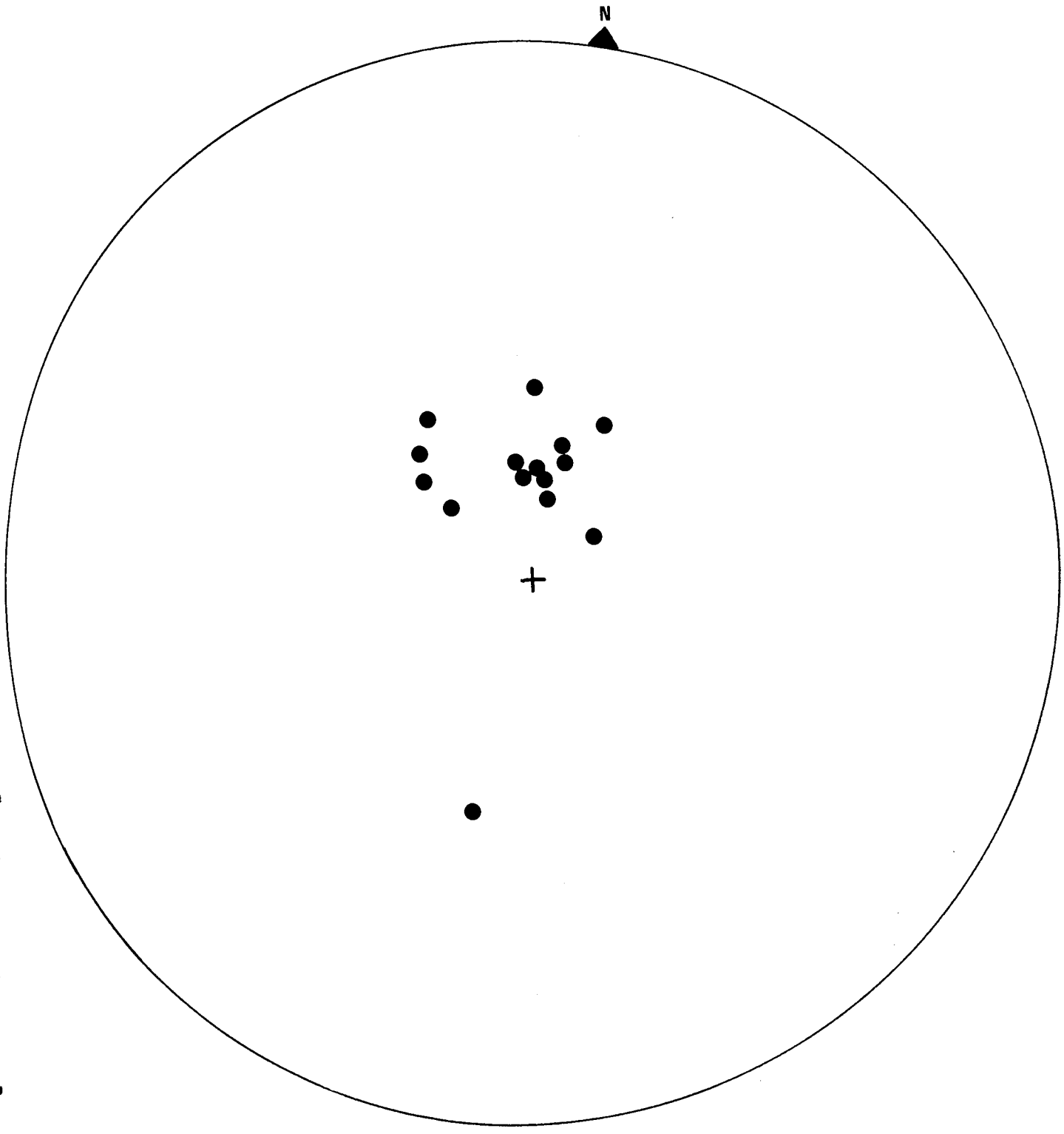

Fig 7.9 Stereographic projection of mean N.R.M. values for sites in the Marlstone Rock-bed

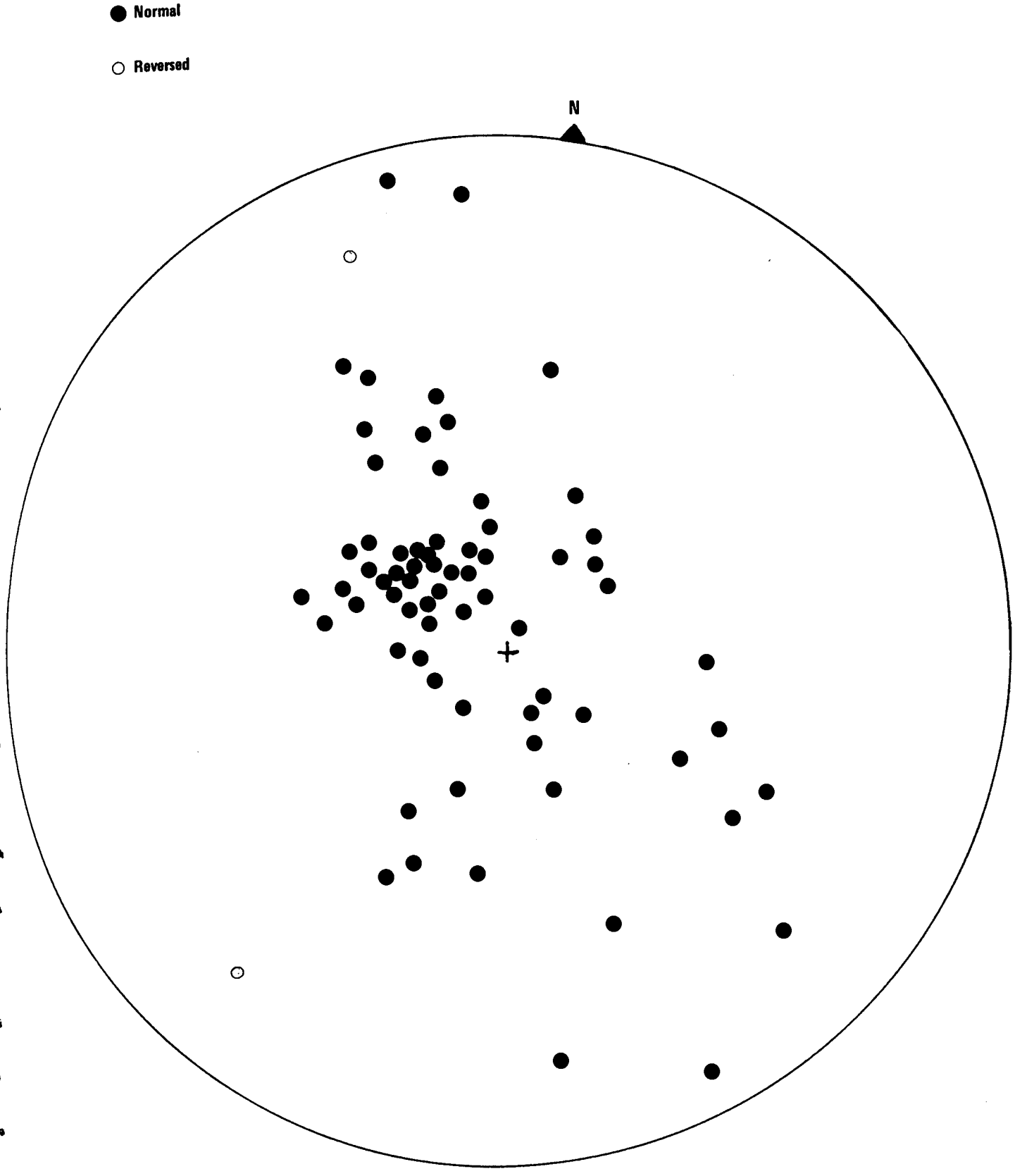

Fig 7.10 Stereographic projection of mean N.R.M. values for sites in the Cleveland Ironstone formation

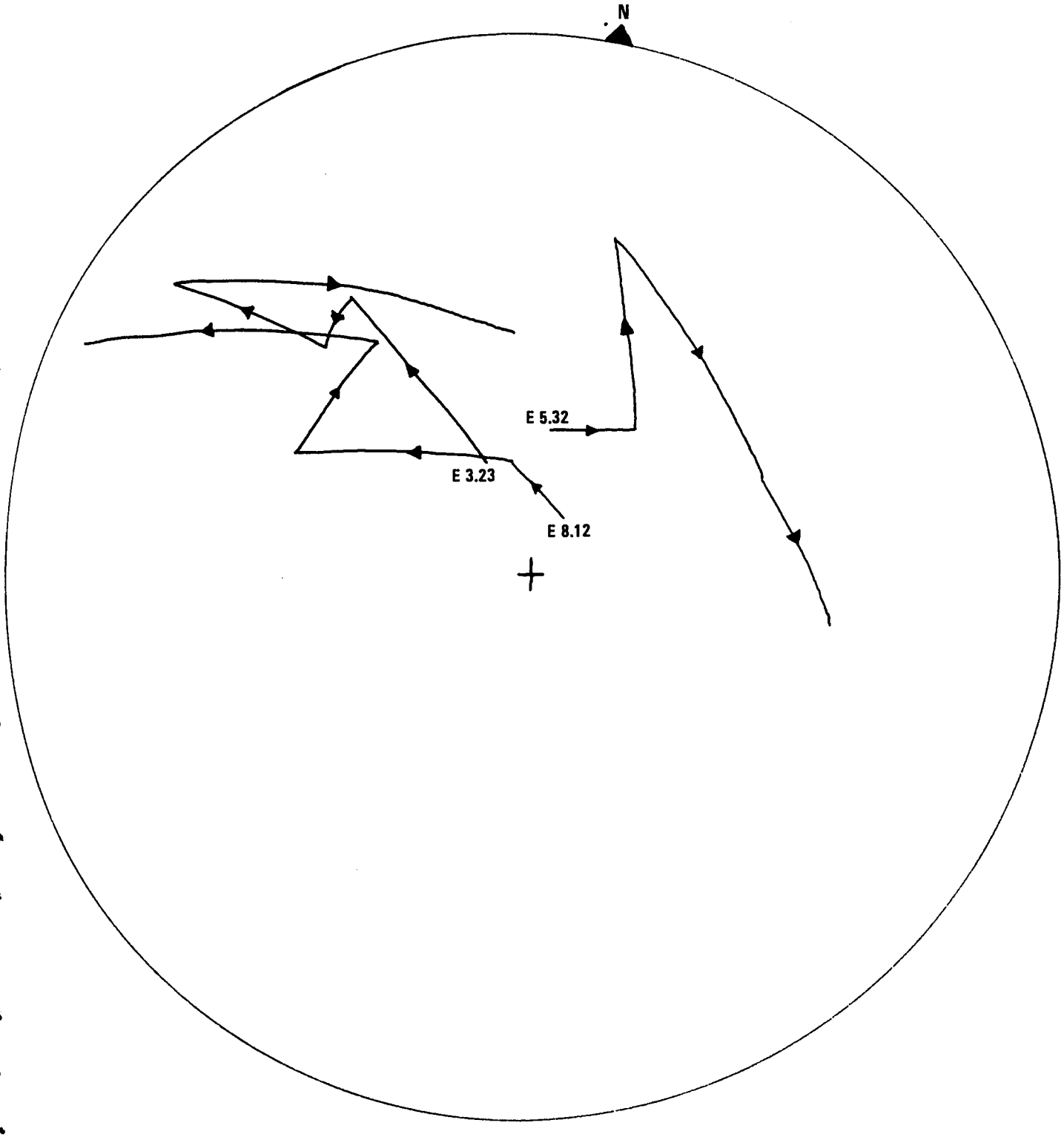

Fig 7.11 Thermal demagnetization pilot study. Marlstone Rock-bed. Temperature progression : Room temperature, 100C, 200C, 300C, 400C

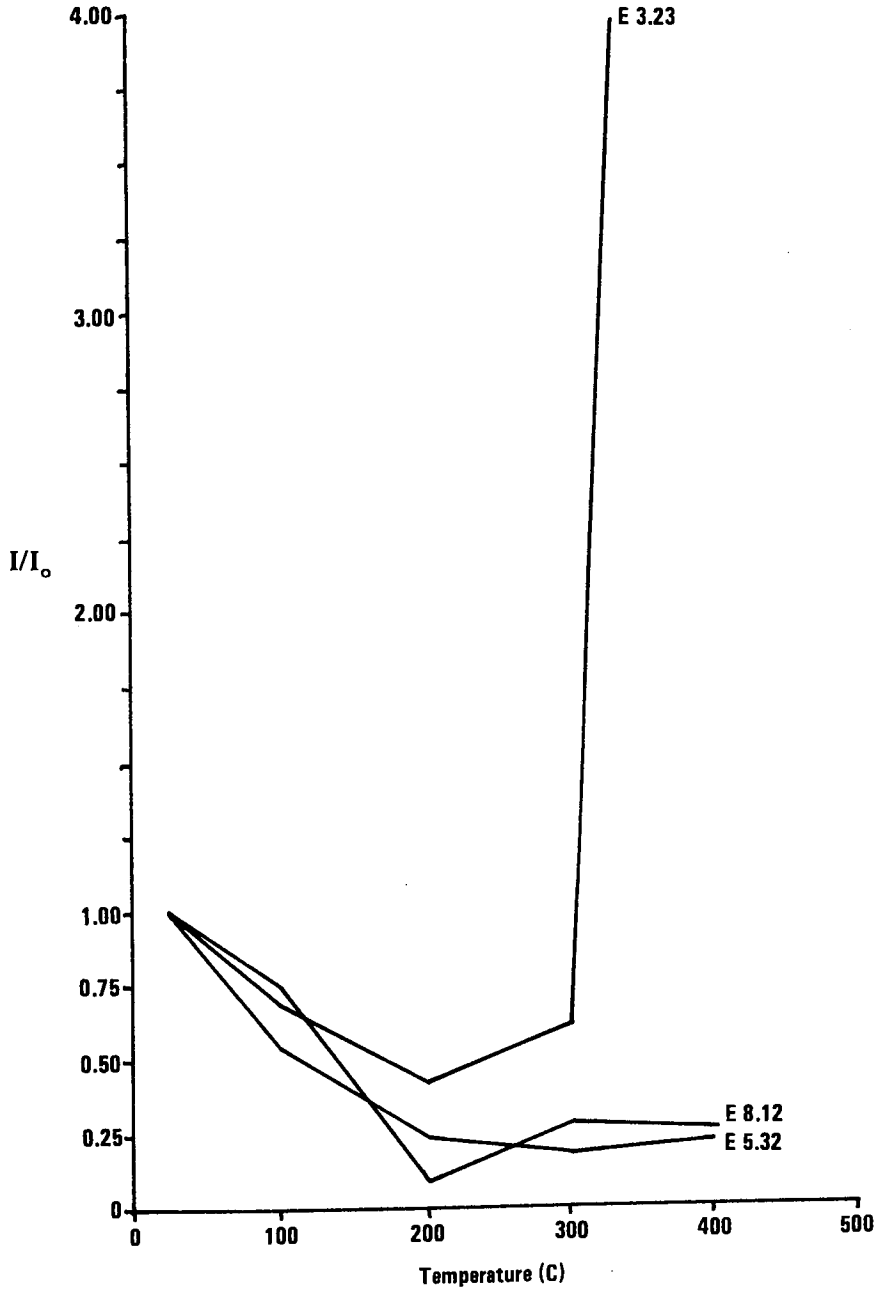

Fig 7.11 Thermal demagnetization pilot study.
Marlstone Rock-bed, Intensity, variation with temperature

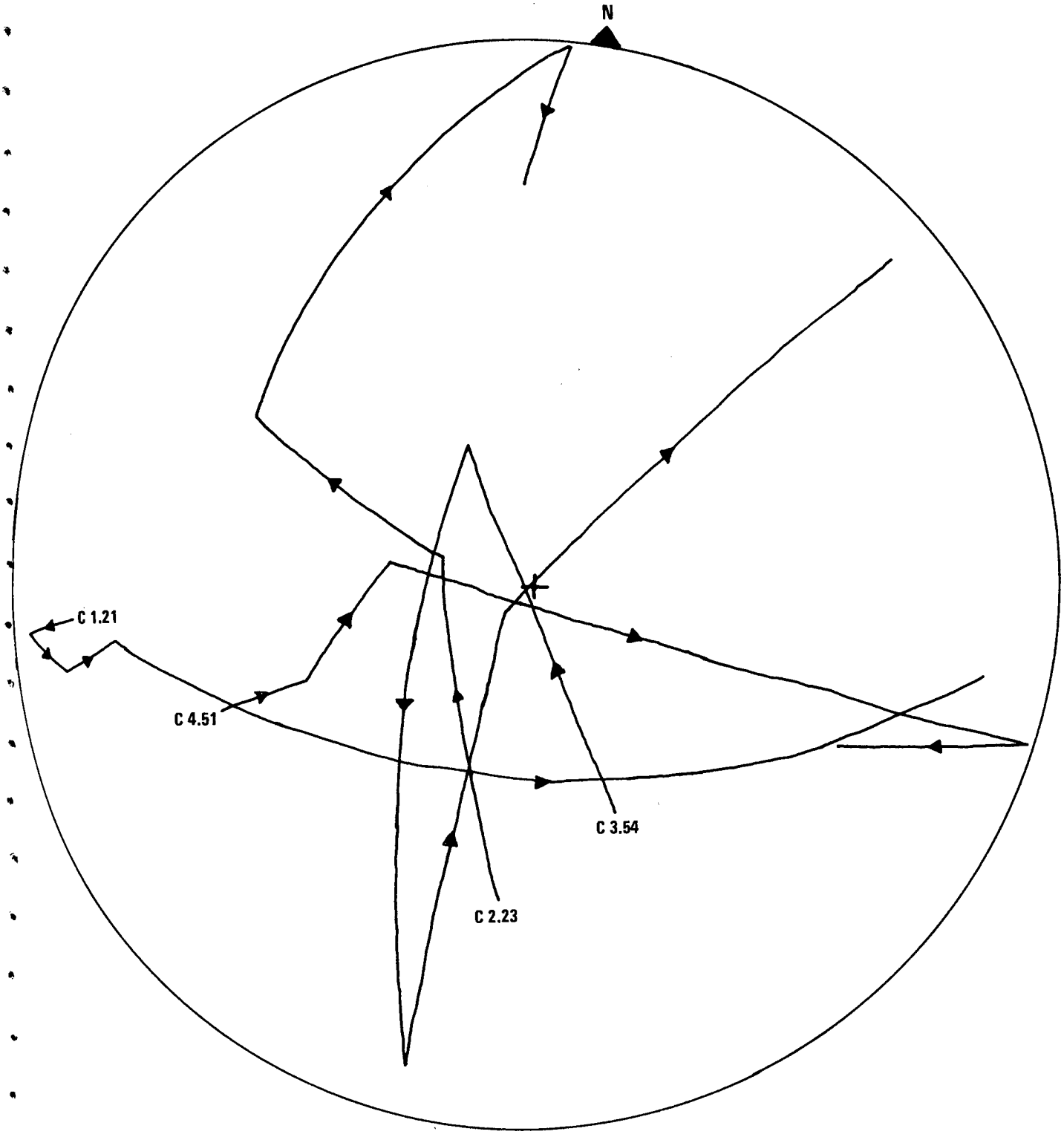

Fig 7.12 Thermal demagnetization pilot study. Cleveland Ironstone
Temperature progression : Room temperature, 100C, 200C, 300C, 400C

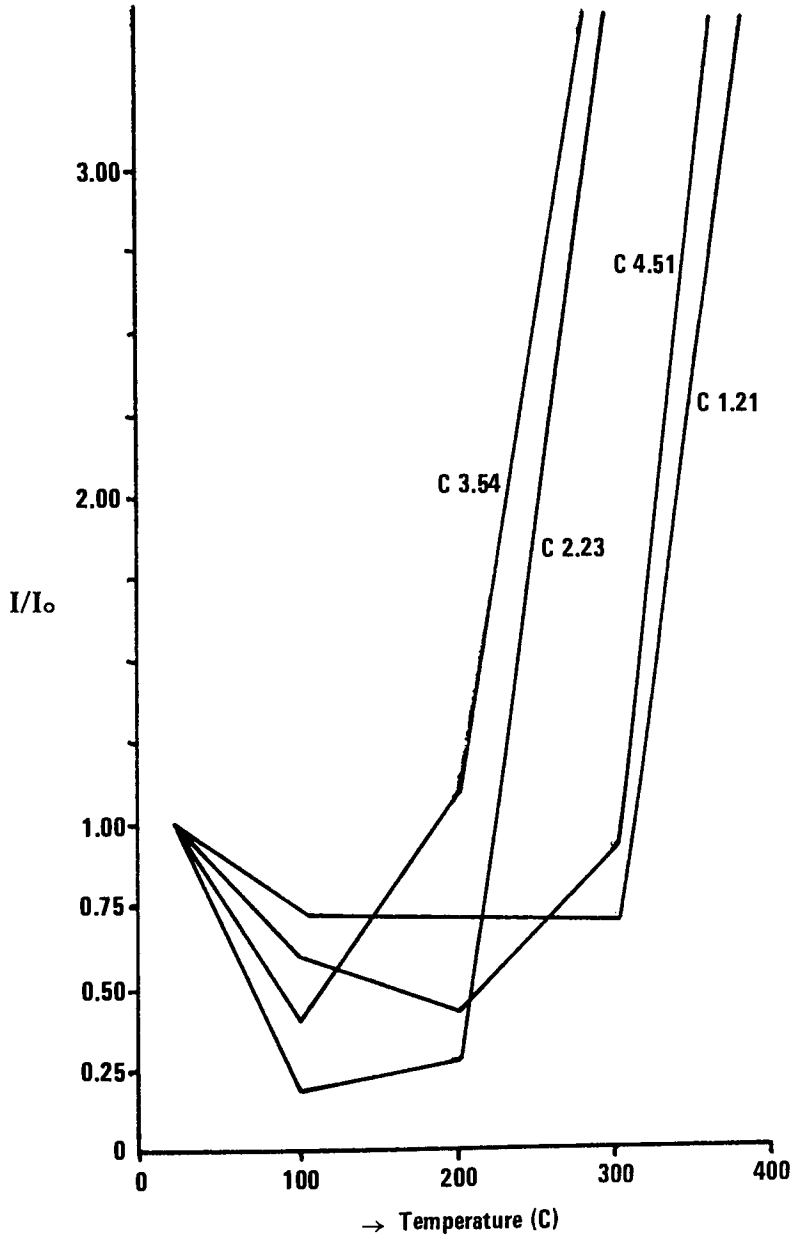

Fig 7.12 Thermal demagnetization pilot study. Cleveland Ironstone. Intensity, variation with temperature

in intensity to almost zero which is followed by a rapid increase. The intensity increase can be explained as the result of the break-down of siderite to magnetite and the formation of a chemical remanent magnetisation due to the presence of some minor residual fields in the laboratory. It is concluded that no stable direction of magnetisation is present within these ironstones and that the measureable natural remanence is viscous in nature.

If viscous remanent magnetisation characterises specimens of these ironstones then some diminution in their intensity should be observable following magnetisation by an applied field greater than that of the earths. This would also be observed as a gradual change in the declination and inclination until values similar to those of the earths field were obtained. A study of this type has been carried out by Kligfield and Channell, (in press). Although a large number of measurements were carried out no such variation was obtained. Thellier (1938) has shown that the change in magnetisation is proportional to the logarithm of time. This suggests that since no change in the magnetisation of the specimens was observed an initial rapid change in magnetisation occurred prior to measurement (Figure 7.13). The total period of study spanned approximately two months. No change in the intensity of magnetisation, declination, or inclination corresponding to the attainment of a viscous component of magnetisation was observed. It would, however, be quite possible for such a component to be obtained over the time period since the formation of the specimens.

Since an intensity of magnetisation of 10-30 micro Gauss was obtained in the above experiment and did not decay with time it seems likely that

minerals capable of carrying a magnetic remnance are present in the Marlstone Rock-bed and Cleveland Ironstones. IRM curves were derived for specimens from these ironstones (Figure 7.14). In all cases a saturation was obtained by the time an applied field of 3 kOe was reached. Such curves are charactersitic of magnetite.

7.4 CONCLUSIONS

(1) The Frodingham Ironstone has a stable remanent magnetism probably carried by goethite. The stable direction corresponds to a palaeopole position of latitude 77.8°, longtitude 78.2° for the Sinemurian stage of the Jurassic.

(2) The Marlstone Rock-bed and Cleveland Ironstones exhibit a large viscous component of magnetisation which is probably carried by magnetite particles.

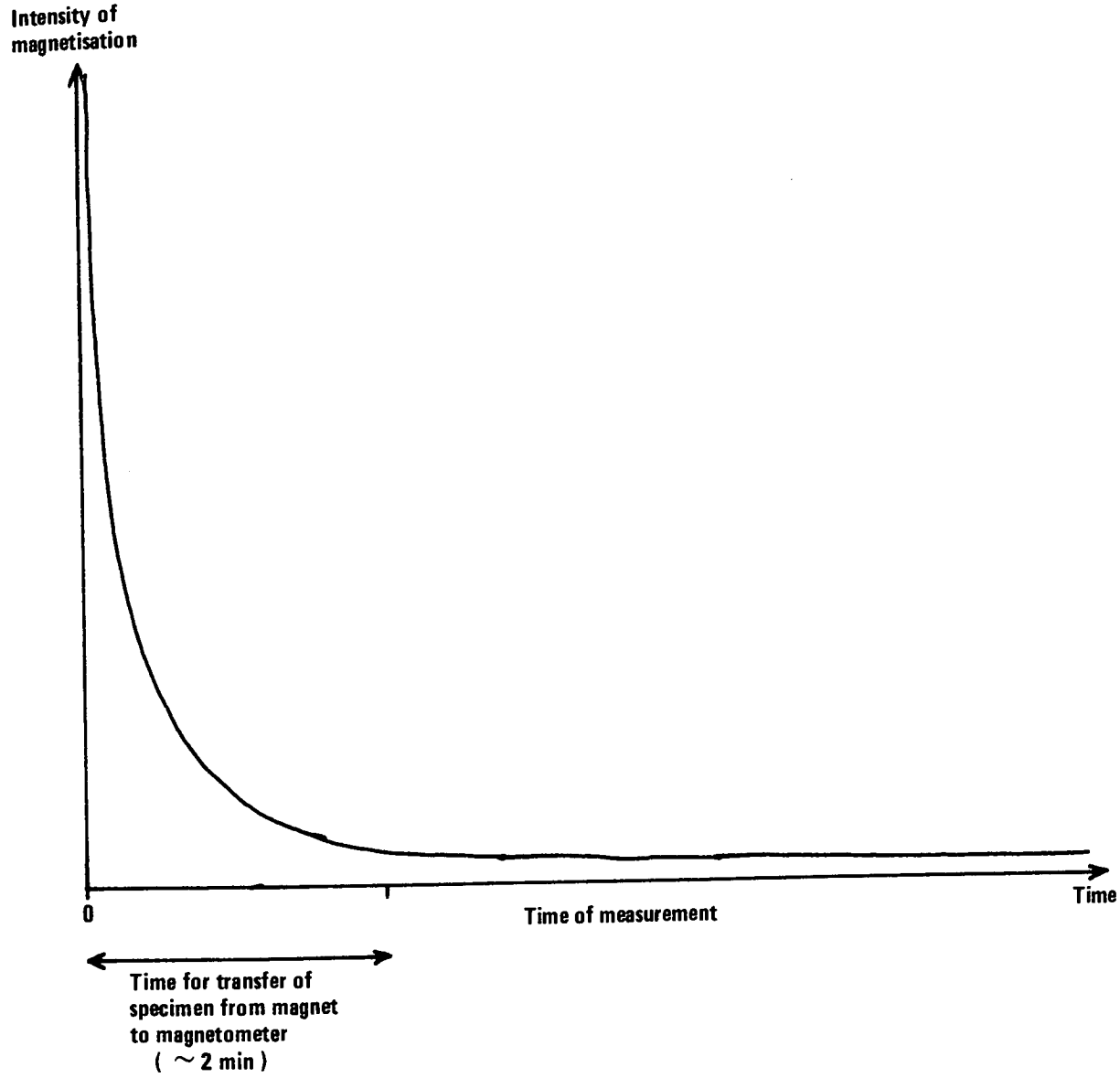

Fig 7.13 Proposed intensity change with time

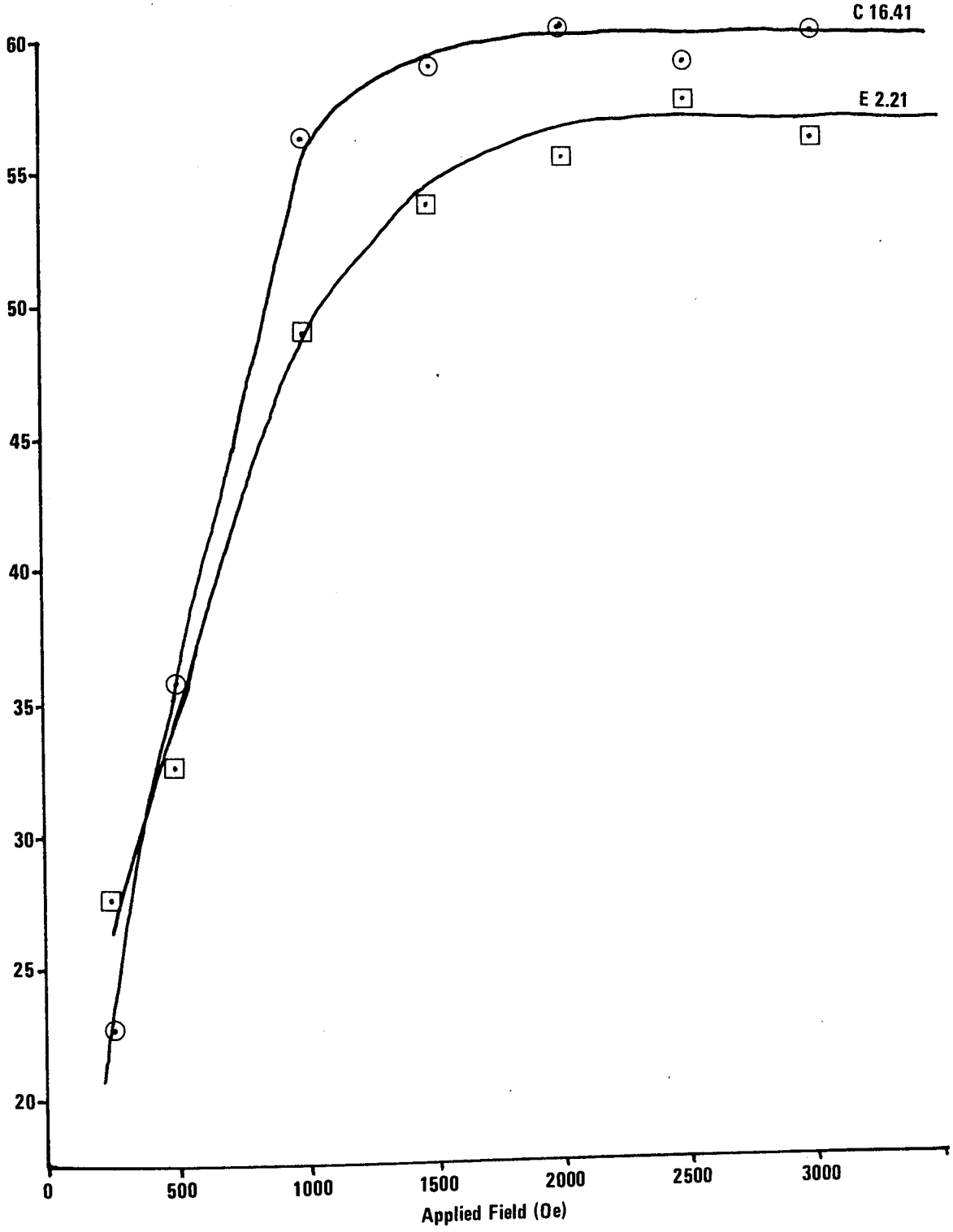

Fig 7.14 IRM curves for Marlstone sample E2.21 and Cleveland sample C16.41

CHAPTER 8

CHEMICAL CONSTRAINTS ON THE DEPOSITIONAL AND DIAGENETIC ENVIRONMENTS OF THE LIASSIC IRONSTONES

CHEMICAL CONSTRAINTS ON THE DEPOSITIONAL AND DIAGENETIC ENVIRONMENTS OF THE LIASSIC IRONSTONES

8.1 INTRODUCTION

From a geochemical standpoint the environment of formation of the Liassic Ironstones can be conveniently subdivided into a depositional and a post-depositional or diagenetic environment. Neither of these environments is represented in present-day sedimentary facies. Thus, the geochemical parameters which define them are unknown. One approach to elucidating the prevalent geochemical conditions during ironstone formation is by considering ironstone mineral assemblages in the context of stability criteria.

8.1.1 Previous Applications Of Stability Criteria

The interpretation of mineral assemblages in terms of their formational physico-chemical conditions was first discussed by Krumbein and Garrels (1952). Garrels (1960) has taken this discussion further by analysing the underlying principles and limitations to the application of chemical thermodynamics to sedimentary systems. Until this analysis, the nature of sedimentary systems had only been considered in terms of Eh and pH. Possibly the most important point made by Garrels (1960) is that the role of dissolved ionic species such as HCO_3^-, SO_4^{2-}, and HS^- in determining the nature of Eh v pH diagrams for mineral assemblages in which carbonates or sulphides are involved should not be ignored. Berner (1963) demonstrated the importance of considering goechemical variables other than Eh and pH in relating the diagenetic

formation of pyrite to the activity of the HS^- and SO_4^{2-} ions in interstitial waters.

Curtis and Spears (1968a) have applied these thermochemical considerations in an appraisal of the environmental controls upon iron mineral formation. In order to assess more precisely the geochemical stability range of iron minerals these workers utilised what is known of geochemical conditions prevalent in Recent sediments by restricting their considerations to pH = 8.0, for depositional waters, and pH = 7.0 for pore waters. They did not restrict Eh as this shows a considerable range of values in Recent sediments. In applying their results to iron-rich sediments, specifically aluminous ironstones, Curtis and Spears (1968a,b) were hampered by the absence of thermochemical data for chamosite which did not allow them to construct stability fields for this mineral. They assumed that since it contains both ferrous and ferric iron its stability fields may be similar to those of magnetite. Tardy and Garrels (1974) have provided a method by which the requisite data may be estimated. Their method has been applied in this work, thus overcoming some of the problems faced by Curtis and Spears (1968a,b). Klein and Bricker (1977) have applied the work of Tardy and Garrels (1974) in a discussion of the sedimentary and diagenetic environments of a Precambrian banded ironstone formation (silicate ironstone). These authors concluded, on the basis of equilibrium mineral assemblages, that the physico-chemical environment prevailing during the formation of this ironstone was not very different from that which obtains in present-day sedimentary basins.

8.1.2 The Nature Of Stability Diagrams

Thermochemical calculations for reactions between dissolved ionic species or between dissolved ionic species and precipitated solids may be plotted graphically as a function of the activities of the dissolved ions. If more than one dissolved species takes part in the reaction, as either a reactant or a product, then the activities of these species are held constant for a given diagram. The calculations which lead to the construction of a stability diagram are for reactions which are assumed to have reached an equilibrium state in a closed system. All sedimentary systems, however, are open and as a result, total internal equilibrium is rarely approached. This is clearly indicated by the presence of mineral phases which are unstable with respect to minerals with which they are associated. Magnetite, for instance, occurs in association with pyrite in the intertidal sediments of the Wash (R. J. Suttill, pers. comm.). The presence of apparently unstable mineral phases may be explicable in terms of reaction kinetics. In the case of the Wash sediments, the rate of formation of pyrite, via iron monosulphides, by the bacterial reduction of SO_4^{2-} and the resultant combination of HS^- with Fe^{2+} is much greater than that of the formation of pyrite by the reduction of magnetite.

In sedimentary systems, therefore, unless it can be demonstrated than an equilibrium mineral assemblage exists, stability diagrams can only be usefully applied in the recognition of potentially unstable phases, which may react, and stable phases which represent reaction products. The recognition of a series of textures representing successive reactions may allow some overall trend in the physico-chemical parameters of the sedimentary system to be revealed.

8.1.3 The Concept of Solid Stability

In closed systems similar in composition to sediment-water systems, the bulk of all chemical species, other than water, tend to occur in the solid phase. The activities of the dissolved ionic species will therefore be controlled by the composition and amounts of the solids present rather than the reverse (Curtis, 1978). At some stage, the activity of a dissolved ion in equilibrium with a particular solid may become so low that the solid becomes immobile or inert towards the system at that time. This is solid stability.

Garrels (1960) places the limit at which a solid becomes stable with respect to coexisting ions arbitrarily at an ionic activity of 10^{-6}. Garrels (1960) notes, on the basis of his own and other researchers work, that this may be taken as the activity of any given ionic species in equilibrium with a solid since there is very little contribution to the stability fields of different ions by other ionic species.

Curtis and Spears (1968a) adopted a solid stability criterion of 10^{-6} for the depositional environment but a criterion of 10^{-3} for pore waters. This follows from the fact that ionic activities are maintained at much higher levels in interstitial fluids. This premise is supported by the fact that higher concentration stability criteria were required to plot the fields of siderite and magnetite over Eh ranges recorded from Recent sediments.

8.2 DETERMINATION OF STABILITY FIELD DIAGRAMS

The methods by which stability field diagrams are obtained are discussed by Garrels (1960) and Vaughan and Craig (1978). The boundaries between any two given phsaes are gradients representing their equilibrium when plotted as a function of ionic activities. These gradients are obtained from thermochemical calculation based on the chemical equilibria existing between the phases. The equilibrium reactions used in this work are given in Table 8.1. The thermochemical calculations require the Gibbs Free Energy of Formation (ΔG_f) of phases. The values of ΔG_f used in this study are listed in Table 8.2. Since these values are quoted in the literature at a standard temperature of 25 C and pressure of 101325 Nm^{-2} the stability diagrams presented are also for these values (i.e. as ΔG_f^{25}).

8.2.1 Estimation Of ΔG_f^{25} For Chamosite Using The Method Of Tardy And Garrels (1974)

The assumption in this method of ΔG_f^{25} estimation is that if the formula of a layer silicate is written in terms of its component oxides and hydroxides, then the ΔG_f^{25} of the silicate is equal to the measured ΔG_f^{25} of the components plus a small indivdual increment which is necessary for them to be incorporated with the other components in a silicate framework. The authors have followed the rule of assigning all hydroxyl components to magnesium. Residual magnesium is expressed as the oxide. From this assumption a series of simultaneous equations can be set up in order to estimate the Δg_f^{25} values of component oxides and hydroxides in silicates. The values of these components are listed in Table 8.3. During the past years, the values of the $\Delta G_f 25$

1) Ferrous chamosite - ferric chamosite.

$2Fe_3Si_2O_5(OH)_4 + 2H_4SiO_4 + H_2O \rightleftharpoons 3Fe_2Si_2O_5(OH)_4 + 2H^+ + 2e^-$

$Eh = 0.164 - 0.059pH - 0.059 \log aH_4SiO_4$

2) Ferrous chamosite - siderite

$Fe_3Si_2O_5(OH)_4 + 3HCO_3^- + 3H^+ \rightleftharpoons 3FeCO_3 + 2H_4SiO_4 + H_2O$

$-\log K = -2 \log aH_4SiO_4 + 3\log a\,HCO_3^- - 3pH$

3) Fe^{2+} - ferrous chamosite

$3Fe^{2+} + 2H_4SiO_4 + H_2O \rightleftharpoons Fe_3Si_2O_5(OH)_4 + 6H^+$

$\log k = -6pH - 3 \log aFe^{2+} - 2 \log aH_4SiO_4$

4) Ferrous chamosite - iron monosulphide

$Fe_3Si_2O_5(OH)_4 + 3HS^- + 3H^+ \rightleftharpoons 3FeS + 2H_4SiO_4 + H_2O$

$\log k = 2 \log aH_4SiO_4 - 3 \log aHS^- + 3pH$

5) Ferrous chamosite - pyrite

$Fe_3Si_2O_5(OH)_4 + 6HS^- \rightleftharpoons 3FeS_2 + 2H_4SiO_4 + H_2O + 6e^-$

$Eh = -0.428 + 0.019 \log aH_4SiO_4 - 0.059 \log aHS^-$

6) Ferric chamosite - goethite

$Fe_2Si_2O_5(OH)_4 + 3H_2O \rightleftharpoons 2FeOOH + 2H_4SiO_4$

$\log K = 2 \log aH_4SiO_4$

7) Fe^{2+} - siderite

$Fe^{2+} + HCO_3^- \rightleftharpoons FeCO_3 + H^+$

$\log K = -pH - \log aHCO_3^- - \log aFe^{2+}$

Table 8.1 - Equilibrium Reactions

Reactant and state	ΔG_f^{25} (kcal mol^{-1})	Source
H_4SiO_4 (aq)	-312.50	1
H_2O (aq)	-56.69	1
H^+ (aq)	0.00	
HCO_3^- (aq)	-140.30	1
$FeCO_3$ (siderite) (s)	-161.00	1
Fe2+ (aq)	-20.30	1
HS^- (aq)	-2.90	1
FeS (iron monosulphide) (s)	-22.30	1
FeS_2 (pyrite) (s)	-38.30	2
FeOOH (goethite) (s)	-117.00	3

Sources: 1 Klein and Bricker (1977)

2 Vaughan and Craig (1978)

3 Tardy and Garrels (1974)

Table 8.2 - Gibbs Free Energy of Formation of Reactants at 25 C (Excluding Silicates) in Order of Appearance in Table 8.1

of several layer-silicates have been experimentally determined. Tardy and Garrels (1974) report good agreement between the observed and estimated values.

Brindley and Youell (1953) have identified ferrous and ferric varieties of chamosite. The distribution of ferrous iron, ferric iron, aluminium, and magnesium within chamosite has been discussed in Chapter 6 and it was concluded that the relative proportions of ferrous and ferric iron in the octahedral sites were the only major variables. It was noted that complete oxidation of ferrous chamosite $Fe^{2+}_3(Si_2O_5)(OH)_4$ without dehydration, would be expected yielding, a chamosite with the structural formula $Fe^{3+}_2(Si_2O_5)(OH)_4$ (Brindley (1951) is reported in Table 8.4. In order to more fully represent natural mineral assemblages on stability diagrams, mineral compositions characteristic of actual mineral phases rather than pure end-members should be used. The equilibrium reactions for natural chamosites, however, would become rather complicated and the stability diagrams rather more difficult to interpret if natural chamosite data were utilised. Equilibrium reactions and thermochemical calculations are therefore based on the ideal formulae. Clearly there will be a disparity between the stability fields for the ideal material and those of the natural chamosites. This is due to the fact that the ideal formulae do not take into account the presence of aluminium, magnesium, and varying proportions of ferrous and ferric iron. The disparity will take the form of smaller stability fields for the ideal chamosites than natural chamosites; the overall geometry of the fields will be unchanged (Klein and Bricker, 1977).

Oxide	ΔG_f^{25} Silicated (kcal mol^{-1})
FeO	-64.10
Fe_2O_3	-177.7
SiO_2	-204.6
H_2O	-59.20

Table 8.3 - Gibbs Free Energy of Formation of Silicated Oxides

(Tardy and Garrels, 1974)

Chamosite Type	Components	ΔG_f^{25} (kcal mol^{-1})
Ferrous Chamosite ($Fe_3^{2+}Si_2O_5[OH]_4$)	$3FeO,2SiO_2,2H_2O$	-719.70
Ferric Chamosite ($Fe_2^{3+}Si_2O_5[OH]_4$)	$Fe_2O_3,2SiO_2,2H_2O$	-705.3

Table 8.4 - Gibbs Free Energy of Formation of Ferrous and Ferric Chamosite (25 C)

8.2.2 Environmental Constants

Following the work of Curtis and Spears (1968a), pH values are restricted to pH = 8 for the depositional environment and pH = 7 for interstitial waters. Eh values are not kept at any constant value. A solid stability criterion of an ionic activity of 10^{-6} is used for depositional waters and 10^{-3} for interstitial waters.

Goethite has been used as the most highly oxidised iron phase as this has been reported as an ooid-forming mineral in Recent sediments (Porrenga, 1967; Lemoalle and Dupont, 1976). Monosilicic acid (H_4SiO_4) is considered to represent the mode of occurrence of dissolved silicon in diagenetic and depositional environments as it is considerably more soluble than species such as SiO_2.

8.3 STABILITY RELATIONSHIPS

The mineral assemblages discussed in the petrographic descriptions of the ironstones may be subdivided into those which formed the primary components of the sediments i.e. chamosite and goethite ooids, intraclasts, chamosite mud, and calcite and aragonite biogenic debris, and those which developed during diagenesis. These include authigenic chamosite, siderite, and ferroan calcite. Textures involving both primary constituents and diagenetic minerals represent diagenetic reactions.

8.3.1 The Depositional Environment

The primary components of the depositional environment can be grouped into those composed of chamosite and those which originated as chamosite, and those which were of either calcite or aragonite. The relationship between seawater and calcium carbonate has received considerable attention in the literature (Bathurst, 1975). The relationship between seawater and chamosite and goethite has not been specifically discussed.

Chamosite is a common mineral throughout the Liassic Ironstones. Although it is considered to have formed as the first authigenic phase it must ultimately depend for its composition on the goechemistry of the seawater. Figure 8.1 illustrates the solubility of ferrous chamosite as a function of pH and the activity of total dissolved Fe. Solubility curves are presented for two dissolved silica activities. These were derived by Eugster and Chou (1973) and Klein and Bricker (1977) for pure greenalite ($Fe_3^{2+}Si_2O_5(OH)_4$). Since ferrous chamosite and greenalite have the same formulae this diagram applies to them both. The maximum concentration of dissolved silica which could have occurred at the time of chamosite formation is that which is in equlibrium with amorphous silica. This has an activity of $10^{-2.7}$. This value for silica saturation is not unreasonable as silica-secreting organisms did not appear until the Cretaceous. (Brasier, 1980). There is no chert associated with aluminous ironstones, however. Lateral equivalents of ironstones are represented by clays, shales, and sandstones. Dissolved silica would therefore be in equilibrium with

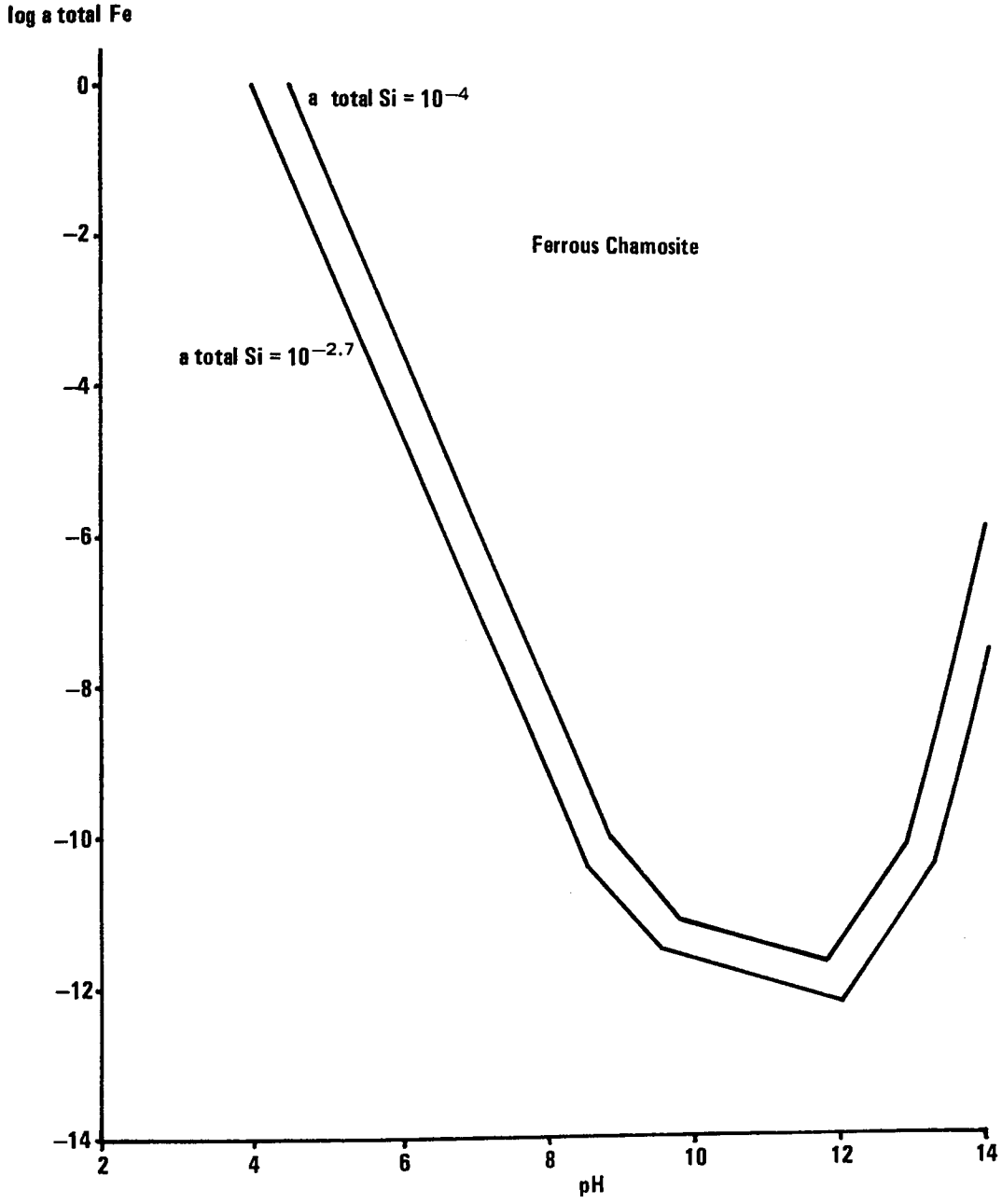

Fig 8.1 Solubility of Ferrous Chamosite

quartz and clay minerals. Sillen (1967) has reported a dissolved silica activity of 10^{-4} for this equilibrium in present-day marine sediments. The solubility of ferrous chamosite at pH = 8 and a dissolved silica activity of 10^{-4} suggests that the total dissolved iron activity was of the order of 10^{-8}. Dissolved iron concentrations in sea-water are of the order of 3 x 10-6 ppm. Lewis and Goldberg, 1954; Spencer and Brewer, 1969). This value approximates to a dissolved iron activity of 10-11. The method by which the dissolved iron concentrations are determined includes iron present as complexes (Turekian and Wedepohl, 1961) in addition to ionic iron in the result. Thus, this value is a minimum value for the total iron concentration in seawater. The complexing of iron also has an affect on the solubility curves for ferrous chamosite in Figure 8.1: These are calculated on the basis of inorganic equilibria in which the possibility of iron-bearing complexes providing a contribution to the total available iron is ignored. The calculated solubilities therefore represent minimum values. A third factor should also be taken into account. This is the concentration of dissolved iron within the sediment where chamosite ooids form. Since this sediment is thought to have consisted, primarily, of chamosite ooids and chamosite mud resulting from the precipitation of iron and silicon from seawater, a boundary situation between early authigenic environments and depositional environments is what should be considered. Interstitial waters at the site of chamosite ooid formation would be expected to exhibit high Fe^{2+} and H_4SiO_4 activities providing an additional source for the components of chamosite by a diagenetic reflux. Due to the absence of any data for dissolved Al3+ activities in seawater it has not been possible to discuss how a Al3+

relates to the solubility of ferrous chamosite and the total dissolved iron activity. Bearing in mind the marine occurrence of silica as quartz and silica and aluminium as clays such data would be expected to support the above discussion.

Studies of ferrous iron: ferric iron ratios of different chamosite specimens indicates that, at the time of chamosite formation, the ferrous iron content was very high relative to the ferric iron content. In contrast, chamosite which has undergone transport is characterised by a much lower ferrous iron level and a much higher ferric iron level. This would suggest that the oxidation of chamosite in the depositional environment was progressive. In the face of this evidence, it seems likely that the transformation from ferrous chamosite ooids to goethite involved two steps: firstly an oxidation of ferrous chamosite to ferric chamosite, and secondly an oxidation of ferric chamosite to goethite. The first of these two reactions has a Gibbs Free Energy of Reaction of -7.59 k cal $mole^{-1}$, the second a value of -16.37 k cal $mole^{-1}$. The alternative transformation i.e. that from ferrous chamosite to goethite, has a value of -28.35 k cal $mole^{-1}$. The natural environment would tend to favour reactions towards an equilibrium state involving a series of small energy changes rather than one large change, assuming that a catalyst promoting a large energy change was absent. It is not possible to construct a stability diagram for the system ferrous chamosite - ferric chamosite - goethite. This suggests that these three minerals cannot coexist together as an equilibrium assemblage, but does not imply that the transformation from ferrous chamosite to goethite via ferric chamosite is kinetically

prohibited (Curtis and Spears, 1968a). The equilibrium between ferrous chamosite and ferric chamosite is illustrated as a function of Eh and the activity of dissolved H_4SiO_4 at pH = 8 in Figure 8.2. This gives some idea of the geochemical conditions under which ferrous chamosite oxidises to ferric chamosite. With decreasing H_4SiO_4 activities the oxidation takes place at progressively higher Eh values. Sillen (1967) reports a dissolved silica activity of 10^{-4} for seawater. Since this value would include dissolved silica-bearing species other than H_4SiO_4 this activity can be taken as a maximum for the activity of H_4SiO_4 in sea-water. Eh values for the oxidation of ferrous chamosite, corresponding to aH_4SiO_4 levels less than 10^{-4}, are similar to the Eh ranges measured in seawater. Curtis and Spears (1968a) conclude that the depositional marine environment may be characterised by an Eh range of -0.1 to +0.5 volts. Ferrous chamosite is the stable phase in waters with negative Eh values whereas ferric chamosite is the stable phase in positive Eh environments. The transition from ferric chamosite to goethite would be expected to occur at dissolved H_4SiO_4 activities of less than approximately 10^{-6} at positive Eh values (Figure 8.2).

8.3.2 The Diagenetic Environment

The petrographic studies of ironstones have concluded that depositional facies are characterised by specific diagenetic mineral assemblages and textures representing diagenetic reactions. In considering these assemblages in terms of stability criteria the nature of interstitial pore fluids must be born in mind. It is generally accepted that the rate of crystal nucleation and growth depends (although not exclusively)

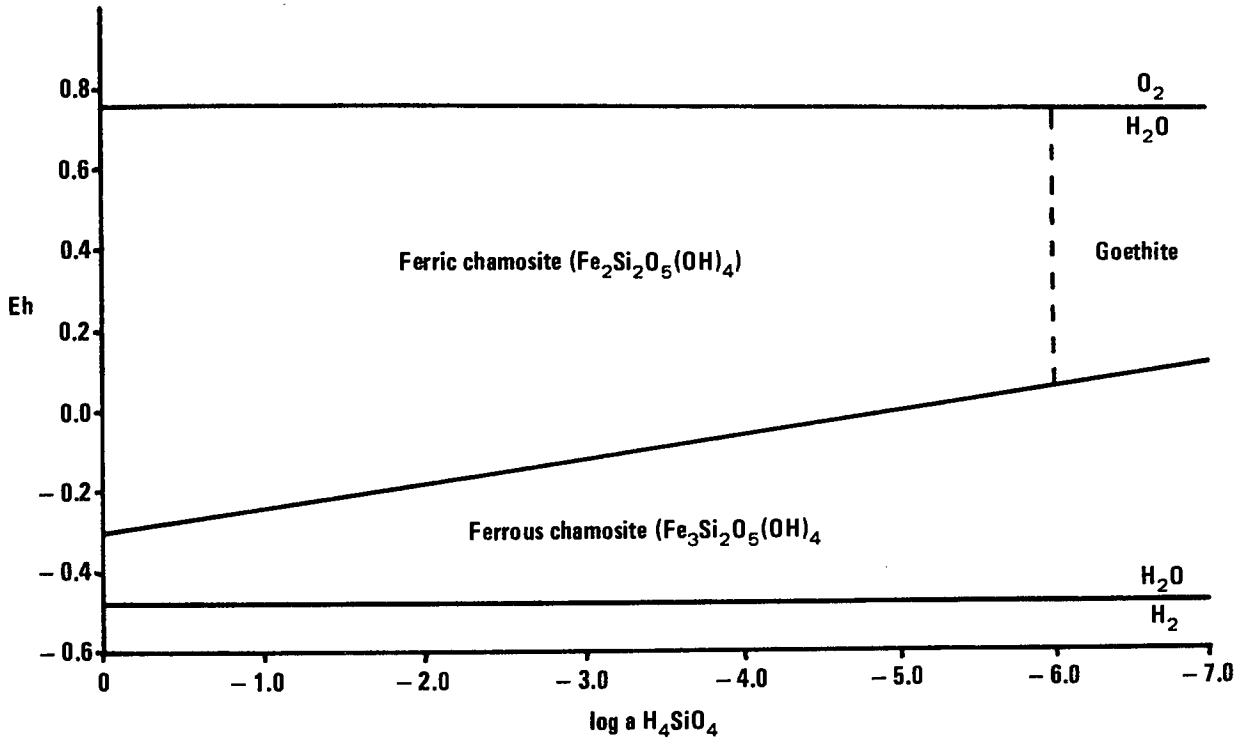

Fig 8.2 Stability of Ferrous and Ferric Chamosite. pH = 8. Dotted line indicates the aH_4SiO_4 value at which ferric chamosite is in equilibrium with goethite

on the degree of supersaturation of the parent pore fluid with respect to the precipitating mineral. Low degrees of supersaturation, for instance, favour growth on existing crystals rather than nucleation and coarsening crystal sizes in sequentially precipitates indicate a diminishing supersaturation level and rate of precipiptation (Curtis, 1978). Although large volumes of aqueous fluids are trapped within sediments at their time of deposition the dissolved species are insufficient to contribute significantly to cements. Aqueous pore fluids must therefore be considered as a medium within which solids may dissolve, be transported, and subsequently be precipitated as solids whose compositions are determined by the physico-chemical conditions existing in the pore fluids. In normal terrigenous sediments cements result from the dissolution of the more soluble components. In ironstones, however, the terrigenous component is extremely small and textural evidence indicates common dissolution of chamosite ooids, aragonite shell debris, and early carbonate cements such as high magnesian calcite or aragonite. It is likely, therefore, that a significant component of the dissolved species within the ironstone pore fluids derived from these sources. Diagenetic mineral assemblages thus depend for their nature on the reactions which cause the entry of different ions into solution, the degree of pore fluid supersaturation which results, and the movement of pore fluids through the system. Curtis (1978) has illustrated this diagrammatically for terrigenous systems. In Figure 8.3 this diagram has been modified with respect to ironstones.

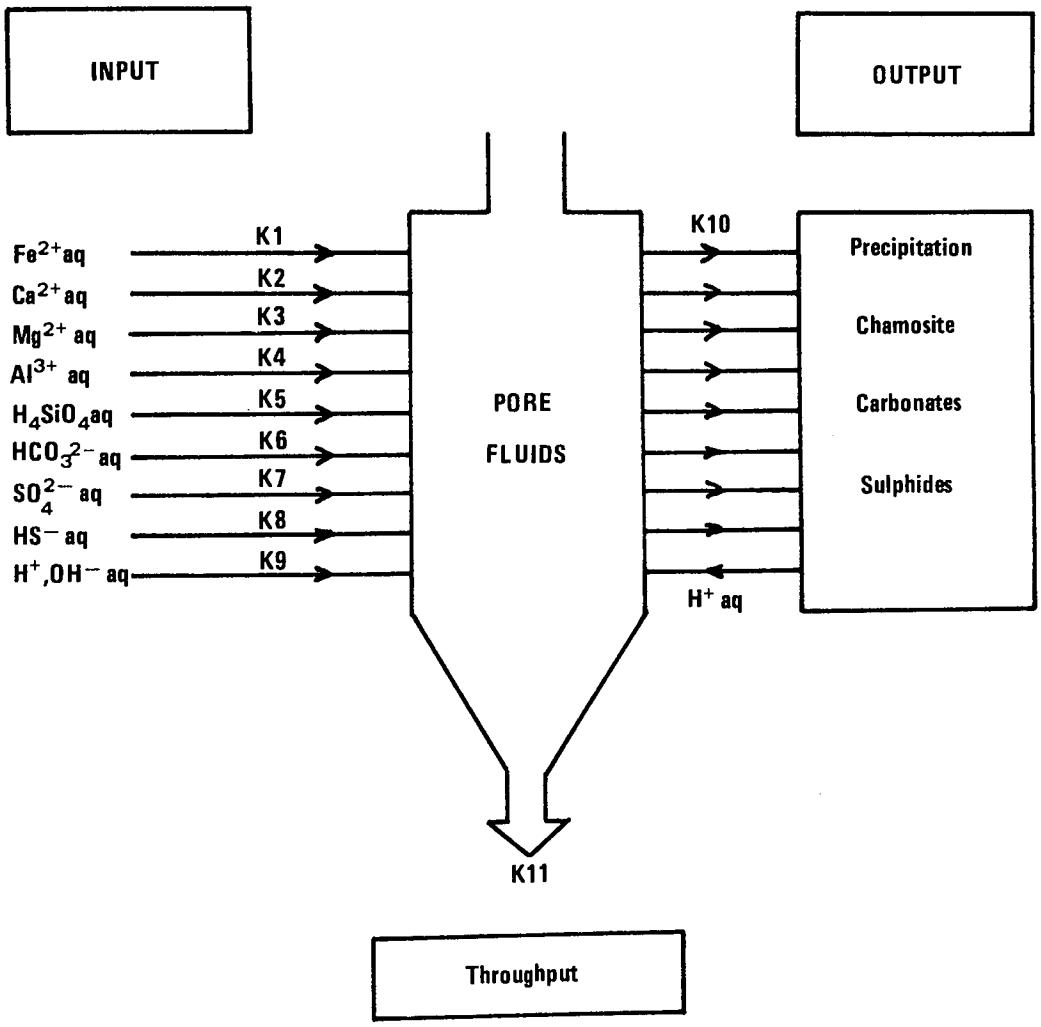

Fig 8.3 K1 – K9; Rate of ions entering solution as a result of decomposition and dissolution reactions

K10; Rate of cement precipitation
K11; Rate of pore fluid migration

8.3.2.i Dissolution. Three frequently occurring textures in the ironstones represent dissolution replacement reactions resulting in chamosite ooids with rims of radial siderite grains and dissolution reactions only in which chamosite ooimoulds are formed and primary chamosite mud is removed. In general the dissolution-replacement occurs first and the removal of chamosite second. Although depositional environments are characterised by a constant pH of approximately 7 (Curtis and Spears, 1968a) it is instructive to consider the system in which these reactions occur as a function of pH. The system in which the dissolution-replacement reaction occurs is ferrous chamosite-siderite-Fe^{2+}-H_4SiO_4-HCO_3^--H^+. The stability fields of Fe^{2+}, siderite, and ferrous chamosite are plotted as a function of aH_4SiO_4 amd pH in Figure 8.4a. For different aFe^{2+} values, slightly more than those suggested for pore waters by Curtis and Spears (1968a), the three phases are in equilibrium at pH values similar to those found in present day pore-waters. The H_4SiO_4 activity is that which might be expected on the grounds that seawater has a total dissolved silica activity of 10^{-4}. This is the situation calculated for an activity of HCO_3aq of $10^{-2.5}$. This is a greater concentration of HCO^{-3} than is found in equilibrium with calcite at the Ca^{2+} activity of normal marine waters (Curtis and Spears, 1968a). The effect of decreasing the HCO_3^- activity (Figure 8.4b) moves the equilibrium point to lower aH_4SiO_4 values. For chamosite to be replaced by siderite via dissolution the geochemical parameters must be very close to the equilibrium point of the two phases. Dissolution of ferrous chamosite would yield Fe^{2+} and the space created would be infilled by the precipitation of siderite thereby redressing the pH imbalance

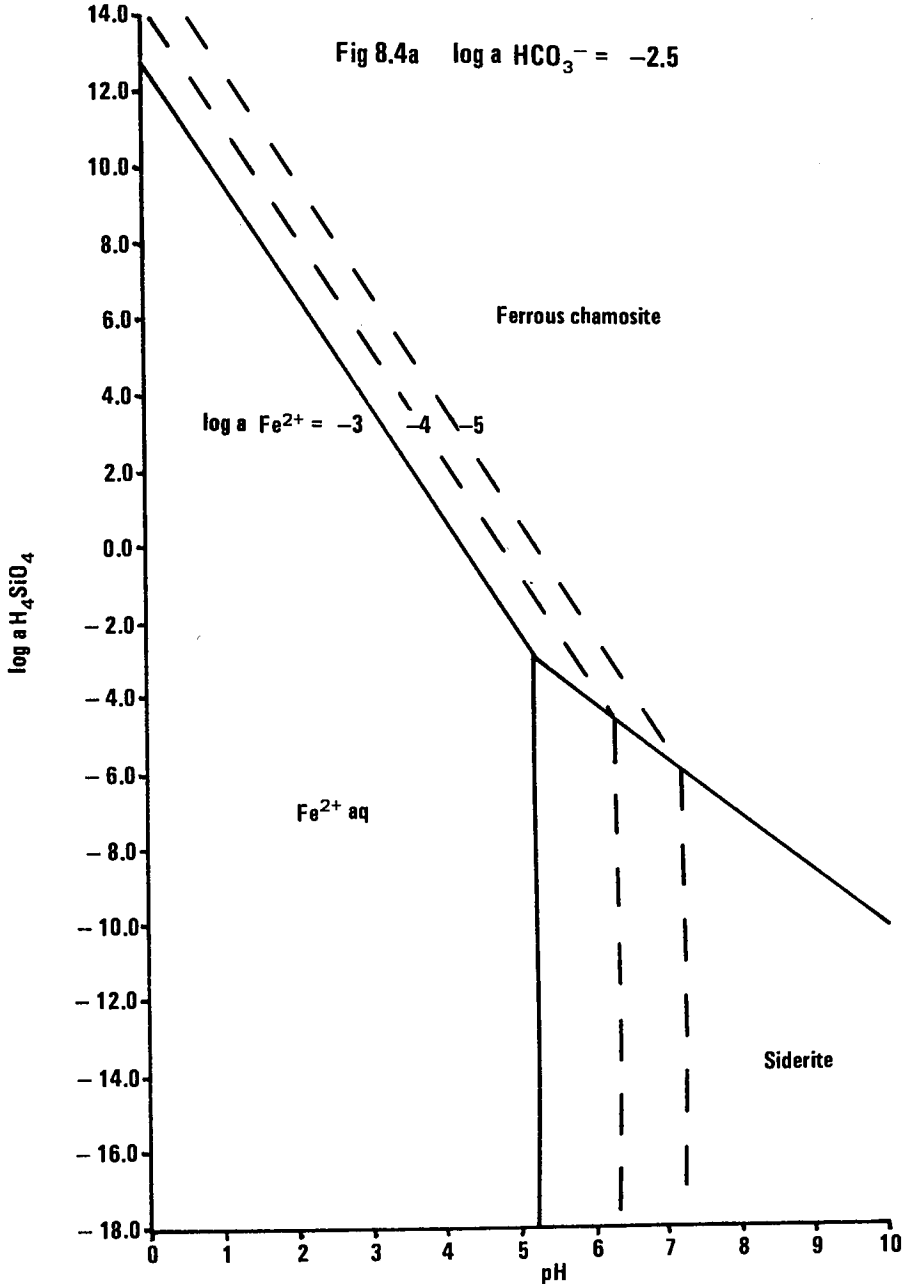

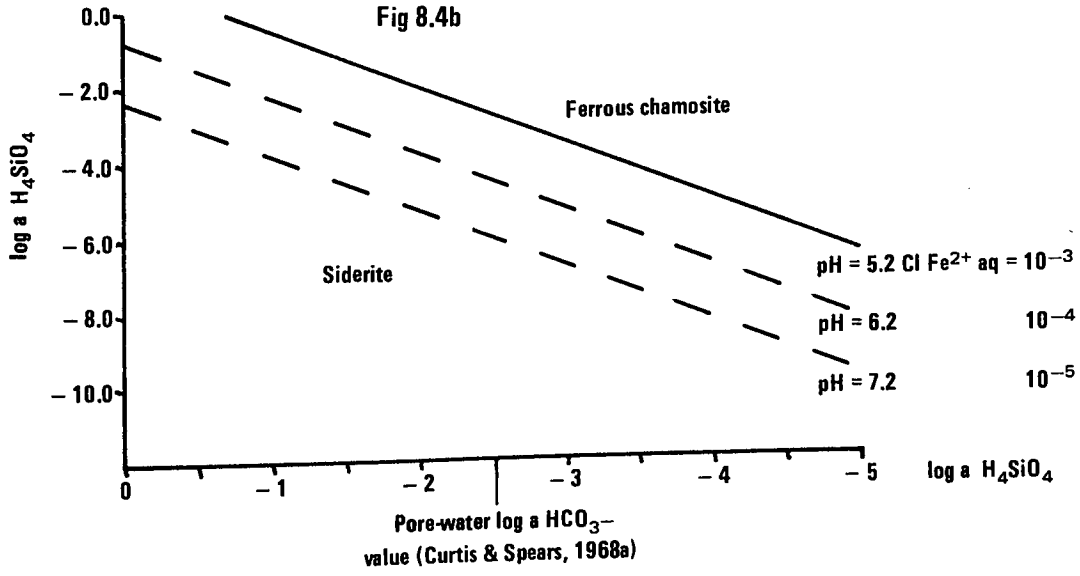

Fig 8.4 Stability relationships between Fe^{2+} aq, Siderite, and Ferrous Chamosite

brought about by the dissolution. The boundary between chamosite and siderite indicates their coexistance under these geochemical parameters. If such parameters were the result of a change from parameters under which only chamosite was stable siderite would precipitate but chamosite would not dissolve. Textures in which chamosite ooids were distorted by siderite crystals would be expected. In this context it is interesting to recall the occurrence of siderite anhedra forming trains, parallel to bedding, in depositional chamosite muds. Their mode of occurrence suggests an easy direction of growth parallel to the dominant (001) bedding-parallel orientation of the chamosite flakes.

There is much evidence to suggest that the formation of ooimoulds and the dissolution of chamosite mud was not accompanied by the precipitation of another mineral. Such textures imply physico-chemical conditions in which chamosite would be near an equilibrium state with some fluid phase. Figure 8.4a suggests that acid pH conditions would be required for chamosite dissolution. The presence of core grain calcite shell fragments in ooimoulds and biogenic debris in areas from which chamosite mud has been removed suggests neutral or slightly alkaline conditions of dissolution. A solid stability criterion of $10^{-4.75}$, or less, for aFe^{2+} would allow such dissolution to occur.

8.3.2.ii Replacement reactions: Several textures have been recognised in which the direct replacement of one phase by another occurs. These include the common replacement of chamosite ooids and chamosite mud by pyrite.

In recent sediments, pyrite forms as a result of the sulphidation of iron monosulphides by HS-. HS- is produced by the metabolic activity of

sulphate-reducing bacteria. The initial combination of HS^- and Fe^{2+} leads to the precipitation of monosulphides (Berner, 1963). The diagenetic production of pyrite in chamosite muds and chamositic chamosite ooilites might be expected to occur in the same way. The textural evidence indicates non-distortive replacement whereas textures indicative of distortive displacive replacement would be expected if pyrite precipitation occurred via a monosulphide phase. Figure 8.5 indicates the stability of pyrite and ferrous chamosite. as a function of Eh and log aHS^- and log aH_4SiO_4. Since a stability diagram for pyrite, iron monosulphide, and ferrous chamosite can only be obtained at an activity of H_4SiO_4 of $10^{-10.5}$ it is thought unlikely that the formation of pyrite from ferrous chamosite involves an intermediate monosulphide stage. The absence of a ferrous iron stability field precludes the possibility of a dissolution-precipitation type of replacement. The boundary between ferrous chamosite and pyrite corresponds to Eh values comparable with those in Recent sediments. Berner (1963), for instance, reports a common Eh range of -0.200v to -0.250v for pore waters in a variety of environments. This range suggests geochemically acceptable values for the activities of HS^- and H_4SiO_4 at which pyrite and chamosite are in equilibrium. Textural evidence implies that the replacement of chamosite by pyrite is a disequilibrium situation at activity values within the pyrite stability field. Thus, the initial chamosite ooids and mud would undergo replacement by pyrite when the geochemical environment changed in favour of pyrite formation. This would be brought about by an increase in the activity of the HS^- ion, a decrease in the

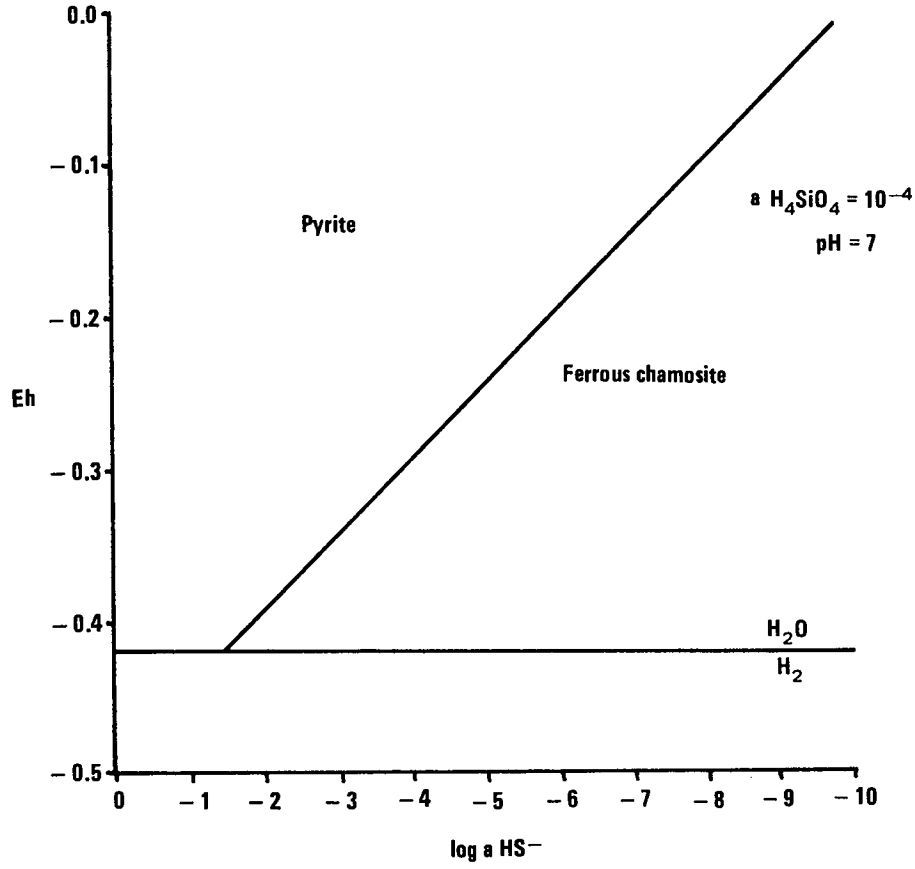

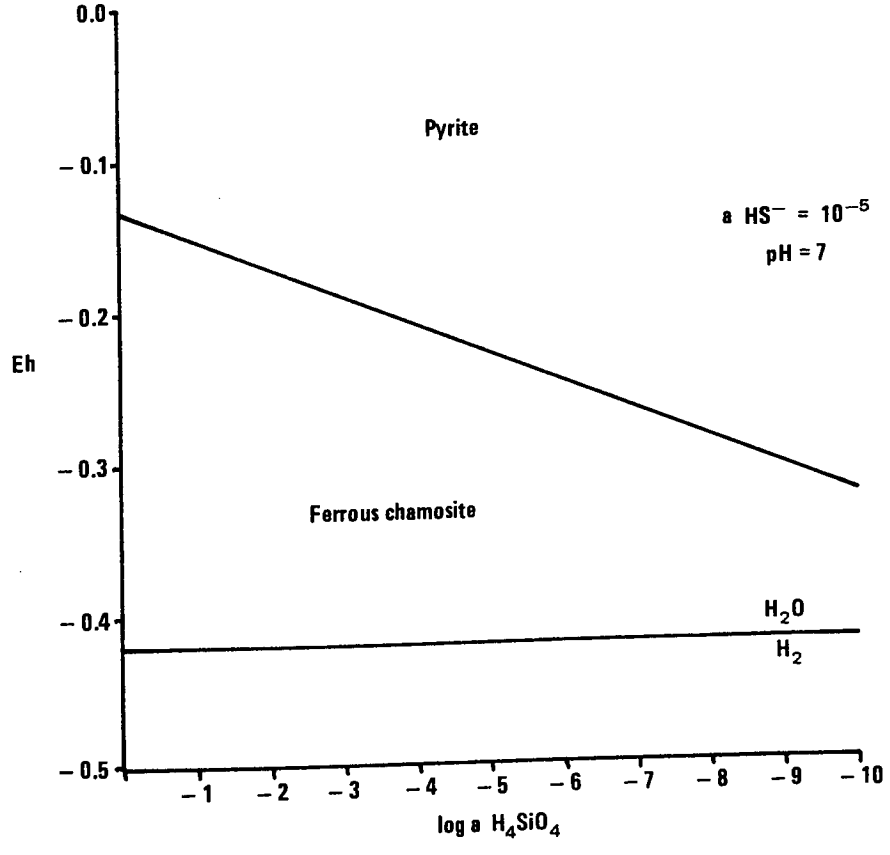

Fig 8.5 Stability relationships between Pyrite and Ferrous Chamosite

H_4SiO_4 activity, or both. Since chamosite oolites and chamosite muds contain organic material bacterial decomposition of this by sulphate-reducing bacteria would be likely to bring about the aSH^- increase required.

8.3.2.iii Cement precipitation: The cements present in ironstones comprise authigenic chamosite, siderite, and ferroan calcite. Some facies may be cemented by only one of these phases, others by a mixture. There is, however, a general trend in the history of cementation which commences with the precipitation of authigenic chamosite. This is followed by iron-rich carbonate (siderite), and this by iron-poor carbonate (ferroan calcite). Thomas (1978) has shown that cement formation in clay and carbonate-cemented sandstones occurs in the same order as that of the ΔG_f^{25} values of the minerals. This assumes precipitation from a single pore fluid. The ΔG_f^{25} of ferrous chamosite (-719.9 kcal $mole^{-1}$) is greater than that of siderite (-161 kcal $mole^{-1}$) suggesting that it is formed and precipitated more easily. Calcite has a value of -269.7 kcal $mole^{-1}$. If all three minerals precipitated from a single pore fluid, calcite would be expected to precipitate between chamosite and siderite. The composition of the pore fluids in fact controls the precipitation of siderite and calcite. A ferrous iron concentration more than 5% greater than that of the calcium concentration favours siderite precipitation (Berner, 1971). The aHS^- is also an important control on the cement as if this is in excess of all other anions, pyrite will precipitate whereas an excess of HCO^{-3} over HS^- allows siderite precipitation (Curtis and Spears, 1968a).

It has been shown that depositional chamosite muds undergo authigenisis with burial. Transport of the chamosite mud would have resulted in partial if not total oxidation to ferric chamosite, as indicated by Mossbauer studies. The presence of organic material in the chamosite mud as a result of the erosion and breakup of chamositic chamosite oolites and also from other sources would cause the development of a negative Eh environment (Curtis, 1978) as a result of its decomposition. Reference to Figure 8.6 shows that at activities of H_4SiO_4 of the order of 10^{-4} Eh levels of -0.3 are required. A lower H_4SiO_4 activity will result in the reduction of ferric chamosite to ferrous chamosite at slightly higher Eh values. Textures such as isopachous authigeneeic chamosite linings to pore spaces indicate the possibility of localised chamosite dissolution and reprecipitation. A further diagenetic change in the lithologies characterised by an 'in situ' authigenic chamosite cement (chamositic limonite oolite sub-type iii) is the removal of chamosite by dissolution. This leaves goethite ooids in a porosity which is infilled by siderite.

Where siderite occurs as a cement to goethite ooids it is commonly distortive with respect to them. As goethite is a ferric compound, its presence in environments where a negative Eh prevailed is, perhaps, difficult to understand. Obviously the $aFe^{3+}aq$ activity would be extremely low thus causing the relative immobility of the goethite ooids. Reactions in which goethite is being dissolved or undergoing dissolution and replacement by a ferrous mineral cannot be convincingly demonstrated (goethite ooimoulds may represent a goethite skin to an originally chamosite core which underwent dissolution). The presence of magnetite in present-day negative Eh

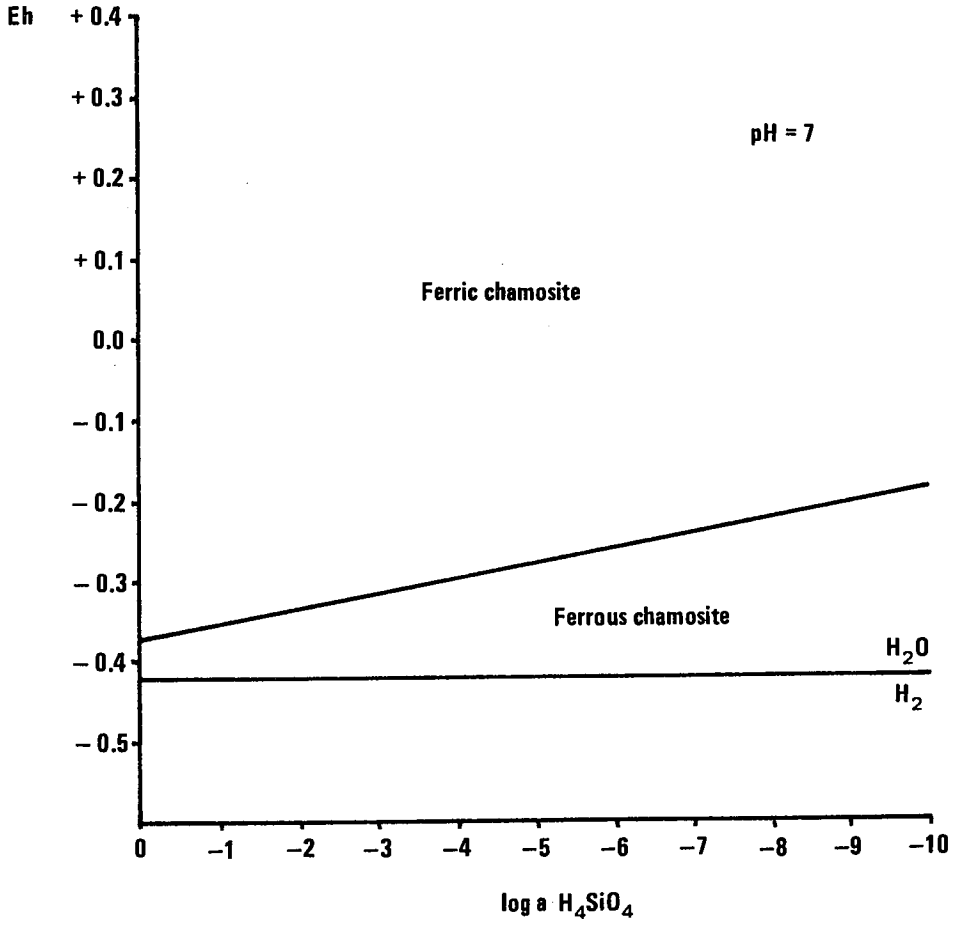

Fig 8.6 Stability relationship between ferrous and ferric chamosite

environments allows the suggestion that the kinetics of reactions bringing about the reduction of goethite are extremely slow. Thus the distortive textures exhibited by siderite and goethite ooids may be ascribed to the pressure of crystallisation of siderite. Reference to Figure 8.4b shows that HCO_3^- activities slightly higher than those at which HCO_3^- is in equilibrium with calcite in seawater, siderite will precipitate at H_4SiO_4 activities less than 10^{-6}. The possibility that siderite cements of this type represent an almost immediate replacement following chamosite dissolution exists. Chamosite dissolution would cause an increase in the H_4SiO_4 activity for a time and siderite precipitation would be impeded until this dropped. In some cases there is textural evidence to suggest that some time interval separated chamosite dissolution from siderite precipitation.

Cement fabrics representing a porosity infilling by an initial authigenic chamosite generation and a subsequent siderite generation, as in siderite chamositic limonite oolites (Frodingham Ironstone) and calcitic sideritic chamosite oolites (Cleveland Ironstone) are explicable by a simple change in the pore fluid chemistry. As discussed by Thomas (1979) and noted above, ferrous chamosite would be the first mineral to precipitate from a pore fluid containing H_4SiO_4aq, $Fe^{2+}aq$, $Ca^{2+}aq$, and HCO_3^-aq. At a pH of 7, high H_4SiO_4 activities and low HCO_3^- activities are required for chamosite precipitation (Figure 8.4b). The loss of H_4SiO_4 from solution would result in a corresponding increase in the HCO_3^- activity until a point was reached at which lower H_4SiO_4 activities allowed the precipitation of siderite. For pH=7 a solid stability criterion of

approximately $aFe^{2+}aq = 10^{-4.75}$ is required for chamosite and siderite precipitation. Such textures are indicative of an initially high and subsequently diminishing level of supersaturation of the pore fluids with respect to chamosite and siderite (Curtis, 1978).

Cements involving authigenic chamosite and siderite as the initial phases also occur in calcitic limonite oolites (Frodinghma Ironstone) and calcitic chamosite oolites (Marlstone Rock-bed and Cleveland Ironstones). Here, however, there is a textural difference in that siderite tends to nucleate as euhedra on echinoid plates and as euhedra on authigenic chamosite pore-linings. The cement paragenesis is the same as that in the preceeding paragraph and probably corresponds to the same pore fluid change. The textural difference may be ascribed to a diminished supersaturation level of the pore fluid with respect to siderite in comparison to the level in the above fluids. This would promote its nucleation on pre-existing crystals.

The precipitation of ferroan calcite is in all cases, with the exception of ironstones replaced by siderite mudstone, the final major diagenetic event. The source of the calcite-precipitating fluids is debateable. They may represent a final Ca^{2+}-rich, Fe^{2+}-poor pore fluid remaining after siderite precipitation or, alternatively, a late stage fluid with the same chemistry percolating into the sediment from overlying shales or clays. The latter is commonly the case in limestones. A final dissolution-precipitation reaction in which chamosite ooids are replaced by ferroan calcite is associated with the precipitation of ferroan calcite cement. This reaction is of the same type as that in which chamosite ooids are replaced by siderite.

The absence of thermochemical data for ferroan calcite, however, precludes the possibility of discussing the physico-chemical parameters governing this reaction. The occurrence of ferroan calcite syntaxial overgrowths to echinoid plates suggests that the calcite-precipitating pore fluids had a low supersaturation level with respect to ferroan calcite.

8.3.3 Conclusions

The construction of stability field diagrams for mineral assemblages representing different geochemical processes in ironstones allow the following conclusions to be drawn:

(1) A consideration of the solubility of ferrous chamosite as a function of total dissolved iron and silicon suggests that the geochemistry of the environment of ironstone formation was not significantly different to that of present-day depositional environments.

(2) Chamosite ooids and chamosite mud which formed initially as ferrous chamosite may be oxidised to ferric chamosite at H_4SiO_4 activities, Eh, and pH values comparable to present-day oxidising depositional conditions. Ferric chamosite is the stable phase at H_4SiO_4 activities greater than 10^{-6}. At values less than this it will tend to transform to goethite. Goethite cannot be formed directly by the oxidation of ferrous chamosite.

(3) Dissolution of chamosite ooids and chamosite mud may occur at pH, aH_4SiO_4, and $aHCO_3^-$ values comparable with conditions in pore waters in Recent sediments.

(4) Chamosite mud authigenesis i.e. ferric chamosite reduction and partial ferrous chamosite dissolution can occur under conditions

similar to those in Recent sediments.

(5) Dissolution reactions bring about an increase in the concentration of H_4SiO_4, Fe^{2+}, Al^{3+}, Ca^{2+}, Mg^{2+}, SO_4^{2-}, HS^-, HCO_3^-, and H^+, OH^- in the pore fluids. This allows cementation of uncemented facies as a function of the activities of these ions the ΔG_f^{25} of successive phases, and the degree of supersaturation of the parent pore fluid with respect to the precipitating phase. It is difficlut to assess the extent of pore fluid movement but the fact that in some facies chamosite is removed in solution and in others, which lacked primary or depositional chamosite, it occurs as a cement implies some degree of movement. Such facies may be separated by one metre or more on a vertical scale. The possibility that pore fluids containing Ca^{2+}, Fe^{2+}, and HCO_3^- originated in facies other than ironstone must be born in mind. All cement precipitates can be considered in context of the present-day diagenetic environment.

(6) Goethite is a more or less totally inert constituent of ironstone.

CHAPTER 9

THE SEDIMENTOLOGY OF THE LIASSIC IRONSTONES : CONCLUSIONS

THE SEDIMENTOLOGY OF THE LIASSIC IRONSTONE : CONCLUSIONS

9.1 INTRODUCTION

In understanding the origins of the Liassic aluminous ironstones three major factors must be considered. These are the origin of chamosite ooids, the sedimentological setting of ironstones, and the source of the requisite ferrous iron, silicon, and aluminium for chamosite formation. Many of the diagenetic features exhibited by ironstones are in common with those of limestones. An understanding of these features may further elucidate the nature of the depositional environment and the setting of chamosite ooid formation. The key to the origin of ironstones lies in the origin of chamosite ooids. It is necessary, however, to have some idea of the sedimentological setting conducive to ooid formation before discussing the possible modes of ooid development.

9.2 THE SEDIMENTOLOGICAL SETTING

The stratigraphic levels at which ironstones occur have been shown to correspond to the minima of regressive events (Hallam and Bradshaw, 1979). This is reflected in their relationship to overlying and underlying sediments (Hallam, 1978). It has been shown that they are condensed sequences by comparing their thicknesses with those of time-equivalent strata elsewhere (Hallam, 1966). The Frodingham Ironstone is condensed with respect to equivalent strata in Yorkshire, and the Cleveland Ironstone exhibits condensation with respect to deposits in its own depositional area. The lateral distances between condensed and non-condensed strata are clearly small. Condensation over short distances

suggests a rapid diminution in water depth which when combined with the shallow-water nature of ironstones (Hallam, 1978; Hallam and Bradshaw, 1979) indicates deposition in inshore areas or on shoals. The general absence of terrigenous detritus has lead a number of workers (Huber and Garrels, 1953; Knox, 1970; Hallam and Bradshaw, 1979) to conclude that oolitic ironstone formation occurred on shoal areas. Deeper marginal areas trapped the clastic components. Talbot (1974), however, has proposed that the Upper Oxfordian ironstones of southern England formed in inshore lagoonal settings when the supply of terrigenous detritus was much reduced. No really detailed facies analysis has been carried out, with the exception of the work of Talbot (1974), to elucidate the possible nature of the depositional environments represented by oolitic ironstones.

The Frodingham Ironstone is made up of a number of distinct depositional or primary facies which are arranged in a cyclic fashion. The results of facies analysis indicate that the ideal cyclothem is a coarsening-upwards sequence representing progressively more energetic and oxygenated environments with diminishing distance from the shallowest marine depositional area. Two red oolite horizons occur which are considered to represent phases of subaerial exposure. Evidence for this is provided by slightly irregular upper surfaces to these horizons and the presence of red chamosite mudstones within them. It is interesting to recall that the Mössbauer spectra of such mudstones is comparable to the spectra of chamosite oxidised by heating (Chapter 6, Section 6.4.3). The presence of such horizons which can apparently be correlated over large distances implies a very shallow water depth and a very low gradient for the sea-bed: Small reductions in sea-level would thus affect widespread areas. Consideration of the sedimentary structures

and other depositional but non-mineralogically controlled features allows a comparison of the Frodingham Ironstone with present-day depositional environments. The closest degree of similarity is to be found in the transition zone from the open shelf to the shore deposits of the Gulf of Gaeta (Reineck and Singh, 1975). By applying this model to the Frodingham Ironstone it was concluded that chamosite mudstones and chamositic chamosite oolites represented shelf deposits, chamositic limonite oolites transition zone deposits, and calcitic limonite oolites and bioclastic limestones shoreface deposits (Figure 2.20). The shelf deposits commence at a depth of 10-20 m in the Gulf of Gaeta (Reineck and Singh, 1975) which is not thought to be an unreasonable depth for the Frodingham Ironstone when it is borne in mind that it passes laterally into clays and shales of deeper water origin. Both the shelf muds of the Gulf of Gaeta and the chamosite mudstones of the Frodingham Ironstone are quartzose. In the case of the Gulf of Gaeta the dominant cause of sediment transport is longshore drift. Since other ironstone facies are non-quartzose it would appear that this is a likely mode of transport for the quartz silt. Periodic erosion of the chamositic chamosite oolites is thought to release chamosite mud and chamosite ooids for incorporation in the other ironstone facies.

Due to the widespread replacement of oolitic ironstone by siderite mudstone in the Cleveland Ironstone Formation the inter-relationships between facies of depositional origin are more or less impossible to see. It is possible to make several observations regarding the depositional environment of this Ironstone. Chowns (1968) has shown that the Ironstone Formation occupies a depositional basin. Its margins are characterised by thin ironstone seams separated by thin shales and silts. In the centre of the basin both are thicker but passing ESE the shales become

much thicker and the ironstones thinner. This is considered to represent a passage into deeper areas of deposition. In the centre of the basin the Main and Pecten seams may be split which is also considered to be indicative of deeper water conditions during ironstone deposition. The Lower gibbosus Shales and the hawskerense Shales both exhibit sedimentary structures which have been reported from depths of 2-10 m off the coast off Georgia (Howard and Reineck, 1972). Both units coarsen upwards and are overlain by ironstones. In the case of the Lower gibbosus shales at Brackenberry Wyke it is the Raisdale Seam which overlies and this is characterised by a basal ball and pillow structure indicative of rapid deposition. A number of the shales exhibit Chondrites sp. which Fürsich (1975) considers to represent depositional facies deeper than the deep sub-tidal. Rhizocorallium jenense (Zenker) is abundant in the Blue Mottle which underlies the Bottom Block of the Main Seam. This trace fossil is charactersitic of the shallow sub-tidal environment (Fürsich, 1975). In the case of the Cleveland Ironstone Formation it can be seen that ironstone deposition follows periods of shallowing which may reduce depths to those of the shallow sub-tidal. The Raisdale Seam was deposited quickly at Brackenberry Wyke and this represents chamosite ooids formed elsewhere during shale-silt deposition. The Main Seam is characteristically always underlain by the Blue Mottle. It is unlikely that the Main Seam represents deposits shallower than the shallow sub-tidal. This therefore suggests a shore-face environment for the Main Seam which includes facies thought to represent sites of chamosite ooid formation and sites of deposition following erosion. Ironstones in the Cleveland Ironstone Formation appear to have formed in shallow marginal areas, possibly at depths corresponding to the shore-face environment. Erosion and redeposition would result in

ironstones such as the Raisdale Seam at Brackenberry Wyke being deposited at greater depths.

Beyond relating the Marlstone Rock-bed and sandrock facies to a depositional basin on the East Midlands shelf it has not been possible to draw any major conclusions regarding the depositional environment of the ironstone. From the thickness data it was suggested that the Sandrock and sandrock facies represented marginal deposits whereas the Marlstone was more centrally situated.

From a number of lines of investigation it is concluded that the Frodingham Ironstone and the ironstones of the Cleveland Ironstone Formation represent environments corresponding to those between the shelf and shoreface. Since the sandrock facies of the Marlstone occurs marginally to the basin and Spinatum zone clays and shales apparently only occur in a small central portion of the basin (Figure 3.5), the Marlstone depositional region may have been sufficiently shallow over large areas to allow chamosite ooid formation in similar depth ranges to those at which they formed in the other two ironstones.

9.3 THE NATURE AND ORIGIN OF CHAMOSITE OOIDS

The origin of chamosite ooids has been the cause of much discussion. Three main schools of thought have emerged; the primary accretionary school, the replacement school, and a school which favours chamosite ooid formation by processes analagous to those which form carbonate ooids.

Hallimond (1925) first suggested that chamosite ooids were primary grains, since, in addition to this mode of occurrence,

chamosite also forms mud matrices and intraclasts. In considering the origin of the ooids this worker considered that the ooid chamosite was directly precipitated around some core grain. Subsequent destruction of the ooids would yield chamosite mud. On the basis that chamosite exhibited a constant composition Hallimond (1925) rejected the possibility that it originated as a gel containing the components of chamosite as such substances would not always be expected to have a constant composition. Caillère and Kraut (1954) and Strakhov (1953) suggest that chamosite ooids formed within a gel by concretion and nucleation at many centres, respectively. Curtis and Spears (1968b) favour the gel hypothesis on the grounds of the minerals which are found in association with chamosite ooids. They argue that opal, reported from the Cleveland Ironstone by Chowns (1968), kaolinite reported from the Northhampton Sand Ironstone by Taylor (1949), and goethite which all occur within, or as ooid-forming minerals reflect an original gel of variable composition. Excess SiO_2 would result in formation of opal, excess Al_2O_3 in the formation of kaolinite, and Fe^{3+} in the formation of goethite. Talbot (1974) has also proposed a gel origin for chamosite ooids in the Upper Oxfordian ironstones of southern England. In contrast to the above proposals which attempt to relate chamosite ooids to some initial precipitate Taylor (1949) and Knox (1970) have assumed that a chamosite mud environment formed a site at which ooids could form by the accretion of chamosite mud around some core grain. Textural evidence for the formation of chamosite ooids from a gel has never been reported. If chamosite ooids formed by a snow-ball effect then illitic and smectitic ooids would be expected to be more abundant in the stratigraphic record (Hallam and Bradshaw, 1979).

Sorby (1857) proposed that the Cleveland Ironstone chamosite ooids were a replacement of originally calcareous ooids brought about by percolating iron and silica-rich ground waters. This hypothesis has recently been applied to the Mid-Cainozoic Paz de Rio iron ore of north-eastern Columbia and an Upper Pliocene ironstone in the Sea of Azov by Kimberley (1974) and subsequently to all aluminous ironstones (Kimberley, 1979). Kimberley (1979) suggests that the replacement of aragonitic oolite by chamosite occurs when aragonitic oolite is overlain by delta topset muds. Leachates rich in iron, aluminium, and silicon are produced by weathering of the topset muds and are carried down into the oolite. Dissolution of aragonite and high magnesian calcite increases the electrolyte concentrations, which aided by a related increase in pH induced the precipitation of chamosite. Many of the stratigraphic and petrographic arguments presented by Kimberley (1979) are at variance with the features of the Liassic ironstones, thereby casting a degree of doubt on the general applicability of this eluviation-replacement model. Bradshaw et al. (1980) have discussed these features with specific reference to this model.

It is strange that in a science dominated by the principle of uniformitarianism discussions of the mode of chamosite ooid formation have not attempted to relate these grains to the well known methods by which present-day carbonate ooids form. Chowns (1968) has briefly discussed similarities and dissimilarities between chamosite ooids and carbonate ooids. He concludes that orientated and unorientated zones of chamosite platelets within chamosite ooids may be related to the activities of algae. His overall conclusions with respect to the origin of chamosite ooids are that chamosite is a direct result of the interaction between ferrous iron and clay minerals such as kaolinite and

montmorillonite. Chamosite formed by this method is directly accreted to a core grain. The one problem with this suggestion is that under conditions of negative Eh ferrous iron is stable in the marine environment (Curtis and Spears, 1968a) and thus chamosite would be expected to be far more abundant in the stratigraphic record.

9.3.1 The Formation of Calcareous Ooids

Calcareous ooids are subdivided into those in which the primary, aragonite, structural elements of the envelope are disposed either tangentially (Illing, 1954), or radially (Friedman et al., 1973; Sandberg, 1976). It has been suggested that the former type represent ooid formation in agitated marine environments, and the latter in quiet water environments (Illing, 1954; Kahle, 1954; Davies and Martin, 1976). Davies et al. (1978) have proposed that these ooids may be end-member types, perhaps resulting from two different mechanisms of formation. Berner (1971) and Lippman (in Bathurst, 1975) both consider that inorganic precipitation plays an important part in ooid formation. Mitterer (1971, 1972) and Suess and Fütterer (1972) have reported the presence of organic material, some of it protein-rich, in calcareous ooids and have demonstrated its importance in the formation of laboratory formed ooids.

Davies et al. (1978) have carried out a detailed laboratory study of the formation of quiet and agitated water carbonate ooids. It was found that the former ooids developed in seawater solutions containing humic acids. Other solutions gave negative results. Ooids form as a result of the creation of membranes around core aggregates. These provide nucleation sites for aragonite. Low molecular weight organic molecules are adsorbed by the aragonite crystals which poison the ooid surface

for any aragonite growth but radial. As the crystals grow this organic matter is pushed ahead of them as a band. When it becomes too thick aragonite precipitation ceases due to the reduction of Ca^{2+}, Mg^{2+}, and CO_3^{2-} supply. The outer band forms a substrate for membrane formation and the growth process commences again. The end product is an ooid with concentric shells consisting of radial aragonite crystals, each shell being separated from the next by a layer of organic material.

In contrast, the agitated water ooids with tangentially oriented aragonite crystals were synthesised under conditions of agitation, supersaturation, and without the direct intervention of organic processes during precipitation. The development of these ooids is divided into three stages: (i) Quartz and other possible nuclei, present in supersaturated, agitated, seawater solutions, cause inorganic heterogenous nucleation of aragonite on their surfaces. An accretionary coat is thus formed. Crystal poisoning by Mg^{2+} and H^{+} brings about the cessation of such growth. This may be removed by abrasion if the proto-ooid remains in the agitated environment. (ii) If the proto-ooid is buried, however, the Mg^{+} and H^{+} ions are removed. Re-entry to the agitated environment causes further heterogenous nucleation of aragonite. Repetition of these agitation and resting stages culminates in a layer of tangentially oriented aragonite grains on which further precipitation does not occur due to the presence of Mg^{2+} and H^{+} ions which cannot be totally removed. (iii) In order to provide a new substrate, enabling further precipitation to occur, organic membranes develop around the proto-ooid. They form in precisely the same way as those which develop in quiet water ooids. Davies et al. (1978) consider that this occurs during a prolonged burial or sleeping stage.

The discussion regarding the origin of Recent carbonate ooids has placed much importance on the role of organic material found within them. Davies et al. (1978) have related radial and tangential aragonite ooids and the occurrence of organic material in their laboratory study. Organic material has been reported from Recent aragonite ooids (Mitterer, 1971, 1972; Suess and Fütterer, 1972). Newell et al. (1960) have carried out acid dissolution of Bahamian aragonite ooids in order to isolate the organic component. It was found to consist of a complex mesh of mucilaginous organic material in which traces of the original form and lamination of the grains were preserved. Shearman et al. (1970) have described aragonite ooids from the Persian Gulf. Many of these ooids were coated entirely with a mucilaginous envelope containing occasional colonies of blue-green algae. The colonies frequently corresponded to pits in the ooid surface and bored into the concentric cell structure of the ooid creating a sub-radial zone of unorientated aragonite in contrast to the surrounding oriented material. In addition to this type of ooid surface ooids with lustrous surfaces were also found and these were characterised by the absence of any organic coatings. Tangentially oriented aragonite forming the outer shell could be seen in this type of ooid surface. Shearman et al. (1970) consider that the mucilaginous material was produced either as a secretion by the blue-green algae or as a result of the autolytic break down of cell walls.

If the laboratory formation of tangentially oriented aragonite ooids (Davies et al., 1978) is considered in context of the nature of organic material present in Recent tangentially oriented aragonite ooids (Newell et al., 1960; Shearman et al., 1970) it seems likely that

during the ooid sleeping stage blue-green algae colonise the surface and produce the requisite organic material for subsequent ooid growth. This takes the form of a mucilaginous envelope. The colonisation of core grains by blue-green algae in quiet water would also be expected to produce a mucilaginous envelope which would act as the nucleation site for aragonite. In order that the mucilaginous envelopes be retained as substrates for tangential aragonite and nucleation sites for radial, the development of mucilaginous envelopes must occur beneath the sediment surface in static conditions thereby reducing abrasion of the envelopes to a minimum.

9.3.2 The Nature of Chamosite Ooids.

Chamosite ooids in the Frodingham, Marlstone Rock-bed, and Cleveland Ironstones have been described in detail. The goethite ooids of the Frodingham Ironstone are identical in nature with its chamosite ooids and are therefore considered to represent the oxidised equivalents of these grains. The relationship between initial core grain shape, ring thickness variation, and final ooid shape is exactly the same in all the ooids which have been examined, regardless of source. The one major difference between the ooids is that those from the Frodingham Ironstone are discoidal in shape and those from the other two ironstones are prolate ellipsoids. A feature which all chamosite ooids have in common is the presence of black organic material. This occurs in three different forms; as rings concordant with the chamosite rings, as filamentous material which is subparallel to the ring structure and dominantly concentrated in the chamosite rings in the region of the ooid long axes, and fine ramifying filamentous material which cross cuts the ooid ring structure. Of these different forms the subparallel

filamentous type is the only form recognised in Frodingham ooids. This form occurs with the ring form in the Marlstone ooids. The Cleveland ooids are characterised by the presence of all three forms.

The ooid fine structure has been investigated with high-power transmission electron microscopy (TEM) by Dr. J. R. Ashworth, and with scanning electron microscopy (SEM).

TEM has elucidated the ooid ring infrastructure. The results of this study are reported in detail in Turner et al. (in prep). They show that the ooid envelope rings are constructed of sub-rings of high and low porosity. Both porosity types have a framework structure formed by small chamosite flakes, less than 0.1 μm in length, with a morphology similar to that of the much larger core books. The flakes have a preferred orientation tangential to the ooid core, thus confirming the deductions made from optical data.

SEM work allows the envelope surfaces to be subdivided into those which are smooth and those which are rough. The former are usually present in considerable excess over the latter. Fractured ooids reveal the same sub-ring structure recognised by TEM work. Exposed ring surfaces may be smooth or rough. Again smooth surfaces tend to predominate. Ooids with generally smooth ring surfaces may contain occasional rings with rough surfaces and vice versa. Chowns (1968) and Knox (1970) report that individual rings are constructed of either randomly or tangentially oriented chamosite flakes. This subdivision has not been recognised. The smooth ring and envelope surfaces are characterised by a generally very low relief with occasional pits (Plate 9.1). In contrast, the rough surfaces have a high relief, and are characterised by a complete coverage of chamosite tubules less than 7 μm in length and 2 μ in diameter (Plate 9.2). Tubular structures such as these

have not been found within the body of the ooid rings (Plate 9.3). The individual tubules have a tangential orientation relative to the ooid surface and core (Plate 9.4). Some ooids have a relatively smooth surface but numerous pits (Plates 9.5a). Such surfaces are found to have a tangential tubular structure in which the upper surfaces of the individual tubules are partially flattened. These tubules are generally less than 4 μm in length and 1 μm in diameter and are generall very closely packed in a matrix of fine chamosite platelets which are oriented with the basal plane tangential to the ooid (Plate 9.5b). Goethite ooids generally show smooth envelope and ring surfaces (Plate 9.6). Rough surfaces rarely occur. Chamosite ooids from the chamositic chamosite oolites of the Frodingham and Marlstone Rock-bed Ironstones and from the chamositic chamosite oolites of the Cleveland Ironstone Main Seam are commonly found to have rough surfaces characterised by the presence of the smaller tubules. Chamosite ooids from burrows in the Marlstone Rock-bed are characterised by the presence of the much larger tubules. Chamosite ooids from other lithologies and the inner rings of the ooids with tubular surfaces tend to have smooth surfaces with occasional rough surfaces.

All the specimens of chamositic chamosite oolite facies which have been examined show that there is a structural relationship between the ooids and the interstitial chamosite mud. This is clearly manifested in several cases as a tangential arrangement of the interstitial chamosite mud flakes around the ooid envelope: The ooid envelope extinctic cross extends into the chamosite mud and this exhibits a positive optic sign in common with the ooid. In cases where this is not so obvious, due to the abundance of siderite, at least some degree of orientation is revealed by the extinction of small areas of chamosite with the extinction of the adjacent ooid envelope. Chamosite ooids which are set in chamosite mud which has a depositional fabric do not exhibit

this relationship with this type of chamosite. The interstitial chamosite mud is characterised by the presence of filamentous organic material similar to that which is found in ooid envelopes oriented subparallel to the ooid ring structure. In some cases the chamosite mud organic filaments are oriented parallel to the adjacent ooid envelope.

9.3.3 Chamosite Ooid Formation

The form and nature of organic material within chamosite ooids is extremely similar in morphology to that reported from recent aragonite ooids by Newell et al. (1960) and Shearman et al. (1970). It is very tempting to assign the subparallel filamentous material to blue-green algal colonies, the ring variety to mucilaginous envelopes, and the ramifying variety to blue-green boring algae extending from muclilginous envelopes, as is seen in the Cleveland ooids. Unfortunately it has not been possible to obtain conclusive proof of either the organic nature of this material or its origin as blue-green algal material. In the absence of any mineralogical characteristics the black material in chamosite ooids has been tacitly assumed to be organic in nature. Staining techniques of the type suggesed by Smith (1970) have been unsuccessful in confirming this. This is probably due to the fact that staining has no effect on carbonaceous material such as carbon films. Several lines of evidence suggest the possibility that the organic material owes its origin to blue-green algae. Palynological studies of both oolitic limestones and oolitic aluminous ironstones show that the blue-green algal content of both is extremely high (Dr. J. Fenton, pers. comm.). Blue-green algae are known to be responsible for the creation of micrite envelopes to shell debris. In the chamositic chamosite oolites shell material is

extensively micritised in comparison to that of other facies. A common diagenetic change in chamositic chamosite oolites is the creation of ooimoulds as a result of ooid chamosite dissolution. Mucilaginous envelopes occur within ooimoulds and have been unaffected by the processes of inorganic dissolution. It is a general rule that inorganic liquids do not dissolve organic solids and vice versa. The balance of the above evidence does tend to suggest the possibility of the organic debris being of blue-green algal origin. Stability relationships between ferrous and ferric chamosite (Chapter 8) suggested that ferrous chamosite would be stable at negative Eh levels. Such levels represent low dissolved oxygen concentrations and this type of environment is one in which blue-green algae would be expected.

The role played by blue-green algae in chamosite ooid formation may be established tentatively from the relationship between chamosite ooids and the interstitial oriented chamosite mud. Since the chamosite mud surrounding the chamosite ooids contains blue-green algae and has the same oriented structure as the ooids it is evident that there is an intimate relationship between these three components. The tubular structures seen at the surface of chamosite ooids with the aid of the SEM correspond in form and size to the filamentous inclusions seen at ooid envelope ring contacts. Blue-green alge are phototropic organisms and filamentous blue-green algae seek light by gliding upwards towards the sun leaving their sheath behind (Brasier, 1980). If the blue-green algae were a catalyst in the combination of ferrous iron, silicon, and aluminium to form and precipitate chamosite their light seeking nature would lead to the precipitation of chamosite as they moved ahead of the substrate, represented by either a chamosite ooid or core-grain, in response to sunlight. The chamosite precipitate would

infill the old sheaths. The abundance of blue-green algal sheaths in ooids is not generally high so flattening of such material would not necessarily result in the formation of an ooid envelope. Mucilaginous envelopes have been observed in a number of ooids. By analogy with aragonitic ooids these may represent the metabolic products of blue-green algae and may bring about a similar effect in crystal orientation. Since the quiet water aragonite orientation is radial the chamosite orientation might be expected to be radial also. However, aragonite is acicular in habit whereas chamosite is a platy clay mineral. The stable orientation due to intra-particulate forces of attraction between individual chamosite platelets would result in a tangential orientation. Thus, as the blue-green algae moved away from the substrate chamosite platelets were precipitated. The platelets were orientated tangentially around the substrate by a combination of intra-particulate forces of attraction and the effect of a mucilaginous envelope, if present. The absence of mucilaginous envelopes from the Frodingham Ironstone chamosite ooids suggests that their presence may not have been a prerequisite for tangential orientation. The production of chamosite in this way would gradually totally infill the interstices of the sediment with chamosite mud thus blocking off much light. If the formation of chamosite ooids occurred in this way the reduction in light levels within the sediment may not pose a major problem. Braiser (1980) reports that blue-green algae occur to depths of 30 cm in soil and have been recorded from depths greater than 1000 m in the oceans.

The mode of chamosite ooid formation proposed above would be expected to produce spherical ooids. The fact that ooids show a gradation from outer rough surfaces at their sites of formation to smooth surfaces in high energy oolite deposits suggests that abrasion

may play an integral part in ooid formation. The provenance of ooids with rough surfaces has been noted. It is significant that they are devoid of current activity. Ooids with smooth surfaces, however, occur in beds which show cross-bedding and contain intraclasts, thus indicating somewhat energetic conditions of deposition. Ooid cores are generally characterised by a non-equidimensional shape. The initial ooid ring will reflect this shape. Abrasion and rounding of the ring would be concentrated at the regions of minimum radii of curvature until these processes had no effect. At this stage its thickness variation will have a minimum in those areas corresponding to the corners of the core-grains. Deposition of a second ring and subsequent abrasion would have a similar results. Thus, the final ooid would be expected to have a broadly similar shape to the core-grain. Over-printed on this is a second mode of abrasion, which could not be obtained from a consideration of ooid thin sections, occurring when the ooid was situated in calmer conditions at the sediment-water interface. Its stable orientation would be with the long axis sub-parallel to the sediment surface. The portions of the ring in contact with the sediment would undergo thinning as a results of gentle rocking and rolling. These two abrasion and rounding modes represent two different ring thickness controls.

There are three differences between the Frodingham Ironstone ooids and those of the Marlstone Rock-bed Ironstone and the Cleveland Ironstone. In the former case the dominant ooid-forming mineral is goethite. No mucilaginous envelopes have been observed in either goethite or chamosite ooids. The shape of these ooids is discoidal. In the latter cases mucilaginous envelopes have often been found. Chamosite is the only ooid-forming mineral. The ooids are dominantly prolate ellipsoids. It seems possible that the absence of mucilaginous

envelopes in the Frodingham ooids might allow easy oxidation of chamosite to goethite in energetic enviroments. These would otherwise act as seals to the chamosite surrounded by them. The envelopes may also have a structural effect in retaining the ooid envelope shape. Without this slight flattening of chamosite ooids prior to oxidation might be expected to occur. Mucilaginous envelopes are not ubiquitons in the chamosite ooids of the Marlstone Rock-bed Ironstone. The rings of these ooids often vary in colour from grass-green to brown. The results of the Mossbauer spectroscopy and X-ray work suggest that green chamosite is high in Fe^{2+} whereas brown chamosite has a relatively higher Fe^{3+} content. These levels are considered to represent differing degrees of environmental oxidation. It is possible that mucilaginous envelopes could be removed by abrasion revealing the underlying chamosite ring which would be partially oxidised before the ooid returned to the site of chamosite ooid formation. If the mucilaginous envelopes corresponded to ring contacts then this would result in the formation of an ooid with only one ring. If, however, a coating of chamosite was added to the ooid before the formation of a mucilaginous envelope then a series of rings could be built up (Figure 9.1). In contrast to the Marlstone, the Cleveland Ironstone ooids are of a uniform green colouration, which may be slightly obscured by boring algae, and all exhibit mucilaginous envelopes.

9.3.4 Summary

Chamosite ooids are considered to form in the following way. This is illustrated in Figure 9.1.

(1) Potential core-grains are colonised by blue-green algae which may cause the formation of a mucilaginous envelope.

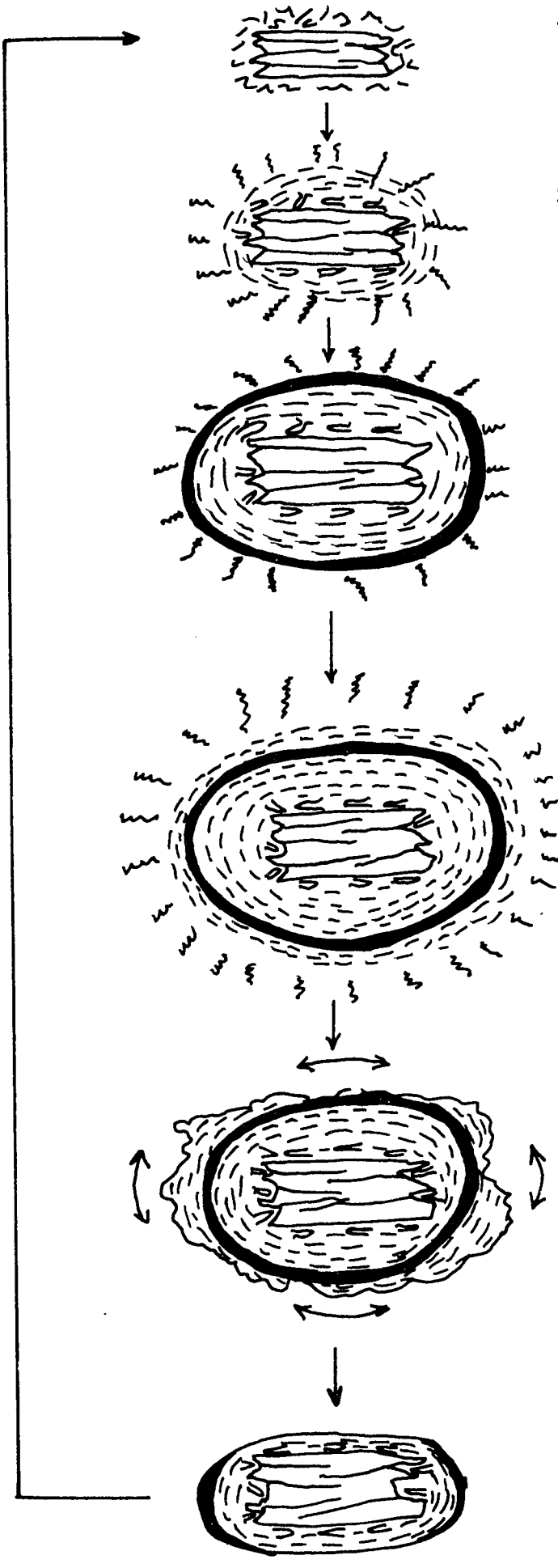

1. Core grain colonization by blue-green algae.

2/3 Algae move away from core-grain precipitating chamosite. Chamosite plates become tangentially oriented.

4. Formation of mucilaginous envelope during resting stage.

5. Algae move outwards precipitating chamosite.

6. Proto–ooid removed from site of formation and rounded.

7. Proto–ooid returns to site of formation at stage 1.

Fig 9.1 Schematic diagram of Ooid formation

(2) Blue-green algae vacate sheaths and move towards the light source and catalyse the precipitation of chamosite from aqueous solution.

(3) Individual chamosite platelets adhere to the core grain, the adhesion perhaps being aided by the presence of a mucilaginous envelope. The stable orientation is with (001) tangential to the core-grain. Vacated sheaths are infilled with chamosite platelets which will tend to follow the orientation of external platelets.

(4) During the outward movement of the algal material there may be a resting stage during which a mucilaginous envelope is formed.

(5) The blue-green algae continue their outward movement precipitating more chamosite.

(6) Currents, occasional in their frequency, passing over the site of ooid formation excavate the proto-ooids. Rounding and abrasion at the sediment surface bring about the ooid ring thickness variations described above. This will remove any sheaths adhering to the outer ooid surface and may extend down to remove a mucilaginious envelope formed at a resting stage. Interstitial chamosite mud excavated with the ooids and removed by abrasion is winnowed away. Partial oxidation of the chamosite may occur. If mucilaginous envelopes were never formed the increased time of subjection to relatively oxygen rich conditions may cause oxidation to and the formation of goethite.

(7) Blue-green algal activity resumes at stage (1).

(8) High energy erosive currents destroy the site of ooid formation or excavate its upper portion and carry the ooids to another environment of deposition.

9.4 DIAGENETIC FEATURES

From a study of the primary, depositional components of ironstone facies and the textures and cements which represent diagenetic changes within them it can be concluded that diagenesis in ironstones is facies-controlled. Textural evidence has been presented in Chapters 2, 3, and 4 to show that each ironstone is represented by similar facies types. The one exception to this is the siderite mudstones of the Cleveland Ironstone. The similarity between facies suggests that depositional and diagenetic conditions of ironstone formation were similar for each deposit. Textures present in a particular facies of one ironstone and absent in another may therefore give some indication of the departure from a norm. A comparison of textures that are common to both ironstones and carbonates may allow some further conclusions regarding the ironstone environment to be drawn.

The balance between dissolution of material present in a sediment at the time of its deposition, the chemistry and flow of pore-waters, and the precipitation of cement minerals has been discussed by Curtis (1978). This has been applied to textures occurring in ironstones in Chapter 8. It was concluded from stability criteria that the physicochemical parameters of the diagenetic environments of ironstones were not dissimilar from those of present-day diagenetic environments.

9.4.1 Dissolution Features

The chamositic chamosite oolite facies is in all cases characterised by the presence of features indicative of dissolution. Since chamosite occurs as a cement in other facies, and this facies type is thought to be the site of chamosite formation, it may be regarded as the source of this cement. The facies is thought to be entirely chemical in origin: The activities

of blue- green algae bring about the precipitation of chamosite from aqueous solution and its concentration in an ooid-forming role. Thus, both chamosite ooids and chamosite mud may be thought of as the first authigenic phase.

Diagenesis proceeds with the formation of a siderite replacement to the outermost portion of ooid envelopes. The siderite may contain ghost ring contacts and does not distort the ooid envelope which it surrounds. The replacement must therefore have been one in which chamosite dissolved at the grain edges and was immediately replaced by siderite. This texture therefore approximates to an equilibrium between chamosite, siderite, and the components of these minerals in solution.

A more vigorous type of chamosite dissolution results in the formation of ooimoulds. This event gradually follows the formation of replacive siderite rims. All gradations occur from a small dissolution cavity at the centre of an ooid to an ooimould lined by a siderite replacement. Intervening stages are represented by dissolution cavities whose edges correspond to ring contacts. These observations have lead to the conclusion that chamosite dissolution commenced in the core region and moved outwards. The presence of occasional forams and shell fragments within the ooimoulds suggest that a neutral or alkaline pH prevailed during this dissolution. In some cases undissolved books of chamosite are present in the ooimould which suggests, as in many chemical reactions, that a very small grain size promoted dissolution. The reason for dissolution commencing in the core region is obscure but may be related to concentration gradients set up within the ooids which, as shown by TEM and SEM work, are porous. The porosity, therefore, does not pose a problem for the removal of chamosite in solution.

A related texture occurs in chamositic limonite oolites sub-type

(ii) of the Frodingham Ironstone. This is the formation of ooimoulds in apparently goethite ooids. It was suggested in Chapter 8 that goethite would be more or less inert in the diagenetic environment. Textures in which goethite occurs as an oxidised rim to chamosite ooids have been reported from this facies. The balance of the evidence would suggest that it is more likely that ooimoulds in goethite ooids represent the dissolution of an originally chamosite interior.

Following ooimould formation a structural reorganisation of the sediment generally occurs. This is indicated by the flattening of ooimoulds to form chain and hooked ooids. These derivatives are often oriented with their long axes perpendicular to bedding thus indicating a load-controlled compression. Another variety of chain and hooked ooimoulds is formed apparently by the mechanical failure of the surrounding chamosite mud. They commonly exhibit siderite replacements at their rims and this is thought to give them an element of strength preventing their flattening. The hooks may be found connecting with thin black lines in the interstitial mud which in the Frodingham and Marlstone Rock-bed Ironstones were suggested to be failure surfaces. In the Cleveland Ironstone, however, although these 'failure surfaces' occurred they were lined by siderite grains and in some cases were relatively wide with a siderite lining and a ferroan calcite infill. This texture was identified as being stylolitic in nature. Since stylolites are a pressure solution feature it seems likely that the black lines in the Frodinhgam and Marlstone cases do not represent mechanical failure of the mud but are dissolution surfaces which allowed slight degrees of lateral movement in the mud allowing the formation of hooked ooids. In the case of the Cleveland Ironstone stylolites the large degree of pressure solution suggests

a more rapid build-up of overburden pressure than was the case in the formation of dissolution surfaces in the Frodingham and Marlstone interstitial muds. This may be correlated with the occurrence of spastoliths, which are abundant in the Cleveland Ironstone, and represent ooid distortion parallel to bedding without the formation of ooimoulds.

Instead of the formation of dissolution surfaces the interstitial chamosite mud may undergo wholesale dissolution. This creates a structural imbalance in the sediment with the resultant collapse of all ooimoulds and the formation of an ooimould melange.

The removal of chamosite in solution increases the level of dissolved ferrous iron, silicon, and aluminium within the pore fluids. Since the dominant direction of flow in a compacting sediment is upwards a proportion of these components would find their way back to the level at which chamosite ooids were being formed and be reprecipitated as chamosite. The presence of horizontal pathways such as dissolution surfaces would promote the lateral movement of pore fluids into other facies where chamosite could precipitate as a cement.

9.4.2 Authigenic Chamosite

Authigenic chamosite occurs in all the ironstone facies as an early cement mineral. It infills echinoid plate stereome systems and forms isopachous pore linings. This mode of occurrence is suggestive of its precipitation from aqueous solution. It is found in this role around originally aragonitic shell fragments. Although forming an infill to algal borings in calcite shell fragments it does not always occur as a surround to these grains.

Authigenesis of chamosite books has been found to occur in the depositional quartzose chamosite mudstones of the Frodingham Ironstone. The books are found to be grass green in colour and pass with optical continuity into adjacent patches of unstructured authigenic chamosite. As would be expected, these grains show no noticeable signs of rounding. Olive green books of a similar size but showing rounding also occur in chamosite muds but are not associated with authigenic chamosite. It is considered that these are reworked equivalents of the authigenic variety. Chamosite books are abundant in the Sandrock and sandrock facies of the Marlstone Rock-bed. They are much larger than those which are found in quartzose chamosite mudstones and are comparable in size to the books which occur as ooid core-grains in the Marlstone ooids. These books do not exhibit the niches at either ends of the cleavage traces or the rounding which characterised core-books. Where occurring between two quartz grains chamosite books often appear to be pinched. This is due to the termination of the outermost cleavage flakes against the quartz grains. These textures lead to the conclusion that such books are also of authigenic origin. The relationship of the Sandrock and sandrock facies with the ironstone facies suggests that reworking of the former would liberate books for incorporation as core-grains in the ooids of the latter.

The Frodingham Ironstone chamositic limonite oolites sub-types (ii) and (iii) are both cemented more or less entirely by authigenic chamosite. Lateral and imperceptible transitions from areas of depositional chamosite mud to areas of authigenic chamosite in sub-type (ii) suggest that these two facies types represent the insitu authigenesis of large amounts of chamosite mud. Textures

involving early high magnesian calcite or aragonite and authigenic chamosite, and pore lining textures shown by the chamosite suggests that the authigenesis involved some degree of chamosite dissolution and reprecipitation in order for it to take up the maximum possible space available. Similar textures occur in areas of depositional chamosite mud present in other ironstone facies. In Chapter 8 it was suggested that this authigenesis might represent the reduction of chamosite ferric iron to ferrous iron under conditions of negative Eh.

9.4.3 Siderite

Siderite occurs most commonly as a replacement of interstitial chamosite muds in chamositic chamosite oolite facies and chamositic limonite oolite sub-type (iii) facies. It also occurs as a pore-filling generation in many facies following the precipitation of authigenic chamosite pore linings.

9.4.4 High Magnesian Calcite and Aragonite

It is possible to say unequivocally that, of the original depositional components of the ironstone facies, high magnesian calcite was present as echinoid plates (Richter and Füchtbauer, 1978) and that aragonite occurred as bivalve shell fragments (Bathurst, 1975). Early cement generations of some carbonate mineral occur as fringes to calcite shell fragments and have been replaced by ferroan calcite. By analogy with recent carbonate sediments this initial generation may have been either high magnesian calcite or aragonite.

Echinoid plates, spines, and crinoid collumals are common in ironstone facies. They are usually of ferroan calcite and are surrounded by syntaxial overgrowths of ferroan calcite of a similar composition.

Occasional plates have been found which exhibit a compositional zonation from ferroan calcite at the grain edges to non-ferroan calcite at the core. Richter and Füchtbauer (1978) have discussed the transition from the initial high magnesian calcite to the later replacement by low magnesian calcite; the stable phase in the diagenetic environment. They consider that the transition occurs by a process of epitaxial replacement in which Mg^{2+} diffuses out from the high-magnesian calcite lattice reducing it to a low magnesian calcite lattice. Thus the low magnesian calcite form pseudomorphs all the original detail of the fragment due to the inherited calcite lattice. Richter and Fuchtbauer (1978) note the common replacement of original high magnesian calcite by low magnesian ferroan calcite and conclude that the loss of Mg^{2+} is accompanied by the uptake of Fe^{2+} from pore waters. On the basis that in limestones a progression of increasingly Fe^{2+} rich cements occur these workers consider that zoned echinoid debris, from iron-rich edges to iron-poor reflects an increasing Fe^{2+} level in the pore waters. Since the diagenetic environments of ironstones would be expected to be rich in Fe^{2+} it is not, therefore, surprising that the majority of echinoid plates are entirely ferroan in nature. Those which exhibit zonation may well record the gradual increase in the Fe^{2+} level of a diagenetic environment which was becoming established.

Lohmann and Meyers (1977) have concluded that microdolomite inclusions in echinoid plates and their surrounding syntaxial overgrowths and in coarse prismatic calcite cements are indicative of a marine environment of diagenesis. No microdolomite textures within syntaxial overgrowths have been found but microdolomite inclusions in ferroan calcite replacements of radial fibrous early carbonate cements in chamositic chamosite oolites

have been. This is thought to be an allied texture resulting from the precipitation of an early radial fibrous high magnesian calcite cement. The subsequent inversion to low magnesian ferroan calcite, by the process discussed by Richter and Füchtbauer (1978), created an environment locally rich in Mg^{2+} and as a result ferroan microdolomite formed (Lohmann and Meyers, 1977). This texture is thought, by analogy, to indicate that diagenesis in this facies, at the time at which the microdolomite formed, was marine in nature. It is interesting to note that Meyers and Lohmann (1978) report the presence of microdolomite inclusions in echinoid plates and syntaxial overgrowths but their absence from prismatic calcite cements in a diagenetic environment representing the metoric-marine mixing zone.

Many radial fibrous fabrics around calcite shell fragments representing an original carbonate cement of either high magensian calcite or aragonite occur in ironstone facies, and are replaced by ferroan calcite. Textural evidence in a number of cases suggests that this cement predates the precipitation of authigenic chamosite. Authigenic chamosite occurs commonly as a rim to originally aragonite shell fragments, suggesting that its precipitation may have predated their dissolution. It very infrequently coats low magnesian calcite shell fragments which usually exhibit the radial fibrous cement. A possible reason for this could be that the initial radial fibrous cement was high magnesian calcite which nucleated on the high magenesian calcite outer layer of calcite shell fragments. (Bathurst, 1979). In the absence of a moulding medium aragonite radial fibrous cements would be expected to dissolve without leaving any trace, in parallel with the behaviour of aragonite shell fragments. Cullis (1904) and Ball (1967) report that radial fibrous aragonite develops only on

aragonitic allochems. Bathurst (1975) has shown that original aragonite cements which have been replaced by calcite result in a radiaxial fibrous calcite cement in which the fast vibration directions converge away from the allochem. This texture has not been observed. Studies of Recent carbonate cements with respect to the mineralogy of the cemented grains have shown that in the early stages of marine diagenesis high magnesian calcite and aragonite cement allochems of similar composition (Cloud, 1962; Purdy, 1964, 1968; Glover and Pray, 1971). Although microdolomite inclusions are absent from the majority of radial fibrous cements it is thought that they represent, in general, original high magnesian calcite resulting from early marine diagenesis.

9.4.5 Ferroan Calcite

In addition to the above modes of occurrence ferroan calcite infills the remaining pore spaces as the final cement generation. In this role it often replaces chamosite ooids.

An important textural type of ferroan calcite is that which is found as grains with a meniscus-like form at the points of contact between allochemical components. This texture is restricted to the red calcitic limonite oolites of the Frodingham Ironstone. Dunham (1971) has interpreted this texture as being characteristic of vadose zone diagenesis. This is important evidence in support of the suggestion that the red oolites represent horizons of subaerial exposure.

9.4.6 Late Stage Replacement By Siderite Mudstone

The Cleveland Ironstone is characterised by the widespread replacement

of oolite facies by microcrystalline siderite mudstone. Curtis and Spears (1968a) note that in order for siderite to form HCO_3^- must be present in greater concentration than HS^-, otherwise pyrite will be precipitated. HS^- is produced in sediments by the bacterial reduction of SO_4^-. Assuming that these conditions are satisfied then siderite will precipitate at negative Eh values. Two possible sources for the requisite HCO_3^- concentrations are organic material, of which there is plenty in the Cleveland Ironstone ironstones, and the dissolution of aragonitic material. In order to reduce the HS^- level the diagenetic environment of the ironstones must be sealed off from the marine environment by some means as the SO_4^- for HS^- production diffuses into the diagenetic environment from the overlying seawater. The dissolution feature stylolites, which are abundant in the ironstones, suggest the rapid build-up of overburden pressures which, in turn, reflect rapid deposition. Clays deposited rapidly on the ironstones would both seal off their diagenetic environments and create large overburden pressures. In order for widespread precipitation of siderite to occur the conditions conducive to this must be developed over large areas. The ironstone seams are overlain and underlain by argillaceous material which would tend to restrict pore fluid circulation to the more porous ironstone seams. Thus, it is logical to conclude that siderite precipitation occurred over large areas due to the relative restriction of HCO_3^-, within the porous ironstones, and from solutions which maintained slight supersaturation with respect to siderite. A similar mode of siderite mudstone formation has been proposed for a clay-band ironstone in the Westphalian (Carboniferous) of Yorkshire by Curtis et al. (1975).

9.4.8 Summary

Diagenetic textures indicate that chamosite dissolution provided a source of dissolved chamosite for reincorporation in ooids and for precipitation as cements.

The creation of distorted ooimoulds and ooids can be related to overburden pressure bringing about structural reorganisation and the formation of dissolution surfaces and stylolites.

It is thought that the first cement mineral was high magnesian calcite indicating marine conditions of diagenesis. In the red oolites vadose zone diagenesis prevailed. Subsequent cement minerals were authigenic chamosite, siderite, ferroan dolomite, and ferroan calcite. Siderite and ferroan dolomite generally occur as replacements after the dissolution of chamosite mud.

The authigenic production of chamosite books in the Sandrock and sandrock facies furnished potential core grains for ooids as a result of reworking.

The final diagenetic change in oolitic ironstones is the production of siderite mudstone, by precipitation from pore fluids, trapped in a porous media containing abundant organic material and maintaining conditions of supersaturation with respect to siderite.

9.5 THE SOURCE OF IRON, SILICON, AND ALUMINIUM

In order for ironstones to form it is necessary that sufficient quantities of iron, silicon, and aluminium be present in the aqueous environment for the precipitation of chamosite by blue-green algae to occur. It is also necessary that these elements should be present in

some easily reacting form. It has been noted, for instance, that detrital magnetite is relatively inert in depositional waters and the diagenetic environment.

Iron is released by weathering of rocks and enters the aqueous environment in the ferric state. This may be as detrital grains of magnetite or haematite, or as suspended particles of ferric hydroxide. Moore and Maynard (1929) have shown that iron may be transported as ferric salts of organic acids adsorped by organic complexes and as ferric oxide hydrosols stabilised by organic complexes. Carroll (1958) has demonstrated that large quantities of iron can be transported in suspension as ferric oxide coatings on clay platelets.

The mode by which aluminium and silicon are transported in the aqueous environment is rather less well understood. They are both relatively immobile in the geochemical environment. Their dominant occurrence is as clay minerals, feldspars, and quartz. As with iron, silicon and aluminium may be transported in reactive forms as organic complexes (Moore and Maynard, 1929).

The work of Eugster and Chou (1973) and Klein and Bricker (1977) was applied to the occurrence of iron, silicon, and aluminium in the marine environment in Chapter 8. It was found that, at a pH of 7, the activities of iron and silicon required for the precipitation of chamosite from aqueous solution were broadly in agreement with what is known of the total dissolved activities of these species in the present day marine environment. Bearing in mind the figure of 10^6 years, which is usually assumed to be the average time span of an ammonite zone, it may well be that the Frodingham Ironstone (three zones), Marlstone Rock-bed Ironstone (one zone), and Cleveland Ironstone (two zones), which are all condensed deposits, were formed within a marine

environment which was not geochemically dissimilar from that which obtains today. Once chamosite ooids had started to form, a diagenetic reflux may have aided further chamosite ooid formation by providing more iron, silicon, and aluminium from chamosite ooid dissolution.

Igneous lithoclasts of volcanic origin occur within the Cleveland Ironstone. They contain quartz grains of a very similar nature to those which occur within the Marlstone Rock-bed and Frodingham Ironstones. It is very tempting to suggest the possibility of contemporaneous volcanic activity increasing the levels of iron, silicon, and aluminium in the marine environment at the time of ironstone deposition. In connection with this possibility it is interesting to recall the analytical work of Catt et al (1971) who discuss the trace element content of chamosite ooids and chamositic shales from the Cleveland Ironstone. They report that these are enriched in Co, Cr, Ni, Pb, V and Zn. Fragments of fossil wood within the ironstone seams were also found to be rich in Co, Cu, Mo, Ni and Pb whereas fossil wood from horizons remote from the ironstone seams contained much smaller quantities of these elements. If a volcanic origin for anomously high levels of Fe, Si and Al in the marine environment during ironstone formation is contemplated then some geochemical signature should be expected within the ironstones, expressed as anomously high levels of trace elements associated with volcanism. The levels of Co, Cr, Ni, Pb, V, Zn and Mo reported by Catt et al (1971) may be an expression of this. Unfortunately, these authors did not analyse their ironstone samples for rare earth elements, anomously high values of which would be expected if volcanism was related to ironstone deposition.

Several authors have considered the possibility of a lateritic origin for the iron, silicon and aluminium concentrated in the Liassic ironstones (Taylor, 1949; Hallam, 1966; Catt et al, 1971). They suggest that laterite formed in the higher areas of landmasses adjacent to the Liassic epeiric seas. There is some support for this suggestion; large amounts of iron and aluminium are transported far out to sea by the Amazon (Gruner, 1922) and by some Asiatic rivers (Krejci-Graf, 1964), all of which drain lateritic areas. Triassic and fresh-water Jurassic microfaunas and microfloras have been found in samples of the Marlstone Rock-bed (Dr. J. Fenton, pers. comm.) which clearly indicate erosion of land areas of Triassic age. Dunham (1960), however, has pointed out that lateritic weathering fixes iron and aluminium whilst all other components are removed in solution. It has been established that ironstones occur at the minima of regressive events. At these times, therefore, active erosion of laterite would be required to introduce the requisite large quantities of iron into the marine environment. When sea level is reduced the most active erosion on landmasses occurs at niche points as the drainage adjusts to the new base level by eroding upstream. Thus, before lateritic iron is liberated, readjustment of drainage as far upstream as the laterite is required. This would appear to involve a considerable time lapse when compared to present-day rates of erosion. Since non-sequences do not occur immediately beneath ironstones, further consideration of the relationship between regression and mechanical release of iron from laterites is required. The possibility of a lateritic or ferricrete origin or iron, aluminium and silicon in the marine environment during ironstone formation cannot be ignored. A further possibility is erosion and weathering of exposed Triassic and Permian red-bed. With specific reference to laterites, however, erosion would be expected to

release kaolinite, lateritic chamosite and possibly garnierite, an Fe-Ni silicate mineral formed during laterite formation for incorporation in marine sediments. Analysis of terrigenous sediments laterally equivalent to ironstones has not been carried out to determine whether lateritic chamosite and grunerite are present.

9.6 CONCLUDING STATEMENT

The origin of chamosite ooids is related to the activities of photosynthesising blue-green filamentous algae. They are thought to catalyse chamosite precipitation from aqueous solution and control its tangential concentration around a substrate of either a core grain or an ooid envelope. In this context the shallow-water, well-illuminated depositional environments suggested for aluminous ironstones are understandable. It is interesting to compare this environment with that of the environment of formation of carbonate ooids which are also characterised by an abundance of blue-green algae. Since aluminous oolitic ironstones represent a very small chemical sediment thickness, accumulated over a long time span, it may well be that excessive levels of dissolved iron, aluminium, and silicon were not required for their formation. The derivative ironstone facies are all characterised by marine diagenesis. Subaerial exposure of the ironstones, however, brought about vadose zone diagenesis.

REFERENCES

Allen, J. R. L. (1970). Sediment of the modern Niger delta: a summary and review. pp 138-151 in Morgan, J. P. (Ed.). Soc. Econ. Palaeontologist Mineraologists, Spec. Publ, 15.

Ann. Rep. I. G. S. (1972). Boreholes in northern England and Wales. pp 45. H.M.S.O.

Bailey, S. W. (1980). Summary of recommendations of the AIPEA Nomenclature Committee. Canadian Mineralogist, 18, 143-150.

Bailey, S. W., Brindley, G. W., Johns, W. D., Martin, R. T. and Ross, M. (1971). Summary of national and international recommendations on clay mineral nomenclature. Clays Clay Minerals, 19, 129-132.

Ball, M. M. (1967). Carbonate Sand bodies of Florida and the Bahamas. J. Sed. Pet., 37, 556-591.

Bancroft, G. M. (1973). Mössbauer Spectroscopy: An Introduction for Inorganic Chemists and Geochemists. pp 238. McGraw-Hill, New York.

Bancroft, M. M. and Burns, R. G. (1967). Applications of the Mössbauer effect to silicate mineralogy - I. Iron silicates of known crystal structure. Geochim. Cosmochim. Acta., 31, 2219-2246.

Bancroft, M. M., Ong, W. K., Prince, R. H. and Stone, A. J. (1967). Mössbauer spectra of iron III diketone complexes. J. Chem. Soc., (A), 1967 A, 1966-1971.

Bathurst, R. G. C. (1975). Developments in Sedimentology. 12. Carbonate sediments and their diagenesis. pp 658. Elsevier, Amsterdam.

Berner, R. A. (1963). Electrode studies of hydrogen sulphide in marine sediments. Geochim. Cosmochim. Acta., 27, 563-575.

Berner, R. A. (1964). An idealised model of dissolved sulphate distribution in recent sediments. Geochim. Cosmochim. Acta., 28, 1479-1503.

Berner, R. A. (1970). Sedimentary pyrite formation. Am. J. Sci., 268. 1-23.

Berner, R. A. (1971). Principles of Chemical Sedimentology. pp 260. McGraw-Hill, New York.

Blake, R. W. (1977). Brachiopod nests from the Marlstone Rock-bed (Jurassic) of Warwickshire. Mercian Geol., 6, No.2, 97-102.

Bradshaw, M. B., James, S. J. and Turner, P. (1980). Origin of oolitic ironstones - Discussion. J. Sed. Pet., 50, No.1, 295-304.

Braiser, M. D. (1980). Microfossils. pp 93. George, Allen and Unwin, London.

Brindley, G. W. (1949). Mineralogy and crystal structure of chamosite Nature. 164, 319-320.

Brindley, G. W. (1951). The crystal structure of some chamosite minerals. Min. Mag., 209, 502-525.

Brindley, G. W. and Youell, R. F. (1953). Ferrous and ferric chamosite. Min. Mag., 30, 57-70.

Bull. Geol. Surv. G.B., (1956). The stratigraphy of the Stowell Park borehole. No.11, 1-47. H.M.S.O.

Bull. Geol. Surv. G.B. (1979). The stratigraphy of two boreholes near Warlaby, Lincolnshire, No.54. 1-50. H.M.S.O.

Catt, J. A., Gad. M. A., Le Riche, H. H. and Lord, A. R. (1971). Geochemistry, micropalaeontology, and origin of the Middle Lias ironstones in northeast Yorkshire (Great Britian). Chem. Geol., 8, 61-76.

Caillére, S. and Kraut, F. (1954). Les gisements de fer du bassin Lorraine. Mem. Mus. Hist. Nat. Paris., (c), 4, 1-175.

Carozzi, A. V. (1961). Distorted oolites and pseudoolites. J. Sed. Pet., 31, No.2, 262-274.

Carozzi, A. V. (1963). Half-moon oolites. J. Sed. Pet., 33, No.3, 633-645.

Carroll, D. (1958). The role of clay minerals in the transportation of iron. Geochim. Cosmochim. Acta., 14, 1, 21-26.

Cayeux, L. (1935). Les Roches Sedimentaires de France, Roches Carbonatées. pp 463.

Chowns, T. M. (1968). Environmental and diagenetic studies of the Cleveland Ironstone Formation of north east Yorkshire . Unpub. Ph.D. thesis . University of Newcastle upon Tyne. pp 432.

Cloud, Jr., P. E. (1962). Environment of calcium carbonate deposition west of Andros Island, Bahamas, U.S., Geol. Surv., Prof. Paper, 350, 1-138.

Coleman, J. M., Gagliano, S. M. and Smith, W. G. (1970). Sedimentation in a Malaysian high tide tropical delta. pp 185-197 in Morgan, J.P. (Ed.). Soc. Econ. Palaeontologists, Mineralogists, Spec. Publ, 15.

Conley, C. D. (1977). Origin of distorted ooliths and pisoliths. J. Sed. Pet., 47, No.2, 554-564.

Cullis, C. G. (1904). The mineralogical changes observed in the cores of the Funafuti borings. pp 392-420 in the Atoll of Funafuti, Bonney, T. G. (Ed.). Trans. Roy. Soc. London.

Curtis, C. D. (1978). Possible links between sandstone diagenesis and depth-related geochemical reactions occurring in enclosing mud-stones. Jl. Geol. Soc. Lond., 135, Pt. 1, 107-119.

Curtis, C. D., Pearson, M. J. and Somogyi, V. A. (1975). Mineralogy, chemistry, and origin of a concretionary siderite sheet (clay-ironstone band) in the Westphalian of Yorkshire. Min. Mag., 40, 385-393.

Curtis, C. D. and Spears, D. A. (1968a). The formation of sedimentary iron minerals: Part 1. Econ. Geol., 63, (3), 257-262.

Curtis, C. D. and Spears, D. A. (1968b). The formation of sedimentary iron minerals: Part II. Econ. Geol., 63, (3), 262-270.

Davies, W. and Dixie, R. J. M. (1951). Recent work on the Frodingham Ironstone. Proc. Yorks. Geol. Soc., 28, 85-96.

Davies, P. J.,Bubela, B. and Ferguson, J. (1978). The formation of ooids. Sedimentology, 25, 707-730.

Davies, P. J. and Martin, K. (1976). Radial aragonite ooids, Lizard Island, Great Barrier Reef, Queensland, Australia, Geology, 4, 120-122.

Davis, J. C. (1973). Statistics and Data Analysis in Geology. pp 550. Wiley, New York.

Dickson, J. A. D. (1966). Carbonate identification and genesis as revealed by staining. J. Sed. Pet., 36, No.2, 491-505.

Donahue, J. D. (1969). Genesis of oolite and pisolite grains: an energy index. J. Sed. Pet., 35, 251-256.

Dunham, K. C. (1960). Syngenetic and diagenetic mineralisation in Yorkshire. Proc. Yorks. Geol. Soc., 32, 229-275.

Dunham, R. J. (1971). Meniscus cement: pp 297-300 in Carbonate Cements, Bricker, O. P. (Ed.). John Hopkins Press, Baltimore.

Edmonds, E. A. and Wilson, V. (1965). Geology of the country around Banbury and Edgehill. H.M.S.O.

Ellison, M. (1955). Palaeogeographical considerations as an aid to mineral exploration. Econ. Geol., 50, 1055-1078.

Englehardt, W von. (1942). Die structuren von thuringit, bavalit, und chamosit und ihre stellung in der chloritgruppe. Zeits. Krist. 104, 142-159.

Eugster, H. P. and Chow, I-Ming,(1973). The depositional environments of Precambrian banded iron-formations. Econ. Geol. 68, 1144-1169.

Evamy, B. D. and Shearman, D. J. (1965). The development of overgrowths from echinoderm fragments. Sedimentology, 5, 221-233.

Evamy, B. D. and Shearman, D. J. (1969). Early stages in development of overgrowths on echinoderm fragments in limestones. Sedimentology, 12, 317-322.

Folk, R. L. (1959). Practical petrographic classification of limestones, Bull. Am. Assoc. Petrol. Geologists, 43, 1-48.

Friedman, G. M. (1965). Terminology of crystallisation textures and fabrics in sedimentary rocks. J. Sed. Pet., 35, 643-655.

Friedman, G. M., Amiel, A. J., Bruan, M. and Miller, D. S. (1973). Generation of carbonate particles and laminates in algal mats - Example from sea marginal hypersaline pool, Gulf of Aqaba, Red Sea. Bull. Am. Ass. Petrol. Geol. 57, 541-557.

Fursich, F. T. (1975). Trace fossils as environmental indicators in the Corallian of England and Normandy. Lethaia, 8, 151-172.

Garrels, R. N. (1960). Mineral equilibria pp 254, Harper and Row, New York.

Glover, E. D. and Pray, L. C. (1971). High magnesian calcite and aragonite cementation within modern subtidal carbonate sediment grains. pp 80-87 in Carbonate Cements, Bricker, O. P. (Ed.).

Goodman, B. A. and Bain, D. C. (1978). Mössbauer spectra of chlorites and their decomposition products. pp 65-75 in Developments in Sedimentology, 27, Int. Clay. Conf.

Gould, H. R. (1970). The Mississippi delta complex pp 3-30 in Morgan, J. P. (Ed.). Soc. Econ. Palaeontologists, Mineralogists, Spec. Publ, 15.

Greensmith, T. J., Rawson, P. F. and Shalabu, S. E. An association of minor fining-upward cycles and aligned gutter marks in the Middle Lias (Lower Jurassic) of the Yorkshire coast. Proc. Yorks. Geol. Soc, 42, 4, 525-539.

Gruner, J. W. (1922). The origin of sedimentary iron formation: the Biwabik formation of the Mesabi Range. Econ. Geol., 17, 407-460.

Hallam, A. (1961). Brachiopod life assemblages from the Marlstone Rock-bed of Leicester: Palaeontology., 4, 653-659.

Hallam, A. (1963). Observations on the palaeoecology and ammonite sequence of the Frodingham Ironstone (Lower Jurassic): Palaeontology, 6, 554-574.

Hallam, A. (1966). Depositional environment of British Liassic ironstones considered in the context of their facies relationships: Nature, 209, 1306-1309.

Hallam, A. (1968). The Lias. pp 188-210, in The Geology of the East Midlands. Sylvester-Bradley, P. C. and Ford, T. D. (Eds.).

Hallam, A. (1978). Eustatic cycles in the Jurassic: Palaeoecology, Palaeobotany, Palaeoclimatology, 23, 1-32.

Hallam, A. and Bradshaw, M. J. (1979). Bituminous shales and oolitic ironstones as indicators of transgressions and regressions. Q.J.G.S., 136, 2, 157-164.

Hallam, A. and Sellwood, B. W. (1976). Middle Mesozoic sedimentation in relation to tectonics in the British area. Geol. Journ. 84, 301-321.

Hallimond, A. F. (1925). Special Reports on the Mineral Resources of Great Britian - Volume XXIX - Iron Ores: Bedded Ores of England and Wales. Petrography and Chemistry. HMSO. pp 100.

Hallimond, A. F. (1939). On the relation of chamosite and daphnite to the chlorite group. Min. Mag., 25, 441-455.

Hayes, M. O. (1967). Hurricanes as geologic agents: case studies of Hurricans Carla, 1961 and Cindy, 1963. Bur. Econ. Geol. Univ. Texas, Rept Invest. 61, 1-50.

Hemmingway, J. E. (1951). Cyclic Sedimentation and the deposition of ironstone in the Yorkshire Lias: Proc. Yorks. Geol. Soc., 28, 67-74.

Hemmingway, J. G. (1974). Jurrasic. In: The Geology and Mineral Resources of Yorkshire. Rayner, D. H. and Hemmingway, J. E. (Eds.). Yorks. Geol. Soc. 161-233.

Hollingworth, S. E. and Taylor, J. M. (1951). The Northampton Sand Ironstone ,Stratigraphy, structure and resources. H.M.S.O.

Howard, J. D. and Reineck, H. E. (1972). Georgia coastal region, Sapelo Island, U.S.A.: Sedimentology and Biology IV. Senckenb. Maritima 4, 81-123.

Howarth, M. K. (1955). Domerian of the Yorkshire coast. Proc. Yorks. Geol. Soc. 30, 147-175.

Howarth, M. K. (1958). The Ammonites of the Liassic Family Amaltheidae in Britain. Palaeontogr. Soc. Monogr. , IXXXVII , 53pp.

Howarth, M. K. (1962). The Jet Rock Series and the Alum Shale Series of the Yorkshire coast. Proc. Yorks, Geol. Soc. 33, 381-422.

Howarth, M. J. (1973). The stratigraphy and ammonite fauna of the Upper Liassic Grey Shales of the Yorkshire coast. Bull. Br. Mus. Nat. Hist. (Geology) 24, 235-77.

Howarth, M. J. (1978). The stratigraphy and ammonite fauna of the Upper Lias of Northamptonshire. Bull. Br. Mus. Nat. Hist. (Geology) 29, 235-88.

Howarth, M. K. and Rawson, P. F. (1965). The Liassic Succesion in a Clay Pit in Kirton in Lindsey, N. Lincolnshire. Geol. Mag., 102, 261-266.

Huber, N. K. and Garrels, R. M. (1953). Relation of pH and oxidation potential to sedimentary iron mineral formation. Econ. Geol. 48, 337-57.

Illing, L. V. (1954). Bahamian calcareous sands. Bull. Am. Assoc. Petrol. Geol., 38, 1-95.

Irving, E. and Opdyke, N. D. (1965). The palaeomagnetism of the Bloomsburg red beds and its possible application to the tectonic history of the Appalachians. Geophys. J. Roy. Astron. Soc., 9, 153-167.

James, H. L. (1954). Sedimentary Facies in Iron Formation. Econ. Geol., 49, 235-281.

James, H. L. (1966). Chemistry of the Iron-rich Sedimentary Rocks. U.S. Geol. Surv. Prof. Paper 440-W.

Kahle, C. F. (1975). Ooids from Great Salt Lake, Utah, as an analogue for the genesis and diagenesis of ooids in marine limestones. J. Sed. Pet., 44, 30-39.

Kent, P. E. (1980). Subsidence and uplift in East Yorkshire and Lincolnshire: A double inversion. Proc. Yorks. Geol. Soc., 42, 4, 505-525.

Kimberley, M. M. (1974). Origin of iron ore by diagenetic replacement of calcareous oolite. Nature, 250, 319-320.

Kimberley, M. M. (1979). Origin of oolitic iron formations. J. Sed. Pet., 49, 111-132.

Klein, C. and Bricker, O. P. (1977). Some aspects of the sedimentary and diagenetic environment of Proterozoic banded iron formation. Econ. Geol., 72, 1457-1471.

Knox, R. W. O' B (1970). Chamosite ooliths from the Winter Gill Ironstone (Jurassic) of Yorkshire, England. J. Sed. Pet., 40, 1216-1225.

Krejci-Graf, K. (1964). Discussion. Proc. Yorks. Geol. Soc., 34, 469.

Krumbein, W. C. and Garrels, R. M. (1952). Origin and classification of chemical sediments in terms of pH and oxidation-reduction potentials. J. Geol. 60, 1-33.

Lemoalle, J. and Dupont, B. (1976). Iron-bearing oolites and the present conditions of iron sedimentation in Lake Chad (Africa). pp 168-178 in Ores in Sediments, Amstutz and Bernard (Eds.). Springer-Verlag, Heidelberg.

Lewis, G. J. and Goldberg, E. D. (1954). Iron in marine waters. J. Marine Res., 13, 183.

Lindholm, R. C. and Finkleman, R. B. (1972). Calcite staining: semi-quantitative determination of ferrous iron. J. Sed. Pet., 44, 428-440.

Lohmann, J. C. and Meyers. W. J. (1977). Microdolomite inclusions in cloudly prismatic calcites: A proposed criterion for former high-magnesian calcites. J. Sed. Pet., 47, 3, 1078-1088.

Mc Elhinny, M. W. (1973). Palaeomagnetism and Plate Tectonics. pp 358. Cambridge University Press.

Mc. Elhinny, M. W. and Cowley, J. A. (1980). Palaeomagnetic directions and pole positions - XVI. Pole numbers 16/1-16/296. Geophys., J.R. A.S., 61, 3, 549-573.

Martinsson, A. (1970). Toponomy of trace fossils. pp 323-330 in Trace Fossils, Crimes, T. P. and Harper, J. C. (Eds.). Geol. J. Spec. Issue 3.

Mason, B. (1966). Principles of Geochemistry. pp 300. Wiley, New York.

Meyers, W. J. and Lohmann (1978). Microdolomite-rich syntaxial cements: Proposed meteoric-marine mixing zone phreatic cements from Mississippian Limestones, New Mexico. J. Sed. Pet., 48, 2, 475-488.

Moore, E. S. and Maynard, J. E. (1929). Transportation and precipitation of iron and silica. Econ. Geol., 24, 272-527.

Nelson, B. W. and Ray, R. (1958). Synthesis of the chlorites and their structural and chemical constitution. Amer. Min., 43, 707-725.

Newell, N. D., Purdy, E. G. and Imbrie, J. (1960). Bahamian oolitic sand. J. Geol., 68, 481-497.

Novak, F. and Valcha, Z. (1964). Zelezity ortochamosit z Hory Svate, Katering v Krusnych horach. Sb. Geol. ved. I.G., 3, 7-26.

Orcel, J., Henin, S. and Caillere, S. (1949). Layer silicates of iron ore minerals. C.R. Acd. Sci. Parid, 229, 134-135.

Poole, E. G., Williams, B. J. and Hains, B. A. (1968). Geology Of The Country Around Market Harborough. H.M.S.O.

Porrenga, D. H. (1967). Glauconite and chamosite as depth indicators in the marine environment. Marine Geol., 5, 495-501.

Purdy,E. G. (1964). Diagenesis of Recent marine carbonate cements. Bull. Am. Assoc. Petrol. Geologists, 48, 542-543 (abstract).

Purdy, E. G. (1968). Carbonate diagenesis: An environmental survey. Geol. Romana, 7, 183-228.

Rastall, R. H. and Hemmingway, J. E. (1940). The Yorkshire Dogger: I, The Coastal Region. Geol. Mag., vol. 77, pp 177-275.

Rayner, D. H. and Hemmingway, J. E. (1974). The Geology and Mineral Resources of Yorkshire. Yorks. Geol. Soc.

Reed, S. J. B. (1975). Electron Microprobe Analysis. pp 350. Cambridge University Press.

Reineck, H. E. and Singh, I. B. (1975). Depositional Sedimentary Environments. Springer-Verlag, New York.

Rhys, G. H. (1974). A proposed standard lithostratigraphic nomenclature for the whole of the U.K. (North Sea). I.G.S. Report No: 74/8.

Richardson, L. Arkell, W. J. and Dines, H. G. (1946). Geology of the Country around Witney. H.M.S.O.

Richter, D. K. and Füchtbauer, H. (1978). Ferroan calcite replacement indicates former magnesian calcite skeletons. Sedimentology, 25, 843-860.

Sandberg, P. A. (1976). New interpretations of Great Salt Lake ooids and of ancient non skeletal carbonate mineralogy. Sedimentology, 22, 497-537.

Seilacher, A. (1964). pp 296-316. In: Approaches to Palaeoecology; Imbrie, J., Newell, N. (Eds.). Wiley, New York.

Selley, R. C. (1970). Studies of sequence in sediments using a simple mathematical device. Q.J.G.S., 125, 557-581.

Shearman, D. J., Twyman, J. and Karimi, M. Z. (1979). The genesis and diagenesis of oolites, Proc. Geol. Ass (Engl), 81, 561-575.

Sillen, L. G. (1967). Gibbs phase rule and marine sediments, pp. 57-69 in Equilibrium Concepts in Natural Water Systems. Washington D.C., Am. Chem. Soc., Advances in Chemistry Series No. 67.

Smith, M. H. (1970). Identification of organic matter in thin sections by staining and a study programme for carbonate rocks. J. Sed. Pet., 40, No. 4, 1350-1351.

Sorby, H. C. (1856). On the origin of the Cleveland Hill ironstone. Polytechnic Soc. West Riding of Yorkshire Proc., 3, 457-461.

Spencer, D. W. and Brewer, P. G. (1969). The distribution of copper, zinc, and nickel in sea water of the Gulf of Maine and the Sargasso Sea. Geochim. Cosmochim Acta 33, 325.

Strakhov, N. M. (1953). Diagenesis and its importance in sedimentary ore formation. Izv. An. S.S.S.R. ser. geol., 5, 12-49. (British Govt. Dept. Education and Science Russian Translating Programme RT.S. 2863, pp 1-74, 1965).

Suess, E. and Fütterer, D. (1972). Aragonitic ooids; experimental precipitation from seawater in the presence of humic acids. Sedimentology, 22, 497-537.

Swineford, A. Leonard, A. B. and Frye, J. C. (1958). Petrology of the Pliocene pisolitic limestone in the Great Plains. Bull. Geol. Surv. Kansas, 130: 97-116.

Talbot, M. R. (1974). Ironstones in the Upper Oxfordian of southern England. Sedimentology, 21, 433-450.

Tardy, Y. and Garrels, R. M. (1974). A method of estimating the Gibbs energies of formation of layer silicates: Geochim. Cosmochim. Acta v. 38, pp 1101-1116.

Taylor, J. H. (1949). Petrology of the Northampton Sand Ironstone Formation. H.M.S.O.

Taylor, J. H. (1963). Geology of the Country Around Kettering, Corby, and Oundle. H.M.S.O.

Thellier, E. (1938). Thesis (Unpublished, University of Paris).

Thomas, J. B. (1978). Diagenetic sequences in low-permeability argillaceous sandstones. Jl. Geol. Soc. Lond., 135, 1, 93-101.

Turekian, K. K. and Wedepohl, K. H. (1961). Distribution of the elements in some major units of the earth's crust: Geol. Soc. Amer. Bull., 72, 175-192.

Turner, P. (1974). Lithostratigraphy and facies analysis of the Ringerike Group of the Oslo region. Norges. geol. Unders, 314, 101-130.

Turner, P. (1977). Ironstones: B.A. Meeting, Section C.

Van Loon, J. C. and Parissis, C. M. (1969). Scheme of silicate analysis based on the lithium metaborate fusion followed by atomic absorption spectrophotometry. The Analyst, 94, 1057-1062.

Vaughan, D. J. and Craig, J. R. (1978). The Mineral Chemistry Of Metal Sulfides. pp 493. Cambridge University Press.

Whitehead, T. H., Anderson, W., Wilson, V. and Wray, D. A. (1952). The Liassic Ironstones. H.M.S.O.

Wilson, V. (1952). The Jurassic ironstone fields of the East Midlands of England. pp 441-449. In: Symp. Gisements Fer Monde, Internat. Geol. Congr., Algiers, II, 1952.

Yershova, Z. P., Nikitina, A. P., Periflev, Yu. D. and Babeshkin, A. M. (1975). Study of chamosite by gamma-resonance (Mössbauer) spectroscopy. Proc. Int. Clay Conference 1975, 221-219.

Youell, R. F. (1955). Mineralogy and crystal structure of chamosite. Nature, 176, 560-561.

Zalinski, E. R. (1904). Untersuchungen über Thuringit und Chamosit aus Thüringen und Umgebung. Neues Jahrbuch Min. B. Bd., 19, 40-84.

Ziegler, P. A. (1978). North-west Europe: Tectonics and basin development. Geol. en. Mijnb., 57 (4), 589-626.